GEOLOGICAL SURVEY OF CANADA
COMMISSION GÉOLOGIQUE DU CANADA

PAPER 80-1B
ÉTUDE

CURRENT RESEARCH
PART B

RECHERCHES EN COURS
PARTIE B

Energy, Mines and Resources Canada
Énergie, Mines et Ressources Canada

1980

Notice to Librarians and Indexers

The Geological Survey's thrice-yearly *Current Research* series contains many reports comparable in scope and subject matter to those appearing in scientific journals and other serials. All contributions to the Scientific and Technical Report section of *Current Research* include an abstract and bibliographic citation. It is hoped that these will assist you in cataloguing and indexing these reports and that this will result in a still wider dissemination of the results of the Geological Survey's research activities.

Avis aux bibliothécaires et préparateurs d'index

La série Recherches en cours *de la Commission géologique paraît trois fois par année; elle contient plusieurs rapports dont la portée et la nature sont comparable à ceux qui paraissent dans les revues scientifiques et autres périodiques. Tous les articles publiés dans la section des rapports scientifiques et techniques de la publication* Recherches en cours *sont accompagnés d'un résumé et d'une bibliographie, ce qui vous permettra, nous l'espérons, de cataloguer et d'indexer ces rapports, d'où une meilleure diffusion des résultats de recherche de la Commission géologique.*

Technical editing and compilation
Rédaction et compilation techniques
R.G. Blackadar
P.J. Griffin
H. Dumych
F.R.W. Neale

Production editing and layout
Préparation et mise en page
Leona R. Mahoney
Lorna A. Firth
Michael J. Kiel

Typed and checked by
Dactylographie et vérification
Debby Busby
Judy Côté
Jane Desautels
Susan Gagnon
Janet Gilliland
Sharon Parnham

GEOLOGICAL SURVEY
PAPER 80-1B

COMMISSION GÉOLOGIQUE
ÉTUDE 80-1B

CURRENT RESEARCH
PART B

RECHERCHES EN COURS
PARTIE B

1980

Available in Canada through

authorized bookstore agents
and other bookstores

or by mail from

Canadian Government Publishing Centre
Supply and Services Canada
Hull, Québec, Canada K1A 0S9

and from

Geological Survey of Canada
601 Booth Street
Ottawa, Canada K1A 0E8

A deposit copy of this publication is also available
for reference in public libraries across Canada

Cat. No. M44-80/1BE Canada: $7.50
ISBN – 0-660-10596-9 Other countries: $9.00

Price subject to change without notice

SCIENTIFIC AND TECHNICAL REPORTS
RAPPORTS SCIENTIFIQUES ET TECHNIQUES

ECONOMIC GEOLOGY/GÉOLOGIE ÉCONOMIQUE

GEOCHEMISTRY/GÉOCHIMIE

GEOCHRONOLOGY/GÉOCHRONOLOGIE

GEOPHYSICS/GÉOPHYSIQUE

PALEONTOLOGY/PALÉONTOLOGIE

QUATERNARY GEOLOGY/GÉOLOGIE DU QUATERNAIRE

REGIONAL GEOLOGY/GÉOLOGIE RÉGIONALE

Appalachian Region/Région des Appalaches

Cordilleran Region/Région de la Cordillère

Precambrian Shield/Bouclier précambrien

Interior Plains/Plaines intérieures

SCIENTIFIC AND TECHNICAL NOTES
NOTES SCIENTIFIQUES ET TECHNIQUES

DISCUSSIONS AND COMMUNICATIONS
DISCUSSIONS ET COMMUNICATIONS

Separates

A limited number of separates of the papers that appear in this volume are available by direct request to the individual authors. The addresses of the Geological Survey of Canada offices follow:

601 Booth Street,
OTTAWA, Ontario
K1A 0E8

Institute of Sedimentary and Petroleum Geology,
3303-33rd Street N.W.,
CALGARY, Alberta
T2L 2A7

Cordilleran Geology Division
100 West Pender Street,
VANCOUVER, B.C.
V6B 1R8

Atlantic Geoscience Centre,
Bedford Institute of Oceanography,
P.O. Box 1006,
DARTMOUTH, N.S.
B2Y 4A2

When no location accompanies an author's name in the title of a paper, the Ottawa address should be used.

Tirés à part

On peut obtenir un nombre limité de "tirés à part" des articles qui paraissent dans cette publication en s'adressant directement à chaque auteur. Les adresses des différents bureaux de la Commission géologique du Canada sont les suivantes:

601, rue Booth
OTTAWA, Ontario
K1A 0E8

Institut de géologie sédimentaire et pétrolière
3303 N. – O., 33rd, ST. N.W.,
CALGARY, Alberta
T2L 2A7

Division de la géologie de la Cordillère
100 West Pender Street
VANCOUVER, Colombie-Britannique
V6B 1R8

Centre géoscientifique de l'Atlantique
Institut océanographique de Bedford
B.P. 1006
DARTMOUTH, Nouvelle-Ecosse
B2Y 4A2

Lorsque l'adresse de l'auteur ne figure pas sous le titre d'un document, on doit alors utiliser l'adresse d'Ottawa.

SCIENTIFIC AND TECHNICAL REPORTS
RAPPORTS SCIENTIFIQUES ET TECHNIQUES

1.

UPPER TRIASSIC STRATIGRAPHY, DEASE LAKE AND TULSEQUAH MAP AREAS, NORTHWESTERN BRITISH COLUMBIA

Project 750015

J.W.H. Monger
Cordilleran Geology Division, Vancouver

Monger, J.W.H., Upper Triassic stratigraphy, Dease Lake and Tulsequah map areas, northwestern British Columbia; in Current Research, Part B, Geological Survey of Canada, Paper 80-1B, p. 1-9, 1980.

Abstract

Upper Triassic volcanogenic strata in northwestern British Columbia comprise a lower sequence of basic extrusives, volcaniclastics and sedimentary rocks, probably of Late Karnian age, and an upper sequence of intermediate and locally acidic volcaniclastics that is in part of Late Norian age. In Tulsequah map area, proximal facies, extrusive and coarse grained volcaniclastics, lie to the southwest, whereas distal facies, commonly finer grained and interbedded with shales, lie to the northeast. This facies trend mirrors that of overlying Lower Jurassic clastic strata of the Whitehorse Trough.

Introduction

This report describes the stratigraphy of mainly Upper Triassic rocks in parts of Dease Lake (104 J) and Tulsequah (104 K) map areas, and is the continuation of earlier work to the east and southeast (Monger and Thorstad, 1978). The work was carried out concurrently with Operation Dease (Gabrielse, 1980) and Jurassic biostratigraphic studies by H.W. Tipper.

Most earlier work in this region is of a reconnaissance nature. Taku River area in Tulsequah map area was mapped on a scale of 1 inch to 2 miles by Kerr (1948). Later Souther (1971) mapped the whole of the Tulsequah map sheet on a scale of 1:250 000, and recognized such major structural discontinuities as the King Salmon Fault. Parts of Dease Lake map area were studied by Kerr (1926), Hanson and McNaughton (1936), and Watson and Mathews (1944). This area was mapped at a scale of 1:250 000 by Gabrielse et al. (1962) and the Cache Creek Group within it by Monger (1969).

The Triassic strata described below lie in three different tectonostratigraphic terranes, separated by major faults (Fig. 1.1). (1) To the southwest, the Stikine block (or Stikinia) has dimensions of at least 1000 km along the trend of the Cordillera and 300 km across it (see Fig. 1 of Monger and Price, 1979). Triassic rocks described herein from the Tulsequah area lie mainly on the northeastern margin of Stikinia. They overlie upper Paleozoic to Middle Triassic strata of the "Stikine assemblage" (Monger, 1977), that were deformed, locally metamorphosed and probably intruded by granitic rocks in the Tahltanian orogeny (Souther, 1971; Anderson, 1978). Disconformably (?) above the Triassic strata are Lower Jurassic (Upper Pliensbachian to Middle Bajocian) conglomerate, greywacke, and shale of the Takwahoni facies of the Laberge Group, that form the proximal part of the southeastern extension of the Whitehorse Trough (Souther, 1971; Tipper, 1978). (2) Northeast, across the King Salmon Fault, is the Hinterland Belt, which is characterized by high strain and by structures directed dominantly southwestward in this region (Wheeler and Gabrielse, 1972; Monger et al., 1978). It consists of two elements, locally separated by the Nahlin Fault. A southerly one, the distal part of the southeastern extension of the Whitehorse Trough (Souther, 1971), contains Lower Jurassic shale and siltstone, the Inklin facies of the Laberge Group, uppermost Triassic carbonate of the Sinwa Formation, probable Upper Triassic volcaniclastics, and local, fault-bounded slices of the Cache Creek Group. The northern element comprises highly deformed Mississippian to probable Middle Triassic strata of the Cache Creek Group, forming the Atlin Terrane. (3) Northeasternmost is the Omineca Crystalline Belt, at these latitudes composed of variably metamorphosed lower Paleozoic and Proterozoic miogeoclinal strata, upper Paleozoic and lower Mesozoic volcanic and sedimentary rocks, and Cretaceous granitic rock. Upper Triassic volcanogenic strata of the Nazcha and Shonektaw formations, discussed herein, together with Laberge-like greywacke, form a narrow belt separated from the Hinterland Belt to the south by a major fault, and have unknown relationships to older strata to the north (Gabrielse, 1978; and personal communication).

Tulsequah Map Area

Triassic strata were examined in an area on both sides of the Taku River (Fig. 1.1, 1.2), between Sutlahine River and Tunjony Lake (Fig. 1.1, T), and west of Sheslay River (Fig. 1.1, S).

Most strata examined in the Taku River area lie south of the King Salmon Fault. Southerly exposures, south of Mount Jeanne, near Stuhini Creek and south of Shustahini Mountain are sparsely fossiliferous massive volcaniclastics and flows whose internal stratigraphy is poorly understood. Northern exposures, well developed along the faulted anticline between Honakta Mountain and Mount Lester Jones (Fig. 1.2), are well stratified, have contrasting lithologies and diagnostic fossils, and thus readily provide reference sections.

The lowest sequence in the core of the anticline north of Mount Lester Jones (Fig. 1.2, Section 2) typically consists of thin bedded graded argillite, siltstone and bedded lithic tuff about 1000 m thick (Fig. 1.3a, b). In its lower part are lenses of dark grey-green pillow basalt (Fig. 1.3g), locally with small feldspar phenocrysts, lapilli tuff, and massive breccia beds containing clasts up to 30 cm across of mainly basic feldspar porphyry and rare fragments of coralline limestone. The base of the sequence is not exposed. At the top of the section is black, calcareous shale and local thin bedded argillaceous limestone containing halobiid clams,

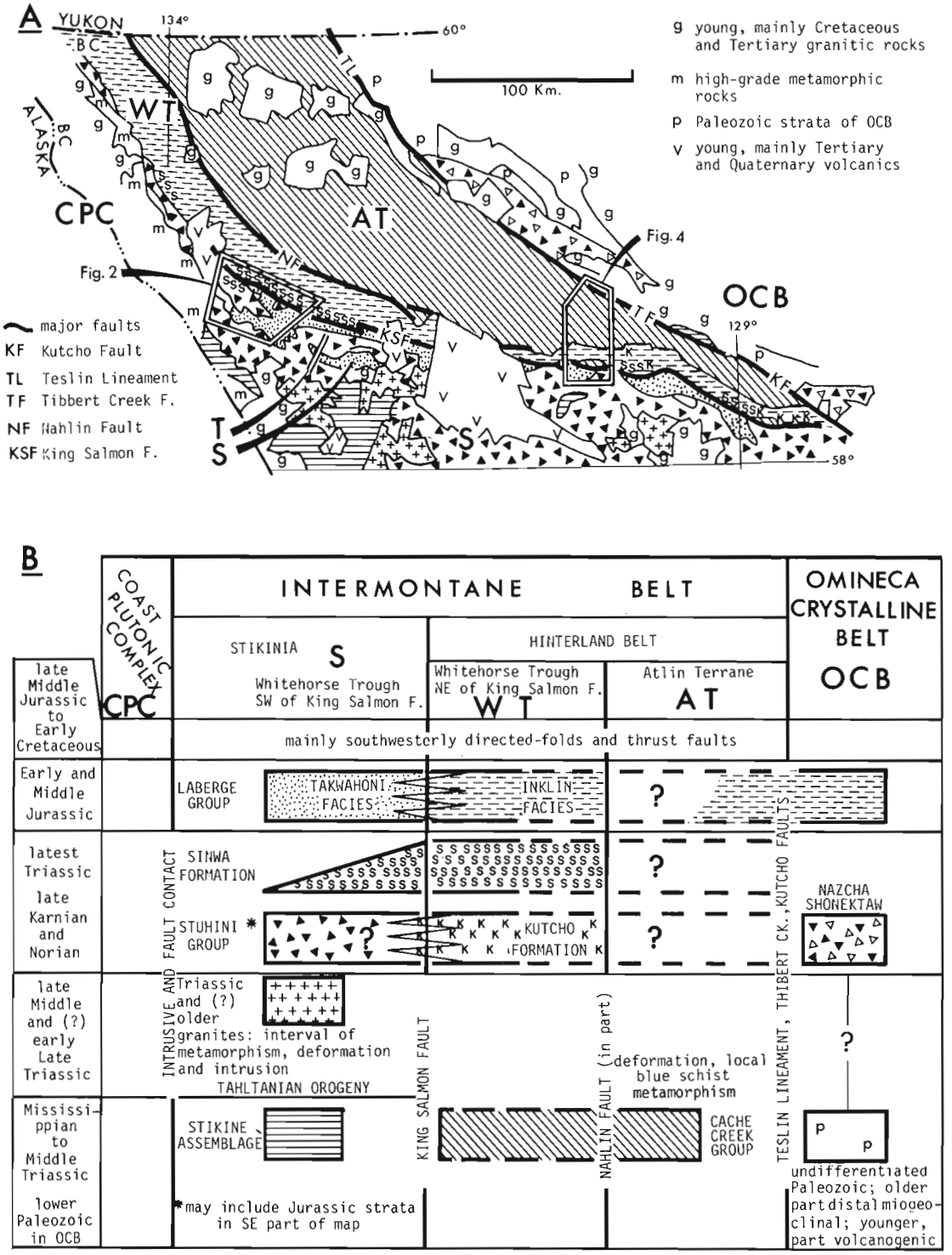

A Index map showing location of areas studied in detail, on a geological sketch map of northwestern British Columbia.

B Tentative correlation chart of upper Paleozoic and lower Mesozoic rock units in northwestern British Columbia, showing intervals of deformation.

Figure 1.1

belemnites and ammonites, whose age, according to E.T. Tozer (personal communication), is Late Karnian (Welleri zone). The unit comprises most of the King Salmon Group of Kerr (1948), which Souther (1971) redefined as a formation within the Stuhini Group. The writer concurs with this change.

Above the predominantly fine grained rocks is a sequence transitional to the uppermost coarse grained volcaniclastic sequence and included by Kerr (1948) in the upper part of his King Salmon Group. It consists of at least five massive breccia and conglomerate units interbedded with shale and siltstone beds containing small halobiid clams and belemnites (Fig. 1.3c, d). The total thickness is about 700 m, with individual coarse clastic units ranging from 30 to 100 m. The massive beds have little apparent internal structure, variable proportions of sandy matrix to cobbles and boulders, and any internal layering is generally apparent only from a distance. The bases of some massive units locally contain contorted argillite and siltstone fragments apparently derived from underlying beds, and one unit appears to cut down markedly into the underlying shale (Fig. 1.3c). The coarse grained units are interpreted as debris flows into the shale basin represented by the intercalated beds.

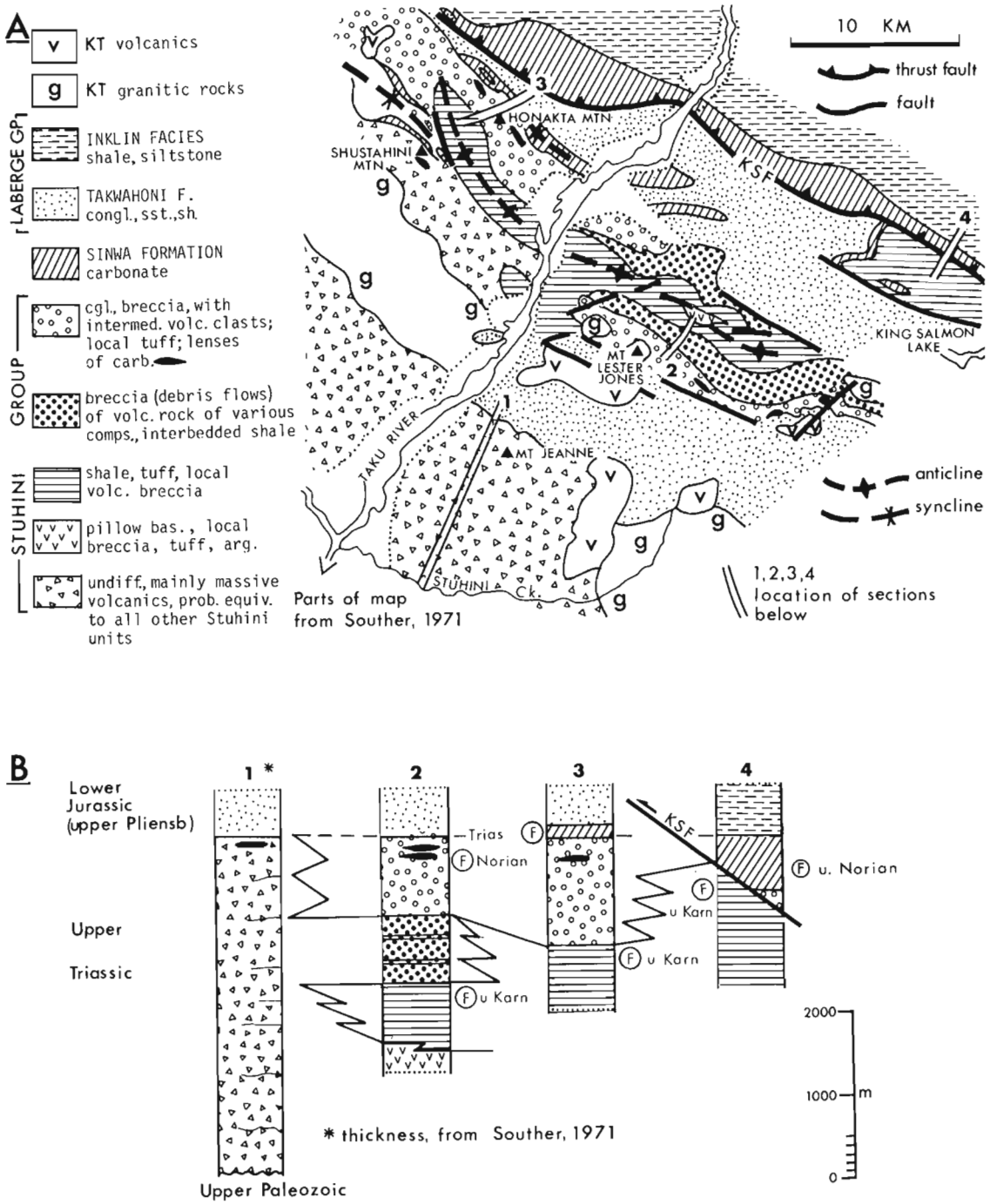

Figure 1.2. Geological sketch map of the Taku River area, northwestern Tulsequah map area, with a local correlation chart of Triassic strata, showing increased sedimentary component in sections towards the northeast.

Figure 1.3. *Features of the Triassic sections near Taku River.*

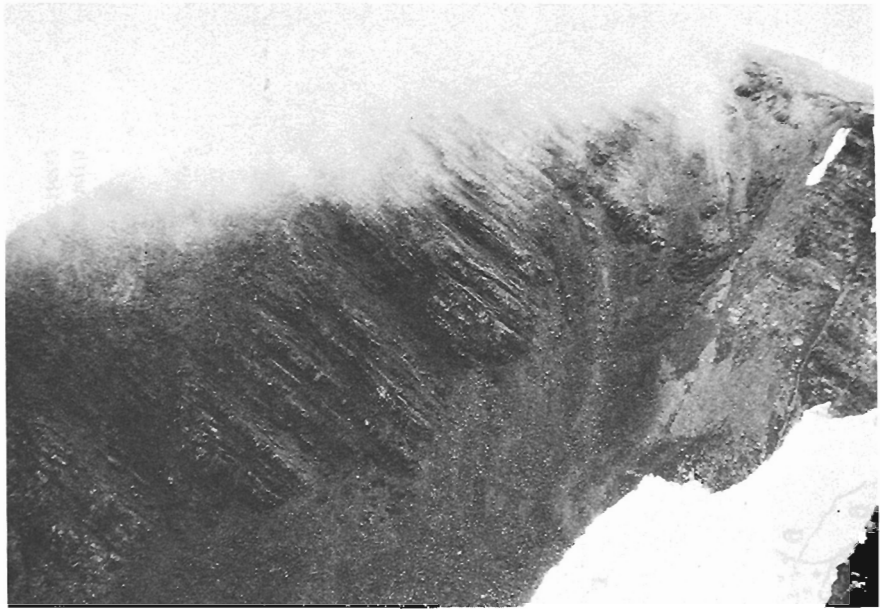

Figure 1.3a. *Characteristically well bedded argillites and fine grained volcaniclastics of the lower part of the Triassic section exposed in the core of the anticline, northeast of Mount Lester Jones.*

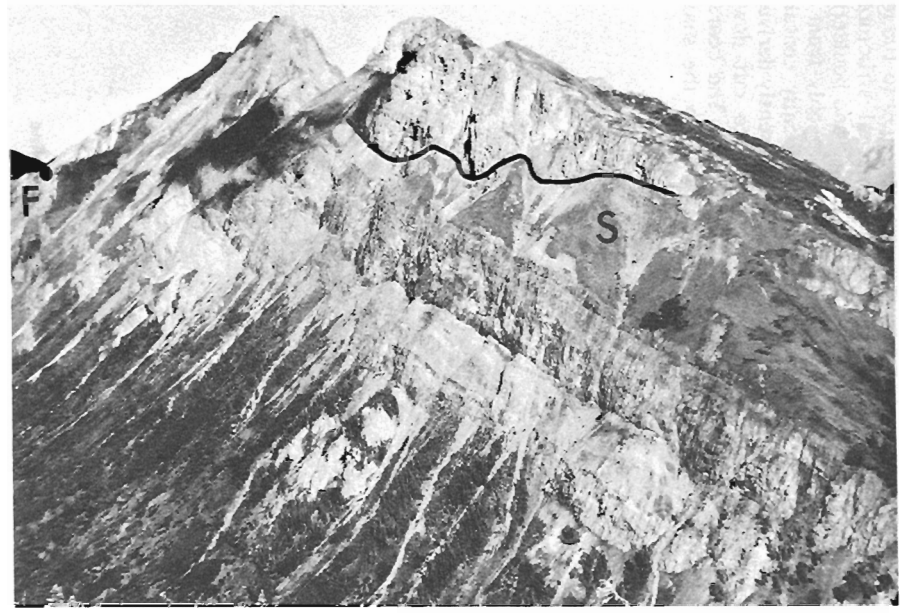

Figure 1.3c. *Massive, debris flows with interbedded argillites and siltstones from northeastern part of Mount Lester Jones area. Note the upper flow cuts into underlying shale section (S). Upper Karnian fossil locality (f) on extreme left of photo.*

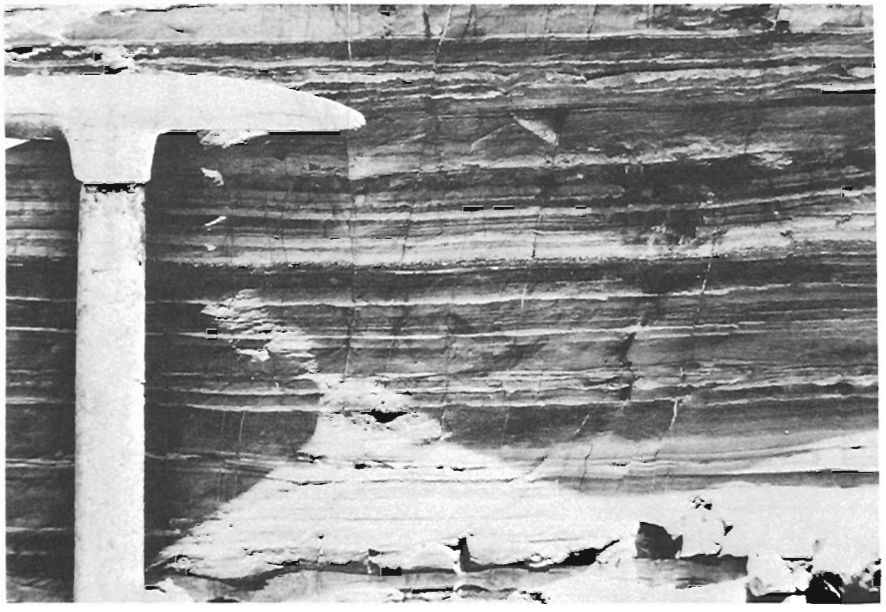

Figure 1.3b. *Detail of finely laminated part of section shown in A.*

Figure 1.3d. *Detail of debris flow: boulders of basic volcanics and carbonate up to 0.5 m across in a volcaniclastic matrix. No internal stratification.*

Figure 1.3e. *Detail from f; breccia of intermediate volcanic clasts.*

Figure 1.3g

Pillow basalt intercalated with lowest part of section in Fig. 1.3a; note contact (arrow) of pillows with underlying part of section.

Figure 1.3f. *Upper part of Triassic section. Massive, locally well bedded conglomerate, and breccia and volcanic sandstone on Honakta Mountain.*

Figure 1.3h. *Relationship of Sinwa Formation to Triassic volcanics. In middle ground, carbonate of the Sinwa (S) lies on Triassic volcanics (V) and is folded into a syncline with Takwahoni conglomerate and sandstone (T) in core. Behind, thicker Sinwa carbonate is thrust on the King Salmon Fault (KSF) over Jurassic Takwahoni conglomerate. North of Honakta Mountain.*

Each coarse grained unit has its own distinctive composition which it maintains over the area north of Mount Lester Jones. (1) Lowermost, and lying sharply but conformably on calcareous shale, is white, buff and pale green feldspathic sandstone or crystal tuff, interbedded with shale, that grades up into massive breccia with a similar matrix and cobbles mainly of light coloured andesite containing small feldspars, and rare limestone. (2) The overlying massive unit is distinctive brown, friable, sandstone (or tuff) and breccia containing pyroxene crystals both as free grains and as pheoncrysts in clasts of porphyritic basalt. (3) Above this is a massive breccia unit containing purple, pink and green clasts of fine grained andesitic feldspar porphyry that closely resembles the youngest Triassic volcanogenic sequence. (4) Uppermost, northeast of the summit of Mount Lester Jones, is a very coarse debris flow with blocks and boulders of pyroxene porphyry, fine grained basalt and limestone (Fig. 1.3d).

The uppermost Triassic volcanogenic unit forms the ridge containing the summit of Mount Lester Jones and is at least 1000 m of massive, pale green, white and red andesite breccia and conglomerate with no interbedded shale, but local red or buff weathering tuffaceous horizons. The colour variation is perhaps due to secondary alteration. Where the rocks are freshest they are commonly red or pink, but in most places they are buff and friable with laumontitic alteration and, near granitic intrusions, bleached white and hard. Clasts are predominantly light coloured, fine grained feldspar porphyry, with or without crystals of hornblende generally altered to magnetite, and rare hypabyssal (?) granitoids. Near the top of the succession are interbedded lenses of grey and pink limestone, generally a few tens of metres thick, that are locally tuffaceous and contain an abundant but poorly preserved, silicified fauna of corals, bryozoans (?), belemnites, rare wood fragments and possible ammonites, and conodonts of Norian age (M. Orchard, personal communication).

This unit is overlain, apparently disconformably, on the southeastern ridge of Mount Lester Jones and on the mountain to the east, by calcareous sandstone and polymictic conglomerate of Early Jurassic (Late Pliensbachian) age of the Takwahoni facies of the Laberge Group.

The succession near Shustahini and Honakta mountains, along trend to the northwest, is divisible into two major volcanosedimentary units (Fig. 1.2, Section 3). Lowermost is well bedded shale and tuff, and locally, more massive beds of lapilli tuff. These rocks contain Late Karnian (Dilleri zone) fossils (E.T. Tozer, personal communication). The overlying unit is massively bedded, white, buff, pink and locally red, andesitic conglomerate, breccia and tuff, with local lenses of limestone containing silicified fossils (Fig. 1.3f, e), equivalent to the uppermost Triassic unit to the southeast and possibly to some of the massive debris flows. Above the upper unit is fine grained, locally laminated limestone that ranges in thickness from 10 to 100 m, and whose base locally is red. This limestone has been correlated by Souther (1971) with the lithologically identical but thicker, Upper Norian Sinwa Formation that lies north of the King Salmon Fault, and contains Triassic conodonts (M. Orchard, personal communication).

Rocks on Shustahini Mountain and Mount Jeanne (Fig. 1.2, Section 1) are lithologically identical with the upper volcanic unit to the north and consist of white, pale green to reddish andesite breccia and local conglomerate and tuff horizons and, on Shustahini, carbonate pods containing silicified fossils. They form the upper part of an apparently entirely volcanic sequence, whose thickness is estimated by Souther (1971) to be about 4000 m, that appears to be equivalent to the entire Triassic section to the north. Lower members in this succession, near Stuhini Creek, include dark basaltic flows, lithologically similar to those at the base of the section north of Mount Lester Jones and local porphyritic basalt with pyroxene phenocrysts. The base of this succession lies unconformably on metamorphic rocks of possible late Paleozoic age (Kerr, 1948).

Other sections, south of the King Salmon Fault, are correlative with the lower part of the Mount Lester Jones section, in that extrusive rocks and volcaniclastic detritus are predominantly basic, and known diagnostic fossils are of Late Karnian age. North of King Salmon Lake and south of the King Salmon Fault (Fig. 1.2, Section 4) the section comprises dark green to dark brown, well bedded lapilli tuff and lithic tuff and argillite containing Upper Karnian (Dilleri zone) fossils. Farther east, between Sutlahine River and Tunjony Lake (Fig. 1.1, T), Triassic strata lie north and south of a faulted syncline containing Lower Jurassic clastics. North of the syncline, the section consists of predominantly well bedded, brown, lithic crystal and lapilli tuff, with minor shale and near the top, more massive dark red and green breccia, and pillow breccia of 'bladed' feldspar porphyry, with coarse (up to 2 cm long) plagioclase laths in a dark green matrix. Upper Karnian (Welleri zone) fossils are in the upper part of this section (E.T. Tozer, personal communication). South of the syncline the section is dominated by extrusive rocks, mainly pillow basalt that is either aphanitic or has small feldspar phenocrysts (similar to basalt in the lower part of the Lester Jones section) and lesser amounts of basalt with pyroxene phenocrysts. The lateral facies variation from proximal in the south to distal in the north seen from Stuhini Creek to Mount Lester Jones, is repeated here.

Rocks west of Sheslay River (Fig. 1.1) are typical of the lower part of the Triassic sequence farther east in Dease and Cry Lake map areas (e.g. Monger and Thorstad, 1978). They comprise porphyritic pillow basalt, with phenocrysts of pyroxene and feldspar, pillow breccia and crystal lithic tuff with abundant pyroxene and plagioclase crystals.

North of the King Salmon Fault, Triassic rocks are mainly the continuous, massive but locally laminated and bituminous, carbonate of the Sinwa Formation. This in places attains a thickness of 800 m and contains early Late Norian (Cordilleranus zone) age fossils (E.T. Tozer, personal communication). North of King Salmon Lake (Fig. 1.2, Section 4) the Sinwa grades down into red tuff and volcanic breccia with clasts of porphyritic andesite containing small feldspar phenocrysts, that is lithologically similar to the uppermost volcaniclastic unit south of the King Salmon Fault. Lower Jurassic argillite and siltstone of the Inklin facies of the Laberge Group lie disconformably on the Sinwa.

Dease Lake Area

The Hinterland Belt at Dease Lake is only 35 km across, compared with 115 km farther west, and has a concomitant increase in the amount of deformation and development of foliation.

South of the King Salmon Fault, Triassic rocks are mainly massive, unfossiliferous, commonly green and rarely red volcanic breccia and crystal tuff, with clasts of porphyritic basalt containing pyroxene phenocrysts. Although no fossils were found in this area, these rocks are typical of Upper Karnian-Lower Norian sequences elsewhere in the Intermontane Belt and of those in the lower part of the succession around the Hotailuh Batholith, 25 km to the southeast (Monger and Thorstad, 1978), and in the Sheslay River section to the west. The Triassic succession is in structural (?) contact with highly deformed Permian carbonate exposed on the south side of Tanzilla River valley and in the Stikine River canyon that is part of the Stikine assemblage of Monger (1977). The Triassic rocks are overlain

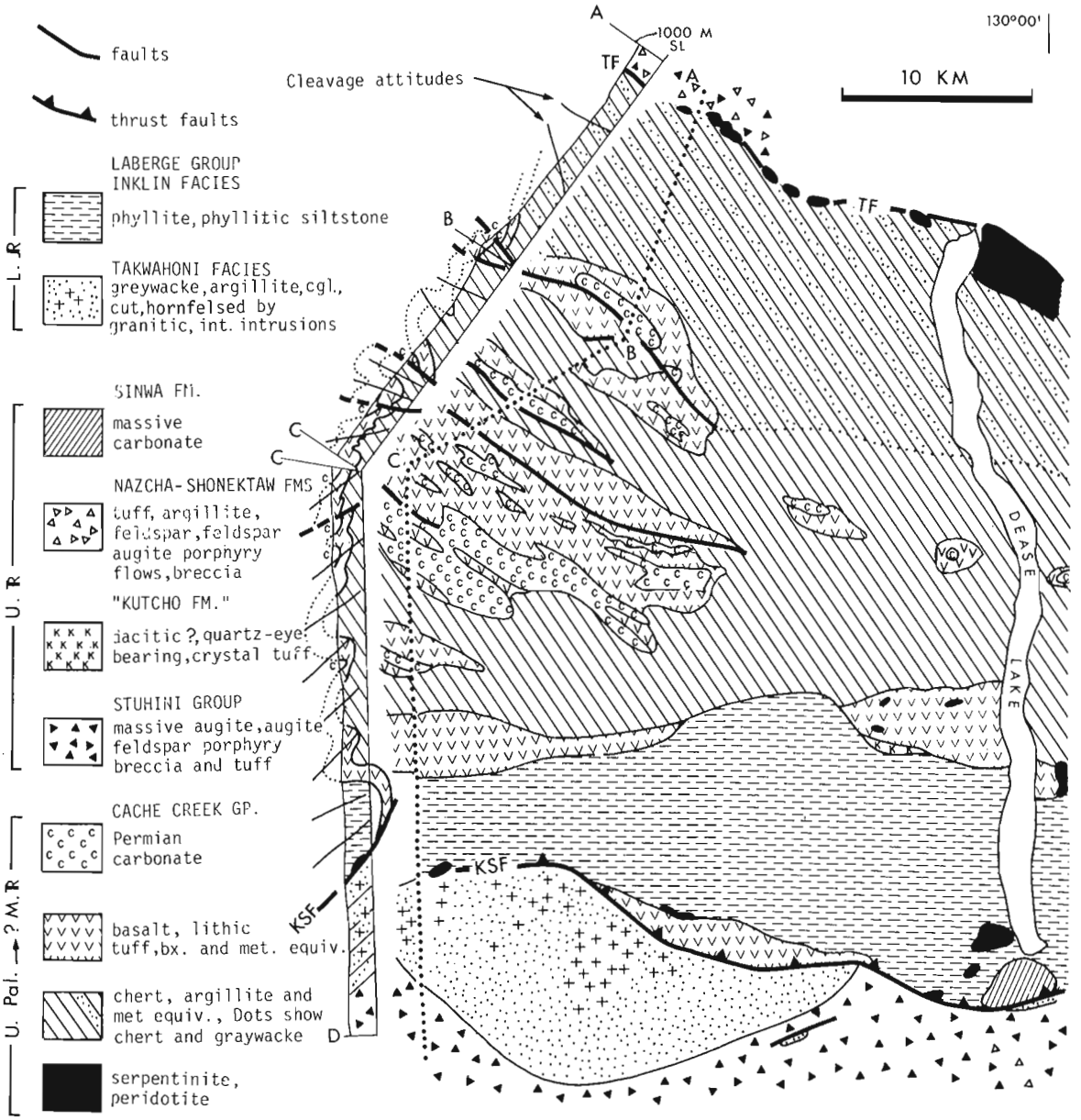

Figure 1.4. *Sketch map of the geology near Dease Lake, with a cross-section. Note that the cleavage is overturned predominantly to the southwest.*

disconformably (?) by probable Lower Jurassic greywacke and conglomerate, correlated with the Takwahoni facies. The latter rocks have no cleavage and are cut and hornfelsed by numerous small granitic and intermediate intrusions, that are absent from contiguous phyllites of the Inklin facies north of the King Salmon Fault in this area, indicating post-intrusive movement of the fault.

The only known Triassic rock in the Hinterland Belt near Dease Lake is carbonate correlated with the Sinwa Formation, exposed at the south end of Dease Lake, from which Kerr (1926, p. 85A) reported Upper Triassic fossils. Possible Triassic rocks are local, minor quartz bearing tuffs and quartz-feldspar porphyry breccias interbedded with phyllite of the Inklin facies near its northern contact with the Cache Creek Group (Fig. 1.4). These quartz bearing rocks are lithologically similar to the possible Upper Triassic "Kutcho formation" farther east in Cry Lake map area that there grades up into the Sinwa Formation (Monger and Thorstad, 1978). It may be that some rocks in the Cache Creek Group in Dease Lake area are as young as Late Triassic, as possible Middle Triassic radiolarians are known in the Cache Creek Group north of Taku River (D.L. Jones, personal communication, in Monger, 1977, p. 1844).

In this area there is no evidence that the contact between the Cache Creek Group and the Inklin facies of the Laberge is the major dislocation, the Nahlin Fault, so prominent east and west along trend. Here, foliation in Cache Creek metabasalt is parallel with cleavage of adjacent Inklin phyllite with no obvious structural break between the two. Cache Creek metabasalt, chert, limestone and serpentinite are exposed along the King Salmon Fault to the south, isolated from the main mass of Cache Creek by Inklin phyllites, as they are locally to the east in Cry Lake map area. It is not known whether the Cache Creek underlies the Inklin, as shown on the section (Fig. 1.4), or is an infolded klippe. The suggestion that the Cache Creek Group underlies distal parts of the Whitehorse trough elsewhere has been made by Souther (1971, p. 50) and, recently by Bultman (1979, p. 229). Speculatively, the high strain features, so characteristic of the Hinterland Belt, could be due to a thin,

incompetent basement of Cache Creek rocks below the Mesozoic strata, in contrast with the more rigid basements of terranes on either side.

Triassic rocks, named Nazcha and Shonektaw formations by Watson and Mathews (1944), are exposed north of the Thibert Creek Fault, northeast of the Cache Creek Group, on the southeastern margin of the Omineca Crystalline Belt. They are massive, green to locally red, fine grained feldspar porphyry and pyroxene feldspar porphyry flows and breccias (Shonektaw) with coeval (?) volcanic sandstone, argillite and minor conglomerate (Nazcha). Ribbed pelecypods, possibly Monotis, were collected by H.W. Tipper from argillaceous rocks in this sequence, and Norian conodonts found in limestone clasts in intraformational conglomerate (M. Orchard, personal communication), where earlier an ichthyosaur vertebra was collected (Watson and Mathews, 1944, p. 19). These indications of age, plus the lithological similarity of the volcanic rocks to those in the upper part of the section near Taku River, suggest a Norian age for this succession. Its relationship to contiguous probable lower Paleozoic strata is not known.

Conclusions

1. The composition of the Triassic volcanics ranges from a basic lower part to an intermediate, locally acid, upper part. The lower part shows some lateral variation as well. Volcaniclastics whose dominant clasts are porphyritic basalt containing prominent pyroxene phenocrysts (augite porphyry), together with local augite porphyry flows, form the lower sequence around the Hotailuh Batholith and much of the succession for 150 km to the west as far as Sheslay River, and outcrop on the other side of the Hinterland Belt, along the southwestern margin of the Omineca Crystalline Belt. However, such rocks form a minor component of the lower parts of the sections between Sutlahine River and Tunjony Lake and near Stuhini Creek, and are found only as clasts in two debris flows on Mount Lester Jones. In these places the dominant extrusive rocks in the lower part of the sections are either aphanitic or fine grained feldspar porphyry basalt. The upper sequence, where present, features intermediate and, rarely, acidic volcaniclastics characterized by fine grained feldspar porphyry. Such rocks form the upper part of the successions around the Hotailuh Batholith, near Taku River, and northwest of Dease Lake, north of the Hinterland Belt. Triassic volcanogenic rocks, in the Hinterland Belt, presumably of Late Triassic age because they grade into limestone correlated with the Sinwa Formation in Cry Lake map area, contain an acidic (dacitic) component with prominent quartz phenocrysts, as well as basic, chloritized pyroxene porphyry (Monger and Thorstad, 1978). Such rocks, extensively exposed near Kutcho Creek, extend at least as far west as the Dease Lake area, although there they are relatively minor.
2. The age of these rocks ranges from Late Karnian to Late Norian. The lower basic sequence near Taku River is Late Karnian. The upper, intermediate succession is Norian, and it is overlain locally gradationally by the Late Norian Sinwa Formation.
3. Facies changes in Triassic sections in Tulsequah map area, south of the King Salmon Fault, vary from a southwestern proximal facies, with flows and massive volcaniclastics to a distal, partly fine grained sedimentary facies to the northeast. These changes mirror those in Lower Jurassic rocks, although the latter are juxtaposed by the King Salmon Fault. Speculatively, they reflect a change from deposition on the Stikine block to the southwest, which was deformed, intruded by granitic rocks and possibly high standing by Late Karnian time, to a basin underlain by Cache Creek rocks to the northeast.
4. The Triassic rocks described in this report appear to lie on three lithologically and faunally different Paleozoic basements (see Monger, 1977), yet Triassic rocks in all three show many similarities. Sinwa carbonate occurs in the Stikine block and the Hinterland belt, and identical volcanics are in the Stikine and on the southwestern edge of the Omineca Crystalline Belt. Does this mean that all three Paleozoic basements were juxtaposed by Late Karnian time, or were the Triassic rocks once part of a single arc, now duplicated by later strike-slip movements, or, as speculatively suggested earlier (Monger, 1977, p. 1854) is the Cache Creek Group in the Atlin Terrane an enormous, rootless nappe lying on a single Triassic volcanogenic terrane? The facies changes reported herein would seem to preclude the latter suggestion, if the distal part of the Laberge Group, now forming the southwestern element of the Hinterland Belt, stratigraphically overlay the Cache Creek Group (as indicated in cross-section, Fig. 1.4), for there is no doubt the southwestern Hinterland Belt can be tied to Stikinia by Late Triassic time.

References

Anderson, R.G.
1978: Preliminary report on the Hotailuh Batholith: Its distribution, age, and contact relationships in the Cry Lake, Spatsizi and Dease Lake map areas, north-central British Columbia; in Current Research, Part A, Geological Survey of Canada, Paper 80-1A, p. 29-31.

Bultman, T.R.
1979: Geology and tectonic history of the Whitehorse Trough west of Atlin, British Columbia; unpublished Ph.D. thesis, Yale University, 284 p.

Gabrielse, H.
1978: Operation Dease; in Current Research, Part A, Geological Survey of Canada, Paper 78-1A, p. 1-4.

1980: Operation Dease; in Current Research, Part A, Geological Survey of Canada, Paper 80-1A, p. 347.

Gabrielse, H., Souther, J.G., and Roots, E.F.
1962: Dease Lake, British Columbia; Geological Survey of Canada, Map 21-1962.

Hanson, G. and McNaughton, D.A.
1936: Eagle-McDame area, Cassiar District, British Columbia; Geological Survey of Canada, Memoir 194.

Kerr, F.A.
1926: Dease Lake area, Cassiar District, B.C.; Geological Survey of Canada, Summary Report 1925, Part A, p. 75A-99A.

1948: Taku River map-area, British Columbia; Geological Survey of Canada, Memoir 248, 84 p.

Monger, J.W.H.
1969: Stratigraphy and structure of Upper Paleozoic rocks, northeast Dease Lake map-area, British Columbia; Geological Survey of Canada, Paper 68-48, 41 p.

1977: Upper Paleozoic rocks of the western Canadian Cordillera and their bearing on Cordilleran evolution; Canadian Journal of Earth Sciences, v. 14, p. 1832-1859.

Monger, J.W.H. and Price, R.A.
1979: Geodynamic evolution of the Canadian Cordillera – progress and problems; Canadian Journal of Earth Sciences, v. 16, p. 770-791.

Monger, J.W.H. and Thorstad, L.
Spatsizi map-areas, British Columbia; in Current Research, Part A, Geological Survey of Canada, Paper 78-1A, p. 21-24.

Monger, J.W.H., Richards, T.A., and Paterson, I.A.
1978: The Hinterland Belt of the Canadian Cordillera: new data from northern and central British Columbia; Canadian Journal of Earth Sciences, v. 15, p. 823-830.

Souther, J.G.
1971: Geology and mineral deposits of Tulsequah map-area, British Columbia; Geological Survey of Canada, Memoir 362, 84 p.

Tipper, H.W.
1978: Jurassic biostratigraphy, Cry Lake map-area, British Columbia; in Current Research, Part A, Geological Survey of Canada, Paper 78-1A, p. 25-27.

Tozer, E.T.
1979: Latest Triassic ammonoid faunas and biochronology, Western Canada; Geological Survey of Canada, Paper 79-16, p. 127-135.

Watson, K. DeP. and Mathews, W.H.
1944: The Tuya-Teslin area, northern British Columbia; British Columbia Department of Mines, Bulletin 19, 52 p.

Wheeler, J.O. and Gabrielse, H.
1972: The Cordilleran Structural Province; in Price, R.A. and Douglas, R.J.W., ed., Variation in Tectonic styles in Canada, Geological Association of Canada, Special Paper 11.

2. GEOLOGY OF THE HOPEDALE BLOCK OF NAIN PROVINCE, LABRADOR: REPORT 2, NAIN-MAKKOVIK BOUNDARY ZONE

Project 780025

Ingo Ermanovics
Precambrian Geology Division

Ermanovics, Ingo, Geology of the Hopedale block of Nain Province, Labrador: Report 2, Nain-Makkovik boundary zone; in Current Research, Part B, Geological Survey of Canada, Paper 80-1B, p. 11-15, 1980.

Abstract

Archean plutonic rocks of the Hopedale block in Nain Province were reworked and intruded by granites during Aphebian time in Makkovik subprovince. The Nain-Makkovik boundary is marked by a zone of cataclastic rocks along Kanairiktok Valley.

Introduction

This report presents results of 1979 field work in the boundary region between Makkovik subprovince and Hopedale block in Nain Structural Province. Taylor (1971) separated Makkovik subprovince from Nain Structural Province on the basis of discordance between, respectively, regional northeast to east and north to northwest structural trends. The boundary between the two (Taylor, 1971, Fig. 5) lies along the prominent lineament of Kanairiktok Valley, and is characterized by a 2 to 3 km wide cataclastic zone in which the rocks range from protomylonite to blastomylonite (Higgins, 1971). Ermanovics (1979) and Ermanovics and Raudsepp (1979) have described the regional geological setting and suggested a tentative subdivision of the Archean rocks in the Hopedale block northwest of this boundary. In this report, these Archean rocks, including the Hopedale Gneiss (Taylor, 1977), are referred to as the Kanairiktok complex. The rocks in Makkovik subprovince include deformed Kanairiktok complex gneiss and Proterozoic granite intrusions, and are collectively termed the Bay of Islands complex. All rocks of both complexes were affected by cataclasis in the boundary zone.

Kanairiktok Complex

Layered amphibolites and grey granoblastic layered feldspathic orthogneiss (Weekes amphibolite and Maggo gneiss) represent the oldest rocks in Kanairiktok complex (Hopedale Gneiss). They display amphibolite facies metamorphism and northwesterly-striking structural trends developed during D_2 deformation (e.g. northwest portion of Fig. 2.1). Designation of deformation as D_2 in these rocks is based on refolded isoclinal folds whose axial planes are parallel to regional gneissic layering. Although the history of these rocks may be more complex, it is assumed that the northwest structural trend is the result of at least two phases of deformation. These gneisses were intruded by granitoids of the Kanairiktok intrusive suite, including mainly leucocratic tonalite and granodiorite. Intrusion of this suite was syn-D_3, which produced a rotation of D_2 layering into northeast-southwest directions. Migmatite, developed at the time of this intrusion, was transposed to form poorly layered migmatite gneiss (Kanairiktok gneiss) and is intercalated with mappable remnants of well layered older gneiss (Fig. 2.2).

Granodiorite and tonalite make up the bulk of the plutonic suite. In plan individual plutons are elongate to the northeast. They become progressively smaller and less crowded together towards the northeast (Fig. 2.1). In the southwest they are homogeneous and free of gneiss inclusions. Heterogeneity of composition and abundance of xenolithic material increases to the northeast. These features suggest that a lower level of emplacement is exposed in the southwest. Granodiorite-tonalite intrudes Florence Lake volcanic rocks just west of the area of Figure 2.1 and there it was determined that D_3 foliation in tonalite and supracrustal rocks was accompanied by greenschist facies metamorphism (Ermanovics and Raudsepp, 1979). Greenschist facies metamorphism is observed as diaphthoresis in older amphibolite facies gneiss.

In a number of places in Kanairiktok complex, northerly-and northwesterly-striking structural trends indicate incomplete transposition to southwest-northeast striking trends during D_3 deformation. These are pseudo-D_2 structures (layering in gneisses and schlieric gneissosity in granitoids) presumed to have been affected by some component of D_3 rotation. In the central area of Kanairiktok Bay this northwesterly trend is still evident in Bay of Islands of Makkovik subprovince (Fig. 2.1). There it is expressed as a weak, locally penetrative foliation in Aphebian Bay of Islands granodiorite and as a much flattened and folded banding in reworked Kanairiktok gneisses. Incomplete, penetrative D_3 deformation may be observed along the southwestern end of Cross Island and elsewhere, where layered, migmatitic, northwest-striking gneisses are sporadically refolded about northeast trending axes (Fig. 2.2).

In a number of places along shorelines of northeast trending bays formed by glacial scouring of less resistant rocks, cataclastic foliation parallel to northeast trending D_3 layering was observed. Whether such localized brittle deformation represents late D_3 or D_5 deformation is not known.

Gabbro and diabase dykes (Kikkertavak dykes) trending 025° to 045°, form a dense swarm west of Kanairiktok Bay. Greater dyke width and swarm density appear to coincide with high intensity D_3 deformation. Gabbroic dykes are commonly altered to subgreenschist and locally to lower greenschist facies. Kikkertavak dykes do not intrude Bay of Islands granite, but may be equivalent to amphibolite dykes in reworked Kanairiktok gneisses in the Bay of Islands complex.

Bay of Islands Complex

Bay of Islands Granite

Porphyroblastic granodiorite and minor coarse grained granite dominate the Bay of Islands complex within the map area. The granitoids form an oval-shaped southwest-northeast trending batholith whose dimensions in plan are 20 by 100 km (Fig. 2.1). The rocks are massive to weakly foliated, except near the margins where screens of layered gneisses are accompanied by pronounced gneissosity in granodiorite. Lit-par-lit migmatite is extensively developed around the southern portion on the pluton where it is dominantly granodioritic. In the northeast the pluton becomes granitic (Fig. 2.3) and intrusive contacts with gneiss are generally sharp (Fig. 2.6) and discordant with extensive

development of granitic pegmatite. This change in plutonic composition and the nature of intrusive relationships suggests that the southwestern portion of the pluton is a synkinematic (D_4) deeper level intrusion compared to the granitic phase of the pluton in the northeast. Although granite and granodiorite appear to be cogenetic, the granite phase may have crystallized later than granodiorite.

The granodiorite is a medium grained, grey biotite + epidote (8 per cent), zoned oligoclase-andesine bearing rock commonly containing porphyroblastic microcline. Microcline is poikilitic, enclosing epidotized plagioclase, chloritized biotite, and quartz, and hence appears to be a late crystal phase in these rocks. Granitic phases (Fig. 2.3) are richer in allanite, zircon, fluorite and sphene than granodioritic members.

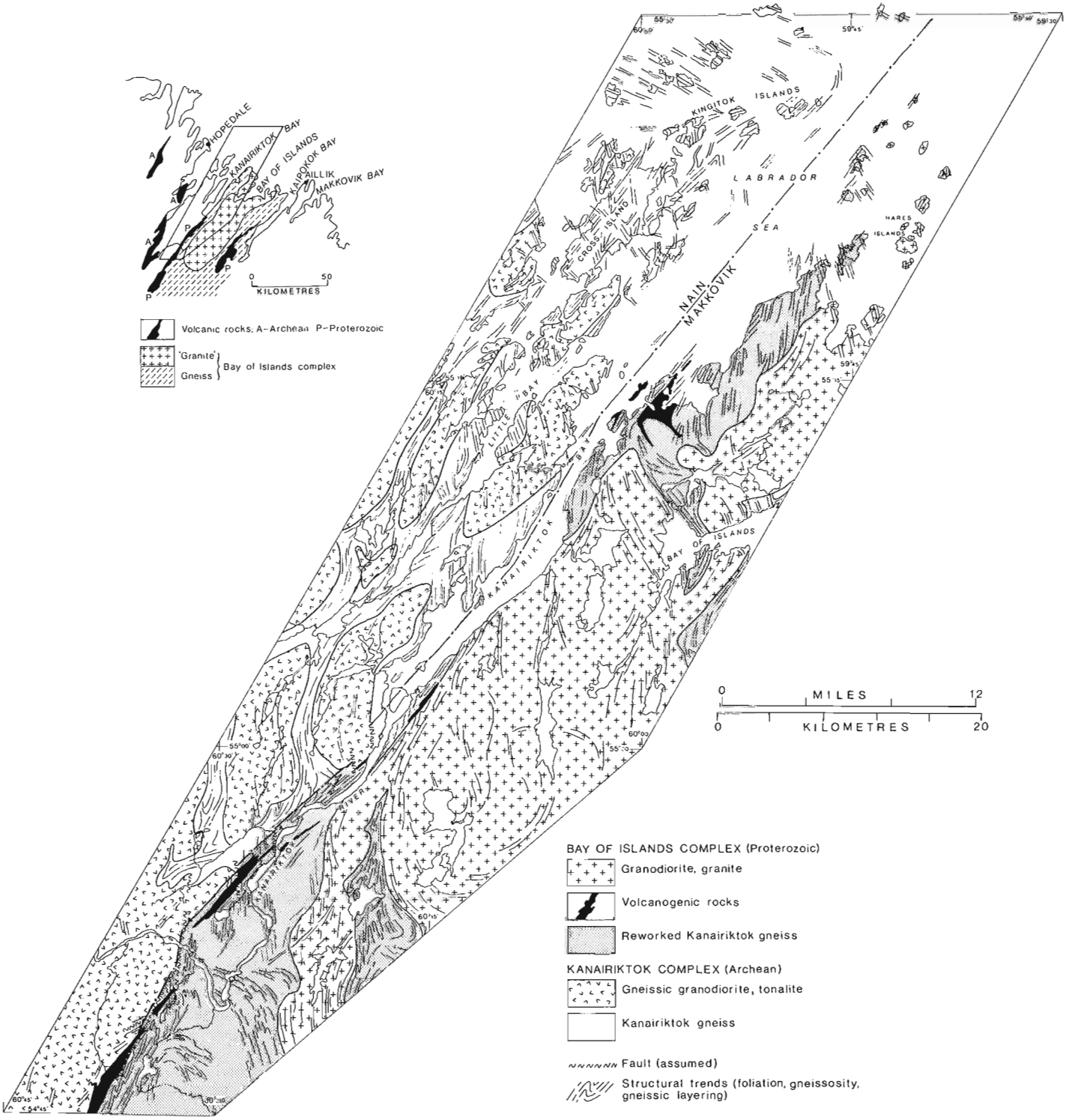

Figure 2.1. *Structural trends in Kanairiktok complex (Nain Structural Province) and Bay of Islands complex (Makkovik subprovince). The complexes are separated by a zone of cataclastic rocks that may be traced from the outer islands southwestward along the east shore of Kanairiktok Bay and along Kanairiktok River mainly east of the volcanic rock remnants.*

Layered Gneiss

Layered gneiss, derived from Kanairiktok gneiss, surrounds the Bay of Islands pluton. Zones of migmatite gneiss and schlieric remnants of gneiss occur within the pluton. The gneisses may be followed southwest from the present map area to where they and Aphebian Moran Group were deformed during 'Hudsonian' Orogeny (Ryan, 1979). It is assumed that in the present area D_4 deformation is 'Hudsonian' also.

The gneisses are well layered (1 to 10 cm wide), variegated grey to white, and include granoblastic granitoid orthogneiss, garnetiferous biotite feldspathic gneiss, and garnetiferous banded amphibolite. Oblique schistosity in most layered gneiss may be a manifestation of late D_4 or D_5 deformation. Amphibolite dykes, thought to be derived from Kikkertavak dykes, cut the gneiss but are folded with them. Agmatite of this gneiss occurs in northeastern portions of the Bay of Islands granite and suggests that D_4 deformation in part preceded granite intrusion. Grade of metamorphism is in amphibolite facies (hornblende, garnet, biotite) but it is not known whether regional or contact metamorphism prevailed.

Supracrustal Rocks

Supracrustal rocks underlie the three areas within the cataclastic boundary zone (Fig. 2.1). South of Kanairiktok River these comprise deformed, banded and schistose pillow lavas, sandstone, siltstone, graphitic schists and felsic schists of unknown derivation. This succession lies unconformably on Kanairiktok granodiorites (exposed on the western contact) and is assigned to Moran Lake Group of Aphebian age (Ryan, in press). Kanairiktok granodiorite at or near the unconformity (west contact) exhibits a weak D_4 foliation parallel to regional D_3 foliation, but is primarily characterized by brittle, poorly indurated rock with white, soft feldspars cut by calcite and quartz veins. On the east side the unconformity is not recognized; instead, Moran Group is in tectonic contact with banded gneisses (D_4 deformation) overprinted by cataclastic foliation (D_5) typical of the boundary zone.

The age of the sliver of supracrustal rock exposed immediately north of Kanairiktok River is problematical, but may be correlative with Florence Lake group (Archean). The succession consists of calcareous, laminated, mafic to intermediate volcanics, calcareous 'quartz-eye' felsic schists and cataclastic felsic schists. The rocks are in shear contact with cataclastic pink leucogranitoids and are locally intruded by rocks thought to belong to Kanairiktok complex.

The age of the northernmost occurrence of supracrustal rocks in Kanairiktok Bay is also problematical, but an Archean age is favoured. It consists of contorted, laminated, fine- to medium-grained mafic rocks, banded tuffs, felsic schist and gneiss, and granitic lenses. This succession is in gradational contact with reworked Kanairiktok gneisses and pink leucocratic granite.

Granitic intrusions are not observed in type Moran Group, but are common in Archean Florence Lake group. Hence assignment of the latter two supracrustal remnants to the Archean is based primarily on the presence of intrusive granitoids. These, however, may derive from Bay of Islands intrusions rather than Kanairiktok intrusions, and hence may be Aphebian in age.

Mesocratic Dioritic Dykes and Sheets

Reddish, medium grained, mesocratic dykes and sheets in various orientations intrude the Bay of Islands granite and gneisses. With rare exception, they are confined to the Bay of Islands complex east of Kanairiktok Bay. They generally dip less than 40 degrees; on Striped Island, they form horizontal sheets in homogeneous granite (Fig. 2.4). Mineralogy comprises 30 to 40 per cent chloritized euhedral pale-brown amphibole, 4 to 8 per cent quartz, and saussuritized euhedral zoned sodic plagioclase. Chilled margins are well developed and some rocks contain abundant sphene and 5 to 15 per cent calcite. The age of these dykes is post-D_4 deformation, and possibly post-D_5.

Nain-Makkovik Boundary Zone

The zone is characterized by protomylonite, mylonite gneiss and blastomylonite derived from rocks of Kanairiktok and Bay of Islands complexes (Fig. 2.5, 2.6, 2.7). Mylonite and ultramylonite are rare, and recrystallization generally appears to have outlasted cataclasis. Recrystallization includes green amphibole, quartz, muscovite, epidote, biotite and feldspars. Cataclastic foliations strike northeast and are generally steeper than 65 degrees to either side of vertical. This cataclastic deformation (D_5) rotated D_3 gneissosity of the Kanairiktok complex and D_4 layering of the Bay of Islands complex into north and northeast trending directions.

In Kanairiktok Bay most cataclastic rocks of the boundary zone are under water. However, the zone may be traced from the northeastern islands (White Mark and Mussel islands, latitude 55°24', longitude 95°45') southwestward along promontories of the eastern shore of Kanairiktok Bay to the mouth of Kanairiktok River at latitude 55°00'. There the zone splays and part of it cuts and follows the margin of the Bay of Islands granite with a southerly trend. The main zone continues southwestward along the river and intersects supracrustal rocks. It then appears to be offset by left lateral fault displacements and continues southwestward within and along the eastern contact of Moran Group.

As the boundary zone is approached from the Bay of Islands complex, foliation curves toward the northeast (Fig. 2.1). This could be interpreted as suggesting a component of right lateral fault displacement between Kanairiktok and Bay of Islands complexes. However, the same argument based on cataclastic foliation trends with left hand curvatures in gneisses south of Kanairiktok River suggests a component of left lateral fault displacement. Compression resulting from opposite sense fault displacement between these two segments in southern Bay of Islands complex may explain the offset and splay (widening) of the boundary zone observed in the Kanairiktok River area (Fig. 2.1). The gneisses in the south, however, may originally have had more westerly trends that were thus rotated to southwesterly trends in response to dominantly northwest-southeast compressive stresses.

Whether the boundary zone represents dominant shear displacement or compression requires structural analysis. That the entire Bay of Islands complex (30 to 40 km wide) may have been an area of compression is suggested by the Kikkertavak dykes which were emplaced in a contiguous area of tension 40 km wide in Kanairiktok complex immediately west of the boundary zone. This interpretation implies that amphibolite dykes in Bay of Islands gneisses are older than Kikkertavak dykes.

Deformation in Makkovik subprovince may be related to closing of a "trough" or "sea" in Makkovik area (Kaipokok Bay, 25 km east of Bay of Islands of Fig. 2.1). In this model (Clark, 1979) Moran Group is correlated with Ketilidian supracrustals in Greenland and closing of the "Makkovik trough" resulted from simple-shear, with right hand lateral displacement, between Nain and Makkovik cratons. If this was so, then the boundary zone in Kanairiktok Bay may represent the final stage of this tectonism.

Figure 2.2. *Kanairiktok gneiss (gneissic granodiorite and layered, dark grey, Maggo gneiss) reoriented from a northwest trend to a northeast strike (right side) during D_3 deformation. From east side of Cross Island. (GSC 177157)*

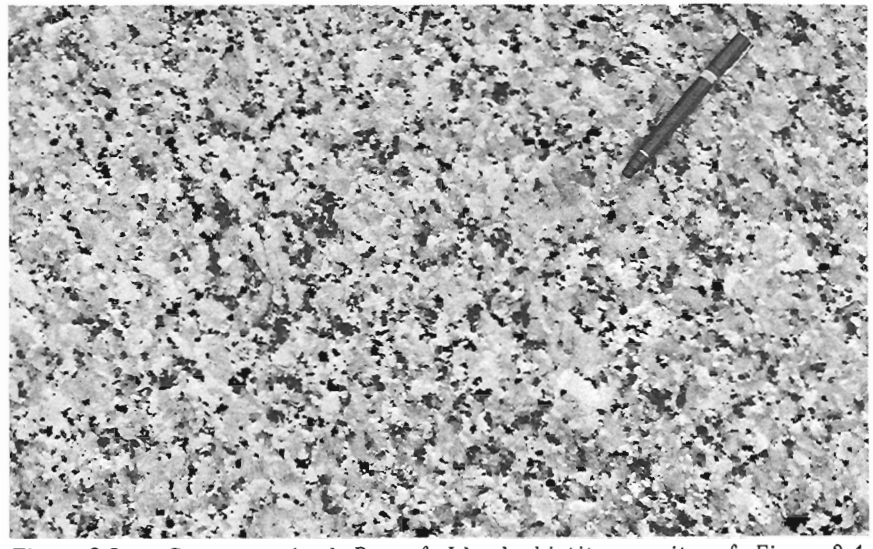

Figure 2.3. *Coarse grained Bay of Islands biotite granite of Figure 2.4. (GSC 177326)*

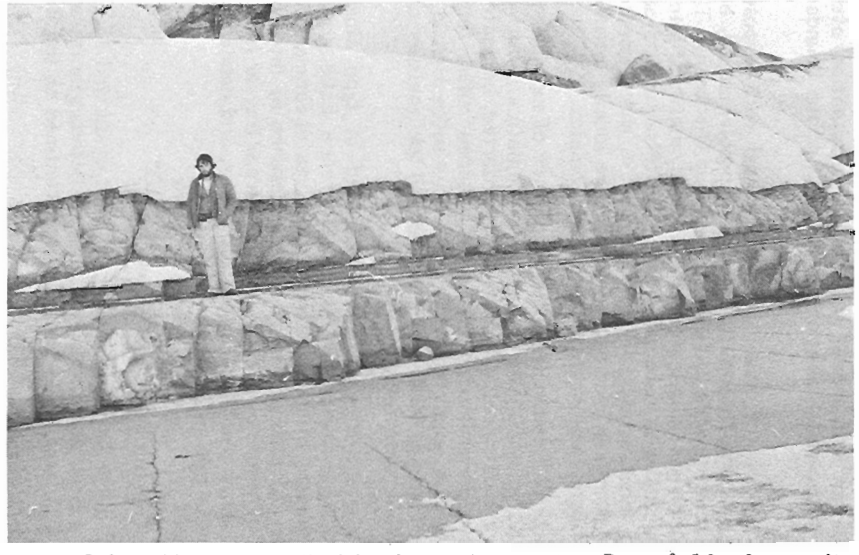

Figure 2.4. *Mesocratic dioritic sheets in massive Bay of Islands granite (Fig. 2.3) from Striped Island (area of Hares Islands, Fig. 2.1). (GSC 177241)*

Figure 2.5. *Reworked Kanairiktok gneiss (D_4 and D_5 deformation) from boundary zone on east shore of Kanairiktok Bay. (GSC 177211)*

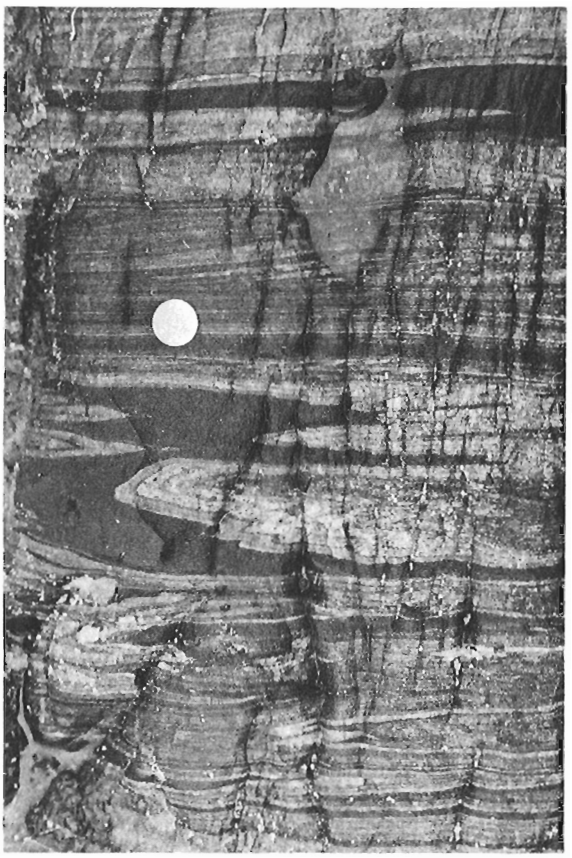

Figure 2.7. Sugary, mylonite gneiss in boundary zone derived from Bay of Islands complex gneiss from west side of Mussel Islands (longitude 59°45', latitude 55°24') in Kanairiktok Bay. Coin is 24 mm in diameter. (GSC 177227)

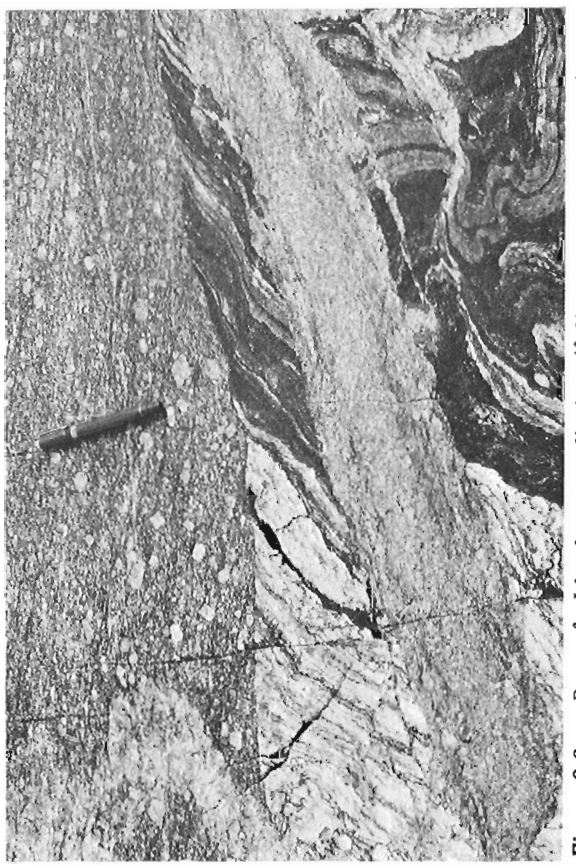

Figure 2.6. Bay of Islands granodiorite (foliate and porphyritic), and reworked (D_4 and D_5 deformation) Kanairiktok gneiss cut by foliated pegmatite that also intrudes the granodiorite. The outcrop occurs in the boundary zone on the east shore of Kanairiktok Bay. (GSC 177303)

Summary

Highly deformed, northwesterly trending granoblastic, layered gneisses of the Hopedale block were refolded about northeast trending axes in late Archean time. Synkinematic intrusions of granodiorite-tonalite were intruded parallel to the northeast trending structural grain and produced poorly layered migmatite gneiss intercalated with older granoblastic layered gneiss.

Rocks of the Kanairiktok complex are recognized east of Kanairiktok Bay where they were flattened and recrystallized in amphibolite facies, probably during early Aphebian time. Synkinematic granodiorite and late synkinematic granite are part of a regionally concordant batholith that was intruded parallel to a northeast trending tectonic grain in Makkovik subprovince. Granodiorite and granite are probably cogenetic, but granite appears to be a late phase compared with the more deformed and metamorphically altered granodiorite.

The last major deformation occurred in a zone between the complexes and produced cataclastic rocks in both complexes in which recrystallization outlasted cataclasis in upper greenschist facies. This boundary zone separates 'Kenoran' from 'Hudsonian' tectonites and hence serves as an appropriate division between the two structural domains proposed by Taylor (1971). However, sharp discordance of structural trends between Nain and Makkovik blocks is not evident in the boundary region.

The tectonic significance and kinematics of the boundary zone is not known and requires structural analysis.

Acknowledgments

I am indebted to my field assistants Irvine Annesley (University of Windsor), Marcia Mazurski (Queen's), Valerie Stenerson (Carleton), Norman Di Perno (Concordia), Joanne Jones (Concordia) and Michael Worthmann (Concordia) for a successful field season during 1979. A. Davidson reviewed the manuscript.

References

Clark, A.M.S.
1979: Proterozoic deformation and igneous intrusions in part of the Makkovik subprovince, Labrador; Precambrian Research, v. 10, p. 95-114.

Ermanovics, I.F.
1979: Adlatok Bay-Florence Lake map-area, Map; Geological Survey of Canada, Open File 580.

Ermanovics, Ingo and Raudsepp, Mati
1979: Geology of the Hopedale block of eastern Nain Province, Labrador: Report 1; in Current Research, Part B, Geological Survey of Canada, Paper 79-1B, p. 341-348.

Higgins, Michael W.
1971: Cataclastic Rocks; United States Geological Survey Professional Paper 687, 97 p.

Ryan, A.B.
1979: Kaipokok River, Labrador; Newfoundland Department of Mines and Energy, Map 7949.

Kanairiktok River, Labrador; Newfoundland Department of Mines and Energy, Map. (in press)

Taylor, F.C.
1971: A revision of Precambrian structural provinces in northeastern Quebec and northern Labrador; Canadian Journal of Earth Sciences, v. 8, p. 579-584.

1977: Geology – Hopedale, Newfoundland; Geological Survey of Canada, Map 1443A.

3. AN ASSESSMENT OF THE URANIUM POTENTIAL OF THE RAFT BATHOLITH AREA, BRITISH COLUMBIA

Project 760043

D.R. Boyle
Resource Geophysics and Geochemistry Division

Boyle, D.R., An assessment of the uranium potential of the Raft Batholith area, British Columbia; in Current Research, Part B, Geological Survey of Canada, Paper 80-1B, p. 17-28, 1980.

Abstract

The uranium potential of the Raft Batholith area of central British Columbia has been assessed using a genetic model developed from research on the formation of basal type uranium deposits in the Okanagan Highlands. A comparison of these two areas has been made using model parameters considered to have the most important influence on the formation of ore, namely – geological setting, age relationships, tectonic history, composition of source rocks, labile uranium in source rocks, composition of host rocks, and preservation of basalt-fluvial sediment assemblages.

Both the Raft Batholith and the Okanagan Highlands Complex have similar geologic settings and would appear to have the same age relationship with an overlying Plateau basalt-fluvial sediment assemblage. There is good evidence to suggest that the same schedule of tectonic events occurred in both areas.

The petrology, major element composition, and total uranium content of these two complexes are very similar. On an experimental basis just as much uranium can be leached from the Raft Batholith as the Okanagan complex and under natural conditions the uranium content of surface waters draining the Raft Batholith is greater than for waters draining the Okanagan Highlands Complex. However, the uranium concentration of groundwaters draining the Raft Batholith is noticeably less than for groundwaters in the Okanagan complex; this may have a direct bearing on uranium potential.

Six main areas underlain by basalts have been identified in the Raft Batholith area. Based on the various model parameters mentioned above, the Upper Mann Creek valley basalt and the Coldscaur Lake basalt appear to offer the best potential for basal type uranium mineralization.

Certain factors which may have a direct bearing on mineral potential are still unanswered and these may only be resolved by subsurface exploration.

The method of assessment used is applicable to many areas of the North American Cordillera and South American Andes where Tertiary volcano-sedimentary assemblages overlie granitic batholith complexes.

Introduction

A logical extension of any study of the genesis of sedimentary hosted uranium deposits is the development of an exploration model based mainly on geological and geochemical characteristics of both source and host rocks which can be applied to areas of unknown potential. Research by the author on the genesis of basal type uranium deposits associated with a granitic basement complex in the Okanagan uranium province of south central British Columbia has led to a number of conclusions which can be incorporated in such a model (Boyle, 1979). The model, described below, has been used to assess the potential of the Raft Batholith area of central British Columbia (Fig. 3.1) for associated sedimentary-hosted uranium deposits. The Raft Batholith was initially chosen as an example for such studies because of its high gamma radioactivity and the spatial relationship shown by Miocene-Pliocene Plateau Basalt formations which act as cap rocks for potential uranium-bearing fluvial sediments. Data from the Okanagan region are used in this assessment for comparative purposes.

Characteristics and Model of Formation of Basal Type Uranium Deposits

Basal type uranium deposits have been recognized in southern British Columbia (Smee and Ballantyne, 1976; Christopher and Kalnins, 1977; Boyle 1979), Washington State (Sherwood Deposit; Becraft and Weis, 1963), Idaho State (Challis Formation; Choate, R., 1962), California (Juniper Mine; Rapp, 1978) and Japan (Katayama et al., 1974 and Doi et al., 1975). The term 'basal-type' was first proposed by Katayama (1960) to represent uranium deposits in Tertiary fluvial sediments resting on or immediately adjacent to granitic basement rocks. Essentially these deposits comprise uranium mineralization in the form of ningyoite, ningyoite-coffinite-uraninite (autunite), ningyoite-autunite-saléeite, uraninite-coffinite (uranophane, phosphuranylite) and adsorbed uranium on carbonaceous matter, clays and zeolites. The mineralization occurs as grain coatings and void fillings in continental fluvial conglomerate-sandstone-mudstone sequences overlying granitic rocks. Pyrite, marcasite and limonite are generally the predominant gangue minerals; occasionally gypsum may be present. The deposits are situated at or near the basement contact and are invariably associated with ancient paleochannels developed along probable Mesozoic-Tertiary fault traces within the granite basement. In many cases where drilling has been extended into the basement a highly fractured and altered fault zone has been encountered. Impermeable mudstones or volcanic lavas act as cap rocks to preserve mineralization. In all cases the granitic rocks associated with these deposits are of Cretaceous age.

An example of the geological setting for this type of mineralization is given in Figures 3.2 and 3.3 for the Blizzard deposit and associated occurrences. The paleotopographies of the Blizzard deposit (Fig. 3.3) and Cup Lake occurrence

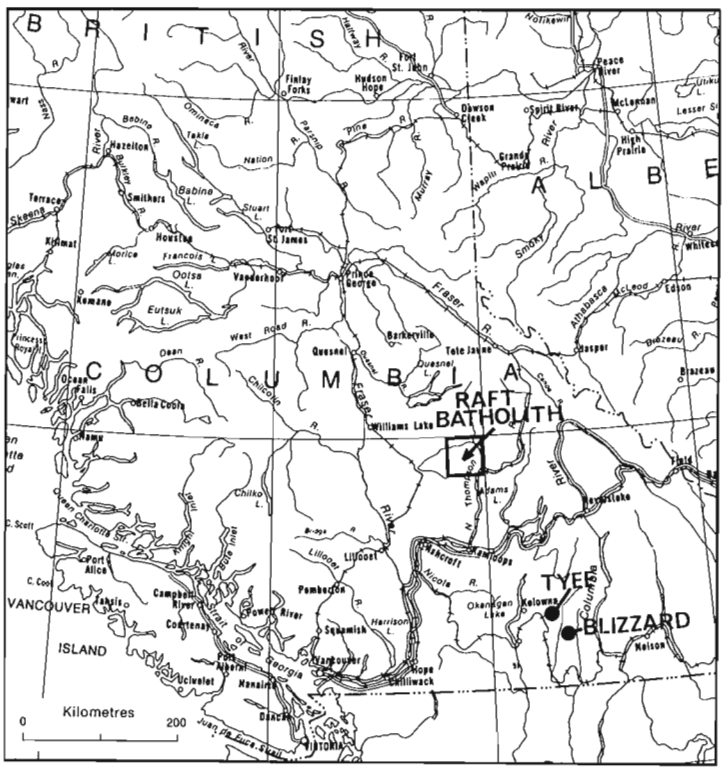

Figure 3.1. *Location of Raft Batholith area and Tyee and Blizzard basal type uranium deposits (Okanagan Region).*

Table 3.1

Uranium in waters draining granitic rocks of the Raft and Okanagan Highlands Complexes

Type of Water and Number of Samples	Range (ppb)	Average (ppb)*
Raft Batholith:		
Streams (165)	0.10- 3.60	0.49 (0.31)*
Springs (26)	0.10- 48.00	4.90
Drillhole (1)	6.80	6.80
Okanagan Highlands Complex:		
Streams (243)†	0.02- 1.70	0.38 (0.27)*
Fault Controlled Waters		
Streams (49)	1.10- 54.0	8.90
Springs (12)	4.00-125.0	25.50
Well Waters (5)	2.80- 75.0	37.00

* Geometric means are given in brackets for regional data
† From Federal-Provincial Uranium Reconnaissance Survey (GSC Open File 409)
Note: lower limit of range represents half the detection limit of 0.05 ppb.

(Fig. 3.2) as well as a partial reconstruction of the Miocene paleovalleys that may have existed during time of formation are also presented in these figures. All of the smaller basalt outliers throughout the Okanagan region display a distinct linearity which correlates well with the northwest-southeast and northeast-southwest structural fabric of this region (see Fig. 3.2). These basalts have been dated as early Pliocene (4.4 ± 0.6 Ma, 5.9 ± 0.6 Ma, author's data; 5.0 ± 0.5 Ma, 4.7 ± 0.17 Ma, Christopher, 1978; all K-Ar whole rock). The occurrence of basaltic plugs and diatremes along these structural trends, such as occurs under the northern part of the Blizzard basalt capping (Fig. 3.2, 3.3) and just to the southwest of the Blizzard deposit (Fig. 3.2), indicates the presence of open structures in the basement complex along which valley basalts have been extruded. Prior to the formation of the Pliocene basalts, the earliest volcanic activity in the area is recorded in the Eocene with the extrusion of alkali and felsic volcanics (Church, 1977). The Oligocene-Miocene series represents a period of compressional and tensional tectonism and subsequent erosion leading in part to the formation of fluvial paleochannels along Mesozoic-Tertiary fault zones and small graben structures. The paleochannels were later capped by Pliocene basalts and in some cases uranium was introduced into the sediments as a result of groundwater infiltration. Mineralization has only been found in basal Miocene sediments overlying granitic rocks of the Okanagan Highlands Intrusive complex – a complex of which monzonite and granite make up approximately 75 per cent by volume (Valhalla intrusives of Little, 1957, 1961), the rest being made up of more mafic granodiorites and diorites (Nelson intrusives of Little, 1957, 1961) and Tertiary syenitic rocks (Coryell intrusives). The Tyee deposit which is situated 30 km to the northwest of the Blizzard deposit rests on a window of Valhalla monzonite within the Shuswap metamorphic complex. Numerous barren paleochannels have been discovered by drilling programs through basalts overlying Tertiary volcanics, Paleozoic greenstones, and the Shuswap metamorphic complex. The localization of this type of mineralization on or immediately adjacent to granitic rocks has also been demonstrated for the Japanese deposits (Katayama et al., 1974; Doi et al., 1975).

Whereas the source for many other types of sedimentary hosted uranium deposits is still very controversial (International Atomic Energy Agency, 1977) there can be little doubt that for basal-type deposits, most of the uranium has been derived from the leaching of granitic basement rocks. For the Okanagan region streams draining granitic rocks of the Highland Intrusive Complex have a higher than average natural background of 0.27 ppb (Table 3.1) compared to a geometric regional mean for the Cordillera of 0.19 ppb (data from Geological Survey of Canada Open Files 409, 410, 514, 515, 516, 517; 11 908 water samples). Waters draining Holocene fault zones in the Okanagan basement rocks have also been found to be highly uraniferous (Boyle and Ballantyne, 1980). These recent fault zones together with their uraniferous waters would appear to be present day analogues of the Mesozoic-Tertiary structural systems in which basal-type mineralization formed (Boyle, 1979). In Japan high concentrations of uranium have also been found in structurally controlled groundwaters draining the granites associated with mineralization (Doi et al., 1975). Recent investigations by the author on the labile uranium content of granitic rocks in the Cordillera indicate that monzonites and granites of the Okanagan Highlands Complex are a reasonably good source of mobile uranium.

Bearing in mind the tectonic history of mineralized areas, the structural and geological setting of these deposits and the leachability of basement rocks, the model outlined in Figure 3.4 is proposed for the formation of basal-type deposits. The model depicts movement of local,

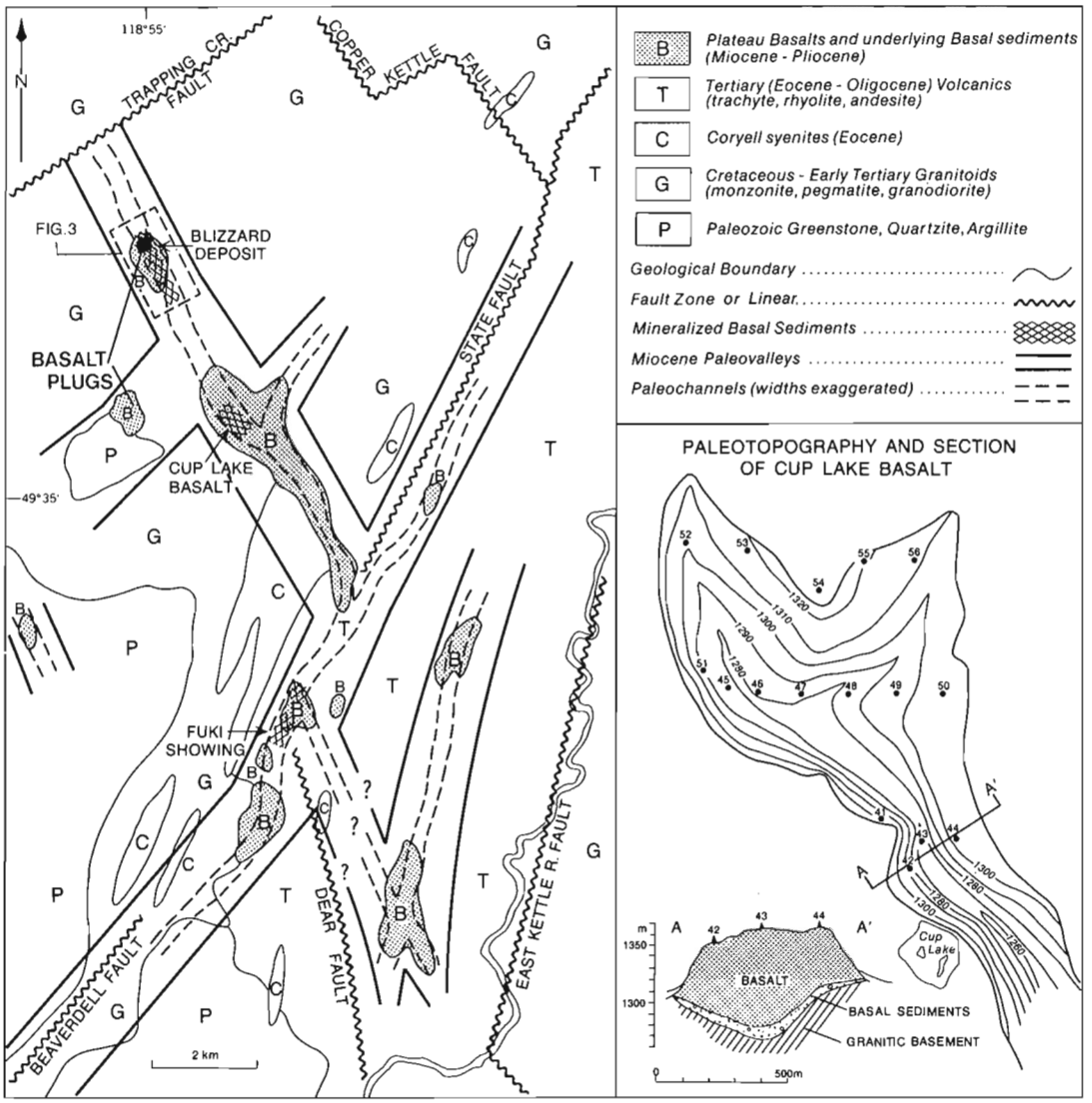

Figure 3.2. *Geological setting of the Blizzard basal type uranium deposit and associated uranium occurrences, south central British Columbia (geology after Okuno, 1972; Christopher, 1978).*

intermediate, and regional groundwaters through a fractured crystalline basement towards major Mesozoic-Tertiary lineaments with eventual infiltration into sediments overlying these structures. The terms local, intermediate, and regional groundwater systems are often used by hydrologists to describe overall conditions of groundwater movement. The levels of U attributed to waters associated with each of these systems in Figure 3.4 have been arbitrarily chosen based on data for stream waters and groundwaters in the Okanagan region and other granitic terranes in the Cordillera.

It is unlikely that only local groundwater flow would give rise to the grades of mineralization observed in the Okanagan for the simple reason that many of the other lithologies in this region, over which only barren paleochannels have been discovered (e.g. Eocene volcano-sedimentary rocks, Paleozoic greenstones; Coryell syenites and Shuswap metamorphic rocks) have associated stream waters which display similar and in some cases greater average U contents than those draining the monzonites and granites of the Highlands Intrusive Complex (Boyle and Ballantyne, in press). It is apparent therefore that a large component of the uranium in these deposits must be derived from infiltration of intermediate and regional groundwaters; some of which probably had a long residence time in the basement complex. It follows therefore that an open basement structure is required for deep seated groundwater movement. In the Okanagan this has been easily facilitated by a period of epeirogenic uplift in Oligocene-Miocene times giving rise to extensive block faulting (tensional) which is most evident in the Tertiary volcanic basins (Church, 1977) and the granitic basement complex.

All of the mineralized zones as well as many of the barren channels contain abundant carbonaceous trash to create reducing conditions. In cases, such as the Tyee deposit, marcasite may be the main reducing agent.

Groundwaters moving up favourable fault zones or graben structures will issue as a continuous set of springs along the basement fluvial sediment contact and will collectively move down the hydrological gradient (usually 1-2%) until favourable conditions for precipitation are met. It should not be expected therefore that the source of these deposits lies directly underneath mineralization.

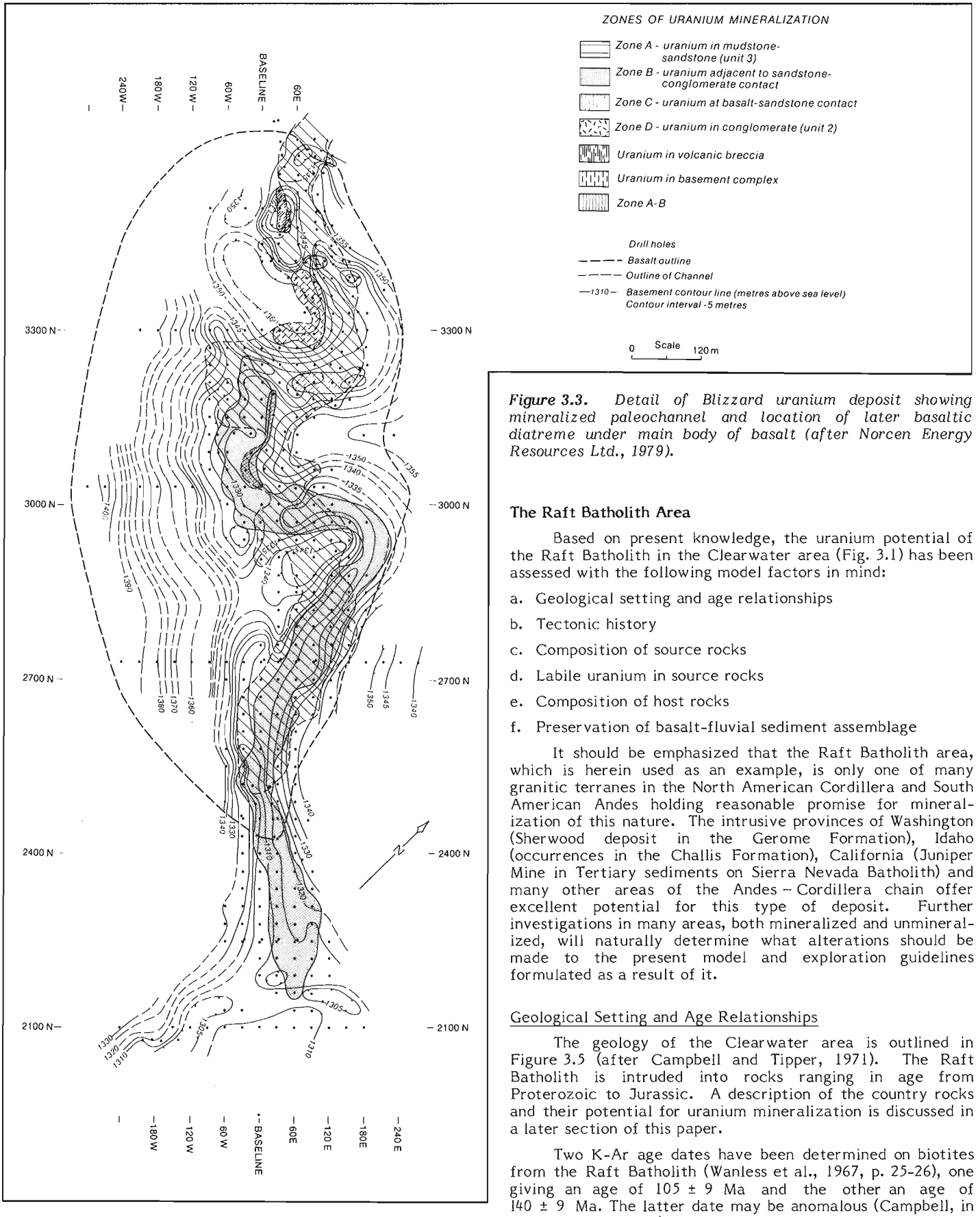

Figure 3.3. Detail of Blizzard uranium deposit showing mineralized paleochannel and location of later basaltic diatreme under main body of basalt (after Norcen Energy Resources Ltd., 1979).

The Raft Batholith Area

Based on present knowledge, the uranium potential of the Raft Batholith in the Clearwater area (Fig. 3.1) has been assessed with the following model factors in mind:

a. Geological setting and age relationships

b. Tectonic history

c. Composition of source rocks

d. Labile uranium in source rocks

e. Composition of host rocks

f. Preservation of basalt-fluvial sediment assemblage

It should be emphasized that the Raft Batholith area, which is herein used as an example, is only one of many granitic terranes in the North American Cordillera and South American Andes holding reasonable promise for mineralization of this nature. The intrusive provinces of Washington (Sherwood deposit in the Gerome Formation), Idaho (occurrences in the Challis Formation), California (Juniper Mine in Tertiary sediments on Sierra Nevada Batholith) and many other areas of the Andes – Cordillera chain offer excellent potential for this type of deposit. Further investigations in many areas, both mineralized and unmineralized, will naturally determine what alterations should be made to the present model and exploration guidelines formulated as a result of it.

Geological Setting and Age Relationships

The geology of the Clearwater area is outlined in Figure 3.5 (after Campbell and Tipper, 1971). The Raft Batholith is intruded into rocks ranging in age from Proterozoic to Jurassic. A description of the country rocks and their potential for uranium mineralization is discussed in a later section of this paper.

Two K-Ar age dates have been determined on biotites from the Raft Batholith (Wanless et al., 1967, p. 25-26), one giving an age of 105 ± 9 Ma and the other an age of 140 ± 9 Ma. The latter date may be anomalous (Campbell, in Wanless et al., 1967) and no explanation can be offered for it.

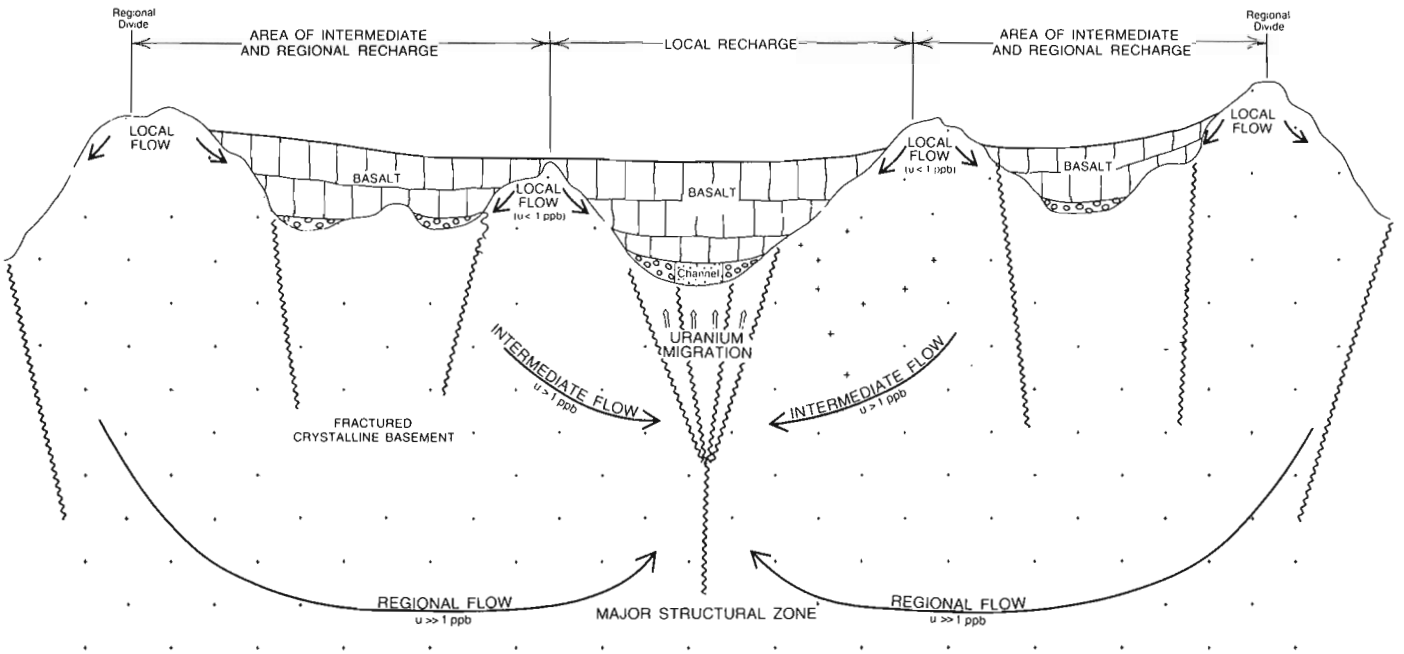

Figure 3.4. *Model of formation for basal type uranium deposits in south central British Columbia.*

The youngest rocks cut by the Raft Batholith are of Middle Jurassic age. The date of 105 ± 9 Ma agrees well with two dates of 96 ± 5 Ma and 80 ± 5 Ma obtained for the Baldy Batholith (Wanless et al., 1966, p. 16-17) located 25 km to the southeast of the Raft. Both these batholiths have similar mineralogy, texture, and geological settings. Granitic rocks of the Okanagan Highlands Intrusive Complex have not been adequately dated due mainly to the influence of a well-recorded Tertiary thermal event of approximately 50 Ma which manifests itself by the presence of Coryell syenites and related felsic volcanic rocks. Dating of biotites and muscovites from quartz monzonite and pegmatite in the vicinity of the Blizzard deposit gave values of 56.7 ± 2.4 Ma, 52.9 ± 2.3 Ma and 52.0 ± 2.3 Ma; (author's data; K-Ar method). The influence of the above thermal event (clock resetting) is evident since these rocks are intruded by Eocene Coryell syenites and must therefore be older than the dates indicated. Although Rb-Sr dating presently in progress may help to alleviate this problem it would appear from stratigraphic evidence and the dates mentioned above that the monzonite-granite-pegmatite phase (Valhalla intrusives) of the Highland Complex is no younger than Paleocene and no older than early-middle Cretaceous. The granodiorite-diorite phase (Nelson intrusives) is probably early Cretaceous in age. Both the Raft Batholith and the more felsic phases of the Okanagan Highlands Complex appear to be representative of a major plutonic event at around 100 Ma which has been well documented for other parts of the Cordillera.

Flat lying, vesicular and massive olivine basalts both overlie and occur adjacent to the Raft Batholith. These rocks which may be included in the Miocene-Pliocene Plateau Basalt formation of the Central Cordillera have a mineralogy and setting which is very similar to the Plateau Basalts capping mineralization in the Okanagan. No age dating has been performed on the basalts in the study area but a good approximate age can be obtained from work in adjacent areas. For a large mass of Plateau Basalts just to the west of the Clearwater area Mathews (1964) obtained ages of 13 ± 2 Ma, 12 ± 2 Ma and 10 ± 2 Ma for ash layers intercalated with the basalts. Ages of 8.3 ± 3 Ma, 7.8 ± 3 Ma and 6.0 ± 3 Ma were determined by Farquharson and Sipp (1969) for basaltic plugs within this mass. These plugs probably represent feeder vents for later basaltic extrusions. Bedded basaltic scoria and breccias, together with extinct cinder cones of late Pliocene to Pleistocene age occur just to the north of the study area. The basalts associated with the Raft Batholith have undergone glaciation and must therefore be older than Pleistocene. Based on age dates obtained in other areas, the Raft basalts must be of late Miocene to early Pliocene age and are most probably early Pliocene. The basalts overlying mineralization in the Okanagan have been dated as early Pliocene (4.4 ± 0.6 Ma, 5.9 ± 0.6 Ma, author's data; 5.0 ± 0.50 Ma, 4.7 ± 0.17 Ma, Christopher 1978; all K-Ar whole rock). It is apparent therefore that the same age relationships between intrusive source and basaltic capping exist for both the Clearwater and Okanagan regions.

Recently basalt formations spatially associated with felsic intrusions have been the main loci of exploration for basal type uranium deposits in the Cordillera and it is convenient therefore to divide the various basaltic bodies in the Clearwater area into six entities based on their relationship to the Raft Batholith. Together with a discussion of their geology and setting the six areas underlain by basalt may be outlined as follows:

a. Upper Mann Creek valley basalt. This is a massive unit of olivine basalt which according to Campbell and Tipper (1971) occupies the valley from Moira Lake to Coldscaur Lake (see Fig. 3.5). Detailed investigations by the author verified the presence of basalt outcrops in the stream bed at both the south and north end of upper Mann Creek (area A, Fig. 3.5), otherwise the presence of a continuous basaltic body is indicated only by numerous large basalt boulders and debris deposited by glaciation – it is presumed that this material was deposited as the result of glacial scouring of the flanks of the valley basalt. This body seems to offer the best potential for the formation of basal type deposits because of its close proximity to source rocks (i.e. Raft Batholith).

b. Coldscaur Lake basalt. Considerable amounts of basalt float north and west of Coldscaur Lake suggests the presence of a large body of flat lying basaltic rocks.

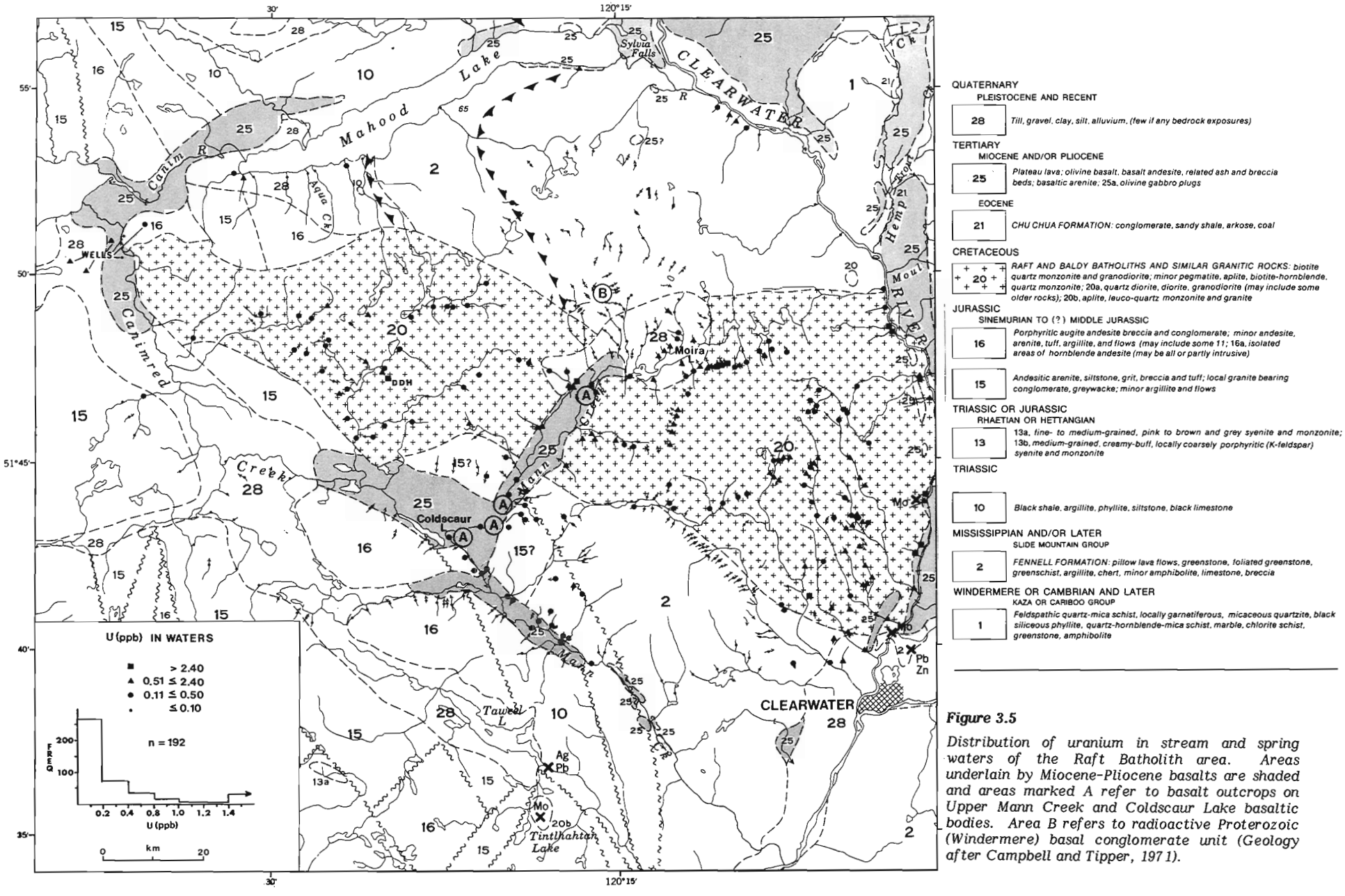

QUATERNARY
PLEISTOCENE AND RECENT

28 — *Till, gravel, clay, silt, alluvium, (few if any bedrock exposures)*

TERTIARY
MIOCENE AND/OR PLIOCENE

25 — *Plateau lava; olivine basalt, basalt andesite, related ash and breccia beds; basaltic arenite; 25a, olivine gabbro plugs*

EOCENE

21 — *CHU CHUA FORMATION: conglomerate, sandy shale, arkose, coal*

CRETACEOUS

20 — *RAFT AND BALDY BATHOLITHS AND SIMILAR GRANITIC ROCKS: biotite quartz monzonite and granodiorite; minor pegmatite, aplite, biotite-hornblende, quartz monzonite; 20a, quartz diorite, diorite, granodiorite (may include some older rocks); 20b, aplite, leuco-quartz monzonite and granite*

JURASSIC
SINEMURIAN TO (?) MIDDLE JURASSIC

16 — *Porphyritic augite andesite breccia and conglomerate; minor andesite, arenite, tuff, argillite, and flows (may include some 11; 16a, isolated areas of hornblende andesite (may be all or partly intrusive)*

15 — *Andesitic arenite, siltstone, grit, breccia and tuff; local granite bearing conglomerate, greywacke; minor argillite and flows*

TRIASSIC OR JURASSIC
RHAETIAN OR HETTANGIAN

13 — *13a, fine- to medium-grained, pink to brown and grey syenite and monzonite; 13b, medium-grained, creamy-buff, locally coarsely porphyritic (K-feldspar) syenite and monzonite*

TRIASSIC

10 — *Black shale, argillite, phyllite, siltstone, black limestone*

MISSISSIPPIAN AND/OR LATER
SLIDE MOUNTAIN GROUP

2 — *FENNELL FORMATION: pillow lava flows, greenstone, foliated greenstone, greenschist, argillite, chert, minor amphibolite, limestone, breccia*

WINDERMERE OR CAMBRIAN AND LATER
KAZA OR CARIBOO GROUP

1 — *Feldspathic quartz-mica schist, locally garnetiferous, micaceous quartzite, black siliceous phyllite, quartz-hornblende-mica schist, marble, chlorite schist, greenstone, amphibolite*

Figure 3.5

Distribution of uranium in stream and spring waters of the Raft Batholith area. Areas underlain by Miocene-Pliocene basalts are shaded and areas marked A refer to basalt outcrops on Upper Mann Creek and Coldscaur Lake basaltic bodies. Area B refers to radioactive Proterozoic (Windermere) basal conglomerate unit (Geology after Campbell and Tipper, 1971).

Campbell and Tipper (1971) have indicated a connection with the Upper Mann Creek flow as well as a possible contact relationship with the Raft Batholith. This contact could not be verified due to lack of outcrop. Most of this basalt flow would appear to be underlain by Jurassic volcano-sedimentary rocks. A contact relationship with the intrusion, to permit influx of igneous derived groundwaters into sediments underlying basalt, would have to be established in order for the Coldscaur basalt to have much potential for mineralization.

c. Lower Mann Creek basalt. Heavily dissected basalts occupy the lower Mann Creek valley and a small tributary into it. These flows have been completely downcut by Mann Creek and they overlie Jurassic volcano-sedimentary units having a low uranium content. It is unlikely, therefore, that any underlying sediments, even if still preserved, would host mineralization.

d. Canim River basalt. A crescent shaped flow occupies the valleys of Canim River and Canimred Creek in the western part of the area. A possible contact between the western extremity of the Raft Batholith and the Canimred portion of this flow is indicated (Campbell and Tipper, 1971). However, no outcrop could be found to verify the presence of basalt on the east side of the Canimred River. The mafic nature (diorite-granodiorite) of the intrusion in the area and the lack of a defined contact relationship would tend to weaken the potential of this area for mineralization.

e. Clearwater River valley basalt. Severe dissection and erosion of an extensive basaltic flow in the Clearwater valley has left a number of 'shoulder remnants' along the eastern edge of the Raft intrusion. These bodies, which are often downcut by easterly flowing streams, do not appear to be related to underlying paleochannel structures and are therefore of questionable potential.

Tectonic History

In the Okanagan six main tectonic events are thought to have a direct bearing on the formation and cessation of mineralizing processes. These events may be summarized as follows:

a. The emplacement of Jurassic and Cretaceous granitic rocks to form part of the Central Okanagan Highlands Complex followed shortly afterwards by the development of a north-south compressive stress system marked by major north-south lineaments (Okanagan Valley, West Kettle River and Granby River lineaments) and conjugate northwest-southeast and northeast-southwest fault and graben structures.

b. Extrusion of Eocene alkali and felsic volcanics (White Lake, Marama, and Marron formations) and emplacement of coeval hypabyssal syenites (Coryell).

c. Gradual uplift in late Eocene-Miocene times with reactivation of the fault-scheme described in (a), unroofing of the basement complex and deposition of fluvial sediments in Tertiary Valleys.

d. Development of extensional stresses in late Miocene – early Pliocene followed by fissure extrusion of basalt along valleys (northwest-southeast and northeast-southwest Mesozoic-Tertiary fault zones) and many upland areas.

e. Late Pliocene uplift of entire area with concomitant block faulting, followed by rapid erosion and eventually glaciation. The valley roots are the only remnants of the Plateau Basalts which have survived this period and they now form linear topographic highs (see Fig. 3.2).

Uranium mineralization in the Okanagan has been deposited in paleochannels underlying valley basalts between periods d and e.

In the Clearwater area there is sufficient evidence to suggest that all of the above mentioned tectonic events have been operative to some degree. Age dating of the Raft Batholith indicates that it was emplaced in Cretaceous times and extensive block faulting of Paleozoic and Mesozoic formations surrounding it has been noted by Campbell and Tipper (1971, see also Fig. 3.5). The stress scheme in this area is similar to that in the Okanagan. Major faults follow northwest-southeast and northeast-southwest directions and although not indicated by Campbell and Tipper (1971) it would appear that the valleys occupied by Upper Mann Creek, Coldscaur Lake and Lower Mann Creek form a conjugate fault system possibly located at the terminus of the major northwesterly trending Louis Creek fault zone which begins at the north end of Okanagan Lake (Holland, 1976) and follows Louis Creek, North Thompson River and eventually into Mann Creek. The Upper Mann Creek valley which appears to have the greatest potential for uranium mineralization occupies a possible northeast-southwest fault zone that bisects the Raft Batholith. Reactivation of tectonic processes followed by erosion must have occurred in Mid-Tertiary times for the batholith to be exposed before the Miocene epoch. Extensive areas just to the southwest of the Clearwater area are covered by Eocene felsic volcanics (Skull Hill Formation) similar to the non-alkaline units in the Okanagan but this tectonic event is not present in the immediate area (Campbell and Tipper 1971). The late Miocene-early Pliocene epoch was characterized by the fissure extrusion of plateau basalts in the Mann Creek, Coldscaur Lake, Clearwater River, and Canim River areas. Late Pliocene movement is evident from extensive faulting and dissection along Clearwater River, Lower Mann Creek, and Canim River but the amount of uplift appears to be less than that observed in the Okanagan. As a result, basaltic bodies such as the Upper Mann Creek and Coldscaur Lake flows, which still appear to be intact, are still in their original valley settings. This is not considered detrimental to uranium potential since this stage of tectonism is one which has caused the cessation of mineralizing processes. In other words, the Okanagan deposits and associated basalt cappings now form topographic highs and are presently wasting, whereas sediments underlying basalts on or immediately adjacent to the Raft intrusion would still be receiving groundwaters draining an igneous source.

Composition of Source Rocks

Both the Raft Batholith and the Okanagan Highlands Complex contain a full range of igneous phases from diorite through to granite. Quartz monzonite and granite accounts for the largest volume of both complexes and are typically coarse grained rocks comprising plagioclase (30-35%), smoky quartz (25-30%), potash feldspar (25-35%) biotite and/or muscovite (5-10%), hornblende (less than 1%) and accessories (sphene, rutile, allanite, apatite). The western part of the Raft Batholith consists mainly of granodiorite and diorite whereas much of the area both east and west of upper Mann Creek and stretching as far as the Clearwater River is underlain by quartz monzonite and granite. Pegmatite and aplite dykes have been observed in all major areas of outcrop.

Tabulation of the major element chemistry of quartz monzonite from the Clearwater and Okanagan areas shows that rocks of the Raft Batholith are slightly more mafic than their counterparts in the Okanagan Highlands Complex but the K_2O and Na_2O contents of rocks for both areas are similar (Table 3.2). High U concentrations in granitic rocks are generally accompanied by increased potash content (Heir

Table 3.2

Composition of quartz monzonite from the Raft Batholith and Okanagan Highlands Complex

	Okanagan Highlands Complex n=13		Raft Batholith n=8	
	Range	Average	Range	Average
SiO_2	64.40-75.70	71.10	58.8 - 71.3	66.50
Al_2O_3	13.70-16.80	15.00	14.0 - 16.8	15.10
TiO_2	0.04- 0.36	0.25	0.25- 0.73	0.42
K_2O	2.73- 6.01	4.42	2.38- 4.10	3.64
Na_2O	3.20- 4.20	3.64	2.30- 4.30	3.56
CaO	0.45- 2.87	1.40	1.84- 5.81	3.36
MgO	0.06- 0.83	0.40	0.71- 2.40	1.43
FeO	0.10- 1.20	0.66	0.90- 2.50	1.79
Fe_2O_3	0.40- 2.00	1.02	0.60- 2.80	1.35
MnO	0.01- 0.09	0.03	0.05- 0.14	0.08
P_2O_5	0.02- 0.16	0.08	0.10- 0.42	0.02
CO_2	0.10- 0.10	0.10	0.10- 2.20	0.75
H_2OT	0.30- 1.00	0.51	0.60- 2.10	1.20
Total	98.00-99.70	98.70	98.70-100.50	99.50

Table 3.3

Uranium in the Raft Batholith and Okanagan Highlands Complex

Rock Type	No. of Samples	U(ppm)* Range	U(ppm)* Average
Raft Batholith:			
Diorite	4	0.1- 0.3	0.2
Granodiorite	4	1.7- 5.4	3.6
Monzonite	5	2.7- 5.7	4.3
Quartz Monzonite	25	2.5- 7.2	4.6
Granite-Pegmatite	8	3.8- 8.8	5.8
Aplite	2	15.4-24.0	20.0
Okanagan Highlands Complex:			
Granodiorite-Diorite	43	0.8- 4.3	2.3
Monzonite	30	1.1-17.7	4.5
Quartz Monzonite	27	0.9-23.7	4.4
Granite	20	1.9-18.0	5.4
Pegmatite	3	3.2- 6.9	5.2
Syenite (Coryell)	76	2.0-36.6	6.2

* Uranium analysis by delayed neutron activation.

and Rogers, 1963; Lyons, 1964 and others), and on an initial basis, granitic rocks rich in potash feldspar, biotite and muscovite can be designated as fertile for the formation of basal type deposits. Granitic rock in both the Raft and Okanagan Highlands Complexes have high K_2O contents (Table 3.2). Those of the Raft Batholith contain considerably more P_2O_5 than those in the Okanagan and it may be presumed therefore that sufficient phosphate would be present in the groundwaters of the Raft area for the precipitation of ningyoite saléeite or autunite – the three principal minerals in basal-type deposits of the Okanagan.

A comparison of the range and average total U contents of the various phases in the Raft and Okanagan Highlands Complexes is presented in Table 3.3. Phases of the Raft Batholith display very similar U contents to comparable units in the Okanagan Complex. On the basis of total U content it is obvious that the Raft Batholith has good potential as a source area. It is interesting to note that the U concentrations of the various rock types in the Raft Batholith increase in the order diorite, granodiorite, monzonite, quartz monzonite, granite, pegmatite, aplite. This also appears to be the general order of increasing potassium content and older to younger age of intrusion.

Labile Uranium in Source Rocks

The amount of labile uranium in source rocks can be determined on a relative basis by a number of methods. Two methods used in this study comprise the leaching of rock powders with bicarbonate waters and the determination of average uranium contents for surface waters and groundwaters draining granitic rocks of the Raft Batholith and of Okanagan Highlands Complex.

Rock powders of quartz monzonite and granite phases of the two above mentioned intrusive complexes were leached for 20 hours using a solution composed of 300, 220, 30, 20, 400, 45 and 20 ppm of HCO_3^-, Na, Ca, Mg, F, Cl and $SO_4^=$ respectively with a pH of 7.0 and a conductivity of 580. The U content of the leaching solution was less than 0.05 ppb. With the exception of a high Na content and a low U concentration the composition of the leaching solution approximates that found for many groundwaters draining granitic rocks in the Okanagan (Boyle and Ballantyne, in press). The leaching solution and sample (20 mL to 1 gm) were continually aerated by allowing air to pass through the funnel holding the sample and solution. All samples were leached in one run and replicate leaching gave a precision of better than ± 20 per cent. The results for this experiment are shown in Table 3.4. The samples from both of these intrusive complexes are listed in decreasing order according to their total uranium content. The final characteristics of the leachate (pH, conductivity, U) together with a determination of the percentage of leachable uranium are also given. There is little correlation between the percentage of U leached and either the total U content of the rocks or their texture. Variations in the partitioning of uranium between accessory minerals and localization along grain boundaries may be the cause of such a poor correlation. Both the range and average percent of U leached from the Raft Batholith (0.3-3.0 and 1.4% respectively) and the Okanagan Highlands Complex (0.3-4.0 and 1.8% respectively) are very similar and it may be concluded therefore that on an experimental basis the Raft Batholith is as good a source area as the granitic rocks associated with mineralization in the Okanagan.

A comparison of the U contents of various types of waters draining these intrusive complexes is perhaps a more representative method of determining their potential as source areas. This is easily justified since for both the areas the paleoclimates during the time of possible ore formation (Miocene-Pliocene; Bell, W.A. in Rice 1960; Piel, 1969; Claque, 1974) and the present day climates are similar. Table 3.1 gives a breakdown of the U content of surface waters and groundwaters draining the two igneous complexes. The average U concentrations of surface waters are very similar for both complexes with the Raft Batholith exhibiting a slightly higher average. However, structurally controlled groundwaters associated with the Okanagan Complex are more uraniferous than those draining the Raft Batholith (Table 3.1), although the average U content of springs draining the latter still exceeds the surface water average by a factor of ten. The differences for groundwaters may be related more to the fact that results for the Raft Batholith were obtained for small fissure controlled springs representing mostly local or intermediate groundwater flow whereas those for the Okanagan represent local, intermediate and regional groundwater flow in much larger fault zones. In

Table 3.4

Labile uranium in igneous rocks of the Raft Batholith (Clearwater Area) and the Okanagan Highlands Complex

Rock Type	Texture	U (ppm)* in Rock	Leachate			% of Total Uranium Leached	
			pH	Conductivity (umhos/cm)	U (ppb)		
Raft Batholith:							
Qtz-Bi-MNZN	fine	6.2	7.9	1360	9.0	1.5	
Bi-GRNT	medium	5.4	8.1	1065	12.6	2.3	
Qtz-Bi-MNZN	coarse	5.3	8.0	1083	7.5	1.4	
Bi-GRNT	coarse	5.2	7.8	691	3.0	0.6	
Qtz-Bi-MNZN	medium	5.0	7.7	792	10.0	2.0	
Bi-GRNT	coarse	4.8	8.1	1177	4.0	0.8	
Qtz-Bi-MNZN	coarse	4.0	7.9	962	6.8	1.7	(Av.=1.4)
Bi-GRNT	coarse	3.6	8.0	882	3.2	0.9	
Ho-MNZN	medium	3.6	7.9	997	1.0	0.3	
Qtz-Bi-MNZN	coarse	3.5	8.1	1340	2.6	0.8	
Bi-GRNT	coarse	3.3	7.8	1310	3.4	1.0	
Bi-GRNT	coarse	2.5	7.8	1350	7.5	3.0	
Bi-MNZN	fine	1.7	9.0	1087	3.6	2.1	
Okanagan Highlands Complex:							
Qtz-Bi-MNZN	medium	23.6	7.8	756	95.0	4.0	
Bi-GRNT	medium	15.0	8.2	627	5.2	0.3	
Qtz-Bi-MNZN	medium	13.1	8.1	659	33.8	2.6	
Qtz-Mu-MNZN	coarse	12.6	7.9	673	36.5	2.9	
Qtz-Bi-MNZN	medium	6.8	8.0	852	16.7	2.5	
Qtz-Bi-MNZN	coarse	6.5	7.9	684	4.0	0.6	
Qtz-Bi-MNZN	coarse	4.8	7.1	727	4.2	0.9	(Av.=1.8)
Qtz-Ho-MNZN	coarse	4.0	7.8	681	1.3	0.3	
Qtz-Bi-MNZN	medium	3.8	7.4	699	4.2	1.1	
Qtz-Bi-MNZN	coarse	3.6	8.0	723	13.5	3.8	
Qtz-Bi-MNZN	coarse	2.8	7.7	635	2.7	1.0	
Qtz-Bi-MNZN	medium	2.3	7.9	644	3.7	1.6	
Qtz-Bi-MNZN	medium	1.8	8.1	659	2.0	1.1	

* Uranium analysis by delayed neutron activation.

terms of size the Raft Batholith is much smaller than the Okanagan complex and of the two noticeable structural zones within it, one (Upper Mann Creek) is heavily overlain by basalts and glacial drift and the other (Clearwater River) is a completely open system flushed by a major river. Spring waters issuing from small fault zones along the western cliff face of the Clearwater River, however, do have anomalously high U contents (see Fig. 3.5). Campbell and Tipper (1971, p. 79) have noted that "the Cretaceous Raft Batholith does not exhibit the closely spaced fractures characteristic of the Thuya and Takomkane batholiths" located to the west of the study area. It is possible therefore that the Raft Batholith lacks the open structure required for deep seated groundwater movement although this is by no means a proven fact. In this context it should also be noted that the levels of U observed for structurally controlled waters in the Okanagan may be well above minimum levels required for ore formation.

Composition of Host Rocks

In the Miocene fluvial sediments of the Okanagan the reducing environment required for precipitation of uranium is produced by abundant amounts of organic trash consisting of both carbonized and uncarbonized tree fragments, leaves and decomposed material. In addition one of the deposits (Tyee deposit) contains high concentrations of marcasite (up to 40%).

A number of palynological and faunal studies of Miocene-Pliocene sediments throughout southern British Columbia indicate that a lush vegetation existed during this epoch in a temperate climate similar to that of today (Bell, W.A. in Rice 1960; Piel 1969; Clague 1974; Mathews and Rouse, 1963).

No exposures of Miocene sediments could be found in the study area but there can be little doubt that basalt flows in the Raft area, provided they are still intact, are underlain by fluvial sediments. Based therefore on the studies mentioned above it should be presumed, until proven otherwise, that sediments in this area contain sufficient organic or sulphide concentrations to precipitate uranium from groundwaters.

Preservation of Basalt-Fluvial Sediment Assemblage

Generally it has been found that basal-type deposits are preserved from later destruction by one or a combination of two processes. Either the basalt cappings remain intact after uplift and faulting because they represent more competent "valley roots" of the Plateau Basalt system (e.g. Blizzard deposit) or the paleochannels when exposed during glaciation have in turn been covered by impervious glaciolacustrine sediments (e.g. Tyee deposit and south end of Blizzard deposit). Preservation such as this is essential since the Holocene hydrological regime after uplift is generally one which promotes leaching of these deposits rather than formation.

In the Raft area the lower Mann Creek basalt is completely downcut to basement and it is unlikely that mineralization if it did form would be preserved. Upper Mann Creek does not downcut the presumed basalt flow in this valley and has been found to actually flow over basalt outcrop in the north and south end of the valley (area A, Fig. 3.5); west of Coldscaur Lake it flows over a basalt escarpment and into lower Mann Creek valley. Similarly much of the Coldscaur Lake and Canimred Creek basalt bodies may still be preserved. The 'shoulder remnants' of the Clearwater River basalt are downcut by small streams and any sediments underlying them would probably be easily leached by groundwaters moving downslope.

Potential For Other Types of Uranium Deposits

Although the main thrust of this assessment has been directed towards possible basal-type deposits something should also be said of the potential for other types of uranium deposits.

No evidence could be found that would suggest the presence of vein type mineralization within the Batholith. Small Mo occurrences are present but these are not strongly radioactive.

Coarse pegmatite phases of the batholith are present in outcrop and extensively in float. The greatest concentration of pegmatites occurs in the portion of the batholith east of Upper Mann Creek. As expected the pegmatites exhibit the highest radioactivity but no recognizable primary or secondary uranium mineralization could be detected in them. The strong anomalies observed in waters southeast and south of Moira Lake may be related to mineralized pegmatites (see Fig. 3.5). Elsewhere in the eastern half of the batholith more isolated anomalies may also reflect concentrations of pegmatites.

Table 3.5

Uranium, sulphur, organic carbon and phosphate contents of triassic shale, greywacke and phyllite near the southern contact of the Raft Batholith (samples in order of decreasing uranium content)

Rock Description	U (ppm)	S(%)	C(%)	P_2O_5 (%)
black shale	6.9	1.13	2.01	0.11
calcitic black shale	6.2	0.36	2.51	1.06
greywacke	4.5	0.06	0.01	0.88
black shale	4.4	0.33	0.70	0.20
silicified phyllite	3.9	0.05	0.30	0.22
grey phyllite	3.8	0.18	0.31	0.10
greywacke	3.3	0.00	0.38	0.15
black shale	3.3	0.12	0.53	0.09
black shale	3.0	0.21	0.56	0.06
grey slate	2.9	0.03	0.37	0.21
silicified greywacke	2.9	0.02	0.26	0.15
silicified greywacke	2.9	0.01	0.20	0.14
black phyllite	2.6	0.05	0.34	0.13
greywacke	2.5	0.02	0.24	0.14
greywacke	2.4	0.08	0.28	0.15
silicified greywacke	2.4	0.34	0.05	0.08
silicified greywacke	2.1	0.03	0.17	0.20
black phyllite	2.0	0.08	0.44	0.07
calcite phyllite	1.8	0.09	0.01	0.07
arkosic shale	1.6	0.11	0.44	0.27
graphitic shale	1.5	0.00	0.65	0.02
Range	1.5-6.9	0.0-1.13	0.01-2.51	0.02-1.06
Average	3.2	0.16	0.33*	0.21

* high values not included in average

Both the age and setting of the Raft Batholith are similar to that of the Loon Lake batholith in northern Washington with which the Midnite and Spokane Mountain uranium deposits are associated. These deposits are composed of uraninite, sulphides and secondary uranium minerals in a roof pendant of Precambrian phyllites at the contact with the Loon Lake intrusion (Nash and Lehrman, 1975; Robbins, 1978). In the Clearwater area Triassic phyllites (Campbell and Tipper, 1971) outcrop near the southern contact of the Raft Batholith (see Fig. 3.5). There is no indication that these rocks are in direct contact with the intrusion. The uranium, sulphur, organic carbon and phosphate contents of these phyllites are given in Table 3.5. The average U content is typical of Phanerozoic shales (average = 0.37, Turekian and Wedepohl, 1961) and no U enrichment in these rocks during emplacement of the batholith is apparent. The sulphur and organic carbon contents are certainly sufficient to create the necessary reducing conditions for precipitation of U from hydrothermal fluids. However, these rocks show very little evidence of either syn- or post-intrusive hydrothermal activity. Two small intrusions similar in composition to the Raft are intruded directly into Triassic phyllites north of Mahood Lake and these may constitute a better environment for this type of mineralization.

A metamorphosed basal conglomerate consisting of sheared pebbles of feldspar and quartz and lenses of pyrite in a medium grained matrix is situated just to the northwest of Moira Lake near the intrusive – Proterozoic contact (area B, Fig. 3.5). This unit possesses the highest radioactivity of any formation within the study area. Uranium analyses of four representative samples however gave values of only 7.6, 10.1, 20.7 and 3.0 ppm U which is much lower than would be expected from radioactive counting if all of the gamma radiation was coming from uranium. Also waters draining this unit contain very low levels of U (less than 0.10 ppb, see Fig. 3.5). These rocks are similar to thorium-rich basal conglomerates in other parts of the British Columbia-Yukon Proterozoic belt and the high Th values accompanied by slightly anomalous U levels can be attributed to the concentration of resistate minerals such as monazite, allanite, sphene and zircon.

Conclusions

The uranium potential of the Raft Batholith area has been assessed using a genetic model developed from research on the formation of basal-type uranium deposits in the Okanagan Highlands. A comparison of these two areas has been made using model parameters considered to have the most important influence on the formation of ore; namely geological setting, age relationships, tectonic history, composition of source rocks, labile uranium in source rocks, composition of host rocks and preservation of basalt-fluvial sediment assemblages.

Both the Raft Batholith and the Okanagan Highlands Complex have similar geologic settings and would appear to have the same age relationship with an overlying Plateau basalt-fluvial sediment assemblage. There is good evidence to suggest that the same schedule of tectonic events occurred in both areas although late Pliocene uplift seems to have been much less severe in the Raft Batholith area; this of course is a post ore forming event and would have a more direct bearing on the cessation of the ore-forming process and the preservation of deposits.

The petrology, major element composition and total uranium content of these two complexes are very similar. On an experimental basis just as much uranium can be leached from the Raft Batholith as the Okanagan complex and under natural conditions the uranium content of surface waters draining the Raft Batholith is greater than for waters draining the Okanagan Highlands Complex. However the uranium concentration of groundwaters draining the Raft Batholith is noticeably less than for groundwaters in the Okanagan complex. This may not be a fair comparison since the latter are associated with major structural zones probably tapping intermediate or regional groundwaters whereas the former only represent small local springs – the major structural zones in the Raft Batholith are either occupied by relatively impervious basalts (e.g. upper Mann Creek valley) or are completely open systems flushed by major rivers (e.g. Clearwater River valley).

Six main areas underlain by basalts have been identified in the Raft Batholith area. Based on such factors as proximity to source rock, preservation of basalt cover and the various model parameters mentioned above the Upper Mann Creek valley basalt and the Coldscaur Lake basalt appear to offer the best potential for basalt type uranium deposits.

Despite the many similarities between these two areas a number of factors which may have a direct bearing on mineral potential are still unanswered. It is not known at this time whether or not

a. the Upper Mann Creek and Coldscaur Lake basalts are continuous bodies;

b. the Coldscaur Lake and Canimred River basalts have a contact relationship with the Raft Batholith in order for igneous derived groundwaters to enter basal sediments;

c. the fluvial sediments underlying the basalts have the proper composition to promote precipitation of uranium;

d. a possible northeast-southwest fault zone along Upper Mann Creek was or still is open to intermediate and regional groundwater flow;

e. the levels of uranium observed for structurally controlled waters in the Okanagan represent a minimum requirement for ore-forming groundwaters. If so the groundwaters associated with the Raft Batholith would appear to fall somewhat short of this requirement.

Many of these unanswered questions can only be resolved by subsurface exploration. A genetic model used in exploration should not be expected to outline mineralizaiton but instead indicate mineral potential, the magnitude of which will depend upon available geological and geochemical information. At the time of completing this work the British Columbia Government imposed a seven year moratorium on exploration for uranium in British Columbia. Although this directly affects any further work in the Clearwater area in the near future, the Raft Batholith is used here only as an example of the application of an exploration model which is applicable to any area where there is an intimate relationship between a granitic basement complex and overlying sediments.

Acknowledgments

The author would like to thank D. Halliwell and B. Henderson for their able assistance in the field. Water analyses were carried out by the analytical staff of the Resource Geochemistry Subdivision, Resource Geophysics and Geochemistry Division under the direction of G.E.M. Hall. Major element analysis of rocks was performed by J.L. Bouvier of the Analytical Chemistry Section of the Central Laboratories and Technical Services Division under the direction of S. Abbey and uranium analyses were done in the laboratories of the Atomic Energy of Canada Ltd. Permission from Norcen Energy Resources Ltd., Calgary to publish Figure 3.3 of this paper is gratefully acknowledged. The authors would also like to thank S.B. Ballantyne, R.T. Bell, and E.H. Hornbrook for critically reviewing this paper.

Addendum

Subsequent to the completion of this paper, results of a uranium exploration program in the Raft Batholith area by Union Oil Company of Canada Ltd. have been made available to the author. This company drilled seven widely spaced reconnaissance drillholes in Upper Mann Creek valley during 1979. Results from this program confirm the presence of a continuous body of valley basalts which are underlain by unconsolidated fluvial sediments consisting of coarse sand, lacustrine silt, conglomerate and mudslide breccia and having a thickness from 2 to 40 m. Gamma ray logs outlined sections of minor anomalous radioactivity but assay results for the sediments range only from 2 to 10 ppm U. These drillholes were sited in order to verify the presence of fluvial sediments underlying the basalt and were to be followed up by more detailed drilling. Based on this initial drilling, the absence of carbonaceous matter and the presence of high U (1.2-3.0 ppb) and PO_4 (avg. 100 ppb) levels in drillhole waters are characteristic of the northern part of the sedimentary aquifer underlying the Upper Mann Creek basalts. These are conditions which are more typical of an aquifer system incapable of precipitating uranium. However, exploration activity has been confined to the northern half of this valley and fluvial sediments underlying basalt in the south may have a greater capacity for precipitating uranium due to an increased concentration of organic matter and/or depletion of dissolved oxygen in groundwaters moving down the aquifer gradient. Clearly more exploration is required in this area before an adequate assessment of uranium potential can be made.

Union Oil Company Ltd. have also carried out a drilling program on basalts overlying the northeast part of the Raft Batholith along the Clearwater River (see Fig. 3.2 for the location of basalts). This program proved the existence of fluvial sediments under the basalts but no anomalous uranium concentrations were encountered.

The author would like to thank J. Schindler of Union Oil Company of Canada Ltd. for allowing him to use data from their company reports.

References

Becraft, G.E. and Weis, P.L.
1963: Geology and mineral deposits of the Turtle Lake Quadrangle, Washington. U.S. Geological Survey, Bulletin 1131, 73 p.

Boyle, D.R.
1979: The formation of basal-type uranium deposits in south-central British Columbia; (Abst.) Canadian Mining and Metalurgical Bulletin, v. 72, no. 803, p. 96 (Abstract).

Boyle, D.R. and Ballantyne, S.B.
Geochemical studies of uranium dispersion in south-central British Columbia; Canadian Mining and Metalurgical Bulletin, in press.

Campbell, R.B. and Tipper, H.W.
1971: Geology of Bonaparte Lake map-area, British Columbia; Geological Survey of Canada, Memoir 363, 100 p.

Choate, R.
1962: Geology and ore deposits of the Stanley area; Idaho Bureau of Mines and Geology, Pamphlet 126, 75 p.

Christopher, P.A.
1978: East Okanagan uranium area (Kelowna to Beaverdell) south-central British Columbia; British Columbia Department of Mines and Petroleum Resources, Preliminary Map 29.

Christopher, P.A. and Kalnins, T.
1977: Exploration for basal type uranium deposits in B.C.; Western Mines, April 1977, p. 75-79.

Church, B.N.
1977: Tertiary stratigraphy in south-central British Columbia; in Geological Fieldwork, British Columbia Ministry of Energy, Mines and Petroleum Resources, 1977, p. 7-11.

Clague, J.J.
1974: The St. Eugene Formation and the development of the southern Rocky Mountain Trench; Canadian Journal of Earth Sciences, v. 11, p. 916-938.

Doi, K., Hirono, S., and Sakamaki, Y.
1975: Uranium mineralization by groundwater in sedimentary rocks, Japan; Economic Geology, v. 70, no. 4, p. 628-646.

Farquharson, R.B. and Stipp, J.J.
1969: Potassium-argon ages of dolerite plugs in the south Cariboo region, British Columbia; Canadian Journal of Earth Sciences, v. 6, p. 1468-1470.

Heir, K.S. and Roger, J.J.W.
1963: Radiometric determination of thorium, uranium and potassium in basalts and in two magmatic differentration series; Geochemica et Cosmochimica Acta, v. 27, p. 137.

Holland, S.S.
1976: Landforms of British Columbia; British Columbia Ministry of Energy, Mines and Petroleum Resources, Bulletin 48, p. 123.

International Atomic Energy Agency
1977: Recognition and evaluation of uraniferous areas: International Atomic Energy Agency Publication, Vienna, 1977, 295 p.

Katayama, N.
1960: Genesis of Uranium Deposits in Sedimentary Rocks; Report of the International Geological Congress, Norden, Part 15, p. 7-14.

Katayama, N., Kubo, K., and Hirono, S.
1974: Genesis of uranium deposits of the Tono mine, Japan; in Formation of Uranium Ore Deposits, Proceedings of Symposium in Athens, International Atomic Energy Agency Publication, Vienna, 1974, p. 437-452.

Little, H.W.
1957: Geology of the Kettle River (East half) area, British Columbia; Geological Survey of Canada, Map 6-1957.

1961: Geology of the Kettle River (West half) area, British Columbia; Geological Survey of Canada, Map 15-1961.

Lyons, J.B.
1964: Distribution of thorium and uranium in three Early Paleozoic plutonic series of New Hampshire; U.S. Geological Survey Bulletin, 1144-F, 43 p.

Mathews, W.H.
1964: Potassium-argon age determinations of Cenozoic volcanic rocks from British Columbia; Geological Society of America Bulletin, v. 75, p. 465-468.

Mathews, W.H. and Rouse, G.E.
1963: Late Tertiary volcanic rocks and plant-bearing deposits in British Columbia; Geological Society of America Bulletin, v. 74, p. 55-60.

Nash, J.T. and Lehrman, N.J.
1975: Geology of the Midnite uranium mine, Stevens County, Washington; U.S. Geological Survey, Open File Report 75-402.

Norcen Energy Resources Ltd.
1979: Phase I Overview. Report of the Royal Commission of Inquiry into Uranium Mining, Province of British Columbia, 11 p.

Okuno, T.
1972: Donen (281 to 360 incl.) Mineral Claims 49°, 118°NW, Greenwood Mining Division, British Columbia; British Columbia Ministry of Energy, Mines and Petroleum Resources Assessment Report 3775.

Piel, K.M.
1969: Palynology of middle and late Tertiary sediments from the central interior of British Columbia; Ph.D. Thesis, Univ. of British Columbia, 1969, 157 p.

Rapp, J.S.
1978: California Division of Mines and Geology, v. 31, ISS: 9, p. 199-202, Ref. 10.

Rice, H.M.A.
1960: Geology and mineral deposits of the Princeton map-area, British Columbia; Geological Survey of Canada, Memoir 243, p. 30.

Robbins, D.A.
1978: Applied Geology in the discovery of the Spokane Mountain uranium deposit, Washington; Economic Geology, v. 73, p. 1523-1538.

Smee, R.W. and Ballantyne, S.B.
1976: Examination of some Cordilleran uranium occurrences; in Report of Activities, Part C, Geological Survey of Canada, Paper 76-1C, p. 255-158.

Turekian, K.K. and Wedepohl, K.A.
1961: Distribution of the elements in some minor units of the earth's crust; Geological Society of America Bulletin, v. 72, p. 175-192.

Wanless, R.K., Stevens, R.D., Lachance, G.R. and Edmonds, C.M.
1967: Age determinations and geological studies K-Ar isotopic ages, report 7; Geological Survey of Canada, Paper 66-17, p. 25-26.

INNUITBEYRICHIA, A NEW SILURIAN OSTRACODE GENUS FROM THE CANADIAN ARCTIC

Project 720072

M.J. Copeland
Institute of Sedimentary and Petroleum Geology, Ottawa

*Copeland, M.J., **Innuitbeyrichia**, a new Silurian Ostracode genus from the Canadian Arctic; in Current Research, Part B, Geological Survey of Canada, Paper 80-1B, p. 29-37, 1980.*

Abstract

*A previously unrecorded microfauna from near the top of the Douro Formation, Devon Island, District of Franklin, contains a unique ostracode genus of the subfamily Beyrichiinae. The morphology of this genus indicates its position intermediate between the genera **Beyrichia**, **Neobeyrichia** and **Calcaribeyrichia** within a Ludlovian beyrichiine lineage previously described from the Balto-Scandinavian region.*

Introduction

A fossil collection made by R. Thorsteinsson from strata of the Douro Formation, Devon Island, District of Franklin contains well preserved, phosphatized specimens of four genera of ostracodes. Three of these, **Tubulibairdia, Neoaparchites** and an unidentified ostracode genus, are long ranging and of limited use in correlation. The presence of the new beyrichiine genus, **Innuitbeyrichia,** and its morphological similarity to established Scandinavian taxa, however, is of significant stratigraphic importance to our understanding of the late Silurian ostracode zonation of the central Canadian Arctic.

Studies from the Baltic area (Martinsson, 1962, 1967; Gailite, 1964) have shown that during the Wenlockian and Ludlovian the morphology of one lineage of beyrichiines developed rapidly in a direction that, by the Pridolian, led to the complete dissection of the lobal elements of the domicilium, in particular the syllobium (i.e. the **Beyrichia-Neobeyrichia-Calcaribeyrichia-Nodibeyrichia** lineage; see Siveter, 1978, table 2). This type of beyrichiacean morphological sequence has not been previously demonstrated from North America because of the relative absence of these beyrichiine elements in the better known eastern endemic Silurian ostracode faunas and the lack of detailed micropaleontological studies of Silurian faunas in the less accessible northern part of the continent. Consequently, our lack of knowledge of the possible occurrence of these Mid- and early Late Silurian beyrichiine ostracodes in North America has restricted our ability to use this stratigraphically important succession of pre-Devonian Baltic ostracode faunas in intercontinental correlation and paleogeographic reconstruction.

Recently, however, a few Siluro-early Devonian ostracode faunas have become documented from northern and northwestern North America (Martinsson, 1960; McGill, 1963; Berdan and Copeland, 1973; Copeland, 1976, 1977, 1978a, b) that give some insight into the stratigraphic successions of beyrichiine taxa in those areas. This sequence of beyrichiacean faunas with dissected and undissected lobation is far from complete, but a beginning may be made to fashion

NORTH AMERICA				NORTHERN EUROPE	
NORTHERN APPALACHIAN FAUNAL PROVINCE	NORTHWESTERN NORTH AMERICA	CENTRAL ARCTIC ISLANDS	MARITIME PROVINCES-NEW ENGLAND	BALTO-SCANDINAVIAN PROVINCE	
Zygobeyrichia Kloedeniopsis Welleria "Kloedenia" Lophokloedenia	Berdanopsis Asperibeyrichia Gannibeyrichia Clintiella Garniella	(Unknown)	Nodibeyrichia Sleia Hemsiella Macrypsilon Kloedenia Frostiella Londinia Beyrichienkalk		Pridoli
Cornikloedenia Pintopsis	Navibeyrichia Beyrichia Berdanopsis Pintopsis	Innuitbeyrichia Berdanopsis	(Unknown, possibly not present)	Calcaribeyrichia Gannibeyrichia Navibeyrichia Neobeyrichia Garniella Beyrichia	Ludlow
Cornikloedenia Drepanellina	Beyrichia	Beyrichia		Bingeria Clintiella Beyrichia Apatobolbina	Wenlock

Figure 4.1. *Distribution of selected Middle and Late Silurian beyrichiacean Ostracoda in northern North America and northern Europe. Heavy black lines enclose endemic faunas.*

a North American framework into which morphological progressions of non-endemic benthonic beyrichiine ostracodes of Balto-Scandinavian type may be placed.

Figure 4.1 shows our present knowledge of the age and stratigraphic occurrence of selected Middle and early Upper Silurian beyrichiacean genera from northern North America and the Baltic region. If the endemic Appalachian faunal province and Beyrichienkalk fauna are excluded, the elements of a northern intercontinental biostratigraphic succession of beyrichiacean ostracodes becomes more apparent. Within this northern province, beyrichiine elements appear to be ascendant in Ludlovian and younger beyrichiacean faunas. The Llandoverian-Wenlockian craspedobolbine beyrichiacean preponderance noted from Gotland and less extensively from Anticosti Island (Copeland, 1974) has not yet been demonstrated from northern Canada where strata of this age tend to be sparingly fossiliferous and few ostracodes (none of them beyrichiaceans) have been reported. The oldest, Wenlockian, beyrichiines recorded from both Scandinavia and northern Canada are species of **Beyrichia** that demonstrate little lobular division or syllobial dissection. The succeeding Ludlovian beyrichiines of the Baltic area show rapid lobular differentiation and dissection through a morphological series represented by genera from **Neobeyrichia** to **Calcaribeyrichia** and culminate in the Pridoli (Beyrichienkalk) with complete lobal dissection of **Nodibeyrichia** type. Such a complete series cannot yet be shown for northern North America but the introduction of **Innuitbeyrichia** into the Canadian Arctic Ludlovian faunas helps to bridge part of the gap between the widespread Wenlockian (and younger) genus **Beyrichia** and the presently restricted Pridolian **Calcaribeyrichia** of Yukon Territory. For some presently unknown reason the Pridolian occurrence of the acme of the beyrichiine morphological sequence in northern North America appears to lag behind that of the Ludlovian acme of this fauna in the Baltic region.

Order Palaeocopida Henningsmoen, 1953

Family Beyrichiidae Matthew, 1886

Subfamily Beyrichiinae Matthew, 1886

Genus **Innuitbeyrichia** gen. nov.

Type species: **Innuitbeyrichia thorsteinssoni** n. sp.

Diagnosis: Beyrichiinae with spinose syllobial cusp; with acroidal, uncular, calcarine(?) and dorsal spines; without velar structure crossing the crumina but with superimposed tuberculation indefinitely aligned on the ventral part of the crumina. L1 (anterior lobe) undivided, nearly isolated by a shallow connection of S1 (prenodal sulcus) with the anteroventral depression. L3 (syllobium) undivided. All lobal parts and crumina with randomly distributed granulation and superimposed tuberculation. Velar ridge broad, strongly spinose, with subvelar spinules.

Remarks: In several respects, such as carapace shape, wide velar ridge and anteroventral depression, **Innuitbeyrichia** is related to **Neobeyrichia** and **Calcaribeyrichia.** It differs from **Neobeyrichia** in lacking marginoventral striations on the crumina and a reported wing-like process on the velum behind the crumina of certain species, and in having calcarine(?) and uncular processes. **Calcaribeyrichia,** a closely related genus, has calcarine and uncular processes but usually shows considerable lobular differentiation and bears marginoventral striations or a velar remnant on the crumina.

One species referred to **Neobeyrichia** (**N. ctenophora** Martinsson) displays an undivided, nearly isolated L1, primitive, undissected L3 and long spines on the velar ridge similar to **I. thorsteinssoni.** Difficulty exists in determining the presence of specialized spines (uncular, calcarine, acroidal) on specimens that bear prominent spines along the velar edge and conical or spinose tubercles, however low, superimposed on the granulation of the lobes. This is well demonstrated by **N. ctenophora** in which syllobial tuberculation is prominent and could obscure identification of a calcarine process; also, the 'caudal' spines of **N. ctenophora** are in the position of the acroidal processes. No species of **Neobeyrichia** bears an uncular lobule or uncular spine similar to that of species of **Calcaribeyrichia,** however, an uncular process without an uncular lobe is present on **I. thorsteinssoni.** This process is broken on all known specimens of **I. thorsteinssoni** and, because of its supravelar position, is indicated by a large hole in the syllobium wall or a robust spine base. An additional tubercle (ventral anterior lobe spine) superimposed on the granulation of **I. thorsteinssoni** is situated in the ventral part of L1 slightly anterior of the anteroventral depression.

PLATE 4.1 (GSC 203201-H)

Figures 1-10. **Innuitbeyrichia thorsteinssoni** n. sp.
Tecnomorphic valves, GSC loc. C-79435.

1-3. Left lateral, x 40, ventral, x 50 and mid ventral view of velar spines and advelar and admarginal spinules, x 220, holotype, GSC 62460.

4. Left lateral view, x 40, paratype, GSC 62461.

5,6. Right lateral, x 50, and mid ventral view of velar spines and advelar and admarginal spinules, x 200, paratype, GSC 62462.

7,8. Left anterior view (45°), x 50 and marginal view, x 300, paratype, GSC 62463.

9,10. Anteroventral marginal view, x 140 and left lateral view, x 50, paratype, GSC 62464.

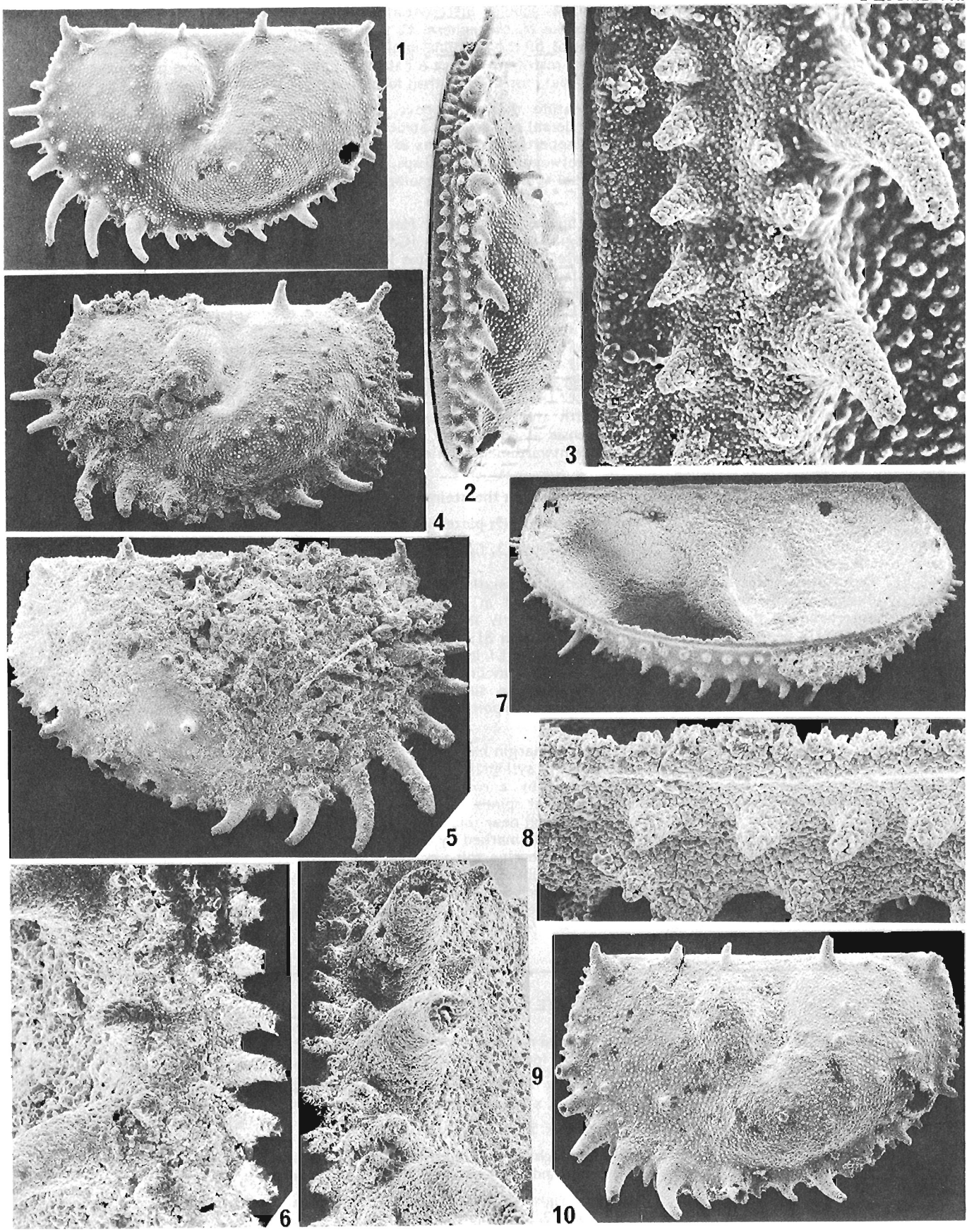
1
2
3
4
5
6
7
8
9
10

Like **N. ctenophora** and **I. thorsteinssoni, Calcaribeyrichia simplicior** Martinsson, a primitive species of **Calcaribeyrichia**, almost lacks lobular differentiation, is heavily tuberculate and bears prominent velar spines. However, unlike **N. ctenophora, C. simplicior** bears calcarine and uncular processes and has no velar ridge ventral of the crumina similar to **I. thorsteinssoni. C. simplicior** appears to differ from **I. thorsteinssoni** mainly in having a callus dividing the syllobium, a prominent calcarine spine and, less importantly, lobal cusps rather than lobal spines.

An interesting morphological feature that may prove of taxonomic value is the consistent presence on **I. thorsteinssoni** of a spine dorsal of L2. This structure does not occur in **Neobeyrichia** or **Calcaribeyrichia** species but has been reported for species of **Beyrichia (Beyrichia)**, some species of which bear 2 spines in this position between the lobal cusps, but only occurs on relatively heavily tuberculate species. Whether the dorsal spine is of morphological value or only an expression of the tuberculation is presently unknown.

N. ctenophora and **C. simplicior** appear in the upper Hemse beds of Gotland (Martinsson, 1962) and **N. ctenophora** occurs in the Pagegiai beds of Latvia (Gailite, 1964; Gailite et al., 1967). The upper Hemse and Pagegiai beds represent the **Saetograptus leintwardinensis** and **S. fritschi linearis** graptolite zones that typify the medial (Leintwardine) and early late (Whitcliff) Ludlovian. The morphological similarities among **I. thorsteinssoni, N. ctenophora** and **C. simplicior**, especially the relative lack of syllobial dissection, indicate a generally similar stage of development for these genera. Conodonts associated with **I. thorsteinssoni** in the same collection (GSC loc. C-79435) have been identified by T.T. Uyeno as follows: "**Oulodus** sp., **Ozarkodina excavata excavata** (Branson and Mehl), **O. confluens** (Branson and Mehl) alpha morphotype of Klapper and Murphy (1975), **Panderodus** sp., **Polygnathoides siluricus** Branson and Mehl. Age: **Polygnathoides siluricus** Zone, above the lowest part of the zone, late Ludlovian age." (Report No. 1-TTU-1980). This serves to more accurately equate the **Innuitbeyrichia** fauna with the **Hoburgiella tenerrima** assemblage rather than the **Neobeyrichia scissa-Neobeyrichia lauensis** assemblage of Gotland (Martinsson, 1967) and thus to an early Whitcliffian rather than a late Leintwardinian position within the Ludlovian.

Innuitbeyrichia thorsteinssoni n. sp.

Plate 4.1, figures 1-9; plate 4.2, figures 1-10;

plate 4.3, figures 1-4

Description: Valve preplete; hinge long, five-sixths greatest length; cardinal angles obtuse; free margin evenly rounded, more broadly curved in posterior half. Bisulcate, S1 shallow, joining anteroventral depression and isolating or nearly isolating L1 (anterior lobe); S2 deeper, curving anteriorly beneath L2 (adductorial node) to join S1; zygal arch; if present, very low, indistinct. L1 and L3 (syllobium) undivided; both lobes broad, L1 low, only slightly more elevated than S1, L3 more highly elevated. L2 ovate, elongate, slightly inclined anterodorsally. All lobal parts and crumina with evenly distributed granulation and sparse superimposed tuberculation. Velar ridge broad, extending along entire free margin of tecnomorphic valve but not passing ventral of the crumina on heteromorphic valve.

Valves with great spinosity. Dorsal margin marked by anterior and posterior acroidal spines, a spine at the dorsal apex of L1 and on the syllobial cusp and a smaller spine on the dorsal margin directly above L2. Velar ridge marked by a row of robust spines, most prominent along the anteroventral edge; velar structure and velar spines not present on or beneath crumina. No uncular lobe, but uncular spine in supravelar position near mid height of posterior margin. On all specimens observed, the position of the uncular spine is marked by a proximal remnant of the spine or a large hole on the syllobium wall. Position of calcarine spine occupied by a tubercle superimposed on the granulation of the syllobium. Two rows of subvelar spinules; the less prominent proximal, advelar row situated below and slightly between the much larger velar spines in meandering fashion, apparently not present beneath the crumina but may be incorporated with and indistinguishable on the densely

---

PLATE 4.2 (GSC 203201-F)

Figures 1-9. **Innuitbeyrichia thorsteinssoni** n. sp.
Heteromorphic valves, GSC loc. C-79435.

1,3. Left lateral view, x 60 and mid ventral view of velar spines and advelar and admarginal spinules, x 300, paratype, GSC 62468.

2. Right lateral view, x 50, paratype, GSC 62469.

4-6. Ventral (70°) and right lateral views, x 50, and mid ventral view (82°) of velar spines and advelar and admarginal spinules, x 180, paratype, GSC 62470.

7,9. Anterior view of right valve, x 80, and anteroventral view of crumina, x 190, paratype, GSC 62472.

8. Interior view of right valve, x 50, paratype, GSC 62471.

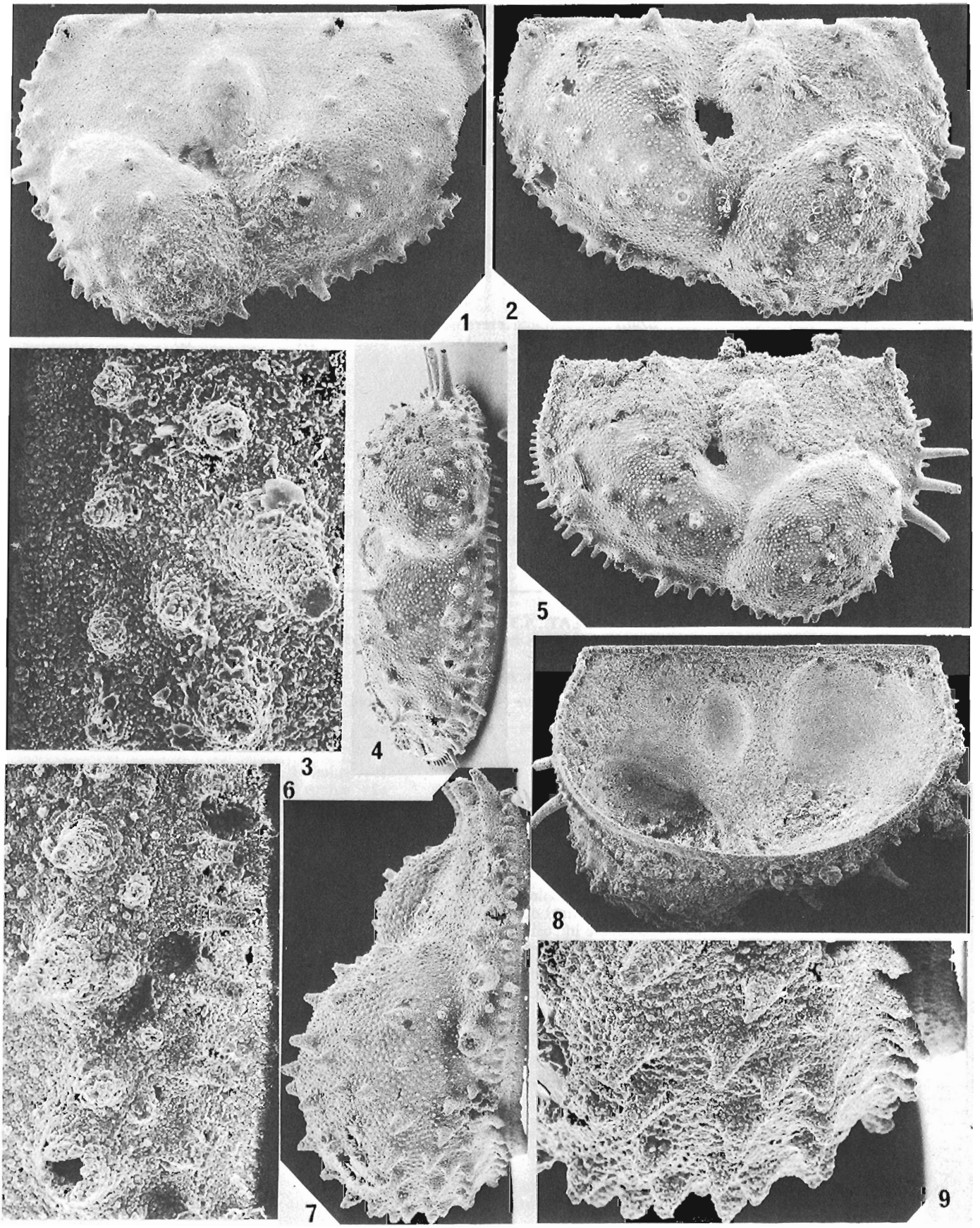
1
2
3
4
5
6
7
8
9

tuberculate ventral part of the crumina; the distal, admarginal row of spines more prominent and regularly aligned parallel to the free edge and continuous along the free margins of valves of both dimorphs. Faint marginal ridge present on both valves.

Heteromorphic crumina ovate, broadly overhanging anteroventral part of valve, sharply set off from domicilium. Ornamentation consisting of evenly distributed granules with superimposed tubercles that increase in density ventrally.

Approximate measurements (mm) of several valves, exclusive of spines:

Type	GSC No.	Dimorph	Length	Height
Holotype	62460	Tecnomorph	1.7	1.0
Paratype	62461	"	1.8	1.1
"	62462	"	1.8	1.1
"	62463	"	1.7	1.0
"	62464	"	1.6	0.9
"	62465	"	1.4	0.9
"	62466	"	1.5	1.2
"	62473	"	1.9	1.1
"	62467	Heteromorph	1.7	1.1
"	62468	"	1.6	1.1
"	62469	"	1.7	1.2
"	62470	"	1.7	1.2
"	62471	"	1.7	1.2
"	62472	"	-	1.1

Number of specimens studied, 28.

Types: Holotype, GSC 62460; paratypes, GSC 62461-62473.

Occurrence: Devon Island, District of Franklin, GSC Locality C-79435, UTM Zone 15X, 548 175E, 8 337 600N, collected by R. Thorsteinsson (TC-615A), 15.25 m below the top of the Douro Formation.

PLATE 4.3 (GSC 203201-G)
(All specimens from GSC loc. C-79435)

Figures 1-4. **Innuitbeyrichia thorsteinssoni** n. sp.

1. Left tecnomorphic valve (45°), x 40, holotype, GSC 62460.

2. Right ventral view of incomplete heteromorphic valve, x 60, paratype, GSC 62472.

as - acroidal spine
vs - velar spine
avs - advelar spinule
ss - syllobial spine
ds - dorsal spine
als - anterior lobe spine
us - uncular spine
ams - admarginal spinule
ad - anteroventral depression
cs - tubercle in position of calcarine spine
s1 - sulcus 1
s2 - sulcus 2
l1 - anterior lobe
l2 - adductorial node
l3 - syllobium
g - granulation
st - superimposed tuberculation
vr - velar ridge
c - crumina
vals - ventral anterior lobe spine

3,4. Left tecnomorphic valves, x 50, paratypes, GSC 62465, 62466.

Figures 5-8. Ostracode indet.

5,6. Dorsal and left lateral views, x 80, figured specimen, GSC 62474.

7,8. Left lateral view, x 50 and adductor and adjustor muscle scars, x 200, figured specimen, GSC 62475.

Figures 9,10. **Neoaparchites franklini** n. sp.
Adductor and adjustor muscle scars, x 200 and right lateral view, x 60, holotype, GSC 62476.

Figure 11. **Tubulibairdia** sp. cf. **T. ordinara** Mikhailova, 1978.
Right lateral view, x 100, hypotype, GSC 62477.

(Scanning electron microscopy by David A. Walker, Geological Survey of Canada)

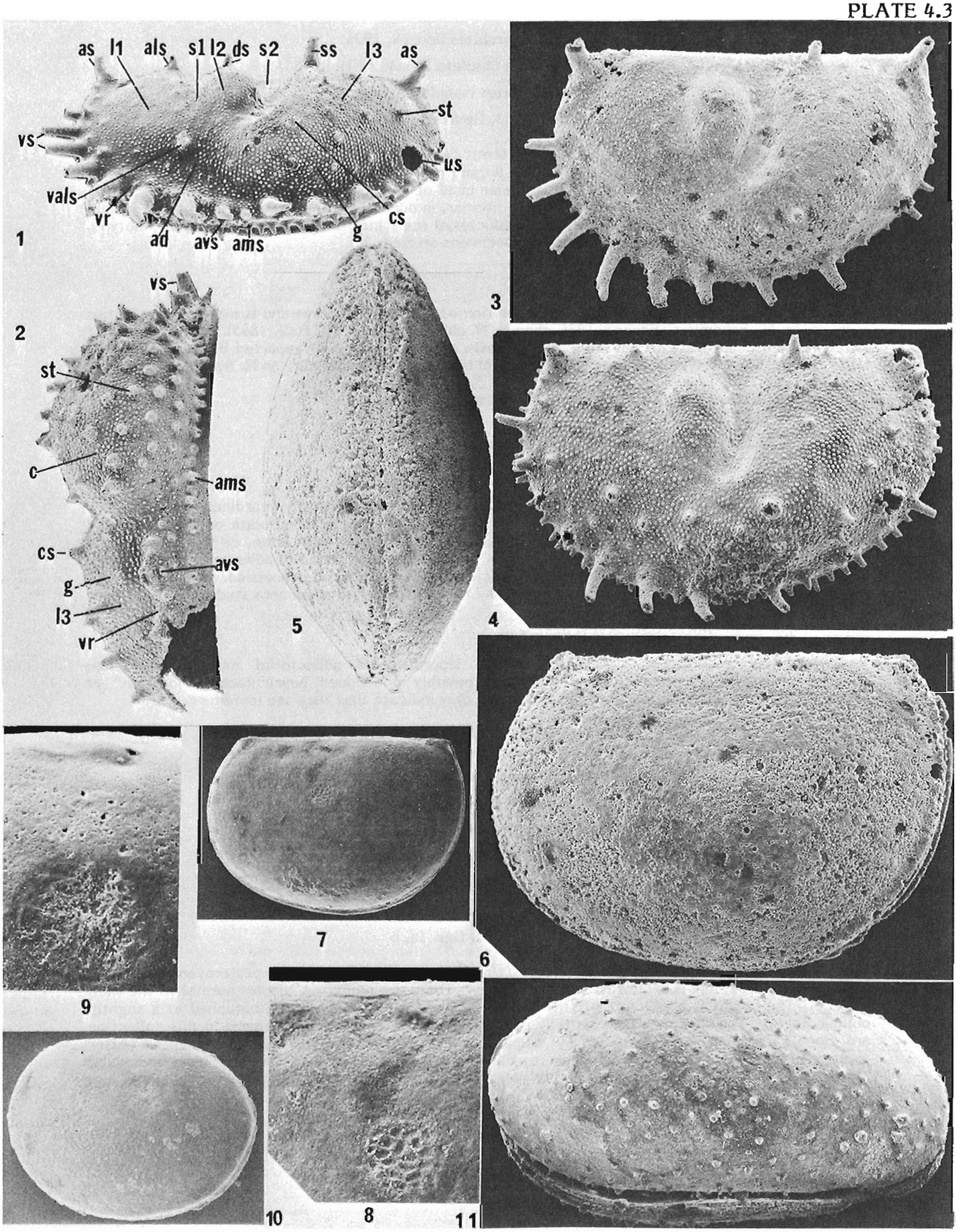
as
l1
als
s1
l2
ds
s2
ss
l3
as
st
vs
us
vals
vr
ad
avs
ams
g
cs
1
vs
2
st
c
ams
cs
avs
g
l3
vr
5
3
4
6
7
9
10
8
11

Family Aparchitidae Jones, 1901

Genus **Neoaparchites** Boucek, 1936

Type species: **Primitia obsoleta** Jones and Holl, 1865

Neoaparchites franklini n. sp.

Plate 4.3, figures 9, 10

Description: Valves subelliptical; hinge short about two-thirds valve length; cardinal angles rounded smoothly into free margin. Free margin of larger, right valve with low velar bend and smooth, subcircular rim that abuts against a similar velar bend of the left valve. Surface of valves faintly reticulate. Adductor muscle impression large, circular, in dorsal half of valve slightly anterior of mid length, with low, near dorsal adjustor ridge. Adductorial scars indistinct. Measurements of holotype, length 0.80 mm; height 0.60 mm. Number of specimens studied, 2.

Type: Holotype, GSC 62476.

Remarks: This species shows very little angulation of the cardinal areas and is more similar in this respect to **N. bohemicus** Boucek, 1936 than to **N. obsoleta** (Jones and Holl, 1865). The drawings of **N. bohemicus,** however, do not show the "slightly raised smooth rim" reported by Jones and Holl (1865, p. 423) for the type species. A low marginal bend and rim also occurs on **N. franklini.**

Occurrence: Same locality as **I. thorsteinssoni** n. sp.

Ostracode indet.

Plate 4.3, figures 5-8

Description: Valves somewhat postplete, right overlapping left ventrally, cardinal angles obtuse. Free margin of each valve with low velar(?) ridge sometimes finely tuberculate on left valve and lacking mid ventrally on right valve. Surface smooth, one specimen with large, circular adductorial spot comprised of about 20 discrete muscle scars. Faint depression dorsal of adductorial spot, a ridge apparently indicating attachment of adjustor muscle and an anterodorsal depression. Measurement of figured specimen 62475, length 0.95 mm, height 0.75 mm. Number of specimens studied, 4.

Types: Figured specimens GSC 62474, 62475.

Remarks: This generalized ostracode bears a leperditicopid adductorial muscle impression, aparchitacean type of velar(?) ridge and very possibly a subdued beyrichiacean "lobation" of **Saccarchites** type. The small size of the specimens may indicate that they are immature.

Occurrence: Same locality as **I. thorsteinssoni** n. sp.

Order Podocopida Muller, 1894

Family Pachydomellidae Berdan and Sohn, 1961

Genus Tubulibairdia Swartz, 1936

Type species: **Tubulibairdia tubulifera** Swartz, 1936

Tubulibairdia sp. cf. **T. ordinara** Mikhailova, 1978

Plate 4.3, figure 11

Tubulibairdia ordinara Mikhailova, 1978, p. 45, pl. II, figs. 1a, b

Remarks: This specimen apparently has left/right valve overlap except posteroventrally; well rounded 'shoulders', and is semiovate in lateral view. There are numerous tubules normal to the shell surface. The height is about three-fifths that of the length (figure 11 is photographed at a slightly oblique angle). The specimen is essentially round in cross-section. Both specimens in this collection are much smaller than those studied by Mikhailova (1978). They may be immature moults. (After photography the figured specimen began to disintegrate as it was being removed from the stub.) Measurements of hypotype, length 0.9 mm; height 0.5 mm. Number of specimens studied, 2. Type: Hypotype, GSC 62477.

Occurrence: Same locality as **I. thorsteinssoni** n. sp.

References

Berdan, J.M. and Copeland, M.J.
1973: Ostracodes from Lower Devonian formations in Alaska and Yukon Territory; United States Geological Survey, Professional Paper 825.

Copeland, M.J.
1974: Silurian Ostracoda from Anticosti Island, Quebec; Geological Survey of Canada, Bulletin 241.

1976: Leperditicopid ostracodes as Silurian biostratigraphic indeces; in Report of Activities, Part B, Geological Survey of Canada, Paper 76-1B, p. 83-88.

1977: Early Paleozoic Ostracoda from southwestern District of Mackenzie and Yukon Territory; Geological Survey of Canada, Bulletin 275.

1978a: Some Wenlockian (Silurian) Ostracoda from southwestern District of Mackenzie; in Current Research, Part B, Geological Survey of Canada, Paper 78-1B, p. 65-72.

1978b: Early Paleozoic ostracode assemblages, northwestern Canada; Geological Association of Canada, Special Paper 18, p. 93-111.

Gailite, L.K.
1964: On the problem of biostratigraphic differentiation of the Upper Silurian in Latvia; Latvijas PSR Zinatnu Akedemijas Vestis, No. 11, p. 65-72, Riga.

Gailite, L.K., Rybnikova, M.V., and Ul'st, R.Zh.
1967: Description of Ostracoda; Chapter 3, in, Stratigraphy, fauna and conditions of formation of Silurian rocks of the Central Baltic Region; Ministry of Geology SSSR, Geological Institute (Riga), p. 89-300.

Jones, T.R. and Holl, H.B.
1865: Notes on the Paleozoic bivalved Entomostraca, No. 6. Some Silurian species (Primitia); Annals and Magazine of Natural History, series 4, no. 16, p. 414-425.

Martinsson, A.
1960: Ostracods; in Boucot, A.J., Martinsson, A., Thorsteinsson, R., Walliser, O.H., Whittington, H.B., and Yochelson, E., A Late Silurian fauna from the Sutherland River Formation, Devon Island, Canadian Arctic Archipelago; Geological Survey of Canada, Bulletin 65, p. 15-20.

1962: Ostracodes of the Family Beyrichiidae from the Silurian of Gotland; Publications from the Palaeontological Institution of the University of Uppsala, No. 41.

1967: The succession and correlation of ostracode faunas in the Silurian of Gotland; Geologiska Foreningens I Stockholm Forhandlingar, v. 89, p. 350-386.

McGill, P.C.
1963: Silurian Ostracoda from Northwest Territories, Canada; Journal of Paleontology, v. 37, p. 1284-1288.

Mikhailova, E.D.
1978: Ostracods in the Border-Land of the Silurian and the Devonian in the West of the Zeravshan Mountain Range; in Stratigraphy and paleontology of the Urals and the Asiatic part of the USSR, Transactions of the Leningrad Mining Institute, v. 73, pt. 2, p. 37-48.

Siveter, D.
1978: The Silurian; in A stratigraphical index of British Ostracoda (R. Bate and E. Robinson, eds.), Geological Journal, Special Issue No. 8, p. 57-100.

5. GEOLOGY OF THE KAMILUKUAK LAKE MAP AREA, DISTRICT OF KEEWATIN, A PART OF THE CHURCHILL STRUCTURAL PROVINCE

Project 790009

Subhas Tella and K.E. Eade,
Precambrian Geology Division

Tella, Subhas and Eade, K.E., Geology of the Kamilukuak Lake map area, District of Keewatin, a part of the Churchill Structural Province; in Current Research, Part B, Geological Survey of Canada, Paper 80-1B, p. 39-45, 1980.

Abstract

The east half of the Kamilukuak Lake map area is underlain by a polydeformed and polymetamorphosed Archean (and Aphebian?) migmatite and granitoid gneiss complex, intruded by diorite, quartz monzonite and syenite, and overlain by volcaniclastic sedimentary and volcanic rocks of the late Aphebian or Paleohelikian Dubawnt Group. The basal unit of the Dubawnt Group, rarely present, is a poorly sorted and sheared polymictic conglomerate, which is disconformably overlain by a sequence of interbedded volcaniclastic sediments, pyroclastics, and mafic and felsic trachyte flows of the Christopher Island Formation, which comprises the bulk of the Dubawnt Group rocks in the area. A poorly bedded volcaniclastic conglomerate unconformably overlies the Christopher Island Formation. Intrustions of mafic syenite, biotite lamprophyre, and high level fluorite-granite cut the Christopher Island Formation. Northwest trending diabase and gabbro dykes (Mackenzie Swarm) cut both the basement complex and the Dubawnt Group rocks.

The basement complex and the cover rocks are transected by three major sets of faults and shear zones. A northeast trending shear zone, in the southeastern part of the map area, is a zone of ductile deformation that shows a variety of mylonitic textures. Numerous east- and northwest-trending faults, some of which are characterized by narrow cataclastic zones, displace all units with dip-slip components. Uranium mineralization is spatially related to the Christopher Island Formation – basement complex contact for the most part and to a lesser extent to the high level fluorite-granite intrusions. Sulphides of minor economic importance occur along narrow shear zones.

Introduction

Kamilukuak Lake map area (65 K), is underlain by two main groups of rocks – an Archean (and Aphebian?) basement complex predominantly composed of migmatite, granitoid gneisses, and associated plutonites, and a late Aphebian or Paleohelikian seqeunce of unmetamorphosed continental sedimentary, volcaniclastic, and volcanic rocks of the Dubawnt Group and late granite-quartz mononite plutons. Mapping in the east-half of the map area at a scale of 1:250 000 was completed during the 1979 field season; the west-half is scheduled for completion in 1980. The distribution of major rock units in the east-half is shown in Figure 5.1, and schematic structural cross-sections in Figure 5.2. Mapping in the area to the east was completed by Eade and Blake (1977) and is in progress in the sheet to the northeast (LeCheminant et al. 1979a, b; 1980). Previous work in the region by Wright (1955, 1967), at a scale of one inch to eight miles, was limited to reconnaissance helicopter traverses.

Archean and Aphebian Basement Complex

The basement complex (units 1 to 4, Figure 5.1) is widely exposed in the southern half of the map area, and to a lesser extent in isolated areas between Dubawnt Lake and Carruthers Lake. Unit 1 is a medium- to coarse-grained migmatite to layered, banded or nebulitic gneiss, and is in part interlayered with thin units of granodiorite gneiss, amphibolite and paragneiss. Sheets and veins of foliated quartz monzonite (unit 3) cut unit 1 at several localities. The migmatitic rocks consist of quartz-plagioclase-biotite-amphibole assemblages with a well developed polygonal granoblastic texture. Apatite, sphene and opaques are present as accessories. Unit 2 is a mixed unit consisting of hornblende-biotite granodiorite gneiss, tonalite gneiss, orthogneiss, potash feldspar augen gneiss, and layered gneiss. Minor layered inclusions of garnetiferous paragneiss and amphibolite are locally present and the unit is cut by massive bodies of quartz monzonite and pegmatite of uncertain age. At two localities along the south shore of Angikuni Lake, inclusions of mafic volcanics and crystal tuff are present in both units 1 and 2. East trending, weakly metamorphosed basic dykes of probable Aphebian age are present in these units.

Orthogneiss (unit 3), pink to grey, medium grained, biotite and/or hornblende bearing, ranges in composition from granodiorite to quartz monzonite. Distinct mineral foliation is typical of these rocks. Inclusions or schlieren of paragneiss, amphibolite, or banded gneiss are locally present.

Unit 4 is a porphyroblastic potash feldspar augen gneiss of granodiorite to quartz monzonite composition that contains numerous inclusions of older rocks (units 1 and 2), and is in turn cut by granite and pegmatite. Abundant coarse, white to pink feldspar augen, up to 3 cm long, are displayed on the weathered surfaces, making rocks of this unit readily recognizable. The unit commonly exhibits localized shear zones.

A suggested sequence of events listed in Table 5.1 is based on field observations, and is subject to revision following completion of detailed petrographic and geochronological studies. Field relations and structural data indicate that the migmatite and granitoid gneiss complex (units 1 to 4) has undergone at least three phases of deformation and possibly two events of (Archean) regional metamorphism. Northeast trending regional foliation is the most common penetrative planar fabric element (S_1) in units 1 to 4, and represents a syntectonic metamorphic fabric developed during the first phase of deformation (D_1). The fabric is defined by the alignment of mafic minerals, biotite and hornblende. Variation in attitudes are not uncommon. First generation folds (F_1) have not been identified at the present scale of mapping. However, a mineral (hornblende) lineation (L_1) recognized in unit 2, at a few localities, is oriented at an oblique angle (with shallow plunges) to the second generation fold (F_2) axes, and may represent relict F_1 fold trends. Mesoscopic to

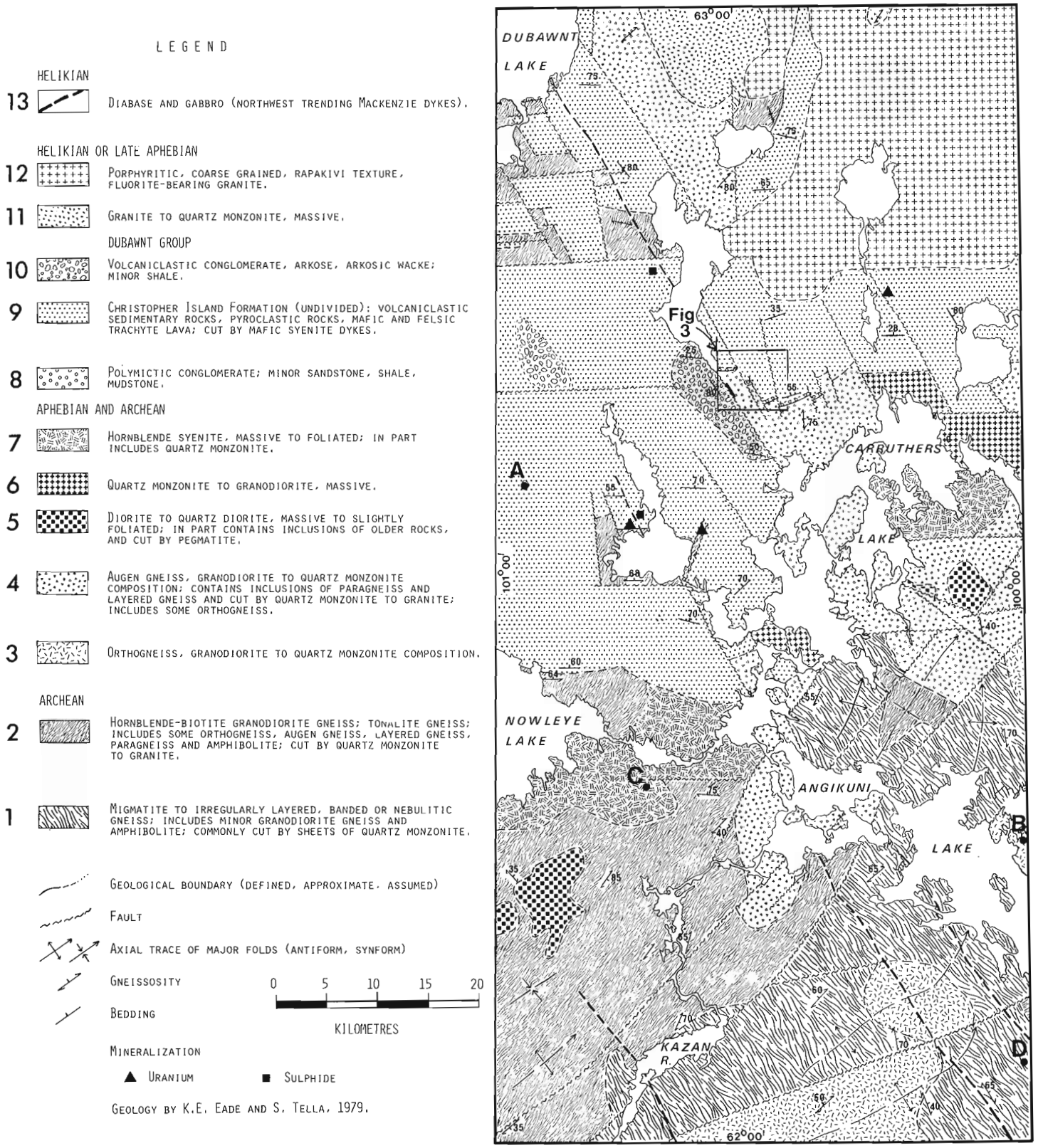

Figure 5.1. *Geological sketch map of Kamilukuak Lake map area (65 K; east-half).*

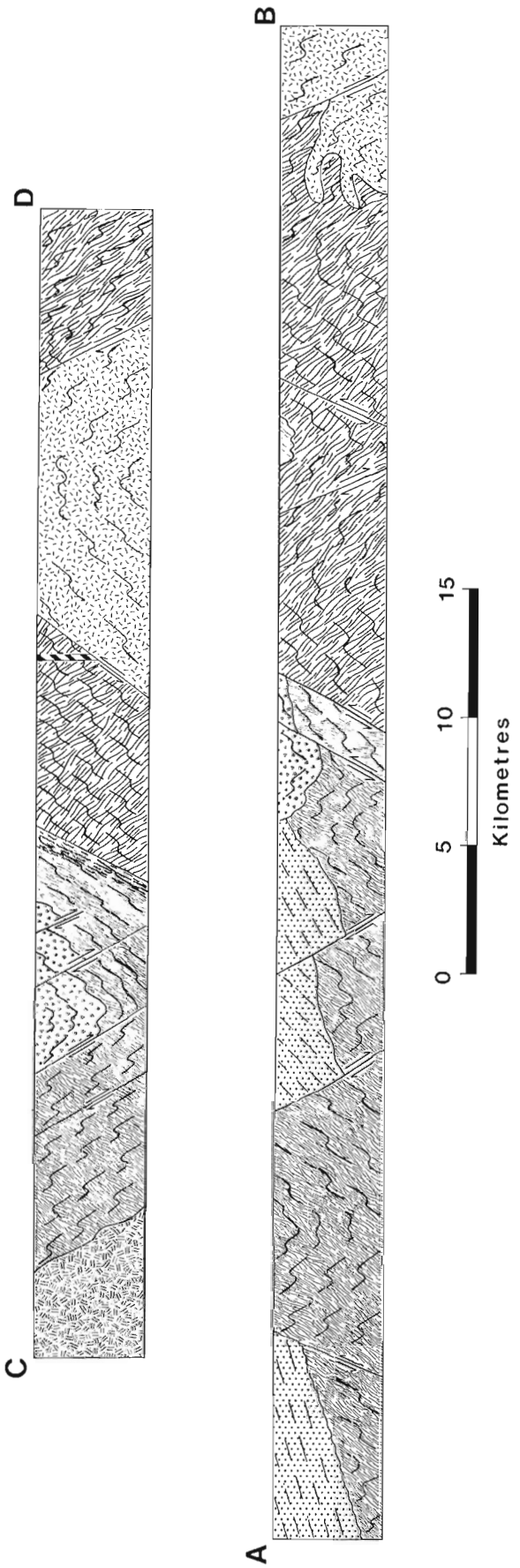

Figure 5.2. Schematic structural cross-sections illustrating major folds and faults (see Fig. 5.1 for location).

macroscopic, upright, open to moderately tight folds (Fig. 5.1, 5.2) with northeast trending axial planes represent the second generation, F_2, folds developed during D_2. Minor folds associated with major F_2 folds commonly show an axial planar crenulation cleavage S_2; i.e., a syntectonic (D_2) metamorphic fabric. Because of the approximate parallelism in strike between S_1 and S_2, the distinction between the two fabric elements in the field is noticeable only at the minor F_2 fold closures, and less obvious in other areas. However, the two fabrics can be distinguished optically. Open, upright folds of local extent with northwest trending axial planes mark the third phase structures. It is probable that the second and third phases are relatively close in age. The regional metamorphic grade during D_2 appears to be within the amphibolite facies conditions. Post D_2 metamorphic effects have been limited to retrogressive alteration of earlier assemblages to epidote, chlorite, and carbonate. In the above descriptions, the structural and metamorphic history of the units is somewhat simplified. The three phases of deformation noted in units 1 to 4 obviously postdate the porphyroblastic augen gneiss (unit 4), and it is possible that units 1 and 2 may have had a complex tectonic and metamorphic history prior to the emplacement of unit 4. A detailed structural analysis on a much smaller scale is a prerequisite for unravelling such a complex polymetamorphic and tectonic history in the basement rocks.

Intrusive Rocks

Two stocks of medium- to coarse-grained diorite to quartz diorite (unit 5) are exposed – one south of Nowleye Lake, and the other southeast of Carruthers Lake. Both bodies contain inclusions of older rocks, and are cut by pink granite and pegmatite. Although the contact relationships with the surrounding units have not been established, the massive character of unit 5, together with the presence of inclusions of older rocks, suggest that this unit post dates units 1 to 4. Fine- to medium-grained, hornblende-biotite bearing, massive quartz monzonite to granodiorite (unit 6) occurs northeast and southwest of Carruthers Lake. Some rocks included in this unit may postdate the Dubawnt Group. A relatively fresh, medium- to coarse-grained, massive hornblende syenite (unit 7) is exposed to the east of Nowleye Lake, and to the south of Carruthers Lake. The unit locally contains sheets of massive quartz monzonite similar in composition to that of unit 6. Locally, the quartz content is higher and the rock is a quartz monzonite. The contact of the syenite with the Christopher Island volcanics to the east of Nowleye Lake is not exposed, and the assigned pre-Dubawnt Group age for the syenite is uncertain.

Paleohelikian or Late Aphebian

Dubawnt Group

Dubawnt Group rocks are exposed in the central and northern parts of the map area and consist of a basal polymictic conglomerate, sandstone, shale succession (unit 8) which is overlain by a sequence of interbedded volcaniclastic sediments, mafic and felsic trachyte flows, and pyroclastics of the Christopher Island Formation (unit 9). Northwest of Carruthers Lake, a poorly bedded, volcaniclastic conglomerate, arkosic wacke, minor shale unit (unit 10) overlies the Christopher Island Formation. The attitude of all units is commonly east-west with northerly dips ranging from 25° to 70°. Northwest trends with northeasterly dips of local extent are also noted in unit 10, where it is deposited in a northwest fault basin. The Dubawnt Group unconformably overlies or is in fault contact with the basement granitoid gneisses. Mafic syenite, bostonite dykes, and fluorite-bearing, high level granite intrude the Dubawnt Group in several places.

Table 5.1

Suggested sequence of events in the east-half of Kamilukuak Lake map area (NTS 65 K/E 1/2)

	STRATIGRAPHY	INTRUSION	METAMORPHISM	DEFORMATION	REMARKS
HELIKIAN		13 Diabase and gabbro dykes	None	Reactivated faulting	Uranium mineralization: Fracture controlled, contact aureole
LATE APHEBIAN OR PALEOHELIKIAN		12 Granite 11 Granite	Contact	Tilting, east and northwest faulting	Calc-alkaline igneous activity
	DUBAWNT GROUP 10 Volcaniclastic conglomerate Unconformity 9 Christopher Island Fm. Disconformity 8 Polymictic conglomerate Unconformity	Syenite & lamprophyre dykes & sills	Regional : None Contact : ?	Reactivated faulting	Alkaline igneous activity
ARCHEAN AND/OR APHEBIAN		7 Syenite 6 Quartz monzonite 5 Diorite Minor eastwest gabbro dykes	Contact ?	Northeast shears; Mylonitization	Some eastwest shears coeval with dyke emplacment
ARCHEAN	2 Granodiorite gneiss, tonolite gneiss 1 Migmatite, layered gneiss, Granodiorite gneiss, etc.	4 Augen gneiss 3 Quartz monzonite	Regional (Amphibolite grade) Local contact ? Regional (Amphibolite grade) ??	Superposed upright folding Superposed folding ?	Northeast and northwest fold trends (D_1, D_2, D_3)

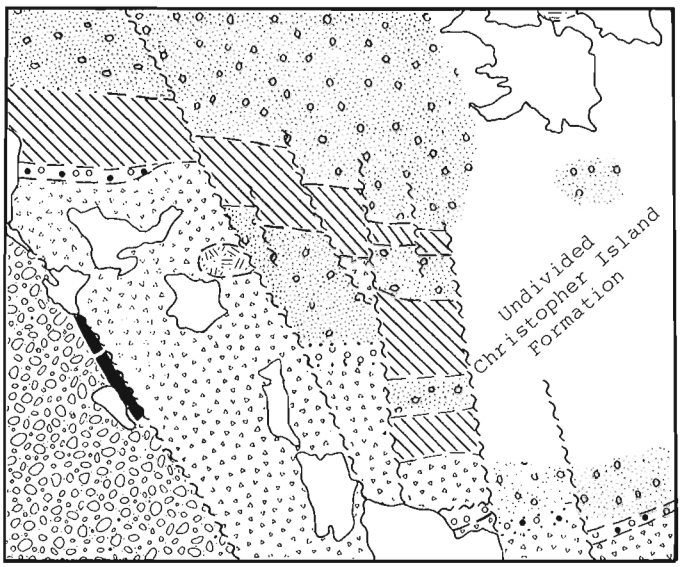

LEGEND

HELIKIAN

Diabase dyke (Mackenzie)

HELIKIAN OR LATE APHEBIAN

Hornblende syenite; massive

DUBAWNT GROUP

Volcaniclastic conglomerate, arkose, arkosic wacke; minor shale.

Christopher Island Formation

Volcaniclastic sedimentary rocks, pyroclastic rocks, lithic and crystal tuff, tuff breccia, tuffaceous wacke; interbedded.

Mafic trachyte lava; brecciated flow tops. phlogopite, pyroxene, feldspar-phyric phlogopite, feldspar-phyric

Polymictic conglomerate (with volcanic clasts); sandstone, shale

Polymictic conglomerate; minor sandstone, shale, mudstone (South Channel Formation)

APHEBIAN AND ARCHEAN

Augen gneiss, granodiorite to quartz monzonite composition; cut by quartz monzonite to granite.

Figure 5.3. *Distribution of Dubawnt Group Rocks in an area north of Carruthers Lake (see Figure 5.1 for location).*

Basal polymictic conglomerate North of Carruthers Lake, two isolated exposures of the unit (Fig. 5.3) contain locally derived and poorly sorted, angular to subrounded clasts of basement granitoid gneiss, feldspar crystals and vein quartz. Volcanic clasts are absent in the unit. The conglomerate has a sheared matrix consisting chiefly of chlorite, carbonate, and sericite. Thin (< 4 cm) arkosic sandstone and shale interbeds are common, and the unit is cut by narrow quartz veins. Northwest and north trending faults systematically offset the unit with apparent right-lateral displacements. The conglomerate unit is correlated with the South Channel Formation (Donaldson, 1965) on the basis of lithological similarities and stratigraphic position.

Christopher Island Formation Interbedded volcaniclastic sedimentary rocks, pyroclastic rocks, lithic and crystal tuff, tuff breccia, and tuffaceous wacke (unit 9, Fig. 5.1) form over 70 per cent of the formation in the map area. Interbeds of phlogopite, clinopyroxene, feldspar-phyric and phlogopite, feldspar-phyric mafic trachytes (Fig. 5.3), and felsic trachyte flows (with locally developed flow top breccias) form approximately 25 per cent of the formation. Both successions overlie the basement rocks unconformably or are in fault contact with them. Discontinuous wedges of immature and poorly sorted, maroon coloured polymictic conglomerate (approximately 100 m thick) occurs conformably below mafic trachyte and volcaniclastic sediments (Fig. 5.3). The conglomerate contains subangular to subrounded clasts of gneissic quartz monzonite, foliated granitoid gneiss (some with mylonitic textures), vein quartz, and mafic trachyte embedded in a fine grained hematitic, sedimentary and volcanic matrix. Note that this conglomerate contains volcanic clasts and the matrix is quite different from that of the previously described basal polymictic conglomerate. The presence of volcanic clasts and the absence of shearing and quartz veining may indicate that is is younger than the basal polymictic conglomerate (South Channel Formation equivalent). As the contacts between the two units are not exposed, it is difficult to establish this relationship with certainty.

The lithological character and stratigraphic relations of the Christopher Island Formation are similar to those described in adjacent areas by Blake (in press), Eade (1976), Eade and Blake (1977), and LeCheminant et al. (1979a, b; 1980), where the lavas and tuffs were interpreted to have been deposited in a subaerial environment and consist of cycles of mafic and felsic alkaline volcanics associated with explosive eruptive centres. No eruptive centres have been found in the present map area.

The volcanic and the sedimentary rocks of the Christopher Island Formation show extensive propylitic alteration. Porphyritic trachytic texture is still preserved in most flows and the groundmass is altered to a mixture of chlorite, carbonate, epidote, sericite. Contact metamorphic effects are present in some mafic lavas near post-Dubawnt Group intrusions, where a radiating, colourless to pale blue-green amphibole overprints the original volcanic flow texture. The Christopher Island Formation is cut by discontinuous northwest and east-west trending biotite-lamprophyre, and biotite-hornblende syenite dykes and sills which are probably cogenetic with the alkaline lavas. Northwest trending, cherry-red brown bostonite dykes (4-6 cm wide) which show anomalous radiometric readings cut the Christopher Island rocks in a few places.

Volcaniclastic conglomerate, arkose, arkosic wacke, and shale The unit consists predominantly of red volcaniclastic conglomerate with minor arkose and shale interbeds (unit 10).

It overlies the Christopher Island Formation in two areas (Fig. 5.1) and is in fault contact with the basement rocks to the east. The clast supported conglomerate is composed mainly of subangular to subrounded, red feldspar trachyte and rare vein quartz clasts which are embedded in a fine grained, reddish green micaceous matrix. The poorly bedded character of the unit suggests rapid deposition of sediment in a fault controlled basin. The conglomerate is lithologically similar to the Kunwak Formation (LeCheminant et al., 1979b), and stratigraphic position suggests that the two are correlative. A slight discordance in attitudes between units 9 and 10 suggests athat unit 10 unconformably overlies unit 9 in the present map area.

Intrusions into the Dubawnt Group

Medium grained, massive and equigranular, pink granite to quartz monzonite (unit 11) is exposed in the northern part of the map area, east of Dubawnt Lake. In thin section, the granite shows a well developed granophyric and myrmekitic texture with scattered phenocrysts of potash feldspar (string perthite). Mafic minerals (mostly biotite) make up less than 3 per cent of the rock, and fluorite, apatite, opaques and zircon are present as accessories. A porphyritic, coarse grained rapakivi textured, fluorite-bearing granite (unit 12) occupies the northeastern corner of the map area. The granite intrudes the Christopher Island Formation, and is characterized by scattered occurrences of ovoid crystals of potash feldspar in a coarse- to medium-grained, greyish white, quartz-feldspar groundmass. Mafic minerals (both biotite and hornblende) represent less than 5 per cent of the total mineral constituents. Accessory minerals include fluorite, sphene, apatite, zircon and opaques. Granophyric and myrmekitic textures are also common. Unit 11, which is free of ovoid crystals, is strikingly similar in composition, but differs in grain size from unit 12 and probably represents a border phase of unit 12.

Helikian

Northwest trending diabase and gabbro dykes (up to 50 m wide; Mackenzie Swarm) with interstitial granophyric phases have been observed throughout the map area. The dykes cut both the basement rocks and the overlying Christopher Island Formation. Some of the dykes appear to have been injected along the northwest trending faults.

Faults

Major northeast trending shear zones, as well as east, northwest, and minor north trending faults, transect the area. Numerous subsidiary cataclastic zones parallel the major structures. Shallow to moderately plunging slickensides on some of the northeast and northwest trending fault surfaces indicate that the last movements on these faults were of oblique slip character. Most faults probably have a history of multiple movements.

The contact between unit 1 and units 2 and 4 (Fig.5.1) is marked in most places by 1-2 km wide, northeast trending, discontinuous shear zone. Granitoid gneisses within the zone exhibit a variety of mylonitic textures which may be classified as protomylonites, mylonite gneisses, and blastomylonites following the classification scheme of Higgins (1971). At one locality north of Angikuni Lake, a small layered inclusion of garnetiferous, clinopyroxene granulite occurs within the mylonitized migmatite and orthogneiss (unit 1). The inclusion, with its granulite facies mineral assemblages, may represent a portion of deeper crust partly assimilated during development of the orthogneiss-migmatite complex or raised along a mylonite zone. Granitoid gneisses to the west of the zone commonly show deep red-brown biotite in their mineral assemblages, whereas brown biotite is present in the rocks to the east; perhaps indicating a higher temperature gradient to the west of the zone (or relative uplift of the block west of the zone). Although the mylonite zone may reflect many movements, the latest mylonitization predates the emplacement of unit 6, because the rocks in this unit do not show mylonitic textures. Brittle deformation may have occurred in the mylonite zone subsequent to intrusion of unit 6.

East trending faults probably postdate the northeast faults but predate the Dubawnt Group rocks. Subsequent movements on them displace the Dubawnt rocks. The northwest trending faults and the minor north faults, which displace the Dubawnt Group rocks, are considered younger than east faults. The northwest trending faults are more abundant on the northwest side of the major northeast trending fault zones. Fault zones on the west half of the map area are commonly filled with barren quartz veins containing scattered fragments of country rocks.

Mineralization

Mineralization was noted in several places within the Christopher Island Formation. Two uranium occurrences – one north-northeast of Nowleye Lake is associated with the basal units of the Christopher Island Formation and a fractured window of basement gneiss, unit 1 (mineralization near unconformity), and the other, located northeast of Nowleye Lake is close to the fault bounded basement rocks and considered to be epigenetic-fracture controlled mineralization. The former occurrence is characterized by secondary uranium minerals – a light yellow sklowdowskite, $Mg(UO_2)_2Si_2O_7.6H_2O$, and a dark yellow solid solution series, compreignacite, $K_2U_6O_{19}.11H_2O$, and becquerelite, $CaU_6O_{19}.11H_2O$ (A.R. Miller, personal communication; mineral identifications by A.L. Littlejohn and A.C. Roberts, Central Laboratories and Technical Services Division. A third occurrence located north of Carruthers Lake, appears to be genetically related to the fluorite-bearing granitic intrusion (unit 12). Two occurrences of sulphides, pyrite with minor chalcopyrite and malachite or chalcopyrite, are associated with small shear zones within the Christopher Island Formation. Several disseminated pyritiferous zones of minor importance are present along various shear zones both in the basement and in the cover rocks.

References

Blake, D.H.
1980: Volcanic rocks of the Paleohelikian Dubawnt Group in the Baker Lake-Angikuni Lake areas, District of Keewatian, N.W.T.; Geological Survey of Canada, Bulletin 309, 50 p.

Donaldson, J.A.
1965: The Dubawnt Group, Districts of Keewatin and Mackenzie; Geological Survey of Canada, Paper 64-20.

Eade, K.E. and Blake, D.H.
1977: Geology of the Tulemalu Lake map area, District of Keewatin; in Report of Activities, Part A, Geological Survey of Canada, Paper 77-1A, p. 209-211.

Eade, K.E.
1976: Geology of the Tulemalu Lake map area (65J), District of Keewatin; in Report of Activities, Part A, Geological Survey of Canada, Paper 76-1A, p. 379-381.

Higgins, M.W.
1971: Cataclastic Rocks; U.S. Geological Survey, Professional Paper 687, 97 p.

LeCheminant, A.N. Lambert, M.B., Miller, A.R., and Booth, G.W.
1979a: Geological studies: Tebesjuak Lake map area, District of Keewatin; in Current Research, Part A, Geological Survey of Canada, Paper 79-1A, p. 179-186.

LeCheminant, A.N., Leatherbarrow, R.W., and Miller, A.R.
1979b: Thirty Mile Lake map area, District of Keewatin; in Current Research, Part B, Geological Survey of Canada, Paper 79-1B, p. 319-327.

LeCheminant, A.N., Miller, A.R., Booth, G.W., Murray, M.J., and Jenner, G.A.
1980: Geology of the Tebesjuak Lake map area, District of Keewatin: A Progress Report with notes on uranium and base metal mineralization; in Current Research, Part A, Geological Survey of Canada, Paper 80-1A, p. 339-346.

Wright, G.M.
1955: Geological notes on central District of Keewatin; Geological Survey of Canada, Paper 55-17.

1967: Geology of the southeastern barren grounds, parts of the Districts of Mackenzie and Keewatin (Operation Keewatin, Baker, Thelon); Geological Survey of Canada Memoir 350.

6. STRATIGRAPHY AND GEOCHEMISTRY OF THE AKAITCHO GROUP, HEPBURN LAKE MAP AREA, DISTRICT OF MACKENZIE: AN INITIAL RIFT SUCCESSION IN WOPMAY OROGEN (EARLY PROTEROZOIC)

E.M.R. Research Agreement 23233-9-0126

R.M. Easton[1]
Precambrian Geology Division

Easton, R.M., Stratigraphy and geochemistry of the Akaitcho Group, Hepburn Lake map area, District of Mackenzie: An initial rift succession in Wopmay Orogen (early Proterozoic); in Current Research, Part B, Geological Survey of Canada, Paper 80-1B, p. 47-57, 1980.

Abstract

The Akaitcho Group consists of 8 to 10 km of metavolcanic and metasedimentary rocks located west of Hepburn Batholith and east of Wentzel Batholith in the central metamorphic core of Wopmay Orogen (Bear Province). Mapping of the Akaitcho Group at 1:50 000 scale in the Hepburn Lake map area revealed the following generalized stratigraphic sequence: (1) a lower basaltic unit of unknown thickness, (2) 3-4 km of arkosic turbidites with 200-300 m of pelite at the base, intruded by sills of rhyolite porphyry, (3) basalt and rhyolite volcanic complexes, and (4) 1-3 km of pelite and tuffaceous sedimentary rocks, locally with abundant basaltic extrusive and intrusive rocks. The upper pelite is conformably overlain by a distinctly different pelite that contains thin quartzite beds diagnostic of the Odjick Formation (Epworth Group) east of Hepburn Batholith. The Akaitcho Group is therefore interpreted to be older than and conformably beneath the western Epworth Group.

The Akaitcho Group metabasalts are LREE enriched tholeiites with geochemical similarities to marginal basin basalts, Group II oceanic basalts and continental flood basalts. The Akaitcho Group rhyolites may originate by crustal melting. The bimodal nature of the volcanism and its association with coarse continent-derived sediments suggest that the Akaitcho Group was deposited in a rift. Its stratigraphic position beneath the lower Epworth Group, a passive continental margin succession, is consistent with the hypothesis that the Akaitcho Group preserves products of inital rifting in Wopmay Orogen.

Introduction

The Akaitcho Group consists of early Proterozoic (Aphebian) metavolcanic and metasedimentary rocks of the Wopmay Orogen located west of the Hepburn Batholith and east of the Wentzel Batholith (Hoffman et al., 1978). The presence of bimodal volcanics in the Akaitcho Group led Hoffman et al. (1978) to suspect that the Akaitcho Group represented products of initial rifting of the Wopmay Orogen. Testing of this hypothesis requires mapping and establishment of the internal stratigraphy, depositional environment and regional stratigraphic position of the Akaitcho Group.

Mapping of the Akaitcho Group in the Hepburn Lake map area (86 J) was begun by the author in 1978 in conjunction with 1:100 000 scale mapping of this area by P.F. Hoffman and M.R. St-Onge (Geological Survey of Canada Project 770019). The current research agreement allowed the author to complete 1:50 000 scale mapping of the Akaitcho Group in the Hepburn Lake map area and to collect samples for geochemistry and geochronology. Studies of these samples will constitute part of a doctoral dissertation at Memorial University.

Regional Geology

Early Proterozoic (Aphebian) rocks of the Bear Province compose the Wopmay Orogen (Hoffman, 1973; 1979; in press). The Wopmay Orogen can be divided into four major tectonic zones. From east to west they are: a foreland platform, a foreland fold and thrust belt, a metamorphic and batholithic core zone, and a volcano-plutonic belt (Hoffman, 1973; in press). The Akaitcho Group is found in the metamorphic core zone and consists of 8 to 10 km of metasedimentary and metavolcanic rocks. The Akaitcho Group is intruded on the east by the Hepburn Batholith and on the west by the Wentzel Batholith (Fig. 34.1, Hoffman et al., 1980). Regional metamorphism of the Akaitcho Group ranges from chlorite (lower greenschist) to above muscovite breakdown (upper amphibolite to granulite) and is spatially related to the two batholiths (St-Onge and Carmichael, 1979; Hoffman, 1980). The dominant structural features in the Akaitcho Group are two broad, north-south trending synclinorium-anticlinorium pairs separated by the Okrark Thrust. Rocks of the Wentzel Batholith and migmatized rocks of the Akaitcho Group are truncated by the Wopmay Fault which juxtaposes these older units against sedimentary and volcanic rocks of the Great Bear Volcano-Plutonic belt. Following uplift and erosion in the orogen, major northeast- and northwest-trending transcurrent faults cut the area (Hoffman, 1980a). Dip-slip reactivation of the transcurrent faults was in part contemporaneous with deposition of the Hornby Bay Group (Hoffman, 1980a). North trending normal faults associated with the intrusion of the Muskox Intrusion and the Mackenzie Set III diabase dyke swarm were the last major geological events occurring in the map area during the Precambrian.

Stratigraphy

A geological map of the Akaitcho Group in the Hepburn Lake map area (86 J) is presented in Figure 6.1. A generalized stratigraphic column for the Akaitcho Group is presented in Figure 6.2. Briefly, the Akaitcho Group consists of a lower basaltic sequence overlain by 200 to 300 m of pelite which is in turn overlain by 3 to 4 km of arkosic turbidites. Basalt and rhyolite volcanic complexes overlie the arkosic turbidites. The volcanic complexes are overlain by 1 to 3 km of pelite and volcaniclastic sedimentary rocks. In some areas, an upper sequence of basaltic volcanic and intrusive rocks is present above the pelites. The upper volcanics are overlain by pelites of the Akaitcho Group. Pelites containing thin quartzite beds characteristic of the Odjick Formation (Epworth Group) conformably overlie the Akaitcho Group. The conformable relation between the Akaitcho Group and the overlying Odjick Formation was the most significant discovery of the summer because it establishes the relative age and stratigraphic position of the Akaitcho Group.

[1]Department of Geology, Memorial University, St. John's, Newfoundland, A1B 3X5

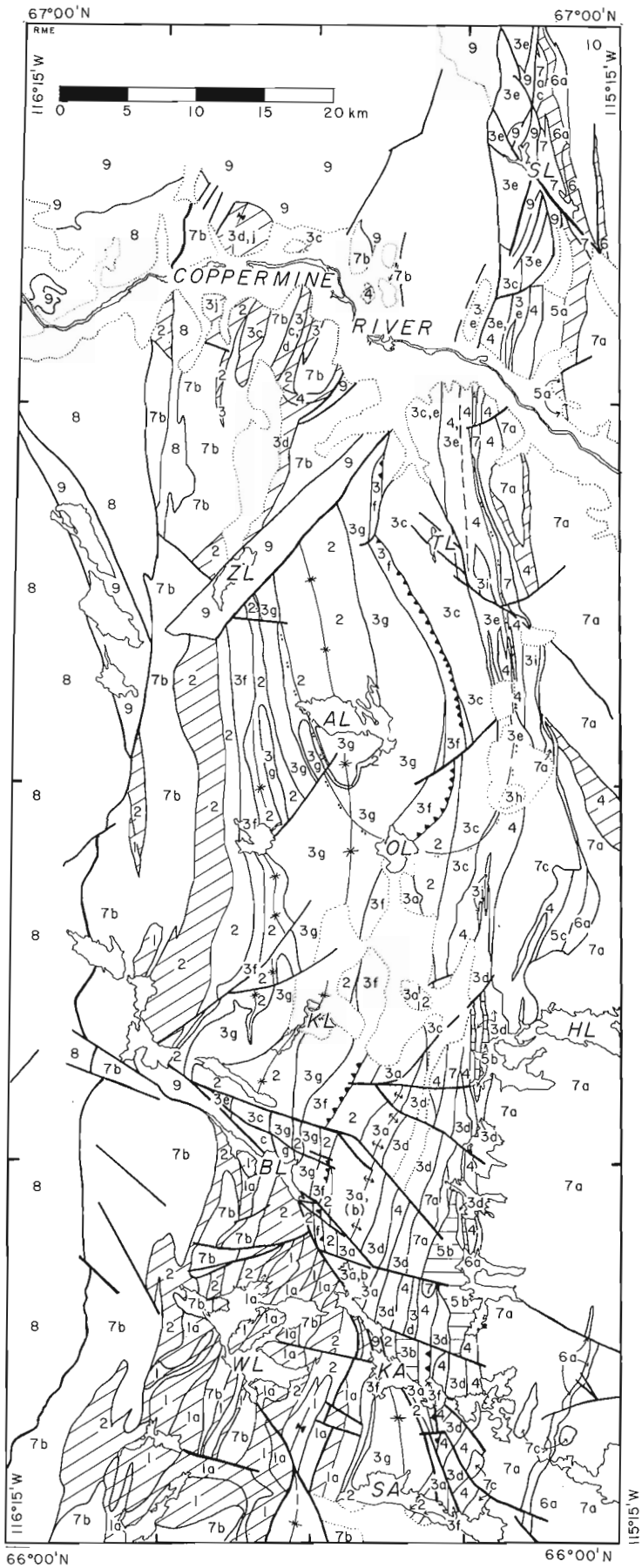

LEGEND

10 MUSKOX INTRUSION

9 HORNBY BAY GROUP sandstone

8 volcanic, sedimentary and plutonic rocks of the GREAT BEAR VOLCANO-PLUTONIC belt

7c younger mafic intrusions of the HEPBURN BATHOLITH

7a HEPBURN BATHOLITH — 7b WENTZEL BATHOLITH

EPWORTH GROUP

6 undivided — 6a Odjick Fm., pelite with thin quartzite bed

AKAITCHO GROUP

5a metabasalt flows — 5b gabbro sills — 5c siliceous metasiltstone

4 olive metapelites and volcaniclastic sediments

3 VOLCANIC COMPLEX LITHOLOGIES

3h metaconglomerate — 3i siliceous metasiltstone — 3j marble, quartzite

3e high Zr, mainly porphyritic rhyolite — 3f plagioclase porphyritic rhyolite sills — 3g orthoclase porphyritic rhyolite sills

3b gabbro sills — 3c massive and pillowed metabasalt — 3d basalt metatuff

3a low Zr, mainly aphanitic rhyolite

2 subarkosic and arkosic turbidites

1 amphibolite (lower volcanic sequence) — 1a pelite

GEOLOGY BY R.M. EASTON, P.F. HOFFMAN, and M.R. ST-ONGE, 1977, 1978, 1979.

fold axis, of bedding, of foliation

fault

Okrark Thrust Fault, teeth on upper plate

biotite isograd, mark on high T side

migmatite (> 30% granitic material)

AL Akaitcho Lake
BL Belleau Lake
HL Hepburn Lake
KA Kapvik Lake
KL Kingarok Lake
OL Okrark Lake
SA Samandre Lake
SL Sinister Lake
TL Tuertok Lake
WL Wentzel Lake
ZL Zephyr Lake

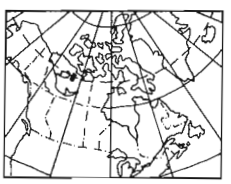

INDEX MAP

Figure 6.1. *Simplified geological map of the Akaitcho Group, Hepburn Lake map area (86 J west half). Okrark Thrust Slice lies west of Okrark Thrust. Marceau Thrust Slice lies east of Okrark Thrust.*

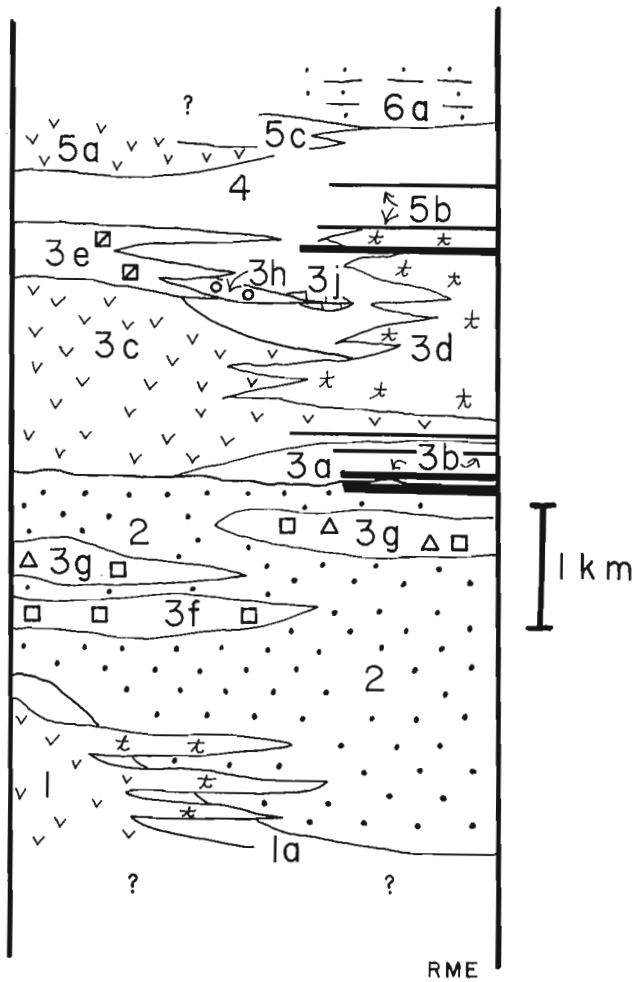

Figure 6.2. Generalized stratigraphic column for the Akaitcho Group in the Hepburn Lake map area (86 J west half). Units are as in Figure 6.1.

The following descriptions are meant to amplify the legend for Figure 6.1 and the generalized stratigraphic column for the Akaitcho Group presented in Figure 6.2 and outlined above.

Akaitcho Group

The Akaitcho Group is inferred to have been deposited on continental crust, as will be discussed later, although basement to the Group has not been observed.

The oldest exposed rocks of the Akaitcho Group are amphibolites and migmatized amphibolites (Unit 1) found in the Wentzel lake area. The thickness of these rocks is unknown, but is probably greater than 500 m. Three types of amphibolite have been recognized, namely: fine grained, compositionally banded amphibolites; medium grained, foliated amphibolite and coarse grained foliated amphibolite which may represent tuffs, flows and gabbros respectively. Areas of extensive outcrop of amphibolite may represent volcanic centres. The amphibolites are overlain by 200 to 300 m of finely banded, dark green or grey, now migmatized, pelite.

The metapelites are overlain by 3 to 4 km of subarkosic to arkosic turbidites (Unit 2). The turbidite beds are 10 to 100 cm thick with 1 to 10 cm thick grey to green weathering argillaceous tops. The basal portions of the turbidite beds are typically composed of medium sand, but locally, coarse sand to gritstone is present. Sedimentary structures are rarely preserved in the turbidite sequence, but complete and partial Bouma sequences were observed in two outcrops north of Akaitcho Lake. Rounded grains of tourmaline, epidote and zircon of probable detrital origin, are common in the coarser turbidites.

Basalt and rhyolite volcanic complexes overlie the arkosic turbidites. Two idealized volcanic complexes are represented in Figure 6.2. The left-hand complex shows the typical stratigraphy found in the volcanic complexes, namely, a basal basalt pile capped by rhyolite. The right-hand complex shows a variant of the typical volcanic complex stratigraphy. Five volcanic complexes have been delineated in the map area – the Sinister, Tuertok, Kapvik, Belleau and Zephyr Volcanic Complexes (Fig. 6.3). The Sinister, Tuertok and Kapvik Volcanic Complexes interfinger with each other, as shown in detail in Figure 6.4, and they can be directly correlated. The Zephyr and Belleau Volcanic Complexes are isolated from, and cannot be directly correlated with the other complexes.

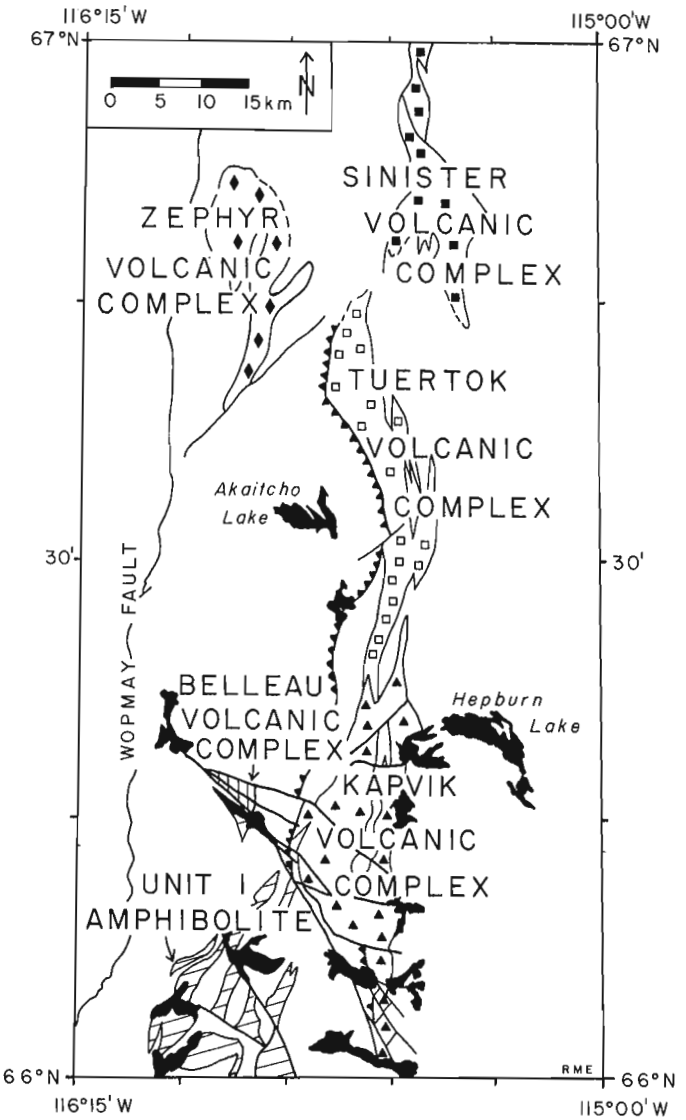

Figure 6.3. Distribution of Akaitcho Group volcanic rocks and location of volcanic complexes in the Hepburn Lake map area (86 J west half).

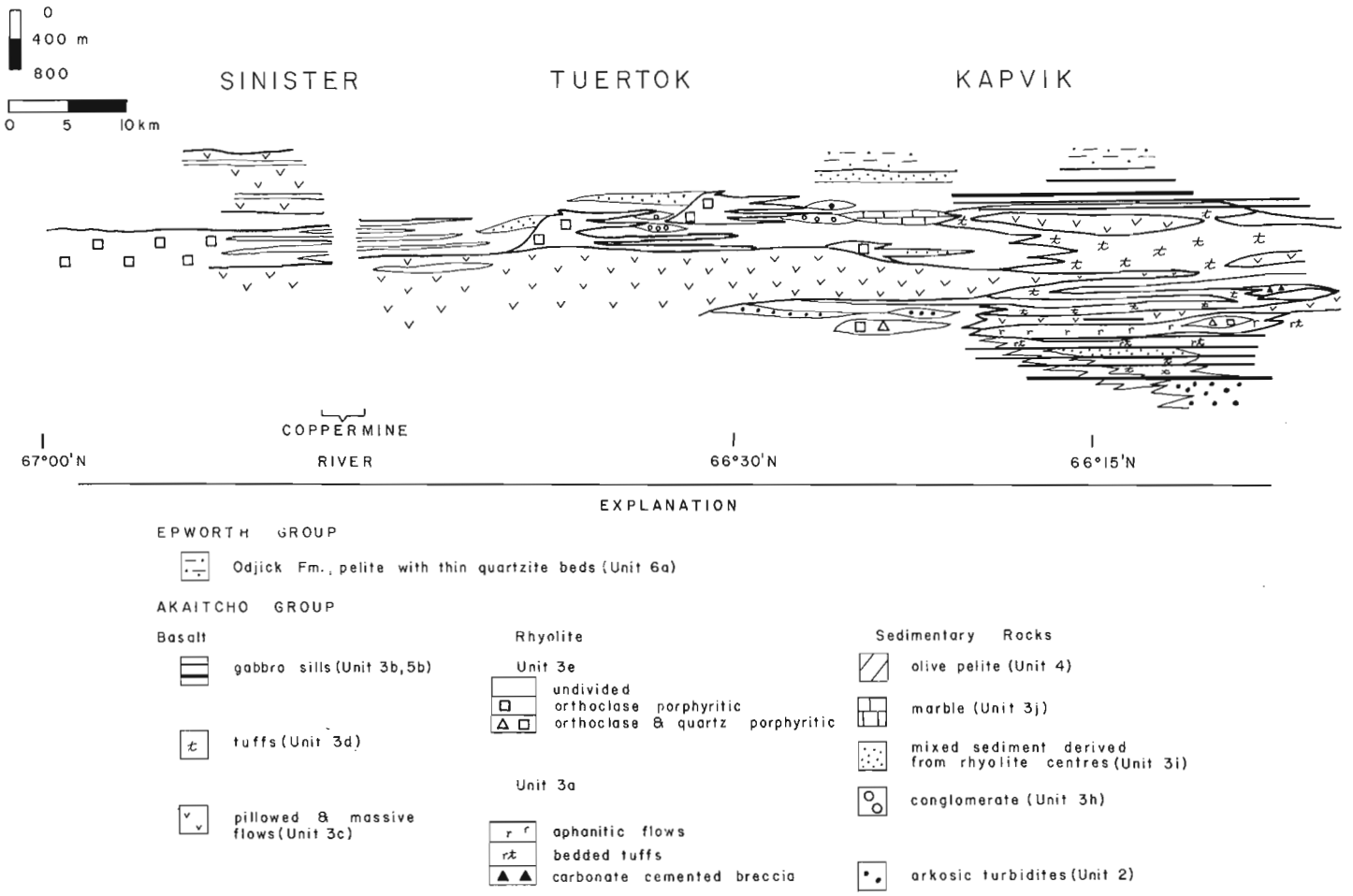

Figure 6.4. *Stratigraphic relations between the Sinister, Tuertok and Kapvik Volcanic Complexes in the Marceau Thrust Slice. Figure represents a simplified cross-section along a north-south line at about 115°35'W.*

The volcanic complexes typically have a 2 km plus thick base of green to dark green weathering, plagioclase porphyritic and nonporphyritic pillowed and massive metabasalts (Unit 3c) and basalt metatuffs (Unit 3d). The proportion of flows to tuffs between the complexes is variable (e.g. compare the Tuertok and Kapvik Volcanic Complexes in Figure 6.4). The basal metabasalts are capped by 1 to 1.5 km of pink and grey weathering, plagioclase, quartz and orthoclase porphyritic metarhyolites (Unit 3e). In cross-section, the metarhyolites form domical shaped accumulations, with massive cores and brecciated margins. The geometry and thickness of these porphyritic metarhyolite accumulations is consistent with their being volcanic domes. Wedges of metasandstone and siliceous metasiltstone (Unit 3i) are typically present on the north sides of the porphyritic metarhyolite domes. Intraformational metaconglomerates (Unit 3j) containing volcanic, quartzite and granitoid clasts, and volcanic breccias consisting of angular blocks of rhyolite in a muddy matrix, possibly lahars, are present on the south side of the porphyritic metarhyolite domes. In addition, beds of rhyolite metatuff can be traced for many kilometres south of the porphyritic metarhyolite domes (e.g., the rhyolite centres overlying the Tuertok Complex in Figure 6.4). Quartzites, marbles, and marble containing 25 to 50 per cent quartz grit are commonly found between the metarhyolite domes.

The only apparent exception to the general volcanic stratigraphy is the Kapvik Volcanic Complex. In this complex, the overlying porphyritic metarhyolites (Unit 3e) are sparse, and, a 1 km thick sequence of aphanatic metarhyolite flows and bedded tuffs (Unit 3a) underlies the basal basalt pile (Units 3c and 3d) (Fig. 6.4). The aphanatic metarhyolites and underlying arkosic turbidites are cut by a gabbro sill swarm (Unit 3b) chemically indistinguishable from the basal basalts. It is possible that aphanatic metarhyolites and gabbro sill swarms underlie the other volcanic complexes, because the bases of thee complexes, except for the southern half of the Tuertok Complex, are not exposed.

Volcanism was mainly subaqueous, although some porphyritic metarhyolites (Unit 3e) may be ash-flow tuffs and hence subaerial. They are massive, 20 to 30 m thick, homogeneous units and contain abundant lithic fragments and broken phenocrysts throughout. These probable ash-flow tuffs are restricted to the upper parts of the volcanic complexes, and probably capped former volcanic islands. The presence of carbonates (Unit 3j) and the greater abundance of tuffs in the upper parts of the volcanic complexes is also consistent with this interpretation.

The metabasalts exhibit a regional facies change from north to south. In the north, large piles of pillowed metabasalt and massive porphyritic metarhyolites are present.

Basaltic and felsic metatuffs are uncommon in the north, but increase in abundance southward (Fig. 6.4). Water depth is an important factor in controlling explosive basaltic eruptions (McBirney, 1963), and the north to south facies change in the metabasalts could be interpreted to indicate increasing water depths to the north. Alternatively, the facies changes could reflect differences in volatile content of the original magmas erupted to form the volcanic complexes.

The Belleau Volcanic Complex is a fault-bounded block of west facing, chlorite grade metavolcanic rocks isolated from the other volcanic complexes by the Belleau Fault System (Fig. 6.3). The lower section of the Belleau Volcanic Complex consists of 1 to 1.5 km of massive metabasalt, cut by gabbro sills, with a few pillowed flows and interbedded metapelites, cherts and basaltic metatuffs. The base of the section is truncated by a fault. A 300 to 500 m thick, compositionally zoned, intermediate composition lithic lapilli tuff with a rhyolitic base, possibly an ash-flow, overlies the metabasalts. Ten metres of chert and volcaniclastic metasedimentary rocks separate the lapilli tuff from an upper basalt section. The base of the upper basalt section is cut by several 50 to 100 m thick gabbro sills. The upper basalt section contains 1 to 1.5 km of hard, pale green, pillowed metabasalt and a few plagioclase porphyritic metabasalt flows. The metabasalts are overlain by metapelites and volcaniclastic metasedimentary rocks and a thick unit of orthoclase, quartz and plagioclase porphyritic metarhyolite, possibly the remains of a volcanic dome. Similar geochemistry of the metabasalts (see later section) and the presence of porphyritic metarhyolite capping the volcanic pile suggests that the Belleau Volcanic Complex is correlative with one or all of the Sinister, Tuertok and Kapvik volcanic complexes.

Metavolcanic rocks of the Zephyr Volcanic Complex are only exposed at sillimanite or higher metamorphic grade. Although the Akaitcho Group lithologies are recognizable at these grades, correlation is difficult, as the Zephyr Volcanic Complex is isolated by the Zephyr Fault and Quaternary cover of the Coppermine River valley from the other volcanic complexes (Fig. 6.1, 6.3). The Zephyr Volcanic Complex contains migmatized amphibolite (flows?) and banded amphibolite (tuffs). Distinct mineral assemblages within the banded amphibolite (tuffs). Distinct mineral assemblages within the banded amphibolite, e.g. garnet or anthophyllite bearing bands, suggests that the bands had primary compositional differences, and hence probably were tuffs. The presence of metarhyolite, marble and quartzite in the Zephyr Volcanic Complex sugggest that the Zephyr Complex is correlative with one or all of the Sinister, Tuertok and Kapvik volcanic complexes. Lithologically, the Zephyr Volcanic Complex most closely resembles the upper part of the Tuertok Volcanic Complex. The Zephyr Volcanic Complex is noteworthy because it contains fuchsite bearing quartzites. The fuchsite bearing quartzites were only observed outcropping in one area 15 km east of the Wopmay Fault, but do not appear to be related to that structure.

Two lithologically distinct, but chemically identical, types of rhyolite porphyry sills intrude arkosic turbidites (Unit 2) in the Okrark Thrust Slice (Fig. 6.5). Most of the sills are orthoclase, plagioclase and quartz porphyritic, red weathering rocks (Unit 3g). Less abundant areally are grey to pink-grey, strongly lineated plagioclase porphyry sills containing less than 10 per cent quartz and orthoclase (Unit 3f). The two types of sills are geochemically indistinguishable from the porphyritic metarhyolites (Unit 3e) which cap the volcanic complexes in the Marceau Thrust Slice (Table 6.1). Thus, Units 3e, 3f and 3g are though to be comagmatic and roughly contemporaneous, and no difference in relative age is inferred.

All of the volcanic complexes (Unit 3) are overlain by and interfinger with 1 to 3 km of olive metapelites (Unit 4). Unit 4 also includes many fine grained, thinly bedded rocks which may be tuffs or volcaniclastic sediments. In thin section, many of these problematic rocks contain more quartz and muscovite than known tuffs, and hence they are probably sedimentary in origin. Rounded epidote grains, probably detrital in origin are found in coarser beds within the sequence. The volcaniclastic sediments and the detrital epidote indicate that many of the pelites were probably derived from weathering of the adjacent volcanic complexes.

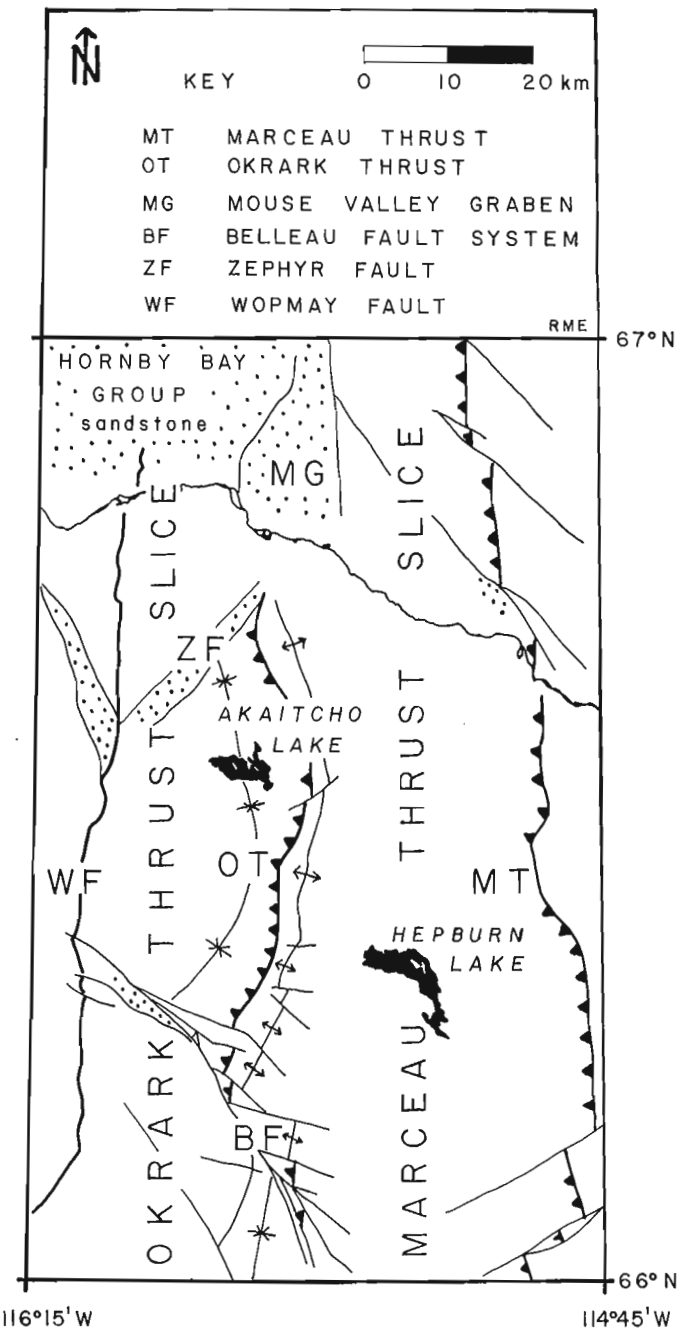

Figure 6.5. Major tectonic elements within the Hepburn Lake map area (86 J). A more detailed map showing the distribution of faults in the area is presented in Hoffman (1980a).

Table 6.1

Average analyses for Akaitcho Group volcanic rocks and recent basalts (modified from Jenner and Fryer, in press)

	K-spar porph. sills (Unit 3g)	Plag. porph sills (Unit 3f)	high Zr rhyolites (Unit 3e)	low Zr rhyolite (Unit 3a)	Belleau Basalt (Unit 3c)	Kapvik Basalt (Unit 3c)	Vaillant Basalt	MORB	IAT	CAB	ICE	90°E	Galapagos Tholeiite	Coppermine River Basalts (Baragar, 1969)	average cont. tholeiite (Manson, 1967)
No. major analyses	2	1	6	5	13	7	2								
SiO_2	68.32	69.42	69.34	75.68	50.72	49.55	49.56	49.61	51.47	50.59	48.01	48.71	48.68	50.84	51.95
TiO_2	.68	.66	.65	.32	1.30	1.31	1.25	1.43	.80	1.05	1.96	2.38	1.96	2.27	1.21
Al_2O_3	13.81	13.35	13.83	12.14	16.83	14.26	14.25	16.01	15.91	16.29	14.05	15.09	15.22	13.63	16.44
FeO*	6.12	6.25	6.00	3.32	13.09	14.16	12.72	12.77	9.50	8.37	11.84	14.78	10.77	12.97	10.51
MnO	.06	.04	.05	.02	.18	.19	.18	.18	.17	.17	.20	.19	.20	.21	.17
MgO	.96	.83	1.50	.40	6.81	6.60	7.30	7.84	6.73	8.96	7.97	6.53	7.01	6.88	5.95
CaO	2.43	2.01	1.13	.27	9.85	10.00	12.00	11.32	11.74	9.50	11.21	9.15	11.72	7.89	9.88
Na_2O	2.25	2.00	2.30	2.74	2.35	2.25	2.35	2.76	2.41	2.89	2.42	2.78	2.55	2.97	2.52
K_2O	5.24	5.33	5.10	5.25	.51	1.42	.35	.22	.44	1.07	.23	.38	.34	1.54	.87
P_2O_5	.13	.14	.14	.02	.10	.15	.12	.14	.11	.21	.21	.19	.24	.22	.21
No. trace analyses	8	6	15	8	16	16	5								
Ba	820	797	855	850	120	155	270	8	75	115	102	45	95		
Rb	204	207	200	125	42	71	15	1.16	5	10	4				
Sr	131	104	145	80	173	170	153	140	207	375	235	265	175		
Y	48	52	46	75	27	34	26	35	19	23	38	26	33		
Zr	270	280	276	202	117	125	75	100	52	106	131	120	126		
Cr	15	10	15	10	51	88	100	296	50	40	135	38	287		
Ni	19	11	17	8	77	53	136	123	30	25	71	51	90		

MORB	average Mid-oceanic Ridge basalt
IAT	average island arc tholeiite
CAB	average calc-alkaline basalt
ICE	average northwest Iceland tholeiite
90°E	average basalt, 90° east ridge, Indian Ocean

A later period of volcanism and intrusion occurred during and after deposition of the metapelites. The metapelites overlying the Sinister Volcanic Complex are overlain by a second pile of basalt, now preserved as amphibolite and migmatized amphibolite (Unit 5a). The top of the second volcanic pile is truncated by the Hepburn Batholith. Gabbro sills (Unit 5b) intrude the upper part of the Kapvik Volcanic Complex and the metapelites overlying the Complex. Again, the gabbro sill swarm and pelite are truncated by the Hepburn Batholith. It is not clear whether these later basalts represent a 'last gasp' of volcanism or a major period of magmatism.

Akaitcho/Epworth Group Relations

Eight kilometres northwest of Hepburn Lake metavolcanics of the Tuertok Volcanic Complex are overlain by 1 km of biotite grade, eastward facing metapelites of the Akaitcho Group (Unit 4). These metapelites grade upward into a 250 to 400 m thick unit of purple tinged, massive, blocky weathering siliceous metasiltstone (Unit 5c). The metasiltstone changes upsection over 100 m into a greenish metapelite containing the distinctive 2 to 5 cm thick quartzite beds diagnostic of the Odjick Formation of the Epworth Group east of Hepburn Batholith (Hoffman et al., 1978). The presence of contorted fine bedding, abundant frost-heaved 'tombstone-shaped' blocks, well developed metamorphic minerals and the distinctive cleavage/bedding pattern of the greenish metapelite all suggest that this unit (Unit 6a) is the Odjick Formaiton. This identification was confirmed in the field by M.R. St-Onge and P.F. Hoffman. The Odjick Formation is east facing, as is the underlying Akaitcho Group, and although the staurolite and andalusite isograds transect the contact at a small angle, the two groups appear to be structurally conformable. A cryptic disconformity cannot be ruled out however.

Similar relationships were also found 20 km south-southwest of Hepburn Lake. East facing metapelites (Unit 4) intruded by gabbro sills (Unit 5b) are apparently overlain by east facing metapelites of the Odjick Formation. Outcrop is poor in this area, with the closest outcrops of the Akaitcho and Epworth groups being 300 m apart. The overall stratigraphy is similar to the sequence preserved northwest of Hepburn Lake.

The conformable contact between the Akaitcho and the Epworth groups indicates:

a. that the Akaitcho Group is older than the Epworth Group; and

b. that the Vaillant Formation metabasalts and the Stanbridge Formation dolomite of the Epworth Group are probably correlative with the uppermost part of the Akaitcho Group. Marbles (Unit 3j) in the upper part of the Tuertok Volcanic Complex are lithologically similar to the Stanbridge Formation dolomite. The Vaillant Formation basalts are chemically similar to the Belleau Formation basalts (Fig. 6.8, Table 6.1).

Structure

The Akaitcho Group in the map area is preserved in two structural slices – the Okrark Thrust Slice and the Marceau Thrust Slice – separated by the westward dipping Okrark Thrust Fault (Fig. 6.5, 6.6). The Okrark Thrust Slice contains an anticlinorium truncated by the Wopmay Fault and a synclinorium with a hinge roughly parallel to the Okrark Thrust (Fig. 6.5, 6.6). The anticlinorium was the locus for intrusion of the Wentzel Batholith (Hoffman et al., 1980). The lower volcanics, the arkosic turbidites, and parts of some of the volcanic complexes are preserved in the Okrark Thrust Slice. The Marceau Thrust Slice also contains a synclinorium-anticlinorium pair, but in this slice, the anticlinorium is truncated against the Okrark Thrust Fault,

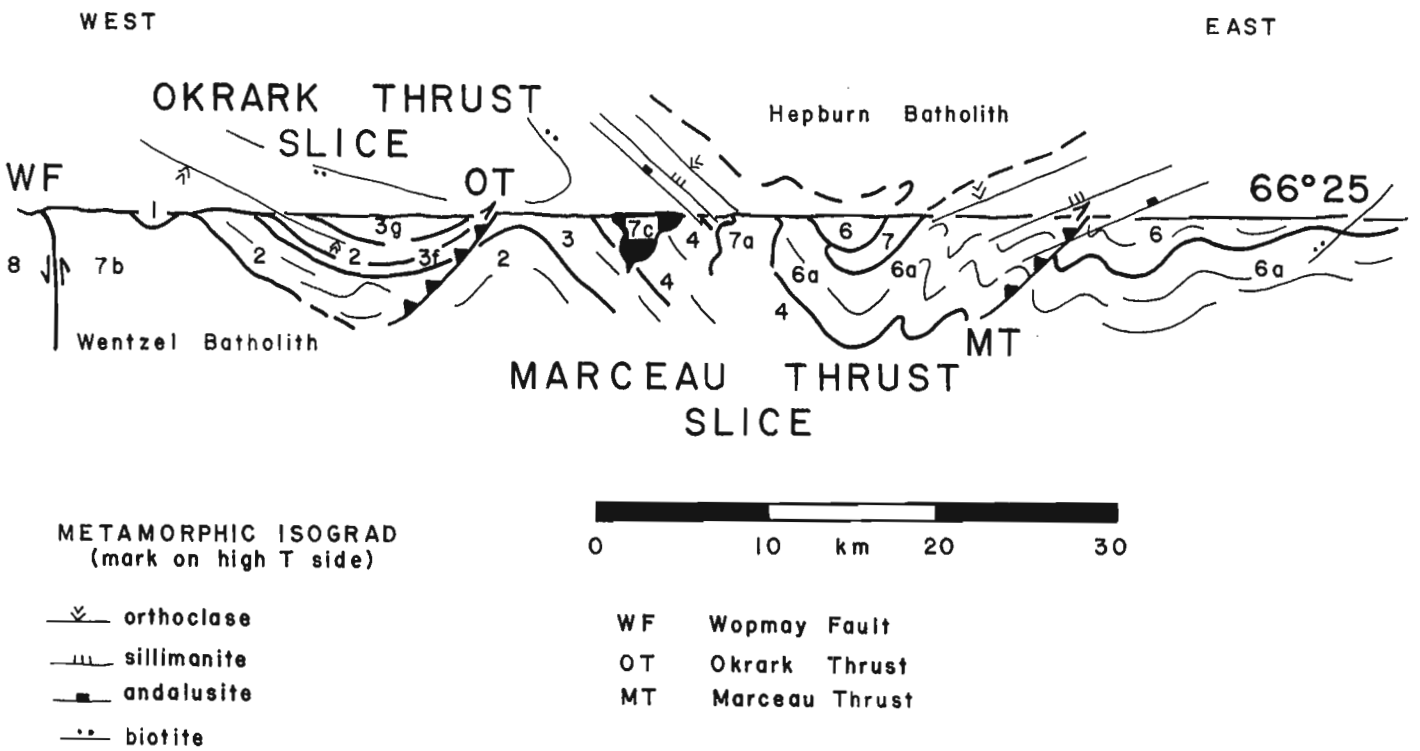

Figure 6.6. Generalized cross-section across the Hepburn Lake map area at 66°25'N, showing synclinoria-anticlinoria pairs and thrusts within the Akaitcho and Epworth Groups. Stratigraphic units as in Figure 6.1. (modified from Figure 27.4, Hoffman et al., 1980).

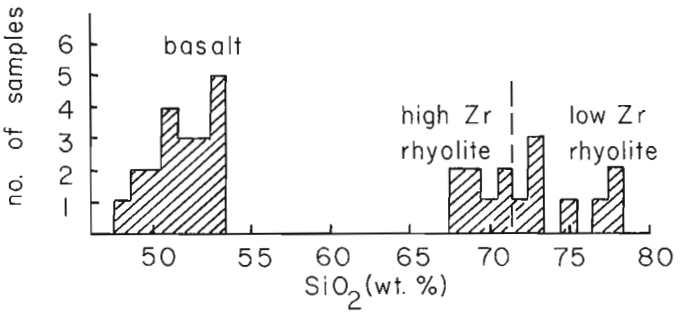

Figure 6.7. SiO_2 versus frequency for flow rocks of the Akaitcho Group showing a distinct bimodal distribution.

and the synclinorium served as the locus for intrusion of the Hepburn Batholith (Fig. 6.6) (Hoffman et al., 1980). The volcanic complexes, the pelites, the later volcanics, and slivers of arkosic turbidites are preserved in the Marceau Thrust Slice. As the two structural slices contain differing stratigraphy, the evidence that the Okrark Fault is a thrust fault is important in establishing the validity of the stratigraphic sequence outlined herein (Fig. 6.2).

The relative age relationships across the Okrark fault have been determined by two means, and both indicate that older rocks preserved in the Okrark Thrust Slice have been thrust eastward over rocks preserved in the Marceau Thrust Slice. This is consistent with the vergence of thrusting east of Hepburn Batholith.

In the Marceau Thrust Slice, subarkosic and arkosic turbidites lithologically similar to the Unit 2 rocks are present below the basal metarhyolite of the Kapvik Volcanic Complex. East of Okrark Lake, arkosic turbidites are also present below the basal basalts of the Tuertok Volcanic Complex (Fig. 6.1, 6.4). Thus, Unit 2 arkoses probably underlie the main volcanic complexes present in Unit 3.

In the Okrark Thrust Slice, rhyolite porphyry sills (Unit 3f and 3g) intrusive into the arkosic turbidites (Unit 2) are chemically indistinguishable from the high Zr porphyritic rhyolites (Unit 3e) present in the upper parts of the Sinister and Tuertok Volcanic Complexes. The restriction of high Zr porphyritic rhyolites to the upper parts of Unit 3 volcanic complexes, plus the chemical homogeneity of the sills and rhyolites argues in favour of Units 3e, 3f, and 3g being comagmatic. Thus, Unit 2 arkoses are older than the volcanic complexes of Unit 3.

The structural history of the Akaitcho Group can be summarized as follows. The Okrark Thrust Slice was transported over the Marceau Thrust Slice and both were broadly folded about northerly trending axes to form the major anticlinorium-synclinorium pairs. It is uncertain whether thrusting preceded or accompanied folding, but thrusting was complete before the peak of metamorphism because metamorphic isograds cross the Marceau Thrust (Hoffman et al., 1980) and possibly the Okrark Thrust (Fig. 6.1). The isograds are related to the early strongly-foliated plutons of Hepburn and Wentzel Batholiths (St-Onge and Hoffman, 1980; Hoffman et al., 1980). The isograds and the early plutons are involved in at least some of the broad folding but the late plutons of Hepburn Batholith are posttectonic. One such pluton, the Rib Granite, has been dated by the Rb-Sr whole rock method as 1750 ± 52 Ma (2σ error, decay constant 1.42×10^{-11} a^{-1}) (Easton, unpublished data). This pluton truncates metamorphic isograds in the Akaitcho Group (Hoffman et al., 1980) and therefore the age obtained is a minimum for the peak of metamorphism. The Akaitcho Group was metamorphosed at about 10 km depth (St-Onge and Carmichael, 1979) but may have been rapidly unroofed as the Wentzel Batholith is onlapped unconformably by sedimentary rocks of the Great Bear Volcano-Plutonic belt (Hoffman and McGlynn, 1977). A 20 km-long outlier of Great Bear sedimentary and volcanic rocks lies unconformably on migmatite derived from the Akaitcho Group at the western edge of the map area south of Coppermine River (Fig. 6.1).

Geochemistry

One hundred and ninety trace and 60 major element analyses of rocks from the map area were made by the author using a Phillips 1450 X-Ray Spectrometer at Memorial University. The results of these analyses confirm that the Akaitcho Group metavolcanic rocks are bimodal (Fig. 6.7).

The Akaitcho Group metavolcanic rocks can be divided into three groups on the basis of silica content (Fig. 6.7): 46 to 52% SiO_2– basalt; 67 to 70% SiO_2– low silica rhyolites; 70 to 75% SiO_2– high silica rhyolites. The absence of rocks in the 52 to 67% SiO_2 range is real, as all likely intermediate composition rocks were sampled and analyzed.

Two chemical and lithological distinct types of rhyolite are present in association with the main volcanic complexes (Unit 3). The oldest are high SiO_2, low Zr (150 to 200 ppm), generally aphanatic rhyolites (Unit 3a) present at the base of the Kapvik Volcanic Complex. The second type is the slightly younger, lower SiO_2, high Zr (250 to 300 ppm) porphyritic rhyolite domes, flows and sills (Units 3e, 3f, and 3g) present in the upper sections of the Sinister, Tuertok and Belleau Complexes and intrusive into arkoses (unit 2) in the Okrark Thrust Slice.

The incompatible trace element contents of both the low and high Zr rhyolites are high for tholeiites, but they do indicate that the rhyolites are not alkaline. The basalts also have high incompatible trace element contents, hence, the rhyolites could be genetically related to the basalts. Alternatively, the high Ba, K, Rb, Y, Fe and Mn contents of both types of rhyolite, the high radiogenic Sr content of the high Zr rhyolites (range: $^{87}Sr/^{86}Sr$ .79 for $^{87}Rb/^{86}Sr$ 2.5 to $^{87}Sr/^{86}Sr$ .89 for $^{87}Rb/^{86}Sr$ 7.5) and the abundance of these high SiO_2 rocks suggest that the rhyolites could be derived from melting of crustal materials. The presence of granitoid cobbles in conglomerates (Unit 3j) at the same stratigraphic level as the porphyritic rhyolites (Unit 3e) indicates that a granitic source area was near, and hence, that crustal materials were available to be melted. REE studies are in progress in an attempt to resolve the question of origin of the rhyolites.

All the analyzed metabasalts plot well into the tholeiite field on an alkali-silica diagram, despite the effects of metamorphism and the high K contents of all rocks in the map area (Easton, unpublished data). Y/Nb ratios for the metabasalts range from 2 to 15, with Nb values ranging from 1 to 18 ppm, indicating that the metabasalts are tholeiitic (Pearce and Cann, 1973). Preliminary REE results indicate that the Akaitcho Group metabasalts are LREE enriched, and hence are either continental tholeiites or LIL enriched oceanic basalts.

The metabasalts can be divided into 2 types on the basis of where they plot on different trace element discrimination diagrams. Type 1 basalts plot only in 'oceanic fields'. Type 2 basalts straddle all fields, but generally fall in 'continental and oceanic fields'. Figures 6.8a and b show the distinction of the two basalt types on a Ti-K-P plot (Pearce et al., 1975) and a Ti-Y-Zr plot (Pearce and Cann, 1973). Only the Belleau and Vaillant metabasalts are Type 1. It should be emphasized that these plots are used only to group the basalts and that they do not necessarily have any significance concerning the tectonic setting into which the Akaitcho Group metabasalts were erupted.

The basalts of each well sampled (20 or more trace element analyses) volcanic complex are distinctive both in major and trace element chemistry, confirming the delineation of the complexes on lithologic grounds. Specifically, the Tuertok Complex is characterized by extremely low Pb values (< 5 ppm), the Kapvik Complex by high FeO^t (> 13%), the Belleau and Vaillant metabasalts by being Type 1 basalts, and the amphibolites in the Wentzel Lake area by low (1 to 5 ppm) Nb contents.

Chemically, there are several modern analogs of the Akaitcho Group basalts. These are: oceanic island basalts, aseismic ridge basalts, back-arc basin basalts and Group II oceanic basalts (Frey et al., 1977) (Table 6.1). In addition, the Akaitcho Group basalts are similar to some continental flood basalts, e.g. the average continental tholeiite of Manson (1967) (Table 6.1). The lack of intermediate rocks, a strong iron enrichment trend on AFM plots, and the limited occurrence of coarse pyroclastic rocks preclude the Akaitcho Group being calc-alkaline. Thus, on the basis of geochemistry, it does not seem possible to designate a specific tectonic setting for the Akaitcho Group LREE enriched tholeiites, but they are not arc-related, they are not alkaline, and they are not depleted tholeiites.

Interpretation

The Akaitcho Group is a bimodal rhyolite/basalt suite containing associated volcaniclastic and continent-derived clastic sedimentary rocks. The following lines of evidence indicate that the Akaitcho Group was probably deposited in a rift.

1. The presence of detrital epidote, zircon and tourmaline in the abundant arkosic turbidites (Unit 2) in the lower part of the Akaitcho Group indicates that a continental source area was near during deposition of this unit.
2. The presence of granitoid and quartzite cobbles in conglomerates associated with the volcanic complexes (Unit 3) indicate that a continental source are was near during deposition of these units.
3. The LREE tholeiitic metabasalts of the Akaitcho Group are associated with rocks indicating the presence of a nearby continental region, hence they are probably continental tholeiites. The geochemistry of the metabasalts is consistent with their being continental tholeiites.
4. The high Ba, Rb, K, Fe, Mn, and Y content of the low and high Zr rhyolites is consistent with these rocks being derived from crustal melting.
5. The bimodal volcanism with a high felsic to mafic ratio (0.2 to 0.3) is consistent with the Akaitcho Group being deposited in a rift.

Basement to the Akaitcho Group has not been observed, but the abundance of continent derived sedimentary rocks in the lower part of the Group, and bimodal volcanism with a high felsic to mafic ratio suggests that the Akaitcho Group in the map area was deposited on continental crust. The thickness of this crust is unknown, but by analogy with recent rift terranes (e.g. Afar in Pilger and Rösler, 1975) probably thinned to the west. The oldest rocks observed in the Akaitcho Group in the map area are tholeiitic basalts, and hence, rifting may have been well advanced by the time these basalts were erupted. Nevertheless, continental terranes were nearby and shed voluminous arkosic turbidites into the Akaitcho basin. As rifting progressed, large basalt volanoes were constructed. The tholeiitic chemistry of the Akaitcho Group basalts suggests significant amounts of partial melting in the basaltic source region. The large volumes of basaltic magma possibly introduced sufficient heat into the crust to cause crustal melting to produce the abundant rhyolites. The abundance of basalt tuffs in some of the volcanic complexes suggest that they formed in shallow water. Possible welded ash-flow tuffs indicate that the upper parts of the volcanoes were probably erupted as islands. Deepening (and widening?) of the depositional basin occurred with time, and the Akaitcho Group was eventually buried by Epworth Group pelites.

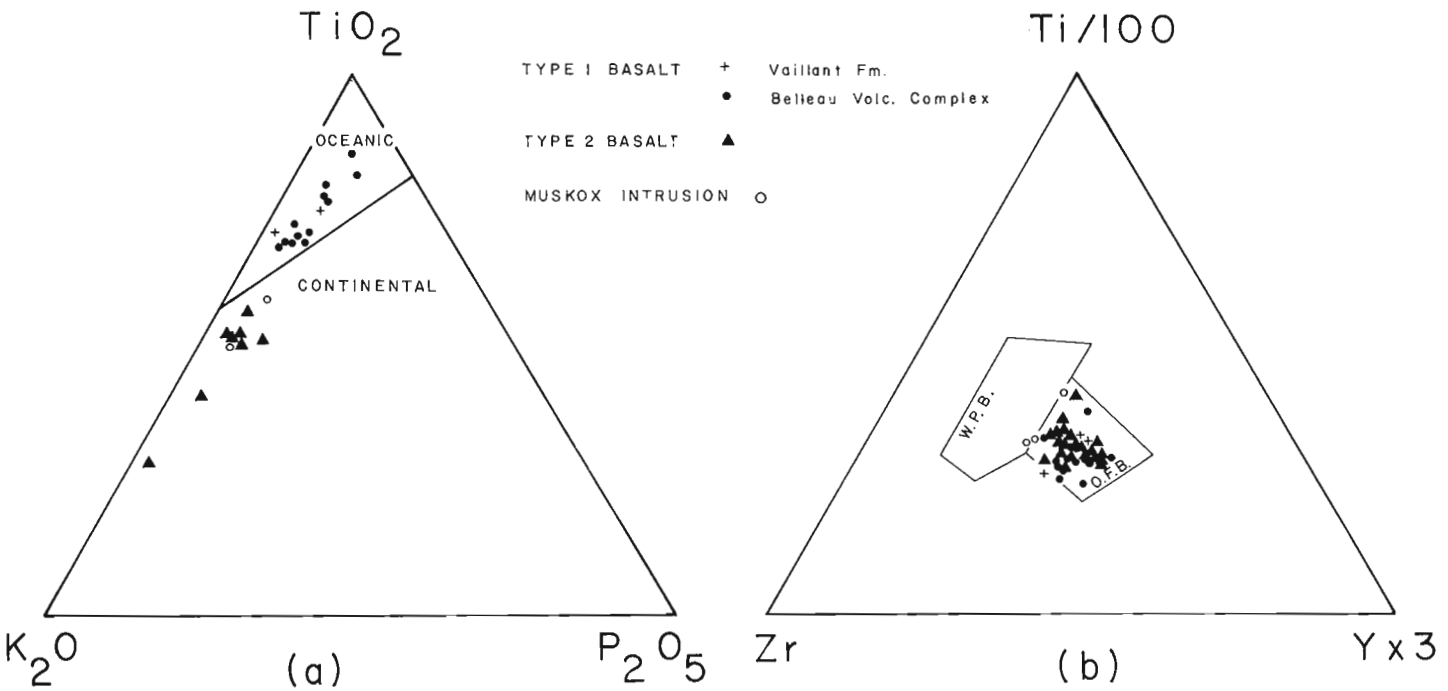

a) Ti-K_2O_5-P_2O_5 plot for Akaitcho Group metabasalts. *b) Ti-Y-Zr plot for Akaitcho Group metabasalts.*

Figure 6.8

The lithologies present in the Akaitcho Group, the geochemistry of the Akaitcho Group metavolcanic rocks, the stratigraphic position of the Akaitcho Group beneath the Epworth Group, and the inferred depositional history are consistent with the Akaitcho Group preserving products of rifting related to the formation of the Coronation continental margin during the Proterozoic, as suggested by Hoffman et al. (1978).

Economic Potential

At first glance, the Akaitcho Group would seem to be a likely exploration target for volcanogenic massive sulphide deposits because of the presence of several areas where a transition from mafic to felsic volcanism occurs in a subaqueous environment. Closer examination shows that:

a. felsic volcanic breccias, which could serve as hosts for ore deposition, are uncommon;

b. associated exhalative deposits, such as bedded chert, and haematite and magnetite facies iron formations are rare;

c. although volcanism was subaqueous, it may not have occurred in a marine setting, particularly in the lowermost sections of the Akaitcho Group;

d. disseminated sulphides and mineral showings in the Akaitcho Group are rare; and

e. the volcanism was tholeiitic, not the calc-alkaline volcanism commonly associated with volcanogenic massive sulphide deposits (Sawkins, 1976).

Little is known about the type of mineral deposits associated with a rift environment, the likely tectonic setting for the Akaitcho Group; although the bimodal volcanism and coarse grained continent derived clastic rocks suggests that if any deposits are present, they should be of the sullivan or Broken Hill Types (Ag, Pb, Zn, Cu) (Sawkins, 1976).

Acknowledgments

D. Press at Memorial University of Newfoundland is in part responsible for the high quality of the geochemical results presented in this report. D.J. Furey provided able assistance in the field. P.F. Hoffman, J.C. McGlynn, R.S. Hildebrand, H. Williams, B.J. Fryer, C.P. Dewey and J. Wynne reviewed earlier versions of this paper.

References

Baragar, W.R.A.
1969: The geochemistry of Coppermine River basalts; Geological Survey of Canada, paper 69-44, 43 p.

Frey, F.A., Dickey, J.S., Jr., Thompson, G., and Bryan, W.B.
1977: Eastern Indian Ocean DSDP sites: Correlations between petrography, geochemistry and tectonic setting; in Indian Ocean Geology and Biostratigraphy, American Geophysical Union, Washington, D.C.

Hoffman, P.F.
1972: Cross-section of the Coronation Geosyncline (Aphebian), Tree River to Great Bear Lake, District of Mackenzie (86 J, K, O, P); in Report of Activities, Part A, Geological Survey of Canada, Paper 72-1A, p. 119-125.

1973: Evolution of an early Proterozoic continental margin: The Coronation Geosyncline and associated aulacogens of the northwestern Canadian Shield; Philosophical Transactions, Royal Society of London, Series A, v. 273, p. 547-581.

Hoffman, P.F. (cont'd)
1979: Wopmay Orogen: Continent-Microcontinent-Continent Collision of Early Proterozoic Age, Bear Province, Canadian Shield; Geological Association of Canada, Program with Abstract, v. 4, p. 58.

1980a: Conjugate transcurrent faults in north-central Wopmay Orogen (early Proterozoic) and their dip-slip reactivation during post-orogenic extension, Hepburn Lake map area, District of Mackenzie; in Current Research, Part A, Geological Survey of Canada, Paper 80-1A, p. 183-185.

1980b: On the relative age of the Muskox Intrusion and the Coppermine River basalts, District of Mackenzie; in Current Research, Part A, Geological Survey of Canada, Paper 80-1A, p. 223-225.

Wopmay Orogen: A Wilson Cycle of Early Proterozoic Age in the Northwest of the Canadian Shield; in Wilson Symposium volume, Geological Association of Canada, Special Paper 20. (in press)

Hoffman, P.F. and McGlynn, J.C.
1977: Great Bear Batholith: a volcano-plutonic depression; in Volcanic Regimes in Canada, W.R.A. Baragar, L.C. Coleman, and J.M. Hall, ed., Geological Association of Canada, Special Paper 16, p. 169-192.

Hoffman, P.F., St-Onge, M., Carmichael, D.M., and deBie, I.
1978: Geology of the Coronation Geosyncline (Aphebian), Hepburn Lake Sheet, Bear Province, District of Mackenzie; in Current Research, Part A, Geological Survey of Canada, Paper 78-1A, p. 147-151.

Hoffman, P.F., St-Onge, M., Carmichael, D.M. Easton, R.M., Grotzinger, J., and Schulze, D.E.
1980: Syntectonic plutonism in north-central Wopmay Orogen (early Proterozoic), Hepburn Lake map area, District of Mackenzie; in Current Research, Part A, Geological Survey of Canada, Paper 80-1A, p. 171-177.

Jenner, G.A. and Fryer, B.J.
Geochemistry of the Upper Snooks Arm Group Basalts, Burlington, Peninsula, Newfoundland: Evidence Against Formation in an Island Arc; Canadian Journal of Earth Sciences. (in press)

Mason, V.
1967: Geochemistry of basaltic rocks: Major elements; in Basalts: The Poldervaart Treatise on Rocks of Basaltic Composition, v. 1, p. 215-269.

McBirney, A.R.
1963: Factors governing the nature of submarine volcanism; Bulletin Volcanologique, v. 26, p. 455-469.

McGlynn, J.C.
1974: Geology of the Calder River map area (86 F), District of Mackenzie; in Report of Activities, Part A, Geological Survey of Canada, Paper 74-1A, p. 383-385.

1975: Geology of the Calder River map area (86 F), District of Mackenzie; in Report of Activities, Part A, Geological Survey of Canada, Paper 75-1A, p.339-341.

Pearce, J.A. and Cann, J.R.
1973: Tectonic setting of basic volcanic rocks determined using trace element analysis; Earth and Planetary Science Letters, v. 19, p. 290-300.

Pearce, T.H., Gorman, B.E., and Birkett, T.C.
1975: The $TiO_2 - K_2O - P_2O_5$ Diagram: A method of discriminating between oceanic and non-oceanic basalts; Earth and Planetary Science Letters, v. 24, p. 419-426.

Pilger, A. and Rosler, A.
1975: Afar Depression of Ethiopia, Inter-Union Commission on Geodynamics Scientific Report no. 14; Schweizerbart'sche Verlagsbuchhandlung, Stuttgart, 416 p.

St-Onge, M.R. and Carmichael, D.M.
1979: Metamorphic Conditions, Northern Wopmay Orogen, N.W.T.; Geological Association of Canada, Program with Abstracts, v. 4, p. 81.

St-Onge, M.R. and Hoffman, P.F.
1980: "Hot-side-up" and "hot-side-down" metamorphic isograds in north-central Wopmay Orogen, Hepburn Lake map area, District of Mackenzie; in Current Research, Part A; Geological Survey of Canada, Paper 80-1A, p. 179-182.

Sawkins, F.J.
1976: Massive Sulphide Deposits in relation to geotectonics; in Metallogeny and Plate Tectonics, D.F. Strong, ed., Geological Association of Canada, Special Paper 14, p. 221-240.

ADDENDUM

REE data are now available for 50 Akaitcho Group volcanic rocks. Unit 1 amphibolites are evolved continental tholeiites. The Kapvik, Tuertok and lower Belleau basalts have sloping REE patterns (La/Yb – 10 to 15) and REE abundances characteristic of continental tholeiites such as the Columbia River basalt (E.G. BCR-1). The upper Belleau basalts have flat REE patterns (La/Yb – 2 to 5) and abundances similar to oceanic basalts. The flat patterns are not LREE depleted. The change in chemistry of the basalts from the older, evolved continental tholeiite to 'oceanic' thoeliites supports the idea that the Akaitcho Group preserves products of rifting related to the formation of the Coronation continental margin. The high and low Zr rhyolites have similar REE patterns and are probably genetically related. The La/Yb ratio of the rhyolites (20 to 22) differs from that for the basalts, REE abundances in the rhyolites are lower than the REE abundances in the most fractionated basalts, and the rhyolite REE patterns are similar to the REE patterns for the upper crust. Combined with the other evidence presented in this report, the REE data indicate that the rhyolites are almost certainly derived from crustal fusion. An Rb-Sr whole rock age of 1881 ± 12 Ma (2σ) has been obtained from 6 samples of a high Zr rhyolite porphyry sill near Kingarok Lake. This age is considered an age of metamorphism.

7.

COMPUTER BASED SYSTEM FOR INTERPRETATION OF AIRBORNE MAGNETIC GRADIOMETER DATA WITH APPLICATION TO KEY LAKE AREA, SASKATCHEWAN

Project 780023

D. Teskey
Resource Geophysics and Geochemistry Division

Teskey, D., Computer based system for interpretation of airborne magnetic gradiometer data with application to Key Lake area, Saskatchewan; in Current Research, Part B, Geological Survey of Canada, Paper 80-1B, p. 59-67, 1980.

Abstract

A semi-automated interpretation system for the vertical gradient of the total magnetic field is described. The system essentially involves manual selection of positions for analysis from the contour map, followed by automatic interpolation and storage of the profiles. Interactive programs using matched filtering or least-squares techniques are then used to estimate the parameters of the causative sources. The least-squares approach can be applied to multibody situations by subtraction.

The effectiveness of the methods is illustrated by their application to the estimation of the depth to magnetic sources in the Key Lake area of Saskatchewan presumed to lie at or near the surface of Archean domes mantled by an Aphebian pelitic to semipelitic basal unit with graphitic horizons. Uranium-nickel orebodies occur in suitable structural traps in the basal unit at the unconformity between the peneplaned domes and the overlying Athabasca formation sandstone.

Interpretation System

A computer-based system has been designed to estimate the dimensions, magnetization strength, and depth of magnetic sources. This system is based on techniques developed earlier (Teskey, 1978) for total field interpretation. However, the present system is intended more specifically for the interpretation of vertical gradient data.

The significant features of the vertical gradient are a decreased sensitivity to depth extent (for bodies more than four times the depth of burial) and improved lateral resolution. The net effect is to accentuate sources near the surface of the crystalline rocks. Lateral offset and termination of anomalies are, of course, indicative of faults and fractures in the basement.

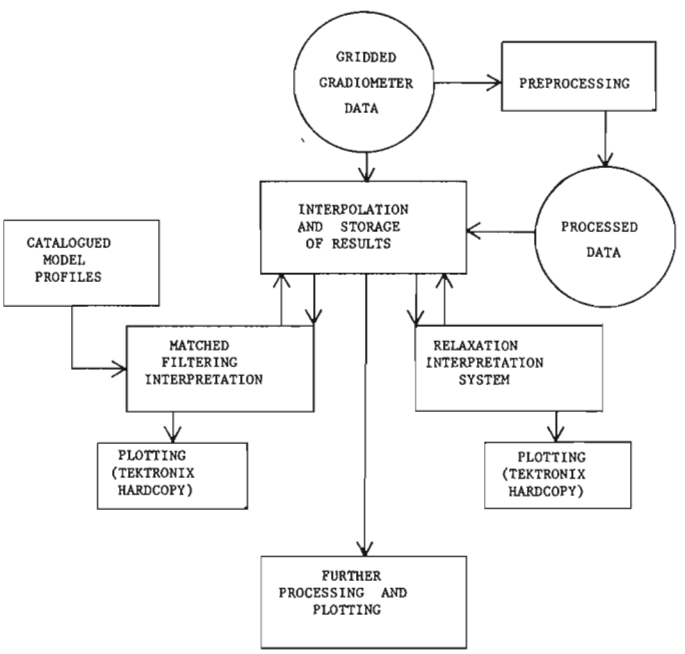

Figure 7.1. *Gradiometer interpretation system.*

The system, shown schematically in Figure 7.1, is described briefly below.

Data Input

The gridded data are taken from the standard output of the Geological Survey of Canada aeromagnetic data-processing system (stored on magnetic tape). These data can be preprocessed in order to enhance or improve the data's interpretability through operations such as continuation, calculation of derivatives or calculation of the vertical component. This is done in all cases by converting to the frequency domain with the fast fourier transform (FFT), applying the appropriate weighting functions and then reconverting the data back to the space domain.

The centre position, angle and number of profile points are selected manually from the contour map and punched on computer cards for each anomaly to be interpreted. Five profiles across the anomaly are then interpolated automatically from the gridded data set and stored on disc along with the above information. These data can then be accessed by the matched filtering or relaxation program through an identification number.

Matched Filtering

The basic operation of the matched filtering technique is the calculation of the cross-covariance between the interpolated data and pregenerated model data calculated over the range of variables. (In this case width (A), strike extent (B), and magnetic dip (α) for a prism model.) This calculation is done over a range of offsets j, such that the cross-covariance

$$C_j = \sum_{i=1}^{N} \frac{(T_i - T_{av}) \times (P_{j-N/2+i} - P_{av})}{V_t \times V_p}$$

where:

- N = number of points chosen for window
- T_i = model values
- P_i = profile values
- V_t = model variance
- V_p = profile variance
- T_{av} = model average
- P_{av} = profile average

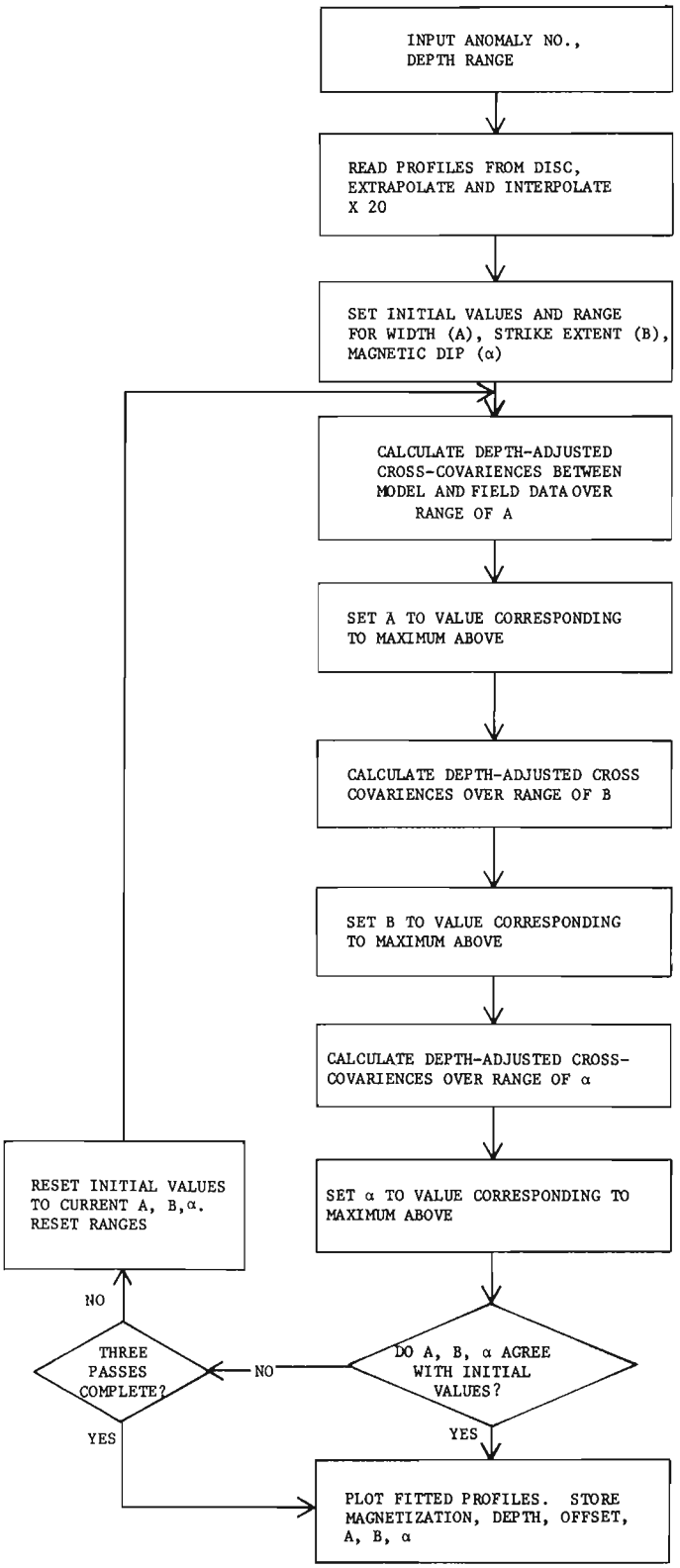

Figure 7.2. *Matched filtering interpretation program.*

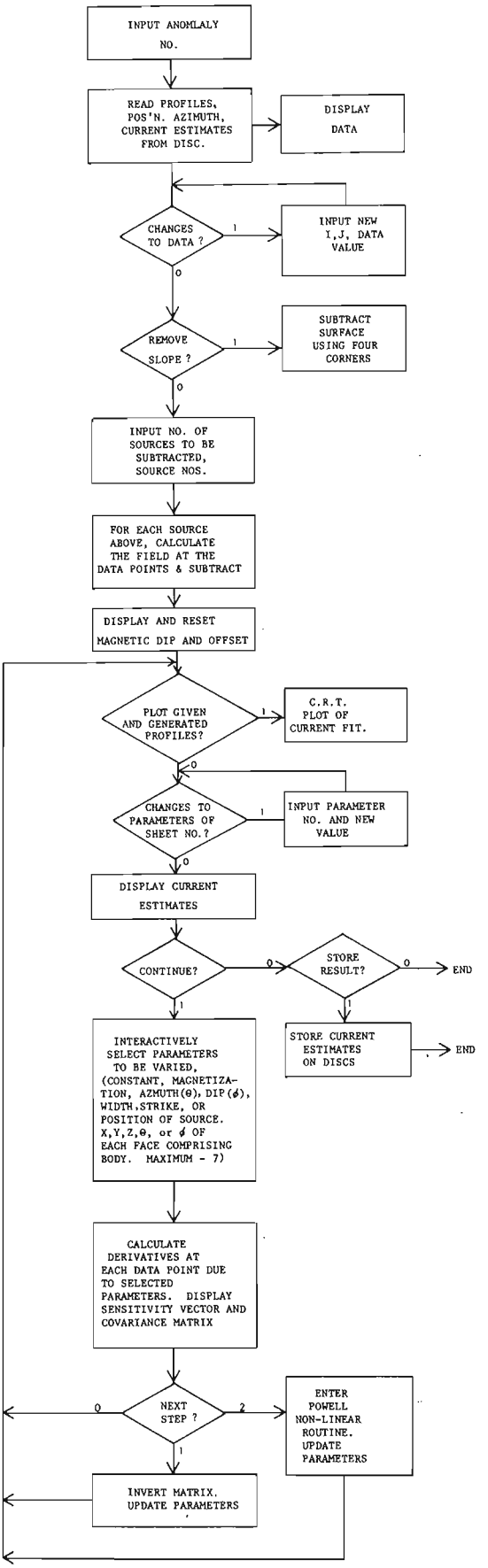

Figure 7.3. *Relaxation program.*

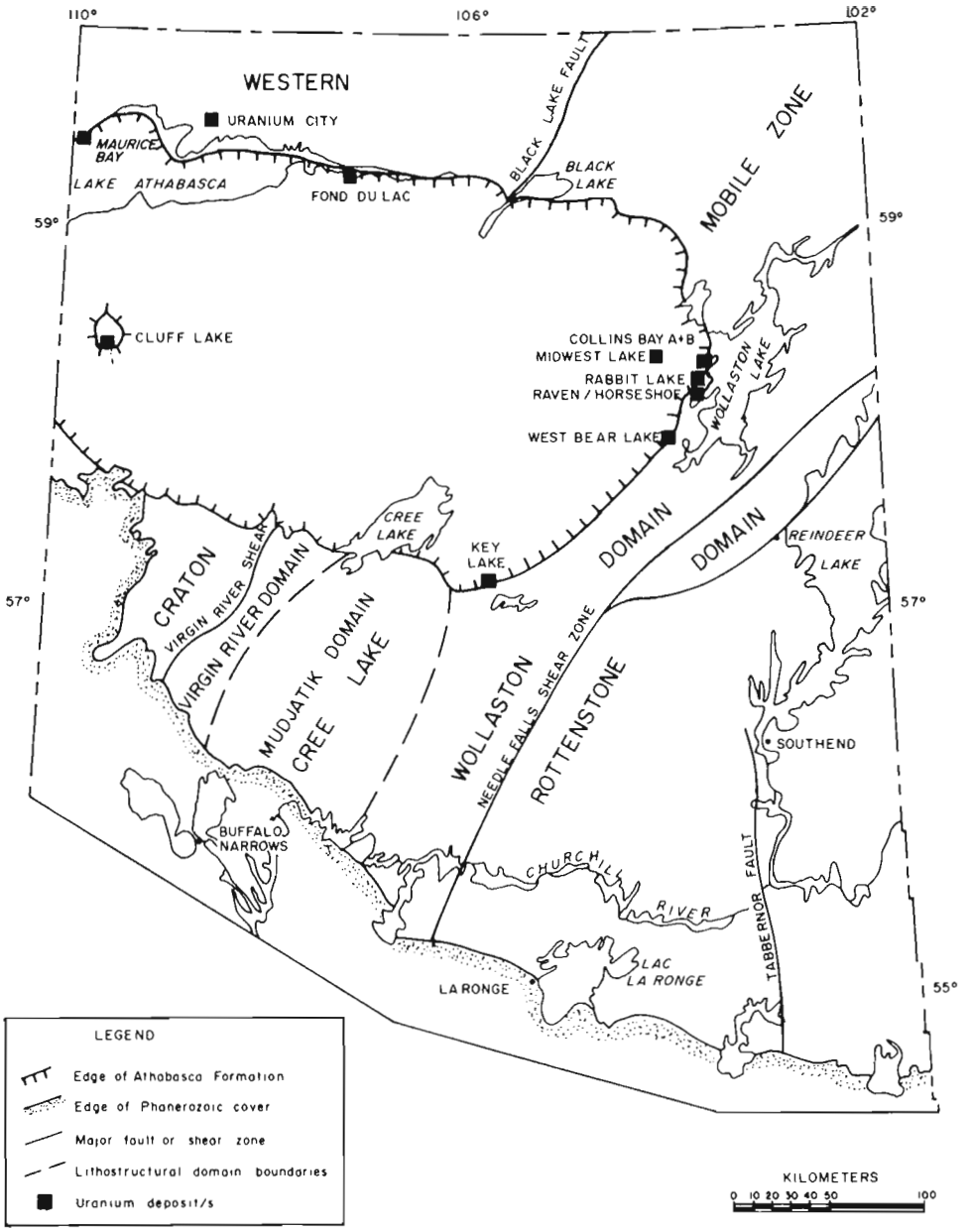

Figure 7.4. *Precambrian Shield of Saskatchewan, showing location of Key Lake (from Hoeve and Sibbald, 1979).*

An exact match will result in a value of $|C_j|=1$, whereas a complete mismatch gives a value of $|C_j|=0$. Thus the criterion for the best match is that the value of $|C_j|$ should be closest to one. The depth of the causative body is found by contracting or expanding the profile to improve the fit. This is accomplished by first interpolating the profile set to twenty times the original number of points, and then sampling the expanded profiles over a range of intervals. The magnetization estimate is obtained from the ratio V_p/V_t. Further description of this technique plus a discussion of the model choice is given in Teskey (1978).

The main advantages of this technique are:

1) No initial estimate of parameters are required.
2) The cost per depth estimate is much less than standard techniques such as nonlinear least squares.

The flow chart for this program is shown in Figure 7.2.

The estimates obtained from the matched filtering program, after being returned to disc can be used as initial input to an interactive relaxation program.

Relaxation

In this program, the magnetization, strike-angle, dip, width, strike-extent and position of the entire prismatic body obtained from the matched filtering program can be varied as well as the strike-angle, dip and position of each side. The parameters to be varied for each pass are selected by the interpreter who then has the option of a linear or nonlinear adjustment. The process can be terminated and the results rejected or returned to disc as desired. The flow chart for this program is shown in Figure 7.3.

Application

Background

A high resolution magnetic total field and gradiometer survey at an altitude of 150 m and with a line spacing of 300 m was flown over the Key Lake area, Saskatchewan in 1977 (Geological Survey of Canada, Open File 529). The location of the area is shown in Figure 7.4 (Hoeve and Sibbald, 1978). Contour maps of the total field and vertical gradient are shown in Figures 7.5 and 7.6. Uranium and nickel mineralization were discovered in this area in 1975 and 1976, and the area has subsequently been the subject of extensive geological and geochemical investigations (Gatzweiler et al., 1979).

The geology of the Key Lake area has been described by Ray (1977). The geological environment felt to be important for the emplacement of the ore is shown in Figure 7.7 (from Ray, 1977). It is felt that circulating hydrothermal fluids in the Athabasca sandstone deposited the minerals in suitable structural traps upon coming in contact with the reducing environment caused by the presence of graphite and sulphides in the basal Wollaston group. The graphite and sulphide horizons also act as electromagnetic conductors. Some major magnetic trends appear to be related to the Archean basement by extrapolation from the portion of the area to the south of the Athabasca unconformity in which some outcrop occurs (Ray, 1977). However the presence of pyrrhotite in the Aphebian basal pelitic zone and up to five per cent by volume magnetite in the Aphebian meta-arkose units would also produce magnetic anomalies. Some presumed Hudsonian intrusives of basic to intermediate composition are also noted in the area.

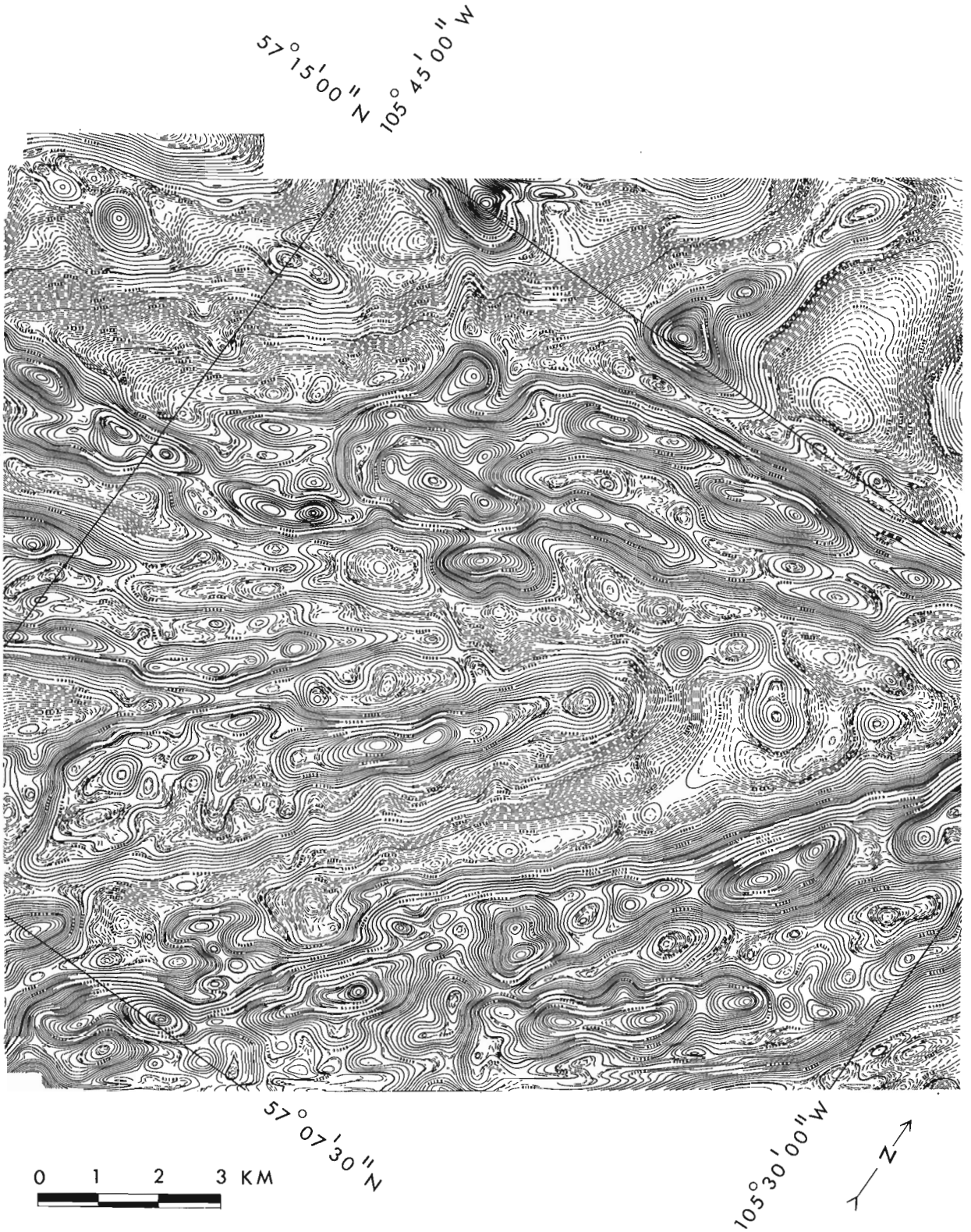

Figure 7.5. *High sensitivity total field magnetic contours, Key Lake, Saskatchewan.*

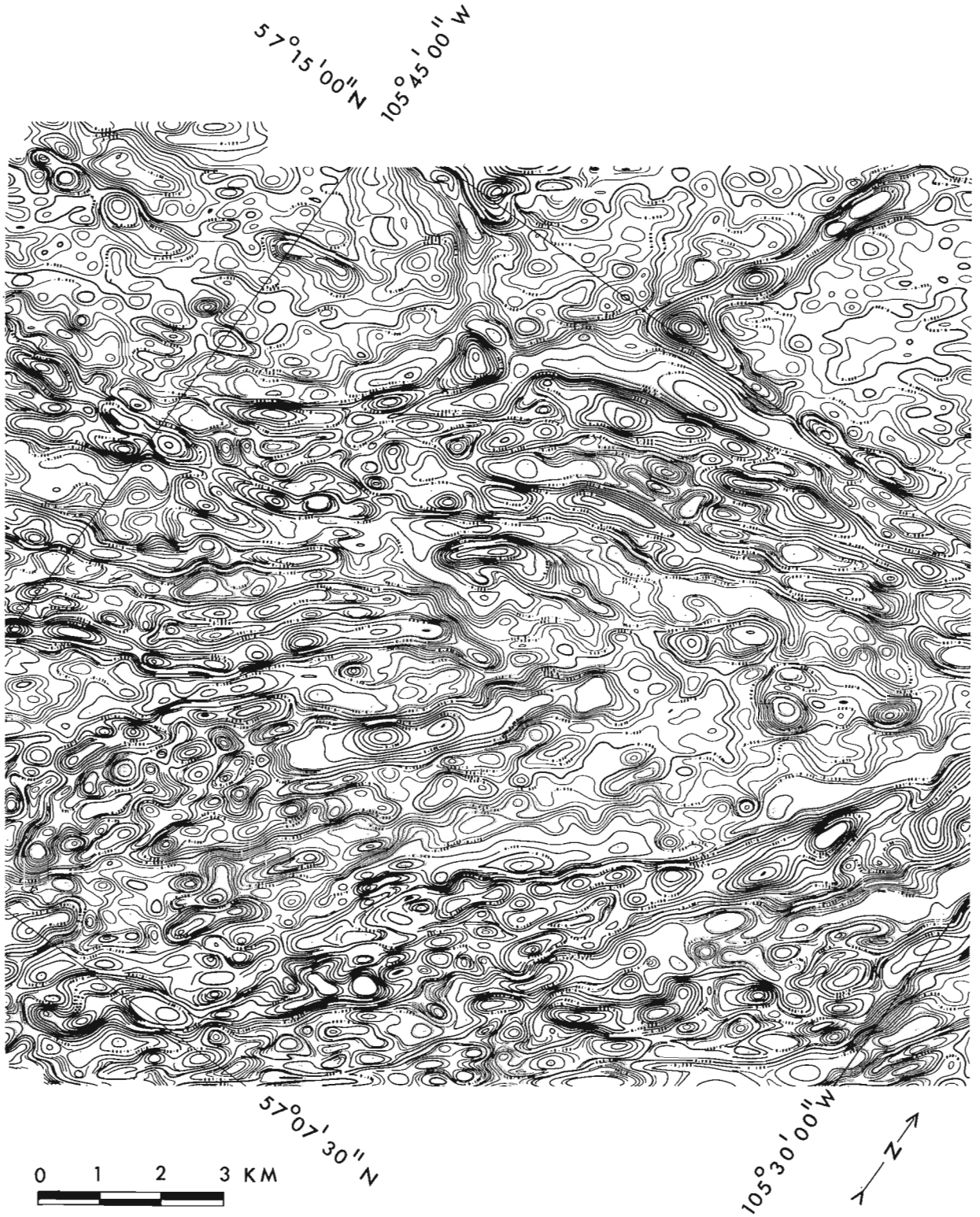

Figure 7.6. *Vertical gradient contours, Key Lake, Saskatchewan.*

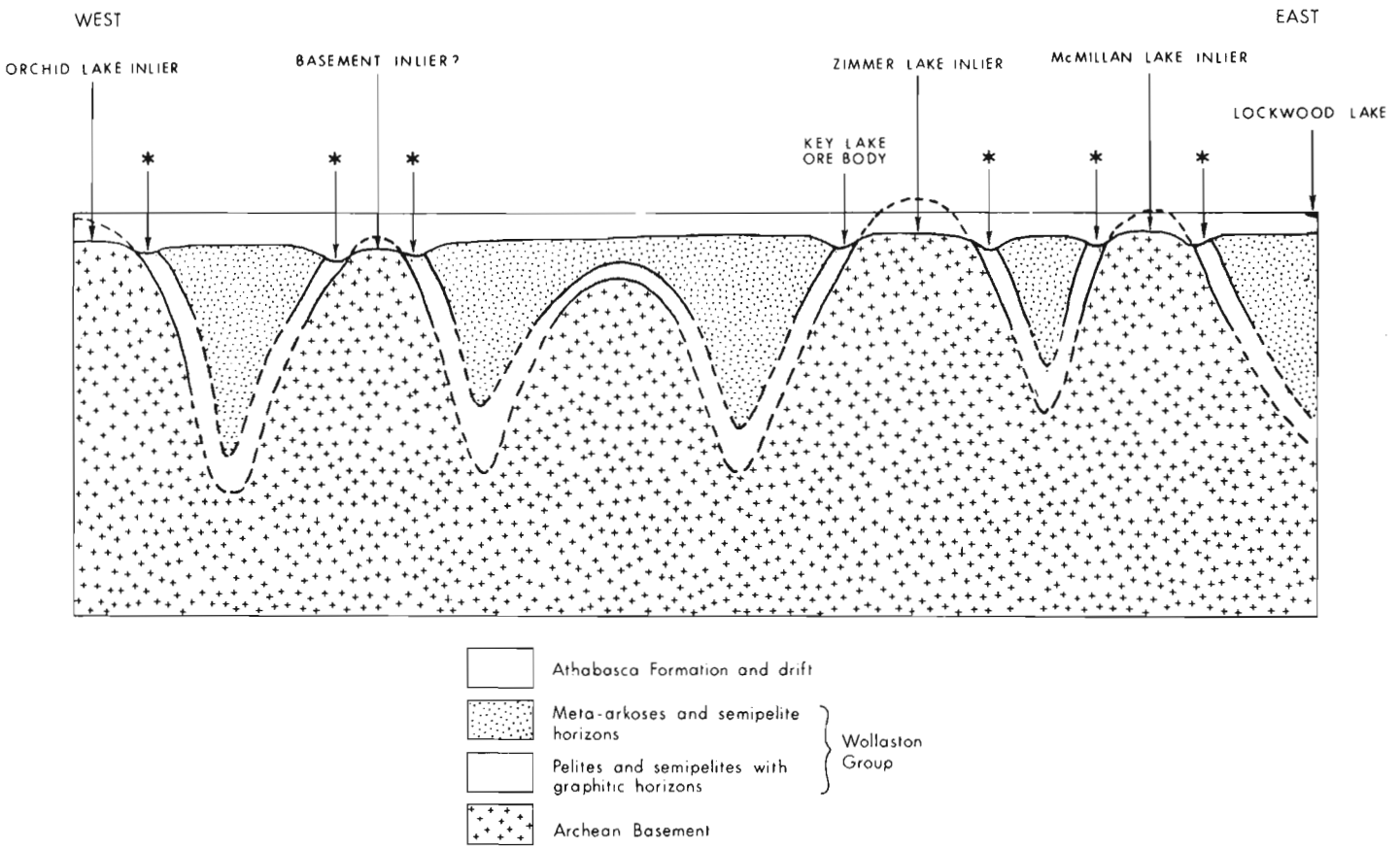

Figure 7.7. *Proposed structure underlying Key Lake area. Sites considered favourable for ore deposition are shown by an asterisk (from Ray, 1977).*

The Key Lake orebodies are found along the intersection of a northeasterly trending fault which extends to the basal graphitic zone, and the sub-Athabasca unconformity, on the northwest flank of a northeastern Archean/Aphebian pericline.

The potential of the gradiometer for outlining the contacts and the depth to periclinal bodies and for locating faults tends to make it, with electromagnetics, a promising method for exploration in this environment.

Interpretation

A preliminary study of the magnetic sources was carried out for the Key Lake area. Anomaly selection and depth estimates were made using the methods outlined in the previous section. Refinement where necessary was done using a modification of the relaxation program which uses only the central profile thus enabling a simplified and much cheaper generating function.

In order to maximize the usefulness of depth estimates it is necessary to have some measure of the confidence to be placed in a particular result. Initially this can be done by examination of the total field and vertical gradient contour maps (Fig. 7.4, 7.5). Clearly anomalies which are distorted or overly affected by neighbouring sources must be given a lower confidence level. The relationship between the total field and vertical gradient anomalies is also indicative of the nature of the source. For example, anomalies that appear strongly in both fields with good correspondence are likely to be due to sources which extend to great depth, whereas anomalies that are strong only in the vertical gradient field are probably due to shallower bodies.

An attempt to provide a numerical measure of the confidence to be placed in a particular result was made by analyzing the minimization surface, which is simply the sum of squares difference between the data and that generated by the model sources for various values of the source parameters. This surface is shown in Figure 7.8 for an anomaly due to a prism with a width and depth of four units and a strike extent and depth extent of one hundred units. The surface was calculated by varying the depth (H) and width (A) from 0.5 to 10.0 units in steps of 0.5, calculating the best least-squares value of the magnetization at each point and then the sum-of-squares difference between the current and ideal model. The correct solution, of course, gives a difference of zero. The zero value can be seen to lie in a narrow trough of low differences, within which the solution is almost as good. Any interference or distortion could cause the minimum to shift along this trough or even for more than one local minimum to occur. As can be seen in Figure 7.8, the residual error increases much more rapidly for depths greater than the true depth. Thus, for the correct choice of model, estimates are much more likely to be less than the actual depth. The slope of the trough axis in the width versus depth plane will also control the portion of the uncertainty which will affect the depth estimate. For the actual anomalies the procedure used was to vary A, from the optimum value and then obtain 'best' values for depth and magnetization, thus providing an estimate of the curvature and slope of the solution trough. The confidence to be placed in a particular solution is determined by (a) the overall quality of fit (from the normalized residual error) and (b) the inverse of the curvature of the surface along the axis of the trough multiplied by the slope in the A-H plane

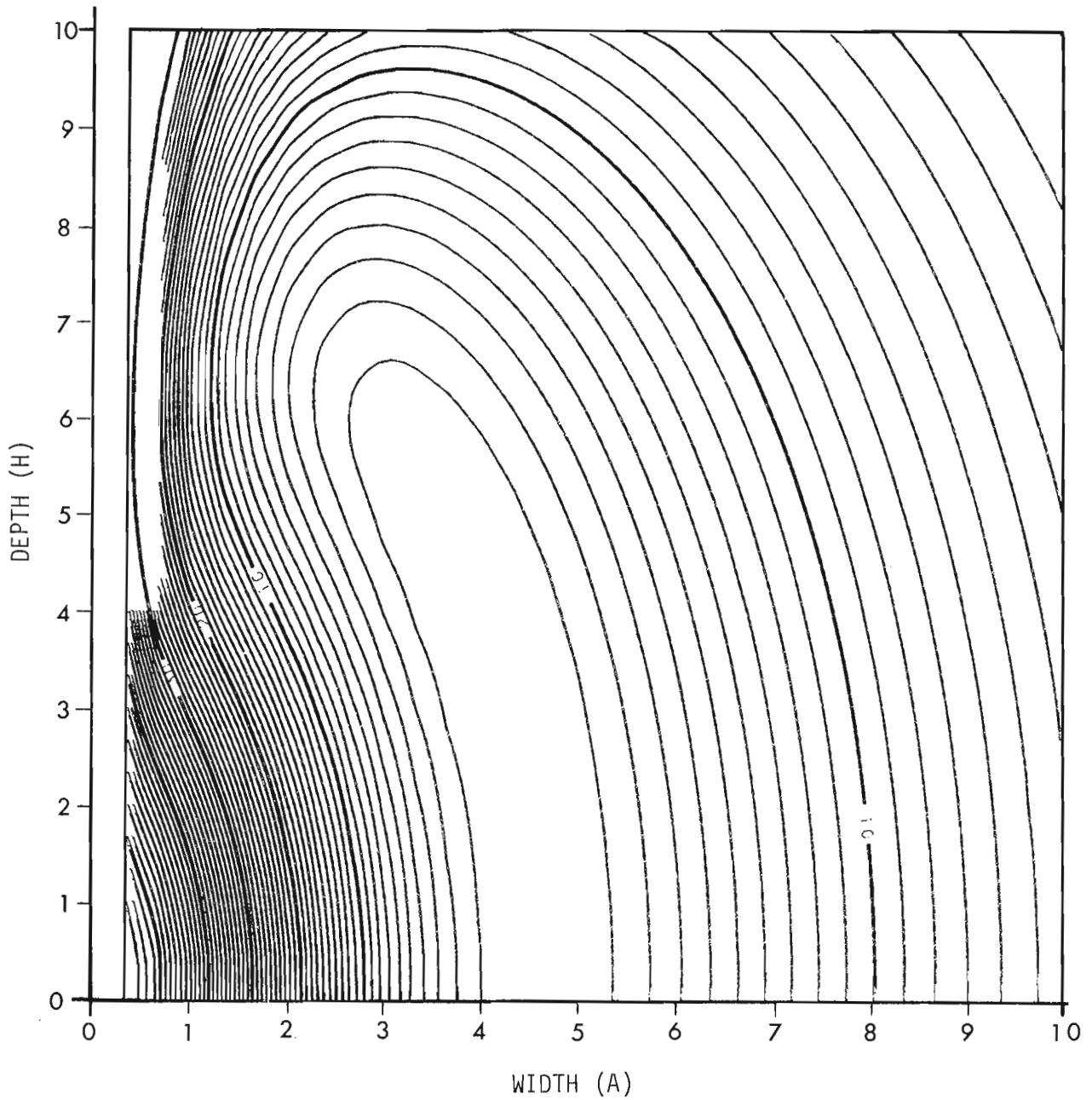

Figure 7.8. *Theoretical minimization surface for a prismatic source of width and depth for units.*

(the resolution parameter). The smaller these values are the better the fit and the higher the confidence for an individual estimate, also taking into consideration the comments at the beginning of this section. These quantities along with the estimated magnetization and depth for each determination are shown in Figure 7.9, where each box contains from top to bottom – the anomaly number, estimated magnetization, estimated depth, quality of fit parameter (residual error), and resolution parameter.

Discussion

For the purpose of discussion the anomalies have been separated into groups which appear to be related to a common geological feature, as shown in Figure 7.9.

Group I

Despite the offset between Anomalies 16 and 17, these appear to be related by a common strike direction (east-west) and character. Except for Anomaly 17, the depths are quite consistent at approximately 100 m below surface (150 m must be subtracted from the depth shown in Figure 7.9 as these values are depth below the flight elevation). Anomaly 16 is very prominent on both the total field and vertical gradient and thus is probably due to a source of great depth extent.

Group II

This group forms a V-shaped pattern with Anomaly subgroup 35, 36, 38 on the east-west arm and Anomalies 39, 77, 40 on the north-south trending arm. The north-south arm

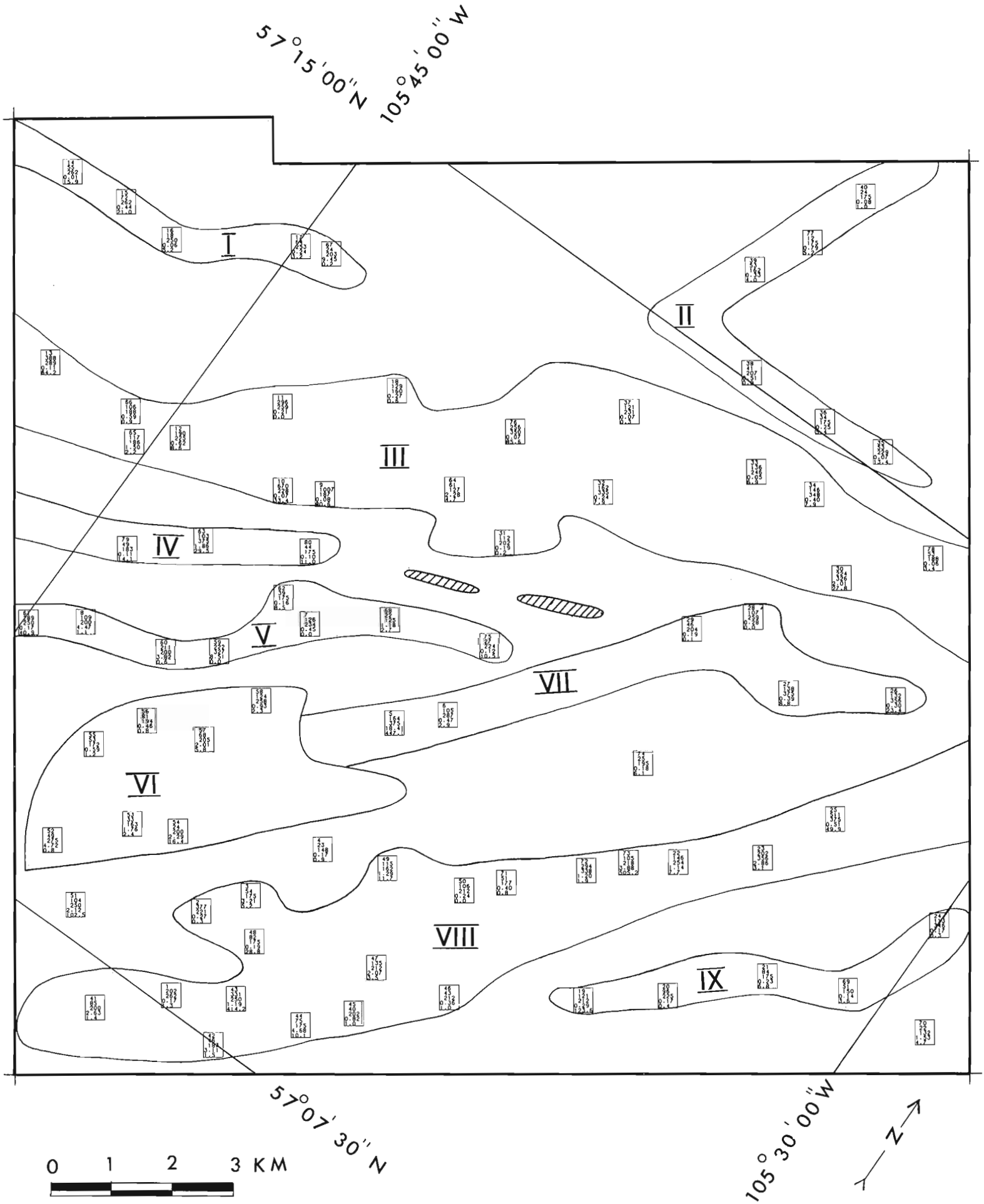

Figure 7.9. *Magnetization and depth estimates for Key Lake area as estimated from vertical gradiometer data. Gartner and Deilmann orebodies are shown as hatched areas.*

is more prominent in the total field and thus is likely to be due to sources of greater depth extent. The estimated depths of this arm are very consistent ranging from 12 m to 25 m below surface. The east-west arm is more erratic ranging from 25 m to 79 m, however the low residual error for 35 and 38 indicates that more confidence should be placed in these.

Group III

Depth estimates in this group range from 36 m to 198 m (Anomaly 64 must obviously be disregarded as it lies above surface). The deeper estimates are concentrated in the eastern portion. Good correlation between total field and vertical gradient data is obtained from all but Anomaly 65 in the western portion. The indication is that there is a break in depth between Anomalies 9 and 18 with contributions from just below surface to 250 m below surface in the east and from surface to approximately 150 m below surface in the western portion.

Group IV

This group includes three anomalies in a southwest-northeast trend below Group III. Anomalies 79 and 80 give depths of 33 and 25 m below surface, whereas Anomaly 63 indicates a depth of 225 m. The residual error for the latter determination is quite high.

Group V

All but Anomalies 62, 68, and 75 show good correlation between the total field and vertical gradient data. The values for Anomaly 68 must be rejected because they indicate a depth above the ground. The remaining estimates vary from 25 m to 139 m, with one determination (Anomaly 59) at 177 m below surface. The residual error for this case is, however, quite high.

Group VI

This group forms a cluster on the southwest end of a longer southwest-northeast trend. Correlation between the total field and gradiometer is poor except for Anomalies 53, 57, and 58. Depth estimates vary from 13 m to 125 m below surface.

Group VII

These anomalies appear on the continuation of Group VI with Anomalies 26 and 27 included because of similar appearance and proximity. Correlation between total field and vertical gradient data is good. Depth estimates range from 54 m to 225 m below surface.

Group VIII

This group lies on a southwest-northeast trend extending across the map area. Anomalies 41, 1, 2, 44, 49, 47, 50, 23 and 25 show good correspondence between the total field and vertical gradient. Depth estimates range from 25 m to 100 m below surface in the western portion with two estimates greater than 200 m on the eastern portion of the trend.

Group IX

This group lies on a southwest-northeast trend to the south of the previous group. All except Anomaly 24 show good correspondence between the total field and vertical gradient gradiometer. Depth estimates range from approximately 25 m to 200 m below surface, the deeper estimates again coming from the eastern extremity.

Comparison with Drillhole Data

Depths to basement were provided by the Saskatchewan Mining Development Corporation from holes drilled by Uranerz in 1979. It was possible to compare the estimated depth to the magnetic sources with the vertical depth to basement at or near 14 anomaly locations. Good agreement was obtained with drillhole trends between Anomalies 29 and 74 and along the orebodies between Anomalies 80 and 28. The estimate from Anomaly 29, however, appears to be shallow by approximately 50 m. Good agreement was also obtained at Anomalies 73, 31, 33 and 37. The estimated depth from Anomalies 61, 6, 73 and 32 appears to be too great by 50 to 100 m, whereas that from Anomaly 38 is shallow by approximately 30 m.

Conclusion

Depths to magnetic sources in the Key Lake map area appear to range from about 50 m below surface on the west to approximately 200 m below surface towards the east. As mentioned earlier, individual determinations cannot be considered as absolute because of the uncertainty depicted in Figure 7.8. On the other hand the maximum depth is fairly well defined and thus in the majority of cases can be taken as the maximum depth for the sources. The Archean basement is probably quite irregular, accounting for some of the variation. Depth extent is primarily shown by good correlation between the total field and vertical gradient and as this condition corresponds to the model, indicates more reliable results. An additional indication of reliability is the residual error and to a lesser extent the resolution parameter. The maximum information from the aeromagnetic data can only be attained by relating anomalies to the causative sources through drillhole information. This information could be used to determine the correct models to be used, thus improving reliability.

Acknowledgments

I would like to thank John Davies of the Saskatchewan Mining Development Corporation for providing the drillhole data, and E. Haley, Magnetic Methods Section of the Geological Survey of Canada, for assistance in preparing the figures.

References

Gatzweiler, R., Lehnert-Thiel, K., Classen, D., Tan, B., Voultsidis, V., Strnad, J.G., and Rich, J.
1979: The Key Lake Uranium-Nickel deposits; Canadian Mining and Metallurgical Bulletin, July, 1979, p. 73-79.

Hoeve, J. and Sibbald, T.I.I.
1978: Uranium metallogenesis and its significance to exploration in the Athabasca basin; in Uranium Exploration Techniques, G.R. Paslow ed., Saskatchewan Geological Society, Special Publication number 4.

Ray, G.E.
1977: The geology of the Highrock Lake-Key Lake vicinity Saskatchewan; Saskatchewan Department of Mineral Resources, Report 197.

Teskey, D.J.
1978: Design of a semi-automated three-dimensional interpretation system for potential field data; Unpublished Ph.D. thesis, Department of Mining and Metallurgy, McGill University, Montreal.

8. TERRAIN DISTURBANCE RESULTING FROM VEHICLE MOVEMENT, LONE GULL LAKE, CENTRAL KEEWATIN

Project 750077

P.A. Egginton and J.P. Ferris[1]
Terrain Sciences Division

Egginton, P.A. and Ferris, J.P., Terrain disturbance resulting from vehicle movement, Lone Gull Lake, Central Keewatin; in Current Research, Part B, Geological Survey of Canada, Paper 80-1B, p. 69-74, 1980.

Abstract

The movement of diamond drills by tracked vehicle and sleighs in central District of Keewatin was studied during the summer of 1979. Drill movement by tracked vehicle in some cases produced ruts up to 15 cm deep and/or completely severed the vegetation mat. In spite of this, in the short-term, the level of disturbance did not increase noticeably beyond that of the primary disturbance. There was no evidence of substantial induced thermokarst subsidence in an area of well drained till.

Loading by the vehicle was not uniform along the length of its track but was higher under the bogie wheels. Patterned ground forms such as ice wedge polygons, hummocks, and mudboils are common in the Lone Gull area. The topographic irregularities produced by these features may be sufficient to induce normal stresses up to 500 per cent higher than those recorded on a flat surface.

Introduction

At Lone Gull Lake, located some 80 km west of Baker Lake, District of Keewatin, a 40-man camp was maintained by Urangesellschaft Canada Ltd. in support of a delineation drilling program (Fig. 8.1). At the request of Department of Indian and Northern Affairs (DINA) a program was initiated primarily to monitor the terrain disturbance resulting from the movement of diamond drilling equipment using a tracked vehicle on different material types and under various conditions throughout the summer. Tests to study the normal stress on the ground surface produced by the vehicle movement also were conducted. The four diamond drills used were commonly moved less than 50 m within a 3 km^2 area. It was originally planned to use a tracked vehicle for the majority of moves; unfortunately, because of a contract dispute, the tracked vehicle was used only to a limited degree, and a helicopter was used in its place. This paper presents preliminary results of the monitoring program. A discussion of all aspects of the 1979 program is presented by Ferris (1980).

Acknowledgments

The authors would like to thank the following for the support provided: D.M. Barnett, K. MacInnes, J. Umpherson, and J. Scotti (DINA) and P. Hesse and K. Greip (Urangesellschaft Canada Ltd.).

Normal Stress Tests

The vehicle used for drill movement was identified by the owner as a Nodwell RN-75, having a single track width of 1.06 m and a length of 3.85 m. These dimensions resulted in an average normal stress on the ground of less than 13.0 kPa.

All normal stress tests were conducted with the empty vehicle only; planned tests with the vehicle under load or moving a drill were not carried out because of contractual problems between Urangesellschaft and the vehicle owner. The tests are not definitive but indicate that topographic irregularities, such as hummocks or other patterned ground forms, may act to localize normal and shear stresses significantly above those expected on the basis of flat ground performance.

The tests were designed to determine the normal stress applied by the vehicle on till. The three tests included: 1) a traverse of flat ground, 2) crossing hummocky terrain headon, and 3) crossing hummocky terrain side-on (Fig. 8.2). A nest of pressure sensors was buried at a selected location, then the vehicle was manoeuvered into position over the sensors. The gauges were read manually as the drive sprocket (S) and each wheel (numbered along one side from the front, W1, W2, W3) and intermediate points between the wheels passed over the sensors (Fig. 8.2, 8.3).

The track of the vehicle had a series of bolts anchoring cleats to the track bottom (Fig. 8.2). The cleats formed a depression for the bogie wheels such that the centre of the track protruded below the main track surface. The pressure sensors were buried at depths of 5 and 10 cm at the track edge and track centre, respectively to avoid sensor damage from the cleats. On the basis of Newmark stress with depth charts (Lambe and Whitman, 1969), the pressure differential recorded at these depths represents about 90 per cent of the actual normal stress generated at the ground surface; however, no corrections were made in the data presented.

Flat Ground Test

For the test on flat ground, one gauge was placed under the central portion of the left track and one under the outer edge of the left track. A graph of normal stress on the ground surface produced when different portions of the vehicle were positioned over the sensors is presented in Figure 8.3. The numbering sequence of the wheels and sprocket form the abscissa of the graph.

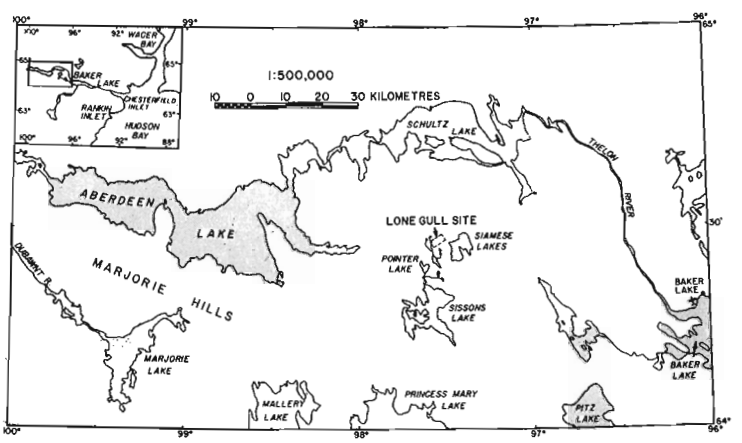

Figure 8.1. *Lone Gull Lake site, the location of the vehicle monitoring program.*

[1] Carleton University, Ottawa, Ontario

In this test and in subsequent tests differential pressures generated when a wheel passed over the sensor were substantially higher than when a portion of the track with no wheel immediately above passed over the sensor. Loads were not distributed uniformly over the entire track; the wheels provided pressure points where stresses were commonly 300 per cent higher than under the rest of the track. This may have resulted in part from incorrect track tension; if the track is too slack the wheels act as pressure points.

Because a ridge protruded along the centre of the track, normal stress was greater under the track centre than under the edge. In spite of this variation, measured differential pressures were essentially the same as those expected on the basis of load and track area computations. Soil compaction was limited as the pressure gauges returned to or near 0.0 kPa after the vehicle had passed over the site (Fig. 8.3).

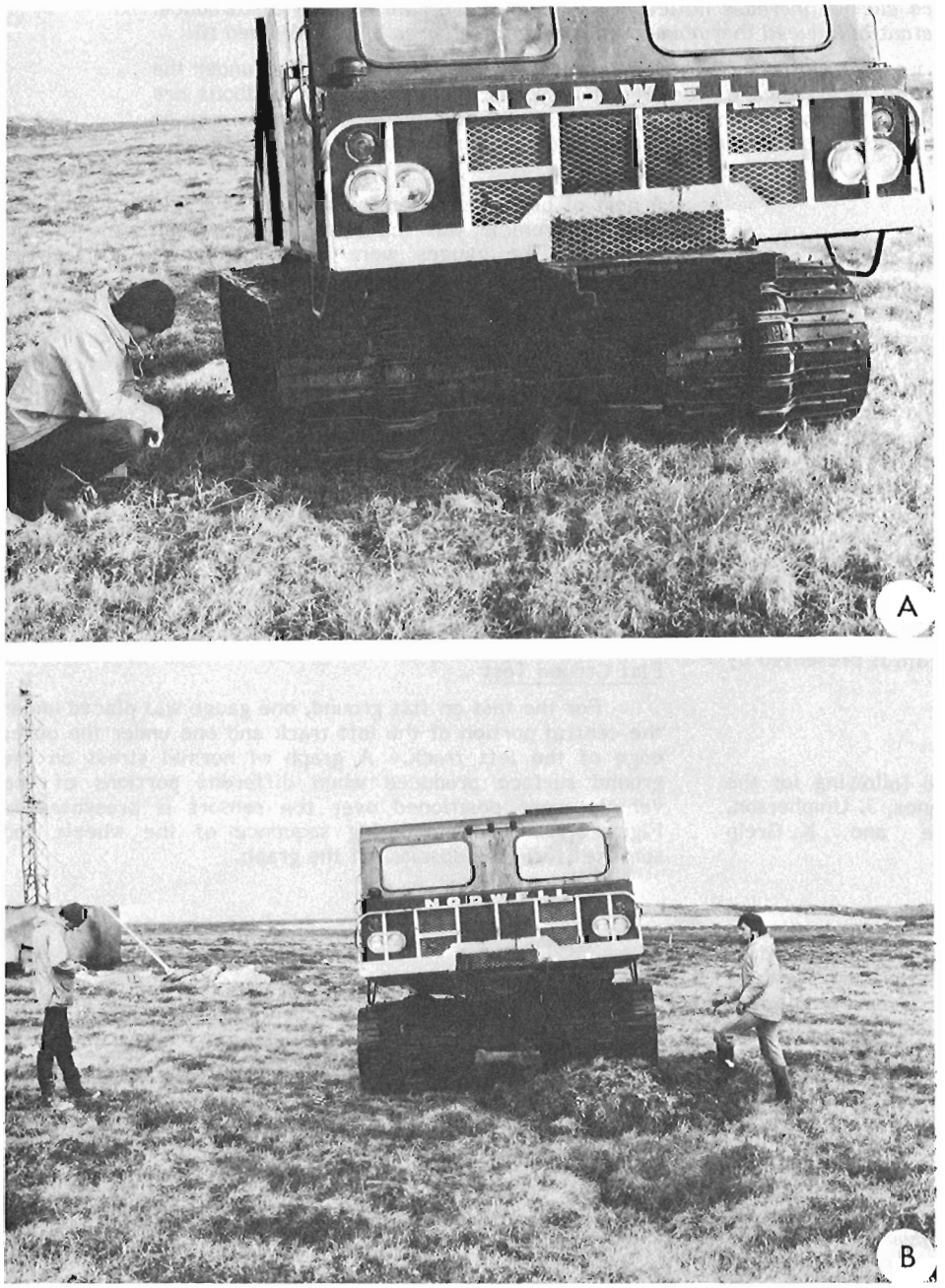

Figure 8.2 *Test sites where normal stresses applied by a tracked vehicle were measured: A, site of the flat ground test. B, site of the hummocky terrain, side-on test. The site of the hummocky terrain, head-on test was similar to that of B. Note the channel formed by the track cleats which act as a guide for the bogie wheels.*

Head-on Hummock Traverse

Three pressure sensors were used for this test: (1) was located on flat ground at the edge of the track; (2) was located on flat ground under the centre of the track, and (3) was located on a hummock top under the track centre (Fig. 8.2, 8.3). Predictably, readings were highest at sensors (1) and (2) when the vehicle began to climb the hummock; differential pressures 100 per cent higher than those recorded in the flat ground test were generated. As the front wheel passed over the hummock, pressures of 55.5 kPa, or 500 per cent higher than the highest values recorded during the flat ground test, were measured. Compaction occurred at sensor sites (2) and (3) as total relaxation (0.0 kPa) did not occur after the passage of the vehicle, and depressions 2 to 15 cm in depth were produced (Fig. 8.2).

Side-on Hummock Traverse

In this test the vehicle listed to one side as it was driven over a hummock. Three sensors were positioned under the lower track: under either edge and in the track centre (Fig. 8.2, 8.3). The highest readings were recorded in the track centre (24.0 kPa), and as might be expected lower readings were recorded under the inside of the lower track than under the outside track edge (maxima of 6.9 and 13.8 kPa, respectively).

Drill Movement

Substantial disturbance resulted from a single drill move by tracked vehicle across an area of till on June 18, 1979. The drill was moved on a wooden skid, 5.5 m long and 3.5 m wide, on three runners 0.15 m wide. The drill with the mast removed was winched onto the skid which then was dragged by Nodwell to the next site. The theoretical average normal stress applied by the loaded skid was less than 13.0 kPa.

The till surface is dominated by bare centre mudboils that have well vegetated borders. Three trips were required to move the drill and its associated equipment between sites, a distance of approximately 50 m. Because the vehicle and skid required a large turning radius, a substantial ground area was traversed by the vehicle (Fig. 8.4).

Little disturbance occurred when the skid was empty, and the vehicle and skid moved forward in a straight line, such as when the vehicle first entered the drilling area (A, Fig. 8.4). The ground-bearing capacity measured by a pocket penetrometer averaged 53 kPa, a value substantially higher

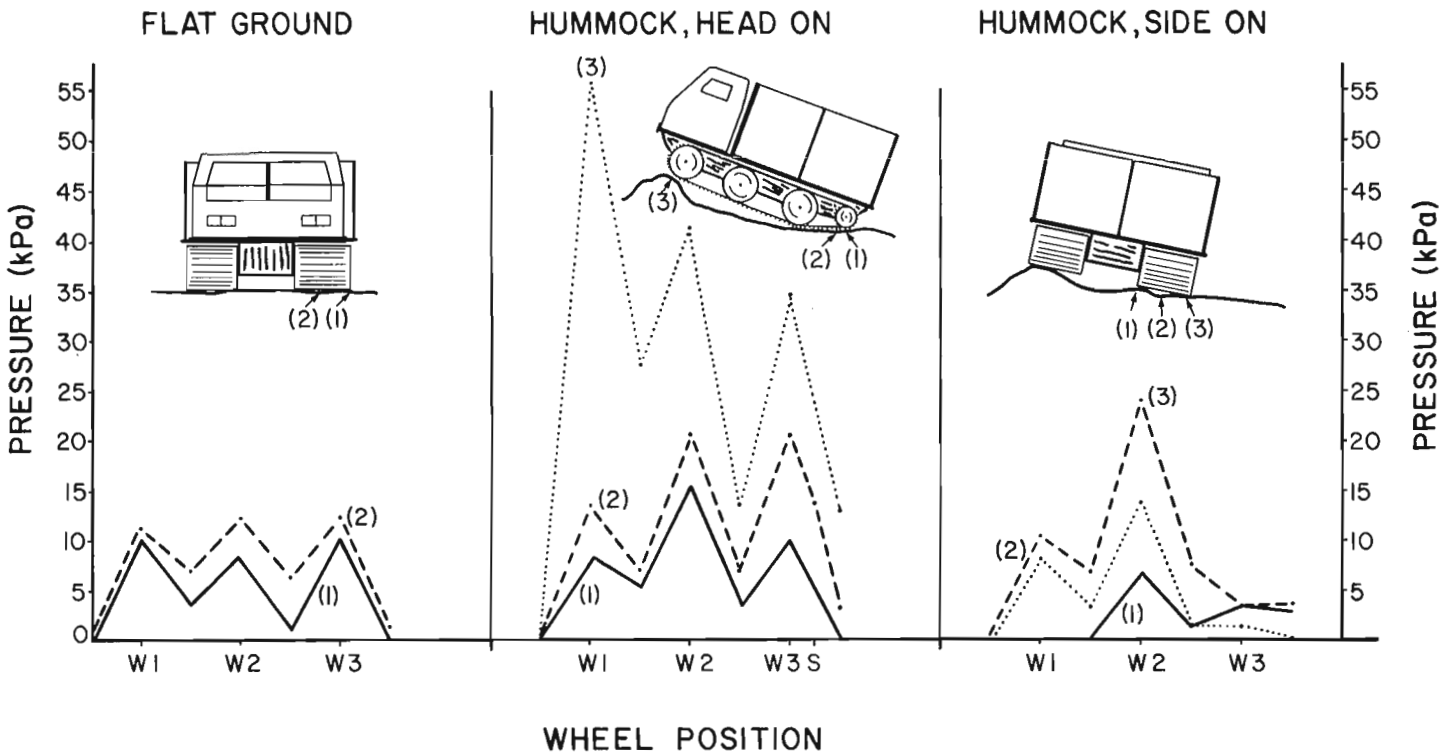

Figure 8.3. *Normal stress on the ground surface produced by a tracked vehicle. The numbers (1), (2), and (3) refer to the location of individual pressure sensors (see text).*

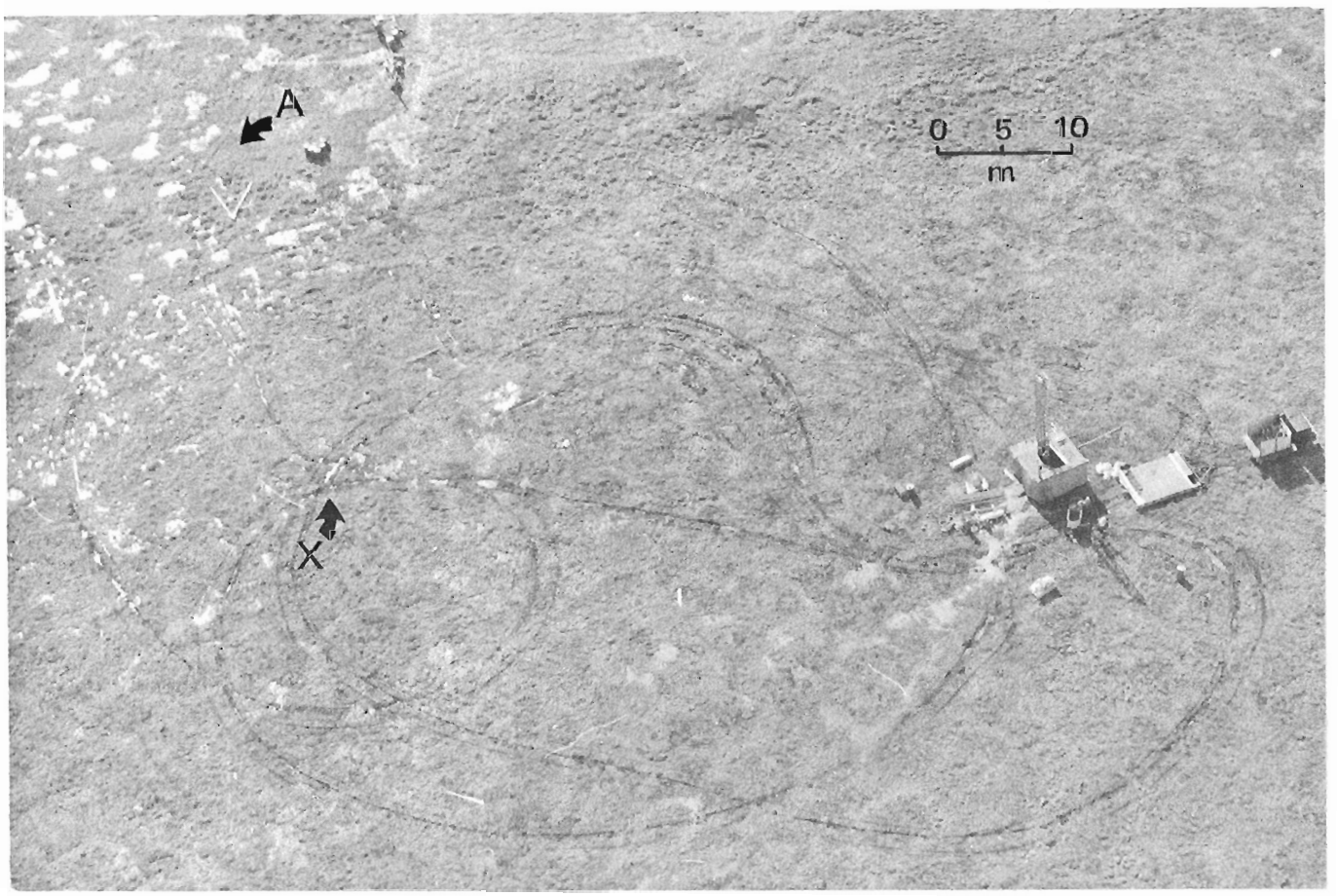

Figure 8.4. *Aerial photograph of vehicle tracks associated with the June 18, 1979 drill move. 'X' locates the position of the drill prior to the move. When the vehicle with the unloaded skid in tow travelled in a straight line, such as at 'A' where it first entered the area, little disturbance occurred. Small radius turns under load caused the greatest terrain disturbance.*

than the static theoretical or measured flat ground normal stress exerted by the vehicle or the skid. In spite of a high bearing capacity, ruts up to 15 cm deep were produced due to track slippage when the drill was moved. Slippage occurred during start-up under load, and sheets of vegetation were sheared from their roots. In some cases the damage appeared minimal, but the vegetation mat could be turned over by hand (Fig. 8.5). Sharp turns resulted in shearing under at least one track, and in addition the ground surface was ploughed by the skid runners as they slipped sideways across the tundra. The latter occurrence was aggravated by cracked joists on the skid which placed undue load on the central runner (Fig. 8.6). The steel cleats of the vehicle cut the vegetation into strips. It is not known whether these strips will reroot or whether they will die; however, the larger severed mats (Fig. 8.5) did not show any signs of recovery by the end of the summer.

Figure 8.5. *An area of apparently limited disturbance. The tracked vehicle moved the drill across this particular site without creating ruts; however, the vegetation mat was severed at the root layer, and pieces of the mat could be flipped over easily by hand.*

Figure 8.6. *An area of rutting associated with sharp turns made by the vehicle moving a drill. The tracks in the foreground were monitored for subsidence by means of bedstead recorder (see text).*

As a result of the disturbance level of this single move, the company decided to suspend drill movement by tracked vehicle until a more suitable skid was obtained. Later, because of a contractual dispute, tracked vehicle movement was suspended completely for the summer.

Track Monitoring

An area of two single vehicle passes associated with the June 18, 1979 drill move was monitored to determine whether the level of disturbance increased over time as a result of thermokarst subsidence (Fig. 8.6). A bedstead recorder was installed to record ground surface movement.

The bedstead consisted of three copper-clad rods, 1.6 cm in diameter and 2.4 m long, which were driven into the permafrost. The rods were arranged in a straight line and spaced 3 m apart. Aluminum tubing was run between and was attached securely to the rods. Holes were drilled perpendicular to the ground surface at 15 cm intervals along the tubing, and aluminum rods were passed through the holes to rest on locators on the ground surface. The change in position of the aluminum rods, relative to the tubing, provided a measure of ground heave or subsidence. The system is similar to one described by James (1971). The bedstead recorder monitored both disturbed terrain, associated with two vehicle passes, and adjacent nondisturbed terrain.

Ground surface movement relative to the ground surface position on June 21, 1979 at the bedstead site is presented in Figure 8.7. During the latter part of June some surface heave occurred as a result of diurnal or short duration freezebacks. Wet areas with high heat capacities, such as the track depressions, generally did not heave in response to these short-term fluctuations about the freezing point (see June 25, Fig. 8.7).

By the end of the monitoring period the ground surface in the tracked areas had subsided to a greater degree than at the nondisturbed sites; however, the variation was small. Typical subsidence values by August 27, 1979 were 5.5 cm in zones of disturbance and 4.0 cm in nondisturbed vegetated areas (Fig. 8.7). The majority of the recorded subsidence resulted from simple active layer thaw progression: During winter freezeback segregated ice forms in the active layer causing the ground to heave, and during summer thaw the ground subsides. The yearly subsidence values are similar to those reported for till in the Henik Lake region, central District of Keewatin (Egginton, 1979). The difference in subsidence between the disturbed and undisturbed sites (1.5 cm) was associated with a thickening of the active layer at the disturbed sites.

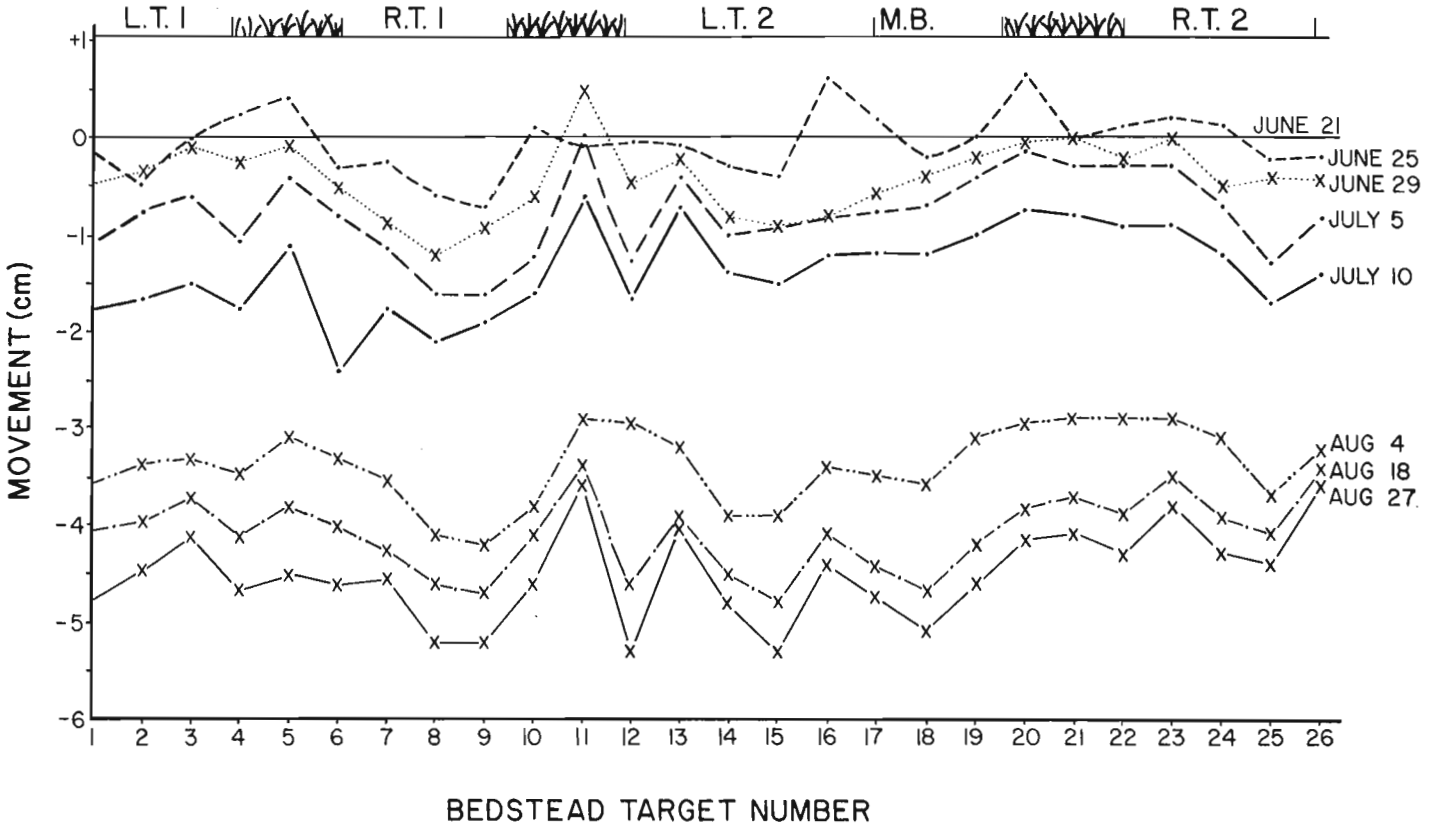

Figure 8.7. *Ground surface movement at the bedstead site 1979 (see Fig. 8.6). Two passes over the same area were monitored. LT1 and LT2 locate the left track during pass 1 and pass 2, respectively. The level of disturbance was not identical for both passes or tracks. M.B. locates a mudboil centre. All movements were measured relative to the position of the ground surface on June 21, 1979.*

The thaw progression of the active layer was periodically measured throughout the summer by probing with a thin metal rod. For two weeks following the June 18, 1979 drill move the depth of thaw increased more rapidly in the terrain disturbed by vehicle passage than in adjacent undisturbed areas (see June 21 and July 1, Fig. 8.8). This rapid increase in thaw depth in the disturbed terrain is associated with a localized decrease in albedo and an associated increase in surface temperature (Ferris, 1980). As the depth of thaw increased beyond 100 cm, the rate of thaw became more uniform at the site as a result of heat dissipation throughout the thawed zone. Depth of thaw in the disturbed areas (≃139.0 cm) was greater than in the nondisturbed areas (≃131.0 cm).

Discussion

The drill move on June 18, 1979 resulted in an increase in the active layer in the tracked areas in comparison to the undisturbed sites. It is assumed that all portions of the bedstead site with similar vegetation cover had the same equilibrium active layer depth (131.0 cm) prior to disturbance. Because up to 15.0 cm of the active layer was removed by rutting and because disturbed sites developed equilibrium active layers typically 8.0 cm (139.0-131.0 cm) greater than nondisturbed sites, some degradation of the permafrost obviously occurred. The total degradation can be calculated as follows: Approximately 15.0 cm of the permafrost degraded to replace that portion of the active layer removed by rutting. The change in surface characteristics (albedo, ground surface temperature, etc.) at the disturbed sites caused the active layer to thicken by an additional 8.0 cm (139.0-131.0). In addition, the difference in subsidence between disturbed and nondisturbed sites, 1.5 cm (5.5-4.0), is attributed to the degradation of ground ice in the permafrost. Therefore, the total degradation of the permafrost in the disturbed till monitored was approximately 24.5 cm (15.0 + 8.0 + 1.5 cm).

In spite of the degradation, it is interesting to note that only limited thermokarst subsidence was associated with it; however, massive ground ice is not typical of till in this region.

A complete program of monitoring vehicle performance on the various terrain types at Lone Gull Lake was not possible in 1979. Cursory observations here and elsewhere in central District of Keewatin suggest that in poorly drained sites, small ponds may form at the junction of two or more sets of vehicle tracks, inducing thermal degradation of the permafrost. Marine or alluvial deposits in low-lying areas overlain by a thick vegetation mat may be particularly vulnerable. These areas can contain significant volumes of segregated and/or foliated ice (ice wedges). The vegetation provides considerable insulation as thaw depths measured in alluvial deposits at Lone Gull Lake were only 25 per cent of those on nearby more sparsely vegetated upland till areas. In 1979, the disruption of the vegetation mat by vehicle movement at test sites in low-lying areas lead to a localized thickening of the active layer by 300 per cent and to some thermokarst subsidence (Ferris, 1980).

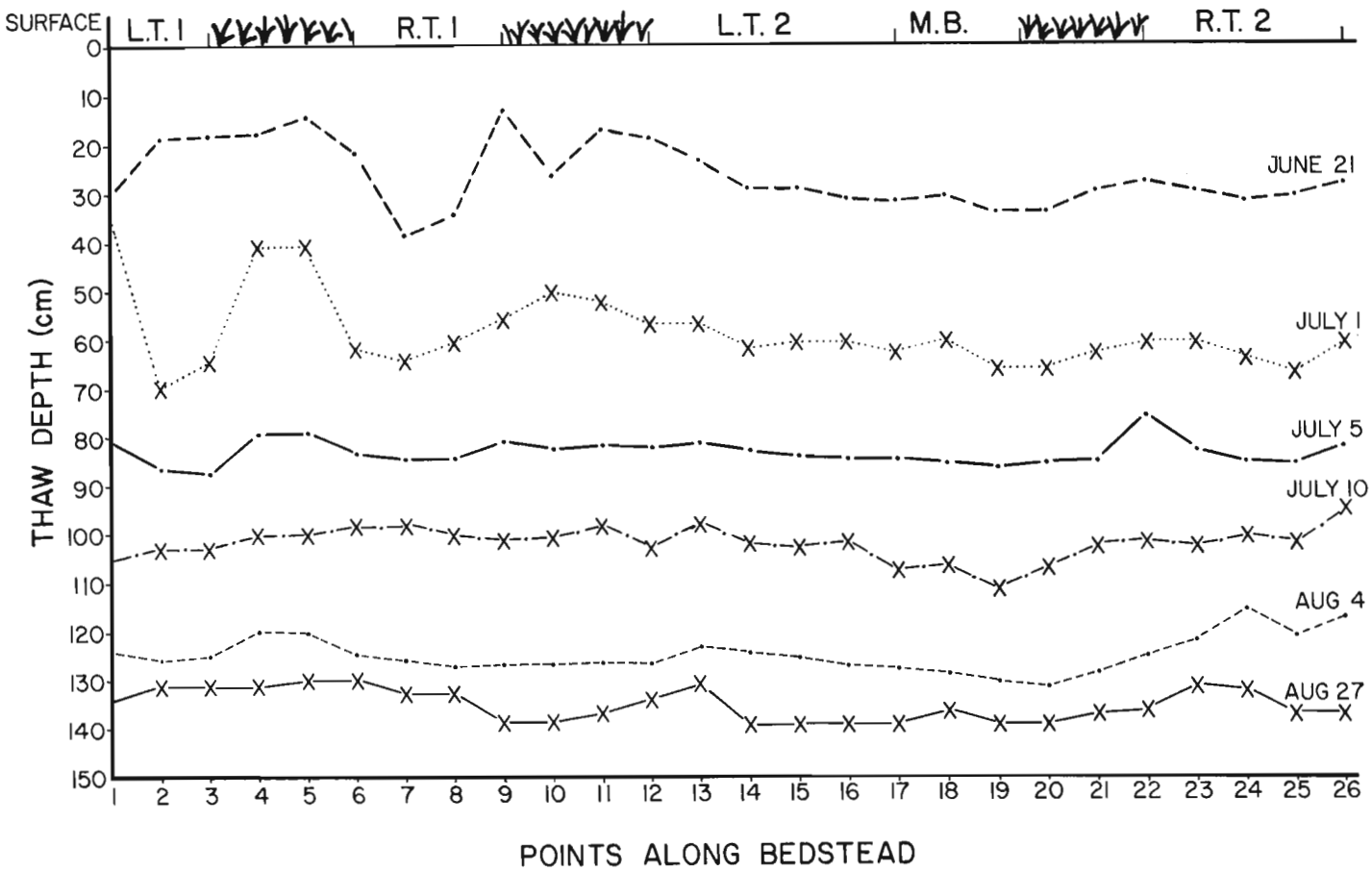

Figure 8.8. *Thaw depth progression associated with the bedstead recorder site. Although the ground surface (0.0) is displayed as being flat, ruts up to 15 cm deep occurred in the track centres, LT1, RT1, etc. (see Fig. 8.6).*

Summary and Future Studies

Small irregularities in the surface topography of more or less flat terrain were sufficient to increase normal stresses produced by a tracked vehicle 500 per cent above those produced on a flat surface. The distribution of shear stresses may be assumed to be similarly affected by local topographic variation. Track tension is important for an even load distribution; a slack track causes undue stress to be placed on the ground surface under the bogie wheels. All stress tests conducted in 1979 were static tests; future tests are planned to include dynamic loading by the vehicle. An attempt will be made to relate vehicle operating procedure, geotechnical properties of the materials, and terrain performance.

To date only limited information on terrain performance is available. A single drill move by the tracked vehicle on June 18, 1979 produced ruts up to 15 cm in depth in an area of well drained till. The vegetation mat was sheared as a result of track slippage during start-up under load. Track slippage also occurred when tight turns were made. In spite of this disturbance, there was no evidence of substantial thermokarst subsidence in an area of well drained till. In future this type of monitoring will be expanded to cover the range of surficial materials present in the area. The effect of single and multiple passes on disturbance levels also will be investigated.

References

Egginton, P.A.
1979: Mudboil activity, central District of Keewatin; in Current Research, Part B, Geological Survey of Canada, Paper 79-1B, p. 349-356.

Ferris, J.P.
1980: Observations on summer vehicle traffic and drilling operations in the District of Keewatin; unpublished report presented to Department of Indian and Northern Affairs, Yellowknife, 43 p.

James, P.A.
1971: The measurement of soil frost-heave in the field; British Geomorphological Research Group, Technical Bulletin, no. 8, 43 p.

Lambe, T.W. and Whitman, R.V.
1969: Soil Mechanics; John Wiley and Sons, New York, p. 97-116.

9. LATE QUATERNARY SEA LEVELS IN THE SOUTHERN BEAUFORT SEA

Project 740086

D.L. Forbes[1]
Terrain Sciences Division

Forbes, D.L., Late Quaternary sea levels in the southern Beaufort Sea; in Current Research, Part B, Geological Survey of Canada, Paper 80-1B, p. 75-87, 1980.

Abstract

Data on late Quaternary sea levels in the Beaufort Sea are extremely limited, yet the sea level chronology in this area is of some importance for studies of continental ice loading, submarine permafrost and ice scour, and deltaic sedimentation. The evidence suggests that deviations from published eustatic curves have occurred in the region, and indeed the concept of local correspondence with a worldwide eustatic pattern appears to be outmoded. A hypothetical history for the Mackenzie Delta is proposed which includes limited isostatic depression due to late Wisconsin ice, minor uplift, and renewed subsidence due to forebulge collapse or sediment loading. A mid-Wisconsin transgression of the order of 10 m higher than present sea level is suggested by evidence in the Mackenzie Delta area and in north Alaska, but no evidence for sea levels higher than present since the late Wisconsin has been found west of Cape Bathurst. Coastal morphology, radiocarbon and archeological dates, and plausible mechanisms suggest a recent and perhaps continuing regional submergence. The tidal record at Tuktoyaktuk is insufficient to resolve the contemporary trend of sea level.

Introduction

This report is an attempt to collate available data pertaining to late Quaternary sea level fluctuations in the Mackenzie Delta area and elsewhere in the southern Beaufort Sea. It is the third in a series of regional summaries, in which the Pacific Coast (Clague, 1975) and the Queen Elizabeth Islands (Blake, 1976) have figured previously. These form part of the contribution of the Terrain Sciences Division to the International Geological Correlation Programme (IGCP) Project 61 on Holocene sea level changes.

Late Quaternary sea levels are perhaps less well documented in the southern Beaufort Sea than in any other major coastal region in Canada. Without a sea level chronology, the duration and areal extent of seafloor emergence in late Quaternary time cannot be established. This data gap presents a serious impediment to studies of submarine permafrost and ice scour processes in the Beaufort Sea, and of the history of the distinctive sedimentary bodies, notably the Mackenzie Delta (C.P. Lewis, 1977), found in the region. Mackay (1963) presented a review of sea level data in the Mackenzie Delta area, and it is noteworthy that few additional ^{14}C dates of relevance have become available since then. However subsequent reinterpretation of late Wisconsin ice limits, some additional stratigraphic and chronological data, and consideration of characteristic lithospheric response in ice-marginal areas, suggest a history involving neither postglacial sea levels higher than present nor exact correspondence with published eustatic curves.

The concept of a 'stable' locality, in which the sea level history can be taken to represent a global or 'eustatic' trend, is suspect (Curray and Shepard, 1972). Indeed it is now clearly evident from recent geophysical studies, particularly that of Walcott (1972a), that deformation of the earth at great distances from former ice sheets may occur in response to the redistribution of load accompanying climatic change. Furthermore, isostatic depression beneath large loads such as the Laurentide Ice Sheet may be accompanied by forebulge uplift in ice-marginal areas; such a feature has been documented in eastern North America (e.g. Grant, 1975; Walcott, 1972b). Therefore it is not possible, in the Beaufort Sea area, to assume that insignificant isostatic adjustments and close correspondence with 'worldwide eustatic' curves have occurred. Unfortunately the data base in the southern Beaufort Sea does not yet permit the establishment of the local history in any but the most general terms.

Regional Setting and History of Wisconsin Glaciation

The physiography of the region is summarized in Figures 9.1 and 9.2. The Beaufort Sea shelf trends roughly east-west and is relatively narrow (40 to 100 km) and shallow, with the shelf break at 100 m depth or less. West of the Mackenzie Delta, the subaerial Arctic Coastal Plain, also narrow (10 to 100 km), is flanked on the south by mountains that form parts of the Romanzoff Uplift and Aklavik Arch. East of the Delta, the Coastal Plain occupies the Tuktoyaktuk Peninsula and merges with an extensive plain south of Eskimo Lakes and Liverpool Bay. The Aklavik Arch trends northeast from the Richardson Mountains beneath the Mackenzie Delta; it was active locally as late as mid-Tertiary time (Norris, 1973). Thick accumulations of Cretaceous and Tertiary clastic sediments are found off the northwest flank of the Aklavik Arch (in the vicinity of Kugmallit Bay) and in structural depressions within the Arch. The Mackenzie Delta occupies a glacially scoured structural depression, developed by late Cretaceous block faulting (Yorath, 1973). This depression extends seaward to Mackenzie Canyon as a partially infilled box-like trough, trending northwest across the shelf to intersect the continental slope at a depth of about 400 m (Canadian Hydrographic Service, 1973a; Shearer, 1972). West of the Delta, the Arctic Coastal Plain merges on the south with an extensive post-Paleocene pediment. This surface and underlying beds rise towards and into the mountains, but appear also to be tilted down towards the northwest (Rampton, in press) with a slope of approximately 0.75 m/km. The date of the presumed tilting has not been established.

Parts of this region were glaciated in early Wisconsin time or earlier by Laurentide ice moving west and northwest along the Mackenzie trough out across the Beaufort Sea shelf and adjacent coastal plain. The early Wisconsin advance has been termed the Buckland Glaciation (Rampton, in press). The limit of this glaciation, plotted in Figure 9.2 (after Hughes, 1972), lies against the northern slope of the Richardson Mountains, along the southern edge of the coastal plain, and across the present coast west of Herschel Island. East of the Mackenzie Delta, the limit lies north of Eskimo Lakes and southern Liverpool Bay, extending north into Kugmallit Bay east of Tuktoyaktuk.

Extensively deformed frozen sediments on Herschel Island, the coastal hills southeast of Kay Point, and elsewhere, are considered to be the result of ice thrusting by

[1] Department of Geography, University of British Columbia, Vancouver, B.C., V6T 1W5

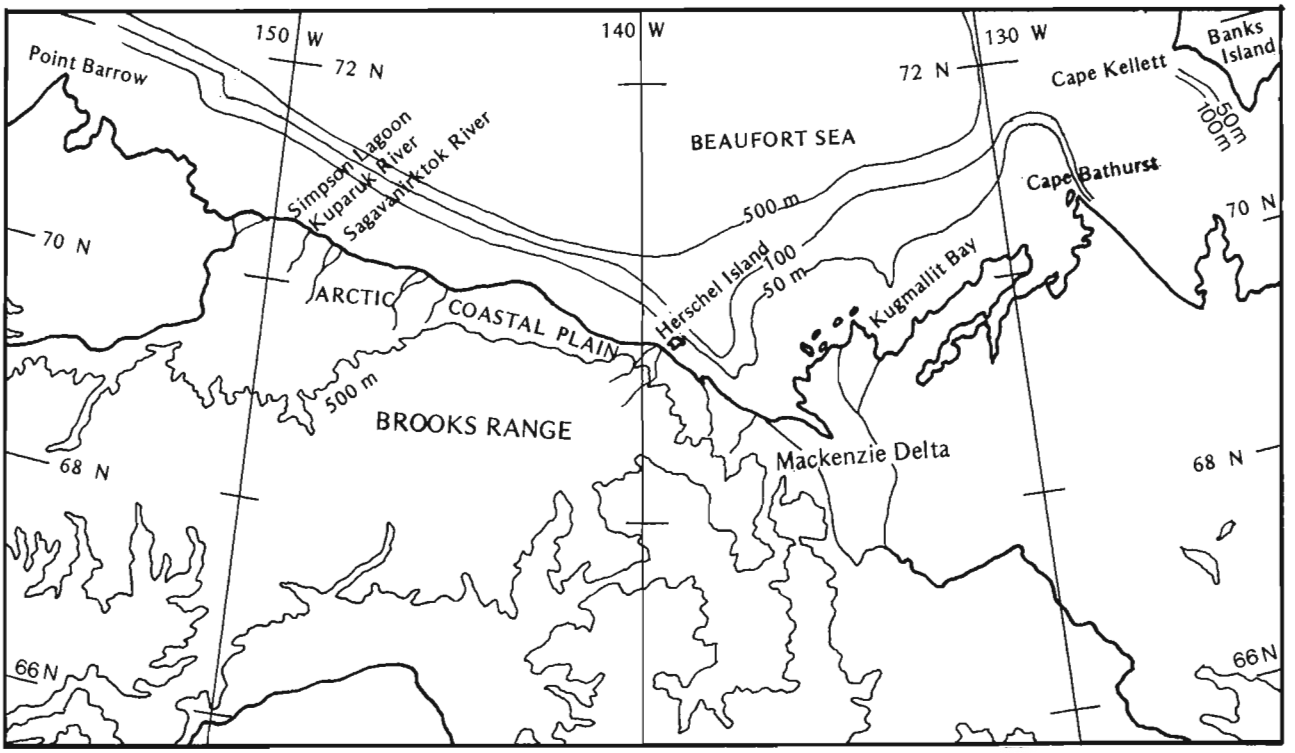

Figure 9.1. *Location map showing Beaufort Sea coast from Point Barrow, Alaska to Banks Island. Note, submarine valley delimited by the 50 m isobath north of Kugmallit Bay, broad shelf north of Cape Bathurst, and partially infilled trough of Mackenzie Canyon trending northwest from the delta front off Herschel Island.*

the early Wisconsin advance (Mackay, 1959). This event appears to be much older than 40 000 years (Mackay et al., 1972) and may be Illinoian (J.R. Mackay, personal communication, 1979). From evidence of a late Wisconsin ice limit descending northward to less than 300 m a.s.l. west of Aklavik (Hughes, 1972) and to less than 200 m near Inuvik (Rampton, in press), it is now thought that late Wisconsin ice did not extend northwest of Shallow Bay (Mackenzie Delta front) and may have been less extensive than previously believed east of the Mackenzie Delta (J.R. Mackay, personal communication, 1979; Rampton, in press). The prominent moraine ridge parallel to the Yukon coast, previously considered to be the probable late Wisconsin limit, recently has been interpreted as the southern margin of a major stillstand or readvance (termed the Sabine phase) of the Buckland (early or pre-Wisconsin) Glaciation (Rampton, in press). The inferred date of maximum late Wisconsin ice extent in this area is between 13 500 and 14 000 years B.P. (Prest, 1969; Mackay et al., 1972).

Chronological Control and Evidence of Varying Sea Level

Radiocarbon and archeological dates relevant to the history of sea level in the southern Beaufort Sea are listed under three regional headings in Table 9.1. Most dates provide circumstantial or negative evidence and very few allow the position of a former shoreline to be fixed with any confidence. In the following discussion, present elevations of shore or other features are given relative to modern datum (e.g., '-10 m' refers to a depth of 10 m below present mean sea level).

Numerous topographic elements point to changes in the relative elevation of land and sea in this region. Emergent terrace or beach features of widely varying age are present, although not prominent, throughout the region. All apparently predate late Wisconsin glaciation. On the other hand, submerged fluvial topography is evident in several places beneath the Beaufort Sea (Mackay, 1963; D.M. Hopkins, personal communication, 1979). A rise of sea level is indicated by many drowned valleys along the coast (Fig. 9.3), including Roland Bay and inlets east of King Point on the Yukon coast, Canyanek Inlet and Tuktoyaktuk Harbour on Kugmallit Bay, and several estuaries and embayments in Liverpool Bay.

Evidence suggesting recent rise of mean sea level comes from archeological sites of Thule culture at Cape Kellett, southwest Banks Island (Fig. 9.1), that in the early 1950s were being undermined by storm tides (Manning, 1953) and from Thule sites on Herschel Island below modern sea level (R.J. MacNeish, cited by Bird, 1967; B. Walker-Yorga, personal communication, 1979). These sites may be less than 1000 years old. At Stokes Point, on the central Yukon coast, a series of old beach ridges, developed under a regime of net southeastward longshore drift, shows evidence of submergence in the older (western) part of the complex (Fig. 9.4). In the absence of subsurface data, however, thaw or other consolidation processes cannot be eliminated as plausible causes of local subsidence. Nevertheless, the entire southern Beaufort Sea coast, dominated by barrier and spit deposits, lagoons, and numerous drowned valleys, presents a classic example of submergent morphology.

Emergent Coastal Features of Mid-Wisconsin Age or Older

Terraces adjacent to Harrowby Bay, Wood Bay, and the Kugaluk River estuary were originally thought to demonstrate marine transgression postdating the last ice advance (Mackay, 1963). This conclusion was strongly supported by the belief that a late Wisconsin ice margin

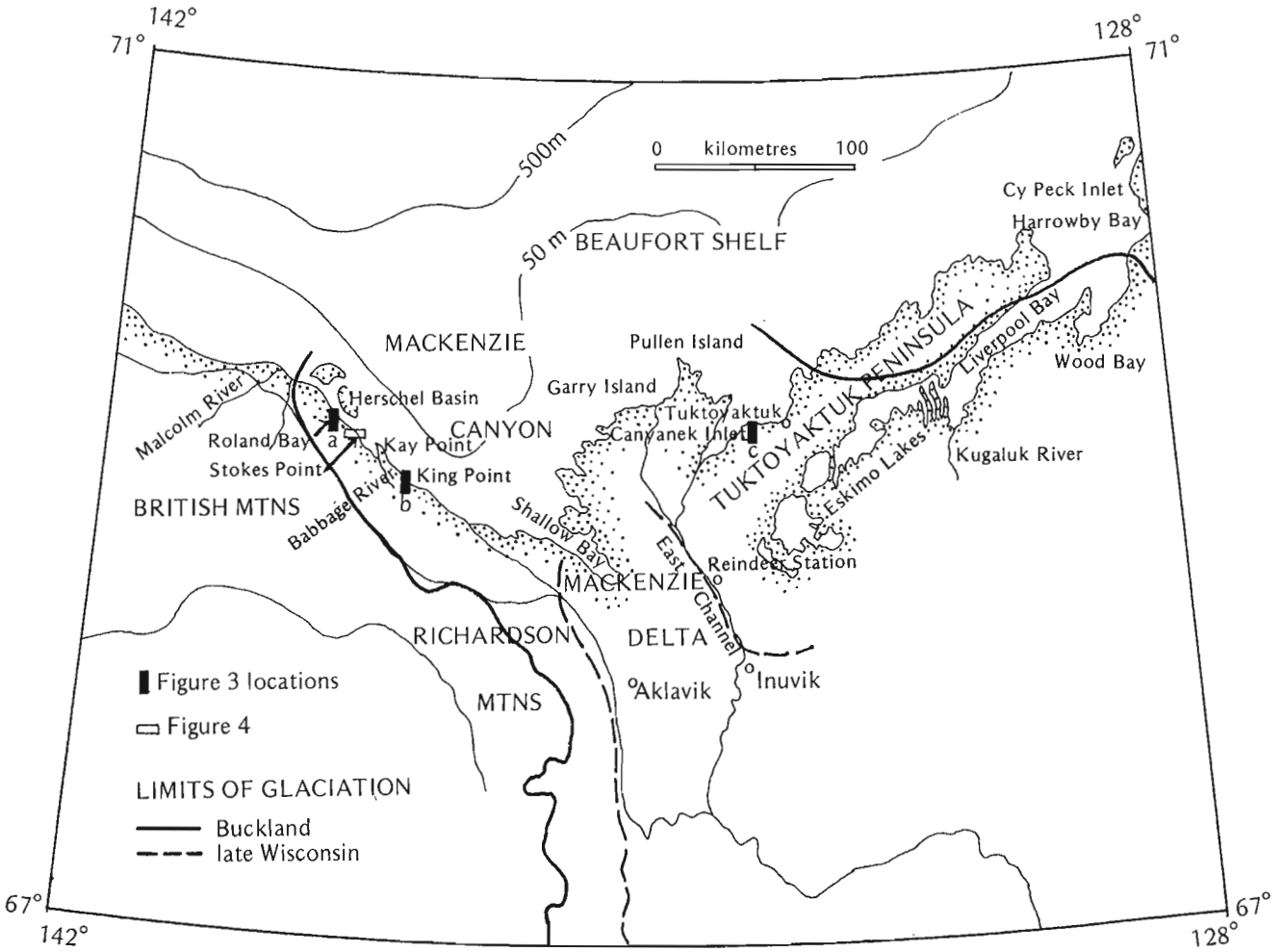

Figure 9.2. *Mackenzie Delta area and Yukon coast, showing limits of Buckland Glaciation and late Wisconsin advance. Locations of Figures 9.3 and 9.4 are indicated.*

existed along Tuktoyaktuk Peninsula, as indicated for example by Mackay et al. (1972). The late Wisconsin ice is now thought to have stopped south of Liverpool Bay (J.R. Mackay, personal communication, 1979), and the terraces may represent a mid-Wisconsin or earlier transgression. Alternatively, they may represent outwash valley train deposits of various ages, graded to sea level at or below present datum; several dates cited in Table 9.1A support this hypothesis (V.N. Rampton, personal communication, 1979).

Other subdued terrace features are present on Garry Island (elevation approximately +8 m) with marine shells dated >35 000 years B.P. (GSC-562; Kerfoot, 1969; revised date in Lowdon et al., 1971). On Pullen Island at +3 m, pelecypod shells from beach gravel cutting older sands were dated >23 000 years B.P. (GSC-1877; Lowdon and Blake, 1976, sample collected by J.M. Shearer). Downstream from Reindeer Station along East Channel, Mackenzie Delta, fluvial or deltaic sediments no younger than early Wisconsin are found up to about +50 m (Mackay and Mathews, 1973).

On the Alaskan coast marine shells in the upper Gubik Formation near Kogru River, with a finite date in the mid-Wisconsin, indicate a sea level about +15 m (E. Reimnitz, personal communication, 1978). In the Point Barrow area, a transgression to +8 m or higher in mid-Wisconsin time has been reported by Sellmann and Brown (1973).

Evidence for Early or Late Wisconsin Marine Regression

Sagavanirktok River valley (Fig. 9.1) extended north and west from the present outlet to a depth of at least -50 m (D.M. Hopkins, personal communication, 1979). Other data kindly provided by Hopkins point to widespread emergence of the Beaufort Shelf north of Alaska; these include a date of 42 000 ± 1440 years B.P. (USGS-249) for an extensive detrital peat layer at about -50 m.

A valley extending northward from Kugmallit Bay (Canadian Hydrographic Service, 1973b) and a broad terrace that may represent a delta at about -50 m (Mackay, 1963) north of Liverpool Bay (Canadian Hydrographic Service, 1974; see Fig. 9.1) may indicate the lowest Wisconsin sea level in this region. The Kugmallit Bay valley is well defined at -70 m, may be present at -80 m, and reappears on the chart as a narrow feature that may have originated as a submarine canyon at -90 m and deeper. Assuming a minimum sea level between -70 and -80 m and a rough estimate of global Wisconsin eustatic depression amounting to -92 m (Flint, 1971, p. 318) or -100 m (Dillon and Oldale, 1978), there is weak evidence of 10 to 20 m of isostatic subsidence during glacial loading of the Mackenzie Delta area. The argument remains tenuous, and it is not known whether the postulated shoreline at or below -70 m dates from early or late Wisconsin time. In addition, the minimum sea level in the region may not necessarily have been contemporary with the global eustatic minimum.

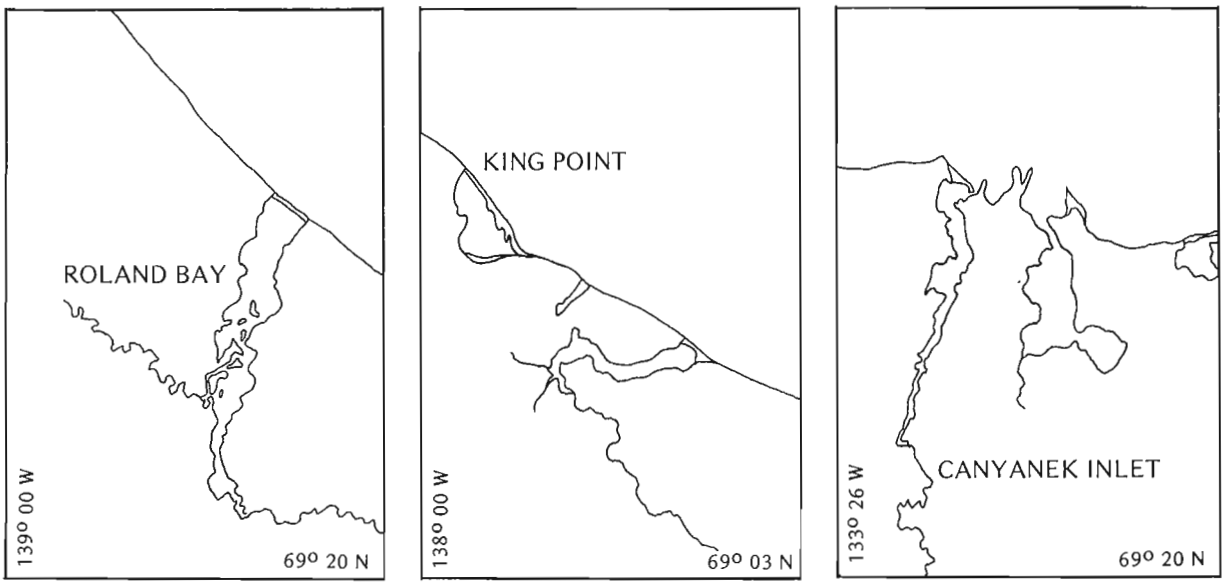

Figure 9.3. *Examples of drowned valleys, southern Beaufort Sea coast. See Figure 9.2 for locations.*

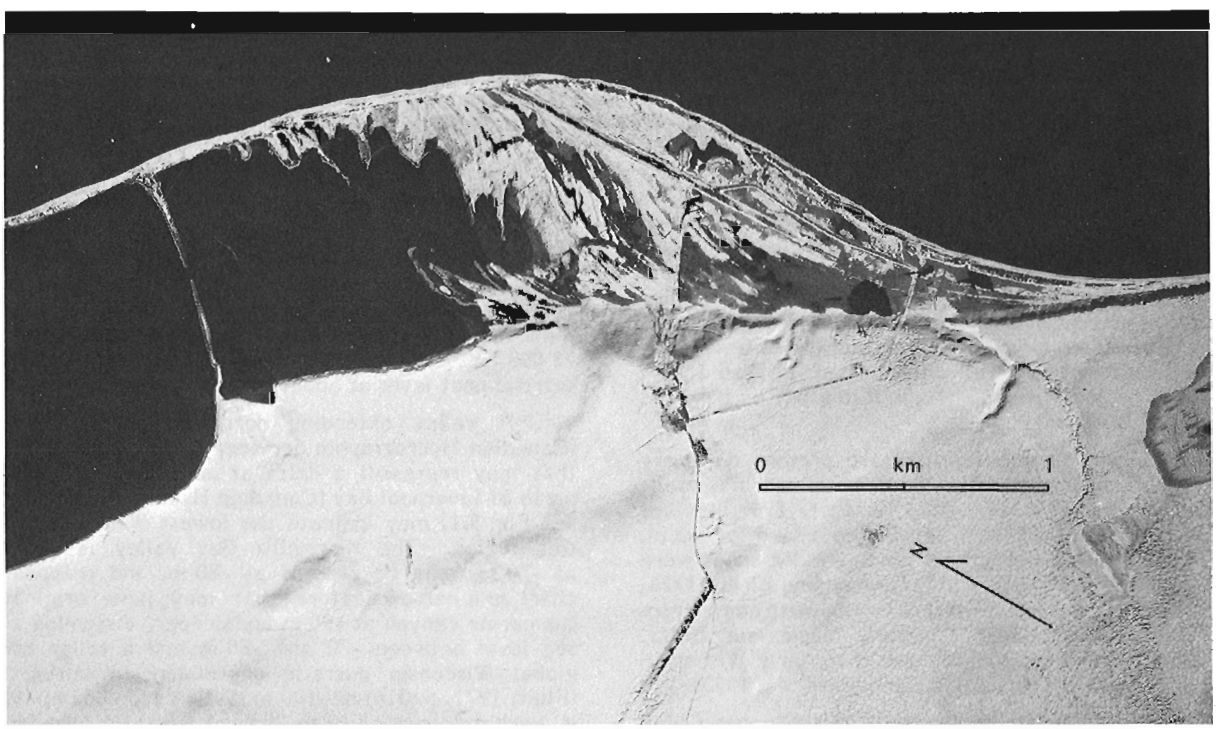

Figure 9.4. *Beach ridges at Stokes Point, Yukon coast. Ridges deposited under net southeastward longshore drift, prograding from left to right. Older ridges at left are partially flooded due to local subsidence, regional submergence, or both. Photograph taken 20 September 1970 following a major storm surge one week earlier. Some flooding at centre right may result in part from surge and impoundment by road between high ground and airstrip. Portion of NAPL photo A22013-13.*

Further evidence of lower sea levels is provided by submarine permafrost and ground ice under the Beaufort Sea (Mackay, 1972). The thickness of offshore permafrost suggests that some areas of the present shelf may have been emergent for at least 50 000 years (J.R. Mackay, personal communication, 1979). In addition, relict ice scour tracks on the seafloor may record a period of lower sea level. At present, ice scour occurs at depths of less than 50 m (C.F.M. Lewis, 1977), but relict scour depressions have been found as deep as -75 m (Pelletier and Shearer, 1972). The age of the deepest features is not known; if they are postglacial, they point to sea level at -25 m or lower, assuming no change in the draught of ice keels has occurred.

Shearer (1971, 1972) reported results of seismic reflection profiling over the Mackenzie Canyon. He described "a fill of well-bedded outwash deltaic deposits overlying a seismically heterogeneous and irregular-shaped basal till-like unit..." and concluded: "The observed stratigraphy can be adequately represented by the irregular advance and retreat of one ice tongue during classical [late] Wisconsin" (Shearer, 1972, p. 180). This basal deposit is here considered to represent the Buckland Glaciation (early Wisconsin or earlier) of Rampton (in press). The age and depositional environment of the bedded fluvial or glaciofluvial deposits overlying the till are not known. These stratified deposits exhibit an upward trend of decreasing seaward slope and are essentially horizontal at the upper contact with overlying muds, considered to be postglacial. The upper part of the stratified valley fill may correspond to a near-minimum late Wisconsin sea level in the Mackenzie Delta area, at about -65 m. The abrupt upward transition to mud reflects an environmental change related either to recession of the Mackenzie ice tongue (ca. 13 000 years ago) or to rapidly rising sea level (date uncertain) or to both (see following section).

Shearer (1971) noted the consistent occurrence of a break in slope where early Wisconsin and older beds are truncated at the top of the western canyon wall. The break occurs at increasingly shallow depths towards the southeast, rising approximately 0.5 m/km. The break in slope might plausibly be interpreted as a synchronous shoreline, tilted following its formation. The slope is comparable to that of the pediment, described above, suggesting a common regional tectonic cause. However, tilting of the hypothesized shoreline would also be consistent with a late Wisconsin ice load and associated isostatic depression to the southeast during formation of the shore. A unit identified as the offshore equivalent of ice thrust deposits along the Yukon coast (Shearer, 1971, his Fig. 3) is truncated by a surface that would then postdate Buckland Glaciation. It may be hypothesized that this surface developed during marine transgression in post-Buckland or Holocene time, in which case a minimum sea level between -60 and -80 m is suggested.

Postglacial Sea Levels

Evidence exists of postglacial transgression on southern Banks Island to +11 m or higher ca. 11 000 years ago (J.G. Fyles in Dyck et al., 1965). Vincent (1978) has described a late Wisconsin or Holocene transgression (termed the Shuyter Point Sea) at +20 m in eastern and southern Banks Island. No indication of an early postglacial sea level higher than present, however, has been found west of Cape Bathurst. Numerous dates at or close to modern sea level in the Mackenzie Delta area and to the west (Tables 9.1A, 9.1B) pertain to subaerial environments, providing collective evidence against a higher postglacial datum in the region. Dates defining postglacial sea level are extremely rare, as are stratigraphic data from the Mackenzie Delta.

Johnston and Brown (1965) reported results of coring near the eastern edge of the trough in the southern Mackenzie Delta near Inuvik. The generalized stratigraphy, from the delta surface at approximately +5 m, was as follows:

0-30 m	thinly stratified organic sandy silt
30-55 m	stratified fine-medium sand with thin organic layers
55-70 m	very dense silty clay with:
	55-63 m no pebbles
	63-67 m scattered pebbles
	67-70 m high concentration of pebbles
70 m	dolomitic limestone (bedrock).

A glaciomarine environment is suggested by high porewater salinity (28 °/₀₀) in the basal silty clay and pebble unit, which has been interpreted as a till (Johnston and Brown, 1965). Although activity characteristics of the clay at the base suggest a freshwater source, marine encroachment against a receding ice front may be hypothesized. This scenario would give a minimum sea level of -65 m at the time of deglaciation in the southern delta (about 12 000 years ago). This estimate is not adjusted for (unknown) depth of sea water at the site and the potentially contrasting effects of postdepositional compaction and ice segregation in delta sediments.

The stratified sand unit overlying the silty clay may be interpreted as a fluvial, deltaic, or estuarine unit deposited at or not far below sea level. A wood fragment found in association with thin peat layers at a depth of 38.3 m yielded a radiocarbon date of 6900 ± 110 years B.P. (GSC-54; Johnston and Brown, 1965). This is a single uncorroborated date and is the only date on organic material at depth in the Mackenzie Delta. Assuming the date is without major error and closely approximates the time of deposition, it indicates sea level no lower than -33 m and probably no higher than about -18 m (Mackay, 1963) ca. 6900 years ago. If, however, the sample comes from a channel-fill deposit, no upper limit can be placed on sea level at the time of deposition. Furthermore, recent data from nine jet drillholes in the modern delta suggest that the stratigraphy described by Johnston and Brown (1965) is not generally representative of the delta (C.P. Lewis, personal communication, 1979).

The only other evidence providing time control for postglacial submergence in the Mackenzie Delta comes from a group of eroded pingos near the delta front (Mackay, 1963; Mackay and Stager, 1966). From one pingo on the modern delta, they report dates of 1470 ± 175 and 2700 ± 200 years B.P. (I-1154, I-1155) on twigs taken from deformed delta sediments. From another pingo nearby, a date of 3210 ± 400 years B.P. (I-1153) was obtained for lake sediment at -0.6 m (corrected). These would seem to suggest relatively recent minor submergence. This may be due to local thaw or compaction, or it may reflect crustal downwarping. Compaction is probably limited at the present time due to the presence of permafrost, an inference supported by the relative absence of morphological features characteristic of local subsidence in deltas.

Wagner (1972) has reported two dates from marine shells collected in the Beaufort Sea. A pelecypod sample obtained 0.2 m below the bottom in 54 m of water (near 70°57'N, 131°25'W), dated 700 ± 180 years B.P. (GSC-1509), clearly postdates the transgression at that location. Another shell sample from a depth of 322 m (near 70°22'N, 137°33'W) yielded a date of 3530 ± 240 years B.P. (GSC-1511). The depth habitat of the animal, tentatively identified as **Buccinum** sp., was estimated less than 50 m by Wagner (1972), who inferred that the elevation of sea level 3500 years ago was approximately -270 m. As has been suggested by W. Blake, Jr. (in Lowdon and Blake, 1973, p. 46-47), this is in contradiction to a large body of evidence, and it is more

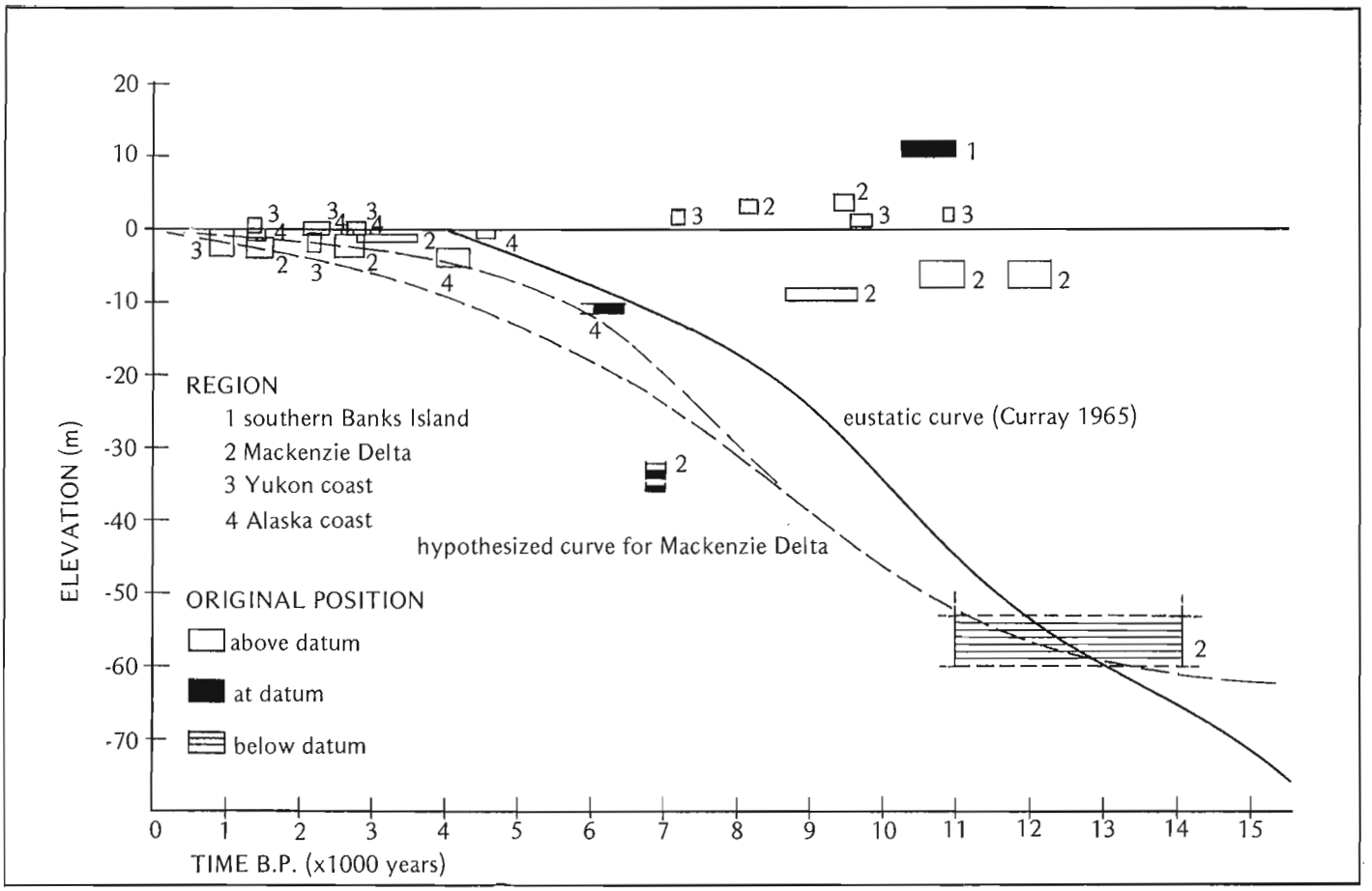

Figure 9.5. *Sea level data and hypothesized history, Mackenzie Delta and adjacent areas. The broken lines indicate a hypothetical envelope of sea level in this region.*

probable either that the shell has been transported from its original habitat or that the animal could tolerate depths much greater than 50 m.

Crustal flexure in response to Mackenzie Delta sedimentation (Richards, 1950) may be responsible for a component of Holocene subsidence in the region. Negative anomalies in the gravity field, -40 mgals or lower, occur over Shallow Bay, Mackenzie Canyon, and Kugmallit Bay, with a positive anomaly over the outer shelf (Hornal et al., 1970), broadly reflecting the pattern expected due to sediment loading at a continental margin (Walcott, 1972c). These anomalies may be due largely to the thick accumulation of Tertiary and Cretaceous clastic sediments in the area (Hornal et al., 1970; Norris, 1973).

An estimate of the lithospheric response to loading by the modern delta alone can be obtained using models of crustal flexure, in which the lithosphere is treated as a thin elastic sheet overlying a fluid asthenosphere. For short-term loads of duration 10^3 to 10^4 years, such as the modern Mackenzie Delta, a combined viscous and elastic response is indicated, with relatively high values of flexural rigidity (Walcott, 1970b). As a first approximation, it may be assumed that the Mackenzie Delta would be supported elastically, with the lithosphere depressed some distance beyond the edge of the load. If the behaviour observed at proglacial Lakes Algonquin and Agassiz is accepted as an appropriate analogue, the flexural parameter of the lithosphere may be taken to be about α = 200 km (Walcott, 1970b). This would allow subsidence to extend about 600 km from the location at which a point load is applied.

Assume ρ_m = 3300 kg.m^{-3} for the density of material below the lithosphere and ρ_c = 1900 kg.m^{-3}, typical of frozen sediments in the modern delta (R.J.E. Brown, cited by Smith and Hwang, 1973), for the overlying material. The area of the load is about 800 km^2, and its average thickness is taken as 100 m. We obtain a load P = 1.5 x 10^{16}N. Now the maximum deflection under a point load P can be computed as (Walcott, 1970a):

$$w(0) = \frac{P}{4\alpha^2(\rho_m-\rho_c)g}$$

This gives an estimate of w = 7 m for the maximum downwarping due to the assumed load. If we apply the solution for a line load given by Gunn (1943, equation 19), taking the delta as a rectangular block of thickness 100 m and width 40 km, we obtain w = 5 m. These computations do not consider the possible ongoing effects of earlier ice-, water-, or sediment-loading in the area, nor do they take into account the complex structure of the Mackenzie trough and adjacent region (Yorath, 1973). It does appear, however, that part of the observed subsidence in the Mackenzie Delta area and over a considerable distance along the coast may be attributable to the sediment load applied since deglaciation.

On the Yukon coast, the earliest sea level data with time control come from organic material in the Babbage Delta. The oldest sample, S-1481 (Table 9.1B), is considered

suspect and may have been reworked from older peat exposures in the area. The same may, of course, be true of other samples also, but two of the dates, 2260 ± 130 years (S-1482) and 2110 ± 90 years (GSC-2691), suggest mean sedimentation rates that are compatible with observed seasonal accumulation at the present time. These dates refer to horizons at present sea level. A date of 2100 ± 80 years (GSC-2323) on peat from -1.3 m (overlying ice and gravel) may indicate a rise of sea level during this interval, if potential ice segregation or thaw are eliminated. Archeological sites on Herschel Island, reported to be as low as -1.8 m (Bird, 1967), suggest a similar trend. A Thule culture winter house site recently has been excavated there and is tentatively dated between 900 and 1100 years B.P. (B. Walker-Yorga, personal communication, 1979). The two older samples (S-1532 and S-1534, Table 9.1B) were obtained from oil-soaked deposits and may be considered to date ca. 400 years younger than indicated, after application of a sea mammal adjustment. "Midden deposits were...excavated at low tide from below the waterline...Additionally, house timbers and midden were observed below water and farther into the bay in the vicinity of the site" (B. Walker-Yorga, personal communication, 1979). These data suggest a sea level no higher than -1 m and probably somewhat lower ca. 1000 years ago; again, however, thaw consolidation may have been a factor. The limited data from the Yukon coast imply a rise of sea level within the envelope of 'eustatic' curves that have been proposed for the Holocene, but in excess of changes attributable to global variation in glacial volume during the past few thousand years (Walcott, 1975).

In northern Alaska, efforts have been made to obtain material from the Beaufort Shelf that would date the transgression, but problems related to stratigraphic interpretation, reworking of sediments, and contamination by anomalously old carbon have prevented any unambiguous conclusions (E. Reimnitz, personal communication, 1978). Driftwood found at -11 m in lagoon sediments near Barrow, Alaska, yielded a date of 6450 ± 200 years (Tx-220; Faas, 1966). In Simpson Lagoon near Kuparuk River, a date of 4118 ± 189 years (AU-91) was obtained on terrestrial organic material found at -5.5 m, but some thaw consolidation is thought to have occurred here (E. Reimnitz, personal communication, 1978). Finally, a set of dates from Point Barrow (Table 9.1C) has been interpreted as evidence both of minor submergence and of short-lived highstands (up to +1 m) within the past 2000 years (Hume, 1965; Brown and Sellmann, 1966). The data suggest a datum at -2 m during occupation of the Birnirk archeological site ca. 1500 years ago (Hume, 1965). Evidence for the higher sea level comes from driftwood within old beach ridges 1 m higher than the highest modern beach. Fluctuations of the sort reported are not inconsistent with the minor eustatic variations suggested by Fairbridge (1961), although the details at Point Barrow do not correspond exactly with Fairbridge's curve. It would seem, however, that ice thrusting of beach sediment, such as has been observed elsewhere on the Beaufort Sea coast, or possible variations in sea-ice distribution and mean fetch, leading to occurrences of higher storm wave or surge height at Barrow, cannot be eliminated as possible causes of the high beach ridges. No other evidence of recent sea level higher than present has been reported from the Beaufort Sea coast.

Tide data for Tuktoyaktuk have been examined for recent trend of sea level. Linear regression against time of monthly mean tide level suggests a rise of 38 mm during the interval 1952-1975; however, the slope of the trend is not significantly different from zero; the standard deviation of the monthly tide is 160 mm.

Discussion

Dates and corresponding elevations for the period since about 15 000 years ago are plotted in Figure 9.5. The following general conclusions are indicated. A hypothetical sea level history for the Mackenzie Delta, within the envelope indicated by the broken lines, is at least as consistent with the limited data as is a selected 'eustatic' curve (solid line) taken from Curray (1965). Departures of the hypothetical history from Curray's curve suggest limited isostatic depression due to late Wisconsin ice prior to 13 000 years ago, followed by uplift and then renewed subsidence, related either to migration and collapse of a forebulge or to depression under sediment loading, or perhaps to both; this subsidence possibly is continuing at present. The pattern of marginal forebulge collapse observed on the Atlantic coast of North America may be a useful analogue.

The proposed Beaufort Sea curve is presented as a working hypothesis to encourage further consideration of the sea level problem in the Mackenzie Delta area. Further exploration of delta stratigraphy would be particularly helpful in elucidating the history of transgression and the nature of the subsidence. The sequence hypothesized here is in keeping with the general pattern predicted by Clark et al. (1978) and with a computed curve, using the model outlined therein, for a point off the Alaska coast (J.T. Andrews, personal communication, 1978). More field data, however, are required to test such a model and to corroborate the existing limited evidence.

Marine transgression and coastal erosion, rapid sedimentation in the Mackenzie Delta and Canyon, and partial removal of the record by late Wisconsin ice have contributed to an extreme paucity of data on late Quaternary sea levels in this region. Additional complications include anomalously old carbon (coal, reworked peat and wood, possibly old ocean water) and reworking of shelf sediment by ice scour. This report, while offering a preliminary interpretation of sea level history in the Mackenzie Delta area, serves primarily to emphasize the need for more data and the danger of assuming a standard eustatic model.

With the exception of the high driftwood at Point Barrow, a broad regional correlation is apparent within the past 3000 years. The coastal morphology, radiocarbon and archeological dates, and plausible mechanisms all point to a recent and perhaps continuing regional submergence. At present it is not possible to discriminate between potential causes, which may include crustal loading, relaxation of late Wisconsin isostatic effects, epeirogenic subsidence, and a possible component of contemporary eustatic change. Nor can the rate of submergence be assessed adequately, although further geological and archeological work and continuation of existing tide gauges may eventually permit a quantitative estimate of the contemporary trend.

Acknowledgments

This work was undertaken in support of research for a dissertation on sedimentary processes in Babbage River delta and estuary, funded by Terrain Sciences Division. I wish to express my thanks to the individuals cited in the text for personal communication of data and interpretations. I am grateful, for critical comments on earlier drafts of the paper, to the following persons: W. Blake, Jr., M. Church, J.J. Clague, C.P. Lewis, J.R. Mackay, B.R. Pelletier, V.N. Rampton, and R.I. Walcott. E. Reimnitz and D.M. Hopkins of the United States Geological Survey were especially generous in providing dates and other information, as was B. Walker-Yorga of the University of Toronto. I thank F. Stephenson, Institute of Ocean Sciences, Patricia Bay, for providing tide data.

Table 9.1A

Radiocarbon dates, Mackenzie Delta area

Location	Elevation (m)	Material	Reference	Lab. No.[1]	Reported age (years B.P.)
Garry Island 69°30'N, 135°40'W	+9	marine pelecypod shells from terrace representing sea level (+9 to +15 m)	Kerfoot, 1969; corrected date in GSC XI	GSC-562	> 35 000
Island south of Kendall Island 69°21'N, 135°22'W	+9	**Astarte** shells from terrace as on Garry Island	GSC XI	GSC-690	> 37 000
Pullen Island 69°46'N, 134°24'W	+3	pelecypod shells from gravel cutting older sands	GSC XVI	GSC-1877	> 23 000
Ibyuk Pingo near Tuktoyaktuk 69°24'N, 133°04'W	?	organic silt in mudflow under lake sediments	GSC XIII	GSC-512	14 130 ± 440
Ibyuk Pingo 69°24'N, 133°04'W	?	peat 0.3 m above GSC-512 in mudflow deposit	GSC XIII	GSC-481	17 860 ± 260
Ibyuk Pingo 69°24'N, 133°04'W	-6 ± 2[2]	driftwood from lake sediments overlying mud flow deposit	Müller, 1962	S-69	12 000 ± 300
Tuktoyaktuk pingo tunnel 69°27'N, 133°01'W	+3.7	woody peat from icy lake silts over gravel and ice	GSC XIII	GSC-1458	9460 ± 140
Eskimo Lakes 69°32'N, 130°55'W	-6 ± 2[2]	wood fragment	Mackay, 1963	I-483	10 800 ± 300
Tununuk Point (Mackenzie Delta) 69°00'N, 134°40'W	+14	peat	GSC XIII	GSC-1286	11 000 ± 160
Tuktoyaktuk Harbour 6.4 km south of DEW Line station 69°23'N, 132°59'W	+3	peat over beach gravel, overlain by colluvium	GSC XVI	GSC-1676	8160 ± 140
Mackenzie Delta NRC borehole near Inuvik 68°18'N, 133°50'W	-38	wood fragment	GSC II; Johnston and Brown, 1965	GSC-54	6900 ± 110

[1] Radiocarbon dating laboratories:

AU - University of Alaska, Fairbanks
GSC - Geological Survey of Canada, Ottawa
GX - Geochron Laboratories, Cambridge, Massachusetts
I - Teledyne Isotopes, Westwood, New Jersey
S - Saskatchewan Research Council, Saskatoon
Tx - University of Texas, Austin
USGS - U.S. Geological Survey, Menlo Park, California
W - U.S. Geological Survey, Reston, Virginia

[2] Estimated original elevation after correction for pingo uplift

[3] Elevation above modern berm

[4] Suggest sea level approximately -2 m

Table 9.1A (continued)

Location	Elevation (m)	Material	Reference	Lab. No.[1]	Reported age (years B.P.)
Shallow Bay 68°55'N, 135°57'W	>-5[2]	wood fragments in peat beds and inter-stratified sand deposited at about +1.5 m?	Mackay and Stager, 1966; Mackay, 1963	I-1154	1470 ± 175
Shallow Bay 68°55'N, 135°57'W	>-5[2]	same	same	I-1155	2700 ± 200
Richards Island 69°25'N, 134°21'W	-0.6[2]	wood in sandy silt with shell fragments; lacustrine?	Mackay and Stager, 1966	I-1153	3210 ± 400
Richards Island 69°25'N, 134°21'W	-5[2]	wood? in lake or shallow marine clay with shells and vein ice	same	I-1152	9155 ± 500
Kugaluk River N of 69°15'N	+10	wood from grey crossbedded sand in terrace	Mackay, 1963	I-482	> 38 000
Kugaluk River 69°20'N, 130°55'W		peat over sand and overlain by sand and gravel in low terrace	GSC XVIII	GSC-1303	10 900 ± 160
Mason River 69°55'N, 128°26'W	+2.1	peat and wood in silty sand; soil within loess	GSC XVIII	GSC-2029	8650 ± 80
Cy Peck Inlet 70°20'N, 127°57'W	+1	wood and bark at base of 4 m of crossbedded sand	GSC XVIII	GSC-1974	33 800 ± 880
Beaufort Sea 70°57'N, 131°25'W	-54	valve of pelecypod **Astarte borealis** 0.2 m below bottom	Wagner, 1972; GSC XIII	GSC-1509	700 ± 180
Beaufort Sea 70°22'N, 137°33'W	-322	gastropod shell (**Buccinum** sp.?) 4.0 m below bottom	Wagner, 1972; GSC XIII	GSC-1511	3530 ± 240

Table 9.1B

Radiocarbon dates, Yukon Coast*

Location	Elevation (m)	Material	Reference	Lab. No.[1]	Reported age (years B.P.)
Backhouse River 3.2 km west of mouth 69°36'N, 140°36'W	+2	wood (**Betula**) from peat in icewedge cast in fan gravel under 0.5 m organic silt	GSC XVI	GSC-1853	10 900 ± 80
7.5 km west of Komakuk Beach 69°35'N, 140°22'W	+5	wood (**Salix**) from peat in fan? gravel under 2 m organic silt	GSC XVI	GSC-1838	10 200 ± 120
2 km east of Roland Bay 69°22'N, 138°52'W	+10	peat pod in oxidized bouldery sand over till, under 4 m lake clay with peat	GSC XVI	GSC-1808	9610 ± 90
Kay Point scarp south of point bordering lagoon 69°17'N, 138°23'W	+1	peat from base of ice-wedge cast in glaciofluvial sand and gravel under peat	GSC XVI	GSC-480	9710 ± 140
Kay Point scarp 1.6 km southeast 69°17'N, 138°22'W	+1.8	peat from base of ice-wedge cast in glacio-fluvial gravel beneath lake sediments, peat, and sand	GSC XVI	GSC-1872	7170 ± 70
Babbage Delta 69°13'N, 137°27'W	0	plant material in delta-plain sediments	unpublished	S-1481	3075 ± 180
				GSC-2691	2110 ± 90
Babbage Delta 69°15'N, 137°27'W	0	peat underlying 0.91 m stratified silt and sand	unpublished	S-1482	2260 ± 130
Babbage lagoon shore south of Niakolik Point 69°15'N, 137°30'W	-0.1	peat extending undetermined depth below sea level	unpublished	S-1479	2775 ± 105
Babbage Delta 69°14'N, 137°27'W	-1.3	peat from base of 2.6 m of peat with excess ice over massive ice over gravel	unpublished	GSC-2323	2100 ± 80
	+0.8	peat from base of active layer	unpublished	GSC-2330	1380 ± 80
Herschel Island 69°34'N, 138°48'W	-0.7	charcoal in basal midden below house floor	B. Walker-Yorga personal communication, 1979	S-1533	990 ± 95
Herschel Island 69°34'N, 138°48'W	-0.7	charcoal in basal midden	same	S-1532	1570 ± 60
Herschel Island 69°34'N, 138°48'W	-0.7	charred fat in basal midden	same	S-1534	1510 ± 90

*See Table 9.1C for footnotes.

Table 9.1C

Radiocarbon dates, north Alaska Coast

Location	Elevation (m)	Material	Reference	Lab. No.[1]	Reported age (years B.P.)
Point Barrow area beach ridge west of Elson Lagoon 71°19'N, 156°36'W	+4.2	thin-layered organics in beach deposits	Sellmann and Brown, 1973	I-1384	25 300 ± 2 300
				W-2676	> 44 000
approximately same	+2	thin organic layer in clean sand	same	I-2359	37 000 $\pm \frac{2\ 900}{2\ 000}$
				W-2679	36 000 ± 2 000
Stefansson Sound 70°42'N, 148°34'W	-50	from widespread detrital peat layer	D.M. Hopkins personal communication, 1979	USGS-249	42 800 ± 1 440
Esatkuat Lagoon near Barrow 71°18'N, 156°47'W	-11	driftwood in lagoon sediment	Faas, 1966	Tx-220	6450 ± 200
Simpson Lagoon off Kuparuk River 70°26'N, 148°47'W	-5.5	tundra vegetation	AU I	AU-91	4118 ± 189
Point Barrow 71°23'N, 156°29'W	< 1[3]	driftwood in beach ridge	Péwé and Church, 1962	I-387	1100 ± 120
				I-388	1090 ± 140
				I-389	10 800 ± 300
Point Barrow 71°23'N, 156°29'W	+1.7	beach ridge	Hume, 1965	GX-0380	1700 ± 110
	+1.4			GX-0381	2365 ± 100
	+2.0			GX-0230	5575 ± 375
Point Barrow 71°21'N, 156°34'W	0	freshwater peat	Brown and Sellmann, 1966	I-1868	2650 ± 160
	-0.8	freshwater peat		I-1949	2860 ± 140
	-1.5	freshwater peat		I-1869	4570 ± 130
Point Barrow 71°21'N, 156°34'W	0[4]	Birnirk culture dwellings	Hume, 1965	estimated from radiocarbon dates on Birnirk sites nearby	[1450]

[1] Radiocarbon dating laboratories:

AU - University of Alaska, Fairbanks
GSC - Geological Survey of Canada, Ottawa
GX - Geochron Laboratories, Cambridge, Massachusetts
I - Teledyne Isotopes, Westwood, New Jersey
S - Saskatchewan Research Council, Saskatoon
Tx - University of Texas, Austin
USGS - U.S. Geological Survey, Menlo Park, California
W - U.S. Geological Survey, Reston, Virginia

[2] Estimated original elevation after correction for pingo uplift

[3] Elevation above modern berm

[4] Suggest sea level approximately -2 m

References

AU I Reeburgh and Young, 1976

GSC II Dyck and Fyles, 1963

GSC IV Dyck, Fyles, and Blake, 1965

GSC XI Lowdon, Robertson, and Blake, 1971

GSX XIII Lowdon and Blake, 1973

GSC XVI Lowdon and Blake, 1976

GSC XVIII Lowdon and Blake, 1978

Bird, J.B.
1967: The Physiography of Arctic Canada; The Johns Hopkins Press, Baltimore, 336 p.

Blake, W., Jr.
1976: Sea and land relations during the last 15 000 years in the Queen Elizabeth Islands, Arctic Archipelago; in Report of Activities, Part B, Geological Survey of Canada, Paper 76-1B, p. 201-207.

Brown, J. and Sellmann, P.V.
1966: Radiocarbon dating of coastal peat, Barrow, Alaska; Science, v. 153, p. 299-300.

Canadian Hydrographic Service
1973a: Natural Resource Series, Map 26606-A, Bathymetry, interpreted by D. Monahan; Canada Department of Environment, Ottawa.

1973b: Natural Resource Series, Map 26602-A, Bathymetry, interpreted by D. Monahan; Canada Department of Environment, Ottawa.

1974: Toker Point to Cape Lyon and Cape Kellett; Canada Department of Environment, Chart 7651.

Clague, J.J.
1975: Late Quaternary sea level fluctuations, Pacific Coast of Canada and adjacent areas; in Report of Activities, Part C, Geological Survey of Canada, Paper 75-1C, p. 17-21.

Clark, J.A., Farrell, W.E., and Peltier, W.R.
1978: Global changes in postglacial sea level: a numerical calculation; Quaternary Research, v. 9, p. 265-287.

Curray, J.B.
1965: Late Quaternary history, continental shelves of the United States; in The Quaternary of the United States, ed. H.E. Wright, Jr. and D.G. Frey, Princeton University Press, p. 723-735.

Curray, J.B. and Shepard, F.P.
1972: Some major problems of Holocene sea levels (abstract); in American Quaternary Association, 2nd National Conference (Miami), p. 16-18.

Dillon, W.P. and Oldale, R.N.
1978: Late Quaternary sea-level curve: reinterpretation based on glaciotectonic influence; Geology, v. 6, p. 56-60.

Dyck, W. and Fyles, J.G.
1963: Geological Survey of Canada radiocarbon dates II; Radiocarbon, v. 5, p. 39-55.

Dyck, W., Fyles, J.G., and Blake, W., Jr.
1965: Geological Survey of Canada radiocarbon dates IV; Radiocarbon, v. 7, p. 24-46; reprinted in Geological Survey of Canada, Paper 65-4.

Faas, R.W.
1966: Paleoecology of an arctic estuary; Arctic, v. 19, p. 343-348.

Fairbridge, R.W.
1961: Eustatic changes in sea level; Physics and Chemistry of the Earth, v. 4, p. 99-185.

Flint, R.F.
1971: Glacial and Quaternary Geology; Wiley, New York, 892 p.

Grant, D.R.
1975: Recent coastal submergence of the Maritime Provinces; in Environmental Changes in the Maritimes, ed. J.G. Ogden and M.J. Harvey, Proceedings of Symposium, Dalhousie University, 1971, Nova Scotia Institute of Science, v. 27, supplement 3, p. 83-102.

Gunn, R.
1943: A quantitative evaluation of the influence of the lithosphere on anomalies of gravity; Journal of the Franklin Institute, v. 236, p. 47.

Hornal, R.W., Sobczak, L.W., Burke, W.E.F., and Stephens, L.E.
1970: Preliminary results of gravity surveys over Mackenzie Basin and Beaufort Sea; Department of Energy, Mines and Resources, Earth Physics Branch, Gravity Maps 117, 118, 119; summarized in Bouguer Anomaly Map of Canada, 1974, Gravity Map 74-1.

Hughes, O.L.
1972: Surficial geology of northern Yukon Territory and northwestern District of Mackenzie, Northwest Territories; Geological Survey of Canada, Paper 69-36, 11 p., map.

Hume, J.D.
1965: Sea-level changes during the last 2000 years at Point Barrow, Alaska; Science, v. 150, p. 1165-1166.

Johnston, G.H. and Brown, R.J.E.
1965: Stratigraphy of the Mackenzie Delta, Northwest Territories, Canada; Geological Society of America Bulletin, v. 76, p. 103-111.

Kerfoot, D.E.
1969: The geomorphology and permafrost conditions of Garry Island, N.W.T.; unpublished Ph.D. dissertation, University of British Columbia, Vancouver, 308 p.

Lewis, C.F.M.
1977: Scouring of the Beaufort Shelf by sea ice (abstract); in Geological Association of Canada, Program with Abstracts, v. 2, p. 32.

Lewis, C.P.
1977: Deltaic processes and delta morphology, Mackenzie Delta, N.W.T. (abstract); in Geological Association of Canada, Program with Abstracts, v. 2, p. 32.

Lowdon, J.A. and Blake, W., Jr.
1973: Geological Survey of Canada radiocarbon dates XIII; Geological Survey of Canada, Paper 73-7, 61 p.

1976: Geological Survey of Canada radiocarbon dates XVI; Geological Survey of Canada, Paper 76-7, 21 p.

1978: Geological Survey of Canada radiocarbon dates XVIII; Geological Survey of Canada, Paper 78-7.

Lowdon, J.A., Robertson, I.M., and Blake, W., Jr.
1971: Geological Survey of Canada radiocarbon dates XI; Radiocarbon, v. 13, p. 255-324; reprinted in Geological Survey of Canada, Paper 71-7.

Mackay, J.R.
1959: Glacier ice-thrust features of the Yukon coast; Geographical Bulletin, no. 13, p. 5-21.

1963: The Mackenzie Delta Area, N.W.T.; Geographical Branch, Memoir no. 8, 202 p.

1972: Offshore permafrost and ground ice, southern Beaufort Sea, Canada; Canadian Journal of Earth Sciences, v. 9, p. 1550-1561.

Mackay, J.R. and Mathews, W.H.
1973: Geomorphology and Quaternary history of the Mackenzie River valley near Fort Good Hope, N.W.T., Canada; Canadian Journal of Earth Sciences, v. 10, p. 26-41.

Mackay, J.R. and Stager, J.K.
1966: The structure of some pingos in the Mackenzie Delta area, N.W.T.; Geographical Bulletin, v. 8, p. 360-368.

Mackay, J.R., Rampton, V.N., and Fyles, J.G.
1972: Relic Pleistocene permafrost, Western Arctic, Canada; Science, v. 176, p. 1321-1323.

Manning, T.H.
1953: Narrative of a second Defence Research Board expedition to Banks Island with notes on the country and its history; Arctic, v. 9, p. 3-77.

Müller, F.
1962: Analysis of some stratigraphic observations and C14 dates from two pingos in the Mackenzie Delta, N.W.T.; Arctic, v. 15, p. 278-288.

Norris, D.K.
1973: Tectonic styles of northern Yukon Territory and northwestern District of Mackenzie, Canada; in Arctic Geology, ed. M.C. Ritcher; American Association of Petroleum Geologists, Memoir 19, p. 23-40.

Pelletier, B.R. and Shearer, J.M.
1972: Sea bottom scouring in the Beaufort Sea of the Arctic Ocean; 24th International Geological Congress (Montreal), Proceedings, Section 8, p. 251-261.

Péwé, T.L. and Church, R.E.
1962: Age of the spit at Barrow, Alaska; Geological Society of America Bulletin, v. 73, p. 1287-1292.

Prest, V.K.
1969: Retreat of Wisconsin and Recent ice in North America; Geological Survey of Canada, Map 1257A, scale 1: 5 000 000.

Rampton, V.N.
Quaternary geology of the Yukon Coastal Plain; Geological Survey of Canada, Bulletin 317. (in press)

Reeburgh, W.S. and Young, M.S.
1976: University of Alaska radiocarbon dates I; Radiocarbon, v. 18, p. 1-15.

Richards, H.G.
1950: Postglacial marine submergence of Arctic North America with special reference to the Mackenzie Delta; American Philosophical Society, Proceedings, v. 94, p. 31-37.

Sellmann, P.V. and Brown, J.
1973: Stratigraphy and diagenesis of perennially frozen sediments in the Barrow, Alaska, region; in Permafrost, North American Contributions, 2nd International Conference (Yakutsk, USSR), National Academy of Sciences, Washington, p. 171-181.

Shearer, J.M.
1971: Preliminary interpretation of shallow seismic reflection profiles from the west side of Mackenzie Bay, Beaufort Sea; in Report of Activities, Part B; Geological Survey of Canada, Paper 71-1B, p. 131-138.

1972: Geological structure of the Mackenzie Canyon area of the Beaufort Sea; in Report of Activities, Part A, Geological Survey of Canada, Paper 72-1A, p. 179-180.

Smith, M.W. and Hwang, C.T.
1973: Thermal disturbance due to channel shifting, Mackenzie Delta, N.W.T., Canada; in Permafrost, North American Contribution, 2nd International Conference (Yakutsk, USSR), National Academy of Sciences, Washington, p. 51-60.

Vincent, J.-S.
1978: Limits of ice advance, glacial lakes, and marine transgressions on Banks Island, District of Franklin: a preliminary interpretation; in Current Research, Part C, Geological Survey of Canada, Paper 78-1C, p. 53-62.

Wagner, F.J.E.
1972: Molluscan fauna as indicators of late-Pleistocene history, southeastern Beaufort Sea; 24th International Geological Congress (Montreal), Proceedings, Section 8, p. 142-153.

Walcott, R.I.
1970a: Isostatic response to loading of the crust in Canada; Canadian Journal of Earth Sciences, v. 7, p. 716-727.

1970b: Flexural rigidity, thickness, and viscosity of the lithosphere; Journal of Geophysical Research, v. 75, p. 3941-3954.

1972a: Past sea levels, eustasy, and deformation of the earth; Quaternary Research, v. 2, p. 1-14.

1972b: Late Quaternary vertical movements in eastern North America: quantitative evidence of glacio-isostatic rebound; Reviews of Geophysics and Space Physics, v. 10, p. 849-884.

1972c: Gravity, flexure, and the growth of sedimentary basins at a continental edge; Geological Society of America Bulletin, v. 83, p. 1845-1848.

1975: Recent and late Quaternary changes in water level; Eos, v. 56, p. 62-72.

Yorath, C.J.
1973: Geology of Beaufort-Mackenzie Basin and eastern part of northern Interior Plains; in Arctic Geology, ed. M.C. Ritcher; American Association of Petroleum Geologists, Memoir 19, p. 41-47.

10.

THE STRATIGRAPHY, STRUCTURE AND METAMORPHISM OF CENTRAL GLOVER ISLAND, WESTERN NEWFOUNDLAND

EMR Research Agreement 2239-4-48/79

Douglas A. Knapp[1]
Precambrian Geology Division

Knapp, Douglas A., The stratigraphy, structure and metamorphism of central Glover Island, western Newfoundland; in Current Research, Part B, Geological Survey of Canada, Paper 80-1B, p. 89-96, 1980.

Abstract

Polydeformed and metamorphosed semipelites, informally termed the Schist group, outcrop on Glover Island in the core of a major south-plunging anticline. These rocks are structurally overlain by the dominantly mafic Glover Formation which is divided into three map units. The lowermost unit is the Glover Island complex which is interpreted as a dismembered ophiolite. It is nonconformably overlain by a conglomerate unit. A volcanic unit stratigraphically overlies the conglomerate unit.

Structures related to five deformational events (D1-D5) are recognized in the Schist group. A chlorite grade, penetrative schistosity (S1) formed during D1 and was overprinted by porphyroblasts of biotite, albite and garnet during the D1 to D2 interkinematic time interval. These porphyroblasts are deformed by a well developed crenulation cleavage (S2). S1 and S2 are subparallel and form a composite schistosity folded by numerous, open, minor F3 folds. All of these structures and rocks are involved in a major, late deformation (D4) which produced the large scale, south-plunging anticline on Glover Island. Minor open folds (F5) and high angle faulting followed this event.

The Glover Formation contains a chlorite grade, composite schistosity (S1'/S2') that has undergone the same D3-D5 structural history as the underlying Schist group. This composite schistosity consists of a penetrative schistosity (S1') overprinted by a crenulation cleavage (S2').

Emplacement of the Glover Island complex occurred before D3 and probably before the D2 deformational event. The complex must have been emplaced before D3 because a major F3 fold involves the Glover Island complex and the underlying Schist group. Furthermore the probable correlation of S2 in the Schist group with S2' in the Glover Formation requires a pre-D2 emplacement age. Absolute age of these structures is unknown.

Introduction

This report summarizes the stratigraphy, structure and metamorphism of central Glover Island (parts of NTS map areas 12A/12, 13), based upon field work and petrography during 1978 and 1979. Important rock units are described and a structural and metamorphic history is presented. The timing of deformation, metamorphism and ophiolite emplacement is an important concept in this structural history and is considered in detail below.

General Geology

Glover Island is located in the southern half of Grand Lake in western Newfoundland. Two major rock groups are exposed on this island (Fig. 10.1). To the west are polydeformed and metamorphosed schists informally termed the Schist group. To the east are dominantly mafic rocks of the Glover Formation. The Glover Formation consists of a basal igneous massif (Glover Island complex) nonconformably overlain by a thin, basal metaconglomerate which is overlain by mafic metavolcanics. The Glover Island complex is interpreted to be a fragment of dismembered ophiolite and the ophiolite-schist contact to be the Baie Verte-Brompton Line (Williams and St-Julien, 1978).

The Schist Group

Rocks west of the Glover Formation consist of polydeformed semipelitic schists with minor amphibolite, marble and gneiss. These previously unnamed rocks are informally termed the Schist group. The group outcrops along the western side of central Glover Island in the core of a major south-plunging anticline (Fig. 10.1); approximately 1 km of its upper part is exposed. True thickness is unknown as the base of the section is not exposed.

The Schist group consists primarily of conglomerate, biotite schist, albite schist, and quartzite. Pebble conglomerate horizons containing granitic and quartz clasts (1-2 cm) are abundant toward the base of the group. These conglomerate units are interlayered with micaceous quartzites and albite schists. Albite schists contain distinctive 2-3 mm porphyroblasts of albite. Biotite schists with 5 mm porphyroblasts of biotite outcrop in the upper part of the section.

A number of distinctive lithologies are present within the group which will eventually be raised to formational status when the Schist group is formally defined. A concordant amphibolite outcrops towards the base and extends throughout the area. A thin (1 m) but laterally extensive marble unit is present in the central part of the group as well. the uppermost section consists of a distinctive, highly graphitic phyllite.

The basal unit in the Schist group consists of a pink, medium grained, concordant quartzo-feldspathic gneiss cut by numerous mafic layers. This gneiss is uniform in composition and contains a prominent schistosity that is roughly concordant with bedding in overlying rocks. It probably represents a pretectonic granitic intrusion cut by later mafic dykes. Its age is unknown, but probably Paleozoic based upon the age of the country rock as discussed in a separate section.

Structure and Metamorphism of the Schist Group

Structures relating to five deformational events (D1-D5) have been recognized and are shown correlated with mineral growth in Figure 10.2 based upon the criteria outlined by Spry (1969). A composite schistosity (S1/S2) composed of a regional schistosity (S1) and a later subparallel

[1] Department of Geology, Memorial University of Newfoundland, St. John's, Newfoundland, A1B 3X5

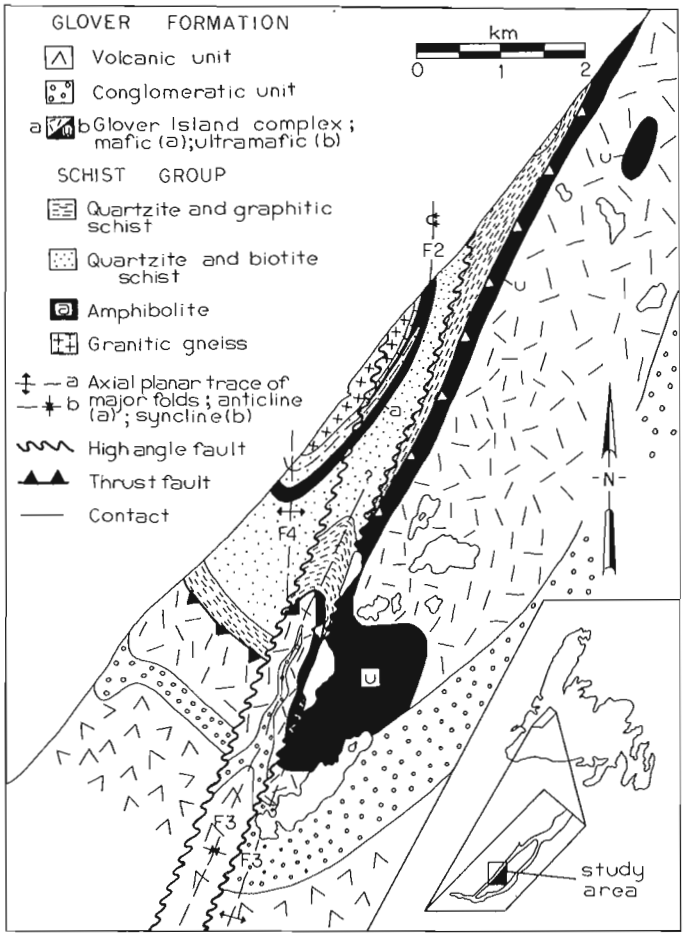

Figure 10.1. *Geology central Glover Island area, Newfoundland.*

crenulation cleavage (S2) was folded throughout the area by minor F3 folds. These structures were subsequently folded into a broad south-plunging anticline (F4) and overprinted by later, open, minor folds (F5). The last recognized deformation in the Schist group involved high angle faulting.

S1/S2 Composite Schistosity An S1/S2 composite schistosity is continuous throughout the Schist group. It consists of a penetrative schistosity (S1) overprinted by a nearly coplanar crenulation cleavage (S2) associated with a well developed mineral lineation (L2). Extensive porphyroblast growth of biotite, albite, and garnet occurred during the interkinematic interval bracketed by D1 and D2 (Fig. 10.2) such that S1 and S2 can be easily distinguished in the field or in thin section. Where porphyroblasts are absent, as within the upper part of the group, a single cleavage is observed and is assumed to be composite in origin.

S1 is a penetrative schistosity defined by lepidoblastic muscovite, chlorite and the long dimension of elongate epidote grains. S1 formed during chlorite metamorphic grade, as is shown by the ubiquitous mineral assemblage muscovite-chlorite-epidote.

S1 is overprinted by posttectonic biotite, albite, and garnet porphyroblasts related to a major, static, metamorphic event which corresponds to the peak of metamorphism in the area. Porphyroblasts of biotite are most abundant. These are randomly oriented and nearly ubiquitous throughout the area. Locally they range up to 5 mm in diameter.

Porphyroblasts of albite are also locally abundant. These contain inclusion trails of quartz, biotite and epidote and are generally less than 2 mm in diameter. Biotite inclusions are randomly oriented and probably represent posttectonic biotites incorporated into the albite porphyroblast early in its growth history.

Microstructures associated with this metamorphic event are typical of those formed during a static metamorphic event. Porphyroblasts are randomly oriented and where inclusion trails are present these trails are generally straight.

A strong gradient in metamorphic conditions existed during this post-D1 metamorphism. The highest grade metamorphic mineral assemblage in the area consists of porphyroblasts of garnet and biotite. This assemblage is only recognized at the very base of the section and is correlated with this metamorphic event. Porphyroblasts of biotite are far more abundant and occur throughout the area except for the very upper part of the section where they are absent. This distribution of metamorphic minerals is interpreted to represent garnet and biotite isograds. Thus post-D1 metamorphic conditions range from chlorite grade in the upper part of the Schist group to garnet grade at its base.

S2 constitutes the dominant cleavage in the area. It crenulates an S1 penetrative schistosity and deforms porphyroblasts of biotite, albite and garnet.

S2 is associated with a well developed lineation (L2) formed by elongate pressure shadows of quartz and muscovite adjacent to porphyroblasts of biotite and albite. This lineation parallels bedding-S2 intersection lineations.

Growth of chlorite, muscovite and albite occurred during D2. Chlorite pressure fringes around relict biotites are oriented parallel to S2 and S2 muscovite locally overprints relict biotites.

Albite porphyroblasts formed during post-D1 metamorphism have straight inclusion trails. Locally these porphyroblasts have rims with curved inclusion trails. Straight inclusion trails in core regions reflect the original orientation of S1. Curved inclusion trails in porphyroblast rim areas reflect synkinematic albite growth during D2 and rotation of S1 into parallelism with S2. This microstructure is observed in albite schists from the hinge of the major F2 fold shown in Figure 10.1. Elsewhere S1 and S2 are subparallel and inclusion trails in porphyroblasts are straight.

Growth of synkinematic chlorite, muscovite and albite during D2 (Fig. 10.2) indicates chlorite grade metamorphic conditions during this event. Locally biotite is partially retrograded to chlorite during D2. Limited postkinematic albite growth occurred after D2 as shown by post-D2 helicitic albites containing F2 crenulations.

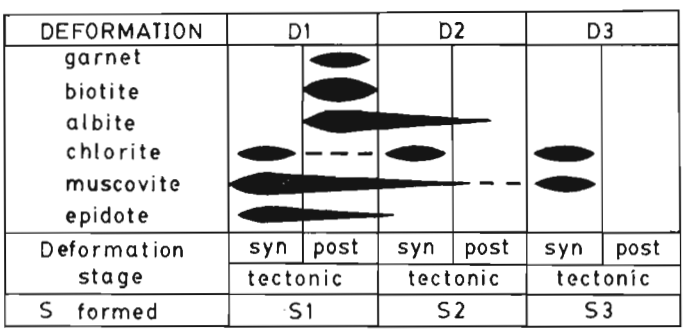

Figure 10.2. *Mineral growth correlated with structural event for rocks of the Schist group.*

Orientation data for S2 and L2 are shown in equal area, stereographic projection in Figure 10.3. S2 data from individual subareas form great circle girdles due to later folding during D3 and D4. This later folding is broadly coaxial as evidenced by the rather consistent orientation of L2.

A major F2 fold is recognized in the Schist group outlined by the thin concordant amphibolite layer shown in Figure 10.1. This structure is an upright isoclinal synform which plunges gently to the south. Graded beds in a quartzite from the less deformed hinge area indicate it is synclinal and west-facing.

D3 Structures D3 is associated with three fabric elements: a heterogeneously developed crenulation cleavage (S3); numerous small scale minor folds (F3); and a well developed intersection lineation (L3). S3 is only recognized in areas of intense F3 folding. It is axial planar to F3 folds and in thin section is a differentiated crenulation cleavage. Muscovite and chlorite locally define S3 but generally little or no mineral growth is recognized. F3 folds are generally upright, tight to open and tend to be chevron in style where contrasting lithologies are involved. L3 is a well developed intersection lineation formed during D3. This intersection lineation plunges moderately to the south (Fig. 10.4) and parallels F3 fold axes.

D3 structures display a strong strain gradient within the Schist group. They are most intense in the upper part of the section where the S1/S2 composite schistosity is locally transposed. In the base of the section D3 structures are far less evident and consist of rare open F3 folds.

Orientation data for S3 and L3 are given in Figure 10.4. In the synoptic diagram (Fig. 10.4d) it can be seen that poles to S3 form a diffuse great circle girdle. This great circle girdle reflects the major south-plunging anticline in the area (F4). In each individual subarea a tailed point maximum pattern is present. Comparison with S2 data for individual subareas (Fig. 10.3) shows that poles to S2 tend to form nearly complete great circle girdles. This contrast in distribution of poles to S2 and S3 is thought to be due to the fact that S2 has been coaxially folded by two generations of folds, F3 and F4. S3 has only been affected by a single generation of folds, F4, producing partial great circle girdles instead of complete girdles as in the case of S2.

This aspect is also demonstrated by the L3 data plotted in Figure 10.4. L3 data for individual subareas exhibit a moderately south-plunging point maximum in all cases. However a great circle girdle pattern intersecting this point maximum is also apparent, especially in Figure 10.4a. Fold axes or intersection lineations formed by folding of a nonplanar surface will be distributed in a great circle girdle pattern corresponding to the axial plane of that fold (e.g. Turner and Weiss, 1963, p. 127). The great circle girdle patterns for L3 data shown in Figure 10.4 are interpreted to reflect the folding of a nonplanar surface formed by deformation related to D2. Thus S3 and L3 both reflect the complex structural history of the area.

A major F3 fold is recognized in the southeastern part of the terrain underlain by the Schist group (Fig. 10.1). This fold is dextral, faces west and plunges moderately south. Its axial plane is upright and trends north-south. Both anticlinal and synclinal hinges are recognized although they are separated by a late, high angle fault. This major F3 fold pair involves the Glover Island complex and the overlying section as well as the Schist group. D3 must therefore postdate movement along the structural surface separating the Glover Island complex from the Schist group.

D4 Structures A major south-plunging anticline with a north-south trending, upright, axial surface is exposed on Glover Island (Fig. 10.1). This major structure controls the distribution of rocks on Glover Island including exposure of the Schist group in its core. Poles to S3 surfaces are folded into a diffuse great circle girdle by this major structure (Fig. 10.4d). Scatter in this data reflects later deformation (D5). Poles to S2 surfaces (Fig. 3) form great circle girdles in each individual subarea due to the effect of D3 deformation. These girdles are progressively rotated about a south-plunging axis by this major F4 anticline as seen in Figure 10.3.

A weak crenulation cleavage which overprints S3 is present in scattered outcrops throughout the Schist group. This cleavage is upright to moderately west-dipping and trends roughly north-south. It is interpreted to represent an axial planar fabric to the major F4 anticline on Glover Island. It is important to note, however, that this interpretation assumes continuity between widely spaced outcrops and must therefore be considered tentative.

D5 Structures All structures in the area are deformed by an episode of broad, open folding about east-west trending axial planes. This is an extremely difficult deformation to characterize because no cleavage or outcrop scale minor folds are associated with it. Folding is very broad and open and only noticeable in areas of nearly complete exposure.

High Angle Faulting The last deformational episode recorded in rocks on Glover Island involves high angle faulting. These faults are vertical and trend roughly north-south (Fig. 10.1). Displacement is dextral from offset of map units but the dip slip and strike slip components of this displacement cannot be determined.

Correlation and Age of the Schist Group

The Schist group resembles polydeformed and metamorphosed schists and gneisses to the west of Grand Lake. These rocks are correlated with the western division of the Fleur de Lys Supergroup on the Baie Verte Peninsula of northwest Newfoundland by most workers (Church, 1969; Williams, 1978).

The Fleur de Lys Supergroup is interpreted to be Cambrian in age based upon its interpretation as a clastic wedge developed along the continental margin of North America following rifting and formation of Iapetus (Stevens, 1970; Bird and Dewey, 1970). A similar age is hypothesized for the Schist group.

The Glover Formation

Rocks west of the Schist group comprise the Glover Formation (Riley, 1957). The Glover Formation is composed of three distinct map units. The basal part consists of an igneous plutonic massif of ultramafic and mafic rocks informally termed the Glover Island complex (Knapp et al., 1979). Overlying this massif are metaconglomerates and mafic metavolcanics. When a formal definition of all units within the Glover Formation can be made, it deserves to be raised to group status.

The Glover Island Complex

The Glover Island complex (Knapp et al., 1979) is a metamorphosed igneous massif composed of variably serpentinized ultramafic rocks, cumulate layered metagabbros and minor metabasalts interpreted to represent a dismembered ophiolite (Williams and St-Julien, 1978). It forms a continuous unit structurally overlying the Schist

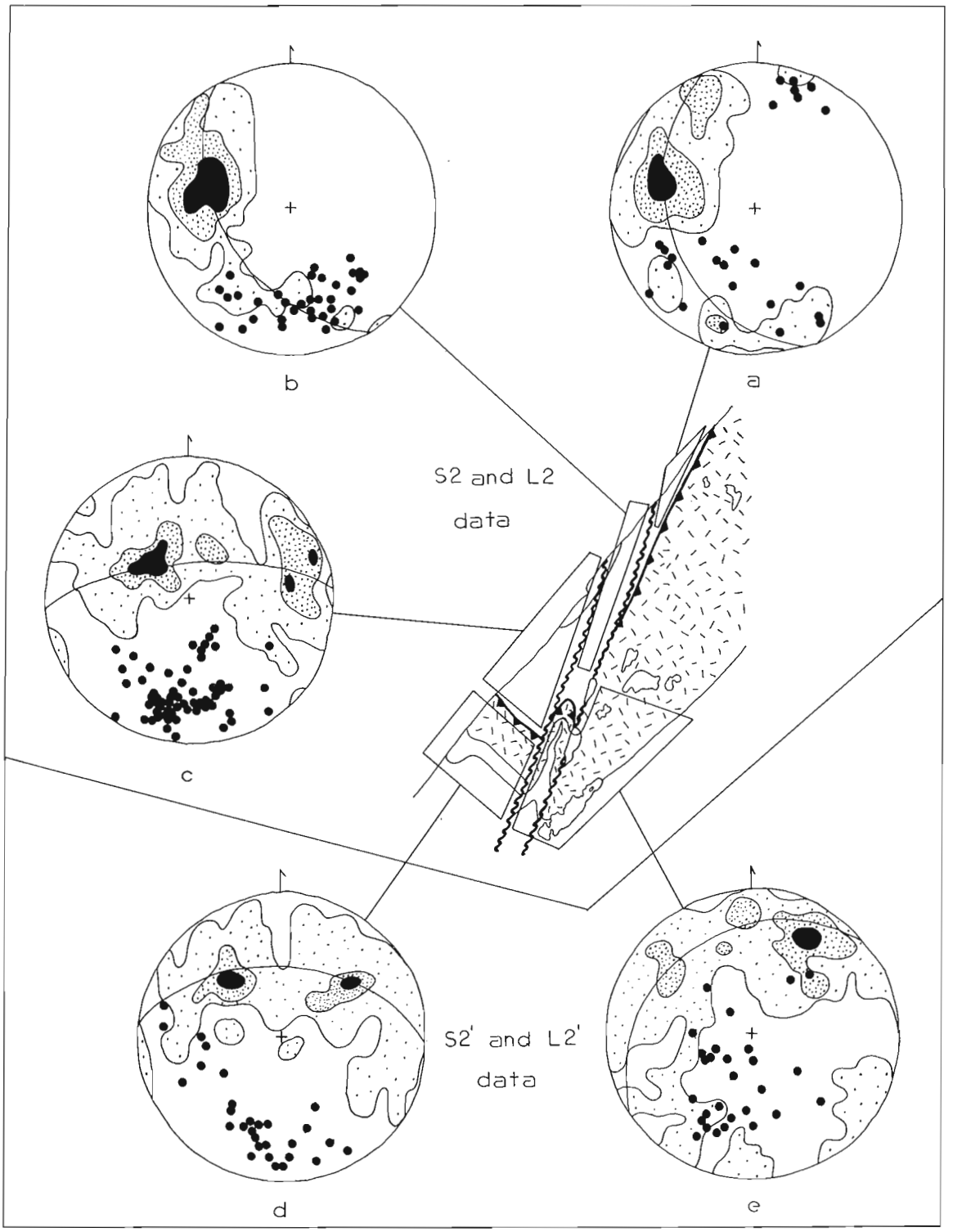

Figure 10.3. *Equal area stereographic projections of D2 and D2' data. Figures 10.3a, 10.3b, and 10.3c show the orientation of poles to S2 surfaces (contoured) and L2 lineations (solid dots). Figures 10.3d and 10.3e show the orientation of poles to S2' surfaces (contoured) and L2' lineations (solid dots). Contour-intervals in per cent per one per cent area, the number of points contoured, and the number of lineations plotted for each figure, are as follows:*

(10.3a) 1, 5, 20; S2=166; L2=21;

(10.3b) 1, 5, 9; S2=110; L2=34;

(10.3c) 1, 5, 8; S2=139; L2=63;

(10.3d) 1, 5, 10; S2'=139; L2'=29;

(10.3e) 1, 5, 10; S2'=154; L2'=28.

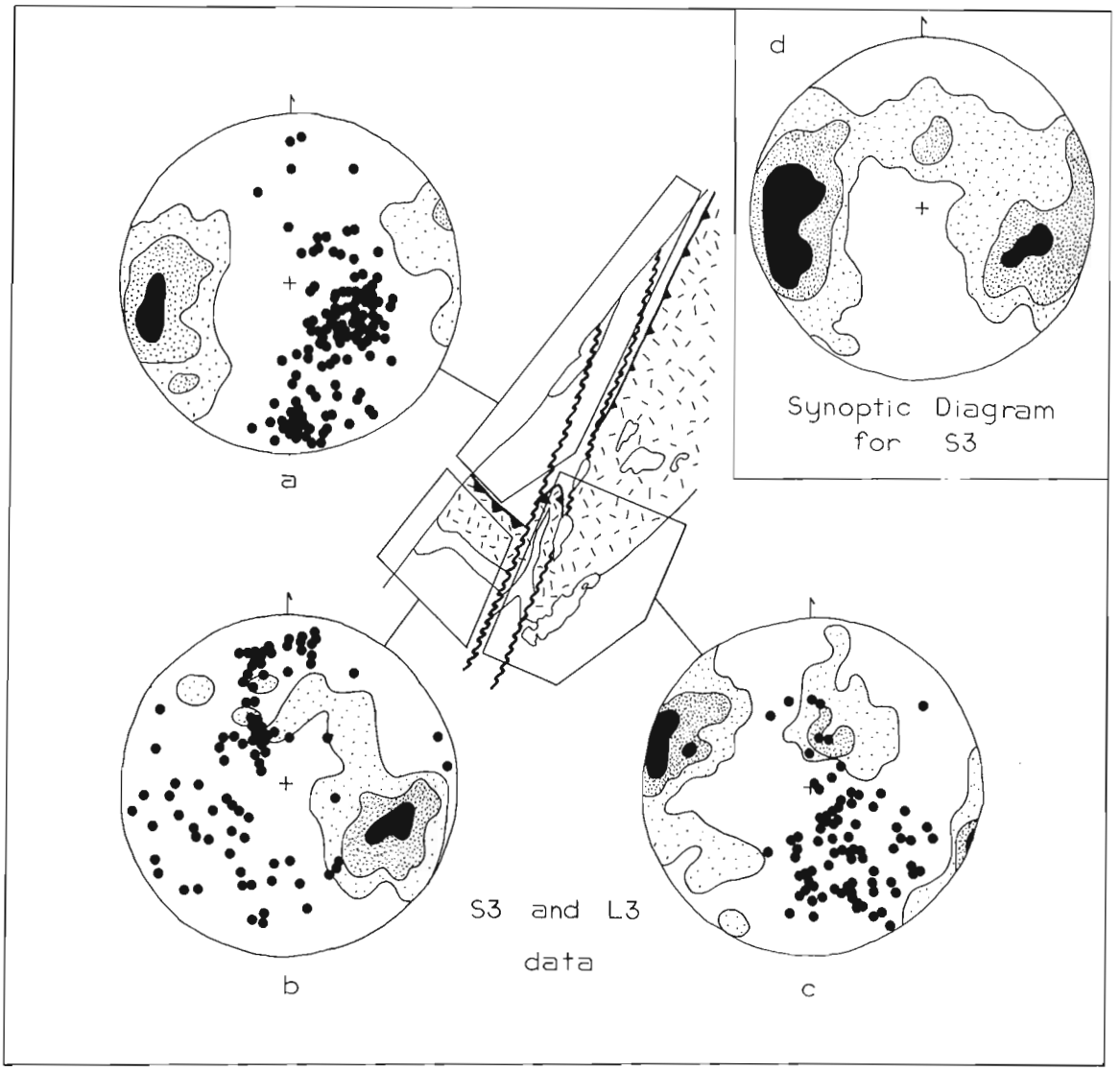

Figure 10.4. *Equal area stereographic projections of poles to S3 surfaces (contoured) and L3 lineations (solid dots). Contour intervals in per cent per one per cent area, the number of points contoured, and the number of lineations plotted for each figure, are as follows:*

(10.4a) 1, 5, 15; S3=116; L3=129;
(10.4b) 1, 4, 9; S3=74; L3=91;
(10.4c) 1, 3, 5; S3=63; L3=81;
(10.4d) 1, 4, 10; S3=256.

ıp and is exposed along the western shoreline of Glover nd at two localities (Fig. 10.1). Total thickness of the ıplex ranges between 500 and 1300 m.

Ultramafic rocks overlie talc-carbonate rocks at the ɜ of the complex at its northern outcrop extent ;. 10.1). These ultramafic rocks are sequentially overlain cumulate layered gabbro and massive leucocratic gabbro. eral grading within cumulate layers indicates the complex ight-side-up. The proportion of metagabbro and meta- alt in the complex increases to the southwest at the ense of ultramafic rocks. Talc-carbonate rocks are ɜent at the base of the complex throughout its extent.

Ultramafic rocks are composed of serpentine, ɔhibole and clinopyroxene. Clinopyroxene is of igneous ;in and contains abundant exsolved orthopyroxene(?) and que material. These relict clinopyroxenes are set in a decussate serpentine matrix. Relict cumulate textures are well preserved. Subidioblastic amphibole is secondary and replaces serpentine and clinopyroxene.

Gabbro is composed of amphibole, clinopyroxene and zoisite. Zoisite aggregates pseudomorph plagioclase. Amphibole is pale olive green in colour and similar in size to clinopyroxene relicts and pseudomorphs of plagioclase. It is probably a metamorphic replacement of clinopyroxene. These minerals form an interlocking granoblastic aggregate interpreted to represent a cumulate igneous texture.

Numerous mafic dykes intrude the massif. Both pyroxene- and amphibole-bearing varieties are present. Excellent subophitic textures are preserved in each. The amphibole-bearing variety is especially distinctive due to cores of euhedral, deep brown amphibole rimmed by a dark green amphibole.

Talc-Carbonate Rocks The base of the Glover Island complex consists of distinctive orange weathering talc-carbonate rocks derived by CO_2 metasomatism of an ultramafic protolith. As the actual contact between unaltered and altered ultramafic rocks is abrupt, it is likely that some postmetasomatism faulting has occurred along this surface.

Rocks in the talc-carbonate zone consist primarily of talc, serpentine, dolomite, magnesite, quartz and white mica in varying proportions. Carbonate minerals generally occur as subidiomorphic porphyroblasts set in a fine grained talc or talc-serpentine matrix. Carbonate-mica and carbonate-quartz rocks are also present.

The Conglomerate Unit

Rocks of the Glover Formation overlying the Glover Island complex can be divided into two distinct map units: a lower, metaconglomerate unit and an upper, dominantly mafic metavolcanic unit. These units are referred to as the conglomerate unit and the volcanic unit, respectively.

The conglomerate unit is distinctive and is located immediately above the Glover Island complex. It consists of an assortment of matrix-supported rounded clasts set in a fine grained metasedimentary matrix. This matrix ranges from a micaceous quartzite to a phyllite and is everywhere thinly layered. Individual layers are generally less than 5 mm thick lending a distinctive laminated appearance to the rock. The conglomerate unit ranges between 160 and 500 m in thickness.

All recognized clasts in the conglomerate unit are igneous in origin. They range from 1 to 10 cm in diameter and average between 2-5 cm. Gabbro clasts are most abundant but fine grained mafic volcanic clasts and clasts of a granitic rock have also been identified. All clasts are well rounded. The largest identified clasts as well as the greatest abundance of clasts occur in the basal part of the unit.

Sedimentological evidence indicates that the contact between the ophiolite and the overlying conglomerate may be erosional in origin. Many of the clasts in the conglomerate consist of gabbro identical to that in the underlying massif. Clasts are coarsest and most abundant near the basal contact as well. This contact is a high strain zone, probably reflecting a mechanical contrast between the crystalline massif and overlying sediments. Thus examination of the contact itself is uninformative with regards to its nature. The clast evidence, however, is significant and strongly suggests that the conglomerate unit nonconformably overlies the Glover Island complex.

The Volcanic Unit

The volcanic unit consists primarily of mafic volcanics and volcaniclastic sediments metamorphosed under greenschist facies conditions. It conformably overlies the conglomerate unit throughout the area shown in Figure 10.1. Igneous textures, and even pillows, are recognizable in low strain areas. Thickness of the volcanic unit is unknown as the top of the section is not exposed. Minimum thickness is 2 km.

The dominant rock type in the volcanic unit is a porphyritic metabasalt. Subophitic textures formed by laths of plagioclase (now albite) enclosed in an amphibole or less commonly a clinopyroxene are widespread. Plagioclase phenocryst pseudomorphs are abundant. These pseudomorphs are composed of an aggregate of albite, zoisite, and minor muscovite. The original shape of the phenocryst is generally well preserved.

The volcanic unit also contains a significant proportion of metamorphosed silicic volcanic rocks. These are porphyritic with euhedral phenocrysts of feldspar and quartz in a fine grained silicic matrix. Minor muscovite and epidote are also present.

The remainder of the volcanic unit is composed of metamorphosed volcaniclastic metasediments and tuffaceous rocks. These fine grained, well bedded rocks are rich in epidote, chlorite and relict feldspar.

The conglomerate unit-volcanic unit contact is interpreted as gradational. Mafic volcanic rocks are interlayered with quartzites in the upper part of the conglomerate and eventually quartzite gives way entirely to mafic volcanics and volcaniclastics.

Structure of the Glover Formation

Structures relating to five deformational events are recognized in the Glover Formation. Three of these (D3-D5) are also recognized in the underlying Schist group and have already been described. The oldest structures recognized in the Glover Formation (S1' and S2') form a composite schistosity. Mineral growth has not been correlated with these events except in a very general way due to the difficulty of separating these two cleavages. The relationship between this composite schistosity and structures in the Schist group bears directly upon the age of emplacement of the Glover Island complex and is discussed later.

S1'/S2' Composite Schistosity S1' and S2' are coplanar cleavages formed under greenschist facies metamorphic conditions. They can only be distinguished in the talc-carbonate zone at the base of the Glover Island complex and in the basal section of the volcanic unit. Higher in the section the single observed schistosity is assumed to be composite.

S1' is a penetrative schistosity formed under greenschist facies conditions. It is defined by muscovite, chlorite, amphibole, epidote and calcite in rocks of appropriate bulk composition.

S2' is a well developed crenulation cleavage associated with a pronounced stretching lineation (L2') which overprints and locally transposes S1' in the basal part of the section. L2' is a strong stretching lineation defined by pressure shadows and pull-apart structures. The orientation of these structures is shown in Figure 10.3.

Correlation of the Glover Formation

Rocks in a similar structural setting to the Glover Formation are present on the Baie Verte Peninsula. Ophiolitic rocks of the Advocate group (Williams et al., 1977) are structurally juxtaposed against polydeformed schists and gneisses of the Fleur de Lys Supergroup (Church, 1969) to the west. To the east are dominantly mafic volcanic rocks of the Flatwater group (Williams et al., 1977). The base of the Flatwater group consists of polymictic conglomerates containing clasts (Kidd, 1977; Williams et al., 1977). The schist-ophiolite contact on the Baie Verte Peninsula has been designated the Baie Verte-Brompton Line (St-Julien et al., 1976; Williams and St-Julien, 1978).

The Baie Verte-Brompton Line is interpreted to be continuous from the Baie Verte Peninsula to Glover Island. Lithologies and structural setting are comparable and rocks along this line must be broadly correlative (Williams and St-Julien, 1978; Knapp and Williams, 1979; Knapp et al., 1979). The Glover Island complex is correlated with the Advocate group and the conglomerate and volcanic units on Glover Island are correlated with the Flatwater group.

Correlation of the Glover Island and Advocate complexes with other ophiolitic rocks in western Newfoundland is a controversial topic. Some workers think that all ophiolitic rocks in western Newfoundland relate to the same cycle of ophiolite generation and are therefore all roughly the same age (Church and Stevens, 1971; Williams, 1975, 1977; Williams, et al., 1977). Others maintain that different ophiolite complexes originated in different basins and may therefore be of different ages (Bird and Dewey, 1970; Dewey and Bird, 1971; Kennedy, 1973, 1975; Kidd, 1977; Kidd et al., 1978).

At Grand Lake a simple cross-section is apparent with schists, gneisses and carbonate rocks separating ophiolitic rocks of the Humber Arm Allochthon (Williams, 1975) from the Glover Island complex (Riley, 1957, 1962; Knapp et al., 1979). The ophiolite-schist contact (Baie Verte-Brompton Line) is the most logical root zone for these transported ophiolitic rocks because no alternative root zone is recognized. The Glover Island complex is tentatively correlated with ophiolitic rocks of the Humber Arm Allochthon.

Age of the Glover Formation

The rocks of the Humber Arm Allochthon are known to be Early Ordovician or older in age (Williams, 1975) and a similar age is proposed for the Glover Island complex based upon the above correlation. The age of the conglomerate and volcanic units overlying the Glover Island complex is uncertain. An Arenig graptolite fauna (Dean, 1976; Williams and St-Julien, 1978) has been recognized in a black shale unit within the Glover Formation as mapped by Riley (1957). The stratigraphic position of this black shale unit in the Glover Formation is not known. Considering the lithological diversity of the Glover Formation, it is premature to assume this age is applicable to the conglomerate and volcanic units. The proposed Early Ordovician or older age for the Glover Island complex limits the age of the overlying rocks to Early Ordovician or younger based upon interpretation of the base of the conglomerate unit as a nonconformity.

Timing of Ophiolite Emplacement

The emplacement of the Glover Island complex against the Schist group is an extremely important event in the structural history of the Glover Island area. Determination of relative age of emplacement rests upon correlation of structures below and above the ophiolite. Structures, which are not present both above and below the ophiolite, must predate emplacement.

Direct evidence demonstrates that ophiolite emplacement predates D3, namely the major F3 fold pair located in the southern part of the area which involves both the Schist group and Glover Island complex. As ophiolite emplacement must predate D3, it is important to determine if D1 or D2 also postdate ophiolite emplacement.

Due to parallelism of the thrust surface at the base of the Glover Island complex with S1, S2, S1' and S2' it cannot be determined if any of these pre-D3 structures directly involve the ophiolite-schist contact. Thus their age relative to the ophiolite-schist contact must be based upon correlation of structures above this surface with those below.

Both S2 and S2' are well developed cleavages containing a strong stretching lineation. The orientation of this lineation as well as the cleavages themselves are shown in Figure 10.3 (compare Fig. 10.3c with 10.3d). It is clear from this figure that these two lineations and cleavages are identical in orientation and may be correlative. This would indicate ophiolite emplacement predates D2 and thus occurred quite early in this structural history. More conclusive evidence for this early emplacement must be sought.

Acknowledgments

The author thanks G. Tobin for assistance in the field and H. Williams for critically reading the paper. Financial support was provided by E.M.R. Research Agreement 2239-4-48/79 and N.S.E.R.C. Operating Grant A5548 to H. Williams and a Memorial University of Newfoundland Fellowship to the author.

References

Bird, J.M. and Dewey, J.F.
1970: Lithosphere plate-continental margin tectonics and the evolution of the Appalachian Orogen; Geological Society of America Bulletin, v. 81, p. 1031-1060.

Church, W.R.
1969: Metamorphic rocks of Burlington Peninsula and adjoining areas of Newfoundland, and their bearing on continental drift in North Atlantic; in M. Kay, ed., North Atlantic – Geology and Continental drift, American Association of Petroleum Geologists, Memoir 12, p. 212-233.

Church, W.R. and Stevens, R.K.
1971: Early Paleozoic ophiolite complexes of the Newfoundland Appalachians as mantle-oceanic crust sequences; Journal of Geophysical Research, v. 76, p. 1460-1466.

Dean, W.T.
1976: Some aspects of Ordovician correlation and trilobite distribution in the Canadian Appalachians; in M.G. Basset, ed., The Ordovician System, Cardiff University of Wales Press and National Museum of Wales, p. 227-250.

Dewey, J.F. and Bird, J.M.
1971: Origin and emplacement of the ophiolite suite: Appalachian ophiolites in Newfoundland; Journal of Geophysical Research, v. 76, p. 3179-3206.

Kennedy, M.J.
1973: Pre-Ordovician polyphase structure in the Burlington Peninsula of the Newfoundland Appalachians; Nature Physical Sciences, v. 241, p. 114-116.

1975: Repetitive orogeny in the northeastern Appalachians – new plate models based upon Newfoundland examples; Tectonophysics, v. 28, p. 39-87.

Kidd, W.S.F.
1977: The Baie Verte Lineament, Newfoundland: ophiolite complex floor and mafic volcanic fill of a small Ordovician marginal basin; in M. Talwani and W.C. Pitman III, ed., Island Arcs, Deep Sea Trenches and Back-arc Basins, Maurice Ewing Volume, American Geophysical Union, p. 407-418.

Kidd, W.S.F., Dewey, J.F., and Bird, J.M.
1978: The Mings Bight ophiolite complex, Newfoundland: Appalachian oceanic crust and mantle; Canadian Journal of Earth Sciences, v. 15, p. 781-804.

Knapp, D.A. and Williams, H.
1979; Ophiolitic rocks along the Baie Verte-Brompton Line at Grand Lake, western Newfoundland; Geological Society of America, Abstracts with Programs, v. 11, p. 20.

Knapp, D.A., Kennedy, D., and Martineau, Y.
1979: Stratigraphy, structure and regional correlation of rocks at Grand Lake, western Newfoundland; in Current Research, Part A, Geological Survey of Canada, Paper 79-1A, p. 317-325.

Riley, G.C.
1957: Red Indian Lake (west half); Geological Survey of Canada, Map 8-1957.

1962: Stephenville map-area, Newfoundland; Geological Survey of Canada, Memoir 323.

St-Julien, P., Hubert, C., and Williams, H.
1976: The Baie Verte-Brompton Line and its possible tectonic significance in the northern Appalachians; Geological Society of America, Abstracts with Programs, v. 8, p. 259-260.

Spry, A.
1969: Metamorphic textures; Pergamon Press Ltd., New York.

Stevens, R.K.
1970: Cambro-Ordovician flysch sedimentation and tectonics in west Newfoundland and their possible bearing on a Proto-Atlantic Ocean; in J. Lajoie, ed., Flysch Sedimentology in North America, Geological Association of Canada Special Paper 7, p. 165-177.

Turner, F.J. and Weiss, L.E.
1963: Structural analysis of metamorphic tectonites; McGraw-Hill Book Co., New York.

Williams, H.
1975: Structural succession, nomenclature, and interpretation of transported rocks in western Newfoundland; Canadian Journal of Earth Sciences, v. 12, p. 1874-1894.

1977: Ophiolitic mélange and its significance in the Fleur de Lys Supergroup, northern Appalachians; Canadian Journal of Earth Sciences, v. 14, p. 987-1003.

1978: Tectonic lithofacies map of the Appalachian Orogen; Memorial University of Newfoundland, Map No. 1.

Williams, H. and St-Julien, P.
1978: The Baie Verte-Brompton Line in Newfoundland and regional correlations in the Canadian Appalachians; in Current Research, Part A, Geological Survey of Canada, Paper 78-1A, p. 225-229.

Williams, H., Hibbard, J.P., and Bursnall, J.T.
1977: Geological setting of asbestos-bearing ultramafic rocks along the Baie Verte Lineament, Newfoundland; in Report of Activities, Part A, Geological Survey of Canada, Paper 77-1A, p. 351-360.

11. AN UNUSUAL TRILOBITE FAUNULE FROM LLANDEILO OR LOWEST CARADOC STRATA (MIDDLE ORDOVICIAN) OF NORTHERN YUKON TERRITORY

Project 500029

Rolf Ludvigsen[1]
Institute of Sedimentary and Petroleum Geology, Calgary

Ludvigsen, R., An unusual trilobite faunule from Llandeilo or lowest Caradoc strata (Middle Ordovician) of northern Yukon Territory; in Current Research, Part B, Geological Survey of Canada, Paper 80-1B, p. 97-106, 1980.

Abstract

An unusual trilobite faunule composed of ***Agerina norrisi*** *n. sp.,* ***Cnemidopyge norfordi*** *n. sp.,* ***Lonchodomas carinatus*** *Cooper, and* ***Robergiella*** *cf.* ***sagittalis*** *Whittington is described from dark limestones within the upper part of a thick carbonate succession near Mount Burgess, northern Yukon Territory. Trilobite-based correlations to Ordovician rocks of Virginia indicate a Llandeilo to earliest Caradoc age for the faunule. The conodonts belong in the upper* ***Pygodus anserinus*** *–* ***Amorphognathus tvaerensis*** *zones. The trilobite faunule has affinity to upper slope faunas of Early and Middle Ordovician age in Spitsbergen and northern Canada, but is completely dissimilar to temporally equivalent faunas on the carbonate platform in the District of Mackenzie.*

Introduction

During stratigraphic investigations of the Geological Survey of Canada's Operation Porcupine in northern Yukon Territory in 1962, A.W. Norris measured a section on an unnamed mountain immediately to the east of Mount Burgess. The section consists of nearly 1100 m of unnamed limestone and dolostone preserved beneath an unconformity at the base of the Devonian Gossage Formation (Fig. 11.1; Norford, 1964, p. 76-80). Fossils are scarce in this section, but a single collection from a 3 m thick unit of brown, finely crystalline, and thinly bedded limestones some 85 m below the unconformity yielded abundant inarticulate brachiopods and trilobites, including well preserved representatives of the genera **Agerina** Tjernvik, **Cnemidopyge** Whittard, **Robergiella** Whittington, and **Lonchodomas** Angelin. This unusual association of trilobites is described in this paper.

Few Ordovician trilobites are known from northern Yukon Territory. Kobayashi (1936) described species of **Geragnostus, Parabolinella,** and **Ptychopleurites** from lower Tremadoc strata of the Yukon River area on the Alaska-Yukon boundary, some 130 km southwest of Mount Burgess. Lenz and Churkin (1966) described species of **Robergia, Cryptolithoides,** and **Ampyxina** from Ashgill strata of the Road River Formation on Snake River, some 300 km east of Mount Burgess. Dean (1973a) described species of **Geragnostus, Ampyxoides, Shumardia, Cybelurus, Carolinites, Remopleurides, Peraspis,** and **Nileus** from Llanvirn strata in the Keele Range, some 120 km northwest of Mount Burgess. A few additional Ordovician trilobites were included in faunal lists by Norford (1964).

Age and Environment of the Faunule

The trilobite faunule from GSC loc. 54290 consists of common to abundant **Cnemidopyge norfordi** n. sp. and **Agerina norrisi** n. sp. and rare **Robergiella** cf. **sagittalis** Whittington and **Lonchodomas carinatus** Cooper, in addition to unstudied fragments of a large cheirurid trilobite. Similar trilobite associations have not been recorded from Ordovician rocks of western North America and, therefore, regional correlations cannot be made.

Closely similar faunas have been recorded only from Ordovician rocks of Virginia. The Effna Limestone contains possible **Agerina norrisi** (that is, **Isbergia virginica** Cooper, 1953, Pl. 1, fig. 21, 22, 27 only; see section on Systematic Paleontology), the lower Edinburg Formation contains **Lonchodomas carinatus** Cooper (Whittington, 1959), and the Liberty Hall facies of the lower Edinburg contains **Robergiella sagittalis** Whittington, 1959. This stratal interval falls within the upper **Pygodus anserinus** – lower **Amorphognathus tvaerensis** conodont zones and the **Nemagraptus gracilis** – lower **Didymograptus multidens** graptolite zones (Bergström, 1971, Fig. 10); that is Llandeilo and early Caradoc in terms of the British series and Chazyan and early Blackriveran in terms of the North American stages. **Cnemidopyge** has not been recorded from other North American localities. In Britain, this genus occurs in Llandeilo and basal Caradoc strata (Hughes, 1969, p. 62). Thus, the trilobite faunule from GSC loc. 54290 suggests a Llandeilo to earliest Caradoc age.

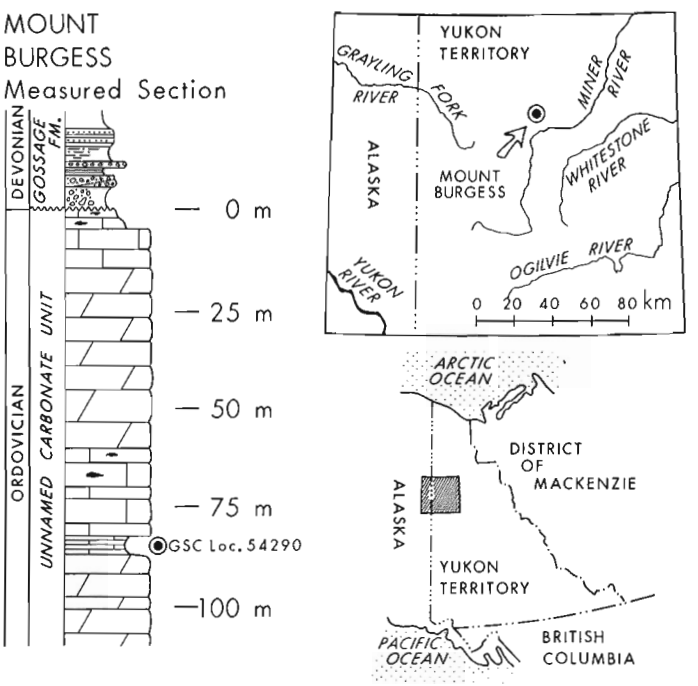

Figure 11.1. Location of measured section on unnamed mountain immediately east of Mount Burgess (66°03'N, 139°35'W). Columnar section of upper part of Ordovician and lower part of Devonian succession is based on Section 16 of Norford (1964, p. 76, 77).

[1]Department of Geology, University of Toronto, Toronto, Ontario M5S 1A1

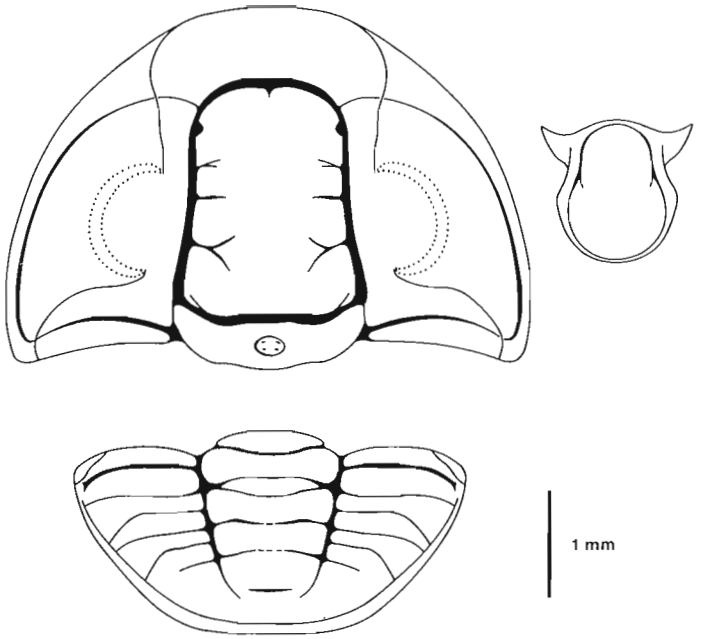

Figure 11.2. ***Agerina norrisi*** *n. sp. Reconstruction of cephalon, pygidium and hypostome.*

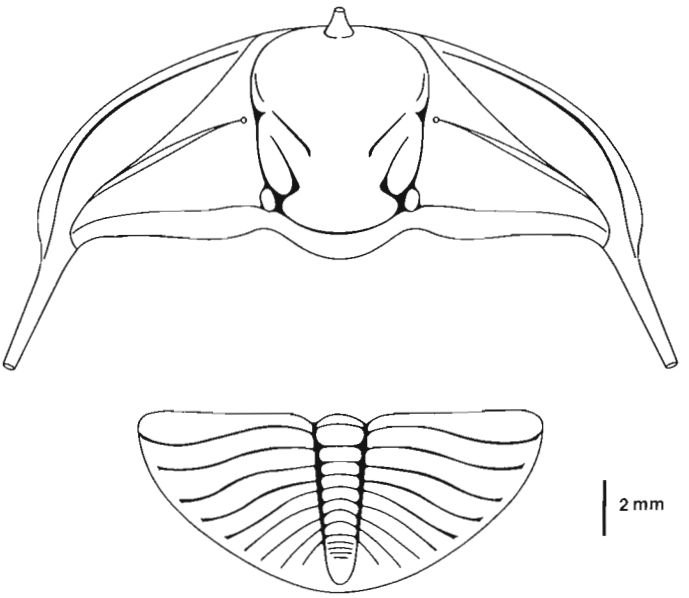

Figure 11.3. ***Cnemidopyge norfordi*** *n. sp. Reconstruction of cephalon and pygidium.*

C.R. Barnes has kindly processed a sample of limestone from GSC loc. 54290 for conodonts. He reports (letter, June 13, 1979):

> "The sample contained several hundred well preserved conodonts of North Atlantic Province affinity. The fauna is of low diversity, being dominated by **Periodon aculeatus** Hadding with several simple-cone multielement genera and a few specimens of **Eoplacognathus elongatus** (Bergström). The latter species has a restricted stratigraphic range (Bergström, 1971, p. 138) in the uppermost **Pygodus anserinus** Zone and the lower part of the **Amorphognathus tvaerensis** Zone. This range corresponds approximately to that of the **Nemagraptus gracilis** graptolite zone (i.e. upper Chazy; upper Llandeilo-lowermost Caradoc)."

The faunal assemblage at GSC loc 54290 belongs in the upper **Pygodus anserinus** – lower **Amorphognathus tvaerensis** zones of the North Atlantic conodont zonation. Second-order correlations of the conodont zones may be made with the **Nemagraptus gracilis** Zone, with Fauna 6 of the midcontinent conodont sequence of Sweet et al. (1971), and finally with the **Ceraurinella nahanniensis** Zone and, possibly, the underlying **Bathyurus granulosus** Zone and overlying **Bathyurus ulu** Zone of the zonation of Middle Ordovician platform carbonates in the District of Mackenzie (Ludvigsen, 1979b).

The complete generic dissimilarity of the **Cnemidopyge-Agerina** assemblage of the Yukon Territory and temporally equivalent platform trilobite assemblages of the District of Mackenzie is striking, but not completely unexpected. In fact, it could have been largely predicted from the recent work on Lower and Middle Ordovician trilobite biofacies by Fortey (1975) and Ludvigsen (1979a). Both of these authors outlined platform trilobite associations which were dominated by bathyurids, cheirurids, illaenids, harpids, and dimeropygids (illaenid-cheirurid community of Fortey and Biofacies I to III of Ludvigsen) and upper slope trilobite associations which include raphiophorids and **Robergiella** among others (nileid community of Fortey and Biofacies IV of Ludvigsen).

In environmental terms, the **Cnemidopyge-Agerina** assemblage can be placed on the upper slope; correlative with both the nileid community and Biofacies IV. Such a position receives support from the dark coloured and slightly bituminous nature of the thinly bedded limestones of GSC loc. 54290 and from the dominance of **Periodon** in the conodont sample prepared by C.R. Barnes. In slightly older rocks of Spitsbergen, the **Periodon** community corresponds to the nileid community (Fortey and Barnes, 1977).

The drastic biofacies change at the edge of the carbonate platform during the Early and Middle Ordovician also indicates a replacement of endemic North American trilobites and mid-continent conodont faunas by widely occurring trilobites and North Atlantic conodont faunas. This faunal replacement was probably localized along a belt which separated warm bottom waters from cold bottom waters (Taylor, 1977; Fortey and Barnes, 1977; Ludvigsen, 1979a).

The 3 m interval of dark limestones within the upper part of a thick dolostone and limestone sequence near Mount Burgess can be viewed as an incursion of Road River sediments caused either by a brief deepening or cooling period during the Llandeilo. A few tens of kilometres to the south and the southeast, the entire Middle and Upper Ordovician carbonate succession passes into basinal sediments of the Road River Formation in the Blackstone Trough (Norford, 1964, Fig. 2; Lenz, 1972, Fig. 6, 7).

Systematic Paleontology

Family BATHYURIDAE

Genus **Agerina** Tjernvik, 1956

Type species: **Agerina erratica** Tjernvik, 1956 from the Upper Planilimbata Limestone (Arenig) of central Sweden (by original designation).

Remarks: **Agerina** was established by Tjernvik (1956) for three species from Tremadoc and Arenig rocks of the Baltic area. Another species was described by Dean (1973c) from Arenig strata of Turkey and one was described by Lu (1975) from Upper Llanvirn strata of Hupeh Province, China. Tripp (1976) questionably attributed a cranidium from Llandeilo strata of Scotland to that genus.

Harrington and Leanza (1957) described a new genus, **Brackebuschia**, from Lower Tremadoc rocks of Argentina. The type and only species, **B. acheila** Harrington and Leanza, has a long (sag.) parallel-sided glabella, flat anterior border, three faint lateral glabellar furrows, and small palpebral lobes located at mid-length of cephalon. The transverse pygidium has a convex axis with four rings and faintly furrowed pleural fields. This species is very similar to both **Agerina praematura** Tjernvik from the Upper Tremadoc of Sweden and **A. norrisi** n. sp. from the Llandeilo of Yukon Territory and it should certainly be assigned to **Agerina**. Thus, **Brackebuschia** is a junior subjective synonym of **Agerina**.

Agerina has not previously been recorded on this continent. The occurrence reported here establishes its presence in Llandello or lowest Caradoc rocks of North America. Moreover, the pygidia attributed to **Isbergia virginica** Cooper from the Effna Limestone of Virginia by Cooper (1953, Pl. 1, fig. 21, 22, 27) probably belong to **Agerina**. Dean (1972) has shown that the holotype cranidium of **I. virginica** is not congeneric with the type species of **Isbergia** and, instead, belongs to the isocolid **Effnaspis** Dean. The pygidia illustrated by Cooper are so similar to those of **Agerina norrisis** n. sp. that they could record an Appalachian occurrence of that species. The Yukon and Virginia localities are of the same age; both belong in the upper **Pygodus anserinus**-lower **Amorphognatus tvaerensis** Zones (Bergström, 1971, Fig. 10, C.R. Barnes, personal communication, 1979).

As presently conceived, **Agerina** is a rare, but widespread, trilobite that occurs in Tremadoc to Llandeilo strata of four of the six main Ordovician continents that were defined by Scotese et al. (1979, Fig. 8):

GONDWANA **A. acheila** (Harrington and Leanza) [Lower Tremadoc]
A. pamphylica Dean [Arenig]

BALTICA **A. erratica** Tjernvik [Arenig]
A. praematura Tjernvik [Upper Tremadoc]
A. woehrmanni (Schmidt) [Arenig]

CHINA **A. elongata** Lu [Llanvirn]

LAURENTIA **A. norrisi** n. sp. [Llandeilo/lowest Caradoc]

In the definitive paper, Tjernvik (1956) assigned **Agerina**, without comment, to the family Bathyuridae. Whittington (in Moore, 1959) questionably assigned this genus to the same family. **Agerina** is most similar to the group of Arenig and Llanvirn bathyurid genera clustered around **Annamitella;** that is, **Annamitella** Mansuy, **Bathyuriscops** Weber, **Proetidella** Harrington and Leanza, and **Monella** Bates. The possibility that these four genera are congeneric was discussed by Whittington (in Neuman, 1964, p. 29, 30) and by Dean (1973b, p. 20, 21). From these genera, **Agerina** can be distinguished by possessing a cephalon with a less inflated glabella (particularly noticeable near the front), smaller eyes, longer (sag.) anterior border, shorter genal spines, and a more transverse pygidium with fewer and less distinct pleural furrows and narrower border. In addition, **Agerina** is considerably smaller than **Annamitella** and its allies.

Agerina first appears in the early Tremadoc and is probably the oldest bathyurid genus. Its distributional pattern though the early part of the Ordovician closely follows that of the trinucleids (Hughes et al., 1972). The earlier species of **Agerina** occur in mid- to high-paleolatitude sites on the fringes of Gondwana and Baltica; later species occur in lower paleolatitude sites in China and Laurentia. Unlike other bathyurids which proliferated in clean, shallow water carbonates with nautiloids, gastropods, and orthid brachiopods during the Arenig and Llanvirn (that is, in the Bathyurid province of Whittington and Hughes, 1972, Table 1); **Agerina** is typically found in clastic rocks or in dark muddy limestones in association with raphiophorid, agnostid, and remopleuridid trilobites and lingulid brachiopods. This suggests that, in low paleolatitudes, **Agerina** was restricted to cold water sites on the slope and platform-edge whereas "typical bathyurids" preferred warm water sites on the platform.

Agerina norrisi n. sp.

Plate 11.1, Figure 11.2

(?) 1953 **Isbergia virginica** Cooper, Pl. 1, fig. 21, 22, 27 (not fig. 20, = **Effnaspis virginica**, see Dean, 1972).

Diagnosis. A species of **Agerina** with a narrow (tr.) convex glabella possessing 3 pairs of faintly incised lateral furrows; 1s furrow is bifid, 2s and 3s are transverse. Lateral glabellar lobes are not inflated. Deep axial furrows converge slightly toward front; include small anterior pit located at mid-length of 4p lobe. A short sagittal furrow occurs on front part of glabella of some specimens. Median occipital tubercle has 4 minute pits arranged in a rectangle. Anterior cephalic border is flat and long (equal to 1/4th sagittal length of cephalon). Genal angles are rounded. Cephalon carries prosopon of minute granules and pits. Hypostome is ovoid, expanding posteriorly; border furrows are complete and median furrow is short; anterior wings are triangular and high. Pygidium is semicircular with a narrow convex border and faint border furrows. Axis narrows evenly towards rear; it does not quite reach posterior border furrow; it consists of 4 or 5 rings (1st and 2nd rings are separated by a lenticular [preannular?] lobe). Pleural field crossed by three pairs of pleural and interpleural furrows; all are faint, with the exception of the first pleural furrow which is deep. Pygidial borders carry prosopon of fine parallel terrace lines.

Holotype. An incomplete cranidium from GSC loc. 54290 (GSC 61349) illustrated on Plate 11.1, figures 1-5.

Paratypes. Cranidia (GSC 61350, 61354, 61355, 61358), pygidia (GSC 61351, 61357, 61359, 61360), free cheeks (GSC 61352, 61353), and a hypostome (GSC 61356); all from GSC loc. 54290.

Name. For A.W. Norris of the Geological Survey of Canada who collected the faunule.

Remarks. Pygidia of **Agerina norrisi** n. sp. are very similar to those illustrated by Cooper (1953, Pl. 1, fig. 21, 22, 27) as **Isbergia virginica** from the Effna Limestone of Virginia. It is quite possible that these pygidia represent **A. norrisi**, but a cranidium is needed for confirmation. The outline of the glabella and the shape and dimensions of the anterior border of the cranidium of **Agerina**? sp. described by Tripp (1976, p. 387, Pl. 4, fig. 10) from the Superstes Mudstone near Girvan, Scotland are reminiscent of **A. norrisi**. The Scottish cranidium apparently lacks the bifid 1s furrow characteristic of **A. norrisi**. The pygidium identified as **Panarchaegonus** sp. by Tripp (1976, p. 389, Pl. 4, fig. 15, 16) may well belong to **Agerina** and, it too, is similar to that of **A. norrisi**. The Scottish locality is within the **Nemagraptus gracilis** Zone and, as such, is about the same age as the Yukon occurrence of **A. norrisi**.

The long anterior cephalic border and the narrow glabella of **Agerina norrisi** effectively distinguishes it from **A. erratica** Tjernvik and **A. praematura** Tjernvik from Sweden and from **A. pamphylica** Dean from Turkey.

The glabellar shape of both **Agerina acheila** (Harrington and Leanza) and **A. elongata** Lu is close to that of **A. norrisi**. Each of these species, however, lacks the long anterior cephalic border and the bifid 1s furrow.

Family RAPHIOPHORIDAE

Genus **Cnemidopyge** Whittard, 1955

Type species. **Trinucleus nudus** Murchison, 1839 from the Upper Llandeilo of central Wales (by original designation).

Remarks. Whittard (1955) assigned **Trinucleus nudus** Murchison, **Ampyx bisectus** Elles, and **Cnemidopyge granulata** Whittard to **Cnemidopyge**. Hughes (1969) redescribed and illustrated **C. nuda** and **C. bisecta**; established a new species, **C. parva**; and suggested that **C. granulata** be considered a subspecies of **C. nuda**. In Britain, **Cnemidopyge** is confined to the **Glyptograptus teretiusculus** and **Nemagraptus gracilis** Zones in central Wales and the Welsh Borderlands; that is, essentially to the Llandeilo and basal Caradoc (Williams et al., 1972). Hughes (1969, p. 62) noted that **Cnemidopyge** has been recorded from the Upper Llanvirn to Caradoc of Scandinavia by Jaanusson.

Plate 11.1

Agerina norrisi n. sp. All from GSC loc 54290, Mount Burgess area, northern Yukon Territory.

Figures 1-5. Cranidium, holotype, dorsal and lateral views, X 9; three views of cranidium, X 18, GSC 61349.
6. Cranidium, paratype, X 22, GSC 61350.
7. Pygidium, paratype, X 11, GSC 61351.
8. Free cheek, paratype, X 18, GSC 61352.
9. Free cheek, paratype, X 13, GSC 61353.
Figures 10. Cranidium, paratype, X 8, GSC 61354.
11. Cranidium, paratype, X 8, GSC 61355.
12,13. Hypostome, paratype, X 18, GSC 61356.
14-16. Pygidium, paratype, X 11, GSC 61357.
17. Cranidium, paratype, X 7, GSC 61358.
18,19. Pygidium, paratype, X 18, GSC 61359.
20. Pygidium, paratype, X 18, GSC 61360.

Plate 11.1

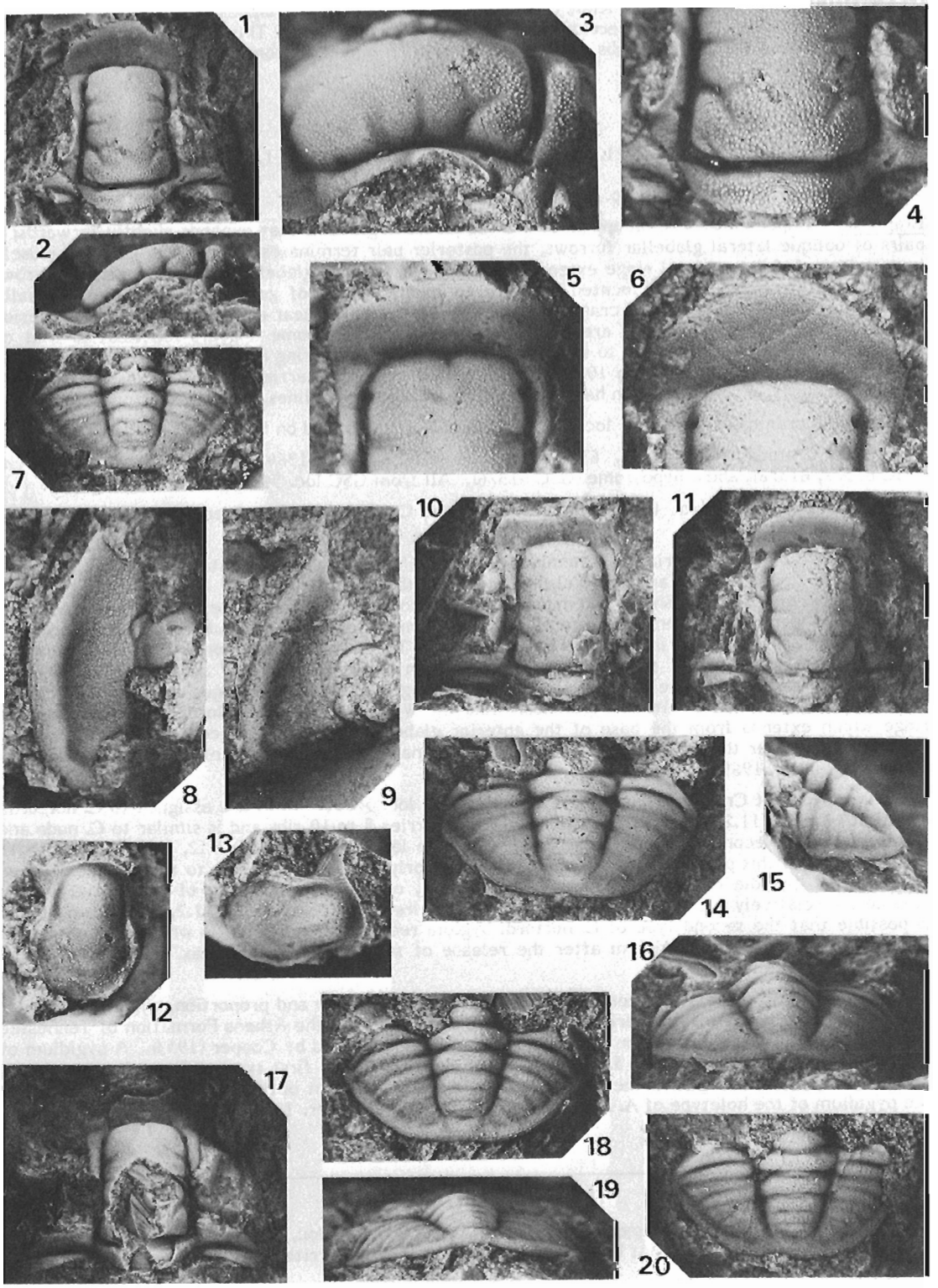

The integrity of **Cnemidopyge** as a genus distinct from its probable ancestor, **Ampyx**, rests merely on the presence of distinct pygidial ribs. Cephalic and hypostomal features cannot, at present, be used to discriminate these genera. Hughes (1969, p. 63) noted that it is possible that the European and North American species of **Cnemidopyge** are results of separate developments from **Ampyx**. The cephalic and pygidial similarity of **C. norfordi** to **Ampyx americanus** Safford and Vogdes (Cooper, 1953, Pl. 5, fig. 5, 8, 9) lends credence to this suggestion. Hughes placed emphasis on the number of pygidial ribs to differentiate species of **Cnemidopyge**. This character must be used advisedly because the pygidial ribs of **C. norfordi** vary in numbers from 8 to 10 and a single large pygidium displays 13 distinct ribs.

Cnemidopyge norfordi n. sp.

Plate 11.2, Plate 11.3, figures 10-13, Figure 11.3

1964 **Cnemidopyge** sp., Norford, p. 132.

Diagnosis. A species of **Cnemidopyge** with a subquadrate glabella that expands slightly forwards; 2 pairs of oblique lateral glabellar furrows, the posterior pair terminates adaxially in circular muscle impression. A faint sagittal ridge extends from base of anterior glabellar spine to occipital furrow. A pair of ovate bacculae are located opposite 1p lobe. A pair of genal ridges diverge gradually toward postero-lateral corner of cranidium from tubercle located near axial furrow opposite anterior end of 2s furrow. Genal spines are long and diverging. Hypostome appears identical to that of **Ampyx**. Pygidium is subcircular to subtriangular with evenly tapering axis which carries 12-17 axial rings. Pygidial ribs number 8 to 10. A single unique pygidium carries 13 ribs. Exoskeleton lacks granules and pits. Pygidial margin has prosopon of parallel terrace lines.

Holotype. A cranidium from GSC loc. 54290 (GSC 61361) illustrated on Plate 11.2, figures 1, 2.

Paratypes. Cranidia (GSC 61362, 61365), pygidia (GSC 61362, 61364, 61366-61368), free cheeks (GSC 61377, 61378), and a hypostome (GSC 61376). All from GSC loc. 54290.

Name. For B.S. Norford of the Geological Survey of Canada who first identified this trilobite as **Cnemidopyge.**

Remarks. All of the material of **Cnemidopyge nuda** (Murchison), **C. bisecta** (Elles), and **C. parva** Hughes from central Wales and the Welsh Borderlands that was descibed by Hughes (1969, p. 62-77, Pl. 2 to 8) is compressed in shales and mudstones. The convex glabellae of these specimens have been flattened to some degree and, therefore, detailed comparisons are difficult with the **C. norfordi** cranidia that are preserved in full relief in limestone. The cranidia of **C. norfordi** n. sp. apparently differ from the cranidia of the three Welsh species in being broader (tr.) across the 2p lobe, in possessing a pair of bacculae opposite 1p lobe, in having a pair of genal ridges on each fixed cheek, and by lacking prosopon of pits and granules. Like the Welsh species, **C. norfordi** possesses a sagittal ridge which extends from the base of the anterior glabellar spine to the occipital furrow, but this ridge is much lower than that of **C. bisecta** and not as narrow (tr.) as the faint ridges of **C. nuda** and **C. parva** (Hughes, 1969, Pl. 5, fig. 1, 8).

Two types of **Cnemidopyge** pygidia occur in GSC loc. 54290. Both are assigned to **C. norfordi.** The first type (Pl. 11.2, fig. 3, 7, 9, 10 and Fig. 11.3) carries 8 to 10 ribs and is similar to **C. nuda** and **C. bisecta.** The second type is represented by a single large pygidium (Pl. 11.2, fig. 11, 12) with 13 distinct ribs. In this pygidium the axis narrows posteriorly to a point and not to a blunt termination as is seen in pygidia of the first type. Furthermore, on the anterior edge of this pygidium, the pleurae are relatively wider (tr.) than in pygidia of the first type (compare Pl. 11.2, fig. 10 and 11). It is possible that the second type of **C. norfordi** pygidia records an individual in which segments were continually added to the pygidium after the release of segments to the thorax had ceased at the initiation of the holaspid stage.

Cranidia and pygidia of **Cnemidopyge norfordi** are, in outline and proportion, extremely similar to some specimens of **Ampyx americanus** Safford and Vogdes from the Athens Formation of Tennessee and the lower Edinburg Formation of Virginia that were illustrated by Cooper (1953). A pygidium of **A. americanus** (Cooper, 1953, Pl. 5, fig. 5) appears identical to the first type of **C. norfordi** pygidium (Pl. 11.2, fig. 3) if one ignores the pygidial ribs. It has a different outline and a narrower axis than the pygidium of the holotype of **A. americanus** illustrated by Cooper, 1953, Pl. 5, fig. 3), but it is also

---

Plate 11.2

Cnemidopyge norfordi n. sp. All from GSC loc. 54290,
Mount Burgess area, northern Yukon Territory.

Figures 1,2. Cranidium, holotype, X 3.5, GSC 61361.
3,4. Pygidium, paratype, X 3 and X 18, GSC 61362.
5,6. Cranidium, paratype, X 2.8, GSC 61363.
7. Pygidium, paratype, X 2.3, GSC 61364.
Figure 8. Cranidium, paratype, X 3.5, GSC 61365.
9. Pygidia, paratypes, X 2.6, GSC 61366a, b.
10. Pygidium, paratype, X 2, GSC 61367.
11,12. Pygidium, paratype, X 2, GSC 61368.

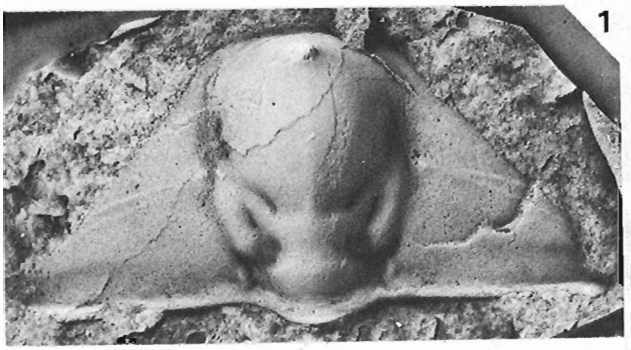
1


2


3

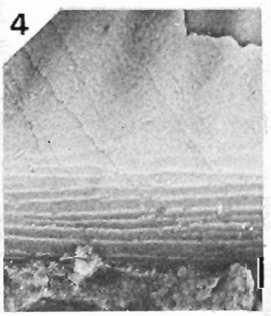
4


5

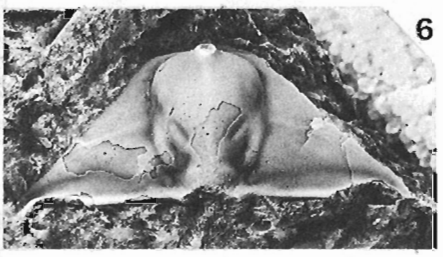
6

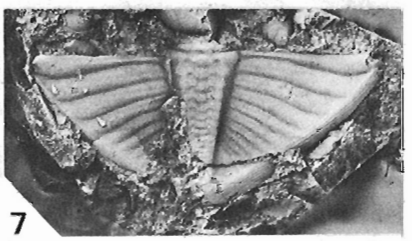
7


8


9


10

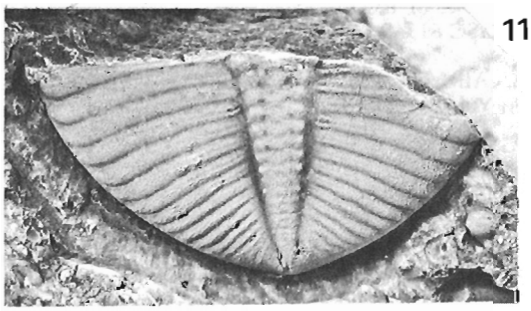
11

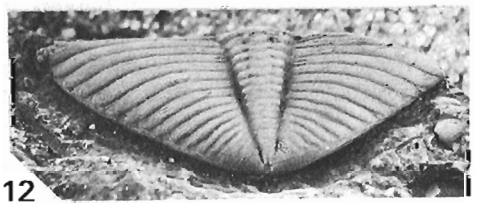
12

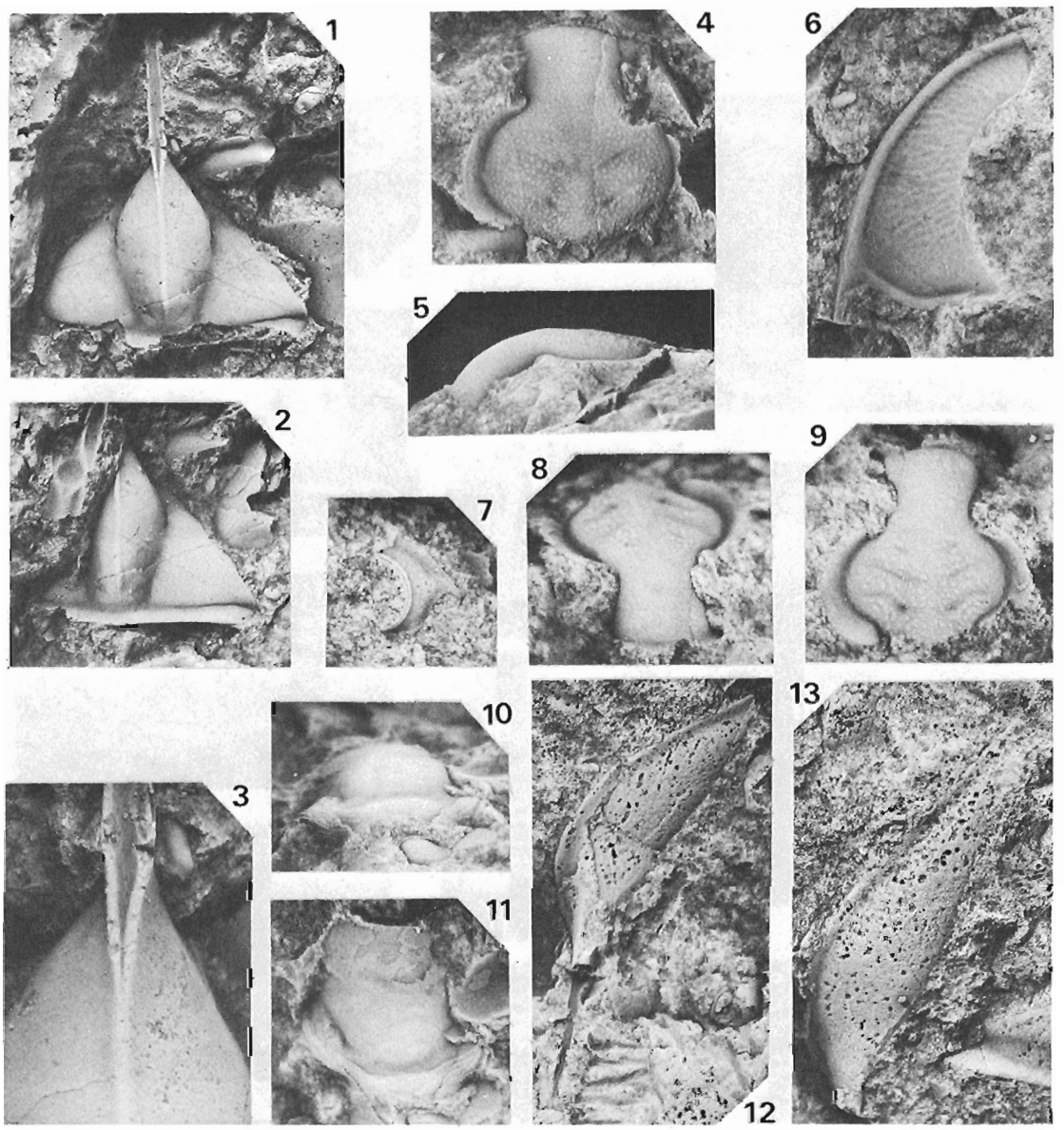

Plate 11.3

Lonchodomas carinatus Cooper. From GSC loc. 54290, Mount Burgess area, northern Yukon Territory.

Figures 1-3. Cranidium, figured specimen, dorsal views of testate specimen and latex impression, X 4, and X 13, GSC 61369.

Robergiella cf. **sagittalis** Whittington. All from GSC loc. 54290, Mount Burgess area, northern Yukon Territory.

Figures 4,5. Cranidium, figured specimen, X 6, GSC 61370.
6. Free cheek, figured specimen, X 8, GSC 61371.
7. Free cheek, figured specimen, X 18, GSC 61372.
8,9. Cranidium, figured specimen, X 18, GSC 61373.

Cnemidopyge norfordi n. sp. All from GSC loc. 54290, Mount Burgess area, northern Yukon Territory.

Figures 10,11. Hypostome, paratype, X 13, GSC 61376.
12. Free cheek, paratype, X 4, GSC 61377.
13. Free cheek, paratype, X 4, GSC 61378.

about half the size (Whittington, 1959, p. 469 noted that Cooper's stated magnification for fig. 3 is in error; it is X 2, not X 5). Similarly, in shape and proportion, the **A. americanus** cranidia (Cooper, 1953, Pl. 5, fig. 8, 9) are very close to those of **C. norfordi.** **Ampyx americanus** and **Cnemidopyge norfordi** are about the same age and appear to be closely related. As Hughes (1969, p. 63) suggested, it is possible that the single North American species of **Cnemidopyge** was derived from a different species of **Ampyx** than the British and Swedish species of **Cnemidopyge.**

Genus **Lonchodomas** Angelin, 1854

Type species. **Ampyx rostratus** Ampyx **rostratus** Sars from the Ampyx Limestone (Llandeilo and early Caradoc), Oslo region, Norway; redescribed and illustrated by Whittington, 1950 (subsequent designation by Raymond, 1925).

Lonchodomas carinatus Cooper, 1953

Plate 11.3, figures 1-3

1953 **Lonchodomas carinatus** Cooper, p. 17, Pl. 7, fig. 12-17, 19-23.

1959 **Lonchodomas carinatus,** Whittington, p. 473, Pl. 32, 33.

1964 ? **Lonchodomas** sp., Norford, p. 132.

Figured specimen. A cranidium (GSC 61369) from GSC loc. 54290.

Remarks. **Lonchodomas carinatus** has been fully described and extensively illustrated by Whittington (1959). As he pointed out (p. 478), **L. carinatus** from the lower Edinburg Formation of Virginia is extremely similar to the type species **L. rostratus** from strata of the same age in Norway. The two species could well be synonymous.

Family REMOPLEURIDIDAE

Genus **Robergiella** Whittington, 1959

Type species. **Robergiella sagittalis** Whittington, 1959 from the Liberty Hall facies of the lower Edinburg Formation (early Caradoc), Virginia (by original designation).

Robergiella cf. **sagittalis** Whittington, 1959

Plate 11.3, figure 4-9

1959 **Robergiella sagittalis** Whittington, p. 432, Pl. 6, fig. 16-32.

Figured specimens. Cranidia (GSC 61370, 61373) and free cheeks (GSC 61371, 61372). All from GSC loc. 54290.

Remarks. The Yukon specimens differ from the Virginia specimens of **Robergiella sagittalis** Whittington in having narrower (tr.) and longer (sag.) anterior cephalic tongues and relatively shorter (exsag.) palpebral lobes. The long anterior tongue also distinguishes **R.** cf. **sagittalis** from the specimens of **Robergiella** from Nevada, District of Mackenzie, and Scotland illustrated by Ross and Shaw (1972, Pl. 2, fig. 1, 2), Ludvigsen (1975, Pl. 5, fig. 22-25), and Tripp (1976, Pl. 2, fig. 21-23).

Acknowledgments

I thank Dr. A.W. Norris and Dr. B.S. Norford of the Institute of Sedimentary and Petroleum Geology for permission to study this faunule and Dr. C.R. Barnes of the University of Waterloo for his report on the associated conodonts. The trilobite reconstructions are by David Sargent.

References

Bergström, S.M.
1971: Conodont biostratigraphy of the Middle and Upper Ordovician of Europe and eastern North America; Geological Society of America Memoir 127, p. 83-157.

Cooper, B.N.
1953: Trilobites from the Lower Champlainian formations of the Appalachian Valley; Geological Society of America Memoir 55.

Dean, W.T.
1972: The isocolid trilobites **Cyphoniscus** Salter, 1853 and **Effnaspis,** gen. nov. in the Appalachian region of Canada and U.S.A.; Canadian Journal of Earth Sciences, v. 9, p. 415-421.

1973a: Ordovician trilobites from the Keele Range, northwestern Yukon Territory; Geological Survey of Canada Bulletin 223.

1973b: Lower Ordovician trilobites from the Summerford Group at Virgin Arm, New World Island, northeastern Newfoundland; Geological Survey of Canada Bulletin 240.

1973c: The Lower Paleozoic stratigraphy and faunas of the Taurus Mountains near Beysehir, Turkey. III. The trilobites of the Sobova Formation (Lower Ordovician); Bulletin of the British Museum (Natural History), Geology, v. 24, p. 279-348.

Dean, W.T. and Monod, O.
1970: The Lower Palaeozoic stratigraphy and faunas of the Taurus Mountains near Beysehir, Turkey. I. Stratigraphy; Bulletin of the British Museum (Natural History), Geology, v. 19, p. 411-426.

Fortey, R.A.
1975: Early Ordovician trilobite communities; Fossils and Strata, no. 4, p. 339-360.

Fortey, R.A. and Barnes, C.R.
1977: Early Ordovician conodont and trilobite communities of Spitsbergen: influence on biogeography; Alcheringa, v. 1, p. 297-309.

Harrington, H.J. and Leanza, A.F.
1957: Ordovician trilobites of Argentina; Department of Geology, University of Kansas Special Publication 1, University of Kansas Press.

Hughes, C.P.
1969: The Ordovician trilobite faunas of the Builth-Llandrindod Inlier, central Wales. Part 1; Bulletin of the British Museum (Natural History), Geology, v. 18, p. 39-103.

Hughes, C.P., Ingham, J.K., and Addison, R.
1972: The morphology, classification and evolution of the Trinucleidae (Trilobita); Philosophical Transactions of the Royal Society of London, B, Biological Sciences, v. 272, p. 537-607.

Kobayashi, T.
1936: Cambrian and Lower Ordovician trilobites from northwestern Canada; Journal of Paleontology, v. 10, p. 157-167.

Lenz, A.C.
1972: Ordovician to Devonian history of northern Yukon and adjacent District of Mackenzie; Bulletin of Canadian Petroleum Geology, v. 20, p. 321-361.

Lenz, A.C. and Churkin, M. Jr.
1966: Upper Ordovician trilobites from northern Yukon; Palaeontology, v. 9, p. 39-47.

Lu Yen-hao
1975: Ordovician trilobite faunas of central and southwestern China; Palaeontologia Sinica, New series B, v. 152, no. 11.

Ludvigsen, R.
1975: Ordovician formations and faunas, southern Mackenzie Mountains; Canadian Journal of Earth Sciences, v. 12, p. 663-697.

1979a: Middle Ordovician trilobite biofacies, southern Mackenzie Mountains; Geological Association of Canada Special Paper 18, p. 1-37.

1979b: A trilobite zonation of Middle Ordovician rocks, southwestern District of Mackenzie; Geological Survey of Canada Bulletin 312.

Moore, R.C., editor
1959: Treatise on Invertebrate Paleontology, Part O, Arthropoda 1; Geological Society of America and University of Kansas Press, Lawrence.

Murchison, R.I.
1839: The Silurian System, Murray, London, 868 p.

Neuman, R.B.
1964: Fossils in Ordovician tuffs, northeastern Maine; United States Geological Survey Bulletin 1181-E.

Norford, B.S.
1964: Reconnaissance of the Ordovician and Silurian rocks of northern Yukon Territory. Geological Survey of Canada Paper 63-39.

Raymond, P.E.
1925: Some trilobites of the Lower-Middle Ordovician of eastern North America. Harvard University, Bulletin, Museum of Comparative Zoology, v. 67, p. 1-180.

Ross, R.J., Jr. and Shaw, F.C.
1972: Distribution of the Middle Ordovician Copenhagen Formation and its trilobites in Nevada; United States Geological Survey Professional Paper 749.

Scotese, C.R., Bambach, R.K., Barton, C., Van Der Voo, R., and Ziegler, A.M.
1979: Paleozoic base maps; Journal of Geology, v. 87, p. 217-277.

Sweet, W.C., Ethington, R.L., and Barnes, C.R.
1971: North American Middle and Upper Ordovician conodont faunas; Geological Society of America Memoir 127, p. 163-193.

Taylor, M.E.
1977: Late Cambrian of western North America. Trilobite biofacies, environmental significance, and biostratigraphic implications; in Kauffman, E.G. and Hazel, J.E., ed., Concepts and Methods of Biostratigraphy, p. 397-425, Dowden, Hutchinson and Ross, Inc., Stroudsburg.

Tjernvik, T.E.
1956: On the Early Ordovician of Sweden, stratigraphy and fauna; Bulletin of the Geological Institutions of the University of Uppsala, v. 36, p. 107-284.

Tripp, R.P.
1976: Trilobites form the basal **superstes** Mudstones (Ordovician) at Aldons Quarry, near Girvan, Ayrshire; Royal Society of Edinburgh Transactions, v. 69, p. 369-424.

Whittard, W.F.
1955: The Ordovician trilobites of the Shelve Inlier, west Shropshire, Part I; Palaeontographical Society [Monographs], v. 109, p. 1-40.

Whittington, H.B.
1950: Sixteen Ordovician genotype trilobites; Journal of Paleontology, v. 24, p. 531-565.

1959: Silicified Middle Ordovician trilobites: Remopleurididae, Trinucleidae, Raphiophoridae, Endymioniidae; Bulletin of the Museum of Comparative Zoology, v. 121, p. 369-496.

Whittington, H.B. and Hughes, C.P.
1972: Ordovician geography and faunal provinces deduced from trilobite distribution; Philosophical Transactions of the Royal Society of London. B, Biological Sciences, v. 263, p. 235-278.

Williams, A., Strachan, I., Bassett, D.A., Dean, W.T., Ingham, J.K., Wright, A.D., and Whittington, H.B.
1972: A correlation of Ordovician rocks in the British Isles. Geological Society of London, Special Report no. 3, p. 1-74.

12.

GEOLOGY AND URANIUM OCCURRENCES OF THE MACINNIS LAKE AREA, DISTRICT OF MACKENZIE

Project 770024

S.S. Gandhi and N. Prasad
Economic Geology Division

Gandhi, S.S. and Prasad, N., Geology and uranium occurrences of the MacInnis Lake area, District of Mackenzie; in Current Research, Part B, Geological Survey of Canada, Paper 80-1B, p. 107-127, 1980.

Abstract

Sedimentary rocks of the Nonacho Group, believed to be of Aphebian age, unconformably overlie predominantly granitic basement in the MacInnis Lake area. They include granite pebble conglomerate, impure arkose, arkose, quartz pebble conglomerate, siltstone, shale, and sandstone, and are folded about north-south trending axes. Gabbroic dykes of Helikian age cut the folded sedimentary rocks. Eight uranium occurrences are known, seven of veintype and one disseminated. Three of the former are hosted by the sedimentary rocks, two others by younger gabbroic intrusions, and two are in amphibolite and gneissic granite of the basement. The disseminated occurrence is in arkose interbedded with quartz-pebble conglomerate; the uranium mineralization is disseminated through the chloritic matrix of detrital heavy mineral concentrations which consist predominantly of magnetite, largely altered to hematite, and contain traces of uranothorite, cassiterite, niobium- and tantalum-bearing minerals and native gold. Field relations and preliminary studies on chemistry, mineralogy and isotopic composition of the mineralized zones, suggest that the disseminated mineralization represents uranium enrichment in the sediments prior to deformation, and that the veins in the sedimentary rocks represent concentrations formed during the deformation. The veins in the gabbroic intrusions were probably formed by deposition from groundwater circulated by convection currents generated by heat of the intrusion, and those in the basement rocks possibly represent supergene concentrations.

Introduction

MacInnis Lake, approximately 240 km southeast of Yellowknife, is in the southwestern part of the Lower Proterozoic Nonacho basin (Fig. 12.1). The study area is approximately 20 km by 10 km. It was first explored for uranium during the 1950s and 1960s. Seven occurrences were discovered, and were investigated by trenching and drilling, but none proved to be economic. The mineralization occurs in the folded sedimentary rocks of the Nonacho Group, in diabase intrusions, and in the basement rocks, mostly as veins but also as dissemination along layers in the sediments.

Elsewhere in the Nonacho Lake area there are some 40 uranium occurrences and these have many features in common with those in MacInnis Lake area. During the last few years there has been a significant surge in uranium exploration throughout the Nonacho Lake area, and several new occurrences, some promising, have been found. The present study was undertaken in 1978 to obtain a better understanding of the uranium mineralization of the MacInnis Lake area, and to develop genetic models to aid in resource evaluation of this and other parts of the Nonacho basin. Observations on the stratigraphy, the structure and the characters of the mineralization, and a discussion of some new isotopic data and genetic aspects, are presented. Some guides for further uranium exploration, based on the present study, are suggested.

Previous Work

Regional mapping of the Nonacho Lake area, on a scale of 1 inch to 4 miles, was carried out by Henderson (1939a, b), Wilson (1941), Stockwell et al. (1968), Mulligan and Taylor (1969), and Taylor (1971). More detailed mapping, on a scale of 1:50 000, of Thekulthili Lake area southeast of MacInnis Lake, was done by McGlynn (1978). The relationship of the Nonacho Group to its basement rocks, and K-Ar isotopic age determinations on rocks from the area, have been discussed by Burwash and Baadsgaard (1962), McGlynn (1971) and Donaghy (1977). A paleomagnetic study of the diabase dykes has been carried out by McGlynn et al. (1974).

Exploration activities in the Nonacho Lake region, including the MacInnis Lake area, are summarized by McGlynn (1971, p. 136-138), Thorpe (1972, p. 22-23), and Gibbins et al. (1977, p. 75). Unpublished reports on the uranium exploration in the MacInnis Lake area are by Meagher (1955), Reid (1955), Campbell Todd (1956), Koehler (1956), MacDonald (1956), McVittie (1956), Stephen (1956), Spencer (1955), Meillon (1956), Hegge and Trigg (1967), Checklin (1968), Makela (1970), Moffat (1974), MacLeod and Brander (1975), and Harrington (1980). Mineralogical and geochemical characters of some uranium occurrences in the Nonacho Lake region, including a few in the MacInnis Lake area, are described by Maurice and Plant (1979). The Nonacho Lake area east of 110°W was covered by a reconnaissance lake sediment geochemical survey by the Geological Survey of Canada (Open Files 324, 325, 326) and follow-up of some of the anomalies was carried out by Maurice (1976, 1977 and 1979).

General Geology

The Nonacho Group rests unconformably on a basement complex consisting predominantly of granitic rocks with bands of metasedimentary and metavolcanic rocks. The metasedimentary and metavolcanic rocks are exposed mainly in the south, and are tentatively regarded as equivalent to the Tazin Group of the Beaverlodge area in northern Saskatchewan (Mulligan and Taylor, 1969; Taylor, 1971; Tremblay, 1972). The basement complex is considered to be Archean, and was affected by the Hudsonian events (approx. 1800 Ma) that also folded the Nonacho Group, and locally reset the K-Ar isotopic equilibrium (Burwash and Baadsgaard, 1962; McGlynn et al., 1974; Donaghy 1977). A further study of the basement complex is being undertaken by Bostock (1980).

The Nonacho Group consists of about 3000 m of basal conglomerate, grey to buff white arkose, local quartz-pebble conglomerate, siltstone, shale and sandstone. The basal conglomeratic rocks are best exposed in the southern part of the basin, where they comprise thick beds interlayered with grey arkose. The lowermost of these include lenses containing large angular clasts of granite gneiss that can be

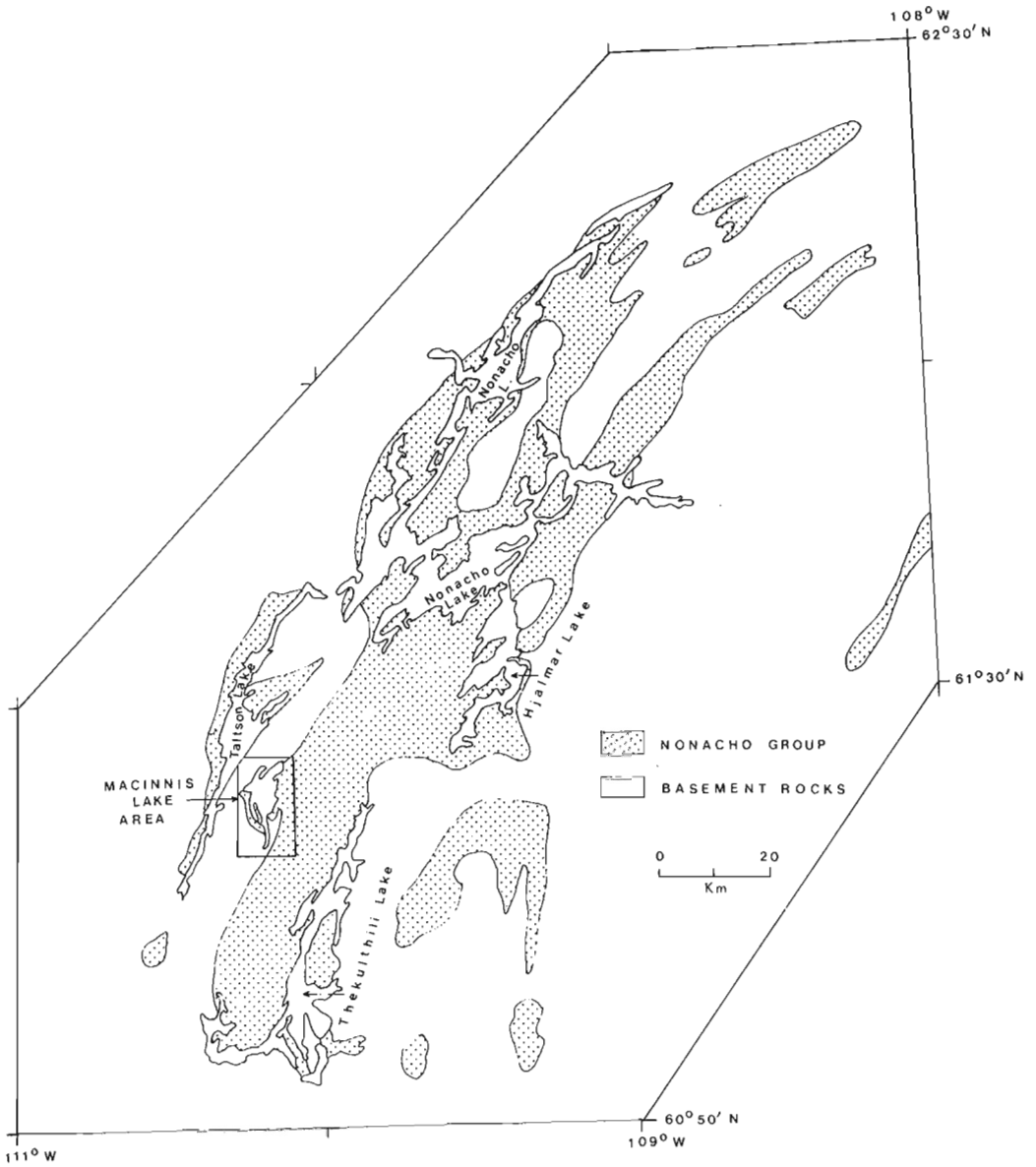

Figure 12.1. *Index map.*

interpreted as talus breccias deposited at base of fault scarps. They are overlain by interbedded arkosic sandstone and thick polymictic conglomerate. The arkosic and conglomeratic strata are overlain by a thin bedded siltstone and shale with interbedded sandstone. These fine grained sedimentary rocks comprise most of the succession in the northern part of the basin. The beds are commonly grey, green and buff white, and include some pale pink to red-maroon beds in the upper part of the sequence. Sedimentary features such as current bedding, ripple-marks, mud cracks, and load-casts are common, and are well preserved at many places. Shale chip conglomerates, and fining upward cycles are also observed. The coarser sedimentary rocks are largely fluviatile. It appears that the Nonacho sediments were laid down in a fault-controlled basin, which received the main influx of sediments from the south, with some contribution from other directions. General fining of the sequence towards the north, and highly variable paleocurrent directions support such a model. (McGlynn, 1971; personal communication, 1978). A more detailed study of the Nonacho sedimentary rocks is being undertaken by L. Aspler towards a Ph.D. thesis at Carleton University, Ottawa.

Nonacho sedimentary rocks are folded into gently plunging open folds along north-northeast trending axes. Minor folds and crenulations are common in siltstone and shale beds, which are relatively more tightly folded than the arkose and conglomerate. Foliation in the basement gneisses and the metasedimentary bands has a regional north to northeast trend, but there are a number of local deviations. Faults parallel to the trend of the basin are located along the margins of the basin and on the flanks of the basement highs within it. Some of the faults predate the deposition of Nonacho sedimentary rocks, and were reactivated during and after the deposition of these rocks. Folding of the rocks may be related to later movements along some of those faults (McGlynn et al., 1974). At several places along the basement-Nonacho boundary, the hornblende- and biotite-rich gneisses have been retrograded to chlorite-rich rocks.

Henderson (1937) mapped some of the granites along the contact of the Nonacho sedimentary rocks as "younger" granites, and described what he regarded as their intrusive relations with, and contact metamorphic effects on, the

sedimentary rocks. McGlynn (1971) on the other hand observed that all plutonic rocks in contact with the Nonacho sedimentary rocks are older, and are therefore part of the basement on which they were deposited, and that in many places, particularly along the western margin of the basin, the unconformity has been destroyed or obscured by faulting. Fieldwork by the writers in the MacInnis Lake area supports McGlynn's observations.

Fresh gabbroic dykes cut all the rocks mentioned earlier, and studies by McGlynn et al. (1974) suggest that many of the dykes were intruded approximately 1700 Ma ago, and that the others probably belong to the younger Mackenzie dyke swarm that was intruded approximately 1200 Ma ago.

Geology of the MacInnis Lake Area

The main lithologic units and structural features of the MacInnis Lake area are shown in Figure 12.2. Eight lithologic units are mapped and are briefly described under A) Basement complex (units 1 and 2), B) Nonacho Group (units 3, 4, 5 and 6), and C) Younger Intrusions (units 7 and 8), followed by a discussion on structural and stratigraphic relations. Outcrops are numerous in this glaciated terrain of low relief. The latest ice movement was from east-northeast.

Lithology

A) Basement Complex (units 1 and 2): Mapping in the basement complex is sketchy and is largely confined to the vicinity of the Nonacho sediments.

Amphibolite (unit 1): A mappbale band of amphibolite is exposed south of MacInnis Lake at the Pyramid Showing (Fig. 12.2 and 12.8). It is intruded by gneissic and massive granites.

Granite gneiss-granite (unit 2): Massive granite predominates and contains inclusions of granite gneiss, amphibolite and rarely of impure quartzite. It is commonly coarse grained with abundant pink potash feldspar, minor quartz, hornblende, and other accessory minerals. Very coarse pegmatitic phases occur locally.

B) Nonacho Group (units 3, 4, 5 and 6): Four lithostratigraphic units are distinguished, namely granite pebble conglomerate (unit 3), impure arkose (unit 4), pure arkose-quartz pebble conglomerate (unit 5) and siltstone-shale-sandstone (unit 6). The stratigraphic position of unit 5 with respect to units 3 and 4 is not certain and their possible relations are discussed later.

Granite pebble conglomerate (unit 3): This conglomerate occurs as a north-northeast trending band east of MacInnis Lake, and is approximately 0.5 km thick. Lenses of impure arkose occur in some places and provide the only evidence of stratification. The beds dip steeply to the east. Clasts in the conglomerate are subrounded, and commonly between 5 to 10 cm in diameter. Granite clasts are most abundant, and they resemble the basement granite. Clasts of other lithologies are scarce and include pegmatite, sheared granite, granite gneiss, vein quartz and what appear to be metasedimentary rocks. The matrix is dark greenish grey, and silt to fine sand in size. Foliation in the matrix is well developed in some places and it trends subparallel to the strike of the unit and dips steeply to the east. The basal contact of the unit is poorly exposed and appears to be sheared.

Impure arkose (unit 4): This unit underlies a large area east of the granite pebble conglomerate. It dips steeply to the east and conformably overlies the granite pebble conglomerate. It is a greenish grey, medium- to coarse-grained lithic sandstone, commonly massive and thick bedded.

Pure arkose-quartz pebble conglomerate (unit 5): A distinctive unit of arkose interbedded with quartz pebble conglomerate, 300 to 400 m thick, nonconformably overlies granitic basement around the shores of MacInnis Lake, and outlines the rim of a structural basin or a syncline. Stratigraphy of this unit based on 1978 fieldwork, is illustrated in Figure 12.3.

Arkose predominates and is coarse to pebbly. The bulk of the arkose is massive but stratification and crossbedding are developed in some beds. Lenses rich in heavy minerals are present locally (Pl. 12.1a). Conglomerate occurs as lenses and beds up to 50 m thick, and contains subrounded to well rounded, matrix supported quartz pebbles in an arkosic matrix (Pl. 12.1b). Some lenses have very well sorted and closely packed pebbles. The lower contact of the conglomerate is commonly well defined but the upper boundary tends to be gradational with the arkose. Weak foliation and imbrication are developed in rocks of the unit and are more conspicuous at the crests of the minor folds.

The basal beds of this unit, where observed, are arkosic, and overlie nonconformably massive granite and gneissic granite. The nonconformity is sharp, except at the north-northwest corner of MacInnis Lake where it is rather poorly defined and appears to be gradational over a 20 m width.

Siltstone-shale-sandstone (unit 6): This is a thinly bedded unit, consisting of grey and pale red siltstone interbedded with greenish grey shales. Fine sandy beds are also present, but are subordinate to the siltstones and shales. Siltstones predominate over shales in the lower part of the unit. At the base of the unit, they are interbedded with the pure arkose-quartz pebble conglomerate of unit 5. The shale beds predominate in the upper part of the unit.

C) Younger Intrusions (units 7 and 8):

Granodiorite dyke (unit 7): Stephen (1956) mapped one dyke, approximately 60 m wide, in the northeastern part of the MacInnis Lake area (Fig. 12.2), and described it as a fine- to medium-grained granodiorite composed of quartz (10-15 per cent), mafic silicates (10 to 30 per cent) and equal amounts of orthoclase and plagioclase. He also noted contact metamorphic effects on the Nonacho sedimentary rocks. Age of the dyke relative to the gabbroic dykes is not known.

Gabbroic instrusions (unit 8): Fresh gabbroic dykes and intrusive bodies cut the basement rocks and deformed Nonacho sedimentary rocks. Dykes in the basement are up to 30 m wide; those cutting the Nonacho sedimentary rocks are relatively thin.

A few small pegmatitic patches cutting siltstone-shale were observed by the writers on a large island approximately 1 km west of the granodiorite dyke. Their origin and relationship to other intrusions are not certain.

Structural and Stratigraphic Relations

Nonacho sedimentary rocks at MacInnis Lake are folded into a north to northeast trending syncline with moderately tight subsidiary folds and an east-northeast trending cross-fold, as seen from the variations in attitude of the pure arkose-quartz pebble conglomerate unit (Fig. 12.2). The

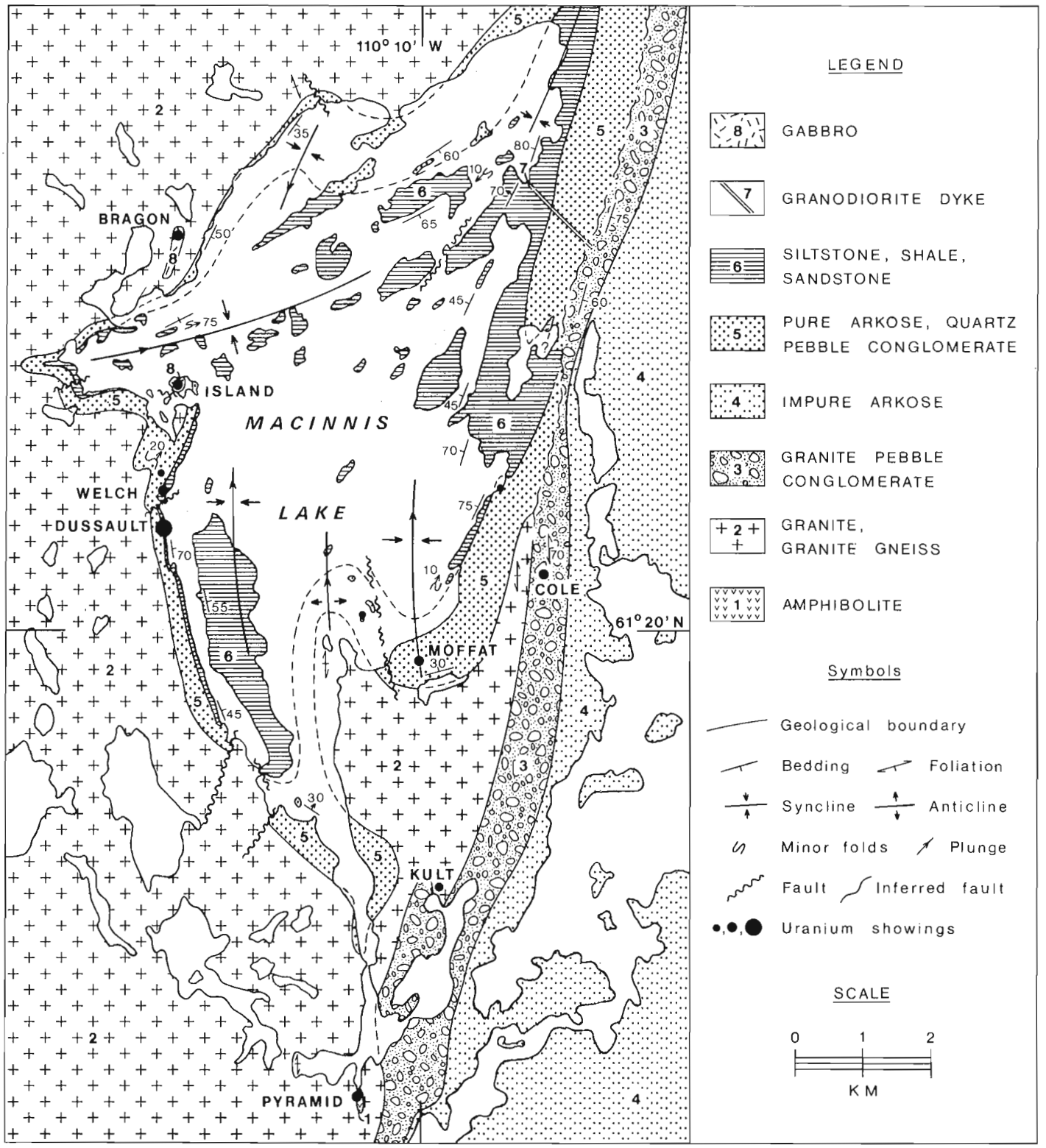

Figure 12.2. Geology and uranium occurrences of the MacInnis Lake area, District of Mackenzie (after Stephen, 1956, Meillon 1965, and Harrington, 1980.)

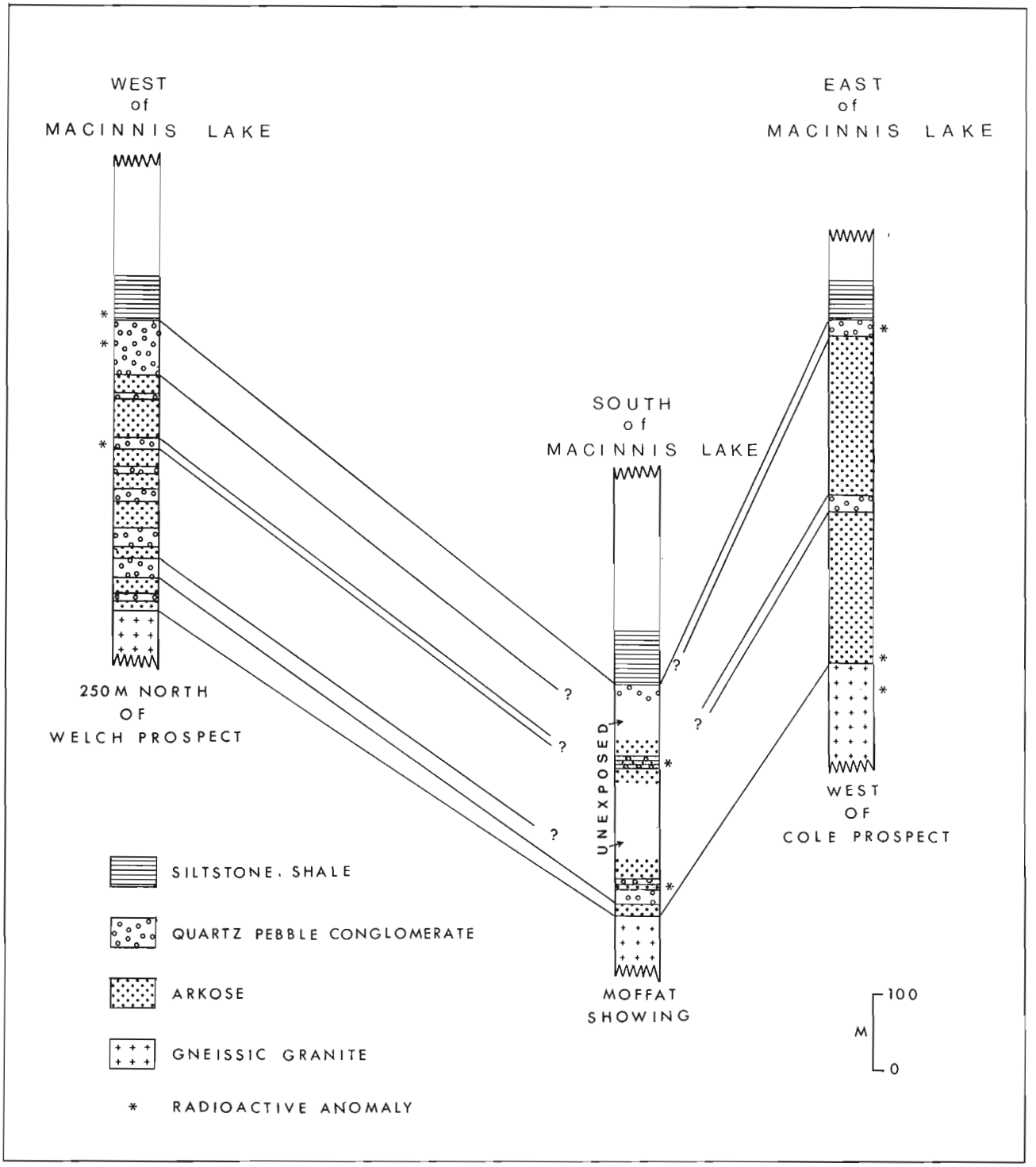

Figure 12.3. *Lithostratigraphy of the arkose-quartz pebble conglomerate unit of the MacInnis Lake area, District of Mackenzie.*

overlying siltstone-shale unit, being relatively less competent, is more complexly folded with numerous drag folds and crenulations. The plunge of the subsidiary and minor folds ranges from gentle to moderate.

The pure arkose-quartz pebble conglomerate is restricted to the synclinal structure. To the northeast, it is juxtaposed with the granite pebble conglomerate (Stephen, 1956; Meillon, 1965). The boundary is mapped as a fault or shear zone by Meillon (1965). In the vicinity of the shear zone, beds dip steeply and away from it, and the rocks are sheared to a varying degree. Furthermore, the juxtaposition of two very different lithologies, one representing mature sediments and the other immature sediments, also implies the presence of a fault, perhaps with a major lateral displacement. The pure arkose-quartz pebble conglomerate extends along the strike a few kilometres to the northeast,

Plate 12.1

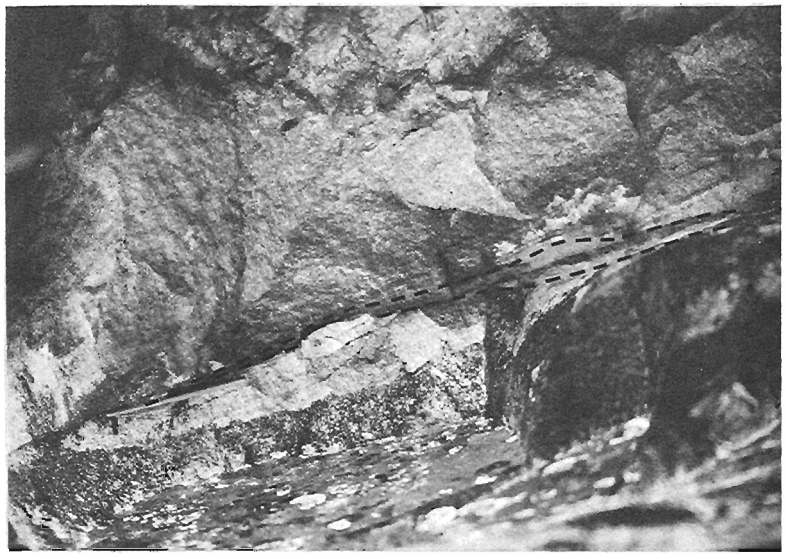

12.1a. A heavy mineral lens in arkose (dashed line), Moffat Showing, Trench-5; Note a dropped quartz pebble in arkose above the centre. (Looking east).

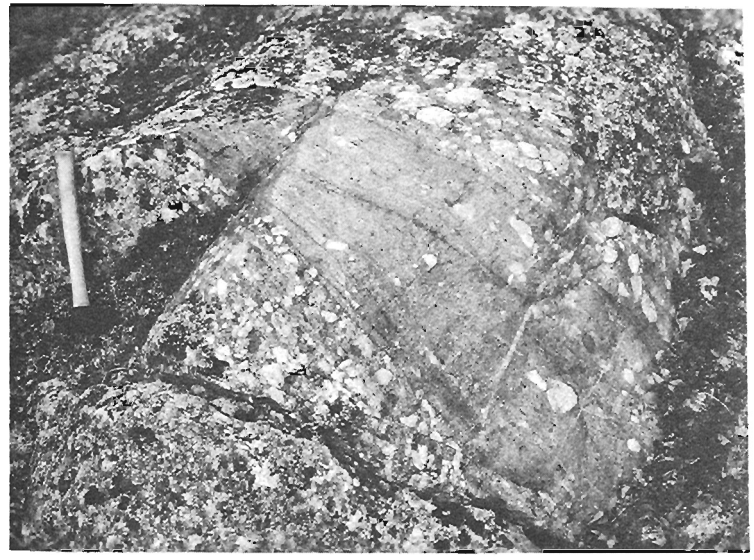

12.1b. Interbedded arkose and quartz pebble conglomerate, east end of the Island Showing (Fig. 12.9).

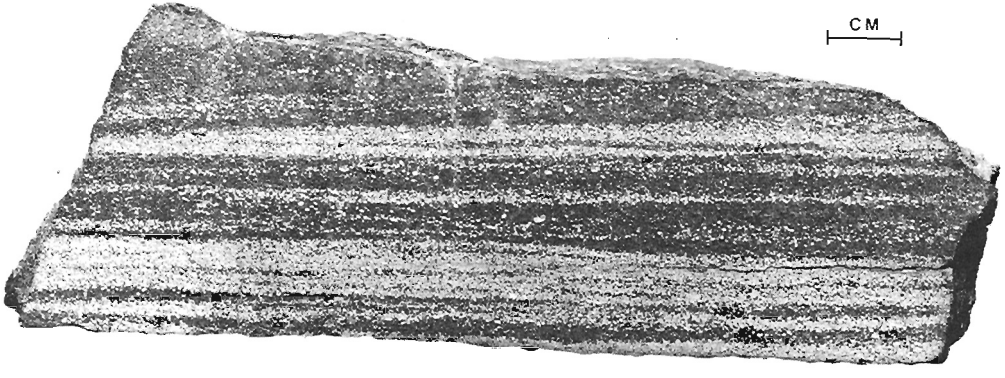

12.1c. Photograph of a polished surface of sample GFA-78-178, trench 5, Moffat Showing.

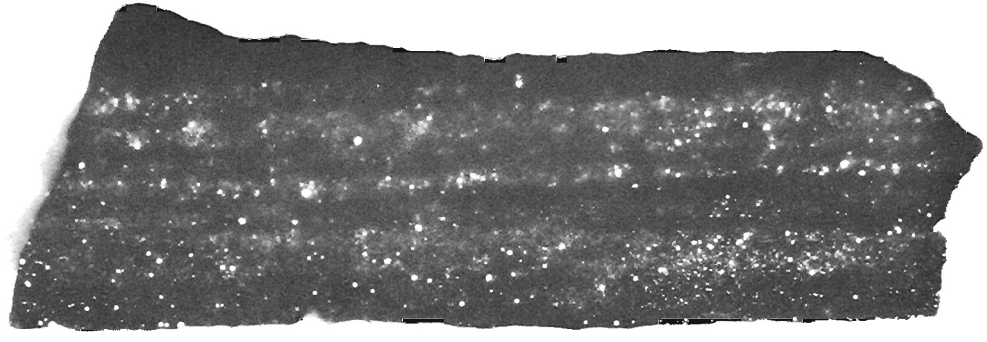

12.1d. Autoradiograph of the sample in 12.1c.

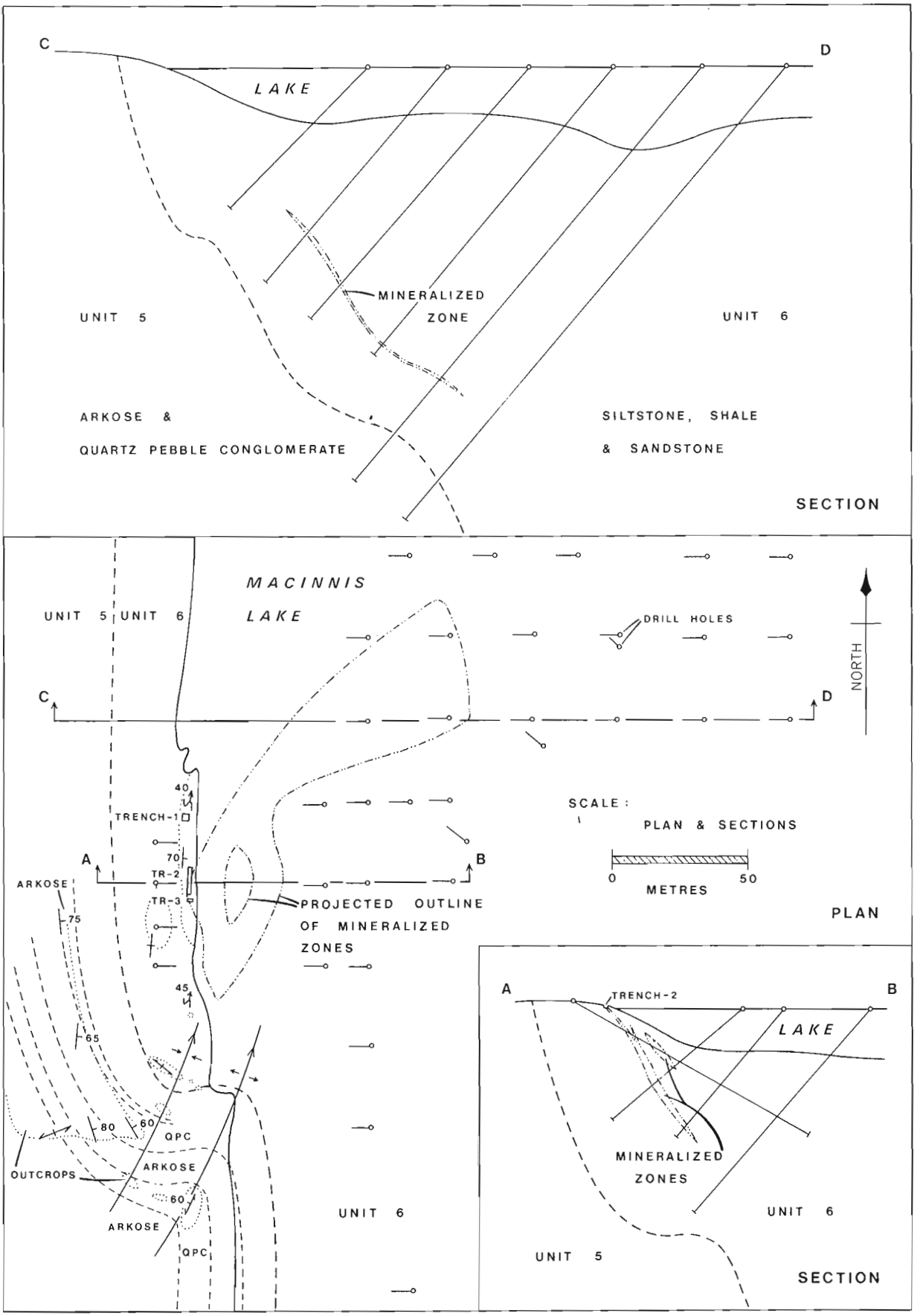

Figure 12.4. *Relationship of stratigraphy, structure and uranium mineralization at the Dussault Prospect (after Makela, 1970).*

but is not known elsewhere in the Nonacho basin. The granite pebble conglomerate and impure arkose on the other hand have a much greater extent. The siltstone-shale-sandstone is also very extensive and conformably overlies the impure arkose elsewhere in the basin. These features suggest that the pure arkose-quartz pebble conglomerate was deposited in a limited area or in a restricted sub-basin, possibly fault-bounded, that had a somewhat different sedimentary regime than the rest of the Nonacho basin, but was later overlain conformably by sediments common to the entire Nonacho basin (unit 6). The impure arkose unit outside the MacInnis Lake area has some relatively pure arkose beds, which also contain lenses rich in heavy minerals, similar to those in the pure arkose of unit 5. This suggests that on a regional scale the two units may in part be related, and represent facies variation. However, additional fieldwork is necessary to define their stratigraphic relationship.

Several other faults were observed in the area, and a few prominent ones are shown in Figure 12.2. They are steeply dipping, and range in strike direction from east-northeast to northwest. Lateral displacement along them is small, in the order of a few metres to a few tens of metres. The more prominent faults cutting Nonacho sedimentary rocks have numerous quartz veins associated with them.

Uranium Occurrences

Veins in Nonacho Sedimentary Rocks – Dussault, Welch and Cole prospects

Dussault Prospect: This prospect on the west shore of MacInnis Lake, and the Welch prospect 600 m to the north, were staked in 1954 by Messrs. Dussault and Baudry and Messrs. Welch and Drever, respectively, following the discovery of the Island and Bragon Showings to the north by Consolidated Mining and Smelting Company of Canada Limited (Cominco Limited). The claims were acquired by Canadian Pipelines and Petroleums Limited, and an intensive exploration program was carried out during 1955 and 1956 which included geological mapping, a scintillometer survey, trenching and drilling totalling 6412 m in 60 holes, of which 50 holes totalling 5194 m were drilled to test the Dussault Prospect and its extension (Reid, 1956; Campbell Todd, 1956; MacDonald, 1956). The drilling outlined a zone containing an estimated 27 000 metric tonnes averaging 0.17 per cent U metal (MacDonald, 1956; Makela, 1970; Checklin, 1970; McGlynn, 1971; Thorpe, 1972). The property has been owned by Scurry-Rainbow Oil Limited, a subsidiary of Home Oil Limited, since the late 1960s.

The geology and the mineralized zones are illustrated in plan and sections in Figure 12.4, based on the study of old drill records and surface mapping done in 1978. The main mineralized lens is 0.5 to 2 m thick, 150 m long and up to 60 m wide, and from the shore dips 40° to 60° to the east beneath the lake. The rake is 40° to the north-northeast, subparallel to the plunge of a small fold approximately 75 m in amplitude. The mineralization consists of pitchblende in veins and as disseminations and aggregates close to the veins, subparallel to the bedding, along a 10 m thick stratigraphic zone of interbedded arkose and siltstone-shale (argillite). The pitchblende veins are up to 0.5 cm thick, but most are much thinner veinlets or stringers. Associated minerals are chlorite, calcite, hematite, quartz, pyrite, chalcopyrite and galena. Chlorite is the most abundant mineral, and is closely related, spatially, to the uranium mineralization. Pyrite occurs in quartz and calcite stringers that also contain pitchblende, and in the wall rocks as disseminated cubes. Secondary yellow uranium minerals are developed at the surface along high grade veins.

Welch Prospect: This prospect was explored concurrently with the Dussault Prospect in 1955 and 1956. Work done included trenching and diamond drilling totalling 1018 m in 10 holes (Reid, 1955; MacDonald, 1956). The uranium mineralization is similar in character, and occurs along the same stratigraphic zone, as at the Dussault Prospect. It is however discontinuous and limited in extent (Fig. 12.5). The host rocks are tightly folded and contorted. Chlorite is abundant, but hematite and pyrite are less common than at the Dussault Prospect. Maurice and Plant (1979, p. 183) reported high contents of Ag, Pb, Ba and Bi, and to some extent Th, in a mineralized sample, and identified uraninite and boltwoodite* and also indicated the presence of minute quantities of a Cu-Pb-Bi sulphide. The thorium could be contained in detrital monazite in the sedimentary host rock but the mineral was not found in the thin sections studied.

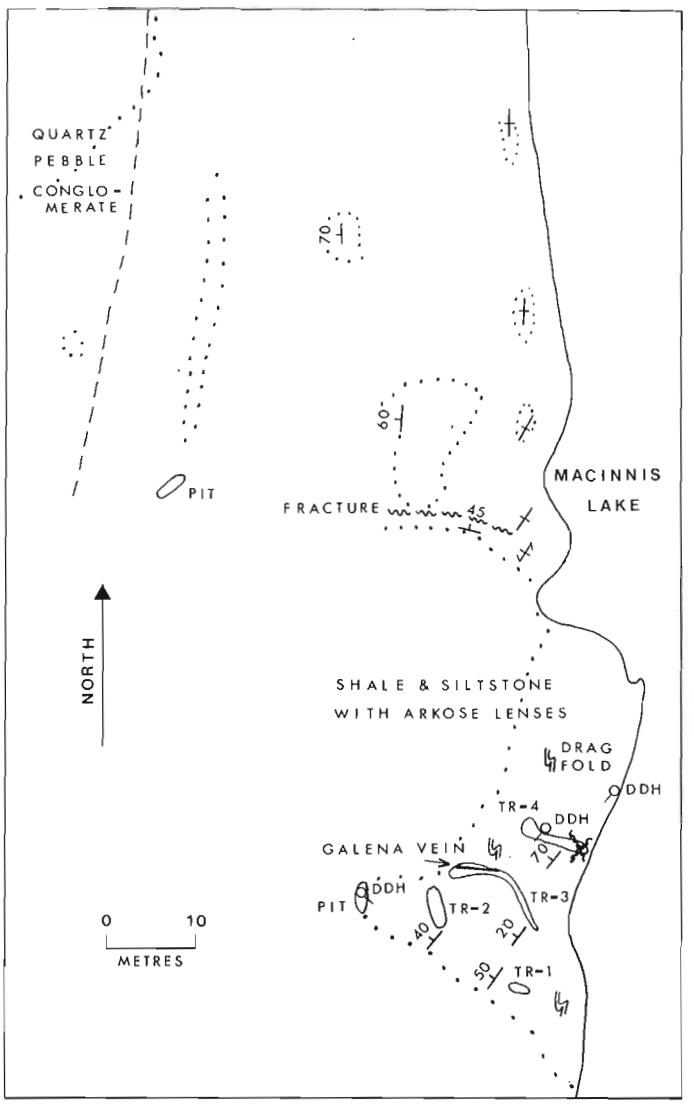

Figure 12.5. Surface geology of the Welch Prospect, MacInnis Lake area.

*$K_2(UO_2)_2(SiO_3)_2(OH)_2 \cdot 5H_2O$

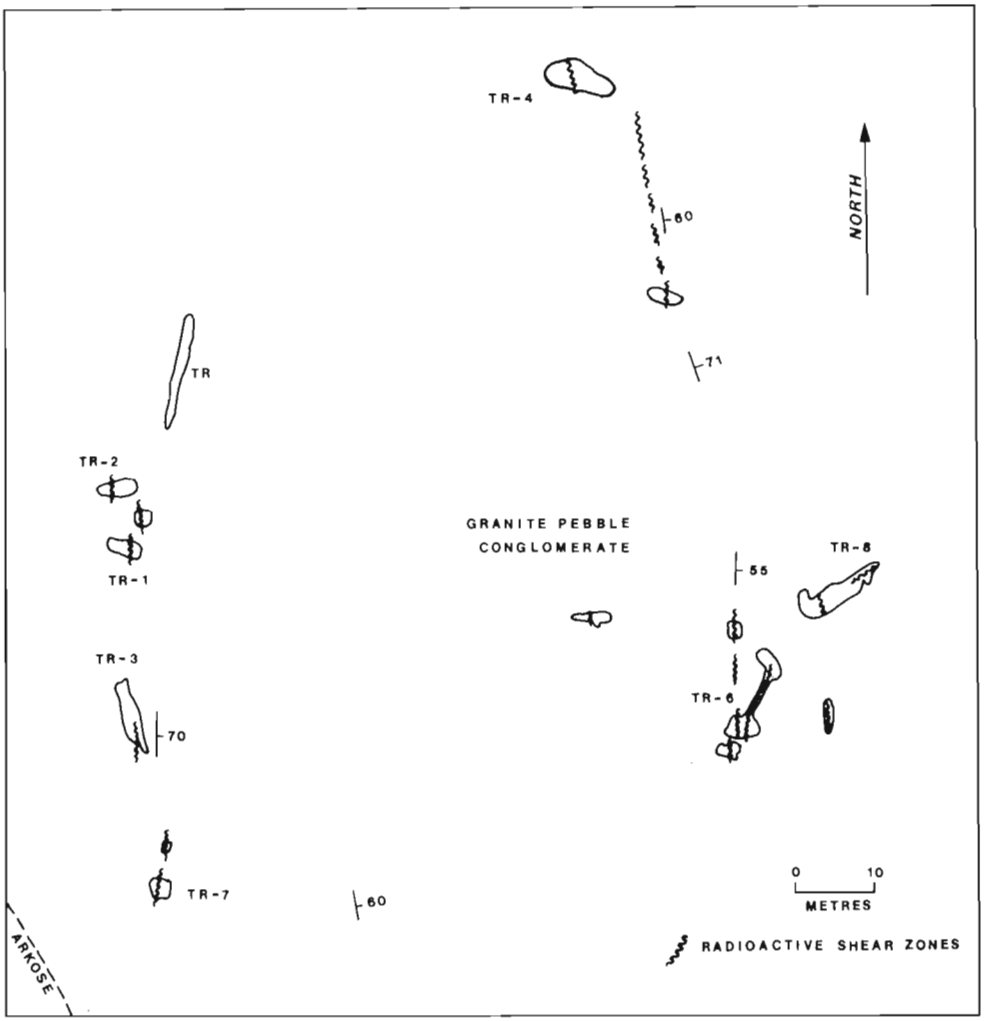

Figure 12.6. *Plan of trenches, Cole Prospect (after MacLeod and Brander, 1975); note: uranium mineralization along shears and fractures exposed by the trenches.*

A veinlet of quartz and calcite carrying galena was seen in one of the trenches. The lead isotopic composition of this galena has been determined and the results are discussed in the section on isotopic ages. Uranium mineralization also occurs in a set of crosscutting fractures on the shore just east of the trenches (Fig. 12.6). The host shale-siltstone beds away from the mineralized zone are light to medium grey-green, and lack pyrite and chlorite, but have a somewhat higher background radioactivity and uranium content (Table 12.1, no. 20 and 21).

Cole Prospect: This prospect was discovered in 1954 by a group of prospectors, and was optioned by William Cole in 1955. He in turn optioned it to Iso Uranium Mines Limited who carried out geological mapping and trenching (Meagher, 1955). It was, however, found that some of the original stakers had grub-staking agreements and ownership was confused. The original claims were apparently allowed to lapse. The property was restaked by prospector Fred Lypka, who optioned it to Consolidated Shunsby Mines Limited, and under a subsequent agreement Shell Canada Limited in 1974 sampled eight of the ten trenches and carried out geological examination, and an airborne radiometric survey of the surrounding region (MacLeod and Brander, 1975; Gibbins et al., 1977). The property is presently owned by F. Lypka estate.

Mineralization occurs in stringers and veins, up to 3 cm wide, in sheared and fractured granite pebble conglomerate. They are concentrated along two zones trending north-south and approximately 75 m apart. The zones can be traced for 100 and 130 m, and are 10 to 30 m wide (Fig. 12.6). A few other isolated veins are present in the vicinity (Meagher, 1955). Foliation in the conglomerate trends north-south with local variations from 330° to 010°, and commonly dips 60 to 70° to the east. The veins are steep and commonly trend north-south and truncate the foliation at low angles. Some of them however cut the foliation at a high angle. The minerals in the veins and stringers are pitchblende, hematite and calcite, and some secondary yellow uranium minerals. Stringers tend to follow foliation in the matrix of the conglomerate, which contains some chlorite and scattered cubes of pyrite. Assay values up to 0.13 per cent U metal over 1.15 m and 2.68 per cent U over 0.15 m have been reported on the trench (No. 8) samples. Some of the samples from the western zone returned minor values of gold along with uranium, the highest being 3.438 ppm (0.11 oz/ton) gold and 0.21 per cent U over 0.76 m in trench 3 (McLeod and Brander, 1975). Grab samples collected by the writers also contain some gold (Table 12.1, no. 7 and 8).

Table 12.1

Concentration of certain elements* in selected mineralized and unmineralized rocks from the MacInnis Lake area, District of Mackenzie.

No.	Location	U ppm	Th ppm	Pb ppm	Au ppm	Ag ppm	Sn ppm	Lithology
	Mineralized Rocks:							
1	Dussault Prospect: Tr-2**	28 700	2430	2000	0.080	30.5		Pitchblende vein in siltstone, unit 5
2	" " : Tr-4	3250	180	5000	<0.005	5.0		Fracture-filling in arkose-siltstone, unit 5
3	Welch Prospect: Tr-4	58 400	1200	4000	0.500	17.0		" " " "
4	" " "	17 000	350	5000	0.010	7.9		" " " "
5	" " : Tr-3	8860	ND†	30 000	0.010	11.0		Pitchblende-galena vein in shale-siltstone
6	" " : Tr-1	2270	180	6000	0.015	2.7		Rusty argillaceous siltstone
7	Cole Prospect: Tr-4	6950	30	6000	2.165	1.4		Pitchblende vein in conglomerate
8	" " : Tr-8	4660	ND	1000	0.510	3.8		" " " "
9	Moffat Showing: Tr-5	1720	740	2000	1.855	0.1	2754	Heavy mineral layers in arkose
10	" " : Tr-4	261	160	ND	0.015	ND	138	" " " " "
11	" " : Tr-1	176	130	ND	<0.010	ND	102	Shale-chip conglomerate
12	1 km NW of no. 11	48	190	ND	<0.010	ND		Heavy mineral layer in arkose
13	15 km south of no. 11	46	160	ND	0.545	0.5	4	" " " " "
14	Bragon Showing: Tr-3	1660	ND	1000	0.010	1.5		Pitchblende-pink calcite vein in gabbro
15	Island Showing: Tr-3	2270	40	ND	0.015	0.6		Pitchblende vein in gabbro
16	" " : Tr-5	111	30	ND	0.035	1.2		" " " "
17	Pyramid Showing: Tr-B	14 000	ND	1000	0.045	11.4		" " " amphibolite
	Unmineralized Rocks:							
18	4.5 km, 080° from no. 14	10.0	100	ND				Shale (argillite)+siltstone, traces of chalcopyrite
19	3.75 km, 095° from no. 14	1.2	ND	ND				Fine grained, pale red sandstone
20	75 m NW of no. 6	17.7	ND	ND			14	Shale at upper boundary of unit 5
21	50 m North of no. 20	14.5	ND	ND				" " " " "
22	20 m West of no. 21	4.6	ND	ND				Quartz pebble conglomerate
23	250 m North of no. 6	11.3	50	ND			116	" " "
24	48 m West of no. 23	9.4	50	ND				Arkose, coarse
25	250 m WSW of no. 1	11.8	ND	ND				Arkose
26	1.5 km NNW of no. 7	5.9	ND	ND			49	Quartz pebble conglomerate
27	Moffat Showing; Tr-1	11.4	ND	ND			17	Arkose, heavy mineral lense, arkose hematized at margin
28	500 m West of no. 7	2.3	ND	ND				Arkose at basal unconformity
29	15 m West of no. 28	2.7	ND	ND				Arkose
30	250 East of no. 15	4.5	ND	ND				Quartz pebble conglomerate
31	1.5 km, 260° from no. 15	9.1	40	ND			25	Arkose
32	4 m SE of no. 8	10.7	ND	ND			7	Granite pebble conglomerate

*U: Delayed neutron activation analyses by Atomic Energy of Canada Limited, Ottawa
Th and Pb: X-ray fluorescence analyses by the Geological Survey of Canada Laboratories, Ottawa; analyst: R.M. Rousseau
Au and Ag: Fire assay + atomic absorption analyses by Bondar-Clegg and Company Limited, Ottawa
Sn: X-ray fluorescence analyses by Bondar-Clegg and Company Limited, Ottawa

**Tr-2: Trench No. 2.

†ND: Not Detected.

Dissemination in Nonacho Sedimentary Rocks – Moffat Showing and Other Occurrences

Moffat Showing: The showing was discovered and staked as WW claims by prospectors Wm. W. Moffat and Jim Barton in 1958 for Murky Fault Metal Mines Limited and Snowdrift Basemetal Mines Limited (Moffat, personal communication, 1980). It was explored by 5 trenches and 6 short X-ray drillholes totalling 227 m. Samples were analyzed for tin, uranium and gold, but no values of economic interest were encountered (Meillon, 1965; Moffat, 1974). The mineralization occurs along stratiform lenses of detrital heavy mineral concentrations in arkose that dips gently to the north.

The relationship between the stratigraphy and mineralization is illustrated in Figure 12.7. The basal arkose is followed by coarse quartz-pebble conglomerate with thin beds and lenses of arkose, which in turn is overlain by pebbly arkose with beds and lenses of conglomerate and also lenses of heavy minerals. The unconformity with the basement gneissic granite is well exposed along the section studied and is sharply defined. Quartz veins up to 3 cm thick and subparallel to gently dipping beds are present along the unconformity. The bedding is poorly developed in the sedimentary rocks, with the exception of parts of the upper arkose containing heavy mineral concentrations (Pl. 12.1b), and the contacts of conglomerate layers which are well defined in many places (Pl. 12.1a).

The lenses rich in heavy minerals are distinctive because of their dark brownish grey to steel grey colour, in contrast to the buff white arkose. The lenses are up to a few centimetres thick, and are traceable for a few metres along the strike and dip. They consist of alternating thin layers, up to 5 m thick, of dark grey heavy minerals and lighter coloured quartz- and feldspar-rich layers. Sedimentary features such as crossbedding, scour and channel-filling and drop pebbles are observed in them (Pl. 12.1a). The crossbedding indicates transport of the sediments from south to north.

Mineralogical studies show that the heavy minerals are magnetite, now largely altered to hematite (very weakly magnetic), cassiterite, zircon, tourmaline, monazite, uranothorite and native gold. The detrital grains are 0.5 to 1 mm in diameter. Magnetite constitutes over 98 per cent of the heavy minerals, and polished sections show nearly complete alteration to hematite except for some small remnants of magnetite in a few grains. Hematite and magnetite also occur in intergranular space as fine grained, blade-like crystals concentrated around the larger hematitized magnetite grains, and also intergrown with a chloritic mineral that forms the matrix. Chemical analysis of one sample (GFA-78-178, see sample no. 9, Table 12.1, for U, Th, Pb and Au values) gave 0.8 per cent Ti, indicating the titaniferous character of magnetite. A few of the magnetite grains examined under the microscope have what appear to be thin ilmenite lamellae. Cassiterite occurs as a few scattered grains, which have a variable deep reddish brown colour in thin section. The sample analyzed contains 2754 ppm Sn. Tin is present in a majority of the heavy mineral lenses encountered during trenching and drilling (Moffat, 1974). Monazite and uranothorite grains can be seen in autoradiograph (Pl. 12.1d) as sharply defined spots: these have been identified during a study of another sample from the same trench from which sample GFA-78-178 was obtained (Maurice and Plant, 1979, p. 185). The autoradiograph also shows a haze in the matrix, but the radioactive mineral phase causing it is too fine grained to identify by optical and X-ray diffraction methods. Electron microprobe study by Maurice and Plant (ibid.) showed that this phase contains 55 to 60 per cent U; Ti, P, Fe and Si are also present. Approximately 85 per cent of the total uranium in the mineralized samples, as determined by delayed neutron activation analyses, is readily leachable by cold 1 N HCl, indicating that much of the uranium is in the matrix phase; the remainder is presumably in the detrital uranothorite, monazite, and zircon.

Five flakes of native gold were discovered by the first author during an examination under a binocular microscope of a -150 mesh heavy fraction of sample GFA-78-178 prepared for isotopic age determination (Table 12.2). No gold was seen in the sections examined under the microscope but analysis by fire assay indicated 1.855 ppm in the sample (Table 12.1; sample no. 9), from which the heavy mineral concentrate was prepared.

Traces of biotite and a small grain of a galena-like mineral were observed in polished thin sections. High contents of Ta (139 ppm), Nb (300 ppm), Ce (104 ppm), La (478 ppm), Y (128 ppm) are present, but the mineral phases containing these elements were not identified. The mineralized sample also contains 624 ppm Zr.

At some places in the vicinity of heavy mineral concentrations, the enclosing arkose shows reddish hematitic coloration in irregular patches and thin layers, and weak radioactivity is commonly associated with it. Traces of pyrite in the arkose-quartz pebble conglomerate are reported by Moffat (1974, p. 92).

Other Occurrences Anomalous radioactivity up to 10 times the background was found in the arkose and quartz-pebble conglomerate at four other localities in the MacInnis Lake area (Table 12.1 nos. 12, 22, 23 and 24.) These are characterized by high Th/U ratios. One of the localities (no. 12, Table 12.1) represents the extension of the Moffat mineralization. It was explored by a 35 m long drill hole which intersected 4 heavy mineral lenses (Moffat, 1974, p. 80). The radioactivity at the other three localities represents high contents of detrital monazite and zircon. Heavy mineral lenses were also intersected in an exploratory drill hole, 40 m long, on an island in the southern narrow extension of MacInnis Lake (Fig. 12.2), known as Pebble Island, and 2 of the 10 lenses carried minor tin values, but no uranium was detected in any of them (Moffat, ibid, p. 81). Pyrite is reported in some of the host arkose and quartz pebble conglomerate beds.

In addition to these, another occurrence similar to the Moffat Showing is reported by Meillon (1965). It is 15 km south of the Moffat Showing, and was examined by the writers in 1979. The dark heavy mineral layers are up to 8 mm thick and occur in medium grained arkose which dips gently to the northwest. The arkose resembles the pure arkose at MacInnis Lake but is part of the impure arkose (unit 4). The heavy mineral layers are well exposed in outcrop and frost-heaved boulders on the shore of a lake for a distance of 100 m. Some layers are in crossbedded lenses, and others are in parallel bedded layers traceable for a few metres. Polymictic conglomerate occurs as thin beds up to 20 cm thick. Meillon (1965) reported a sample assay of 0.030 per cent U and 0.045 per cent Sn over a thickness of 7.6 cm. Analyses of another sample, representing a 1 cm thickness of heavy minerals, collected by the writers, are given in Table 12.1 (no. 13). Close similarities between this occurrence and the Moffat Showing suggest that this type of disseminated uranium mineralization in arkosic beds may be more common than known to date. It is not certain, however, whether or not it occurs preferentially along a definable stratigraphic horizon or is distributed over a considerable stratigraphic thickness.

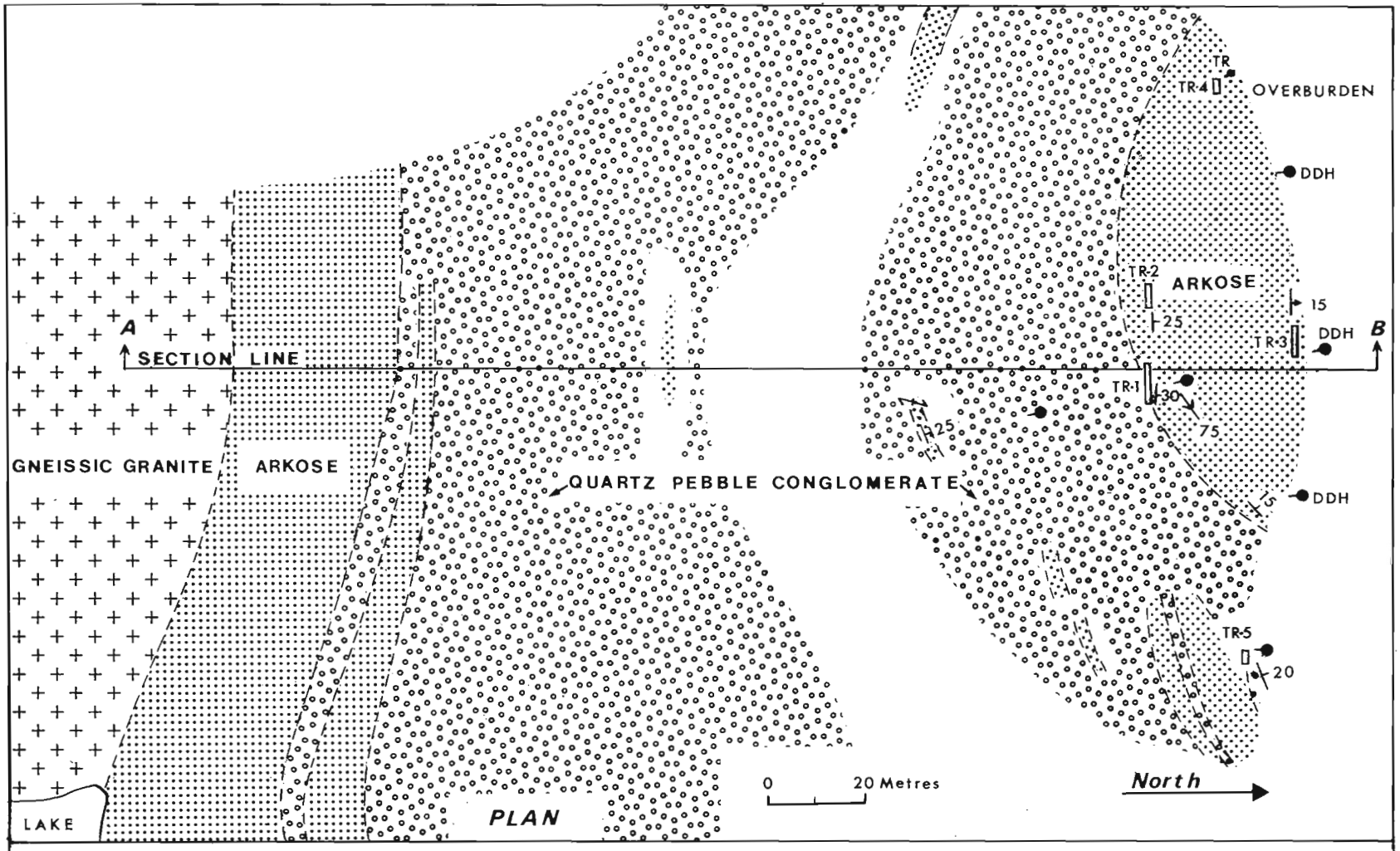

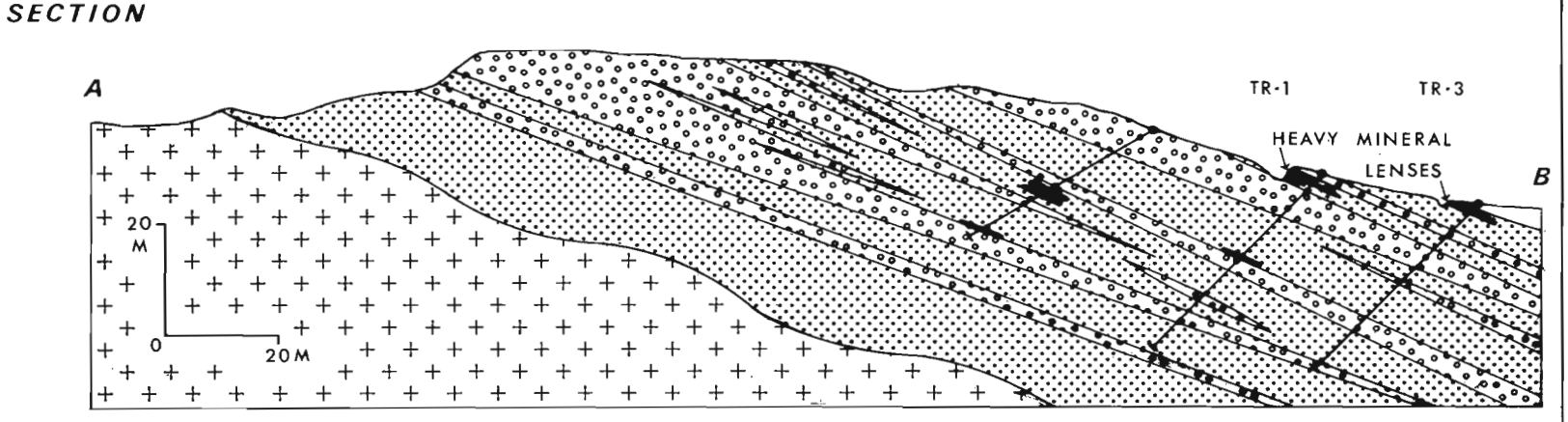

Figure 12.7. *Geology of the Moffat Showing, MacInnis Lake area (after Moffat, 1974).*

Table 12.2

Pb-U isotopic analyses of uranium-bearing samples from the Nonacho Lake area, District of Mackenzie

Sample Number	Location	Sample Weight (mg)	Weight U	Per Cent Pb	Pb Atomic Weight Per Cent Measured 204	206	207	208	Isotopic Ratios $^{206}Pb/^{238}U$	$^{207}Pb/^{235}U$	$^{207}Pb/^{206}Pb$	Age in Million Years $^{206}Pb/^{238}U$	$^{207}Pb/^{235}U$	$^{207}Pb/^{206}Pb$
GFA-77-161	Dussault Prospect ¢1°20.8'N; 110°14.2'W	235.8	32.248	0.862	0.251	83.005	7.817	8.927	0.02457	0.169	0.05002	156	159	196
GFA-78-178	Moffat Showing ¢1°19.8'N; 110°09.9'W	142.8	9.544	0.740	0.176	69.871	6.654	23.299	0.06042	0.490	0.05882	378	405	560
LF-71-27	BEN Claims ¢1°57'N; 109°46'W	12.1	50.90	1.68	a) 0.0352	91.250	7.358	1.357	0.03483	0.361	0.07516	221	313	1073
					b) 0.1729	84.600	8.817	6.410	0.03143	0.326	0.07519	199	286	1074
THEK-4	Steve Showing ¢1°01.8'N; 110°09.4'W	260.0	36.68	3.58	0.014	90.356	9.194	0.438	0.10235	1.406	0.9961	628	891	1671

Analyses by Teledyne Isotopic Laboratories, Westwood, New Jersey, U.S.A.,
a) with correction for 10 per cent blank (0.075 µg Pb).
b) with correction for 0.1 per cent blank (0.075 µg Pb).

Isotopic ratios corrected for the presence of common lead using the lead isotopic composition of a galena sample from Basille Bay, East Arm of Great Slave Lake, reported by Robertson and Cumming (1968), and processing the analytical data by computer program "CONCORD" written by R.I. Thorpe of the Geological Survey of Canada.

Sample LF-71-27 collected by H.W. Little of the Geological Survey of Canada in 1971 from a showing on 'BEN' claims held by Imperial Oil Limited.

Sample THEK-4 collected by M.J. Kreczmer of SMD Mining Company Limited, a subsidiary of Saskatchewan Mining Development Corporation, in 1978 from the Steve Showing on 'THEK' claims held by the company. All sample concentrates prepared at the Geological Survey of Canada, Ottawa; Analytical data on sample THEK-4 provided by SMD Mining Company Limited.

Veins in the Basement Rocks – Pyramid and Kult Showings

The Pyramid Showing is south of MacInnis Lake (Fig. 12.2) and was first staked by S. Yanik in 1966 (Thorpe, 1972, p. 22-23). The claims known as the Pyramid group, were subsequently acquired by Territorial Uranium Mines Limited, and the showing was explored in 1967 by 6 trenches and 10 holes totalling 796 m of drilling (Hegge and Trigg, 1967; Fig. 12.8). The original claims were allowed to lapse. The area around the showing was staked again in 1979 as the Kult group of claims by PNC Exploration (Canada) Limited, a subsidiary of Power Reactor and Nuclear Fuels Development Corporation of Japan. A new showing was discovered in 1979 approximately 3 km north-northeast of the Pyramid Showing (Harrington, 1980), and it is referred to as the Kult Showing in this paper.

Pyramid Showing: Uranium mineralization occurs along veins and fractures in sheared chloritic zones on the west side of a northtrending amphibolite band, surrounded by granite. The band is up to 200 m wide, and varies in character from weakly foliated gabbroic rock to highly chloritized sheared mafic rock. It is intruded by a quartz-rich potassic granite, and the boundary as seen in outcrops and drill core is a wide zone of layers, lenses and irregular patches of the granite alternating with the chloritized and locally granitized amphibolite. Foliation in the amphibolite trends north, and commonly dips vertically or steeply to the west. Some granite gneiss and pegmatite dykes are present in the vicinity of the amphibolite. The granitic complex is considered by the authors to be older than the Nonacho Group, rather than younger as it was regarded by Hegge and Trigg (1967).

Uranium mineralization occurs in veins and fractures for 40 m along one zone and locally in a subsidiary zone 30 m to the east. Both zones are sheared and partly brecciated, and carry abundant fine grained chlorite and some disseminated pyrite. At places the host rock resembles argillite. Drillholes did not encounter any uranium mineralization, but indicated that the main zone has a sinuous north to northeast trend and is traceable for approximately 400 m (Hegge and Trigg, 1967). This zone is up to 5 m wide but is narrower at depths of 50 to 75 m. It dips 70 to 85° to the west. The subsidiary zone is subparallel to the main zone, traceable for only 40 m along strike and pinches out at shallow depth. Most veins trend approximately parallel to the shear zones and are commonly steep. A few veins trend across the shear zone at high angles. The veins contain quartz, white and pink calcite, hematite, pyrite and chalcopyrite in different proportions, and locally yellow secondary uranium oxides were seen in the trenches. Analyses of one high-grade sample is given in Table 12.1 (no. 17). The uranium mineral has been identified as pitchblende from the polished section study and X-ray diffraction.

Kult Showing: Uranium mineralization occurs as veinlets and fracture-fillings in gneissic granite, and at one place in what appears to be a sheared conglomerate in the gneissic granite (Harrington, 1980).

Veins in Gabbroic Intrusion – Island and Bragon Showings

Samples from these showings, first collected in the fall of 1954 by prospectors C. Brock and D. Bagan of Consolidated Mining and Smelting Company of Canada Limited, returned significant uranium values, and they were staked in May 1955, and were mapped and explored by trenching and drilling during 1955, 1956, and 1957 (Spencer, 1955; McVittie, 1956; Koehler, 1957; McGlynn, 1970, p. 136-137). The claims were subsequently allowed to lapse.

The host rocks at both the showings are gabbroic to dioritic in composition, and have chilled margins against the granite and granite gneiss they intrude. Locally at the mineralized zones the intrusive relationship is not clear because of brecciation, shearing and chloritic alteration, and granite appears to be intrusive into the mafic rock. At the Island Showing, the contact zone exposed in southeastern trenches has some lenses of granite material and red feldspar aggregates in the highly chloritic mafic rock. It is possible that high temperature gabbro intrusions locally produced a hybrid zone or rheomorphic effects and back veining. The altered mafic rock grades into the fresh-looking massive gabbro at both showings. At the Island Showing, the gabbro cuts Nonacho sedimentary rocks (Spencer, 1955; Koehler, 1957). At the Bragon Showing, it does not come in contact with the sedimentary rocks, but it is reasonable to assume that it is younger than them.

Island Showing: Mineralization occurs at the margin of a gabbro body of irregular outline, that forms a small hill in the northwestern part of an island (Fig. 12.9). The lower contact with granite is exposed on the north side and dips moderately to the southwest, and has a chilled zone which is somewhat sheared. The contact is very irregular to the southeast where the main mineralized zone is located. Seven trenches were blasted in 1955 and two holes totalling 120 m were drilled in 1957 (Spencer, 1955; Koehler, 1957). The main zone is approximately 70 m long, and has mineralized fractures and veins trending west-northwest and dipping approximately 60° to the southwest. They are cut by a number of short cross fractures which carry some mineralization. The minerals present are pitchblende, quartz, chlorite, hematite and traces of calcite, pyrite and chalcopyrite. Channel samples assayed up to 0.17 per cent U over 2 m, but others ranged between 0.05 and 0.14 per cent over narrower widths. Drillholes did not encounter any mineralization and intersected gabbro near surface and granite at depth (Koehler, 1957). Some radioactivity is present along joint planes and fractures in the massive fresh gabbro on the north side of the small hill. Northwest trending barren quartz veins also occur here. Another small, high-grade occurrence is reported 215 m northeast of the main zone, and a grab sample from it returned 0.81 per cent U. It is a short vein up to 3 cm wide in granite gneiss near a gabbro body, and contains massive and botryoidal pitchblende. The massive granite to the southeast of the main zone is coarse to pegmatitic and locally has radioactivity that is two to three times higher than background.

Bragon Showing: The showing occurs in a dyke-like gabbro body approximately 25 m wide, that strikes north-south. The gabbro is fresh, massive medium- to coarse-grained, with a rather high proportion of accessory magnetite. It cuts massive granite. Pegmatite patches and dykes are common in the granite.

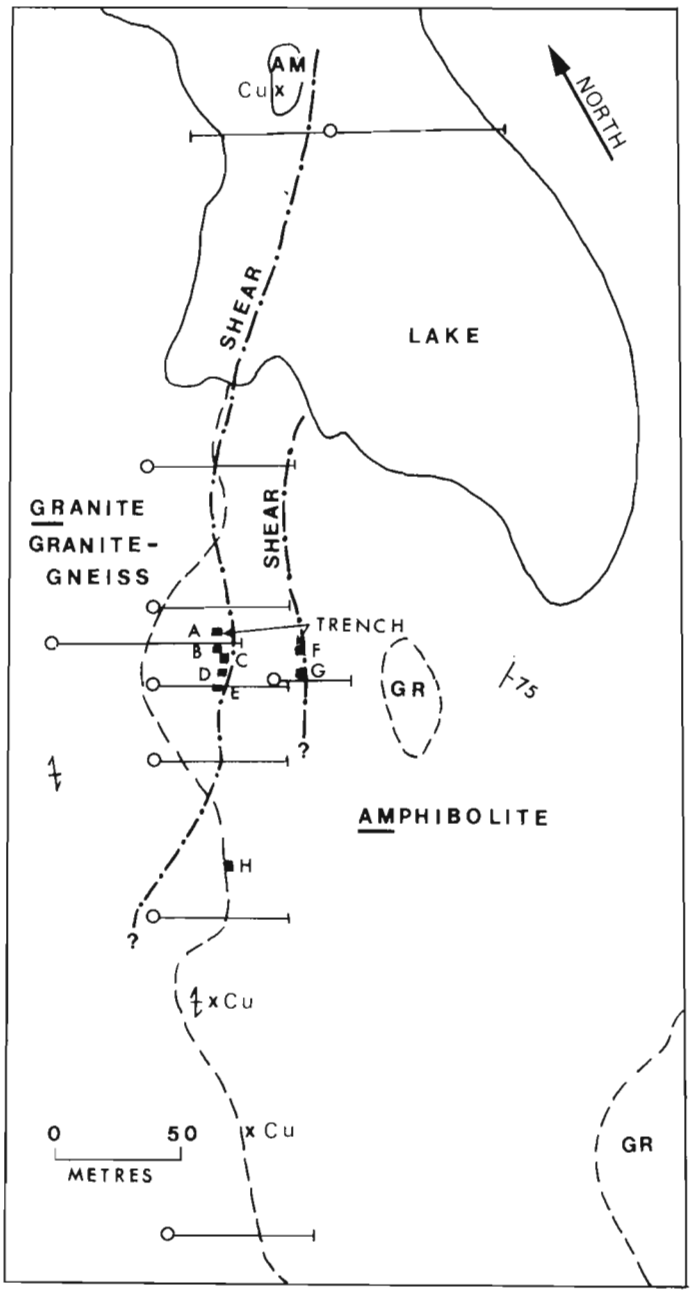

Figure 12.8. Geology of the Pyramid Showing, MacInnis Lake area (after Hegge and Trigg, 1967).

Uranium-bearing veins and fractures occur in an area approximately 50 m by 30 m (Fig. 12.10). They are steeply dipping, and trend in various directions, the most common being east-west and north-south. There is no well defined single fracture zone. Individual fractures range in length from a few metres to a few tens of metres. Radioactivity is traceable along them for lengths up to 8 m. Exploration work in 1955 and 1956 included 7 trenches and 14 short X-ray drillholes totalling 150 m (Fig. 12.10; Spencer 1955, McVittie, 1956). Channel samples gave a maximum assay of

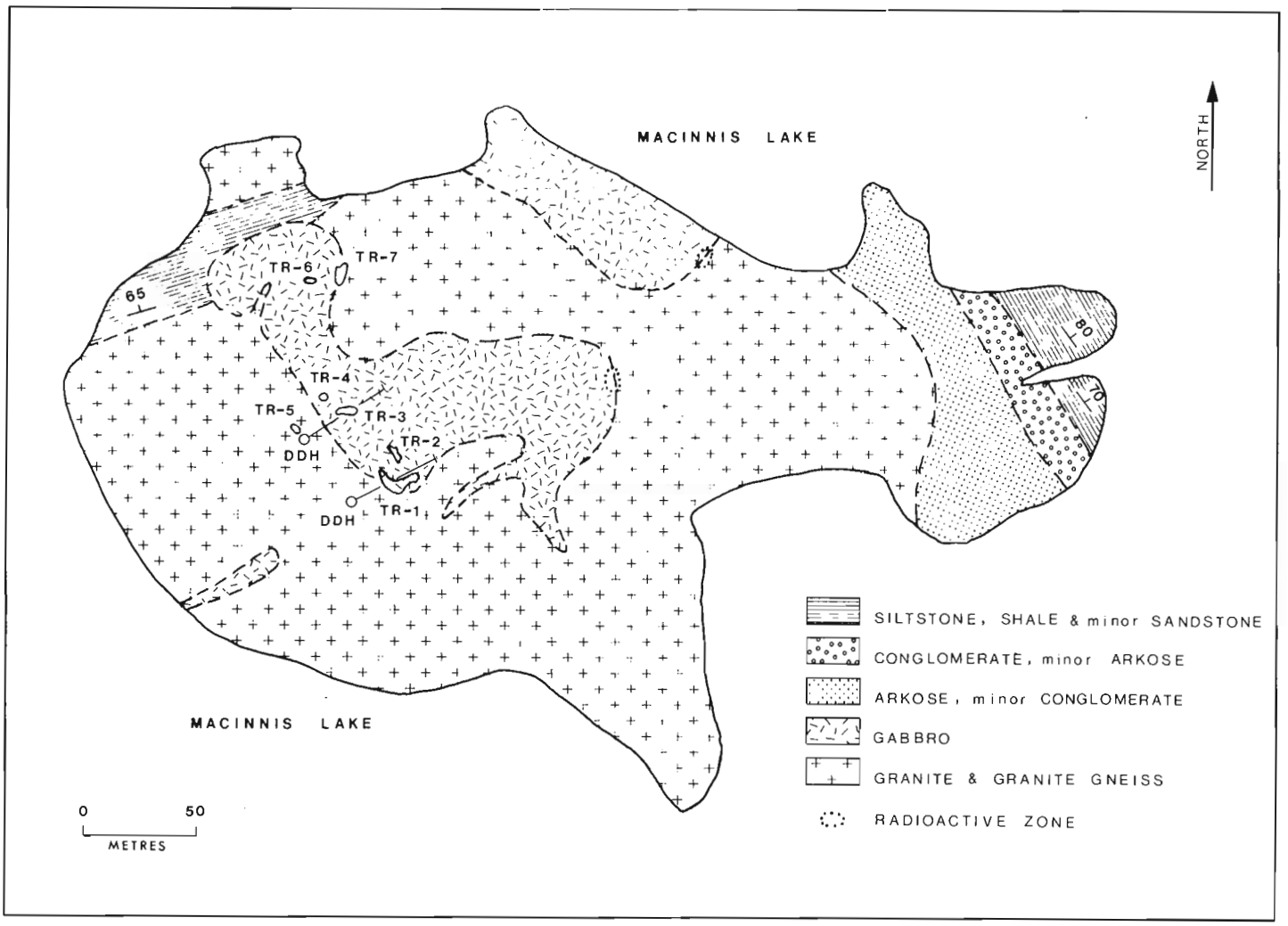

Figure 12.9. *Geology of the Island Showing, MacInnis Lake area (after Spencer, 1955 and Koehler, 1957).*

0.18 per cent U over 1.67 m, and other values ranged from 0.04 to 0.09 per cent U over narrower widths. Assays on drill core samples ranged from 0.04 to 0.13 per cent U over 0.1 to 0.2 m lengths. The uranium mineral was identified as pitchblende and this has been confirmed by Maurice and Plant (1979, p. 183). It is accompanied by hematite, pink and white calcite, chlorite, quartz and locally secondary yellow uranium minerals. There is extensive chloritization of the wall rocks in the vicinity of some of the veins. Some of the calcite aggregates are crenulated.

Isotopic Age Determinations

Several K-Ar isotopic age determinations on granitic rocks and diabase dykes from the Nonacho Lake area have been published by Burwash and Baadsgaard (1962), Wanless et al. (1968) and McGlynn et al. (1974). These are briefly reviewed below, and new data on four Pb-U and two Pb-Pb isotopic analyses are presented.

The granitic rocks dated are from the Thekulthili Lake area in the southern part of the Nonacho basin (Fig. 12.1), and include hornblende-plagioclase gneiss, granite, pegmatite, granitic boulders in conglomerates of the Nonacho Group and sheared granite, all of them representing the basement. A hornblende-plagioclase gneiss sample gave an age of 2240 ma on hornblende. A relatively little deformed granite yielded an age of 2175 Ma on muscovite. Three granitic boulders in Nonacho conglomerates yielded muscovite ages of 2440, 2260 and 1940 Ma. Muscovite from a pegmatite cutting gneiss has been dated at 1845 Ma. Four samples of gneissic to intensely sheared granitic rocks in the vicinity of deformed Nonacho sediments are 1850, 1800 (and 1790), 1785 and 1745 Ma old as determined by analyses of muscovite and biotite (and sericite) concentrates from them. These data suggest that deposition of Nonacho sediments occurred between 2000 and 1800 Ma ago, and that they were deformed approximately 1700 Ma ago.

The deformed Nonacho sedimentary rocks are cut by fresh diabase dykes, referred to as 'Sparrow' dykes. Whole rock K-Ar isotopic analyses of three of these from the northern and southern parts of the basin yielded ages of 1550, 1480 and 1390 Ma. Somewhat older ages, between 1550 and 1750 Ma have been obtained on four diabase dykes by the $^{40}Ar/^{39}Ar$ isotopic method, and the range of ages is supported by paleomagnetic studies (McGlynn et al., 1974).

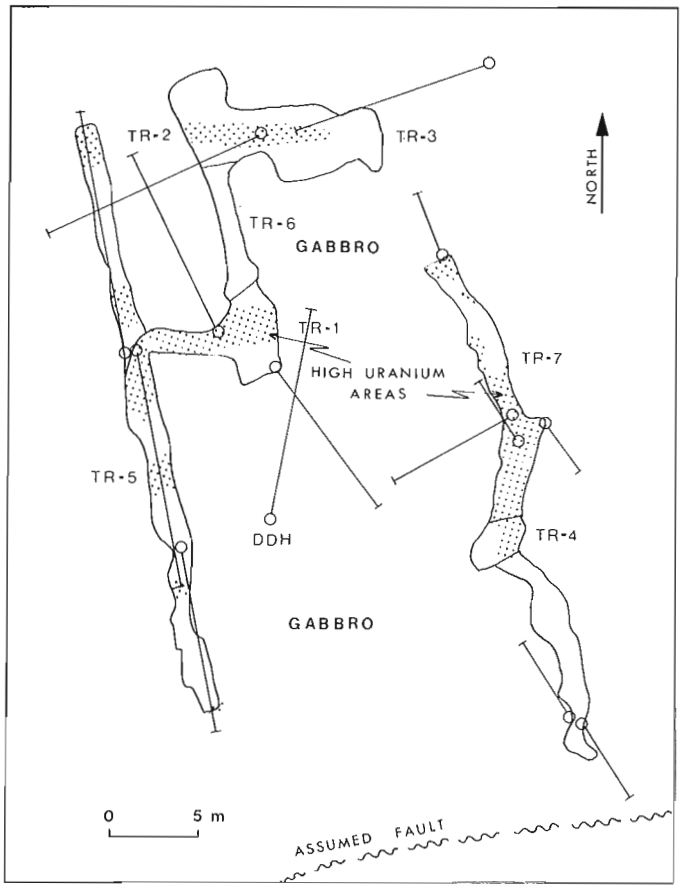

Figure 12.10. *Plan of trenches and drillholes, Bragon Showing, MacInnis Lake area (after Spencer, 1955 and McVittie, 1956).*

Pb-U isotopic analyses on four samples from uranium occurrences are presented in Table 12.2. Two samples are from the MacInnis Lake area, and two others are from localties north and south of it (see latitude and longitude in the table), and are included here for comparison. The results are plotted on a concordia diagram in Figure 12.11. It can be seen from the figure that the ages, except for the youngest, are discordant, due to loss of lead from the system or gain of uranium since the initial deposition of the uranium mineral. The $^{207}Pb/^{206}Pb$ ratios yield ages that cover a wide range.

The oldest age of 1617 Ma is obtained for sample THEK-4 from Steve Showing, located approximately 120 km south of MacInnis Lake. Uranium occurs as pitchblende, which is disseminated along a sinuous zone, up to 10 cm wide and traceable for 2 m, in an impure medium grained arkose interbedded with polymictic conglomerate. The mineralized zone transgresses the bedding; it trends north-south and dips steeply, whereas the beds strike northeast and dip approximately 30 degrees to the southeast. The eastern margin of the zone is marked by red hematite stain, and the mineralization gradually decreases in intensity towards the west. A representative sample assayed 5000 ppm U, 95 ppm Th and 470 ppm Pb. The host beds are folded. The folds are broad, open and trend north-northeast. The deformation is weak. It is possible that the mineralization predated the deformation, and was little affected by it.

Sample LF-71-27 is from a showing located approximately 250 km east-northeast of MacInnis Lake, and represents a pitchblende vein cutting granitic gneiss of the basement, close to the unconformity at the base of the Nonacho Group, according to notes by H.W. Little who collected the sample. The mineralization also occurs along fractures in the Nonacho sediments according to Gibbins et al. (1975, p. 76). The $^{207}Pb/^{206}Pb$ age of 1073 Ma for this sample thus represents a minimum age for the vein type mineralization, and may be extrapolated to similar mineralization in the MacInnis Lake area at the Dussault, Welch and Cole prospects. Sample GFA-77-161 form the Dussault Prospect however yielded a much younger and nearly concordant age of 196 Ma. This may in part be due to the loss of radiogenic lead by weathering processes, as the sample is from a trench at the lake shore and carries some yellow uranium oxides along several minute fractures. The Pb:U ratio in the sample is 1:37.4 (Table 12.2). This sample was concentrated for the isotopic analyses by heavy liquid separation (methylene iodide) of -150+200 mesh and -200 mesh fractions. A portion of the -200 mesh fraction prior to the separation was reserved for analyses by other methods, as reported in Table 12.1, no. 1. The Pb:U ratio on this portion of the sample is 1:14.4 which is significantly higher than the one obtained on the sample concentrate for the isotopic analysis. It is possible that the heavy fraction analyzed isotopically contains less than a true representative proportion of the radiogenic lead, resulting in a relatively young age.

Sample GFA-78-178 from the Moffat Showing was prepared to obtain a concentration of readily leacheable uranium from the matrix. This was carried out by repeating steps of heavy liquid separation and magnetic isodynamic separation of the -200 fraction. A fraction which sinks in methylene iodide (sp.gr. 3.3) and is nonmagnetic at a 0.1 amp. and magnetic at a 0.5 amp. setting on the Franz isodynamic separator was chosen. It should ideally contain the highest concentration of chlorite, the mineral with which uranium is closely associated in the matrix, and be devoid of the uranium-bearing detrital minerals namely uranothorite, monazite and zircon. This concentrate was analyzed, using cold 1N HCl leach, by the fluorimetric method, and gave 1300 and 1100 ppm U in duplicate analyses. This content is only slightly higher than 1200 and 1100 ppm U reported on the whole rock sample analyzed similarly. This suggests that the proportion of uranium-bearing matrix in the concentrate is only slightly higher than in the rock sample as a whole, and probably results from the loss of the matrix to the finer fractions and to other fractions as particles attached to detrital grains. The lead content of the concentrate is 300 ppm compared to 2000 ppm for the whole rock. The concentrate was repeatedly run through the isodynamic separator. For the isotopic analysis, the final concentrate was leached in 1N HCl. The results given in Table 12.2 show that the Pb/U ratio is lower that that in the whole rock, indicating a loss of lead relative to uranium during the mineral separation. Furthermore the high ^{208}Pb content of the leached lead suggests that lead derived from thorium decay is present. The age of 560 Ma represents the minimum age of emplacement of readily leachable uranium.

The points representing three of the samples, namely THEK-4, LF-71-27 and GFA-77-161 lie approximately on a straight line (Fig. 12.11). The join of these points intersects the concordia at 1800 Ma and 100 Ma. This suggests that the initial uranium mineralization could be as old as 1800 Ma, and may have evolved by loss of different proportions of radiogenic lead at about 200 Ma ago. Sample GFA-78-178 is

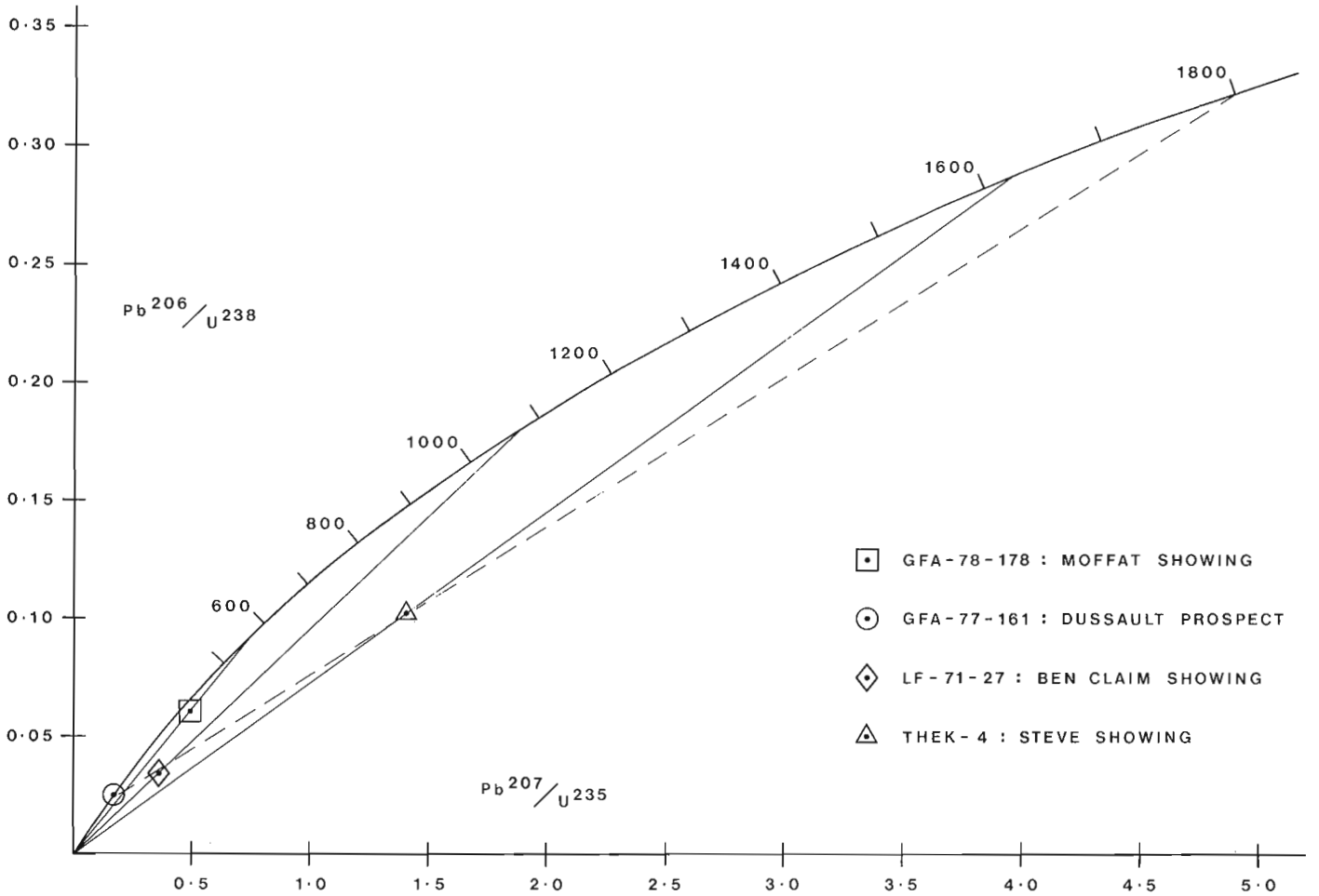

Figure 12.11. *Concordia plot of pitchblendes from the Nonacho Lake area, District of Mackenzie.*

from a different type of mineralization and may have evolved in a somewhat different manner. These isotopic data, however, are insufficient to draw any firm conclusions regarding the time of origin and subsequent evolution of the mineralization.

Lead isotopic analyses of two galena samples from the Nonacho Lake area are given in Table 12.3. One is from the galena vein at the Welch Prospect, mentioned earlier, and is closely associated with pitchblende veins. It has had a uranogenic lead component added to it, otherwise the $^{208}Pb/^{204}Pb$ ratio would be higher than that obtained. The latter ratio is most similar to that reported by Robertson and Cumming (1968) for galena from Basille Bay, East Arm of Great Slave Lake, approximately 100 km northwest of MacInnis Lake. Assuming that the lead at the Welch Prospect evolved from an initial composition identical to the Basille Bay lead, the normal $^{207}Pb/^{204}Pb$ versus $^{206}Pb/^{204}Pb$ plot gives a $\Delta^{207}/\Delta^{206}$ slope of 0.097, and a plot of $^{207}Pb/^{208}Pb$ versus $^{206}Pb/^{208}Pb$ gives a slope of 0.1006. These yield calculated ages of 1570 Ma and 1635 Ma respectively. These ages coincide approximately to the time of deformation of the Nonacho Group, and suggest remobilization of uranium and radiogenic lead at that time.

The galena sample from the Thekulthili Lake area is from a massive galena occurrence in the basement gneiss. It was first reported by prospectors R.J. Menard (Mineral Occurrence Map, NTS 75D, Fort Smith; Department of Indian and Northern Affairs, Yellowknife, N.W.T.), and was examined by the writers in 1979. The host gneiss is fine- to medium-grained with alternating felsic and mafic folia, from 0.5 to 2 mm thick, rich in pink feldspar and in chlorite, hornblende and biotite. The mafic minerals constitute approximately 30 per cent of the rock. The foliation is well developed, regular, and strikes 030° and dips 65° to the northwest at the showing. The dip becomes gradually shallower to the northeast. The lenses of massive galena, up to 0.4 m thick occur parallel to the foliation along a strike length of 15 m, and are exposed by four closely spaced trenches. Minor sphalerite is associated with the galena. Epidote occurs in the gneiss in the vicinity. Pods of pegmatite also occur in the gneiss. Quartz veins with traces of pyrite are found to the west of the showing. Some of the veins, and pegmatitic patches as well as the galena lenses, have a crude to well defined foliation subparallel to that in the gneiss. The isotopic analysis of sample GFA-78-101 (Table 12.3) gives an age of 2150 Ma according a two-stage model proposed by Stacey and Kramers (1975) and 2132 Ma according to a lineal model proposed by Cumming and Richards (1975; R.I. Thorpe, personal communication, 1979).

Table 12.3

Lead isotopic analyses of two galena samples from the Nonacho Lake area.

Sample Number	Location	$^{206}Pb/^{204}Pb$	$^{207}Pb/^{204}Pb$	$^{208}Pb/^{204}Pb$	Remarks
Welch-77-1[a]	Welch Prospect; Trench 3; MacInnis Lake; 61°21.3'N 110°14.0'W	18.318	15.639	35.375	Galena and pitchblende vein in siltstone-shale at the upper boundary of unit 5.
GFA-78-101[b]	Thekulthili Lake, Big Pine Narrows; 60°58'N 110°15.5'W	14.711	15.034	34.971	Galena lenses along foliation in the basement gneiss

(a) Sample Welch-77-1 collected by W.A. Padgham and W.A. Gibbins of the Department of Indian and Northern Affairs, Yellowknife, in 1977, and analyzed in 1978 at the University of British Columbia, Vancouver, by B. Ryan.

(b) Sample GFA-78-101 collected in 1978 by M.J. Kreczmer of SMD Mining Company Limited and analyzed in 1979 at the Geological Survey of Canada, Ottawa, by W.D. Loveridge.

Nonacho sedimentary rocks unconformably overlie the host gneiss, and the model age probably represents the maximum age of the Nonacho Group.

The two Pb-Pb ages thus suggest that sediments of the Nonacho Group were deposited sometime after 2150 Ma and were deformed approximately 1650 Ma ago. This is in general agreement with the isotopic ages obtained by K-Ar methods and paleomagnetic studies.

Genetic Hypotheses

The disseminated and vein type uranium occurrences of the MacInnis Lake area constitute two genetically different types of mineralization.

The disseminated mineralization, exemplified by the Moffat Showing, is stratiform and is related to the paleoplacer accumulation of detrital heavy minerals which included monazite, zircon and uranothorite as the uraniferous minerals. The readily leachable uranium, which accounts for approximately 85 per cent of the total, is in the matrix, is apparently younger, and was probably emplaced during diagenesis. The mechanism of uranium precipitation is not clear. There is a notable lack of strong precipitating agents such as organic matter. Traces of pyrite are reported in the host rocks but the mineral is not intimately associated with the uranium mineralization. Extensive oxidation of magnetite to hematite may have created reducing environments in which uranium could be deposited from circulating uranium-bearing solutions. It is also likely that the chloritic matrix acted as an adsorption medium, and uranium and other associated elements namely titanium, iron, phosphorus and silicon, were deposited in it. These elements could have been derived during diagenesis from the minerals present, namely uranothorite, zircon, apatite, magnetite and quartz. Uranothorite, which contains up to 10 per cent uranium, tends to be metamict, and may release part of its uranium under favourable conditions. Monazite and zircon contain smaller amounts of uranium (less than 1 and 3 per cent respectively) and are relatively more stable. The proportion of these three detrital minerals, however, is too small, less than 0.1 per cent each, to contribute significantly to the readily leachable uranium in the matrix. It is therefore suggested that circulating waters during sedimentation and diagenesis provided most of the uranium in the matrix. The $^{207}Pb/^{206}Pb$ age of 560 Ma obtained is much younger than would be expected from this genetic model. It can, however, be attributed partly to radioactive disequilibrium in an open system in which uranium is weakly bonded to the matrix of the host rock and partly to loss of radiogenic lead relative to uranium during sample preparation. The initial mineralization is probably as old as the mineralization at the Steve Showing which yielded a discordant age of 1671 Ma (Table 12.2). Other isotopic age determinations discussed earlier suggest that this is close to the time of deformation of Nonacho sedimentary rocks. The deformation most likely resulted in reconstitution of the uranium minerals, and the age of initial mineralization, if older than this event, would be difficult to obtain by the Pb-U isotopic method.

The presence of native gold, cassiterite, and niobium- and tantalum-bearing minerals in the paleoplacer is suggestive of a source area such as the Yellowknife-Blachford Lake area north of Great Slave Lake, where native gold occurs in veins and shear zones in an Archean greenstone belt (Boyle, 1961), cassiterite occurs in pegmatites in metamorphic aureoles of younger Archean granites (Moffat, 1974; Mulligan, 1975), and niobium- and tantalum-bearing minerals occur in late stage veins and alteration zones in a perakaline intrusive complex dated at 2057 Ma by the K-Ar isotopic method (Davidson, 1978). It is interesting to note that garnet is not found in the paleoplacer, and it is not a common mineral in this probable source area. The area is between 150 and 250 km northwest of MacInnis Lake. Current bedding in the sediments at MacInnis Lake indicate that paleocurrents were from south to north. McGlynn (1970, p. 94) has, however, pointed out that they probably do not correspond to sedimentary transport direction, and the source areas, in addition to nearby basement highs, may have been in the north, as quartzite boulders in one of the polymictic conglomerate beds in the Nonacho Group are lithologically similar to the quartzites of Late Archean or Early Aphebian Wilson Island Group exposed on islands in Great Slave Lake. The Nonacho conglomerates near Thekulthili Lake contain sparsely distributed large, well rounded pebbles of an altered porphyritic intermediate rock, with high contents of niobium, tantalum, thorium and uranium (Maurice and Plant, 1979), and their source may be the same as that of the detrital minerals carrying these elements in paleoplacers. The area within several hundred kilometres to the south, southwest and west of MacInnis Lake has no known occurrences of native gold, cassiterite or niobium- and tantalum-bearing minerals that could be regarded as possible sources for the paleoplacer.

The vein type occurrences are primarily controlled by minor fractures and shears. Maurice and Plant (1979, p. 183) suggested that the occurrences on the west shore of MacInnis Lake are distributed along a north-south trend and that the mineralizing activity may have occurred along a single fracture system. Field observations by the authors however do not support the interpretation of a single fracture system. No major fault or thrust could be recognized that might in any way be related to the mineralized fractures and shears. The apparent linear distribution of the occurrences is therefore considered to be coincidental. The mineralized fractures and shears, except for those in the younger gabbroic intrusions, may have existed since the major deformation of Nonacho sedimentary rocks approximately 1700 Ma ago. Younger faults which displace the folded sedimentary rocks, and associated minor fractures, are characterized by abundant quartz veins and stockworks. Quartz is scarce or absent in the uranium-bearing veins.

A model invoking remobilization of uranium from Nonacho sedimentary rocks is favoured here for the genesis of the veins in these rocks. As mentioned earlier, some of the sedimentary rocks are enriched in uranium, which may have been introduced during sedimentation or soon after, but prior to the major deformation. It is thus reasonable to postulate that some uranium in the sedimentary rocks was available for remobilization and concentration during the deformation. This migration and deposition would tend to occur along the source beds, as appears to have been the case at the Dussault and Welch prospects. The stratigraphic control of mineralization here is crude but recognizable in the surface exposures, according to the mapping done by the writers. Outlines of the mineralized zones based on the drillhole data (Makela, 1970) show that they are subparallel to the host beds. A further study of the drill logs by the writers revealed that some of the holes intersected the boundary between units 5 and 6, and this led to the structural interpretation presented in Figure 12.4, in which the stratigraphic control of mineralization is much more evident.

Makela (1970) postulated that uranium is primarily syngenetic sedimentary in origin, and invoked metamorphism and intrusion of younger granite as causes for remobilization of uranium. The sedimentary rocks, however, show little metamorphic effects, and there is no field evidence for younger granite. It is therefore suggested here that deformation of these rocks alone may have sufficed to mobilize connate waters and uranium. The maximum concentration of uranium has occurred along the hinge zone of northward-plunging minor folds at the Dussault and Welch Prospects. Uranium probably migrated up the plunge of the folds from a more tightly folded zone at depth to the north and northeast of the prospects. At the Cole Prospect, the structure is simpler but there is some variation in the attitude of foliation in the matrix of the host granite pebble conglomerate.

There is a possibility that uranium in veins may have come from older concentrations along the unconformity at the base of the Nonacho Group or in the basement, at the time of the deformation of rocks of this group. No positive evidence for unconformity-related uranium concentration in the Nonacho basin has yet been reported. The possibility, however, does exist in view of the favourable geological setting of the basin. The basement may have contained some uranium concentrations that predated the Nonacho sediments. It is, however, difficult to see how uranium could have been mobilized from them, since the basement responded differently to the deformation than Nonacho sedimentary rocks, mainly by faulting and shearing instead of folding.

In case of the veins associated with the gabbroic intrusions, an attractive genetic hypothesis is one in which it is postulated that the intrusions have served as a source of heat, set up convective currents in the groundwater in the country rock, and that the heated water leached uranium from the country rock and deposited it in the veins. Makela (1970) pointed out the similarity in geology of the MacInnis Lake area to the Paukkajanvaara area in Finland where several uranium occurrences are found at the margins of diabase dykes that cut a conglomerate-arkose-sandstone sequence of early Proterozoic age, and one of them produced 52 000 metric tonnes of ore in 1960 and 1961 (Piirainen, 1968; Frietsch et al., 1979). The sequence also contains small, low grade occurrences in the sedimentary rocks (Piirainen, ibid.), which resemble to some extent the Moffat Showing. The gabbro intrusions at the Island and Bragon showings may have caused convection cells in the groundwater that could have encompassed Nonacho sedimentary rocks above the present erosion surface, and could have formed the vein type mineralization seen at the showings.

A supergene model for the veins in amphibolite at the Pyramid Showing was proposed by Hegge and Trigg (1967). It is supported by the erratic nature and lack of depth extension of mineralization. This type of deposition can be expected in any uranium district where surface waters are at least locally enriched in uranium. Presence of reducing agents such as iron and copper sulphides, chlorite etc., along the fractures would facilitate deposition of uranium. This model may work for Kult Showing but when it is applied to other occurrences of the area, it does not adequately explain their greater vertical extent, is not in agreement with the determined timing of mineralization, and cannot be readily reconciled with the known stratigraphic and structural relations.

Conclusions

Sediments of the Aphebian Nonacho Group in the MacInnis Lake area were enriched in uranium at the time of deposition or at a later date prior to major deformation that took place at the close of the Aphebian era. Synsedimentary deposition is represented by detrital uranothorite, monazite and zircon with abundant magnetite and some cassiterite, native gold and niobium- and tantalum-bearing minerals in paleoplacers. A possible source area of these minerals is the Yellowknife-Blachford Lake region situated 150 to 250 km northwest of MacInnis Lake. Uranium was also precipitated in the matrix of the Nonacho sediments as disseminations, and is locally preserved in this form. Elsewhere uranium may have been mobilized during deformation to form vein type occurrences hosted by the sedimentary rocks. The new Pb-Pb and Pb-U isotopic age determinations, together with the published K-Ar ages and paleomagnetic studies, suggest that deposition of sediments of the Nonacho Group occurred between 2000 and 1800 Ma ago and that they were deformed approximately 1700 Ma ago. Uranium in veins at margins of younger gabbro intrusions was probably deposited from the groundwater in convection currents set up by heat of the intrusions, and was derived partly or wholly from the sedimentary rocks. Uranium has also been mobilized by surface oxidation at the present and/or past erosion surfaces, and deposited locally under reducing conditions.

Guides for Further Exploration

Uranium, gold and tin in detrital concentrations in the arkose-quartz pebble conglomerate unit are widely distributed, and search for larger concentrations of this type may prove rewarding. Vein type uranium occurrences,

particularly those hosted by Nonacho sedimentary rocks, and where some stratigraphic control is apparent, merit further exploration. Of particular interest is the stratigraphic zone at the base of the siltstone-argillite-sandstone unit. Hinge zones of minor folds and small fractures in tightly folded sediments are favourable structural sites for exploration. The unconformity at the base of the Nonacho Group merits examination for possible uranium concentrations. Highly chloritic zones, either in the basement rocks, Nonacho sedimentary rocks, or the gabbroic intrusions are potentially favourable locales for uranium concentrations.

Acknowledgments

Permission to present unpublished company information was kindly granted by Mr. A.W. Dean of Scurry-Rainbow Oil Limited, Dr. L.A. Clark of SMD Mining Company Limited, Mr. J.A. Climie of AGIP Canada Limited, Mr. S. Kay of International Mine Services Limited, Mr. M. Suginohara of PNC Exploration (Canada) Limited, and also by Cominco Limited. The writers benefitted greatly from discussions with Drs. J.C. McGlynn, R.I. Thorpe, S.M. Roscoe, Y.T. Maurice, R.W. Boyle and H.H. Bostock of the Geological Survey of Canada, Dr. W.A. Gibbins of Department of Indian and Northern Affairs, Messrs. M.J. Kreczmer and R.J. Beckett of SMD Mining Company Limited, J.D. Murphy and K.R. Bond of Uranerz Mining and Exploration Limited, and E. Harrington of PNC Exploration (Canada) Limited. Mr. C.G. Lamontagne assisted in the field work.

References

Bostock, Hewitt, H.
1980: Reconnaissance geology of the Fort Smith-Hill Island Lake area, Northwest Territories; in Current Research, Part A, Geological Survey of Canada, Paper 80-1A, p. 135-155.

Burwash, R.A. and Baadsgaard, H.
1962: Yellowknife-Nonacho age and structural relations; in J.S. Stevenson (Editor), Tectonics of the Canadian Shield, Royal Society of Canada, Special Publication 4, p. 22-29.

Boyle, R.W.
1961: The geology, geochemistry and origin of the gold deposits of the Yellowknife District; Geological Survey of Canada Memoir 310, 193 p.

Campbell Todd, R.
1956: Report on Exploration on the MacInnis Lake property of Canadian Pipelines and Petroleum Limited; Scurry-Rainbow Oil Limited, unpublished report, 20 p.

Checklin, G.A.
1968: MacInnis Lake project (AFE 2-27); Scurry-Rainbow Oil Limited, unpublished report, 14 p.

Cumming, G.L. and Richards, J.R.
1975: Ore lead isotope ratios in a continuously changing earth; Earth and Planetary Science Letters, v. 88, no. 2, p. 155-171.

Davidson, A.
1978: The Blachford Lake Intrusive Suite: An Aphebian alkaline plutonic complex in the Slave Province, Northwest Territories; in Current Research, Part A, Geological Survey of Canada, Paper 78-1A, p. 119-128.

Donaghy, T.J.
1977: The petrology of the Thekulthili Lake area, Northwest Territories; unpublished M.Sc. thesis, University of Alberta, 140 p.

Frietsch, R., Papunen, H., and Vokes, F.M.
1979: The ore deposits in Finland, Norway and Sweden – a review; Economic Geology, v. 74, no. 5, p. 975-1001.

Gibbins, W.A., Seaton, J.M.B., Laporte, P.J., Murphy, J.D., Hurdle, E.J., and Padgham, W.A.
1977: Mineral industry report, 1974, Northwest Territories, Department of Indian and Northern Affairs, EGS 1977-5, document no. N 061742, 267 p.

Harrington, E.
1980: Thekulthili Lake Project, Northwest Territories; Assessment Work Report-1979; PNC Exploration (Canada) Limited; unpublished report.

Hegge, M.R. and Trigg, C.M.
1967: Results of diamond drilling on claim no. 22, Pyramid group, MacInnis Lake, Northwest Territories; Territorial Uranium Mines Limited; Department of Indian and Northern Affairs document no. N 019973, 5 p.

Henderson, J.F.
1937: Nonacho Lake area, Northwest Territories; Geological Survey of Canada, Paper 37-2, 22 p.

1939a: Taltson Lake, District of Mackenzie, Northwest Territories; Geological Survey of Canada Map 525A.

1939b: Nonacho Lake, District of Mackenzie, Northwest Territories; Geological Survey of Canada Map 526A.

Koehler,G.J.
1957: Geological Report, MacInnis Property, Island Zone; Mackenzie Mining District, N.W.T.; Consolidated Mining and Smelting Company Limited, unpublished report, 2 p.

MacDonald, B.C.
1956: Report on exploration on the MacInnis Lake property of Canadian Pipelines and Petroleums Limited, Northwest Territories; Scurry-Rainbow Oil Limited, unpublished report, 6 p.

MacLeod, W.A. and Brander, J.M.
1975: Assessment report: Mining claims BM 1-36, claim map no. 75E-8 (Lat. 61°20'; Long. 110°10') August 1, 1974-October 1, 1974; Shell Canada Limited, Department of Indian and Northern Affairs, document no. N 080170, 8 p.

Makela, K.
1970: MacInnis Lake property evaluation; Scurry-Rainbow Oil Limited, unpublished report, 4 p.

Maurice, Y.T.
1976: Detailed geochemical investigation for uranium and base metal exploration in the Nonacho Lake area, District of Mackenzie; in Report of Activities, Part C, Geological Survey of Canada, Paper 76-1C, p. 259-262.

1977: Follow-up geochemical activities in the Nonacho Lake area (75 F,K), District of Mackenzie; Geological Survey of Canada, Open File 489, 10 p.

Maurice, Y.T. (cont.)
1979: Methods of interpretation and follow-up of reconnaissance lake sediment data in the northern Canadian Shield; Proceedings of 7th International Geochemical Exploration Symposium (J.R. Watterson and P.K. Theobald, ed.) Denver, 1978, p. 117-128.

Maurice, Y.T. and Plant, A.G.
1979: Some mineralogical and geochemical characteristics of uranium occurrences in the Nonacho Lake area, District of Mackenzie: in Current Research, Part B, Geological Survey of Canada, Paper 79-1B, p. 179-188.

McGlynn, J.C.
1970: In Geology and economic minerals of Canada, 5th ed. (R.J.W. Douglas, ed.), Geological Survey of Canada, Economic Geology Report No. 1, p. 92-94.

1971: Stratigraphy, sedimentology and correlation of the Nonacho Group, District of Mackenzie; in Report of Activities, part A, Geological Survey of Canada, Paper 71-1A, p. 140-142.

1971a: Metallic mineral industry, District of Mackenzie, Northwest Territories; Geological Survey of Canada, Paper 70-17, 194 p.

1971b: Stratigraphy, sedimentology and correlation of the Nonacho Group, District of Mackenzie; in Report of Activities, Part A, Geological Survey of Canada, Paper 71-1A, p. 140-142.

1978: Geology of the Nonacho Basin, District of Mackenzie; Geological Survey of Canada, Open File 543.

McGlynn, J.C., Hanson, G.N., Irving, E., and Park, J.K.
1974: Paleomagnetism and age of Nonacho Group sandstones and associated Sparrow dikes, District of Mackenzie; Canadian Journal of Earth Sciences, v. 11, no. 1, p. 30-42.

McVittie, G.A.
1956: Report on Packsack Drilling: Bragon Zone; Consolidated Mining and Smelting Company of Canada Limited, unpublished report, 3 p.

Meagher, J.T.
1955: Report on the BAG claim group, MacInnis Lake, Northwest Territories, Iso Uranium Mines Limited, Department of Indian and Northern Affairs document no. N 017070, 7 p.

Meillon, J.J.
1965: Report on the Nonacho project, Summer 1965; International Mine Services Limited, unpublished report, 16 p.

Moffat, G.W.
1974: An investigation of the radioactive mineral occurrences of the Great Slave Lake-Athabasca Lake region of the District of Mackenzie in the Northwest Territories; unpublished B.Sc. thesis, University of Toronto, 115 p.

Mulligan, R.
1975: Geology of Canadian tin occurrences; Geological Survey of Canada, Economic Geology Report no. 28, 155 p.

Mulligan, R. and Taylor, F.C.
1969: Hill Island Lake, District of Mackenzie; Geological Survey of Canada Map 1203 A.

Piirainen, T.
1968: Die Petrologie and Uranlagerstätten des Koli-Kaltimogebiets im finnischen Nordkarelien; Finlande, Commission géologique, bulletin no. 237, 99 p.

Reid, J.D.
1955: MacInnis Lake: Report on area for exploration; Scurry-Rainbow Oil Limited, unpublished report, 8 p.

Robertson, D.K. and Cumming, G.L.
1968: Lead and sulfur-isotope ratios from the Great Slave Lake area, Canada; Canadian Journal of Earth Sciences, v. 5, no. 5, p. 1269-1276.

Spencer, R.J.
1955: MacInnis Group: Engineering Report No. 1 (Mine Series No. 5831) Consolidated Mining and Smelting Company of Canada Limited, Unpublished report, 4 p.

Stacey, J.S. and Kramers, J.D.
1975: Approximation of terrestrial lead isotope evolution by a two-stage model; Earth and Planetary Science Letters: v. 26, p. 207-221.

Stephen, H.C.
1956: Geological report on the WALT claim group, MacInnis Lake, Taltson Lake map area, District of Mackenzie, Northwest Territories; Newkirk Mining Corporation Limited; Department of Indian and Northern Affairs, document no. N 017080, 9 p.

Stockwell, C.H., Henderson, J.F., Brown, I.C., Wright, G.M., and Barnes, F.Q.
1967: Reliance, District of Mackenzie; Geological Survey of Canada Map 1123 A.

Stockwell, C.H., Brown, I.C., Barnes, F.Q., and Wright, G.M.
1968: Christie Bay, District of Mackenzie; Geological Survey of Canada, Map 1122 A.

Taylor, F.C.
1971: Nonacho Lake, District of Mackenzie; Geological Survey of Canada, Map 1281 A.

Thorpe, R.I.
1972: Mineral Exploration and Mining Activities, Mainland Northwest Territories, 1966 to 1968; Geological Survey of Canada, Paper 70-70, 204 p.

Tremblay, L.P.
1972: Geology of the Beaverlodge mining area, Saskatchewan; Geological Survey of Canada, Memoir 367, 257 p.

Wanless, R.K., Stevens, R.D., Lachance, G.R., and Edmonds, C.M.
1968: Age determinations and geological studies, K-Ar isotopic ages, report 8; Geological Survey of Canada, Paper 67-2, Part A, 141 p.

Wilson, J.T.
1941: Fort Smith, District of Mackenzie, Northwest Territories; Geological Survey of Canada, Map 607 A.

13. THE GOLD CONTENT OF INTERFLOW METASEDIMENTARY ROCKS FROM THE RED LAKE AREA, ONTARIO – A PRELIMINARY EVALUATION

E.M.R. Research Agreement No. 177-4-79
P. Cowan[1] and J.H. Crocket[1]

Cowan, P. and Crocket, J.H., The gold content of interflow metasedimentary rocks from the Red Lake area, Ontario – A preliminary evaluation; in Current Research, Part B, Geological Survey of Canada, Paper 80-1B, p. 129-133, 1980.

Abstract

The gold content of ultramafic to mafic metavolcanic rocks and siliceous and ferruginous interflow metasedimentary rocks from the Red Lake area, northwestern Ontario was determined by radiochemical neutron activation analysis.

The interflow metasedimentary rocks consist mainly of chert and iron formation, the latter including oxide, silicate and sulphide varieties. The ultramafic to mafic metavolcanic rocks are pyroxenitic to basaltic komatiites and tholeiitic basalts. A statistical comparison of the gold content of the volcanic and sedimentary suites indicates a similarity in average gold content and dispersion of gold values. Gold contents range from approximately 0.1 to 380 ppb with arithmetic and geometric means of approximately 28 and 5.7 ppb respectively. The background gold value for the region is 3.5 ppb. There are some significant differences among the various rock types making up each group. The oxide iron formation is richer in gold compared to other interflow sediments. The volcanic rocks are relatively consistent in gold content, although tholeiitic basalts, particularly iron-rich tholeiites are rich in gold relative to the other volcanic rock types.

Introduction

Red Lake is an economically important gold mining camp in the Uchi greenstone belt of Northwestern Ontario (Fig. 13.1). Two producers, the Campbell Red Lake and Dickenson (including the Robin Red Lake), are currently active and the area hosts several significant past producers (Fig. 13.2). The geology of Dome and Balmer townships, which host the most important gold deposits, and of Bateman and McDonough townships, according to the detailed mapping of Pirie and Grant (1978a, b), Pirie and Sawitzky (1977) and Ferguson (1966), is shown in Figure 13.2. The predominant rock types are ultramafic to mafic and intermediate metavolcanics, and felsic stocks and batholiths. Minor lithologies present in the ultramafic and mafic metavolcanic portion of the pile are siliceous and commonly ferruginous metasedimentary rocks, termed here interflow sediments. The regional grade of metamorphism is greenschist facies, although grades up to lower amphibolite facies can be found near intrusive bodies. The objective of this study is to characterize the interflow sedimentary rocks and mafic to ultramafic metavolcanic rocks with respect to their gold contents.

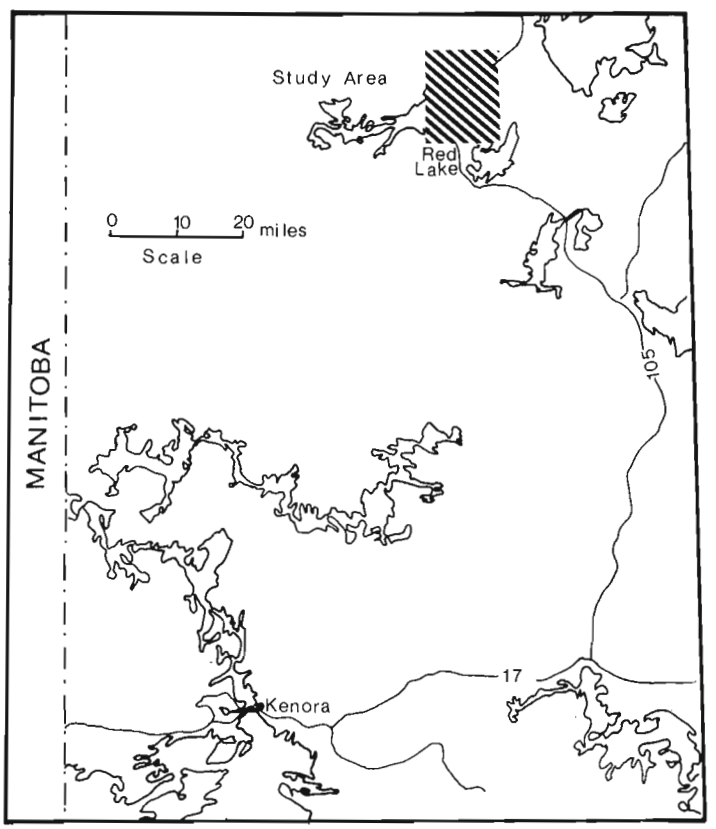

Figure 13.1. *Location map of the Red Lake area.*

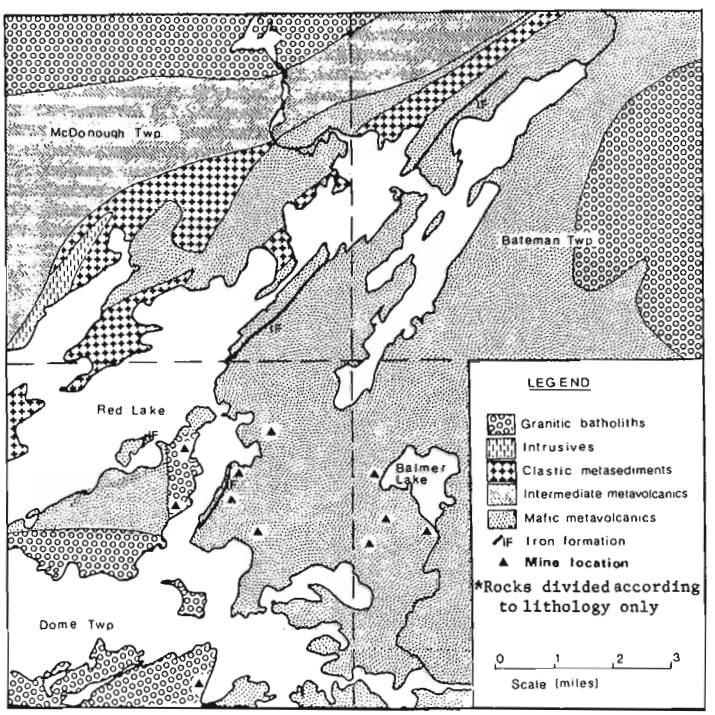

Figure 13.2. *Generalized geology of Balmer, Bateman, Dome and McDonough townships (after Ferguson, 1966; Pirie and Sawitzky, 1977; Pirie and Grant, 1978a, b).*

[1] Department of Geology, McMaster University, Hamilton, L8S 4M1

The interflow sediments are of interest for two reasons. In the first place, highly siliceous and commonly laminated rocks occur at the Dickenson Mine (J.M. Franklin, personal communication), one of the two producing gold mines in the area. Secondly, these rocks were presumably deposited during breaks in active volcanism and thus possibly constitute a record of both volcanic exhalation and leaching of the volcanic pile. There is little basis as yet for speculation on the possible role of interflow sediments in gold metallogeny, and this study attempts to characterize the gold content of these sediments and their associated volcanics.

Interflow Metasedimentary Rocks

The sampling locations for the interflow metasedimentary rocks and mafic to ultramafic metavolcanic rocks are shown in Figure 13.3. The interflow sediments usually occur as thin discontinuous beds between volcanic flows, but can constitute thick, extensive, mappable units conformable with the volcanic rocks (see maps by Pirie and Grant, 1978a, b). The two main types of interflow sedimentary rocks are chert and iron formation with subordinate greywacke. Iron formation is represented by oxide, silicate, sulphide and mixed oxide-silicate facies. In addition to these predominantly chemical sediments a few ferruginous interflow sediments appear to consist of both chemical and clastic components. The principal textural, mineralogical and chemical properties of interflow sediments are summarized in Table 13.1.

Chert

The cherts are massive rocks exhibiting conchoidal fracture. For classification purposes chert contains more than 80 per cent SiO_2, an iron content of up to 15 per cent and very low contents of other components including Al_2O_3. The principal mineral is quartz with minor magnetite and accessory chlorite and calcite. Recrystallization during metamorphism has produced a fine grained mosaic of polygonal quartz grains commonly with interstitial iron staining.

Iron Formation

The iron formations have been classified according to James (1954) and are considered simply sedimentary rocks that contain more than 15 per cent total iron. They are

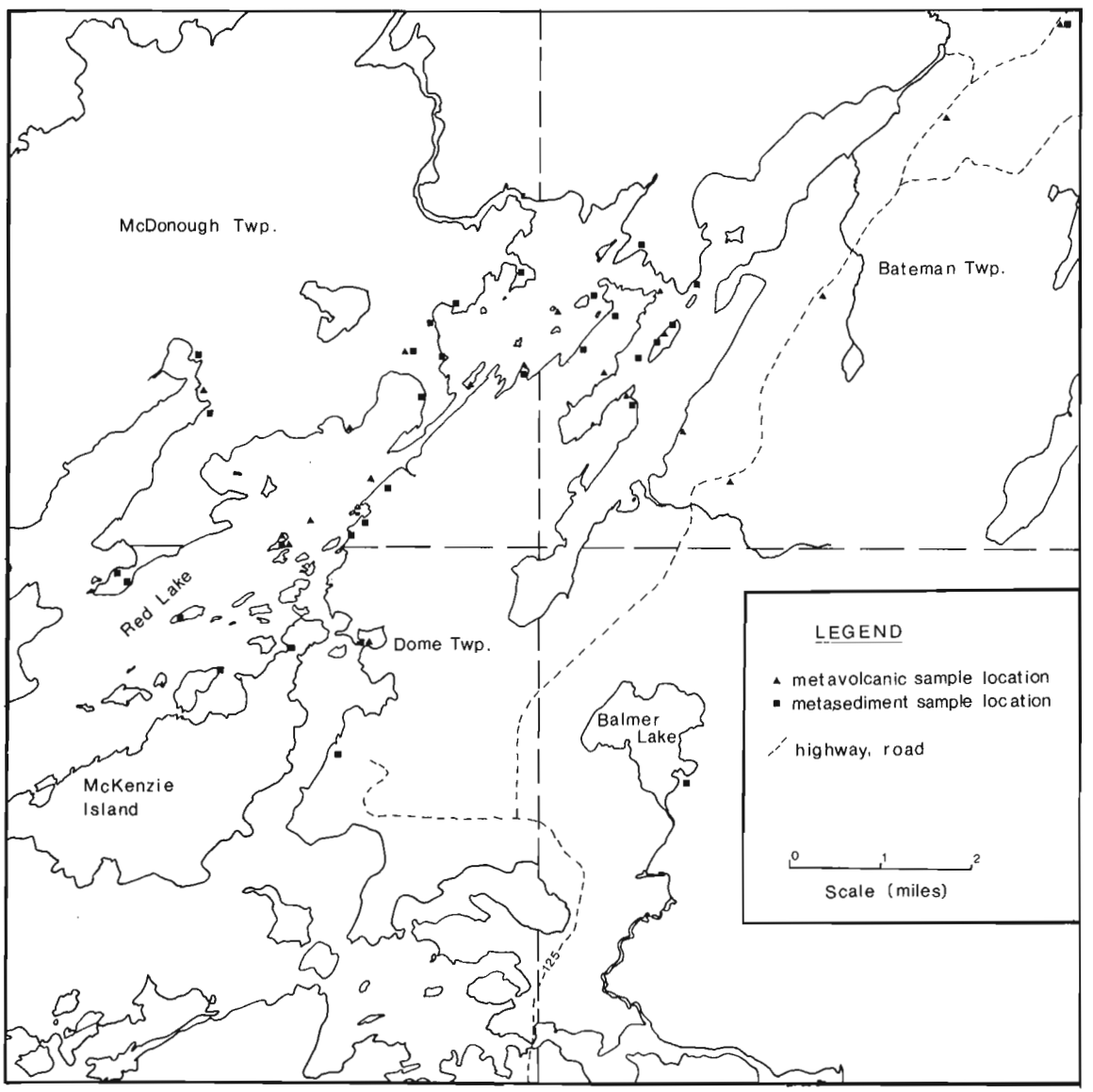

Figure 13.3 *Location map showing sampling sites.*

further subdivided, according to the major mineralogical host of the iron into the various types listed in Table 13.1. There is no implication, however, that these types of iron formation here represent different facies controlled by shoreline proximity as argued by James (1954) for iron formation of Superior type. In fact, our sampling is from a provenance dominated by volcanic rocks. We regard the iron formation to be of Algoman type (Gross, 1965).

(a) Oxide iron formation: The most common iron formation is oxide iron formation which consists of inter-banded magnetite-rich and quartz-rich layers. Acicular amphiboles are associated with the magnetite-rich layers, and in most samples iron and silica together constitute 90 per cent or more of the rock.

(b) Sulphide iron formation: Sulphide iron formation consists of interbanded sulphide-rich and quartz-rich layers. The main sulphides present are pyrite, chalcopyrite and pyrrhotite which usually occur as coarse grained, occasionally euhedral crystals. Fine grained arsenopyrite was observed in one sample.

(c) Silicate iron formation: A few silicate iron formations consisting of silicate-rich and quartz-rich bands were found. The main mineral constituents of the silicate bands are fine grained amphiboles, occasionally present as acicular radiating crystals. Chlorite commonly replaces the amphibole. Iron and silica are the principal chemical constituents of these rocks, as in oxide iron formations, but the proportion of alumina and magnesium is higher.

(d) Mixed silicate-oxide iron formation: In several specimens fine intermixing of light coloured silicate-rich and dark coloured oxide-rich bands occur.

(e) Mixed clastic and chemical interflow sediments: This group of rocks consists of interflow sediments that have both a chemical and a clastic component. They are finely banded and quartz-rich, with amphiboles and magnetite forming dark bands.

Metavolcanics

Ultramafic and mafic metavolcanic rocks dominate the volcanic suite, although a few andesites and felsic volcanic units are also present. The ultramafic rocks are pyroxenitic komatiites that in some cases contain spinifex texture. Komatiitic and tholeiitic basalts represent the main group of volcanic samples. Petrographic nomenclature follows the classifications of Jensen (1976) and Arndt et al. (1977). The Jensen system of nomenclature is shown on a $FeO + Fe_2O_3 + TiO_2 - Al_2O_3 - MgO$ plot (Fig. 13.4). This diagram breaks the rocks into groups according to the mafic chemical components. Figure 13.5 illustrates the grouping of the samples collected from the Red Lake area. In general the chemical compositions of the different volcanic rock types correspond very closely to representative compositions presented by Jensen (1976) and Arndt et al. (1977). One distinctive difference, however, is that some of the Red Lake basalts are characterized by a marked depletion (<1%) in Na_2O. This is also found in all metavolcanic rocks from the Dickenson mine.

Gold Content

The gold contents of the major rock types are summarized in Table 13.2. A range of 0.1 to 380 ppb gold is found for the entire volcanic-interflow sediment suite. In general, the gold distribution in a given rock group is characterized by a large range of values with a significant skewness toward high values. Consequently the arithmetic

Table 13.1

Principal features of interflow sediments

Rock Type	Chemistry		Mineralogy	Distinguishing Features
Chert	SiO_2	> 80%	quartz 80-100%	generally very fine grained
	Fe_2O_3	< 15%	iron staining between quartz crystals	polygonal boundaries of quartz
	Al_2O_3	< 2%	Accessory calcite chlorite and magnetite	conchoidal fracture
	MgO	< 2%		grey, massive
Oxide Iron formation	Fe_2O_3	15-40%	magnetite 20-50%	banded magnetite-quartz rock
	SiO_2	50-60%	quartz 50-75%	bands up to 4 cm thick
	Al_2O_3	0-8%	amphibole/chlorite 10-40%	fine grained
	MgO	0-2%		breaks readily along bands
	TiO_2	0-.7%		
Sulphide Iron formation	S	2.5%	pyrite, pyrrhotite 5-50%	coarse grained sulphides
	SiO_2	65-70%	quartz 40-75%	fine grained quartz
	Fe_2O_3	15-25%	grunerite 10-30%	friable when weathered
	Al_2O_3	1-5%		sulphide usually massive and no banding present
Silicate Iron formation	SiO_2	40-65%	amphibole/chlorite 40-60%	fine grained
	Fe_2O_3	20-45%	quartz 5-35%	grey-green/light grey banded
	Al_2O_3	0-9%	magnetite 0-30%	often acicular amphibole crystals
	MgO	0-5%		
	TiO_2	0.1-0.6%		
Mixed-Oxide Silicate Iron formation	variable		composite of oxide and silicate iron formations	bands of oxide and silicate iron formation intermixed
				bands vary from 1 mm to 10 mm thickness
				bands not always discrete

Table 13.2

Gold contents of rock types from the Red Lake area

Rock Type	No. of Samples	Range ppb	Arithmetic Mean ppb	Geometric (Logarithmic) Mean ppb	Median ppb	P_{10} ppb	P_{90} ppb
		Dickenson Mine, Levels 22 and 30					
Mainly interflow metasedimentary rocks	22	3.1 - 15 000	1040	33	16	4.3	6970
		Metavolcanic and Interflow Metasedimentary Rocks (McDonough, Bateman, Dome and Balmer Townships)					
Volcanics							
Pyroxene komatiites	5	0.1 - 1.3	5.3	2.5	4.6	-	-
Basaltic komatiites	7	0.5 - 15	4.1	2.1	1.7	0.5	4.8
High Mg tholeiites	3	6.2 - 279	98	26	6.2	-	-
High Fe tholeiites	8	4.3 - 380	61	15	21/4.8	4.3	44
Andesites	4	1.3 - 6.7	4.2	3.4	-	-	-
Amphibolite	1	7.0	-	-	-	-	-
All volcanic rocks	28	0.1 - 380	31	5.6	4.8	0.9	44
Interflow Sedimentary Rocks							
Chert	8	0.4 - 10	3.1	2.0	2.3	0.4	3.8
Iron formation							
-sulphide	3	5.0 - 14	10	9.2	10	-	-
-oxide	19	0.7 - 363	78	22	55	0.9	197
-silicate	5	1.3 - 6.0	8.8	13	10	-	-
-mixed oxide silicate iron formation	6	0.8 - 6.0	3.4	2.7	3.2	0.8	6.0
Chemical-detrital interflow sedimentary rock	9	0.8 - 43	8.3	4.1	3.7	0.8	7.9
All interflow sedimentary rocks	50	0.4 - 363	26	6.1	4.3	0.9	83

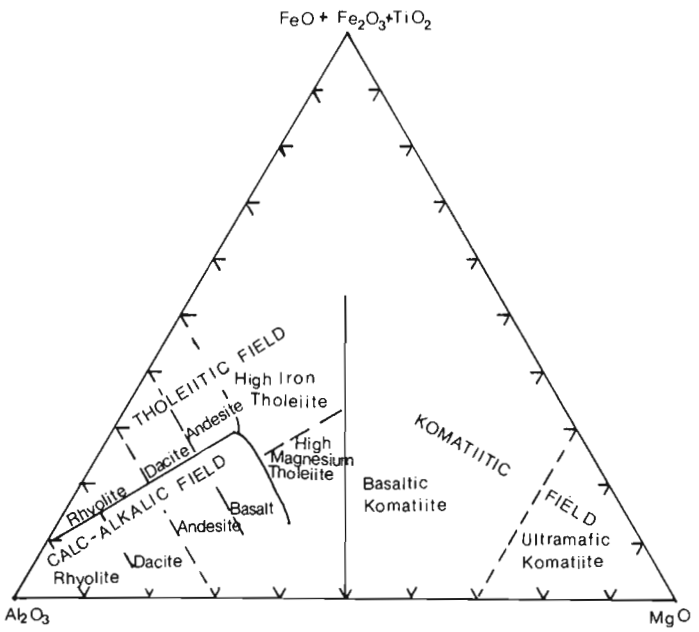

Figure 13.4. *Jensen Cation Plot.*

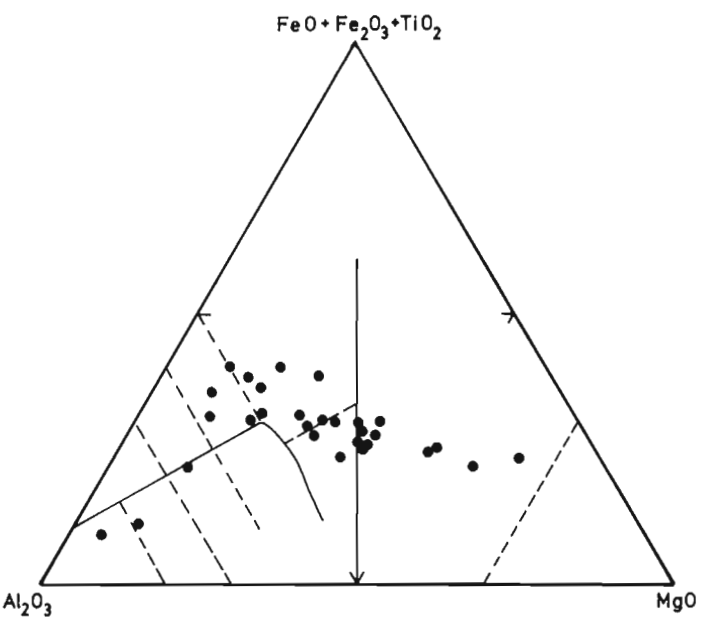

Figure 13.5. *Classification of volcanic rocks according to Jensen Cation Plot.*

mean is strongly influenced by a small proportion of the total samples, and other measures of central tendency including the geometric (logarithmic) mean and median are also listed in Table 13.2 to further indicate the nature of the gold distribution.

If the entire suite of interflow metasedimentary rocks and metavolcanic rocks is considered, there is considerable similarity of gold content between these two groups of rocks. Of the statistical parameters noted in Table 13.2, only the gold content representing the 90th percentile is significantly different, and it is much lower for the volcanic rocks. If the specific rock types belonging to either the sedimentary or volcanic group are compared, then significant differences in gold content become apparent. In particular, oxide iron formation is more auriferous than any other type of interflow sediment included in the study. As indicated in Table 13.2, the high average value for gold in the oxide iron formation, 78 ppb, is not due to a few samples that are anomalously rich in gold. The sulphide iron formation, which averages 10 ppb gold (arithmetic), is unexpectedly poorer in gold than oxide iron formation. However, there are only three samples in the sulphide iron formation suite, and this difference may not be statistically significant. The lack of sulphide iron formation samples reflects their paucity in the study area.

The volcanic suite, as previously noted, includes pyroxenitic komatiites, basaltic komatiites, high magnesium tholeiites, high iron tholeiites, and andesites. The tholeiites are apparently higher in gold than other types of volcanic rocks but little significance can be attached to the statistics for the magnesium tholeiites as the group includes only three samples. The iron-rich tholeiites, however, are significantly higher in gold than other volcanic rocks. All the statistical parameters for this class of basalt demonstrate their high gold content. Half the suite of eight samples contain more than 20 ppb of gold, a concentration well above the 3.5 ppb background estimated for the Red Lake basic-ultrabasic volcanic rocks or the 2 ppb background for gold in the Kakagi Lake volcanic pile suggested by the study of Kwong and Crocket (1978).

The best criteria to use in estimating background gold values are not obvious. However in view of the marked similarity of the two main groups of samples, the interflow sediments and volcanics, the gold content with the highest frequency of occurrence was considered the best estimate of background. This gives a background value of approximately 3.5 ppb, although this differs slightly for different rock types.

Conclusions

The volcanic and interflow sedimentary rocks are remarkably similar in average gold content and in the distribution of gold values within each of these classes of rocks. Because of the intimate spatial relationship between the two, it seems plausible that the interflow sedimentary rocks inherit their gold from the volcanic pile. The mechanisms involved are not obvious, but outgassing of volcanic fluids and vapours during a hiatus in lava extrusion and/or leaching of the pile by seawater could be viable mechanisms. The Na_2O depletion in some of the volcanic rocks, while not correlating directly with gold content, suggests leaching of the volcanic pile.

The significance attached to gold enrichment in oxide iron formation depends very much on processes postulated for deposition of the iron formation. We suggest that these rocks are essentially chemical sediments, noting that the very low alumina contents, usually less than 1.0 per cent Al_2O_3, require an extremely low input of clastic material. If iron oxides form directly in the marine environment it seems highly probable that gold is also derived directly from the same source, possibly by being scavenged or coprecipitated on an iron-bearing precipitate. It does appear that ferruginous chemical sediments deposited during hiatuses in volcanism are, in a geochemical sense, concentrators of gold.

Acknowledgments

We are grateful to Drs. J.M. Franklin and J. Pirie for much helpful discussion and for assistance in the field. Early availability of Dr. Pirie's preliminary field maps of the area are warmly acknowledged.

References

Arndt, N.T., Naldrett, A.J., and Pike, D.R.
1977: Komatiitic and iron-rich tholeiitic lavas of the Munro Township, northeastern Ontario; Journal of Petrology, v. 18, p. 319-369.

Ferguson, S.A.
1966: Geology of Dome Township; Ontario Department of Mines Report 45.

Gross, G.A.
1965: Geology of iron deposits in Canada, Vol. 1: General geology and evaluation of iron deposits; Geological Survey of Canada, Economic Geology Report No. 22.

James, H.L.
1954: Sedimentary facies of iron formation; Economic Geology, v. 49, p. 235-293.

Jensen, L.S.
1976: A new cation plot for classifying subalkalic volcanic rocks; Ontario Division of Mines, Miscellaneous Paper 66, 22 p.

Kwong, Y.T.J. and Crocket, J.H.
1978: Background and anomalous gold in rocks of an Archean greenstone assemblage, Kakagi Lake area, northwestern Ontario; Economic Geology, v. 73, no. 1, p. 50-63.

Pirie, J. and Grant, A.
1978a: Balmer Township area, District of Kenora (Patricia Portion); Ontario Geological Survey, Preliminary Map 1976a.

1978b: Bateman Township, District of Kenora (Patricia Portion); Ontario Geological Survey, Preliminary Map P1569.

Pirie, J. and Sawitzky, E.
1977: McDonough Township, District of Kenora (Patricia Portion); Ontario Geological Survey, Preliminary Map P1240.

14. METALLOGENY OF THE GOLD DEPOSITS IN THE DICKENSON MINE, RED LAKE, NORTHWESTERN ONTARIO – A PRELIMINARY REPORT

E.M.R. Research Agreement No. 177-4-79

R.T.M. Kusmirski[1] and J.H. Crocket[1]
Economic Geology Division

Kusmirski, R.T.M., and Crocket, J.H., Metallogeny of the gold deposits in the Dickenson Mine, Red Lake, northwestern Ontario – A Prelimianry Report; in Current Research, Part B, Geological Survey of Canada, Paper 80-1B, p. 135-144, 1980.

Abstract

The Dickenson mine, a gold producer in the Red Lake, Ontario, volcanic belt, consists of veins and conformable gold-enriched zones in Archean volcanic and sedimentary rocks. Studies of the 17, 25 and 30 levels in the mine reveal that most of the gold-bearing zones are in layered fragmental rocks. These have been derived from a biomodal source, with basaltic komatiites and high-iron tholeiite as dominant source rocks, and felsic volcanic and cherty sedimentary strata as less dominant source rock. The fragmental strata are characterized by high Mg, Ni and Cr contents, and high, but variable gold contents. Gold-enriched quartz-carbonate veins do not have adjacent gold haloes. In general, gold-enriched fragmental strata formed by syngenetic deposition along with sulphides and arsenides. Gold was further redistributed into gold-rich quartz-carbonate veins during deformation and metamorphism.

Introduction

The Dickenson Mine, in west central Balmer Township, is one of the two current gold producers in the Red Lake camp. Much of the Dickenson ore occurs in well defined quartz-carbonate veins which are both conformable and disconformable to volcanic stratigraphy. During the summer of 1978, samples were collected from three levels in the Dickenson Mine in crosscuts that are roughly perpendicular to the strike of the ore zone, and represent profiles traversing the stratigraphy above and below the ore. Some additional samples were provided by Dr. J.M. Franklin, of the Geological Survey of Canada. These samples were analyzed for major and minor elements (S, Ni, Rb, Sr, Y, Zr, Nb, Cr, Co, Pb, Zn, Cu, and As) by X-ray fluorescence, for gold by radiochemical neutron activation, and were examined in thin section and polished section. The principal objectives of the project are: a) to determine whether there is any systematic variation in gold or other elements about the mineralized zone, and b) to obtain a better understanding of the lithologies near the ore. The implications of the preliminary data presented here are considered briefly in terms of mechanisms for formation of the gold ores.

Previous Work

A review of the literature (Ferguson, 1962, 1965, 1966, 1968; Pirie, 1977, 1978) indicates that gold deposits in the Red Lake area occur in essentially five settings: a) generally discordant sets of quartz-carbonate veins with associated veinlets and stringers, in carbonatized mafic metavolcanic rocks which locally are pillowed and in places variolitic (Campbell Mine); b) quartz and quartz-carbonate veins and stringers which are commonly conformable with and enclosed by volcanic strata (Dickenson Mine); c) as narrow laminations within primary interflow sulphide sedimentary rocks and accompanying cherty material (Dickenson Mine); d) quartz filled fractures related to basic to intermediate intrusions (Mackenzie Mine, Howey Mine); e) massive to weakly banded "tuffs" which locally are garnetiferous (Madsen Mine).

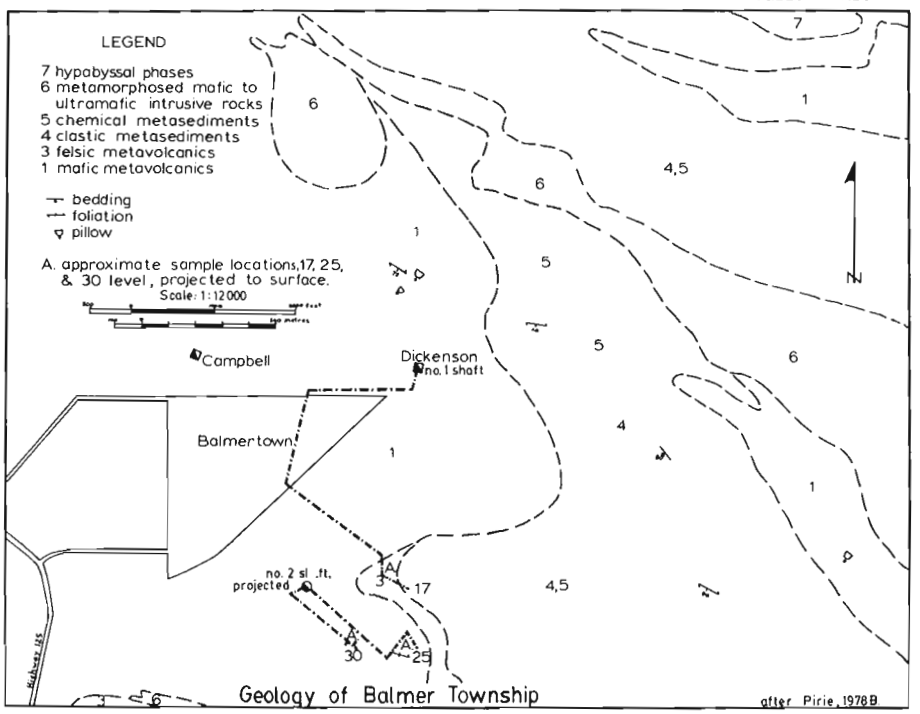

Figure 14.1

Geology of Balmer Township after Pirie and Grant 1978.

[1] Department of Geology, McMaster University, Hamilton, L8S 4M1

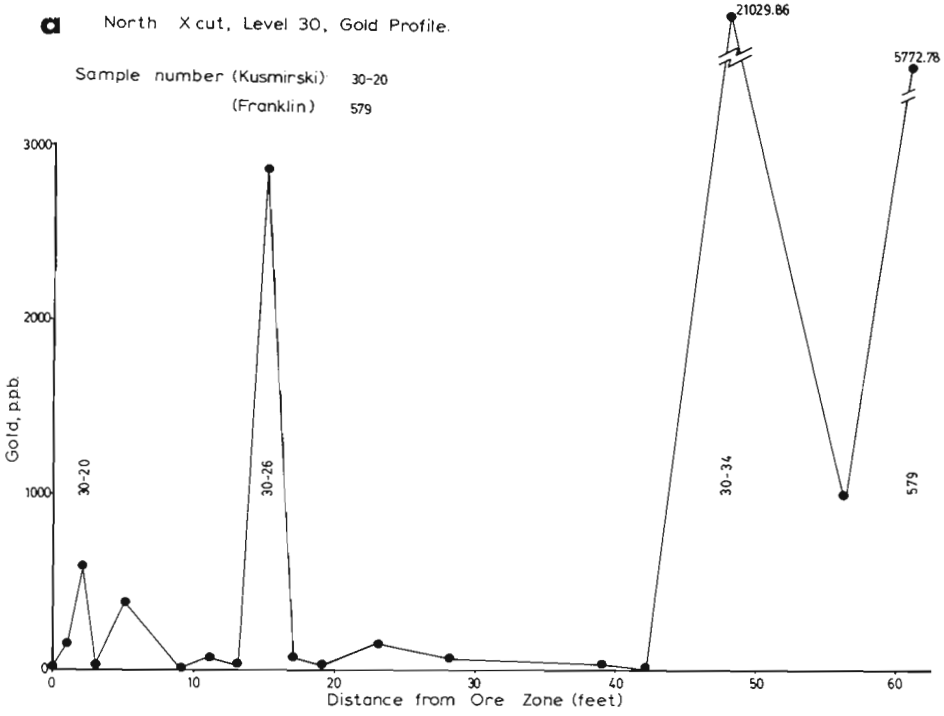

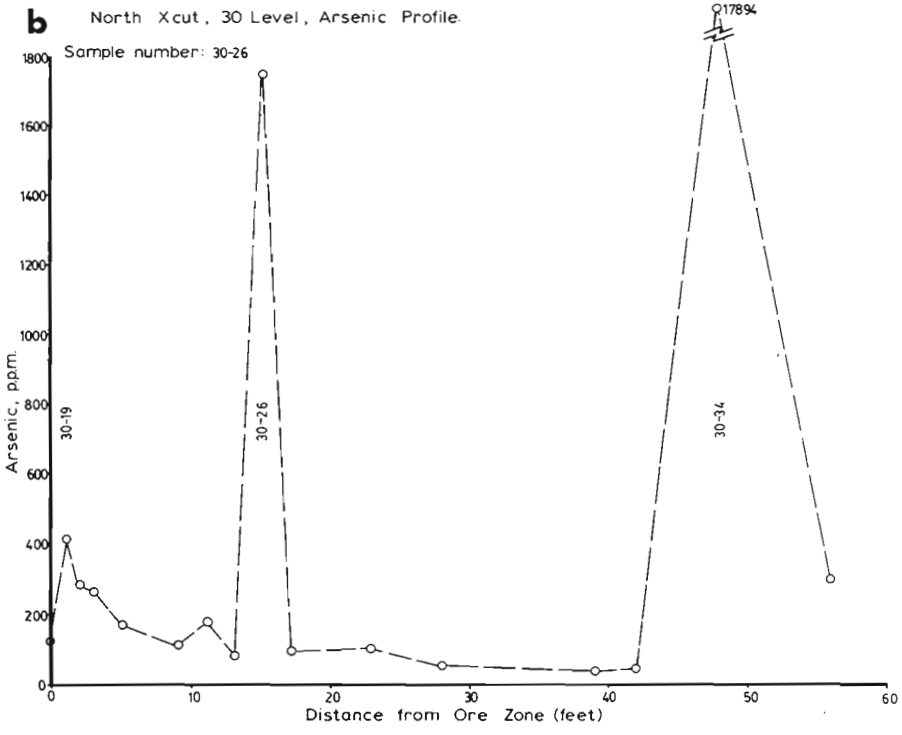

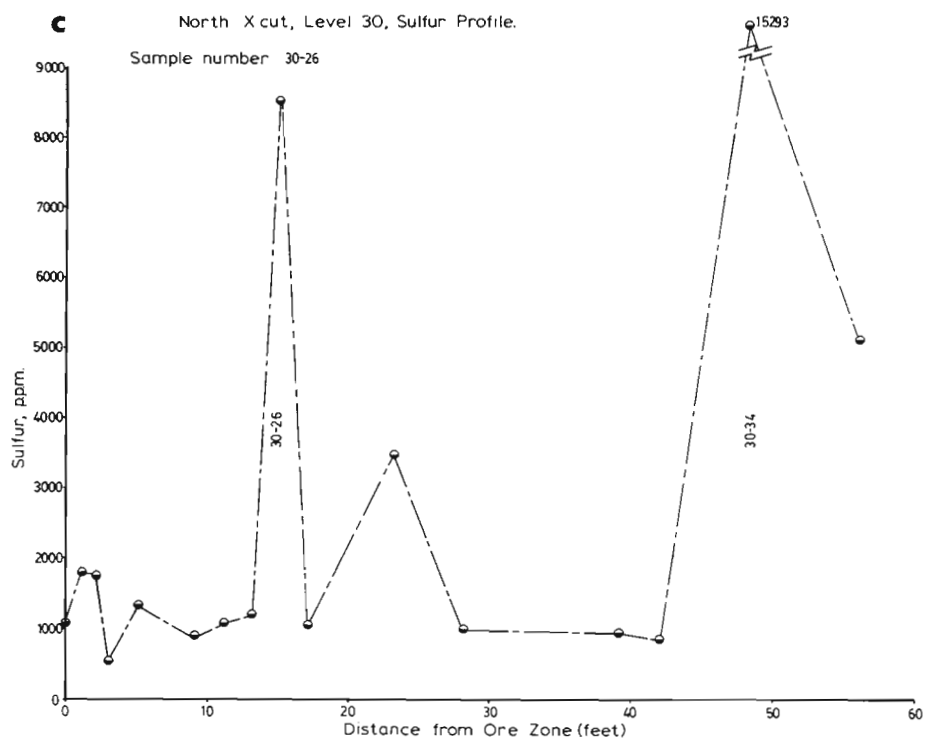

Figure 14.2a. *North crosscut, Level 30, Gold Profile.*

Figure 14.2b. *North crosscut, Level 30, Arsenic Profile.*

Figure 14.2c. *North crosscut, Level 30, Sulphur Profile.*

Part of the most recent geological map that includes the geology around Dickenson Mine (Pirie and Grant 1978), is reproduced as Figure 14.1 with deletion of the boundaries of individual outcrop area. The Dickenson No. 1 shaft and mine buildings sit on a unit of altered (silicified) pillowed mafic metavolcanic rocks. A second shaft sunk from the 22nd level is located approximately 900 m south-southwest of the No. 1 shaft. The contact between these pillowed flows and a thick sequence of clastic and chemical metasediment rocks (units 4 and 5), is approximately 400 m east of both shafts and provides a convenient datum. Bedding within the metasedimentary strata generally trends northwest with a steep southwesterly dip. Just south of the No. 2 shaft is a 500 m thick unit of felsic to intermediate, locally reworked, quartz and feldspar porphyritic pyroclastic rocks with minor felsic flows.

Results

Metal Profiles

Before discussing the lithologies and chemical trends on individual levels, some broad generalizations are presented. Profiles of gold, arsenic and sulphur about the ore zone on Levels 30 and 17 are shown in Figures 14.2, 14.3, and 14.4. All three elements are strongly correlated in a spatial sense, particularly for the 30 Level suite. Samples high in gold are also high in arsenic and sulphur. Spatial correlations on the 17 Level are not as strong, although both gold and sulphur are high in the same samples. There is no suggestion of a systematic gradient of values away from the ore zones. The 17 Level profile north of the ore zone (Fig. 14.4) shows significantly higher gold within 3.5 m of the ore than farther away, but the main feature of the profiles is irregular high gold values in a single or a few adjacent samples.

Lithologies

Samples from the 17 Level were obtained approximately 900 m south of the No. 1 shaft. Those from the 25 and 30 Levels were obtained from 400 to 500 m east to southeast of the No. 2 shaft. Thus, sampling is from the vicinity of the contact between the mafic metavolcanic flows and a major unit of chemical and clastic metasediment rocks. Textural observations of polished slabs and thin sections, together with chemical analyses, indicate that most samples are fragmental (Fig. 14.5 and 14.6). Rocks illustrated in Figures 14.5a, 14.6a, 14.6b and 14.6c consist of ovoid masses of fine grained polygonized quartz in a matrix of volcanic material. The fragmental character is particularly obvious in Figure 14.6a. The lack of any cataclastic texture argues against shearing of quartz vein material or a silicified flow as an origin for these rocks. Textural and compositional characteristics (discussed below) indicate that these rocks are derived from the erosion of a volcanic pile with minor input of pyroclastic material. Recent observations by J. Pirie (personal communication), indicate that some of these rocks may represent hyaloclastites and pillowed flows. Further field work will be necessary to delineate these units.

Specimens shown in Figures 14.5b and 14.5c are fine grained, laminated to thinly bedded rocks with occasional ovoid masses of quartz. They represent distinct units that commonly contain garnets which are largely confined to specific bands.

Chemistry

The compositional features of note in these rocks are the large variations in bulk composition, particularly Si, Mg, Al, Fe, and Ti over distances of 0.5 to 1 m, low alkali contents and high Ni and Cr (Fig. 14.7). Na_2O and K_2O are commonly less than 0.5 and 1.0 weight per cent and Ni and Cr, in addition to being highly variable in some samples, exceed 1000 to 2000 ppm respectively. These Ni and Cr contents suggest that a significant ultramafic to mafic volcanic component is present. As a guide to provenance the samples were plotted on the cation diagram of Jensen (1976), which places approximately 33 per cent of the suite in the basaltic to ultramafic komatiite field (Fig. 14.8). These samples also show a komatiitic character in a TiO_2 vs MgO plot (Fig. 14.9, Arndt et al., 1977). These features indicate that a significant component of the source area that was weathered to give these detrital rocks contained mafic to ultramafic rocks of a komatiitic kindred.

Tables 14.1 and 14.2 illustrate the range and averages in major and trace element values for some of the major lithologies recognized on Levels 30, 25 and 17.

30 Level

Rocks on this level can be subdivided into three distinct types.

Most samples exhibit a fragmental character (Fig. 14.5a) and lie in the magnesian tholeiite to basaltic komatiite field in Figure 14.8. As seen in thin section, individual ovoids of polygonized quartz with minor feldspar are enclosed in a matrix of anhedral quartz, amphibole, micaceous minerals, carbonates and finely disseminated opaques. These ovoids, which are commonly rimmed by opaque minerals, vary in size up to 1 cm and occur in various proportions throughout the strata. It is also common to find stratigraphic units with 1 to 5 mm angular to subangular quartz grains which have either been polygonized or fractured and are set in an aphanitic matrix. In thin section the dominant mafic mineral is a colorful fibrous actinolite. Minor slightly discordant carbonate ± quartz veins were also observed. SiO_2 in these rocks averages 56.5 weight per cent with a range of 45 to 60 weight per cent (Table 14.1). We suggest that these rocks are mainly proximal volcaniclastites composed largely of basaltic material; however, it is also possible that they represent chemically and tectonically altered pillowed flows.

Intercalated with these fragmental rocks are fine grained, laminated, metasedimentary rocks (Figure 14.5b) that contain actinolite, biotite, chlorite, garnet and quartz as essential minerals. Rare ovoids of recrystallized quartz are present. Garnets have incorporated numerous minute grains of opaque minerals. The opaque minerals include pyrite and pyrrhotite, and minor chalcopyrite, arsenopyrite and magnetite. The average composition together with the compositional range of these rocks is presented in Table 14.1. The metamorphic grade implied by the mineral assemblage is probably lower amphibolite facies. A more specific statement cannot be made as the garnet composition is unknown. If they are spessartine-rich, then upper greenschist facies is implied (Winkler, 1976). This is still higher than the regional grade which is lower greenschist (J. Pirie, personal communication). The most significant compositional aspect of these sediments is that they contain very high gold values, up to 21 ppm.

Two finely laminated cherty horizons with nearly 80 weight per cent SiO_2 and 15 to 20 weight per cent Al_2O_3 also occur on this mine level. High chromium (621 to 1412 ppm) and TiO_2 (1.07 to 1.27 wt. %) values indicate a significant detrital input in these rocks.

Two crosscuts were sampled on the 30 Level. Data from the south crosscut are incomplete; profiles from the north crosscut (Fig. 14.2a, b, c) show an extremely good spatial correlation between Au, As and S. There is no correlation between Au and any other major ore trace element, nor is there any systematic variation in the concentration of Au, As and S with distance from the ore zone. This may indicate a stratabound control for these metals, as their values are highest in the sediments on this level.

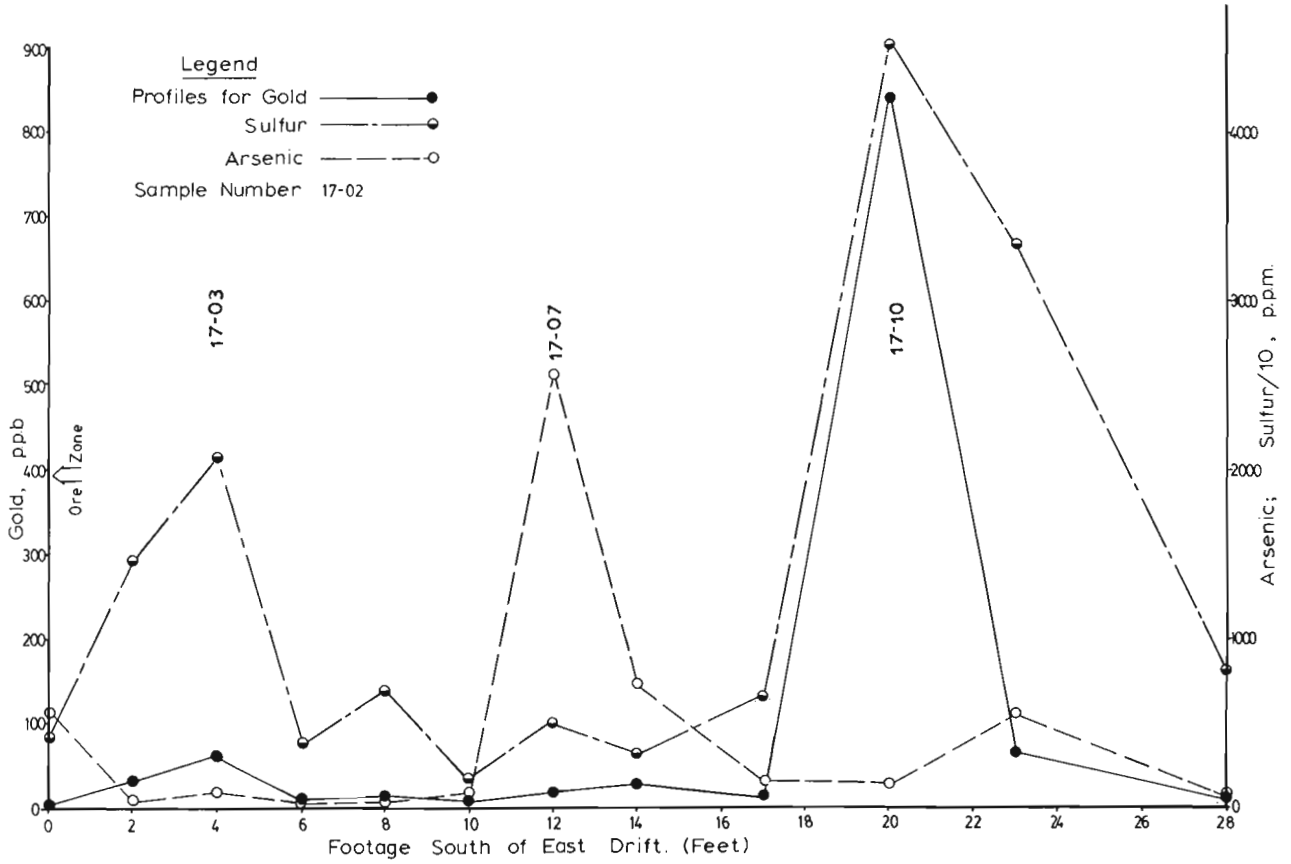

Figure 14.3. *Profiles, South of East Drift, Level 17, Dickenson Mine.*

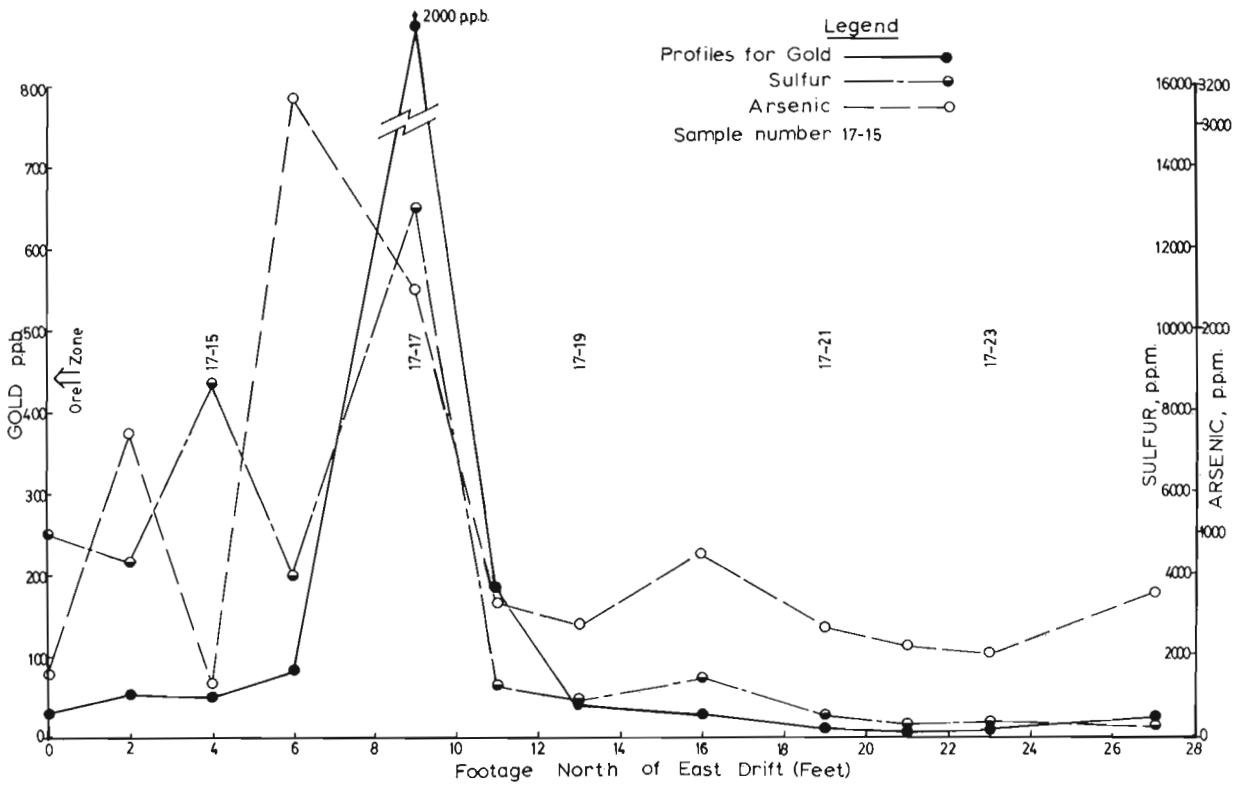

Figure 14.4. *Profiles, North of East Drift, Level 17, Dickenson Mine.*

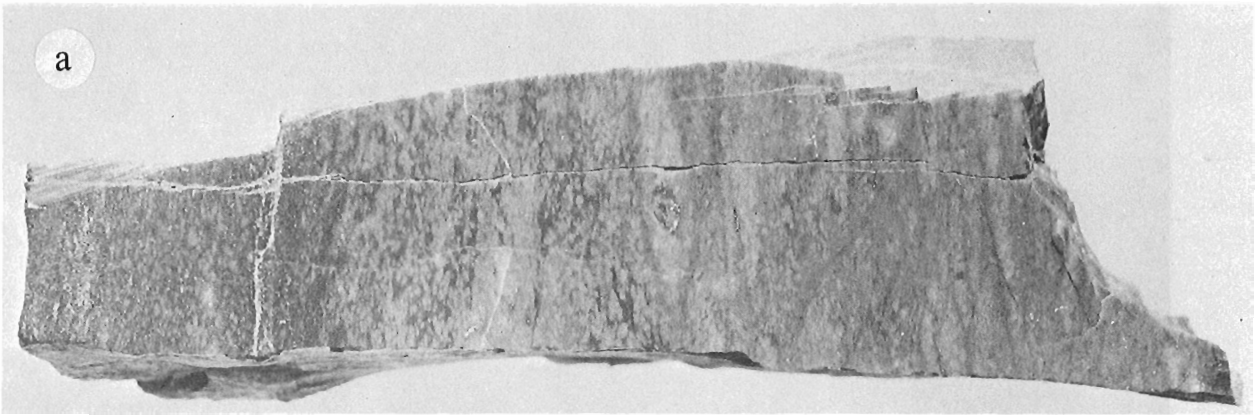

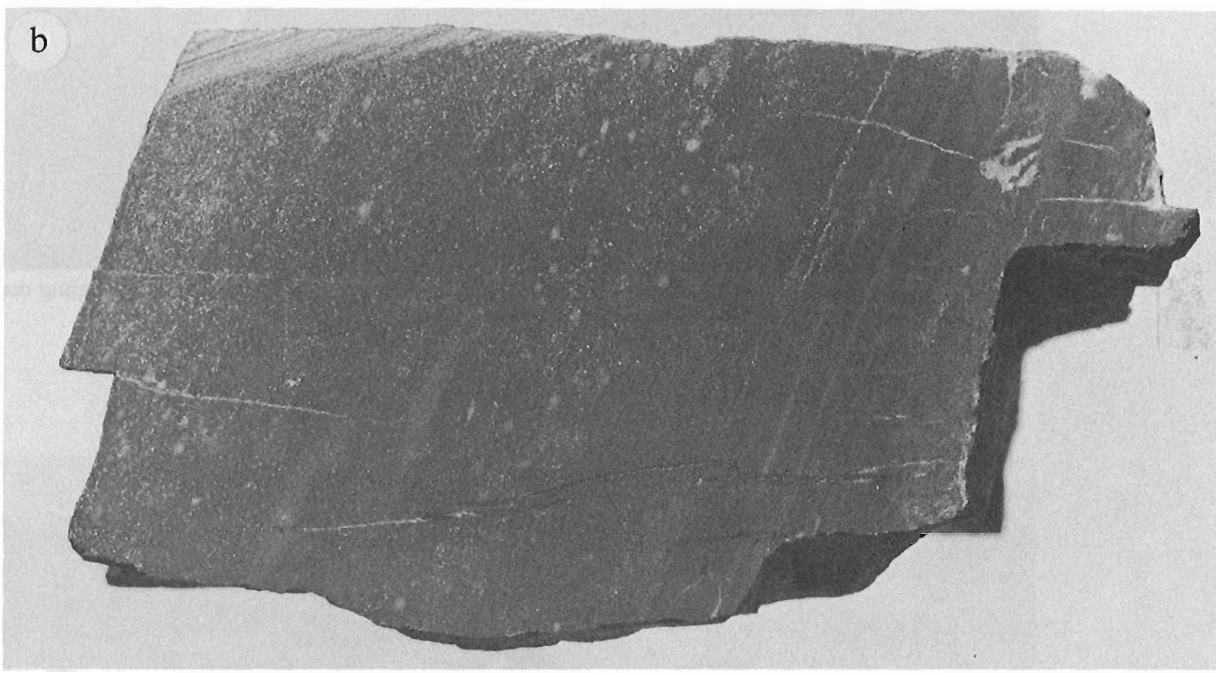

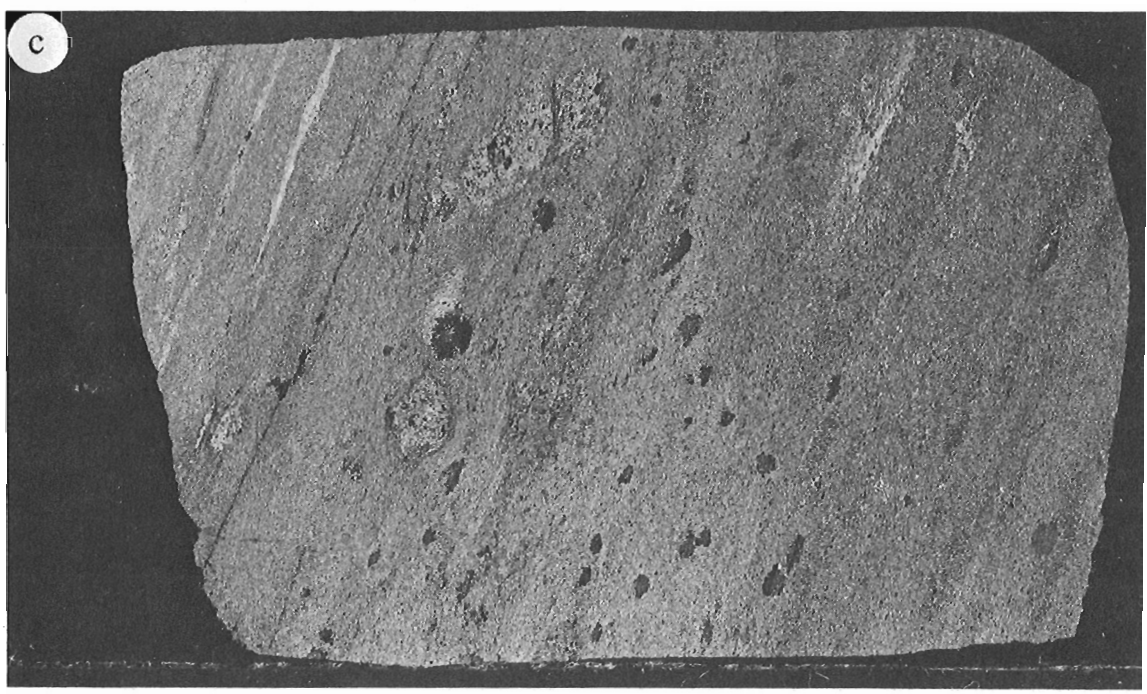

Figure 14.5a

Quartz-rich fragmental rock (sample 30-47, length 9 cm).

Figure 14.5b

Finely laminated garnetiferous sedimentary rock. Garnets are light coloured, coarse grained, subrounded. Sample 30-38, length 5.5 cm.

Figure 14.5c

Finely laminated garnetiferous sedimentary rock. Garnets are black clots. Note polygonized quartz ovoids. Sample 30-38, magnification is 4X, crossed nicols.

Figure 14.6a. *Photomicrograph of a fragmental rock. Note two possible bedding contacts. Sample 17-19, magnification is 4X, crossed nicols.*

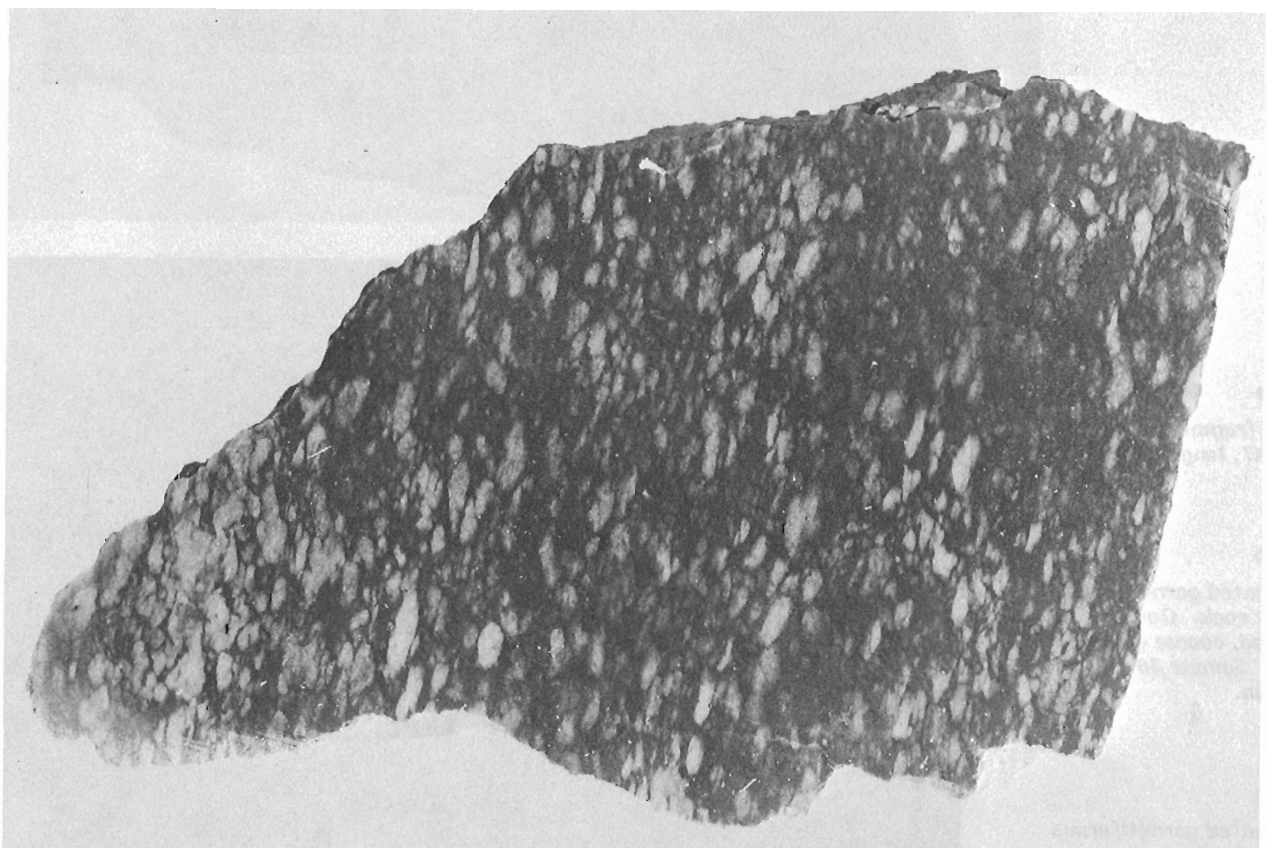

Figure 14.6b. *Quartzofeldspathic fragmental rock. Sample 17-24, length 6.5 cm.*

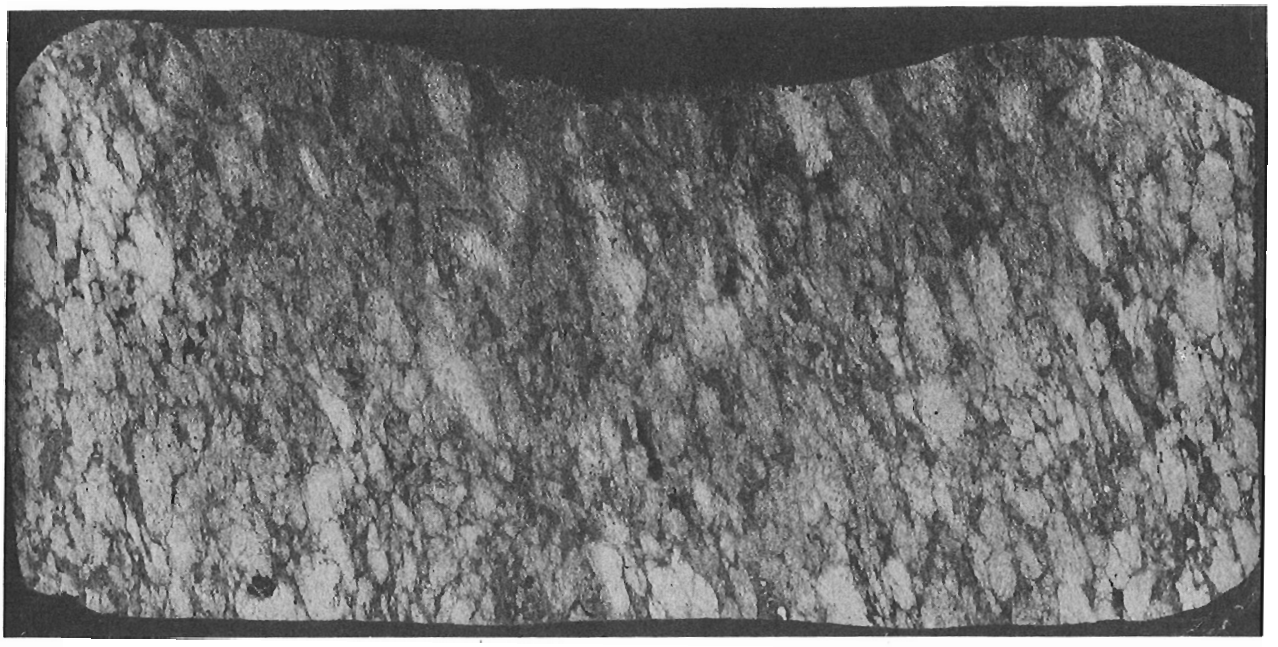

Figure 14.6c. *Photomicrograph of quartzofeldspathic fragmental rock. Black interstitial material is sulphide. Sample 17-24, magnification is 4X, crossed nicols.*

Table 14.1

Variations in major and trace elements for main lithologic units on Levels 30 and 25

	1		2		3	4	
			In Weight Per cent				
SiO_2	45.28-59.70	(56.62)	49.35-69.68	(58.85)	76.11-79.39	57.63-72.55	(64.14)
Al_2O_3	9.64-13.84	(11.94)	6.64-14.66	(11.47)	15.58-19.26	10.84-13.15	(12.17)
Fe_2O_3	7.57-12.77	(10.32)	8.89-17.21	(12.00)	1.96- 4.10	11.06-22.78	(17.54)
MgO	7.56- 9.58	(8.64)	4.04- 9.11	(7.27)	0.85- 1.10	1.95- 7.22	(4.45)
CaO	8.21-16.67	(12.90)	3.70-12.47	(8.85)	0.62- 0.97	0.43- 1.11	(0.69)
Na_2O	<0.20		<0.20		<0.20	<0.20	
K_2O	0.21- 2.70	(1.01)	0.08- 2.28	(0.95)	0.18- 0.22	0.94- 1.80	(1.40)
TiO_2	0.76- 1.04	(0.86)	0.43- 1.06	0.81)	1.07- 1.27	1.07- 1.29	(1.19)
MnO	0.12- 0.34	(0.24)	0.16- 0.35	(0.25)	0.04- 0.27	0.25- 0.67	(0.44)
P_2O_5	0.01- 0.05	(0.02)	N.D.- 0.20	(0.01)	0.02- 0.03	0.02- 0.04	(1.03)
CO_2	1.42-11.82	(5.93)	0.67- 8.56	(3.55)	0.38- 0.78	0.36- 2.40	(1.17)
			In ppm				
S	568-1984	(1271)	825-15 293	(3922)	404-819	962-13 516	(6525)
As	52-414	(133)	30-17 894	(2080)	96-245	295-3610	(1960)
Ni	72-200	(97)	50-272	(123)	57-82	98-345	(185)
Rb	2-67	(19)	<20- 60	(21)	9	9-34	(21)
Sr	89-169	(129)	67-142	(97)	37-49	41-101	(64)
Zr	7-97	(29)	49-74	(65)	71-86	56-104	(70)
Cr	225-717	(384)	129-763	(510)	621-1412	298-585	(433)
Co	20-44	(33)	11-62	(44)	15	39-109	(77)
Pb	10-15	(12)	0-15	(9)	0	<15	
Cu	89-135	(117)	36-148	(114)	112-170	133-241	(153)
Zn	50-257	(83)	44-1296	(160)	27-35	73-642	(265)
			In ppb				
Au	11.6 -881	(144)	8.5 -21 030	(1500)	15.0 -19.0	5.1 -8170	(1411)

1. Range in chemical composition of 17 fragmental rocks, 30 Level.
2. Range in chemical composition of 16 sedimentary rocks, 30 Level.
3. Range in chemical composition of 2 cherty horizons, 30 Level.
4. Range in chemcial composition of 10 sedimentary rocks, 25 Level.

Values in parentheses are average compositions.

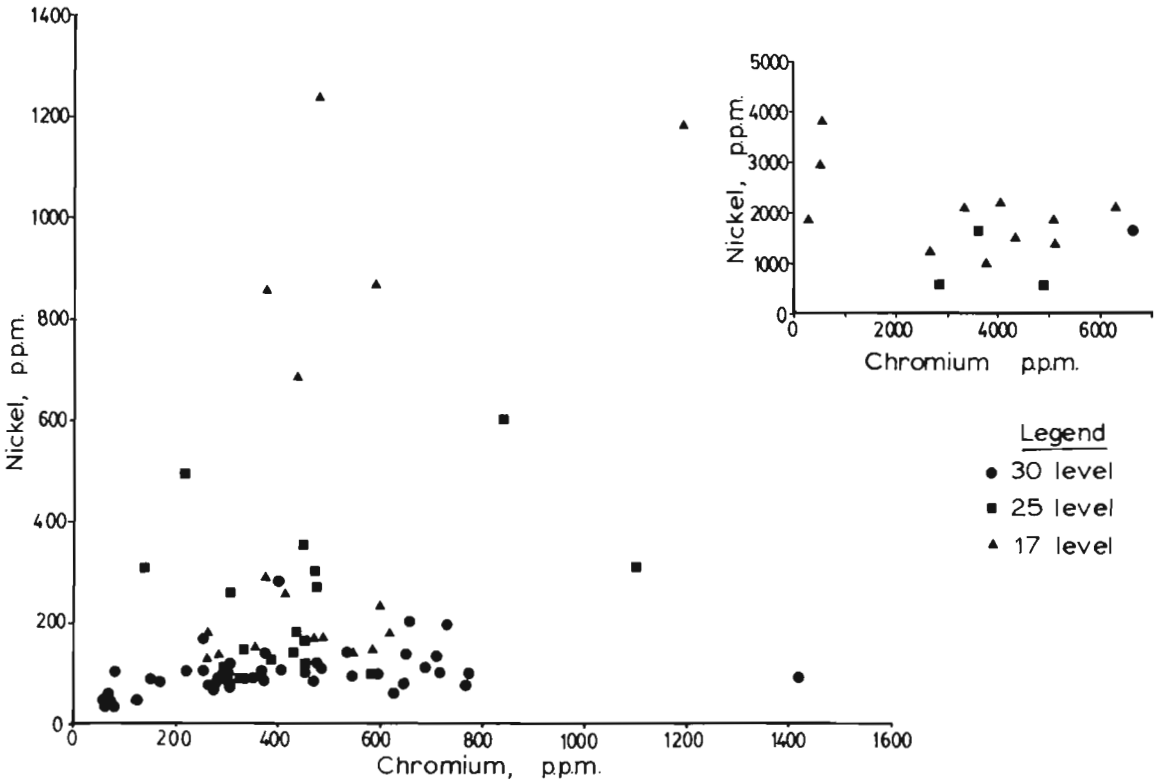

Figure 14.7. *Chromium vs Nickel; 17, 25 and 30 Levels, Dickenson Mine.*

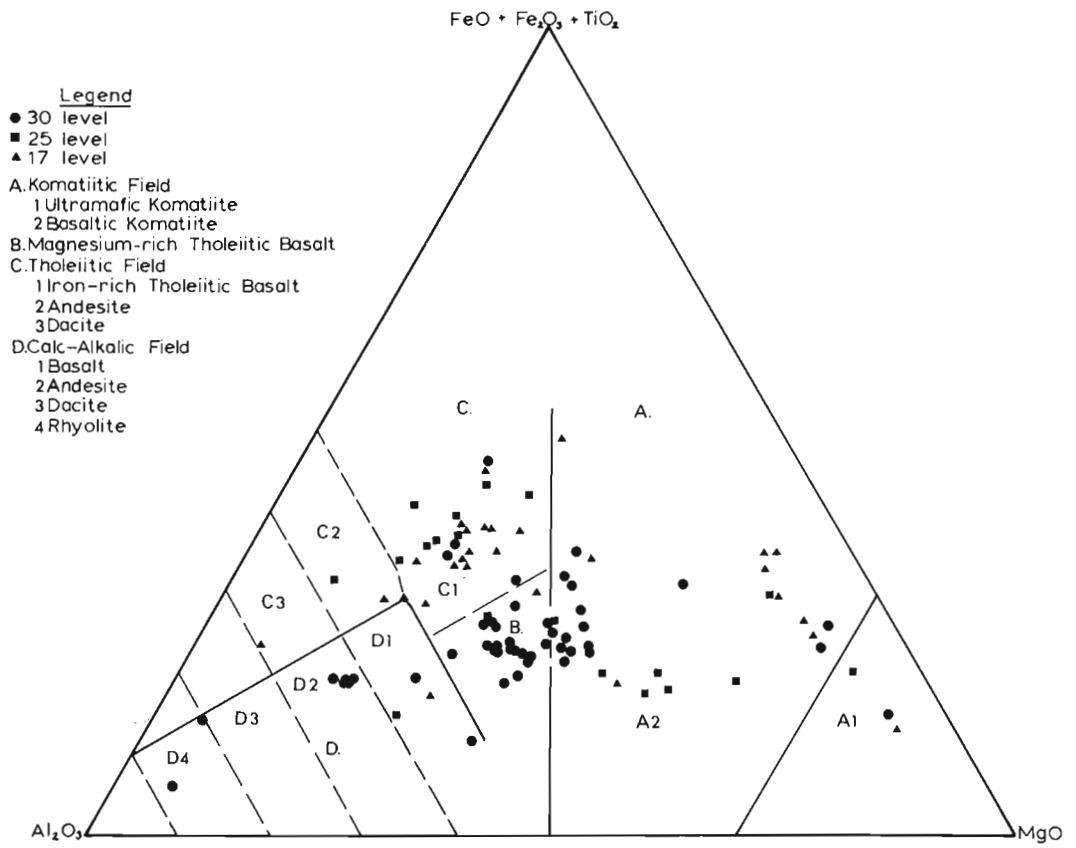

Figure 14.8. *Jensen Cation Plot.*

Table 14.2

Variations in major and trace elements for main lithologic units on Level 17

	1		2		3
	In Weight Per cent				
SiO_2	52.83-76.42	(66.09)	32.66-62.73	(42.71)	77.45
Al_2O_3	8.23-15.79	(11.70)	2.69- 7.38	(4.46)	14.05
Fe_2O_3	9.93-25.98	(16.09)	5.93-21.71	(16.01)	7.41
MgO	3.51-11.50	(5.54)	8.22-26.12	(17.09)	1.00
CaO	0.29- 2.90	(0.74)	3.74-26.96	(12.73)	0.39
Na_2O	<0.20		<0.20		0.10
K_2O	0.00- 1.67	(0.55)	0.13- 1.23	(0.42)	0.35
TiO_2	0.27- 1.02	(0.75)	0.17- 0.58	(0.32)	0.96
MnO	0.21- 0.64	(0.33)	0.28- 1.13	(0.61)	0.09
P_2O_5	N.D.- 0.03	(0.02)	N.D.		N.D.
CO_2	0.77-11.39	(3.07)	8.45-27.30	(19.74)	1.62
	In ppm				
S	8.62-45 600	(10 887)	247-2078	(662)	8161
As	78-2627	(760)	268-889	(497)	6110
Ni	133-2858	(770)	900-2100	(1590)	854
Rb	<35		N.D.-54	(15)	N.D.
Sr	16-119	(42)	47-78	(54)	30
Zr	13-69	(52)	28-48	(37)	70
Cr	264-681	(463)	3300-6300	(4636)	585
Co	47-471	(162)	45-151	(102)	38
Pb	<20		<15		N.D.
Cu	34-250	(130)	21-80	(38)	103
Zn	16-1157	(270)	48-254	(135)	44
	In ppb				
Au	5.6 -2140	(204)	10.0 -43.0	(19.1)	4525

1. Range in chemical composition of 17 fine grained fragmental rocks.
2. Range in chemical composition of 6 basaltic komatiitic volcaniclastic rocks.
3. Chemical composition of sample from East Drift ore zone.

Values in parentheses are average compositions.

25 Level

Several samples were obtained from an ore zone (East South C) on this level which is distinctive in that the gold is not localized in quartz-carbonate veins or stringers. The samples are mainly fine grained laminated garnet-bearing rocks with bands of disseminated sulphide. Much of the sulphide is very fine grained pyrite, pyrrhotite and chalcopyrite. Magnetite is also present. These rocks, many of which are highly auriferous, are considered by us to be sedimentary.

The chemical composition of this group, whose mineralogy is similar to that just noted for the fine grained sedimentary rocks on the 30 Level, is presented in Table 14.1. It suggests that if these rocks are mainly detrital, the source region contained both felsic and mafic rocks. The average SiO_2 content, 64 weight per cent, suggests the occurrence of felsic metavolcanic or cherty metasedimentary rocks in the source region. Other compositional properties, particularly the FeO, TiO_2 and average chromium contents suggest that mafic volcanic rocks may also have contributed to these sediments. In particular, the iron and titanium contents are typical of iron-rich tholeiites. Thus, a bimodal source is suggested. A source region dominated by silicified iron tholeiite is unlikely, because such alteration would result in loss of iron, titanium, magnesium and manganese (Gibson, 1979).

The gold contents of these sediments are relatively high in that six samples contain more than 100 ppb gold and three of these contain 1 to 8 ppm gold. The auriferous rocks are high in arsenic (900 to 3600 ppm) and sulphur (2000 to 13 500 ppm), and are higher in total iron (up to 23 wt. %), manganese, nickel, cobalt, copper, and zinc than gold-poor rocks.

A second lithology sampled on the 25 Level is approximately 2 m thick and consists of four discrete, mutually conformable units, which in mine terminology are known as "chicken feed". The term was first used by Chisholm (1951) to denote a felsic fragmental rock which he classified as a rhyolite tuff, and which graded into an agglomeratic unit. This tuff was observed underground at the New Dickenson Mine where it provided an excellent marker horizon, separating mafic volcanics from Timiskaming-type sedimentary strata. The term has since been used to denote altered and carbonatized felsic to intermediate metavolcanic rocks (reported in Pirie, 1977).

Three of the "chicken feed" units lie in the komatiitic field in Figures 14.8 and 14.9. They are heavily carbonated and characterized by high contents of MgO (19 to 24 wt. %), chromium (2800 to 4845 ppm), and nickel (500 to 1600 ppm) with low SiO_2 content (19 to 28 wt. %). These clearly ultramafic compositions contrast with that of the fourth, a finely laminated rock with 68 weight per cent SiO_2, 6 weight per cent MgO, 1.34 weight per cent TiO_2, and 6569 ppm chromium.

The hypotheses for the derivation of these units are suggested. They may be in situ carbonated ultramafic flows capped by a siliceous interflow sediment. Alternatively, they may be of volcaniclastic origin, with a source material of mainly ultramafic composition. Evidence supporting the latter interpretation is the well bedded nature of the units and the presence of discrete bands of disseminated opaque minerals, fine grained carbonate laminations which may be primary, and ovoids (clasts ?) of polygonized quartz.

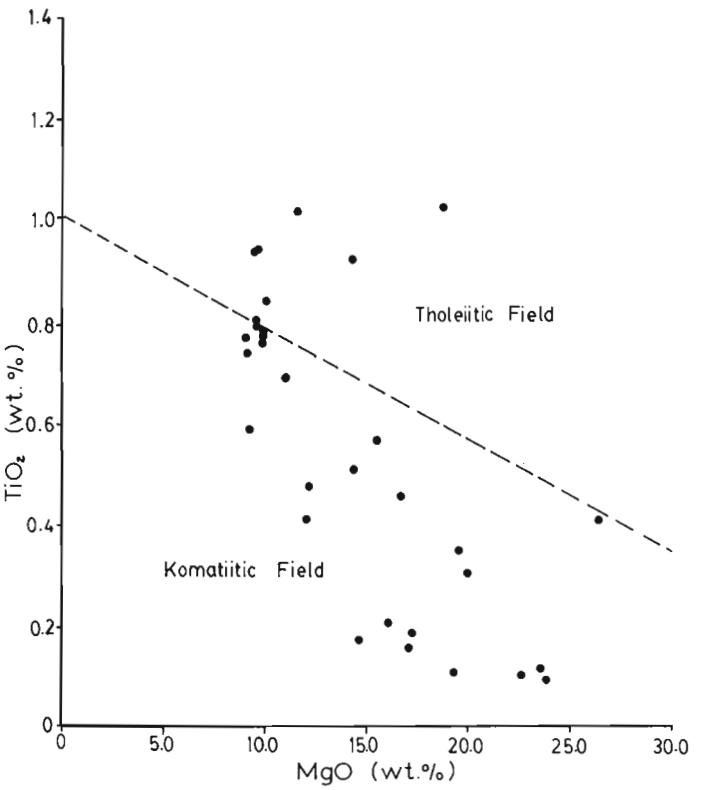

Figure 14.9. *TiO_2 vs MgO.*

17 Level

The 17 Level rocks can be divided into two major distinct groups on the basis of their texture and composition. Their chemical bariations are presented in Table 14.2.

The majority of the samples on the 17 Level are fine grained, siliceous fragmental rocks, commonly garnetiferous and rarely finely laminated. They plot in the iron tholeiite field of Jensen (Figure 14.8). Carbonate alteration is generally not as extensive as on the deeper levels and only occurs in two samples which have also undergone a second episode of sulphide emplacement associated with crosscutting veinlets. These samples were collected south of the East Drift in crosscut 17-1582 SXC, and those in the first 3.5 m north of the East Drift.

There is a spatial correlation between Au and S, but no relationship with As is evident (Figs. 14.3 and 14.4).

Coarse fragmental rocks that plot in the basaltic komatiite field (Fig. 14.8) were obtained north of the East Drift on the 17 Level, and are characterized by high Ni (900 to 2100 ppm), Cr (3300 to 6300 ppm), MgO (8.22 to 26.2 wt. %) and CO_2 (8.45 to 27.30 wt. %) values. Their fragmental nature is illustrated in Figures 14.6a, b, c. The layering in Figure 14.6a appears to be primary. These are probably proximal volcaniclastic rocks of basaltic komatiite composition, or they may be in part tectonized basaltic komatiite flows.

A third minor unit separates the coarse and fine fragmental rocks, and is a fine grained, laminated, highly aluminous (24 wt. %) rock, with low SiO_2 (37 wt. %) and CO_2 (<1.00 wt. %) and high Ni (1170 ppm) and cr (1180 ppm).

The chemical analysis for a sample from the East Drift ore zone is also presented in Table 14.2.

Sulphides on this level are disseminated throughout the matrix and also occur in crosscutting veinlets. Pyrrhotite is the dominant opaque mineral accompanied by minor chalcopyrite and pyrite and accessory magnetite and sphalerite. Gold occurs as discrete grains associated with the sulphides but was rarely observed.

Discussion

Most of the auriferous rocks included in this study of the 17, 25 and 30 Levels at Dickenson mine are layered on a scale of millimetres to a few centimetres. They exhibit a slight range in chemical composition and our preliminary assessment is that they are of sedimentary origin. The non-auriferous rocks exhibit a wide range of chemical composition and are dominantly volcaniclastites although pillowed flows and komatiites may also be present. We suggest that the volcaniclastites were produced by erosion, during periods of quiescence, with a volcanic provenance containing high-iron tholeiitic to basaltic komatiitic rocks with some quartz-rich volcanic rocks or siliceous sedimentary members. Some chemical exhalative activity is also envisaged.

High gold contents may be accompanied by high sulphur and high arsenic values. There are no smooth gradients of gold away from the quartz-carbonate ore zones. High gold, arsenic and sulphur contents are erratically distributed about the vein ore. These localized auriferous zones are commonly in fine grained, laminated, locally garnetiferous rocks, and where present in economically significant quantities, are mined (25 Level). The gold ore seems to be associated with the very fine grained banded sulphides. We suggest that this gold is probably syngenetic and that in a permeable volcano-sedimentary sequence the redistribution of such gold (on a local scale) by geothermal fluids may be one mechanism by which the epigenetic quartz-carbonate vein ore is formed. Further remobilization of gold during subsequent deformation and metamorphism is probable.

Acknowledgments

The project acknowledges the financial support of the Geological Survey of Canada. The authors wish to thank Dr. Jim Franklin (Geological Survey of Canada) and Dr. Jim Pirie (Ontario Geological Survey) for numerous useful discussions. Mr. Wayne Valliant (previous mine geologist) assisted in the preliminary familiarization with the mine, and we are especially grateful to Mr. Valliant and the Dickenson Mines Limited management for their co-operation.

References

Arndt, N.T., Naldrett, J.J., and Pyke, D.R.
1977: Komatiitic and iron-rich tholeiitic lavas of Munro Township, northeast Ontario; Journal of Petrology, v. 18, no. 2, p. 319-369.

Chisholm, E.O.
1951: Geology of Balmer Township; Ontario Department of Mines, vol. 60, part 10, p. 1-62.

Ferguson, S.A.
1962: Geology of the south half of Bateman Township, District of Kenora; Ontario Department of Mines, Geological Report no. 6, 31 p.

1965: Geology of the Eastern part of Baird Township; Ontario Department of Mines, Geological Report no. 39, 47 p.

1966: Geology of Dome Township, District of Kenora; Ontario Department of Mines, Geological Report no. 45, 98 p.

1968: Geology of the northern part of Heyson Township, District of Kenora; Ontario Department of Mines, Geological Report no. 56, 54 p.

Gibson, H.L.
1979: Silicification in a detailed section of Amulet rhyolite, Noranda; P.Q.; Geological Association of Canada, Program with Abstracts, v. 4, p. 53.

Jensen, L.S.
1976: A new cation plot for classifying subalkalic volcanic rocks; Ontario Division of Mines, Miscellaneous Paper 66, 22 p.

Pirie, J.
1977: Bateman-Balmer Townships area, District of Kenora, Patricia portion; in Summary of Field Work, 1977, Ontario Geological Survey, Miscellaneous Paper 75, p. 12-17.

1978: Byshe, Ranger, and Willans Townships Area, District of Kenora, Patricia portion; in Summary of Field Work, 1978, Ontario Geological Survey Miscellaneous Paper 82, 235 p.

Pirie, J. and Grant, A.
1978: Balmer Township. District of Kenora (Patricia Portion); Ontario Geological Survey, Preliminary Map P. 1976-A, Geological Series, scale 1:12 000 or 1 inch to 1000 feet.

Winkler, H.J.F.
1976: Petrogenesis of Metamorphic Rocks; 4th edition, Springer-Verlag, New York, 334 p.

15.

THE URANIUM CONTENT OF THE EXSHAW FORMATION AND BELLOY GROUP IN ALBERTA

Research Contract OST78-00090

F.A. Campbell[1]
Economic Geology Division

Campbell, F.A., The uranium content of the Exshaw Formation and Belloy Group in Alberta; in Current Research, Part B, Geological Survey of Canada, Paper 80-1B, p. 145-148, 1980.

Abstract

Cores from 22 wells of the Exshaw Formation and 3 from the Belloy Group were sampled and analyzed for uranium, nickel, and zinc.

The mean and standard deviation for 155 samples from the Exshaw Formation is 10 ± 2 ppm uranium. Uranium, nickel, and zinc are concentrated at the base of the formation, have a sympathetic relationship, and decrease upward. Cores channel-sampled over two foot lengths average up to 31 ppm uranium over a thickness of 5 feet with individual 2 foot sections up to 37 ppm uranium. Sampling at 0.5 foot (0.15 m) lengths yields similar average results with individual values ranging as high as 57 ppm.

Nineteen samples from Belloy Group cores yield an average of 8.3 ± 7 ppm uranium with a range from 0 to 33 ppm. The Belloy Group of the Alberta basin does not appear sufficiently phosphatic to concentrate uranium.

Introduction

Black shale and phosphatic sedimentary units have long been recognized for their anomalously high concentrations of uranium (Bell, 1978). Two units in Alberta, the Exshaw Formation and the Belloy Group have some characteristics similar to the Chattanooga and Phosphoria in the United States which are noted for relatively high concentrations of uranium (Bates and Strahl, 1958; Swanson, 1960). The study most relevant to the uranium content of the Exshaw Formation is that of Harvard (1967) who reported an average of 6 ppm from 164 samples and 20 ppm for 32 black shale samples.

Method of Study

The study involved sampling 22 wells that cored portions of the Exshaw Formation and 3 wells with core from Belloy Group. The wells involved in the study and the intervals sampled are shown in Table 15.1.

The cores were channel sampled initially in two foot intervals using a diamond wheel grinder. Detailed sampling was then repeated in 6 inch intervals to validate sections with relatively high uranium values and to provide further information respecting uranium distribution. In addition to uranium the samples were analyzed for nickel, zinc, copper, rubidium, strontium, and potassium. Only the uranium, nickel, and zinc results will be discussed in this report.

Powders of the samples were pressed at 30 000 p.s.i. with rims and backing of cellulose powder. The anlayses were carried out by X-ray fluorescence using a Phillips Norelco unit with a molybdenum tube, a LiF 220 crystal, and a scintillation counter. The elements were determined by the method described by Reynolds (1963) which enables the matrix correction to be based on Compton scattering.

Table 15.1

Sample locations

Well	Interval (feet)	Unit	Well	Interval (feet)	Unit
7-30-31- 3W4	2831-2835	Exshaw	10- 1-20- 1W5	9472-9480	Exshaw
11- 3-30- 3W4	2881-2885	Exshaw	1-34-56- 1W5	4760-4770	Exshaw
2-35-10-13W4	3946-3951	Exshaw	15-10-58- 5W5	4531-4551	Exshaw
4-21-18-18W4	4756-4772	Exshaw	14-29-48- 6W5	6974-6994	Exshaw
4-15- 7-19W4	4738-4745	Exshaw	9- 6-52-11W5	8022-8026	Exshaw
2- 9-20-19W4	4992-5036	Exshaw	1-12-74-22W5	5729-5779	Exshaw
16-34-37-20W4	4580-4588	Exshaw	12-11-74-22W5	5675-5687	Exshaw
10-30-20-25W4	7120-7127	Exshaw	13-18-80-23W5	5731-5747	Exshaw
8-18-44-25W4	5190-5196	Exshaw	4-23-72-10W6	11645-11705	Exshaw
1-20-46-26W4	5150-5154	Exshaw	16-19-77-10W6	7262-7335	Belloy
4-12-15-27W4	8776-8780	Exshaw	4- 8-74- 5W6	6814-6896	Belloy
14-14-48-27W4	4988-4998	Exshaw	11-16-77-10W6	7337-7447	Belloy
12-19-18-29W4	9621-9659	Exshaw			

[1]Department of Geology and Geophysics, The University of Calgary, Calgary, Alberta

The Exshaw Results

The samples studied were cored as a result of exploration of the underlying Wabamun for oil and gas. It follows that the core includes the lower portion of the Exshaw Formation more frequently than units higher in the formation. The most useful datum therefore is the base of the Exshaw Formation; it is shown as a westerly sloping surface in Figure 15.1.

The 155 2-foot (0.6 m) samples analyzed for uranium are plotted on frequency diagrams in Figure 15.2. Figure 15.2a shows the distributions typical of trace elements, with a low frequency of high values and a high frequency of low values. The mean and standard deviation for the samples is 10 ± 2 ppm Figure 15.2b shows the same data plotted with log uranium values. It shows the log normal distribuiton and has a mean and standard deviation of 13 ± 8 ppm. The most frequently occurring value as indicated in Figure 15.2b is 12.6 ppm.

As the samples with the highest uranium content are of particular interest three core sections were resampled with channel lengths of 0.5 feet (0.15 m). Comparisons of the results of the 2 foot (0.6 m) and 0.5 foot (0.15 m) sample program are shown in Table 15.2.

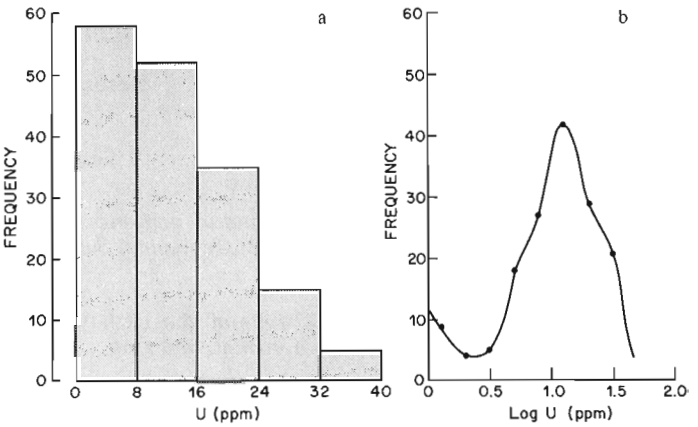

Figure 15.2. *Frequency plots for uranium in the Exshaw two foot (0.6 m) samples; (a) shows frequency and μ (ppm), (b) shows the distribution with Log μ (ppm).*

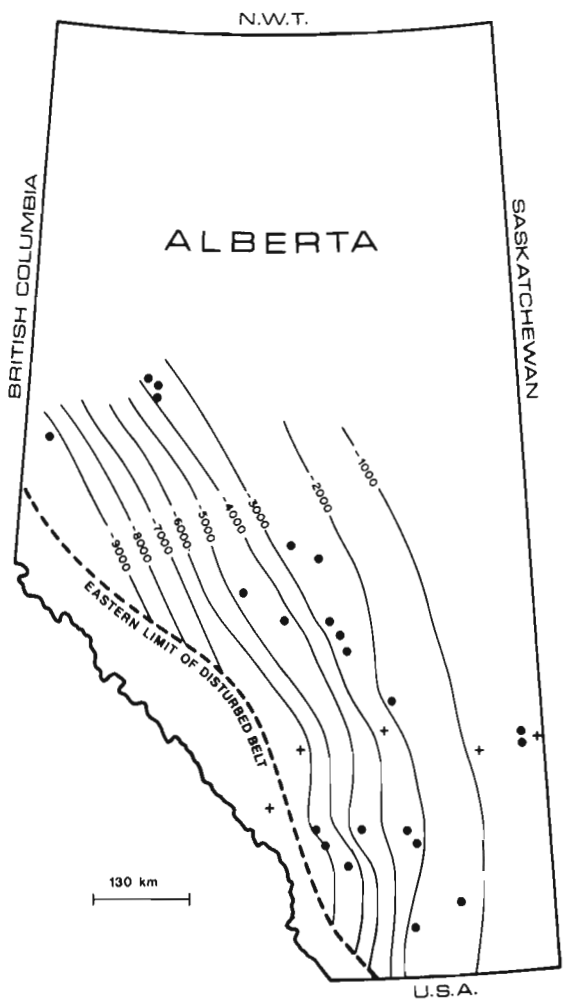

Figure 15.1. *Contours of the base of the Exshaw Formation in feet below sea level. Dots are wells in this study, the crosses are sections studied by Havard (1967).*

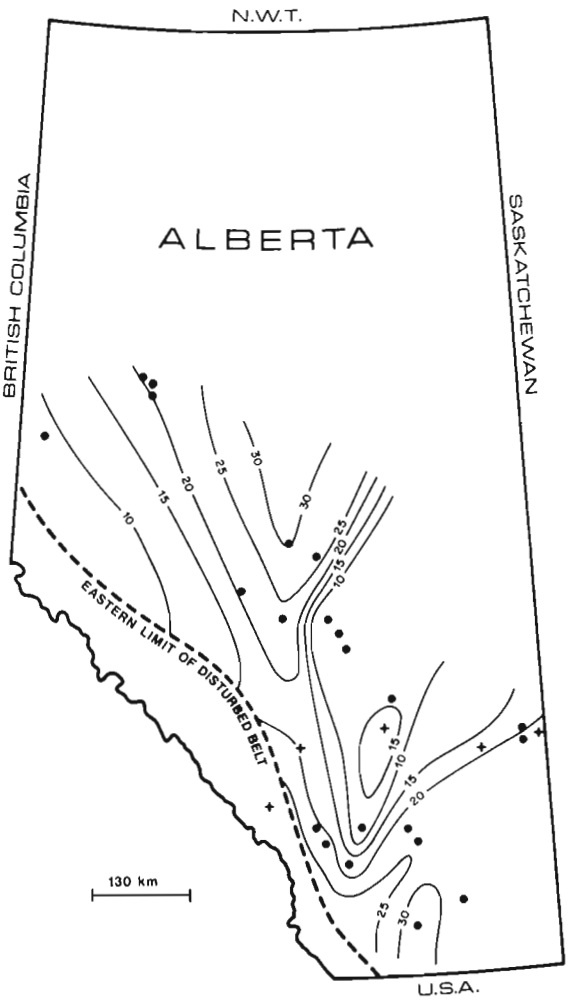

Figure 15.3. *Contour map of the basal 4 feet (1.2 m) of the Exshaw Formation, values in ppm.*

Table 15.2

Comparison of sample length data

Well	Interval	2 foot sample (ppm) (0.6 m)		0.5 foot sample (ppm) (0.15 m)	
		Mean	Maximum	Mean	Maximum
4-15- 7-19W4	4738-4745	28	37	27	51
2-35-10-13W4	3946-3951	31	33	36	57
2- 9-20-19W4	5028-5036	26	29	23	36

It will be noted from this table that the mean values over the intervals remained similar while as might be expected, the maximum values were greater when the 0.5 foot (0.15 m) interval was used. It does demonstrate the reproducibility of the sampling and analytical approach.

The average for the 4 foot (1.2 m) interval immediately above the base of the Exshaw Formation was calculated for each core and is plotted on Figure 15.3. This illustrates the lateral variability, with values greater than 30 ppm encountered locally, despite the mean of 10 ppm calculated above.

A plot of data for each core indicates a general tendency for the uranium to be concentrated at the base of the formation and to decrease upward. The nickel and zinc values varied sympathetically with the uranium. To illustrate this tendency the average values for uranium, nickel and zinc were calcualted for each two foot (0.6 m) interval above the base. The data, shown in Figure 15.4, clearly illustrate the general relationship. They also show that on the average the black shale at the base approximates the 20 ppm value calculated by Havard (1967).

The Belloy Results

The units sampled are highly siliceous consisting largely of cherty siltstones with interbeds of carbonaceous and arenaceous material. The phosphate content of these rocks is not as high as Montana and Idaho phosphatic formations which were analyzed and gave values of 130 ppm. The reconnaissance sample program consisted of 19 samples from 3 wells (see Table 15.1); they yield a range of values from 0 to 33 ppm uranium and a mean value of 8.3 ppm and standard deviation of 7. Other Belloy Group cores were examined and as the lithologies were similar no further sampling was done.

Discussion

The Exshaw Formation like the Chattanooga represents a black shale with a uranium content well above the Clarke value of 2 ppm. The nickel and zinc contents are close to the averages for shale. It is apparent from the data that samples must represent widths to be meaningful. This study suggests the concentration of uranium is well below that of economic interest but supports the potential of this horizon as a source bed for redistribution and concentration. The distribution of uranium and other metals suggests a syngenetic or early diagenetic concentration probably by organic material in a euxinic environment. However the Exshaw Formation caps the porous brine-charged Wabamum Formation and the diffusion of complexed metals up through the semi-permeable organic rich shale could provide a mechanism for a similar distribution with the brine providing the metals and the shale the reducing environment. The presence of nickel and zinc is of interest in this respect as nickel is concentrated with uranium in some unconformity type deposits, and zinc is concentrated in porous carboante hosts. The syngenetic model is currently the more attractive but the brine transport mechanism with sulphate or carbonate complexing of uranium remains a possibility.

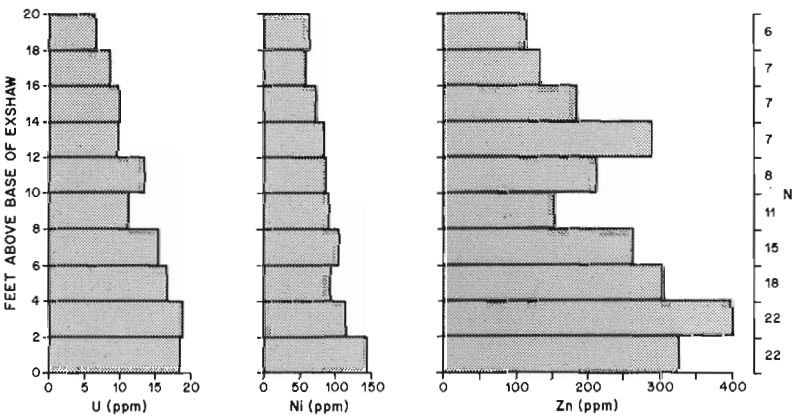

Figure 15.4. *The average values for each two foot (0.6 m) interval above the base of the Exshaw Formation. The number of samples (N) averaged is shown for each interval.*

References

Bates, T.F. and Strahl, E.D.
1958: Mineralogy and chemistry of uranium-bearing black shales; in 2nd United Nations International Conference on Peaceful Uses of Atomic Energy, Geneva 1958, v. 2, p. 407-411.

Bell, R.T.
1978: Uranium in black shales – A review; in Short Course in Uranium Deposits: Their Mineralogy and Origin, M.M. Kimberley, ed., Mineralogical Association of Canada, Short Course Handbook, v. 3, p. 307-329.

Havard, K.R.
1967: Mineralogy and Geochemistry: Exshaw Formation, southern Alberta; unpublished M.Sc. Thesis, Department of Geology and Geophysics, The University of Calgary.

Reynolds, R.C., Jr.
1963: Matrix corrections in trace element analysis by X-ray fluorescence: Estimation of mass absorption coefficient by Compton scattering; American Mineralogist, v. 48, p. 1133-1143.

Swanson, V.E.
1960: Oil yield and uranium content of black shales; U.S. Geological Survey, Professional Paper 356-A, p. 1-44.

16.

NAHANNI INTEGRATED MULTIDISCIPLINARY PILOT PROJECT GEOCHEMICAL STUDIES PART 1: GEOCHEMISTRY AND MINERALOGY OF SHALES, CHERTS, CARBONATES AND VOLCANIC ROCKS FROM THE ROAD RIVER FORMATION, MISTY CREEK EMBAYMENT, NORTHWEST TERRITORIES

Projects 790033, 770044, 740107

W.D. Goodfellow[1], I.R. Jonasson[1], and M.P. Cecile[2]

Goodfellow, W.D., Jonasson, I.R., and Cecile, M.P., Nahanni Integrated Multidisciplinary Pilot Project. Geochemical Studies Part 1: Geochemistry and mineralogy of shales, cherts, carbonates and volcanic rocks from the Road River Formation, Misty Creek Embayment, Northwest Territories; in Current Research, Part B, Geological Survey of Canada, Paper 80-1B, p. 149-161, 1980.

Abstract

Geochemical and mineralogical studies of Section 44 through the Road River Formation were used to substantiate and define chemically earlier divisions as well as to subdivide further each unit. A period of volcanic activity represented by mafic tuffs and flows in unit RRc in Section 40 was recognized in Section 44 by high contents of TiO_2, Na_2O and MgO present in leucoxene, plagioclase and chlorite, respectively. Associated with this volcanic event are cherts and carbonaceous metalliferous shales, interpreted as resulting from the influx of nutrients and base metals during hydrothermal activity.

A second period of volcanism, reflected by high contents of TiO_2, Na_2O and MgO, is interpreted to have occurred during the Middle Cambrian in unit RRs. As in unit RRc, the lower portion of this unit is characterized by anomalous contents of Zn, Cu, Ni, Ag, Mo, As, Hg, Sb and V accompanying carbonaceous shales.

The Lower to Middle Ordovician mafic volcanic rocks and hypabyssal equivalents present in Section 40 are intensely altered, most likely alkali in composition, and characterized by above average contents of F, Pb, Co, As, Sb, Ba, Ce, V, La and Be. The Ba forms clear crystals of celsian that commonly are situated adjacent to K-feldspar

Introduction

A stratigraphic-depositional study of the Lower Paleozoic carbonate-to-shale transition was carried out by Cecile (1978). During the course of this study, the Misty Creek Embayment was outlined and defined and numerous stratigraphic sections were measured and described. In Section 44 (Fig. 16.1), more than approximately 1200 m of Road River Formation were sampled for chemical and mineralogical analysis. In addition, two samples of Lower Paleozoic volcanic rocks from Section 40 (Fig. 16.1) were analyzed to give preliminary data on the composition of these rocks. The objectives of this phase of the overall study were: (1) to characterize precisely the mineral and chemical composition of the sedimentary rocks in one stratigraphic section in an effort to understand the origins of the different mineral phases; (2) and to assess the use of geochemistry in stratigraphic studies.

These studies form part of the geochemical contributions to the Nahanni Integrated Multidisciplinary Pilot Project (NIMPP).

Stratigraphy and Petrology

The Misty Creek Embayment is a Lower Paleozoic paleogeographic feature located in the northeastern part of the Selwyn Basin (Fig. 16.1). Isopachs of total stratigraphic fill in the Embayment show it to be a 100 x 150 km, rectangular northwest trending depression which, on three sides, contrasts 200-600 m thick platform dolomite successions with 900->3000 m thick basin and transitional strata. The fourth side connects across a paleo-submarine ridge, with the Selwyn Basin (Fig. 16.1). The geometry and linear facies belts of the Embayment, together with the type of associated volcanic rocks, reported on here, indicate an extensional origin for the Embayment beginning in late Early Cambrian time and persisting to at least the end of Early Silurian (Cecile, in preparation).

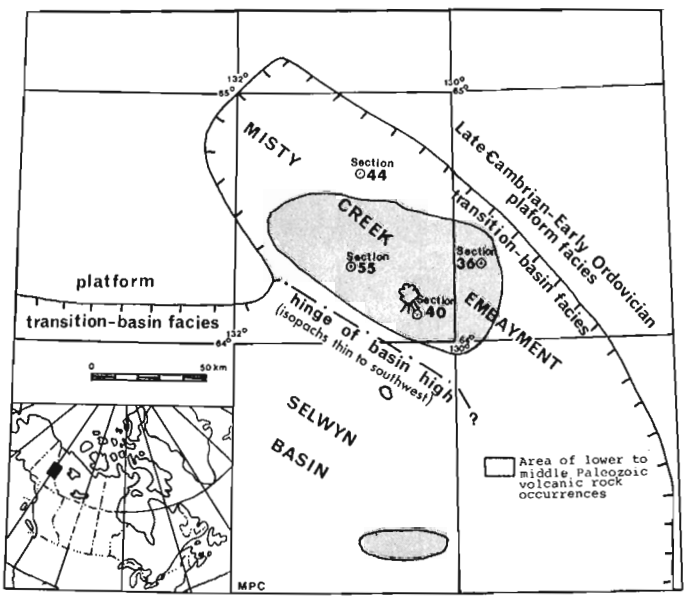

Figure 16.1. *Location map of the Bonnet Plume map area showing the outline of the Misty Creek Embayment, the transition from platform to basin facies and stratigraphic sections. The area of Lower to Middle Paleozoic volcanic rocks is also outlined.*

Basin strata in the Embayment have been mapped and described by Aitken et al. (1973), Aitken and Cook (1974), Blusson (1971, 1974) and Cecile (1978) as the Road River Formation comprising calcareous and carbonaceous shale, silty limestone and dolomite, chert, volcanic tuffs and flows and minor barite that are underlain by the Lower Cambrian Sekwi carbonates and overlain by Silurian-Devonian Mount Kindle carbonates (Fig. 16.2).

[1] Resource Geophysics and Geochemistry Division

[2] Institute of Sedimentary and Petroleum Geology, Calgary

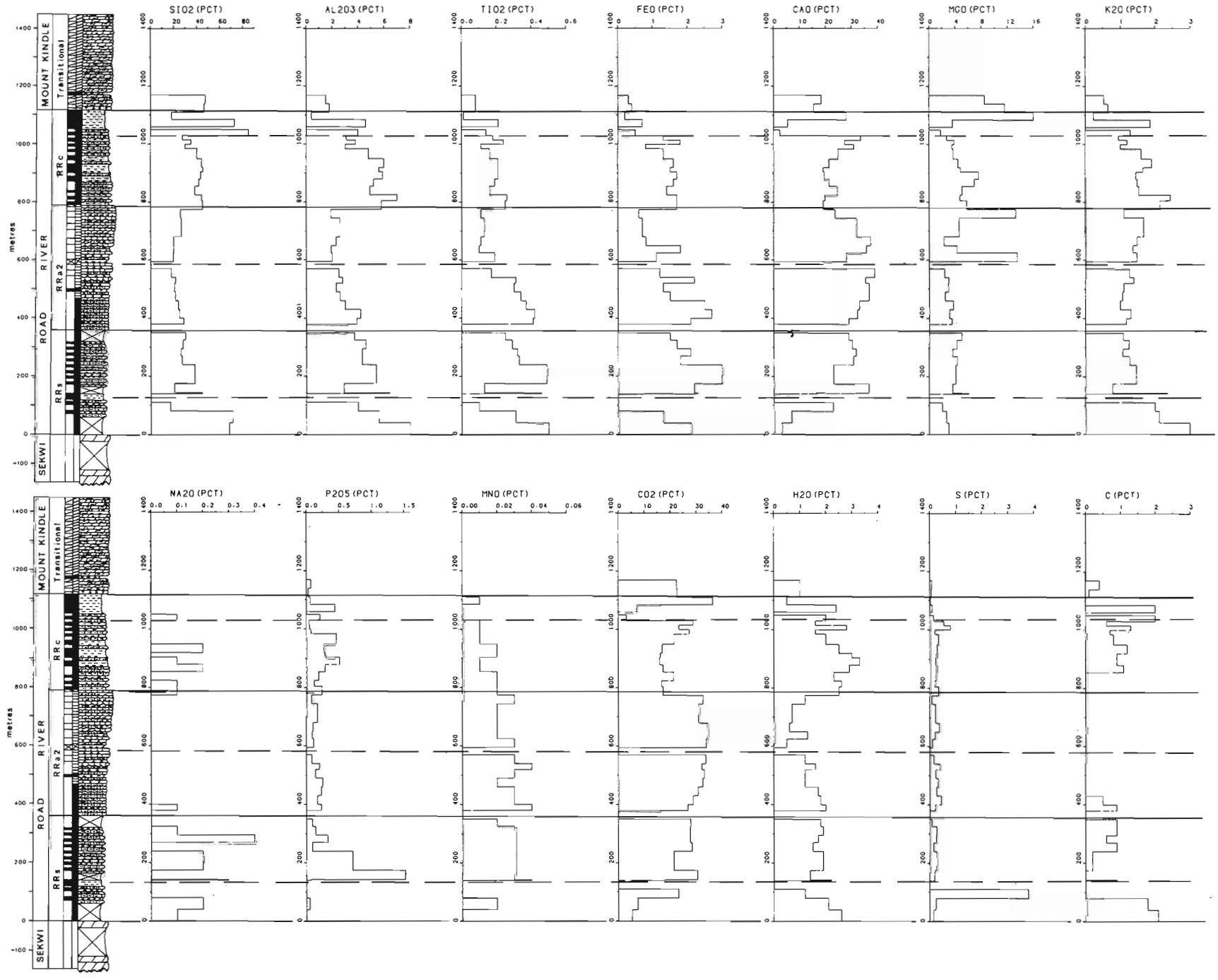

Figure 16.2. *Geochemical profiles showing the distribution of major and minor elements in sedimentary rocks collected from Section 44 which is situated in the Misty Creek Embayment (refer to Fig. 16.1 for the location of Section 44).*

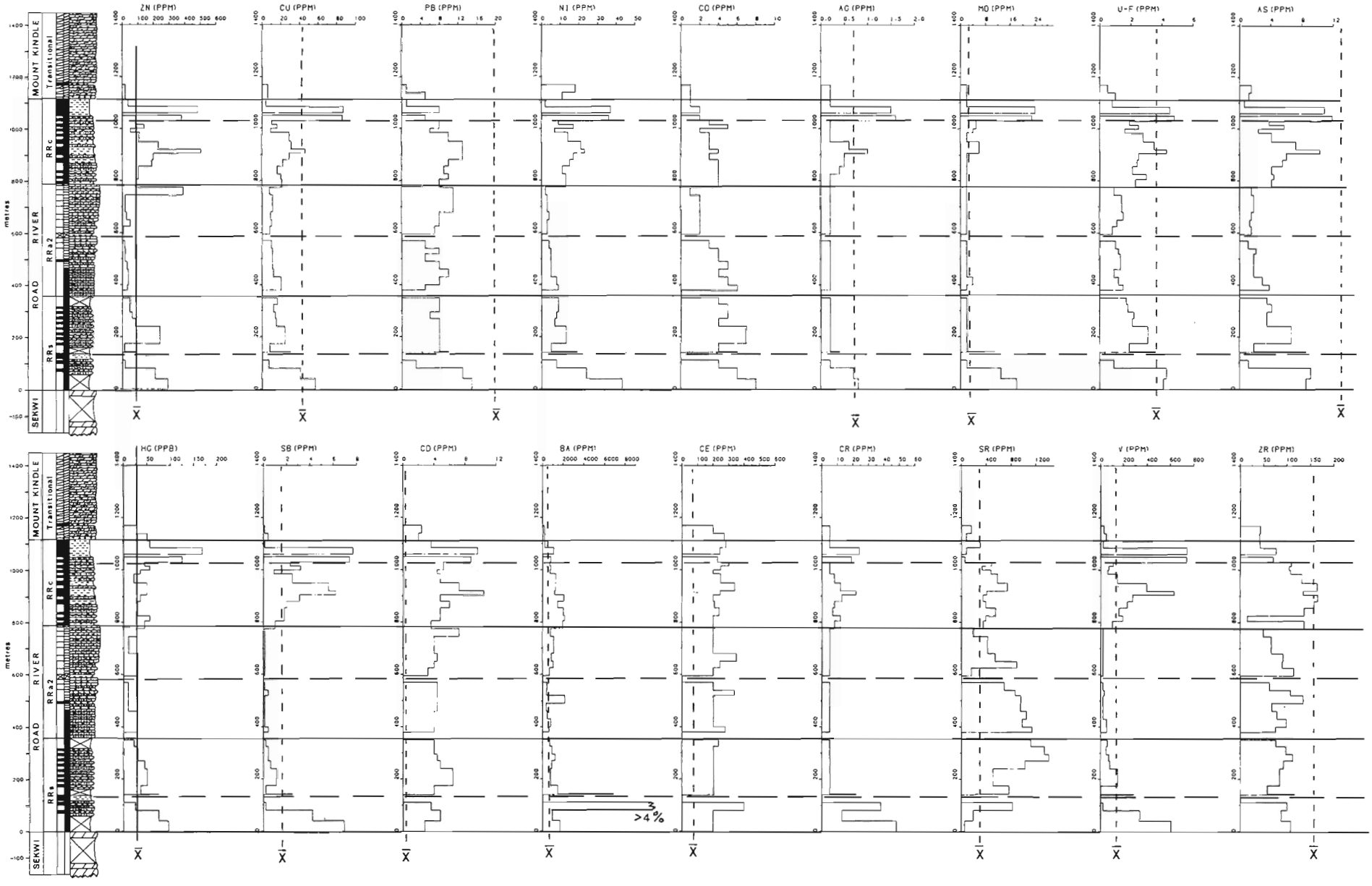

Figure 16.3. *Geochemical profiles showing the distribution of trace and minor elements in sedimentary rocks collected from Section 44. Average shale (x) from Turekian and Wedepohl (1961) except for Hg which is from Cameron and Jonasson (1972).*

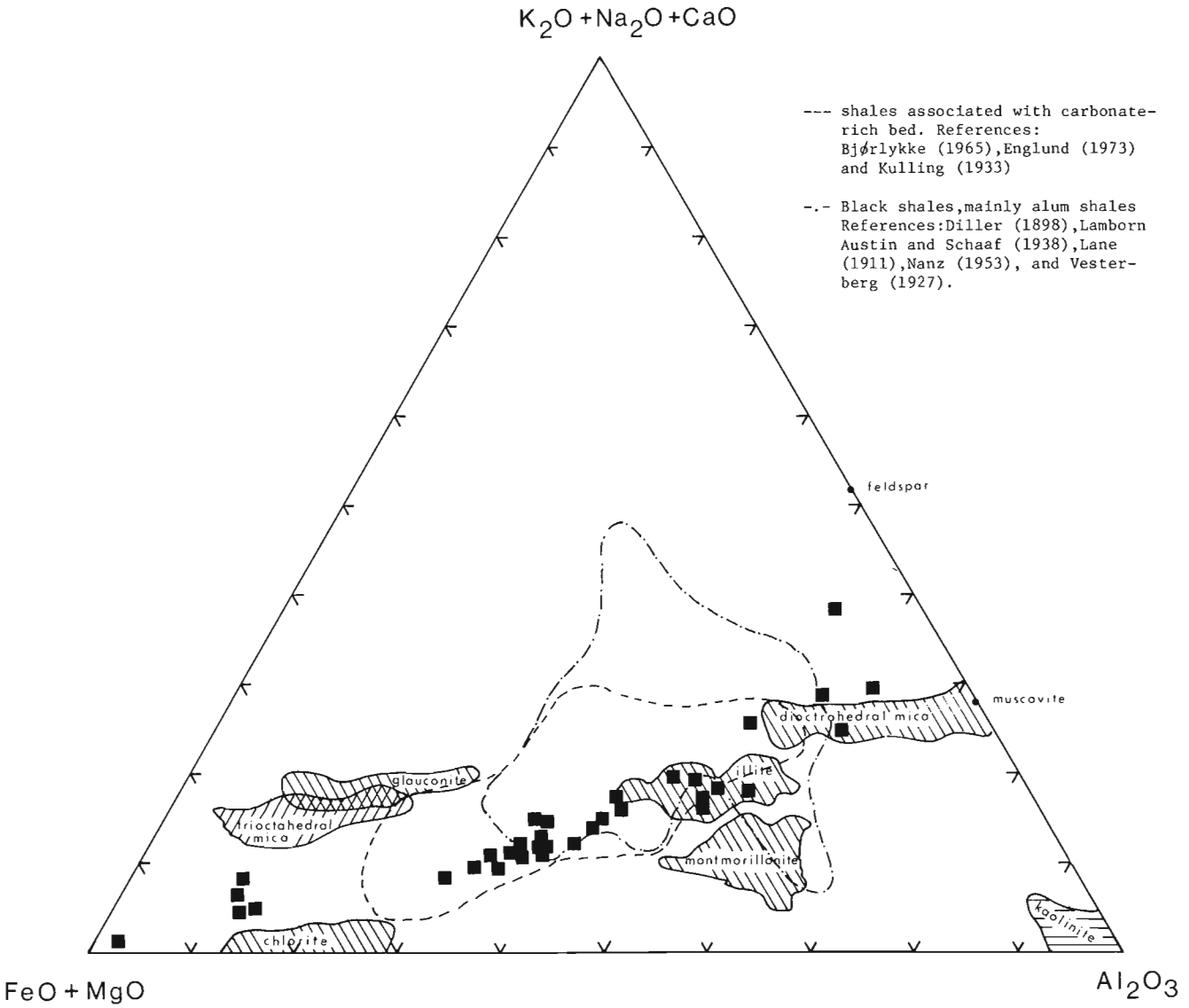

Figure 16.4. *Ternary $(FeO+MgO) - (K_2O+Na_2O+CaO) - Al_2O_3$ plot showing the distribution of common sedimentary minerals, black shales and shales associated with carbonate rocks described elsewhere, and shales and cherts from Section 44 normalized to a carbonate-free basis (Section 44 shales and cherts represented by black squares).*

In the Misty Creek Embayment the Road River Formation has been described and divided by Cecile (1978) into four units ranging in age from late Early to Middle Cambrian to late Early Silurian or younger Silurian. The four mappable units described in ascending order are: a lower shale unit (RRs); a yellowish weathering silty limestone unit, the Rabbitkettle Formation (Cecile, 1978); a shale-chert unit (RRc); and an upper sooty grey thin bedded limestone unit (RRl). The last unit is missing in Section 44 and is not described here.

Shale Unit (RRs)

This unit is composed of 100-2500 m of light grey-brown weathering, dark grey calcareous silty shale and silty limestone. In the lower parts of the unit at Section 44, carbonaceous material gives the rock a sooty appearance. Interbedded with 2 m of limestone in the middle of this unit are beds of medium to light grey barite about 3 to 4 cm thick composed of a fine grained core with coarsely crystalline margins and beds with scattered megacrysts. Immediately above are phosphatic strata. This unit grades generally from a calcareous shale at the base to an argillaceous carbonate at the top (Fig. 16.2) and is mainly of Middle Cambrian age (Fritz, Norford and Tipnis, in preparation). X-ray diffraction (XRD) analyses show that the lower parts of this unit are composed of abundant quartz, minor dolomite, illite and feldspar (mostly plagioclase) and traces of chlorite. In addition to these minerals, variable amounts of carbonaceous matter are present although the degree of maturation is unknown.

As noted above, megacrysts of grey barite have been observed by Cecile (1978) to form sedimentary layers interstratified with argillaceous limestone in the middle of the RRs unit. In the phosphatic shales at the base of this unit, fluorapatite has been identified. Although no sphalerite was observed in unit RRs of Section 44, small amounts of sphalerite were found filling fractures over a 10-m stratigraphic interval in Lower Ordovician transitional strata in Section 36 situated on the northeast side of the Embayment (Fig. 16.1).

Table 16.1

Comparison between mafic igneous rocks from the Misty Creek Embayment and average basalts described elsewhere

	Misty Creek Embayment Bonnet Plume, Yukon		Ocean Ridge Basalts (Engel et al., 1965)		Basalts (Turkian and Wedepohl, 1961)
	CJA77-40-7	CJA77-40-4	Tholeiitic	Alkali	undifferentiated
per cent					
SiO_2	41.8	50.0	49.34	47.41	49.2
Al_2O_3	11.6	15.0	17.04	18.02	14.7
TiO_2	3.59	2.00	1.49	2.87	2.3
FeO	0.0	8.4	6.82	5.80	-
Fe_2O_3	10.3	1.0	1.99	4.17	-
FeO_T	9.3	9.3	8.62	9.55	11.1
CaO	7.5	1.0	11.72	8.65	10.6
MgO	7.5	8.0	7.19	4.79	7.6
K_2O	3.01	3.00	0.16	1.66	1.0
Na_2O	0.0	0.0	2.73	3.99	2.4
P_2O_5	0.76	0.60	0.16	0.92	0.25
MnO	0.03	0.10	0.17	0.16	0.19
CO_2	5.0	0.6	-	-	-
H_2O	5.2	5.9	1.27	1.40	-
C	0.4	0.2	-	-	-
S	1.19	0.10	-	-	0.03
ppm					
F	1100	1920	-	-	400
Cl	160	130	-	-	60
Zn	142	103	-	-	105
Cu	98	45	77	36	87
Pb	32	1	-	-	6
Ni	43	161	97	51	130
Co	105	43	32	25	48
Ag	0.2	0.2	-	-	0.11
Mo	4	2	-	-	1.5
As	14.7	1.1	-	-	2
Hg*	20	10	-	-	900
Sb	0.9	0.1	-	-	0.2
Cd	2.8	2.8	-	-	0.22
Li	171	164	-	-	17
Rb	97	56	<10	33	30
Cs	3.3	3.9	-	-	1.1
Sr	804	398	130	815	465
Ba	17400	>40000	14	498	330
U	1.2	0.6	-	-	1.0
Ce	574	581	-	-	48
Cr	65	363	297	67	170
V	500	365	292	252	250
Y	70	45	43	54	21
La	167	167	-	-	15
Zr	351	277	95	333	140
Be	4.8	4.	-	-	1.0
Th	2	2	-	-	4

*Hg in ppb

The upper portions of this unit contain abundant calcite and minor dolomite, chlorite, illite and quartz. The stratigraphic distribution of these minerals is reflected in the major-element chemistry with SiO_2, Al_2O_3 and K_2O decreasing and CaO, MgO and CO_2 increasing upwards (Fig. 16.2).

Using a ternary (Al_2O_3)-(MgO+FeO)-(K_2O+Na_2O+CaO) plot proposed by Englund and Jorgensen (1973) to classify argillaceous sediments, most of the rocks from the Road River Formation, after being normalized to a carbonate-free basis, plot on a line between muscovite and chlorite (Fig. 16.4). The chlorite may be derived from the weathering of volcanic rocks extruded in the basin. Compared to shales described elsewhere (see Fig. 16.4), rocks from the Misty Creek Embayment plot mainly in a field outlined by shales associated with carbonate-rich beds. The field of black shales (Fig. 16.4) intersects the field of shales from the Road River Formation but is extended towards the feldspar and montmorillonite fields and away from the chlorite field.

Rabbitkettle Formation (Unit RRa2)

The shale unit (RRs) is conformably overlain by as much as 750 m of thin bedded yellowish weathering light to medium grey silty limestone. The limestone is comparable in composition, texture and age to the Rabbitkettle Formation of Gabrielse et al. (1973) mapped in the Southern Mackenzie Mountains (Cecile, in preparation). Fritz, Norford and Tipnis (in preparation) have dated this unit in the Embayment as Late Cambrian to Early Ordovician. Within this unit at Section 44, there is gradation from silty rocks at the base to more carbonate-rich rocks at the top. This gradation is shown clearly by the distribution of CO_2, Al_2O_3, TiO_2 and H_2O in geochemical profiles of Section 44 (Fig. 16.2). From microscopic examinations and XRD analysis, silty carbonates situated in the lower portions of this unit are composed of major calcite and minor dolomite, quartz, chlorite and illite. Towards the top of this unit, the proportion of dolomite to calcite increases and illite cannot be detected by XRD methods.

Chert-Shale Unit (RRc)

This unit comprises 100 to 400 m of interstratified black chert, siliceous shale, black shale and light brown or yellow weathering silty limestone rhythms and thin bedded silty limestone. It ranges in age from Early to Middle Ordovician (Fritz, Norford and Tipnis, in preparation). In Section 44 (Fig. 16.2), this unit grades from a silty limestone at the base to a black sooty shale and chert at the top. X-ray diffraction studies show that the basal portions are composed of calcite and quartz with monor chlorite, dolomite and illite. Towards the top, the amount of calcite decreases while quartz and illite increase. Barite was not detected by XRD in this unit in Section 44 although local accumulations of megacrystalline barite nodules were found in unit RRc at Section 55 (Fig. 16.1).

Volcanic Rocks

Minor units of Lower and Middle Paleozoic volcanic rocks comprising lapilli and fine grained tuffs, breccias and amygdaloidal flows and hypabyssal equivalents are found in the basinal sections of the Misty Creek Embayment intertongued predominantly with unit RRc. A small volcanic centre was identified at Section 40. Here the RRc unit is overlain by close to 500 m of volcanic tuffs, flows and sediments and minor limestone intruded by several dykes and sills. In both intrusive and extrusive rocks, primary minerals have been largely altered to carbonate, chlorite, quartz, tremolite-actinolite, talc, kaolinite and leucoxene. Chemical analyses (Table 16.1) show that these mafic igneous rocks are most characteristically alkaline although the alkalis have been changed by metasomatic processes and are therefore of little use in classifying the volcanic rocks. For example, the low Na content in CJA77-40-7 and CJA77-40-4 is not typical of either tholeiitic or alkali basaltic rocks forming ocean ridges (Table 16.1) demonstrating the pronounced removal of Na during alteration. The content of the relatively more stable elements such as Ti and Zr may be more representative of the primary composition of typical basalts described elsewhere (Table 16.1).

One of the chemical characteristics of both volcanic and hypabyssal rocks from the Misty Creek Embayment is the high Ba which exceeds 4 per cent in sample CJA77-40-4. The site of Ba in this sample has been identified by XRD as celsian ($Ba\{Al_2Si_2O_8\}$). The celsian occurs throughout the rock as clear crystals often adjacent to K-feldspar. In addition to Ba, these igneous rocks contain higher than normal levels of Ce, Li, La, F and V (Table 16.1). Sample CJA77-40-7 taken from the mafic flows is enriched also in the chalcophile elements Cu, Pb, Zn, Co, As and Sb.

Celsian in igneous rocks from the Misty Creek Embayment represents a rather uncommon association. Celsian that occurs elsewhere in the world is associated most commonly with either manganese deposits, such as those

located at Jakobsberg, Sweden or with calc-silicate skarns (Gay and Roy, 1968). Celsian associated with interlocking barite grains also occurs in sulphide-bearing sugary quartz rock that is interbedded with the Rosh Pinah stratabound and stratiform Pb-Zn deposit situated in South West Africa (Page and Watson, 1976). Salmon-coloured fine grained celsian is also found in the matrix of breccia clasts. The feldspars present in the quartzite, microquartzite and argillite are enriched in barium near the massive sulphides. Results from preliminary microprobe investigations indicate that the orthoclase has been replaced by hyalophane in the quartzites (Page and Watson, 1976).

Barium occurring in igneous rocks is present usually as Ba-orthoclase or Ba-sanidine and not as an end member Ba-feldspar. Barium ranging up to 880 ppm has been described for Cenozoic alkali basalts forming seamounts along the Northeast Bank, Southern California Borderland (Hawkins et al., 1971). The Ba is most likely present in alkali feldspar that occurs as patches distributed throughout a fresh aphanitic basaltic rock.

The conditions under which celsian formed in igneous rocks from the Misty Creek Embayment have not as yet been determined. Possible origins would include (1) a crystallization product during cooling of a Ba-rich basaltic magma although the paucity of thermodynamic data for Ba-feldspars precludes determining the behaviour of Ba during cooling. However, under hydrous conditions (2000 bars H_2O pressures), potassium-barium feldspars have been synthesized at temperatures in the 500° to 700°C range (Roy, 1967); (2) the celsian may have formed by the replacement of potassium in orthoclase by later Ba-rich fluids; or (3) the celsian may have been produced from the reaction of barite or witherite with kaolinite. The last mechanism has been proposed by Bjørlykke and Griffin (1973) to explain the origin of authigenic hyalophane found in Lower Ordovician shales of the Oslo region, Norway.

From experiments carried out in ceramic systems, Segnit and Gelb (1970) demonstrated that heating a mixture of kaolinite and barite in the presence of a reducing agent, in this case carbon, produced celsian at 800°C. If witherite was used instead of barite, a reducing agent was not required. The following was proposed as an empirical reaction scheme for the formation of celsian from barite and kaolinite and may well apply to the Misty Creek setting.

1. $BaSO_4 + 4C \rightarrow BaS + 4CO$,
   where C is represented by carbonaceous matter from enclosing shales.
2. $3BaSO_4 + BaS \rightarrow 4BaO + 4SO_2$
3. $BaO + (Al_2(Si_2O_5)(OH)_4) \rightarrow (Ba(Al_2Si_2O_8)) + 2H_2O$

Although the experimental temperatures were much higher than those expected for the formation of authigenic Ba-feldspar, it is possible that these reactions would proceed at lower temperatures, particularly if Ba was present in forms other than the insoluble sulphate.

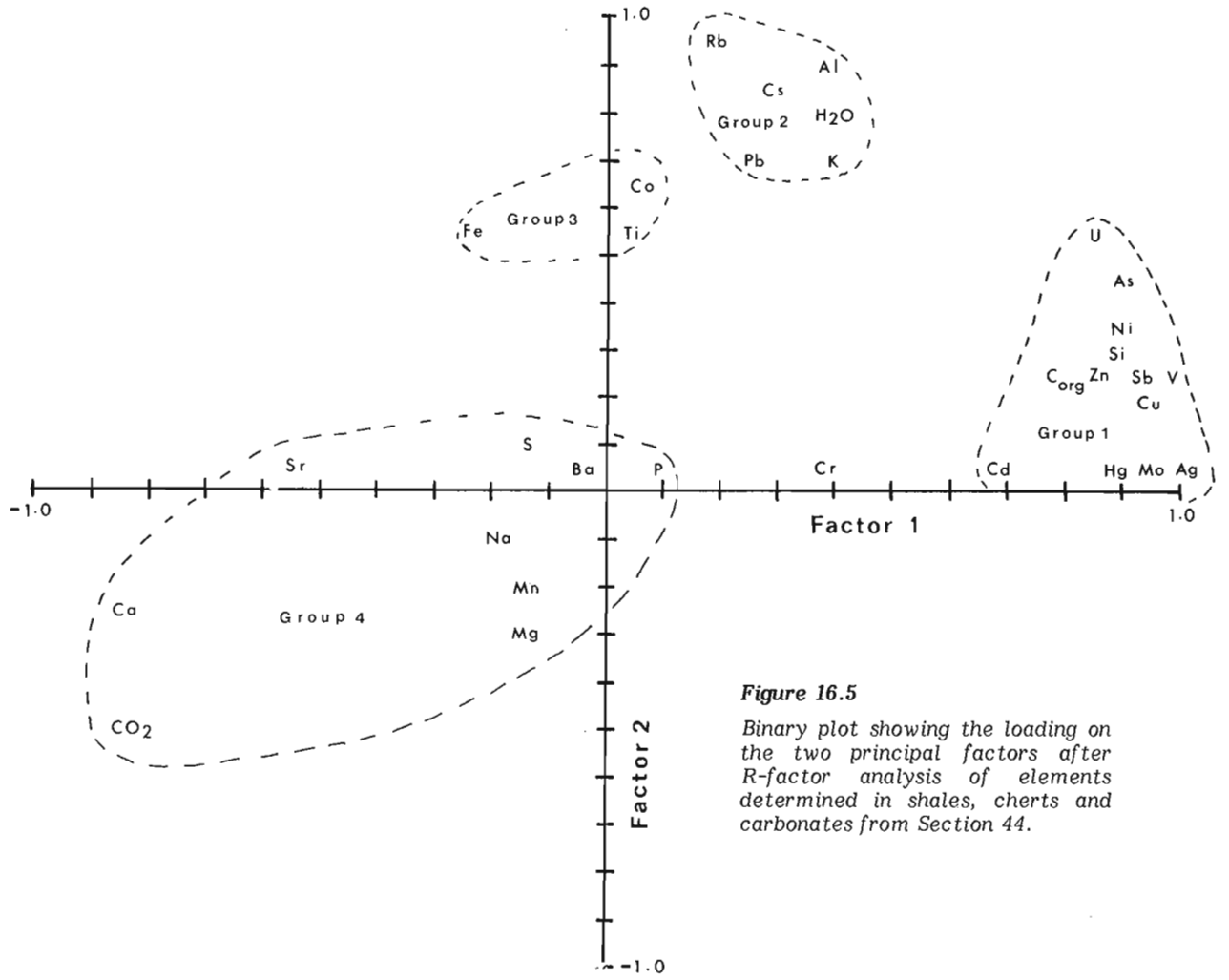

Figure 16.5

Binary plot showing the loading on the two principal factors after R-factor analysis of elements determined in shales, cherts and carbonates from Section 44.

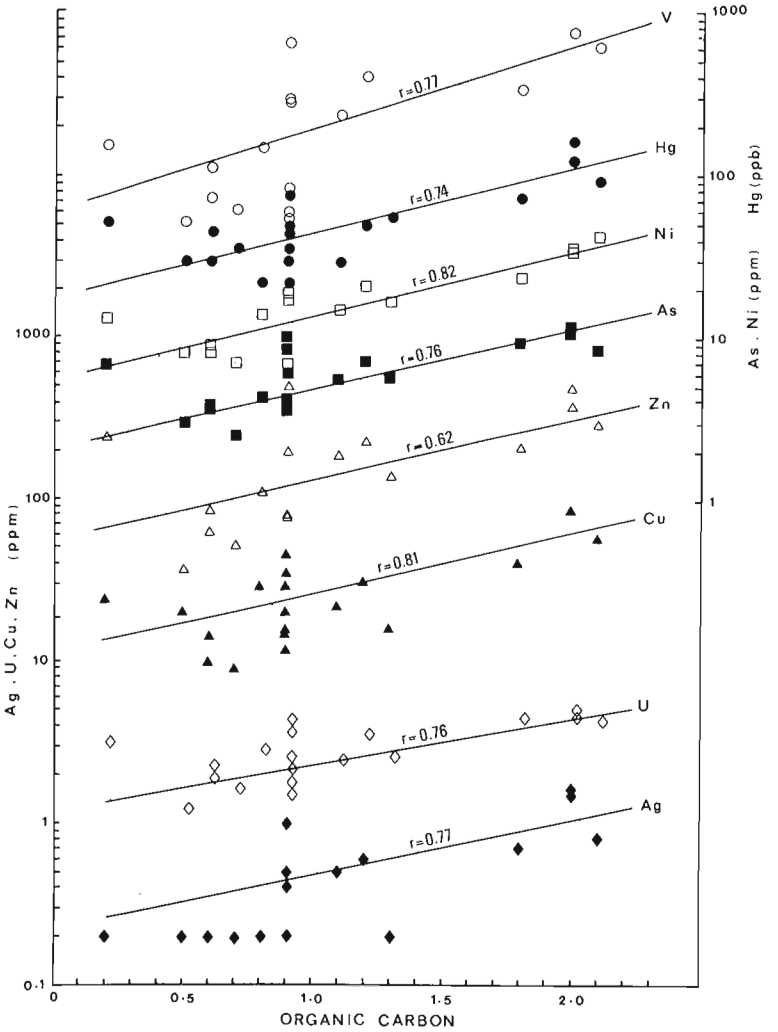

Figure 16.6. *Binary plots of V, Hg, Ni, As, Zn, Cu, U and Ag against organic carbon for shales from Section 44 (r = correlation coefficient).*

In the case of igneous rocks from the Misty Creek Embayment, all the ingredients for this type of reaction are present except that barite or witherite have not been identified in these rocks. The fact, however, that kaolinite is still present indicates that all the barite (or witherite) may have reacted to form celsian. The reducing agent, if required, may be pyrite or carbonaceous matter since up to 0.4 per cent carbon has been found in these igneous rocks (Table 16.1).

The presence of celsian in mafic extrusive and hypabyssal rocks of the Misty Creek Embayment may aid in understanding the origins of sedimentary barite that occurs throughout the Selwyn Basin in rocks of Middle Cambrian to Late Devonian age. The association of celsian with mafic volcanic rocks associated with an extensional feature, the Misty Creek Embayment, supports the hypothesis that at least some of the sedimentary barite owes its origin to volcanic-related processes.

Geochemistry

Sample Collection, Preparation and Analytical Methods

Small rock chips were collected every 50-100 cm over stratigraphic intervals ranging up to 100 m and then reduced to minus-200 mesh. Sample powders were analyzed for Zn, Cu, Pb, Ni, Co, Ag, Mo, As, Sb and Cd by atomic absorption spectrometry after decomposition with strong $HF-HCLO_4-HNO_3$ acid mixture. Mercury was determined using methods described by Jonasson et al. (1973). Fluorometric methods were used to measure U. Most of the remaining trace and minor elements were determined by optical emission spectroscopy.

Major element determinations were made by X-ray fluorescence (XRF) on a glass pellet made by fusing 1 g of sample with lithium metaborate. Thorium was determined by XRF on pelletized rock powders.

Distribution of Elements in Sedimentary Rocks

The distribution of elements in Section 44 is controlled by the relative proportions of the various mineral phases. These are composed of (1) detrital minerals identified by XRD as quartz, plagioclase, mica, ilmenite or leucoxene, hematite, chlorite and clay minerals such as illite; (2) chemically or biochemically precipitated minerals such as calcite, dolomite, chert, barite and fluorapatite; (3) diagenetic or authigenic minerals such as pyrite, other sulphides, clays, plagioclase and barite. In addition to these three mineral groupings, carbonaceous matter is a significant constituent reflecting important processes of biological accumulation of certain elements during sedimentation and in the fixation of others during diagenesis of shales.

Element profiles through the Road River Formation are presented in Figures 16.2 and 16.3. In general, the distribution of elements has been affected by one or more of the following parameters: Composition of rocks that supply detritus to the ocean basin, composition of the sea water, lithologic facies and environment of deposition, volcanism and associated fumarolic activity and the type of organisms present. In the Misty Creek basin, the main factors controlling the distribution of elements are the source rocks (i.e., carbonate versus silicate rocks), volcanism which supplies both epiclastic and pyroclastic material plus nutrient elements and base metals to the basin, and the organic carbon content which reflects the level of nutrient supply. The elements have been grouped on the basis of these factors and represented mathematically by factor analysis. The major groupings outlined on the basis of the two principal factors (Fig. 16.5) are discussed below.

Group 1: Elements comprising this group are chalcophile elements such as Zn, Cd, Hg, As, Cu and Sb, and elements such as V and Ni that are considered to play an important role in metabolic processes of certain organisms. The association of chalcophile elements with organic carbon (Fig. 16.6) may reflect the importance of decaying organic matter as a nutrient source for bacterial reduction of sulphate during diagenesis. The presence of U in this group may reflect a strong affinity for carbonaceous matter and subsequently its stability in the U(IV) valence state. The association of Si with the above mentioned elements and carbon most likely reflects the influx of Si during thermal events associated with volcanism (Maksimova, 1978) or may have precipitated subsequently as radiolarian tests that are found scattered throughout the chert in unit RRc. Because of the surface active nature of colloidal silica either inorganic in origin or derived from micro-organisms, organic colloids and accumulated trace elements could become attached to these particles and be deposited with chert during subsequent seawater-induced flocculation of silica.

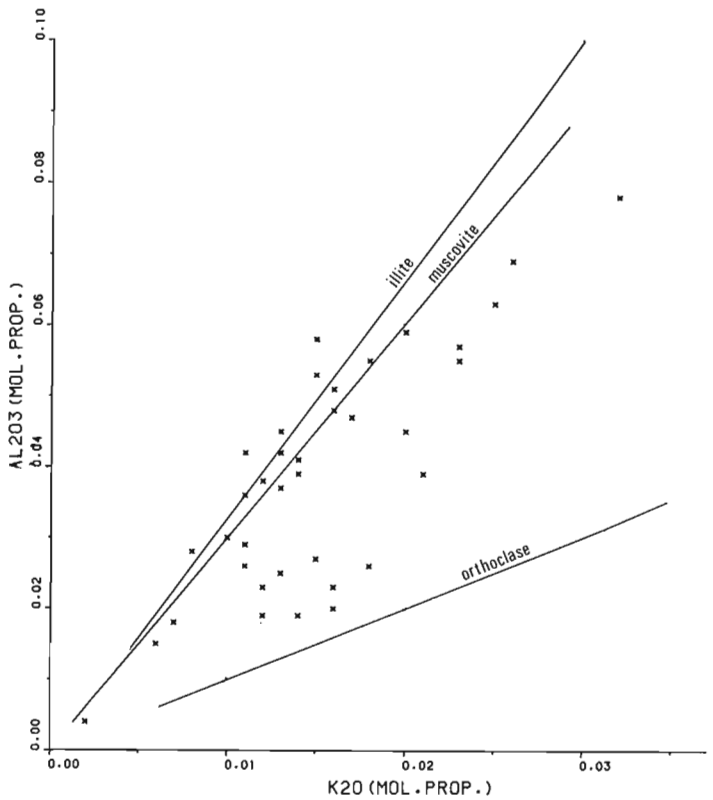

Figure 16.7. *Binary plot of the molecular proportions of Al_2O_3 and K_2O in shales, cherts and carbonates from Section 44. The stoichiometric compositions of illite, muscovite and orthoclase are also plotted.*

Group 2: Elements falling within the group form, or substitute readily into the lattice of feldspar and illite. The association of H_2O with Al, Rb, Cs and Pb indicates that illite is probably the dominant host mineral. This interpretation, which is based on a binary plot of Al_2O_3 and K_2O (Fig. 16.7) that shows all samples plotting between the stoichiometric compositions of illite and orthoclase, is supported by XRD analyses which show that illite is the only major mineral hosting K_2O present. Small amounts of K-feldspar are indicated from Figure 16.7 although none was detected by XRD methods.

Group 3: This group of elements consisting of Fe, Co and Ti form very stable refractory oxides such as leucoxene which are most likely derived from the weathering of alkali basalts that occur within the sequence. Volcanic rocks comprise submarine lapilli tuffs, volcanogenic siltstones, sandstones and conglomerates with some massive flows. The volcanic siltstones, sandstones and conglomerates have been found in numerous areas of the embayment demonstrating that there has been considerable reworking of these volcanic rocks.

Group 4: This group of elements form or are incorporated into carbonates, sulphates and possibly minor silicates. The high Sr accompanies the carbonates (mostly calcite) in unit RRa2 and also the barite in unit RRs. Although P also plots within this group and has been identified as fluorapatite in the shale unit (RRs); its mineral form in the other units is unknown.

The positioning of Mg and Mn in the same quadrant somewhat removed from the calcite field may result from the presence of these elements in chlorite as well as dolomite. Plagioclase, which has been identified in the shales, is considered the main mineral hosting Na. The association of Na with Mg and Mn is most likely due to a common volcaniclastic origin for much of the chlorite and plagioclase.

Comparison Between Misty Creek Shales and Average Shales

Compared to average shales described elsewhere (Vine and Tourtelot, 1970; Turekian and Wedepohl, 1961; Green, 1959), shales from Section 44 through the Road River Formation of the Misty Creek Embayment are enriched overall in Ag, Sb, Cd, Ba, V, Ce and possibly Zn and Mo (Table 16.2). The content of trace and minor elements for each unit in Section 44 is compared with average shales (Turekian and Wedepohl, 1961; Cameron and Jonasson, 1972) in Figure 16.3. The shales and interbedded cherts located at the top of unit RRc have a high abundance of Zn, Cu, Ag, Mo, Hg, Sb, Cd, V, Ce and Ba whereas the lower portions of this unit comprising mostly silty carbonates are concentrated only in Zn, Sb, Ba, Ce, Sr and V.

Unit RRa2 representing mostly silty carbonates is depleted in most of the trace and minor elements except for Sr which substitutes readily into calcite. Although the carbonate component will have a tremendous dilution effect, this factor alone cannot account for the low contents of all elements.

The lower portions of unit RRs are slightly enriched in Zn, Mo, Hg, Sb, Cd, Ba and V, at least when compared to the average shale estimates of Turekian and Wedepohl (1961). Barite occurs in this unit and is overlain by shales that are enriched in P_2O_5 (Fig. 16.2).

Stratigraphic Geochemistry

One of the major objectives of carrying out geochemical and mineralogical studies of a stratigraphically controlled section was to assess the use of geochemistry in supporting stratigraphic studies. This objective is of importance in situations where it is advantageous to understand the physicochemical processes affecting the source, transport and deposition of elements in marine basins. For example, the trace element contents and the manner in which they are fixed in the shales can give valuable information on the Eh and pH, temperature, provenance of sediments, salinity and the nature of volcanic activity. The recognition of periods of volcanism or related hydrothermal activity, even though their contribution to the sedimentary sequence may be very small, is extremely important considering the common association of volcanic rocks and sediment-hosted stratabound sulphide deposits.

Geochemical and mineralogical studies of shales carried out elsewhere include Middle Ordovician shales from Norway (Bjørlykke, 1965), Ordovician shales from Wales (Bjørlykke, 1971), Cambrian alum shales, Sweden (Armands, 1973), lower Paleozoic shales from Scotland (Stephens et al., 1975) and lower Cretaceous shales from western Canada (Cameron, 1965). Most of these studies, carried out on stratigraphically controlled sections, assessed the various factors influencing the composition of the shales.

In the Misty Creek Embayment, the broad lithostratigraphical divisions described by Cecile (1978) for the Road River Formation are supported by geochemical profiles in Section 44 (Fig. 16.2, 16.3). Compared to shales described elsewhere (Table 16.2), shales and silty carbonates are characteristically enriched in Ba, Ce and, to a lesser extent, Cd and V. The remaining trace elements are about the same or lower due partly to the dilution effect of carbonate. Each unit with its characteristic element associations and possible subdivisions is discussed below.

Table 16.2

Estimates of element abundance in shales, cherts and carbonates from the Road River Formation, Yukon and average shale and black shale described elsewhere

	Road River Formation			Average black Shale	Average Shale	
	Shales (RRs)	Argillaceous Carbonates (RRa2)	Shale and Chert (RRc)	Vine and Tourtelot, 1970)	Turekian and Wedepohl (1961)	Green (1959)
Element (%)	n=9	n=12	n=12			
SiO_2	37.8	22.9	44.2	-	17.1	50.7
Al_2O_3	5.0	2.8	4.7	13.2	15.1	14.7
TiO_2	0.33	0.26	0.19	0.33	0.33	0.73
FeO_T	2.06	1.62	1.30	2.58	6.07	5.53
MgO	3.7	4.2	5.1	1.16	2.59	3.15
CaO	22.5	33.7	20.9	2.10	3.09	7.28
Na_2O	0.22	0.10	0.13	0.94	1.29	0.88
K_2O	1.70	1.28	1.54	2.41	3.20	3.37
MnO	0.030	0.027	0.016	0.019	0.110	0.865
P_2O_5	0.42	0.16	0.23	-	0.160	-
CO_2	21.10	31.58	18.93	-	-	9.63
H_2O	1.83	1.30	2.34	-	-	-
C org.	1.06	0.77	1.15	3.2	-	0.65
S	0.61	0.25	0.28	-	0.24	-
Element (ppm)						
Zn	116	28	217	<300	95	80
Cu	23	12	31	70	45	38
Pb	8.8	7.6	9.4	20	20	20
Ni	15.1	5.3	16.8	50	68	21
Co	5.4	3.6	3.1	10	19	12
Ag	0.34	0.20	0.54	<1	0.07	0.09
Mo	6.0	2.2	6.2	10	2.6	0.74
As	5.2	2.1	5.9	-	13	-
Hg*	51.2	21.0	55.4	-	400	-
Sb	1.8	0.16	3.3	-	1.5	-
Cd	4.3	4.1	6.2	-	0.3	-
U	2.7	1.2	2.8	-	3.7	-
Ba	6073	779	1291	300	580	800
V	198	29	275	150	130	130
Ce	222	236	236	-	59	-
Cr	16.2	<5.0	11.0	100	90	160
Sr	706	815	384	200	300	299
Zr	96	89	112	70	160	200

*Hg measured in ppb; n number of samples

Shale Unit (RRs)

This unit can be subdivided into a lower argillaceous unit where dolomite is the dominant carbonate (Fig. 16.8) and an upper calcareous unit. The lower unit is characterized by abundant Si, K, C, Cu, Pb, Ag, Mo, As, Hg, Sb and V when compared to the upper unit that contains relatively higher contents of Mg, P, Mn and Sr. The presence of chalcophile elements associated with high Ba, V, Ni and organic carbon may be evidence for a hydrothermal event, possibly accompanying the formation of the basin due to faulting. The increase of carbonate in the upper portions of RRs may be controlled by shallowing of the basin or may reflect an increased proportion of carbonate detritus derived from platform areas. An increase in the content of chlorite in the upper portions of unit RRs is considered to reflect a period of volcanic activity. Additional evidence for a minor volcanic event in this unit is the high ratio of Mg and Fe to total alkalis (Fig. 16.9). The presence of Na (Fig. 16.2) as plagioclase identified by XRD methods may also prove very useful

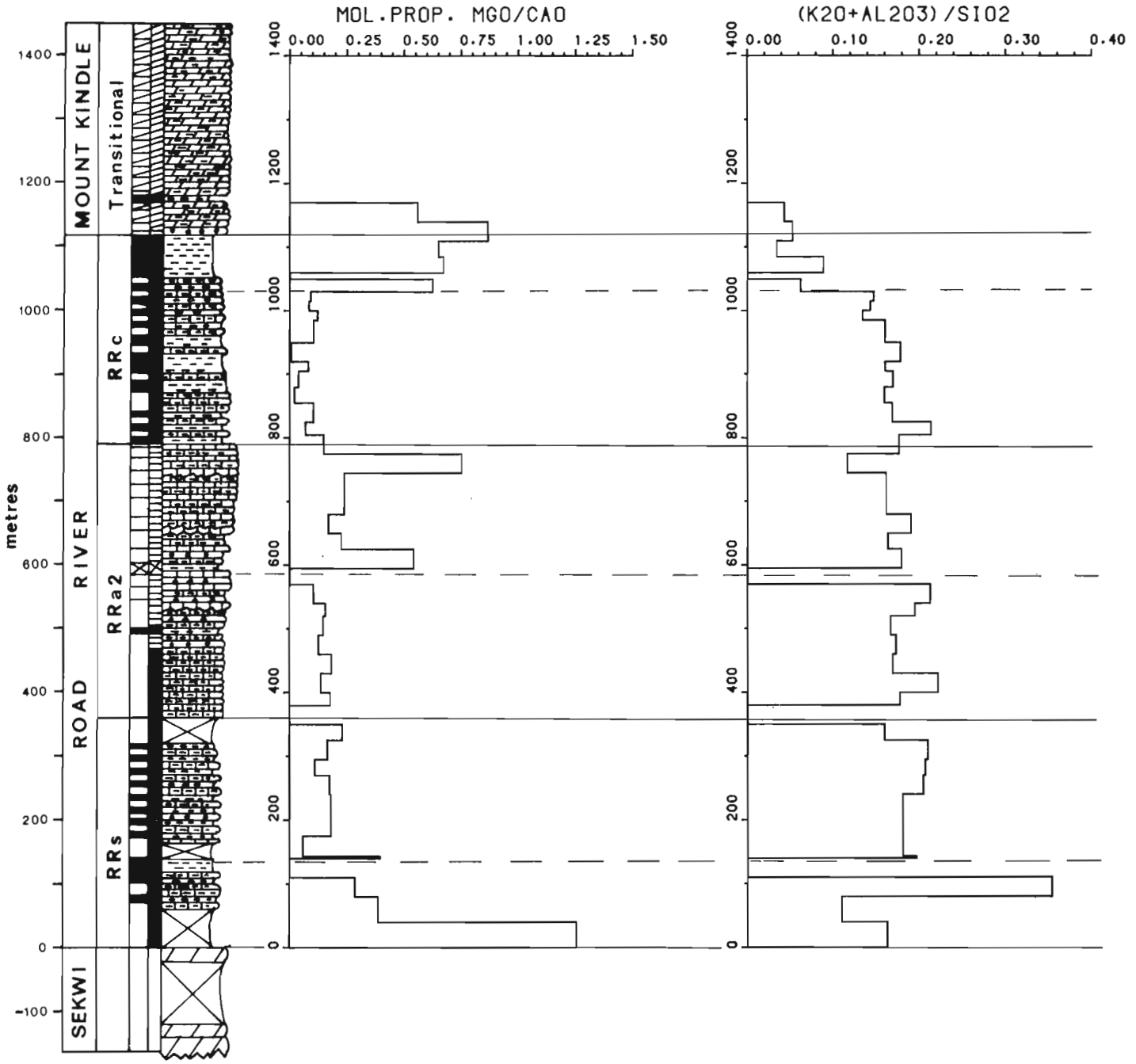

Figure 16.8. *Plots of the distribution of the ratio of the molecular proportions of MgO and CaO and the ratio of $K_2O+Al_2O_3$ and SiO_2 on Section 44.*

in defining a volcanic event if the plagioclase represents a pyroclastic or epiclastic component of a volcanogenic sediment and is therefore not an authigenic mineral.

Rabbitkettle Formation (RRa2)

This unit is composed primarily of limestone and dolomite and can be subdivided into a lower terrigenous unit and an upper carbonate unit. The upper unit differs from the lower unit by having a higher proportion of dolomite to calcite (Fig. 16.8) and lower contents of elements such as Al, Ti, Fe and Co that are found in clays and refractory oxides.

Chert-shale (RRc)

This unit is characterized by a lower silty limestone and a thin upper unit composed of shale and chert. The lower limestone contains minor amounts of dolomite (Fig. 16.8) and abundant illite contributing to high contents of Al and K. Volcanic activity that extruded basaltic tuffs and flows at Section 40 (Cecile, 1978) is reflected in Section 44 by high contents of Ti, Cr, Mg, Na and perhaps indirectly by chalcophile elements such as Zn, Cu, Ni, Co, Ag, As and Sb. The organic carbon content increases rapidly in this unit and remains high in the overlying unit.

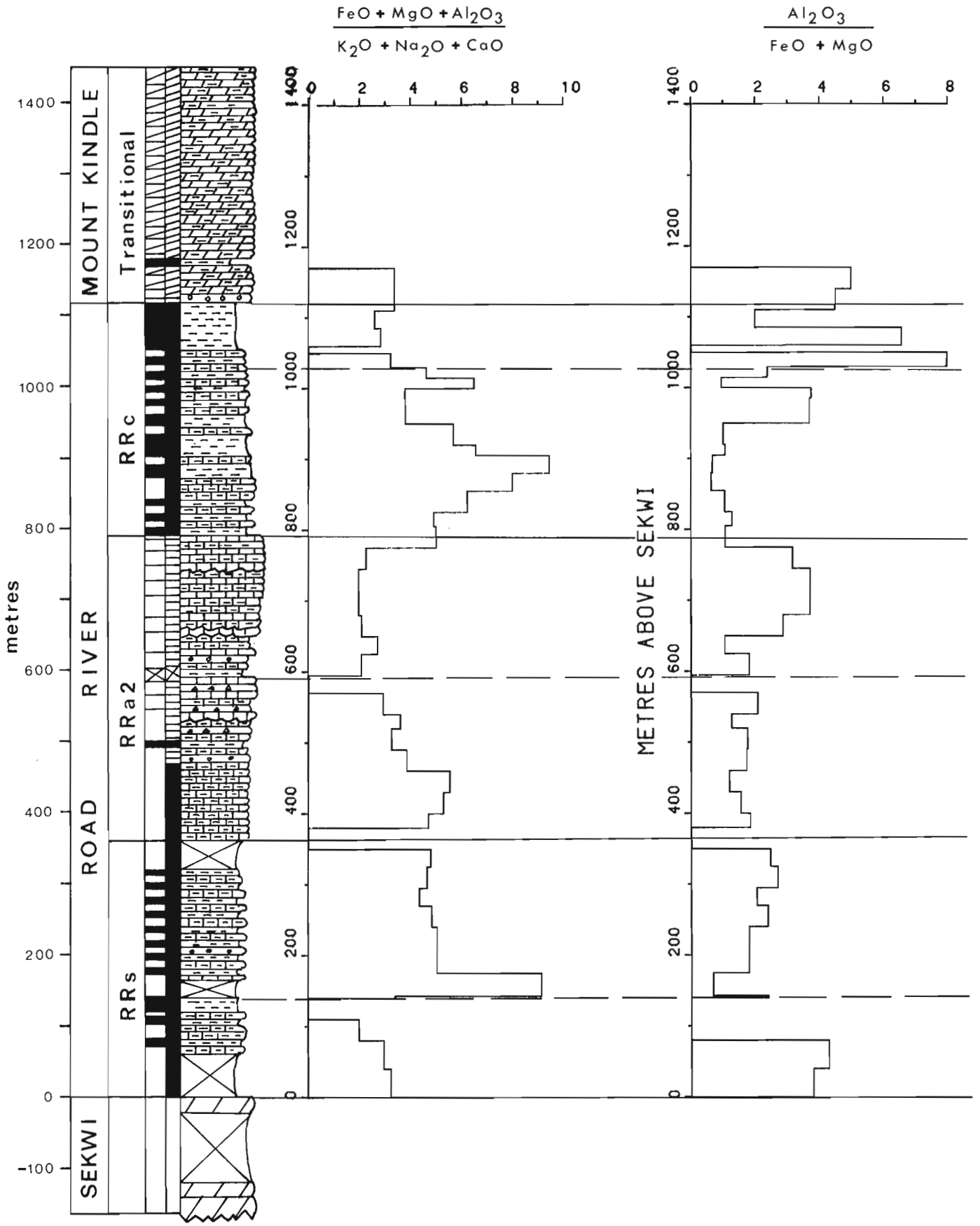

Figure 16.9. *Element oxide ratios calculated on a carbonate-free basis for Section 44 that were used by Englund and Jorgensen (1973) to classify argillaceous sediments.*

The upper unit is composed primarily of shale and chert. The carbonate component, albeit minor, consists of dolomite with minor calcite (Fig. 16.8).

Conclusions

The following conclusions are drawn from geochemical and mineralogical data from Section 44 through the Road River Formation interpreted in light of the overall stratigraphy and geological history of the Misty Creek Embayment.

1. Using the trace and minor element chemistry of rocks from Section 44, it was possible to define chemically and to substantiate the divisions of Cecile (1978) as well as suggest further subdivisions within each unit. Major element assemblages were readily interpreted in terms of the mineralogy determined by XRD methods. Trace element assemblages could also be accommodated according to their expected behaviour in the various mineral phases.
2. The volcanic event represented by mafic tuffs and flows at the base of unit RRc could also be recognized chemically in Section 44 although no visible volcanic rocks were present. Moreover, geochemical evidence for a hydrothermal event associated with minor volcanic activity is interpreted to be present in unit RRs.
3. The trace and major element chemistry of the volcanic rocks indicated that they were alkaline in composition, high in certain rare earth elements, Ti and Ba and are considered characteristic of basalts formed in extensional tectonic environments. Certain elements such as Ba, Zn, Sb, Cd and V that are high in the volcanic rocks and in the sedimentary strata on the same stratigraphic horizon some distance from the volcanic rocks are interpreted as having a common origin.

Acknowledgments

The following individuals are thanked for either supervising or carrying out chemical analysis of rocks: G. Lachance and H. Champ of the Central Laboratories and Technical Services Division; and G.E.M. Hall, A. MacLaurin and G. Gauthier of the Resource Geophysics and Geochemistry Division. A.G. Plant confirmed by XRD methods the occurrence of celsian in the igneous rocks. XRD identifications of silicate and carbonate minerals in the shales were made by R. Delabio. A computer program for plotting chemical data on stratigraphic sections was written by N.G. Lund.

References

Aitken, J.D. and Cook, D.G.
1974: Geological maps showing bedrock geology of the northern part of Mount Eduni and Bonnet Plume map areas, District of Mackenzie, N.W.T.; Geological Survey of Canada, Open File 221.

Aitken, J.D., Macqueen, R.W., and Usher, J.L.
1973: Reconnaissance studies of Proterozoic and Cambrian stratigraphy, lower Mackenzie River area (Operation Norman), District of Mackenzie; Geological Survey of Canada, Paper 73-9.

Armands, G.
1973: Geochemical studies of uranium, molybdenum and vanadium in a Swedish alum shale; Stockholm Contributions in Geology, v. 27, p. 1-148.

Bjørlykke, K.
1965: The Middle Ordovician of the Oslo Region, Norway. No. 20. The geochemistry and mineralogy of some shales from the Oslo region; Norsk Geologisk Tidsskrift, v. 45, p. 436-456.

1971: Petrology of Ordovician sediments from Wales; Norsk Geologisk Tidsskrift, v. 51, p. 123-139.

Bjørlykke, K.O. and Griffin, W.L.
1973: Barium feldspars in Ordovician sediments, Oslo region, Norway; Journal of Sedimentary Petrology, v. 43, p. 461-465.

Blusson, S.L.
1971: Sekwi Mountain map-area, Yukon Territory and District of Mackenzie; Geological Survey of Canada, Paper 71-22.

1974: Five geological maps of the northern Selwyn Basin (Operation Stewart), Yukon Territory and District of Mackenzie, N.W.T. (105N, O; 106A, B, C); Geological Survey of Canada, Open File 205.

Cameron, E.M.
1965: Application of geochemistry to stratigraphic problems in Lower Cretaceous of western Canada; American Association of Petroleum Geologists Bulletin, v. 49, no. 1, p. 62-80.

Cameron, E.M. and Jonasson, I.R.
1972: Mercury in Precambrian shales of the Canadian Shield; Geochimica et Cosmochimica Acta, v. 36, p. 985-1005.

Cecile, M.P.
1978: Report on Road River stratigraphy and the Misty Creek Embayment, Bonnet Plume (106B), and surrounding map-areas, Northwest Territories; in Current Research, Part A, Geological Survey of Canada, Paper 78-1A, p. 371-377.

Diller, J.D.
1898: The educational series of rock specimens collected and distributed by the United States Geological Survey; U.S. Geological Survey Bulletin, v. 150, p. 1-400.

Engel, A.E.J., Engel, C.G., and Havens, R.G.
1965: Chemical characteristics of oceanic basalts and the upper mantle; Geological Society of America Bulletin, v. 76, p. 719-734.

Englund, J.O.
1973: Studies on the latest Precambrian and Eocambrian rocks in Norway. No. 12. Geochemistry and mineralogy of pelitic rocks from Hedmark Group and the Cambro-Ordovician sequence, southern Norway; Norges Geologiske Undersoleilse, v. 286, p. 1-60.

Englund, Jens-Olaf and Jorgensen, Per.
1973: A chemical classification system for argillaceous sediments and factors affecting their composition; Geologiska Foreningen i Stockholm Foerhandlingar, v. 95, p. 87-97.

Gay, P. and Roy, N.N.
1968: The mineralogy of the potassium-barium feldspar series. III: subsolidus relationships; Mineralogical Magazine, v. 36, p. 914-932.

Gabrielse, H., Blusson, S.B., and Roddick, J.A.
1973: Geology of the Flat River, Glacier Lake and Wrigley Lake map-areas, District of Mackenzie and Yukon Territory; Geological Survey of Canada, Memoir 366.

Green, Jack
1959: Geochemical table of elements for 1959. Geological Society of America Bulletin, v. 70, no. 9, p. 1127-1183.

Hawkins, J.W., Allison, E.D., and MacDougall, D.
1971: Volcanic petrology and geologic history of Northeast bank, southern California borderland; Geological Society of America Bulletin, v. 82, p. 219-228.

Jonasson, I.R., Lynch, J.J., and Trip, L.J.
1973: Field and laboratory methods used by the Geological Survey of Canada in geochemical surveys: No. 12, Mercury in ores, rocks, soils, sediments and water; Geological Survey of Canada, Paper 73-21.

Kulling, O.
1933: Bergbyggnoden inom Bjorkvattnet Virisen-omradet i Vasterbottenfjellens centrala del; Geologiska Foreningen i Stockholm Foerhandlingar, v. 55, p. 167-422.

Lamborn, R.E., Austin, C.R., and Schaaf, D.
1938: Shales and surface clays of Ohio; Geological Survey of Ohio, Series 4, Bulletin 39, 20 p.

Lane, A.C.
1911: The Keweenaw series of Michigan; Michigan Geological Survey Division, Publication 6, Series 4.

Maksimova, S.V.
1978: Biogenic silicites: an index of activation of abyssal fracture; International Geology Review, v. 21, p. 869-876.

Nanz, R.H.
1953: Chemical composition of pre-Cambrian slates with notes on the geochemical evolution of lutites; Journal of Geology, v. 61, p. 51-64.

Page, D.C. and Watson, M.D.
1976: The Pb-Zn deposit of Rosh Pinah Mine, South West Africa; Economic Geology, v. 71, p. 306-327.

Roy, N.N.
1967: The mineralogy of the potassium-barium feldspar series II. Studies on hydrothermally synthesized members; Mineralogical Magazine, v. 36, p. 43-49.

Segnit, E.R. and Gelb, T.
1970: Reactions of kaolinite with barium carbonate and barium sulphate; Australian Journal Ceramic Society, v. 6, p. 12-18.

Stephens, W.D., Watson, S.W., Philip, P.R., and Wier, J.A.
1975: Element associations and distributions through a lower Paleozoic graptolitic shale sequence in the Southern Uplands of Scotland; Chemical Geology, v. 16, p. 269-294.

Turekian, K.K. and Wedepohl, K.H.
1961: Distribution of elements in some major units of the Earth's crust; Geological Society of America Bulletin, v. 72, p. 175-192.

Vesterberg, K.A.
1927: Undersokningar over alunskiffer; Ingenjörsveten-skapsakademien Handlingar, no. 62, Stockholm 1927, p. 1-47.

Vine, J.D. and Tourtelot, E.B.
1970: Geochemistry of black shale deposits – a summary report; Economic Geology, v. 65, p. 253-272.

17.

NAHANNI INTEGRATED MULTIDISCIPLINARY PILOT PROJECT
GEOCHEMICAL STUDIES PART 2: SOME THOUGHTS ON THE SOURCE, TRANSPORTATION AND CONCENTRATION OF ELEMENTS IN SHALES OF THE MISTY CREEK EMBAYMENT, NORTHWEST TERRITORIES

Projects 790033, 770044, 740107

W.D. Goodfellow[1], I.R. Jonasson[1], and M.P. Cecile[2]

Goodfellow, W.D., Jonasson, I.R., and Cecile, M.P., Nahanni Integrated Multidisciplinary Pilot Project. Geochemical Studies Part 2: Some thoughts on the source, transportation and concentration of elements in shales of the Misty Creek Embayment, Northwest Territories; in Current Research, Part B, Geological Survey of Canada, Paper 80-1B, p. 163-171, 1980.

Abstract

Paleozoic shales and cherts from Section 44 in the Misty Creek Embayment are enriched in Ba, Ce, V, Ni and chalcophile elements such as Zn, As, Hg, Cd, Sb and Ag. The chalcophile elements correlate strongly with carbonaceous matter than can range up to 2.1 per cent in the shale unit (RRs). Although certain marine organisms can accumulate metals many times their content in seawater, it is considered unlikely that this mechanism alone can explain the high levels of all elements found in the shales. The enrichment in the volcanic rocks of the same elements found in the interbedded shales supports the view that at least some of the metals owe their origin to hydrothermal fluids expelled into the seawater during volcanic activity. The presence of celsian in both the volcanic rocks and hypabyssal equivalents indicates that at least some of the Ba present as barite in the Selwyn Basin in rocks ranging in age from Cambrian to Late Devonian may be derived from fluids vented onto the seafloor.

The behaviour of metal-rich fluids away from points of discharge is affected by several factors that include water depth, basinal chemical environment, and fluid chemistry. In the Misty Creek Embayment near Section 40, the water was shallow at the time of the volcanic event. As a result, boiling of thermal fluids would most likely occur promoting the rapid oxidation of dissolved reduced sulphur species. Elements such as Ba that form insoluble sulphates would be precipitated whereas others such as Zn, Ni, V, Co and Ag that can be accumulated by micro-organisms or degrading carbonaceous matter would be expected to be dispersed away from the conduit. The low level of Pb in the Misty Creek shales compared to shales and siltstones hosting the nearby Tom Pb-Zn-Ba deposit may be attributed to chemical conditions prevalent in the basin at the time of thermal fluid discharge which restrict its geochemical mobility.

Introduction

Goodfellow et al. (1980) discussed the geochemistry and mineralogy of shales, cherts and carbonates from Section 44 and volcanic rocks from Section 40 through the Road River Formation, Misty Creek Embayment, Northwest Territories. Compared to other units the shales and cherts comprising unit RRc and the shales comprising unit RRs are characterized by relatively higher contents of the following elements: Zn, Mo, As, Hg, Cd, Sb, Ag, Ba, Ce, V and Ni. The chalcophile elements correlate strongly with carbonaceous matter that can range up to 2.1 per cent in the shales. Although world averages for shales vary tremendously depending on the particular shales selected, the shales from the Misty Creek Embayment are clearly enriched in Zn, Ag, Mo, Sb, Cd, Ba, V, Ce and Sr when compared to average shales described elsewhere (Vine and Tourtelot, 1970; Turekian and Wedepohl, 1961; Green, 1959). The Hg content of the Misty Creek shales is also anomalously high when compared to its average content (40 ppb) in Phanerozoic shales (Cameron and Jonasson, 1972) which is one tenth that determined by Turekian and Wedepohl (1961) for all shales.

Although certain marine organisms can accumulate metals many times their content in seawater, it is considered unlikely that this mechanism alone can explain the high levels of certain elements found in the Misty Creek shales. The enrichment in the volcanic rock of some of the same elements found to be high in the interbedded shales and cherts (e.g. Zn, Ni, Mo, Sb, Cd, Ba, Ce, V and Ag) supports the view that at least some of the metals owe their origins to hydrothermal fluids expelled onto the seafloor during volcanic activity. This mechanism of metal supply and accumulation is active on ocean ridges and other tectonically active areas where geothermal fluids are supplying elements that are concentrated in the associated sediments. It is the intention of this paper to discuss possible sources of the elements noted above and to suggest mechanisms by which they might be dispersed from presumed spring-vent discharge areas into the sediments of the Misty Creek paleobasin.

Possible Sources of Metals

In geothermal areas, springs active on the seafloor have been shown to supply metals that accumulated locally in the seawater and accompanying sediments. Areas where metalliferous fluids have been expelled onto the seafloor include the East Pacific Rise (Toth, 1980; Bostrom and Peterson, 1966) and Galapagos Rift (Edmond et al., 1979a, b; Corliss et al., 1979), the Red Sea trough (Miller et al., 1966; Craig, 1969) and East African Rift (Bonatti et al., 1972), Matupi Harbour, New Britain (Ferguson and Lambert, 1972), and along the coast of Southern California (Lonsdale, 1979; Vidal et al., 1978). In most of these areas, the conduits are localized along faults or structures intersecting either oceanic or continental crust. The fluids debouched onto the seafloor contain generally high contents of Cu, Pb, Zn, Ba, Ag, Mn, Fe, SiO_2 and dissolved salts when compared to average seawater (Table 17.1). The higher temperature fluids can carry in addition to these elements high contents of As, Bi, Sb, Hg and Au (White, 1965). Temperatures vary considerably depending on whether brine pools or fluids trapped in geothermal reservoirs such as the Salton Sea are measured. In the latter case, temperatures in excess of 300°C have been measured (White, 1965) whereas the Red Sea brines have had time to cool at 56°C in the Atlantis II Deep (Miller et al., 1966) and to 44.7°C in the Discovery Deep (Swallow and Crease, 1965).

[1] Resource Geophysics and Geochemistry Division

[2] Institute of Sedimentary and Petroleum Geology, Calgary

Table 17.1

Compositions of some geothermal fluids and average seawater

	A	B	C	D
Ore metals deposited	-	Cu,Ag,Fe As,Sb,Bi	Zn,Cu,Pb Ag,Sb,Bi	Zn,Cu,Pb Mn,Fe
Temperature	-	>300°C	56°C	65°C
Element content (g/L)				
Cu	2×10^{-6}	0.010	0.00026	0.00005
Pb	3×10^{-8}	0.104	0.00063	0.00009
Zn	5×10^{-6}	~0.300	0.0054	0.00253
Ag	28×10^{-8}	0.001	-	-
As	26×10^{-7}	0.015	-	0.00002
Mn	1×10^{-6}	2.0	0.082	0.111
Fe	1×10^{-6}	3.2	0.081	0.097
Ba	15×10^{-6}	0.2	0.009	0.097
				-
Na	10.8	64	92.8	13.6
K	0.39	32	1.87	0.756
Ca	0.41	51	5.15	0.395
Mg	1.30	0.92	0.764	1.34
SO_4	2.72	0.071	0.84	5.42
Cl	19.5	234	155.5	22.5
SiO_2	6.2	~0.1	0.059	-
Al	0.001	0.45	-	-

A. Average composition of seawater (after Turekian, 1969; Miller et al., 1966).

B. Salton Sea, geothermal brine (White, 1965).

C. Atlantis II Deep, Red Sea (after Craig, 1969; Miller et al., 1966).

D. Tavurvur Shore, Matupi Harbour, New Britain (after Ferguson and Lambert, 1972).

In the Misty Creek Embayment, the metalliferous carbonaceous shales from the Road River Formation are associated with volcanism in the chert-shale unit (RRc) and possibly in the lower shale unit (RRs) (Goodfellow et al., 1980). In the shale-chert unit (RRc), altered lapilli and fine grained tuffs occur adjacent to extensional structures. Although both the volcanic rocks and feeder intrusions are intensely altered, the stable element chemistry indicates that they were most likely derived from an alkaline magma (Schwarzer and Rogers, 1974).

The mafic volcanic rocks and feeder intrusions have been shown to be intensely altered to chlorite, kaolinite, tremolite-actinolite and carbonate (Goodfellow et al., 1980) most likely by hydrothermal fluids. The suite of enriched elements (e.g. Ba, Cs, La, Ce, Zn, Pb, Co, As, Hg, Sb, Cd, V and F) includes most of the elements enriched in hydrothermally altered volcanic rocks located off the coast of Northern Baja California (Vidal et al., 1978). Here, hot metalliferous springs escaping into seawater along major faults have intensely altered associated volcanic rocks and deposited pyrite and up to 7000 ppm As, 3.0 per cent Ba, 7000 ppm Hg, 1000 ppm Sb, 1500 ppm Sr, 700 ppm Tl and 150 ppm Zn. The thermal springs are acid and enriched in Fe, Mn, Zn, Ba and As demonstrating that elements such as Sb, Hg, Cd, Tl and Sr are being precipitated completely from solution at the orifices as a result of a rapid temperature drop.

In the igneous rocks from the Misty Creek Embayment, the Ba is present as celsian which occurs as clear crystals often situated adjacent to K-feldspar. At this time barite has not been identified in these samples. Other than pyrite, the minerals hosting the chalcophile elements have not been identified although the association with high S (up to 1.19%) combined with their insoluble character as sulphides indicates that they most likely formed or are incorporated in sulphides.

Several sources for the metals enriched in the volcanic rocks are possible and without isotopic evidence, it is difficult to choose one over the other. Nevertheless, it may be useful to discuss the possible sources of metals in the light of existing information. These would include: (i) the upper mantle which is considered by Gast (1968) to be the site of generation of alkaline magmas; (ii) the underlying sedimentary rocks that may have been leached of their metals by migrating connate water; or, what seems more likely, (iii) a combination of both. The enrichment of large radius elements (e.g. Ba, K, Sr, Cs, La and Ce) in the mafic igneous rocks from the Misty Creek Embayment could be due to magma derivation from a previously undifferentiated mantle source or equilibration of magma depleted in large radius elements with wall rocks enriched in these elements (Gast, 1968). Field observations, however, indicate that the feeder intrusions are essentially free of xenoliths and probably not contaminated extensively with crustal material.

Elements that are incompatible in the high pressure and temperature region of the mantle and therefore are considered mantle rejects by Mercy (1967) include: (i) constituents with large ionic radii (e.g. Ba, Sr, K, Cs, Tl and the rare earths); (ii) constituents with high vapour pressures (e.g. CO_2, H_2O, Sb, Hg, As, HCl and fluoroborates); and (iii) constituents with high aqueous solubilities (e.g. NaCl, KCl).

In addition to being enriched in major elements with large ionic radii, the Misty Creek volcanic rocks contain above average contents of Fe, Cl, Zn, Pb, Co, As, Hg, Sb, Cd, Be, CO_2 and H_2O. Using the criteria for mantle rejection discussed above, it is possible that enriched elements such as Ba, Cs, La, Ce, F, Cl, Hg, As all originated in the mantle. It is interesting to note that this suite of elements, with the possible exception of Hg and As, is characteristic of carbonatites that form along continental rifts and are considered to be derived from the mantle (Heinrich, 1966; Tuttle and Gittins, 1966).

Other elements, however, that are not normally considered mantle rejects (e.g. Pb, Zn, Co, Sb, Cd, Be) and possibly some of the elements that are considered mantle rejects, may have been leached from the underlying sediments by migrating connate fluids. Waters laden with metals and trapped in the underlying sedimentary rocks under considerable load pressure would most likely escape along the same extensional structures that served as conduits for the extrusion of magma.

Mechanisms of Metal Transport and Accumulation in Misty Creek Shales

In sediments of the Misty Creek Embayment unusually high levels of certain elements, viz., Ba, Zn, Cd, V, Sr, and Ce have been measured. Others such as Pb are of lower abundance than for an average shale. It has been demonstrated here that thermal waters already enriched in these elements can provide the prime source of supply. It remains to account for their relative distribution, with respect to presumed points of fluid discharge, in terms of likely mechanisms of accumulation involving both organic and inorganic moieties.

Firstly, a comparative inspection is required of available data on the behaviour of fluids away from points of discharge in some of the thermal zones already described here. Whether or not these situations are relevant to the Misty Creek setting is also worthy of attention.

The chemical behaviour of fluids away from points of discharge has been investigated near Santorin Volcano in the Aegean Sea (Pushkina, 1967; Smith and Cronan, 1975), the Atlantis II Deep and Nereus Deep in the Red Sea (Bignell et al., 1976), the East Pacific Rise (Bostrom and Peterson, 1966; Corliss et al., 1979) and the Salton Sea geothermal area (White, 1965). In discharge pipes from erupting Salton Sea geothermal brine, high contents of Cu, Fe, Ag, Sb, As and Bi were deposited as sulphides (White, 1965). The ore minerals identified were bornite, digenite, djurkite, pyrite, chalcopyrite, stromeyerite, native silver, tetrahedrite, arsenopyrite, galena and fluorite. From the high temperature (~220°C) discharge fluids, the relatively insoluble sulphides of As, Sb and Bi were deposited. The soluble components including Zn, nearly all the Pb, and most of the Fe, Ba and Mn were transported on beyond the sites of deposition in the discharge pipes.

Near the Galapagos Rift in the East Pacific Ocean, the geothermal fluids are concentrated in Ba, H_2S, Fe, Mn, CO_2 and SiO_2 and low in Cu, Ni and Cd, due to the presence of hydrogen sulphide which leads to the precipitation of these metals along with iron sulphides within the altered ocean floor basalts (Corliss et al., 1979). On the seafloor, mounds are formed by warm circulating fluids that precipitate Fe and SiO_2 in the reducing interiors, Mn at the surface, and carry significant flux of Mn and Ba into the bottom waters. The Ba and Mn are then dispersed by currents and deposited over large areas adjacent to the East Pacific Rise (Bostom, 1973). In other areas along the East Pacific Rise, however, pyrite, marcasite, sphalerite and chalcopyrite in association with amorphous silica and iron oxides occupy troughs along the axial zone (Francheteau et al., 1979). Other metals associated with these sulphides are Co, Ag, Pb and Cd.

The studies carried out on the Galapagos Rift (Corliss et al., 1979; Edmond et al., 1979a, b) provide valuable information not only on physical and chemical behaviour of the expelled fluids but also on the stimulative influence of these fluids on the biological activity in the areas of discharge. Flourishing marine organisms reflect the abundance of sulphur-oxidizing bacteria at the base of the food chain that feed on H_2S expelled by the thermal springs.

In the Aegean Sea, SiO_2, Mn, Fe, P, CO_2 and H_2S are expelled into the seawater by acid and reducing thermal springs that are active on the floor of the Santorin caldera (Pushkina, 1967). Upon interaction with the seawater, the pH and Eh increase rapidly, Fe hydrolyzes and is precipitated near the points of discharge whereas Mn is dispersed away from the vent as sols of manganous hydroxide (Smith and Cronan, 1975). Eventually Mn^{+2} is oxidized to MnO_2 and deposited with sorbed Zn in the ocean sediments.

The fractionation of Mn and Fe is also reflected in sediments associated with sulphide deposits in the Atlantis II Deep. Near the points of discharge within the brine pool, sulphides of Fe, Zn, Cu and Pb and iron silicates are precipitated, followed by limonite then manganite towards the flanks of the basin (Backer and Richter, 1973). In the sediments surrounding the Atlantis II sulphide deposit, Hg, Zn, Cu and Mn are anomalously high forming a halo that extends up to 10 km away from the edge of the deposit (Bignell et al., 1976). The seawater overlying the Atlantis II Deep is likewise enriched in these elements (Holmes and Tooms, 1973).

Although geothermally active ocean ridges can provide valuable information on the chemical and physical behaviour of fluids expelled onto the seafloor, they are not suitable as recent analogues of the Misty Creek Embayment, particularly in terms of geologic setting. The Misty Creek Embayment has been interpreted (Cecile, in preparation) as representing a fault-bounded possibly restricted basin that formed adjacent to the continental margin. The geometry and linear facies belts of the Embayment together with the alkaline composition of the mafic volcanic rocks indicate an extensional origin beginning in late Early Cambrian time and persisting to at least the end of Early Silurian. Although volcanic activity associated with extensional structures occurred during Ordovician and possibly Cambrian time, rifting did not occur to the extent where oceanic crust was generated. Therefore, the ocean rifts such as those occurring along the East Pacific Rise or the Red Sea are not suitable recent analogues of the Misty Creek Embayment, at least not in terms of the geologic setting. The Black Sea which is an elliptical anoxic basin characterized by a high geothermal gradient along the axis and interpreted to be underlain by a basaltic layer (Neprochnov et al., 1974) might be more closely analogous to the Misty Creek basin. The metal levels in the sediments (Hirst, 1974), however, are generally lower than those found in shales and cherts from units RRs and RRc.

Although it is unlikely that a modern basin that is similar in all respects to the Misty Creek Embayment can be found, the series of northwesterly trending troughs and ridges off the coast of Southern California appear similar in terms of the tectonic setting, composition of the volcanic rocks that are localized along structures, and the chemistry of hydrothermal fluids debouching onto the seafloor (Hawkins et al., 1971; Hawkins, 1970). The volcanic rocks are represented by seamounts composed of basalts and hyaloclastites of alkaline composition and characterized by high contents of Ba (up to 880 ppm). Some of the basaltic rocks are intensely

altered to chlorite, iddeingsite and hematite, and the vesicles are filled with chlorite or carbonate or both (Hawkins et al., 1971). The composition of these Upper Cenozoic volcanic rocks from Southern California and Baja California is interpreted to have resulted from the fractional crystallization under hydrous conditions in the upper mantle (Hawkins, 1970). Since all the Late Cenozoic volcanism shows a close spatial relation to fault zones, a genetic relation between faulting, regional dilation and volcanism is inferred.

Along the San Clemente fault zone at the foot of an escarpment formed by strike-slip faulting, columns and irregular piles of white crystalline barite (Lonsdale, 1979) are aligned along structures. Ba is believed to have been expelled onto the seafloor along faults similar to those controlling the site of hydrothermal activity in the Salton Sea geothermal area (White, 1965) and at Punta Banda (Vidal et al., 1978). In the latter case, thermal springs at temperatures in excess of 100°C precipitate pyrite and gypsum in the littoral zone.

All of these examples have one feature in common, the fluids are discharged into oxygenated ocean waters and the chemistry of element migration and deposition are influenced accordingly. Consequently they are not directly analogous to the Misty Creek Setting although certain aspects of the chemistry that relate to sites of fluid discharge rather than the nature of the overlying ocean water column will be applicable. It is likely that the Misty Creek Embayment contained bottom waters that were essentially anoxic and very likely reducing near points of discharge due to the presence of free hydrogen sulphide. Not only are the shales heavily carbonaceous, indicative of such conditions at sediment-seawater interface, but also they are commonly pyritic. Under these circumstances it is unlikely that stable accumulation of Fe and Mn oxides will be found. To date they have not been recognized. Trace elements migrating through the seawater which are trapped and coprecipitated by suspensions of these oxides e.g., V, Ni, Co, Zn, Pb, must accumulate in sediments by other mechanisms in the absence of these oxides. In the case of Pb and Zn, the first requirement is that they escape the sulphide-enriched zones near spring vents. These are likely analogous to zones of sulphide precipitation in basalts described by Corliss et al. (1979) in the Galapagos Rift system.

The factors, which are considered here to be the most important in determining dispersion and migration patterns for trace elements in the Misty Creek shales, are: i) the nature of discharging fluids, probably brines, carrying metals, ii) the interaction between brines and Misty Creek Embayment seawater, and iii) the involvement of organic matter both living and dead.

Organic Factors

Elements commonly enriched in shales (e.g. Cu, Zn, Ni, Hg, As, Sb, U and V) are characteristically associated with organic matter that is presumably derived originally from living organisms (Vine and Tourtelot, 1970; Swanson, 1961; Armands, 1973). Living organisms can accumulate specific elements in their cellular structures (e.g. C, S, Si, Ba, Ca, P). A number of other elements, especially metals, are considered essential elements (e.g. Mg, Co, Zn, and perhaps V). Some of each of these groups e.g., P and Fe are involved in biochemical energy transfer processes within cells or act as catalysts in enzyme-moderated reactions. Other metals such as Ni, Mo, and U are not considered important in biological processes but because of their strong adsorptive and complexation affinities towards carbonaceous matter are accumulated in dead and decaying organisms by replacement of, for example, Mg in chlorophyll. Other elements may be complexed directly by amino acids, lipids and humic acids which are degradation products of organism decay (Berner, 1968). The levels of enrichment for Ni, V, Zn, and Co in brown algae and marine animals (Table 17.2a) has been studied by Black and Mitchell (1952). In the case of brown algae, the enrichment of these elements commonly exceeds their concentration in seawater by more than three orders of magnitude. The enrichment of these elements in other marine micro-organisms can be even greater as shown in Table 17.2b (Trudinger and Bubela, 1967; Baas-Becking, 1959).

Micro-organisms may also affect dissolution and desorption of metals from clays and other sediment particles leading to an accumulation of those metals (Trudinger and Bubela, 1967). Such processes might be of particular importance where sediments comprise metal-rich ash and clay, other volcanic debris or iron oxides of hydrothermal origin. Micro-organisms interacting in these ways with sediment-bound metal generate sulphide minerals as products of reaction (Devigne, 1977).

In addition to directly accumulating metals in living organisms, organic matter may play an indirect role in the mobilization and fixation of certain metals dissolved in pore waters and trapped in the sedimentary sequence. The decaying organisms not only provide an excellent nutrient source for sulphate-reducing bacteria but also generate anoxic and even reducing conditions. Most chalcophile elements that form insoluble sulphides (e.g., Cu, Pb, Zn, As, Hg, Ag) would be precipitated as sulphides while other elements that form insoluble oxides in the reduced state (e.g. UO_2) would be fixed in the sedimentary sequence. An important byproduct of decaying organisms is CO_2 and it is often ignored in terms of the role it plays in adjusting pore water pH and in the formation of calcite during diagenesis (Berner, 1968). The common association of calcite, especially in nodular and concretionary forms, with organic-rich shales is most likely due to this process.

The sediments of the Misty Creek paleobasin have been shown to be enriched in a number of these elements whose dispersion behaviour is strongly affected by the presence of organic materials and especially by water soluble organic acids. In particular, Ni, V (as VO^{++}), Cu, Hg, Zn, As, Mo, Pb, U (as UO_2^{++}) form stable, soluble humates and fulvates (Jackson et al., 1978). Those which are not immediately precipitated as sulphides near spring discharge areas are rapidly sequestered by dissolved humic-acids and will remain in the water column until these complexes, sols and colloids are precipitated into organic rich shales. It is suggested that broad dispersions of Ni, V, and Zn observed in the Misty Creek shales formed in this way but were originally derived from the spring discharge areas.

The potential impact of colloidal processes in anoxic, reducing waters should not be ignored. Not only can metal ions or hydroxyions undergo complexation by dissolved and colloidal-size organic acids but molecular species such as metal sulphides can also be stabilized in colloidal "solution". Horzempa and Helz (1979) investigated the solution conditions under which a sol of CuS (covellite) could be stabilized in solutions of seawater composition. It was observed that simple sols of CuS were not protected from coagulation by divalent ions such as Ca^{++} or even Na^{+} at conditions typical of seawater and that it was necessary to protect these sols sterically with stable sheaths of humic acids for them to survive. Similarly, formation of humic-protected colloids of clays can stabilize them from coagulation and precipitation (Narkis and Rebhin, 1975) and the formation of SiO_2-organic adducts described by Fotiyev (1971) may also be attributed to these processes. The humic acid concentrations (5 mg-C/L) used in these experiments with CuS sols are quite reasonable for normal seawater.

If the same stabilization processes can be shown to apply to sols of say ZnS, PbS, FeS then it can be argued that this is a potentially important process for dispersing low concentrations of these metals through a sulphidic, anoxic environment. In basins starved of suspended particulates of clays, other metal oxides, which might act as adsorbers or counter-colloids (opposite surface charge), these protected colloids might remain in the water column for considerable periods of time before coagulation. Other colloids likely to be important in starved basins include silica and perhaps aluminosilica. In Misty Creek it is argued with some supporting literature evidence (Maksimova, 1978) that silica now present as chert was largely derived from the same spring vents that debouched base metals. Moreover colloidal or amorphous silica accumulations are commonly enriched in residual organic matter, perhaps an indication of interactions between colloidal silica and colloidal humic acids. Any trace ions with a strong affinity for humic acids, e.g., Ni^{++}, UO_2^{++}, Mo^{4+} and VO^{++} may also collect in resulting carbonaceous cherts. The distribution of Ni and V in Misty Creek shales may be influenced in this way.

Inorganic Factors

Barite has been identified by Cecile (1978) to occur at three stratigraphic levels within the Road River Formation in the Misty Creek Embayment. The mineral hosting Ba enriched in the shales in units RRc and RRs has not been identified although the high correlation of Ba and S (r=0.96) in these rocks suggests that it is barite. This is not unexpected considering that barite is the only significant Ba-phase in East Pacific Rise sediments (Bostrom et al., 1973). The barium occurs there as small (1-3 μm) crystals dispersed throughout the pelagic sediments (Church, 1970).

The mechanisms governing the migration of Ba away from the areas of fluid discharge have been studied in sediments along the East Pacific Rise. Brongersma-Sanders (1966) argued that Ba-carrying diatoms dispersed away from the rift zone along current directions and deposited the Ba in pelagic sediments. The siliceous diatoms may be destroyed easily which would explain the poor correlation between Ba and the host organisms. However, Bostrom et al. (1973) argued that some correlation between total mass of diatoms and Ba should exist although the total count of siliceous remnants of organisms revealed no such correlation. As an alternate explanation, the Ba derived from the thermal springs interacted with oxygenated seawater and precipitated barite directly on the seafloor.

The occurrence of barite at various stratigraphic intervals in the Misty Creek basin indicates that at least part of the basinal environment above the seawater-sediment interface was oxygenated. The presence and size of vesicles in basalts that are situated at the base of unit RRc suggest that they have been deposited in less than 500 m of water (Moore, 1965). It should be pointed out, however, that several factors other than the water depth will affect the size of vesicles. These include vapour pressures of dissolved gases and the composition and temperature of the magma. Assuming that the 500 m water depth is a reasonable

Table 17.2a

Concentration of trace elements in marine organisms

Element	Enrichment factor from brown algae (fresh weight)		Enrichment factor for marine animals (dry weight)	
	Black and Mitchell (1952)	Noddack and Noddack (1939)	Black and Mitchell (1952)	Noddack and Noddack (1939)
Ni	200-1000	1600-8000	5000	41 000
V	10-300	>160-5000	17 000	>280 000
Zn	400-1400	400-1400	32 500	32 000
Co	(<4500)	(13 000)	>7000	21 000

Table 17.2b

Concentration of elements from seawater by micro-organisms

Element	Concentration Factor (after Baas-Becking, 1959)	Element	Concentration Factor (after Baas-Becking, 1959)
Na	10^{-2}	Si	10^3 to 10^5
Cl	10^{-2}	P	10^4 to 10^6
Mg	0 to 10^{-2}	Li	10^{-1}
Ca	10 to 10^2	Ba	0 to 10^2
S	10	Zn	10^3 to 10^4
K	0 to 10^2	Mn	10^3 to 10^4
C	10 to 10^4	Cu	10^3 to 10^4
Br	10^{-1} to 0	Fe	10^4 to 10^6
B	10^{-1} to 10^2	Ni	10^3 to 10^6
Sr	10^{-2} to 10^2	Se	10 to 10^5
Al	0 to 10^3	V	10^3 to 10^5
F	10 to 10^3	Ag	10^4 to 10^5
N	10^4 to 10^6	Co	10^5 to 10^6

estimate, a brine solution containing 5 weight per cent NaCl would boil at temperatures in excess of about 250°C (Haas, 1971). Since fluids associated with volcanic events have temperatures generally in excess of 300°C (White, 1965; Corliss et al., 1979) it is expected that volcanic fluids expelled into the Misty Creek Embayment would boil is a manner similar to Type III ore-forming solutions described by Sato (1972). Rapid boiling would promote mixing and oxidation of reduced sulphur species, cooling of the fluid and the dispersion and dilution of other elements into the seawater. Elements such as Ba that form very insoluble sulphates would be precipitated and form part of the sedimentary sequence under oxygenated conditions. If anoxic conditions prevailed at that time in the Misty Creek Embayment, whether or not barite would precipitate is dependent on the activities of Ba^{++} and $SO_4^{=}$.

Factors influencing the Sr content of barite include temperature, the content of chloride, and the relative activities of other anions in solution e.g., carbonate. The solubilities of barite and celestite in H_2O and H_2O-NaCl solutions between 20 and 350°C (Fig. 17.1) have been determined experimentally by Scherp and Strubel (1974). With increasing temperature, barite becomes slightly more soluble and celestite becomes considerably less soluble. Both celestite and barite are more soluble in NaCl solutions. At about 350°C in a 2N NaCl solution, the solubility curves for celestite and barite meet whereas at 25°C, celestite is about 40 times more soluble than barite. As a result, barite crystallizing under low temperatures can be expected to incorporate very little Sr into its lattice. The low Sr content (0.08 weight per cent) of barite from unit RRs in the Misty Creek Embayment indicates that the conditions of formation were low temperature, characteristic of the conditions expected distant from the immediate area of discharge of thermal fluids.

The behaviour of Ba and Sr which can escape from hydrogen sulphide bearing waters to form bedded barite some distance from source vents is quite different from Zn and from Pb in particular. Elements such as Pb which is an important constituent of the Red Sea metalliferous sediments and older sediment-hosted stratabound sulphide deposits are relatively immobile in the oxygenated waters surrounding the brine pools. Lead is also very low in the Misty Creek shales whereas elements such as Zn, Cu, Ni, V, As, Hg, Sb, and Cd are anomalously high (Goodfellow et al., 1980). The fractionation of Pb and Zn in marine sediments is shown by a ternary Cu-Pb-Zn plot (Fig. 17.2) for shales from the Misty Creek Embayment and shales and siltstones interbedded with the Tom Pb-Zn-Ba occurrence (Carne, 1979) which is situated 125 km south in the Selwyn Basin of the Yukon Territory. The shales from the Misty Creek Embayment have Pb:Zn ratios comparable to shales described elsewhere (Fig. 17.2) whereas shales and siltstones from the Tom occurrence have much higher Pb:Zn ratios. Although the mineral(s) hosting the small quantities of Pb in sediments interbedded with the Tom Zn-Pb-Ba occurrence has not been identified, the Pb is most likely present as a sulphide or sulphate.

The separation of Zn from Pb in marine sediments surrounding points of fluid discharge may reflect the ability of certain marine organisms to accumulate and disperse Zn relative to Pb. However there are a number of other factors to consider. The movement of Pb is more restricted by decreasing seawater acidity conditions than Zn whose simple cation has considerable amphoteric character. Lead forms a number of sparingly soluble salts, e.g., chloride, sulphate and relatively insoluble salts, e.g., sulphide and carbonate and as a result is readily coprecipitated into carbonate rich sediments. Hydrolyzed Pb ions are also subject to strong adsorption by Mn-Fe crusts or colloids. Thus the movement of Pb in normal oxic seawater is limited by essentially inorganic factors. On the other hand equivalent Zn salts are more soluble and solution stable under these conditions. This is evident in tables of normal seawater abundance when Zn concentration exceeds Pb by two orders of magnitude (Table 17.1).

Under anoxic conditions and especially in the presence of hydrogen sulphide, conditions presumed to be more characteristic of the depositional setting of the Misty Creek paleobasin, Pb is very restricted compared with Zn although both form insoluble sulphides. It is usual for Pb to precipitate from acid waters as a sulphide before permitting Zn to separate completely from Pb. However in more alkaline waters or when hydrochloric acid formed in the sulphidization of Pb can be neutralized by carbonate-rich sediments, as at Misty Creek, Pb and Zn will tend to precipitate together. It is predictable that in the Misty Creek Embayment Pb and Zn may become separated by purely inorganic mechanisms with Pb remaining near to the discharging springs. Another important consideration deals with the possible influence of organic matter both dissolved and particulate. Bivalent Pb is generally considered to form stronger complexes with humic acids, solid and dissolved (Jackson et al., 1978), than bivalent Zn, but the Pb complexes formed show a much greater tendency to flocculate and precipitate. In this way the residence time of Pb in seawater is reduced significantly compared with Zn.

Summary

Anoxic, sulphidic, organic waters might be expected to prevail in the deeper parts of the Misty Creek paleobasin and under these circumstances all factors described simplistically above would be expected to favour Zn dispersion over Pb. As a result Pb may be restricted to the area of fluid discharges whereas other elements with a different chemistry (e.g., Cd, Ni, Hg, As, Sb, V) can be dispersed from the conduit to be incorporated into organic-rich sediments some distance away depending on depositional conditions noted above. However the formation of certain very insoluble sulphosalts perhaps by direct reaction with complex sulphur ions may cause retention near the vent of another group of elements, viz., Cu, Ag, As, Sb and Hg. These conditions would also have a further restrictive effect on Pb dispersion. It should not be surprising that Zn, Ni and V in particular are most commonly enriched in sulphidic carbonaceous shales that are distributed over large areas such as the Misty Creek Embayment whereas the distribution of others discussed here are comparatively more localized.

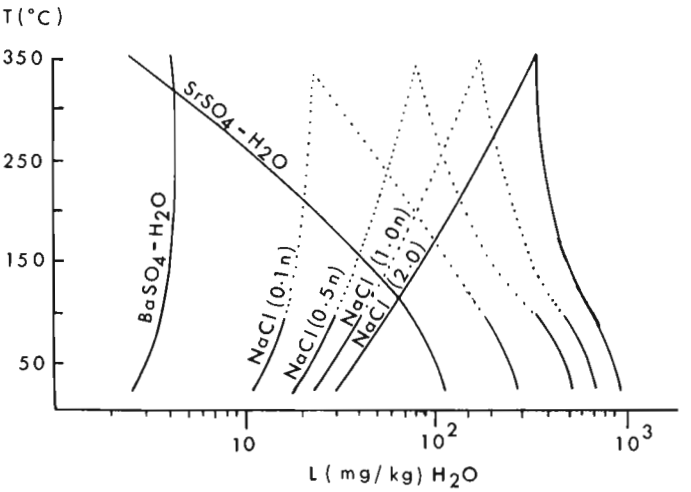

Figure 17.1. Solubilities of barite and celestite in H_2O and H_2O-NaCl solutions between 20° and 350°C temperature (after Scherp and Strubel, 1974).

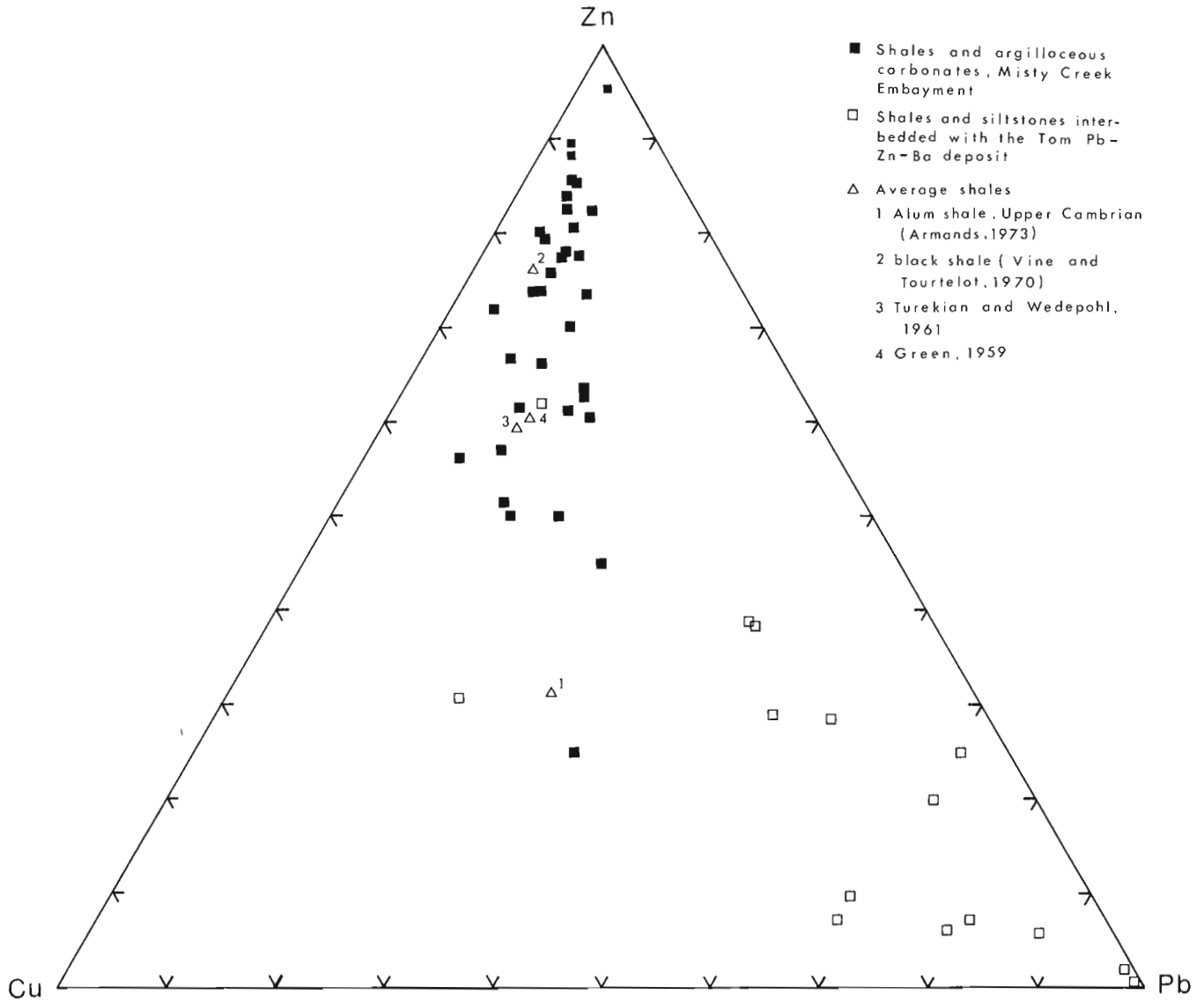

Figure 17.2. *Ternary Cu-Zn-Pb plot for shales and argillaceous carbonates from the Misty Creek Embayment, shales and siltstones interbedded with the Tom Pb-Zn-Ba deposit and average shales described elsewhere.*

Conclusions

The base metal elements, viz., Zn, Pb, Hg, As, Cd and Sb, which are found to be enriched in carbonaceous shales of the Misty Creek Embayment, Selwyn Basin, are considered to have originated in thermal fluids which have been vented onto the seafloor. The timing of fluid discharges likely coincides with periods of volcanic activity recorded in sedimentary units RRs and RRc. The same thermal events also gave rise to discharges of Ba, SiO_2, H_2S and perhaps CO_2. It may also be argued that P, Ni, V, Mo originate with these same springs and indirectly from the volcanic rocks themselves. The mechanisms of dispersion of these elements are considered to be primarily inorganic in chemical character for Ba, Zn, Pb, Cd, SiO_2, Hg and As with hydrogen sulphide in the deeper bottom waters of the paleobasin exerting a strong control over the mobility of the base metals in particular. The relative mobilities of Pb and Zn are influenced by the presence of sulphide, presence of CO_2 and therefore by the pH of the waters. Soluble organic complexors or organic colloids may have some added influence on restricting the dispersion of Pb out of a reducing, anoxic seawater while promoting the escape of Zn.

On the other hand, interaction of colloidal silica with colloidal organic matter may account for the close association of these substances in certain cherty sediments. It might be anticipated that elements which have a much stronger affinity for organic compounds and colloids would be associated ultimately with these same sediments. This appears to be the case for V, Ni and Mo and to a lesser extent for Zn. Since the distributions of all these elements depend ultimately on relative interactions between metal, organic moieties, carbonate, chloride and sulphide ions it is interesting to observe that elements which are not readily precipitated at low concentrations as sulphides in anoxic waters are those that form the strongest attachments with carbonaceous matter. P may act as a final fixer of some of these (V, Mo) in organic-rich sediments.

The geochemical behaviour of elements that are commonly associated with or constitute shale- and chert-hosted stratiform base metal deposits (i.e., Pb, Zn, Cu, As, Hg, Sb, Cd) is important in the interpretation of distribution of these metals in carbonaceous shales and to the application of these data to mineral exploration strategy. Because of the

limited mobility of Pb away from areas of fluid discharge, either in oxic or anoxic waters, it may be used to successfully identify these points of discharge and thereby facilitate exploration for stratabound deposits. Other trace elements found to be enriched in the Misty Creek Embayment sediments, e.g., As, Sb and Ba, may prove similarly useful.

References

Armands, G.
1973: Geochemical studies of uranium, molybdenum and vanadium in a Swedish alum shale; Stockholm Contributions in Geology, v. 27, p. 1-148.

von Backer, and Richter, H.
1973: Die rezente hydrothermal-sedmentare Lagerstatte Atlantis-II-Tief in Roten Meer; Sonderdruck aus der Geologischen Rundschau, v. 62, p. 697-741.

Baas-Becking, L.G.M.
1959: Geology and microbiology; New Zealand, Department of Scientific and Industrial Research, Bulletin 22, p. 48-64.

Berner, R.A.
1968: Calcium carbonate concretions formed by the decomposition of organic matter; Science, v. 159, p. 195-197.

Bignell, R.D., Cronan, D.S., and Tooms, J.S.
1976: Metal dispersion in the Red Sea as an aid to marine geochemical exploration; Institution of Mining and Metallurgy, Transactions, Section B, p. B274-B278.

Black, W.A.P. and Mitchell, R.L.
1952: Trace elements in the common brown algae and in sea-water; Journal Marine Biological Association, v. 30, no. 3, p. 575-584.

Bonatti, E., Fisher, D.E., Joensuu, O., Rydell, H.S., and Beyth, M.
1972: Iron-manganese-barium deposit from the Northern Afar Rift (Ethiopia); Economic Geology, v. 67, p. 717-730.

Bostrom, K.
1973: The origin and fate of ferromanganoan active ridge sediments; Stockholm Contributions in Geology, v. 27, p. 149-243.

Bostrom, K. and Peterson, M.N.A.
1966: Precipitates from hydrothermal exhalations on the East Pacific Rise; Economic Geology, v. 61, p. 1258-1265.

Bostrom, K., Joensuu, O., Moore, C., Bostrom, B., Dalziel, M., and Horowitz, A.
1973: Geochemistry of barium in pelagic sediments; Lithos, v. 6, p. 159-174.

Brongersma-Sanders, M.
1966: Barium in pelagic sediments and in diatoms; Koninke Ned. Akad. Wetensch. Proc. B70, p. 93-99.

Cameron, E.M. and Jonasson, I.R.
1972: Mercury in the Precambrian shales of the Canadian Shield; Geochimica et Cosmochimica Acta, v. 36, p. 985-1005.

Carne, R.C.
1979: Geological setting and stratiform mineralization, Tom Claims, Yukon Territory; Indian and Northern Affairs, Canada EGS, 1979-4, 30 p.

Cecile, M.P.
1978: Report on Road River stratigraphy and the Misty Creek Embayment, Bonnet Plume (106B), and surrounding map-areas, Northwest Territories; in Current Research, Part A, Geological Survey of Canada, Paper 78-1A, p. 371-377.

Church, T.M.
1970: Marine barite; Ph.D., University of California at San Diego, San Diego, California.

Corliss, J., Diamond, J., Gordon, L.I., Edmond, J.M., von herzen, R.P., Ballard, R.D., Green, K., Williams, D., Bainbridge, A., Crane, K., and van Andel, T.H.
1979: Submarine thermal springs on the Galapagos Rift; Science, v. 203, no. 4385, p. 1073-1083.

Craig, H.
1969: Geochemistry and origin of the Red Sea brines; in Hot Brines and Recent Heavy Metal Deposits in the Red Sea, ed. E.T. Degens and D.M. Ross, Springer-Verlag, New York, p. 208-242.

Devigne, J.P.
1977: Pourquoi les micro-vegetaux participent-ils a la genese des mineraux et des minerais sedimentaires? Mineraux Fossiles, Guide Collectioneur No. 29 (BRGM), p. 20-32.

Edmond, J.M. and others
1979a: Ridge crust hydrothermal activity and the balances of the major and minor elements in the ocean: the Galapagos data; Earth and Planetary Science Letters, v. 46, p. 1-18.

1979b: On the formation of metal-rich deposits at ridge crests; Earth and Planetary Science Letters, v. 46, p. 19-30.

Ferguson, J. and Lambert, I.B.
1972: Volcanic exhalations and metal enrichments at Matupi Harbour, New Britain, T.P.N.G.; Economic Geology, v. 67, p. 25-37.

Fotiyev, A.V.
1971: Nature of aqueous humus; Doklady, Adademiya Nauk SSSR 199(1), p. 198-201.

Francheteau, J. and others
1979: Massive deep-sea sulphide ore deposits discovered on the East Pacific Rise; Nature, v. 277, p. 523-528.

Gast, P.W.
1968: Trace element fractionation and the origin of tholeiitic and alkaline magma types; Geochimica et Cosmochimica Acta, v. 32, p. 1057-1086.

Goodfellow, W.D., Jonasson, I.R., and Cecile, M.P.
1980: Nahanni Integrated Multidisciplinary Pilot Project, Geochemical Studies, Part 1: Geochemistry and mineralogy of shales, cherts, carbonates, and volcanic rocks from the Road River Formation, Misty Creek Embayment, Northwest Territories; in Current Research, Part B, Geological Survey of Canada, Paper 80-1B, report 16.

Green, J.
1959: Geochemical table of elements for 1959; Geological Society of America Bulletin, v. 70, no. 9, p. 1127-1183.

Haas, J.L., Jr.
1971: The effect of salinity on the maximum thermal gradient of a hydrothermal system at hydrostatic pressure; Economic Geology, v. 66, p. 940-946.

Hawkins, J.W.
1970: Petrology and possible tectonic significance of Late Cenozoic volcanic rocks, Southern California and Baja California; Geological Society of America Bulletin, v. 81, p. 3323-3338.

Hawkins, J.W., Allison, E.C., and MacDougall, D.
1971: Volcanic petrology and geologic history of Northeast Bank, Southern California Borderland; Geological Society of America Bulletin, v. 82, p. 219-228.

Heinrich, E.W.
1966: The geology of carbonatites; Rand McNally and Company, Chicago, 555 p.

Hirst, D.M.
1974: Geochemistry of sediments from the Black Sea cores; in The Black Sea – Geology, Chemistry and Biology, D.A. Ross and E.T. Degens, ed., American Association of Petroleum Geology, Memoir 20, p. 430-455.

Holmes, R. and Tooms, J.S.
1973: Dispersion from a submarine exhalative orebody; in Geochemical Exploration 1972, Jones, J.J. ed., Institute of Mining and Metallurgy, p. 193-202.

Horzempa, L.M. and Helz, G.R.
1979: Controls in the stability of sulphide sols: colloidal covellite as an example; Geochimica et Cosmochimica Acta, v. 43, p. 1645-1650.

Jackson, K.S., Jonasson, I.R., and Skippen, G.B.
1978: The nature of metals-sediment-water interactions in freshwater bodies with emphasis on the role of organic matter; Earth Science Review, v. 14, p. 97-146.

Lonsdale, P.
1979: A deep-sea hydrothermal site on a strike-slip fault; Nature, v. 281, p. 531-534.

Maksimova, S.V.
1978: Biogenic silicites: an index of activation of abyssal fracture; International Geology Review, v. 21, p. 869-876.

Mercy, E.L.P.
1967: Geochemistry of the mantle; in The Earth's Mantle, ed. T.F. Gaskell, Academic Press, London, p. 421-443.

Miller, A.R., Densmore, C.D., Degens, E.T., Hathaway, J.C., Manheim, F.T., McFarlin, P.F., Pocklington, R., and Jokela, A.
1966: Hot brines and recent iron deposits in deeps of the Red Sea; Geochimica et Cosmochimica Acta, v. 30, p. 341-359.

Moore, J.G.
1965: Petrology of deep-sea basalt near Hawaii; American Journal of Science, v. 263, p. 40-52.

Narkis, N. and Rebhin, M.
1975: The mechanism of flocculation processes in the presence of humic substances; Journal of American Water Works Association, v. 67, p. 101-108.

Neprochnov, Y.P., Neprochnova, A.F., and Merlin, Y.G.
1974: Deep structure of the Black Sea basin; in The Black Sea – Geology, Chemistry and Biology, D.A. Ross and E.T. Degens ed., American Association of Petroleum Geology, Memoir 20, p. 35-49.

Noddack, I. and Noddack, W.
1939: Die Haufigkeit der Schwermetallen in Meerestieren; Arkiv. Zool., V32 A, No. 4.

Pushkina, Z.V.
1967: Iron, manganese, silicon, phosphorous, boron and aluminium in seawater in the area of Santorin volcano caldera (Aegean Sea); Lithology and Mineral Resources, No. 6, p. 218-225.

Sato, T.
1972: Behaviour of ore-forming solutions in seawater; Mining Geology (Tokyo), v. 22, p. 31-42.

Scherp, A. and Strubel, G.
1974: Hydrothermal investigation of the system $BaSO_4$-SrO_4-NaCl-H_2O and its bearing on Ba-Sr mineralizations. Problems of Ore Deposition, Fourth IAGOD Symposium, Varna 1974, Volume III, p. 23-28.

Schwarzer, R.R. and Rogers, J.J.W.
1974: A worldwide comparison of alkali olivine basalts and their differentiation trends; Earth and Planetary Science Letters, v. 23, p. 286-296.

Smith, P.A. and Cronan, D.S.
1975: The dispersion of metals associated with an active submarine exhalative deposit; Oceanology, Proceedings of International Conference, Brighton, 1975, p. 111-114.

Swallow, J.C. and Crease, J.
1965: Hot salty water at the bottom of the Red Sea; Nature, v. 205, p. 165-166.

Swanson, V.E.
1961: Geology and geochemistry of uranium in marine black shales – a review; U.S. Geological Survey, Professional Paper 356-C, p. 67-112.

Toth, J.R.
1980: Deposition of submarine crusts rich in manganese and iron; Geological Society of America Bulletin, Part 1, v. 91, p. 44-54.

Trudinger, P.A. and Bubela, B.
1927: Micro-organisms and the natural environment; Mineral Deposita, v. 2, p. 147-157.

Turekian, K.K.
1969: The oceans, streams and atmosphere; Handbook of Geochemistry, K.H. Wedepohl, ed., Springer-Verlag, Berlin, Volume 1, p. 310.

Turekian, K.K. and Wedepohl, K.H.
1961: Distribution of elements in some major units of the Earth's crust; Geology Society of America Bulletin, v. 72, p. 175-192.

Tuttle, O.F. and Gittins, J., ed.
1966: Carbonatites; Interscience, New York, 591 p.

Vidal, V.M.V., Vidal, F.V., and Isaacs, J.D.
1978: Coastal submarine hydrothermal activity of northern Baja, California; Journal of Geophysical Research, v. 83, p. 1757-1774.

Vine, J.D. and Tourtelot, E.B.
1970: Geochemistry of black shale deposits – a summary report; Economic Geology, v. 65, p. 253-272.

White, D.W.
1965: Metal contents of some geothermal fluids; in Problems of Postmagmatic Ore Deposition, II, A Symposium, p. 432-443. Academy of Science, Prague.

18.

A COMPARISON OF BISMUTH GERMANATE, CESIUM IODIDE, AND SODIUM IODIDE SCINTILLATION DETECTORS FOR GAMMA RAY SPECTRAL LOGGING IN SMALL DIAMETER BOREHOLES

Project 740085

J.G. Conaway, P.G. Killeen, and W.G. Hyatt
Resource Geophysics and Geochemistry Division

Conaway, J.G., Killeen, P.G., and Hyatt, W.G., A comparison of bismuth germanate, cesium iodide, and sodium iodide scintillation detectors for gamma ray spectral logging in small diameter boreholes; in Current Research, Part B, Geological Survey of Canada, Paper 80-1B, p. 173-177, 1980.

Abstract

Preliminary studies comparing a 19 x 76 mm bismuth germanate scintillation detector ($Bi_4Ge_3O_{12}$, commonly called BGO) to thallium activated sodium iodide (NaI(Tl)) and sodium activated cesium iodide (CsI(Na)) detectors of the same size have been completed. The potential advantage of BGO in gamma ray spectrometry is due to its high density (7.13 g/cm^3), which is almost twice that of the most commonly used detector material, NaI(Tl) (3.67 g/cm^3). The increased stopping power for high energy gamma rays of the high density BGO is evident in both the gamma ray logs and gamma ray spectra recorded in the model boreholes at the Geological Survey's calibration facility at Bells Corners, Ontario. The calibration factors (stripping factors and proportionality constants) for the three types of detectors are tabulated and compared both for the standard set of energy windows commonly used in portable spectrometers and for a set of wider energy windows which offer improved accuracy under some circumstances. The relative performance of the three detectors for determining uranium concentrations (using both sets of windows) was computed and tabulated for a range in U/Th concentration ratios from 10:1 to 1:10. A reduction of more than 50% in statistical errors in uranium determinations was found in comparing the BGO detector to NaI(Tl). CsI offers a more modest improvement of about 10%. In hardrock mining applications where the borehole diameter imposes a severe detector size restriction, the BGO detector appears to offer considerable advantages for uranium exploraton and evaluation.

Introduction

A problem that is well known in gamma ray spectrometry for geophysical exploration is the low gamma ray count rate measured in the high energy windows utilized for thorium (2.62 MeV) and uranium (1.76 MeV) determinations, leading to large statistical uncertainties in computed radioelement concentrations. Two approaches to solving this problem are to increase the counting time in any given location, or increase the detector volume. In gamma ray spectral logging the counting time depends on the logging speed, and extremely slow logging speeds are economically unattractive. The detector size, on the other hand, is limited by the diameter of the borehole. In hardrock mining and exploration, boreholes with diameters of 60 mm or less are common; often the logging must be done inside casing or drill rod, which further decreases the available space. Commonly a scintillation detector of diameter on the order of 19 mm must be used for gamma ray spectral logging, and these small detectors are extremely inefficient at high gamma ray energies (see Killeen and Bristow, 1976). Greater efficiency may be obtained with a detector which has higher density and/or atomic number (Z). Tests over the past few years with sodium activated cesium iodide detectors (CsI(Na)) which have a density of 4.51 g/cm^3 have shown a significant improvement over thallium activated sodium iodide (NaI(Tl)), (density 3.67 g/cm^3) in counting statistics for the high energy windows. In addition CsI(Na) detectors are more resistant to both thermal and mechanical shock than NaI(Tl). Another scintillating material, bismuth germanate ($Bi_4GE_3O_{12}$, commonly called BGO), has recently become available in sufficiently large sizes to be used for borehole logging. With a density of 7.13 g/cm^3 it would seem to have considerable promise for borehole applications.

Table 18.1 shows some of the physical properties of the three scintillating materials considered in this study. The gamma-scintillation efficiency is a measure of the light output of the scintillating crystal. CsI(Na) has a light output nearly 85 per cent of NaI(Tl). However the light output of BGO is only 8 per cent that of NaI(Tl) and hence the energy resolution will be poorer. BGO, like CsI(Na), is a rugged scintillating material; in addition BGO is not hygroscopic, unlike the other two detector materials. The energy resolution measurements (based on a ^{137}Cs source) for the three 19 x 76 mm detectors used in this study are also given in Table 18.1. BGO detectors with better energy resolution than the one used in this study are possible as indicated by the work of Nestor and Huang (1975).

The decay constant, also given in Table 18.1, is comparable for all three detector materials. Note that thallium activated cesium iodide CsI(Tl) (not considered here) has different properties from CsI(Na) including a longer decay constant and lower light output. A long decay constant will impose an upper limit on the count rate to which the detector may respond. When a gamma ray causes a scintillation in the detector before the previous scintillation has decayed, the two events cannot be distinguished.

Experimental Apparatus

A series of experimental measurements were made with each of the three 19 x 76 mm scintillation detectors, NaI(Tl), CsI(Na), and BGO. The NaI(Tl) detector was considered the standard for comparison. The GSC DIGI-PROBE logging system was used for all the measurements. This minicomputer-based, truck-mounted logging system has been developed for such R and D work by the Geological Survey, and is described briefly by Killeen et al. (1978), and in greater detail by Bristow (1980). The logging system is built around a 16-bit minicomputer operated interactively via a keyboard with a CRT display having alphanumeric and graphic capabilities. The system can record 256 or 1024 channels of gamma-ray spectral logging data on 9-track tape as often as every 0.25 s. For the purpose of this investigation, 256 channel (12 keV per channel) gamma ray spectra were recorded.

Table 18.1

Properties of the three detector materials compared in this paper, as specified by the supplier, Harshaw Chemical Co.

Material	Decay Constant (μS)	Density (g/cm^3)	Relative γ Scintillation Conversion Efficiency (%)	Side-On Energy Resolution (%)
NaI(Tl)	.23	3.67	100	11.2
CsI(Na)	.63	4.51	85	12.6
$Bi_4Ge_3O_{12}$	.30	7.13	8	24.5

The energy resolution of the detectors was measured by the authors with a small ^{137}Cs source alongside the detector.

All measurements were made by interchanging detectors in the same borehole probe. In this way no parameters except those due to the detector and its integral-mount photomultiplier tube changed during the comparison tests.

Calibration checks were made before and after each measurement to minimize the potential problem of gain shifts. Because of the versatility made possible by full spectral recording it is possible to reproduce gamma ray spectral logs using energy windows of any desired widths or positions in the gamma ray energy spectrum. Comparisons were therefore made with two sets of energy windows as shown in Table 18.2. The 'standard' windows represent those commonly used in portable and airborne gamma ray spectrometers. The 'wide' uranium window has the advantage of including the 2.24 MeV gamma ray peak from the uranium decay series, but the disadvantage of an increased scattered thorium component in the uranium window. This requires a larger stripping factor α (see Conaway and Killeen, 1980; Killeen, 1979) to remove the thorium component from the uranium window. The wide thorium window is useful when working with BGO because of the poorer energy resolution of this material.

Experiments in Model Boreholes

All measurements were made with the above described logging system in the model boreholes at the Geological Survey's calibration facilities at Bells Corners, near Ottawa. These model boreholes consist of a set of nine concrete columns 3.9 m in height, each with a simulated ore zone 1.5 m thick sandwiched between upper and lower barren zones. Each test column contains three boreholes of diameters 48 mm (size A) 60 mm (size B) and 75 mm (size N) intersecting the ore zones. Three of the test columns contain 'ore' zones of different concentrations for potassium, three for thorium and three for uranium. These are described in more detail by Killeen (1978); Killeen and Conaway (1978) and Killeen (1979).

Gamma ray spectral logs were run in the high grade U, Th, and K model holes using each of the three detectors; also a 5 minute gamma ray spectrum was accumulated and recorded with each detector with the logging probe stationary in the centre of the 'ore' zones. All tests were performed in the B-size holes, water filled. From these data, all of the required calibration fractors for a gamma ray spectral logging probe were derived (see Conaway and Killeen, 1980) for the three detectors for each of the two sets of energy windows shown in Table 18.2. The results are given in Table 18.3. The meaning of each of these factors has been discussed by Conaway and Killeen (1980) and is summarized below.

Table 18.2

Window energy limits (keV) used to determine the calibration factors in this paper

Window	TC	K	U	Th
Standard	400-3000	1360-1560	1660-1860	2410-2810
Wide	400-3000	1360-1560	1610-2300	2400-3000

Stripping Factors

α = ratio of Th gamma rays in U window to Th gamma rays in Th window

β = ratio of Th gamma rays in K window to Th gamma rays in Th window

γ = ratio of U gamma rays in K window to U gamma rays in U window

a = ratio of U gamma rays in Th window to U gamma rays in U window

b = ratio of U gamma rays in Th window to K gamma rays in K window

g = ratio of K gamma rays in U window to K gamma rays in K window

Total Count Window Proportionality Constants
(CPS = counts/second)

K_K = % K/CPS in total count window

K_U = ppm U/CPS in total count window

K_{Th} = ppm Th/CPS in total count window

K, U, and Th Window Proportionality Constants

C_K = % K/CPS in K window

C_U = ppm U/CPS in U window

C_{Th} = ppm Th/CPS in Th window

Note that the factor K_U is equivalent to the so-called 'K-factor' commonly used in gross count gamma ray logging where all the gamma rays are assumed to originate from the radioactive decay series of uranium.

These K-factors and C-factors are used as the constant of proportionality K in the equation (Scott et al., 1961):

$$\bar{G}T = KA \qquad (1)$$

depending on which radioelement is causing the anomaly, and which spectral window is being used. In equation (1), $\bar{G}$ is the average grade over a zone of thickness T. A is the area under the corresponding anomaly on the gamma ray log. In the centre of a uniform ore zone of effectively infinite thickness, equation (1) reduces to

$$G = KI \qquad (2)$$

where I is the measured gamma ray intensity.

The CsI(Na) detector used in these studies was implanted with an ^{241}Am stabilization source emitting alpha particles exhibiting gamma equivalent energies on the order of 4 MeV. A small fraction of these alpha particles exhibited gamma-equivalent energies in the 0.4-3 MeV energy range of interest in these studies. This 'background' count rate was quite low compared to the observed intensities in the U and Th model ore zones, and those data were easily corrected. In the case of potassium, however, the background was on the same order as the count rate in the potassium model, and hence values of the calibration factors determined in that borehole are not listed in Table 18.3 for CsI(Na).

Table 18.3

Calibration factors obtained for 3 different detector materials, each detector having dimensions 19 x 76 mm.

Windows →	Standard			Wide		
Detector Material →	NaI	CsI	BGO	NaI	CsI	BGO
↓ Calibration Factor						
α	1.5	1.2	0.65	5.0	3.7	1.9
β	2.1	1.6	0.92	2.0	1.5	0.85
γ	1.8	1.6	1.2	1.0	0.87	0.65
a	0.04	0.05	0.07	0.02	0.03	0.04
b	0.05	*	0.02	0.05	*	0.03
g	0.03	*	0.04	0.12	*	0.13
K_K	0.39	*	0.16	-	-	-
K_U	0.91	0.80	0.33	-	-	-
K_{Th}	1.9	1.6	0.81	-	-	-
C_K	4.7	*	1.2	-	-	-
C_U	39	31	10.5	22	17	5.6
C_{Th}	128	73	25	122	70	23

Asterisks indicate factors which could not be determined for the CsI detector because of background problems, as described in text.

Horizontal dashes indicate instances where the wide windows are identical to the standard windows

From Table 18.3 it is easy to see that the BGO detector has much lower stripping factors (α, β, γ) than NaI(Tl), and that the values for CsI(Na) are intermediate. The reason for the decrease in stripping factors is the higher detection efficiency of CsI(Na) and especially BGO at the high energies. This is evident in the comparison of gamma ray spectra shown in Figure 18.1. These spectra were recorded as 5 minute stationary measurements with each of the three detectors in the centre of the 350 ppm thorium 'ore zone' of the model holes. The spectra shown in Figure 18.1 are linear plots with the same vertical count-rate scale; note that these plots are in CPS/channel. The high energy peak at 2.615 MeV from ^{208}Tl in the thorium decay series is much larger in the spectrum observed with BGO than in the spectrum observed with NaI(Tl), and even the CsI(Na) shows an improvement over NaI(Tl).

Figure 18.2 shows the spectra recorded with the three different detectors positioned in the centre of the 950 ppm uranium ore zone in the high grade uranium test column. The 1.76 MeV peak from ^{214}Bi which is generally used for uranium determinations is obviously greatly enhanced by the BGO detector, and to a lesser extent by the CsI(Na). This improvement in count rate in the uranium window is even more apparent in the three uranium logs shown in Figure 18.3. These three logs through the 950 ppm uranium model ore zone represent the deadtime corrected gamma ray count rate in the uranium channel using 'standard' energy windows (see Table 18.2). The uranium log obtained with the CsI(Na) detector shows about a 25 per cent increase in count rate over NaI(Tl) and the BGO detector shows a count rate increase by a factor of about 4 over NaI(Tl). Since there is no appreciable thorium in this ore zone the relative count rates shown in Figure 18.3 are true indications of the higher efficiency of the BGO detector at high energies.

Table 18.4

Computed performance of the three 19 x 76 mm detectors for determining uranium concentrations in a mixed U-Th environment.

Concentration Ratio U/Th	Standard Windows			Wide Windows		
	NaI	CsI	BGO	NaI	CsI	BGO
10	1.00	0.90	0.51	0.81	0.72	0.39
1.0	1.00	0.91	0.47	0.93	0.83	0.39
0.1	1.00	0.93	0.42	1.06	0.94	0.39

Values given are error limits (one standard deviation) in the uranium computations normalized to the NaI standard windows for each radioelement concentration ratio. Clearly, the smaller the relative error, the better the detector's performance.

The comparison can be put in more quantitative terms if the C-factors in Table 18.3 are compared. These figures represent the number of parts per million (or percentage in the case of potassium) required to produce one count per second for each radioelement in the appropriate energy window. Thus, using the standard windows, C_U for NaI, CsI, and BGO detectors are 39, 31 and 10.5 respectively, which indicates that BGO is 3.7 times as sensitive to uranium as NaI(Tl). Even CsI(Na) is 1.26 times as sensitive as NaI(Tl). The thorium window proportionality constant C_{Th} for the three detectors shows improvements over NaI(Tl) by a factor of 1.75 times and 5.1 times for CsI(Na) and BGO respectively. For the wide windows the improvement factors for uranium C_U are 1.3 and 3.9 for CsI(Na) and BGO, and for thorium C_{Th} the improvement factors over NaI(Tl) are 1.74 and 5.3 for CsI(Na) and BGO respectively. Thus a similar improvement is observed for both 'standard' and 'wide' windows.

Statistical Errors in Uranium Determinations

What effects do these improvements in count rate and changes in the stripping factors have on the determination of uranium concentrations in a mixed U-Th environment? Using the calibration factors in Table 18.3 and the statistical analysis described below we can arrive at some conclusions about the degree of improvement over NaI(Tl) which is possible with CsI(Na) and BGO detectors.

Ignoring the contribution of K, which would be negligibly small even in a low grade uranium ore zone, we can extend equation (2) to the case of a mixed U-Th zone by writing the equations

$$G_U = C_U (I_U - \alpha I_{Th}) \tag{3}$$

$$G_{Th} = C_{Th} (I_{Th} - a I_U) \tag{4}$$

where G_U is uranium grade, I_U is the gamma ray intensity in the unstripped uranium window, G_{Th} is thorium grade and I_{Th} is the gamma ray intensity in the unstripped thorium window; a and α are stripping factors described earlier. Solving equations (3) and (4) for I_U and I_{Th} we get

$$I_U = \frac{1}{1-a\alpha} \left[\frac{G_U}{C_U} + \frac{\alpha G_{Th}}{C_{Th}} \right] \tag{5}$$

$$I_{Th} = \frac{1}{1-a\alpha} \left[\frac{G_{Th}}{C_{Th}} + \frac{a G_U}{C_U} \right] \tag{6}$$

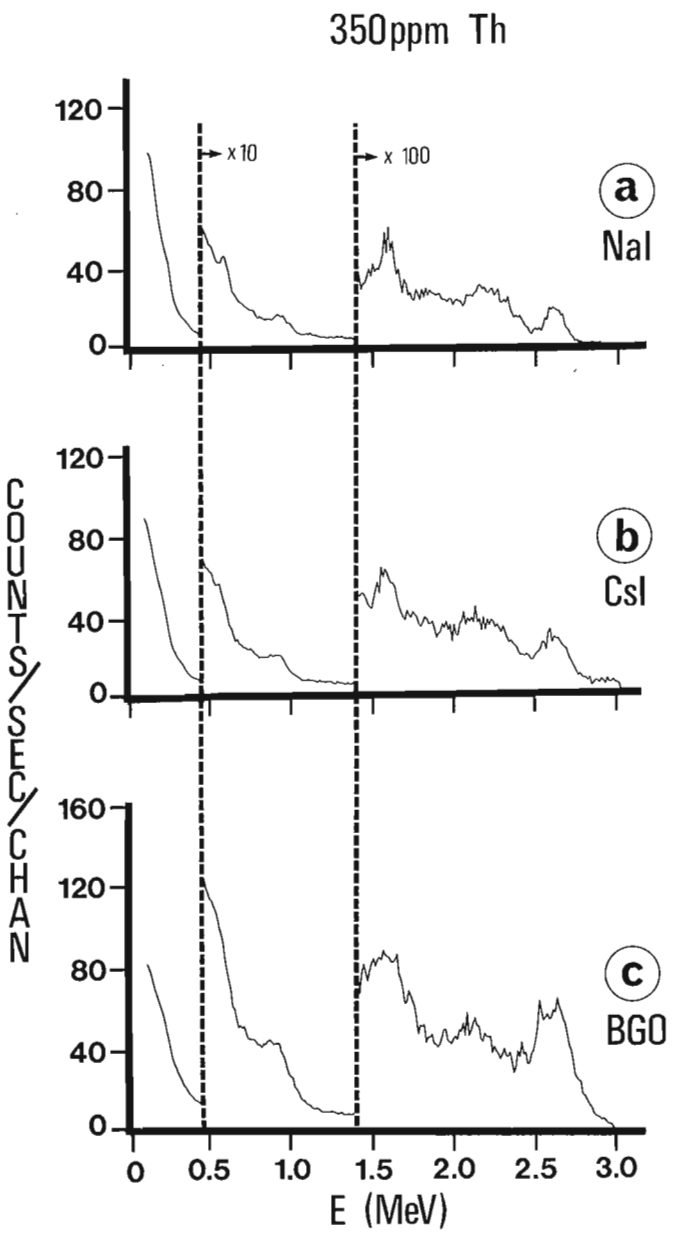

a. 256 channel gamma ray spectrum (12 keV per channel) recorded in 350 ppm thorium model ore zone using a 19 x 76 mm NaI(Tl) detector.

b. Same as (a) but using a 19 x 76 mm CsI(Na) detector. Note that at the high energy end of the spectrum the count rate does not drop to zero as in the NaI(Tl) spectrum (a). This is due to the implanted ^{241}Am source, as explained in text.

c. Same as (a) but using a 19 x 76 mm BGO detector.

Figure 18.1

Using these equations it is possible to compute the expected count rate in a given spectral window for a specified concentration of uranium and thorium. We are concerned here with the statistical errors in the uranium window count rate, after stripping. The count rate in the stripped uranium window I_{Us} is (ignoring potassium)

$$I_{Us} = I_U - \alpha I_{Th} \tag{7}$$

The standard deviation σ of the statistical noise in the stripped U window is (e.g. Chase and Rabinowitz, 1968):

$$\sigma = (I_U + \alpha I_{Th})^{1/2} \tag{8}$$

and thus the relative error E in the uranium determination is given by

$$E = \frac{\sigma}{I_{Us}} = \frac{(I_U + \alpha I_{Th})^{1/2}}{(I_U - \alpha I_{Th})} \tag{9}$$

If desired, E may be multiplied by 100 to give percentage error. The relative errors for the three detectors were computed from equation (9) for three U/Th ratios, 10:1, 1:1, and 1:10. These results are given in Table 18.4, normalized to the error for the NaI(Tl) detector (standard windows) for each U/Th ratio.

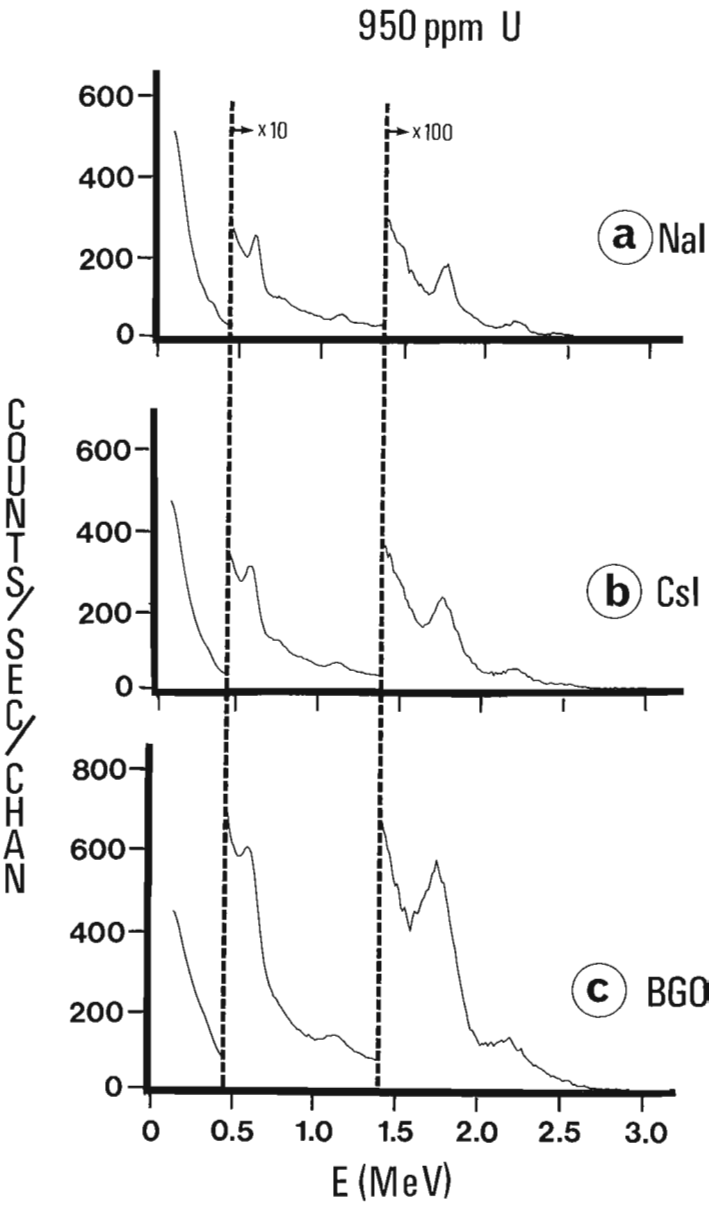

Figure 18.2. *256 channel spectrum recorded in 950 ppm uranium model ore zone using*

a. NaI(Tl) detector,

b. CsI(Na) detector and

c. BGO detector

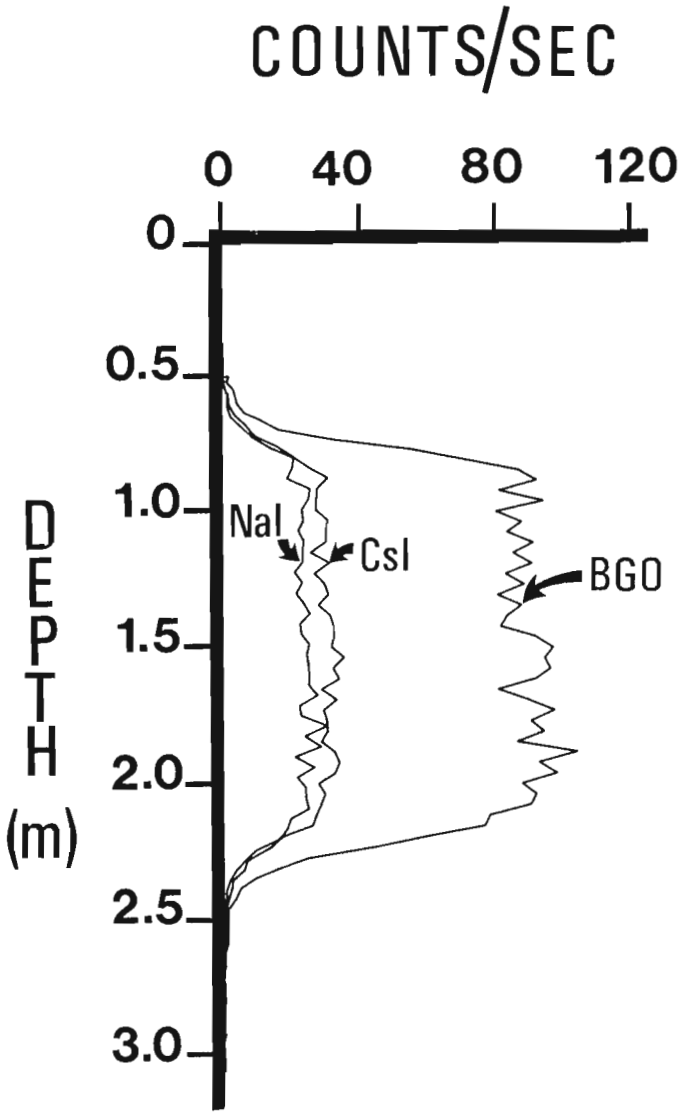

Figure 18.3. Plot of gamma ray intensity as a function of depth using the standard uranium spectral window and three different detector materials, as indicated.

Several conclusions can be drawn from Table 18.4 for the 19 x 76 mm detector size.

1. The wide windows are better than the standard windows for all 3 detector materials for U/Th ratios of 10:1 and 1:1. For BGO the wide windows are also better for the 1:10 U/Th ratios, but this is not true for NaI(Tl) or CsI(Na).
2. CsI(Na) exhibits a relative error improved by about 10% compared to NaI(Tl) with the same window widths.
3. BGO produces an improvement in relative error on the order of 50 per cent or more under all conditions.

Conclusion

It is clear that BGO is the best of the three detector materials tested for slim hole gamma ray spectral logging. BGO's improved ruggedness compared with NaI(Tl) is also an advantage. At present the price of BGO is on the order of double the price of the other detector materials, however, this price differential is still not high enough to rule out the use of BGO in spectral logging, considering its great advantages in slim probes.

Note that the results obtained in these tests are dependent on probe characteristics, detector size, and borehole conditions. It may be expected that the observed advantages of BGO will in general decrease with increasing detector size.

References

Bristow, Q.
1980: NOVA-based airborne and vehicle mounted systems for real-time acquisition, display and recording of geophysical data; in Proceedings of the 6th Annual Data General Users Group Meeting, New Orleans, Dec. 4-7, 1979.

Chase, G.D. and Rabinowitz, J.L.
1968: Principles of radioisotope methodology; Burgess Pub. Co., Minneapolis, 633 p.

Conaway, J.G. and Killeen, P.G.
1980: Gamma-ray spectral logging for uranium; Canadian Institute of Mining and Metallurgy Bulletin, v. 73, no. 813, p. 115-123.

Killeen, P.G.
1978; Gamma-ray spectrometric calibration facilities – a preliminary report; in Current Research, Part A, Geological Survey of Canada, Paper 78-1A, p. 243-247.

1979: Gamma ray spectrometric methods in uranium exploration – application and interpretation; in Geophysics and Geochemistry in the Search for Metallic Ores; Peter J. Hood, Editor; Geological Survey of Canada, Economic Geology Report 31, p. 163-229.

Killeen, P.G. and Bristow, Q.
1976: Uranium exploration by borehole gamma-ray spectrometry using off-the-shelf instrumentation; in Exploration for Uranium Ore Deposits, Proceedings Series, International Atomic Energy Agency, Vienna, p. 393-414.

Killeen, P.G. and Conaway, J.G.
1978: New facilities for calibrating gamma-ray spectrometric logging and surface exploration equipment; Canadian Institute of Mining and Metallurgy Bulletin, v. 71, no. 793, p. 84-87.

Killeen, P.G., Conaway, J.G., and Bristow, Q.
1978: A gamma-ray spectral logging system including digital playback, with recommendations for a new generation system; in Current Research, Part A, Geological Survey of Canada, Paper 78-1A, p. 235-241.

Nestor, O.H. and Huang, C.Y.
1975: Bismuth germanate: a high-Z gamma-ray and charged particle detector; Institute of Electrical and Electronics Engineers Transactions on Nuclear Science, NS-22, p. 68-71.

Scott, J.H., Dodd, P.H., Droullard, R.F., and Mudra, P.J.
1961: Quantitative interpretation of gamma-ray logs; Geophysics, v. 26, no. 2, p. 182-191.

19. # REVISION OF THE TERTIARY REINDEER FORMATION IN THE CARIBOU HILLS, DISTRICT OF MACKENZIE

Project 770050

L.L. Price, D.H. McNeil, and N.S. Ioannides
Institute of Sedimentary and Petroleum Geology, Calgary

Price, L.L., McNeil, D.H., and Ioannides, N.S., Revision of the Tertiary Reindeer Formation in the Caribou Hills, District of Mackenzie; in Current Research, Part B, Geological Survey of Canada, Paper 80-1B, p. 179-184, 1980.

Abstract

Field study of the predominantly terrestrial Tertiary Reindeer Formation in the Caribou Hills was undertaken to resolve variance in use of the name "Reindeer Formation" in the Beaufort-Mackenzie basin. Consequently, beds from the lower and upper parts of the formation have been reassigned after consideration of the observed lithologic divisions, refinements in stratigraphic correlation, and previous nomenclatural usage. The section is now divided into the Paleocene Moose Channel Formation (64 m) made up of sandstone, pebbly sandstone, and minor dark claystone interbeds; the revised Paleocene-Early Eocene Reindeer Formation (657 m) comprising carbonaceous claystone and shale, lignite, and lesser amounts of sand and pebbly sandstone; an unnamed white-clay unit (40 m), tentatively dated Oligocene, composed of silty and sandy kaolinitic claystone with minor gravelly sand, carbonaceous clay, and lignitic beds; and the Beaufort(?) Formation (439 m), of probable Miocene age, consisting of poorly exposed limonitic gravels or conglomerates and sandstones with minor lenses of whitish claystone.

Significant stratigraphic relationships in the section include: Tertiary overstep of Cretaceous rocks; conformity between the Paleocene Moose Channel Formation and the Paleocene-Eocene Reindeer Formation; unconformity between the Reindeer Formation and the white-clay unit; and a rapid northward thickening of the Reindeer Formation.

Introduction

The Caribou Hills lie along the eastern margin of the Mackenzie Delta within the Beaufort-Mackenzie basin (Young et al., 1976), the site of active petroleum exploration and geological investigation for more than two decades. The hills offer numerous but poorly exposed outcrops (Fig. 19.1) of weakly indurated Tertiary shale, claystone, siltstone, sandstone, conglomerate, and lignite, as well as Cretaceous shale exposed only at the south end of the hills. The sequence attains importance as a standard for subsurface comparison and as the site of the stratotype for the Reindeer Formation erected by Mountjoy (1967). The importance of these rocks coupled with developing inconsistency in use of the term "Reindeer Formation" has precipitated a need for clarification of the litholigic sequence and standardization of the nomenclature applied. Thus, in August of 1978, a detailed geological investigation of the Caribou Hills was carried out as part of the Survey's on-going Mackenzie-Beaufort project. The preliminary results of this field study are presented here.

History of the Use of the Name "Reindeer Formation"

Mountjoy (1967, p. 10) proposed the name "Reindeer Formation" for the "non-marine silty shales, siltstones, coarse sands, conglomerates and coal" exposed on the southwestern face of the Caribou Hills, designating two sections (3 and 4 of his report; 32 and 15 of this paper, see Fig. 19.1, 19.2) as representative of its lithology. Palynological evidence led Mountjoy (op. cit., Fig. 2, p. 11) to assign a Paleocene-Eocene age to the formation. Also, Mountjoy (op. cit., p. 8) established the Moose Channel Formation, defined from exposures of loosely consolidated sandstone outcropping along Big Fish River on the west side of the Mackenzie Delta. He considered (op. cit., p. 10) that the Moose Channel extended northeastward (from its type locality) beneath the Delta and that its upper part was an equivalent of the lower Reindeer. Young (1975, p. 11-15) examined the type Moose Channel Formation in more detail and established two members, at the same time excluding from the Moose Channel Formation coaly beds which outcrop along Aklak Creek. The excluded beds were assigned to the Reindeer Formation and named the Aklak Member of the Reindeer Formation. The lower member of Young's revised Moose Channel Formation was named "basal sandstone member"; the upper unit was named "Ministicoog Member", composed predominantly of mudstone.

Young et al. (1976) presented the first comprehensive report on the stratigraphy of the Beaufort-Mackenzie basin. They mapped the "Reindeer Formation" (interpreted as Paleocene to Eocene in age) extensively in the subsurface of the Mackenzie Delta and Tuktoyaktuk Peninsula. In the Mackenzie Delta, they (op. cit., Table 1) indicated that the "Reindeer Formation" was underlain by the Late Cretaceous Tent Island Formation and overlain in succession by an informal "Eocene shale unit", unnamed Paleogene and Neogene units, and the ?Beaufort Formation. The Moose Channel Formation, at that time dated as Maestrichtian, was reported to be overlain by the Reindeer Formation in the neighbouring Yukon Coastal Plain and to be a facies equivalent of an upper part of the Tent Island Formation in the subsurface of the Mackenzie Delta. It is important to note that part of the stratigraphic scheme of Young et al. (1976) has been revised; the Moose Channel Formation is now dated as Paleocene and is not considered to be a facies equivalent of the upper part of the Tent Island as depicted (op. cit., Table 1), but rather (Young and McNeil, in press) to extend widely through the Mackenzie Delta as a discrete unit between the "Reindeer Formation" and the Tent Island Formation. In the Caribou Hills, Young et al. (op. cit., p. 35) divided the Reindeer Formation into a basal mudstone member, a medial arenaceous member, and an upper pelitic member. They further stated that (in the Caribou Hills) the "Reindeer Formation is overlain abruptly, and probably unconformably, by lithic gravel and sand of probable Neogene age", thus restricting Mountjoy's concept of the formation by excluding the gravel that outcrops along the northernmost part of the Caribou Hills escarpment. The gravel and sand were assigned questionably to the Beaufort Formation (originally described from the northwestern coastal area of the Arctic Archipelago by Tozer, 1955).

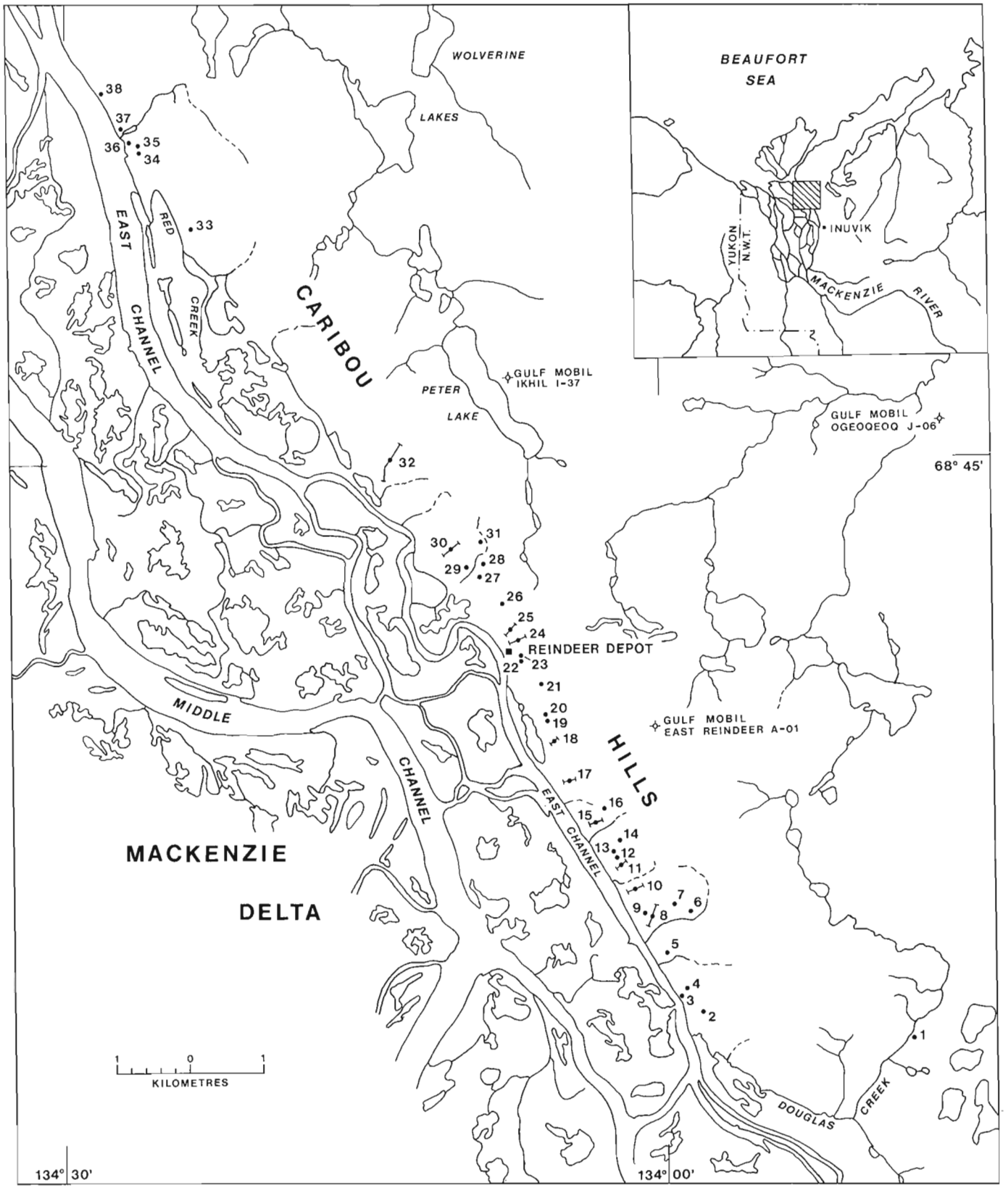

Figure 19.1. *Index map for locations to measured sections 1 to 38 and abandoned wells in the Caribou Hills and environs.*

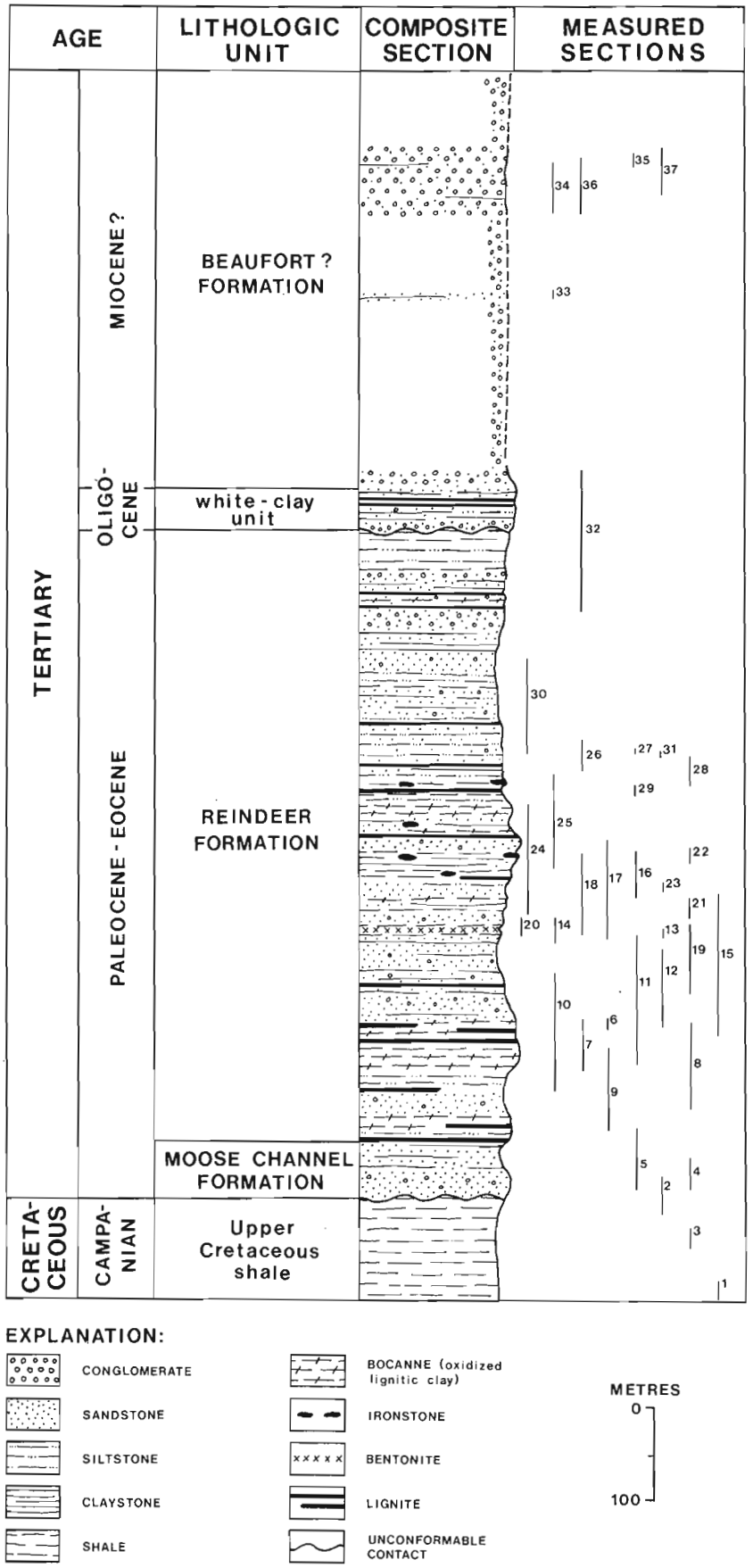

Figure 19.2. *Generalized composite type section of the Reindeer Formation and associated units in the Caribou Hills. In general, siltstones and sandstones are recessive relative to claystones and bocannes, as indicated by profile on right side of column. For locations of measured sections, see Figure 19.1.*

Brideaux and Myhr (1976) described the stratigraphy and palynology of the Parsons N-10 well, assigning interval "?100 - 5005 feet" to the Reindeer Formation dated Paleocene to Middle Eocene, overlying the Tent Island Formation and overlain by Quaternary sand and gravel. Also in 1976, Doerenkamp et al. reported on the palynology and stratigraphy of the Caribou Hills applying the name Reindeer Formation in the sense of Mountjoy (1967). They recognized a lower member of sand, brown shale, lignite and coal dated Paleocene to Eocene and an upper member of coarse and conglomeratic sands with rare grey shales dated Miocene to Recent.

Young (1978a, p. 52) recounted the studies of Mountjoy (1967) and Doerenkamp et al. (1976) and presented a five-fold lithogenetic division of the exposed Tertiary succession in the Caribou Hills:

e. upper gravel unit

d. upper nonmarine unit

c. medial shallow marine unit

b. lower nonmarine unit

a. basal sandstone and shallow marine unit

Citing palynological and lithological evidence, Young (1978a, p. 53-57) assigned units (d) and (e) to the Beaufort Formation, consistent with an earlier modification of the formation introduced by Young et al. (1976), but eliminating the upper nonmarine unit as well as the upper gravel unit from the Reindeer Formation. In the same publication, Young and Norris (1978, p. 6) presented a composite stratigraphic column for the Mackenzie Delta illustrating the "Reindeer Formation" overlying the Moose Channel Formation and overlain in turn by the "Eocene shale unit". They identified two members in the Reindeer: the Aklak, consisting of various nonmarine sediments and coals overlain by the "Taglu" member (Shawa, 1978), consisting of sandstone interbedded with mudstone, and minor conglomerate and containing major hydrocarbon reserves. In that context, Young (1978b, p. 38-39) further described the "Reindeer Formation" in a summary of the Tertiary of the Mackenzie Delta and illustrated the formational sequence (Moose Channel, Reindeer, unnamed Eocene shale, etc.) in a correlation of subsurface sections.

The Proposed Revision

The historical sketch summarizes progressive restriction of the Reindeer Formation (see also Table 19.1) by exclusion of the upper gravels or conglomerates (Young et al., 1976) and by exclusion of the "upper nonmarine unit" (Young 1978a). We support the modifications to the upper boundary introduced by Young et al. (1976) and Young (1978a) and, furthermore, recognize the Moose Channel Formation in the Caribou Hills (see Fig. 19.2). Retention of the name "Reindeer Formation" is justified by usage cited in the historical review, although strict interpretation of the North American Code of Stratigraphic Nomenclature would call for either its abandonment or its elevation to group rank.

Table 19.1

History of nomenclature for the Reindeer Formation and associated units in the Caribou Hills and the Yukon Coastal Plain

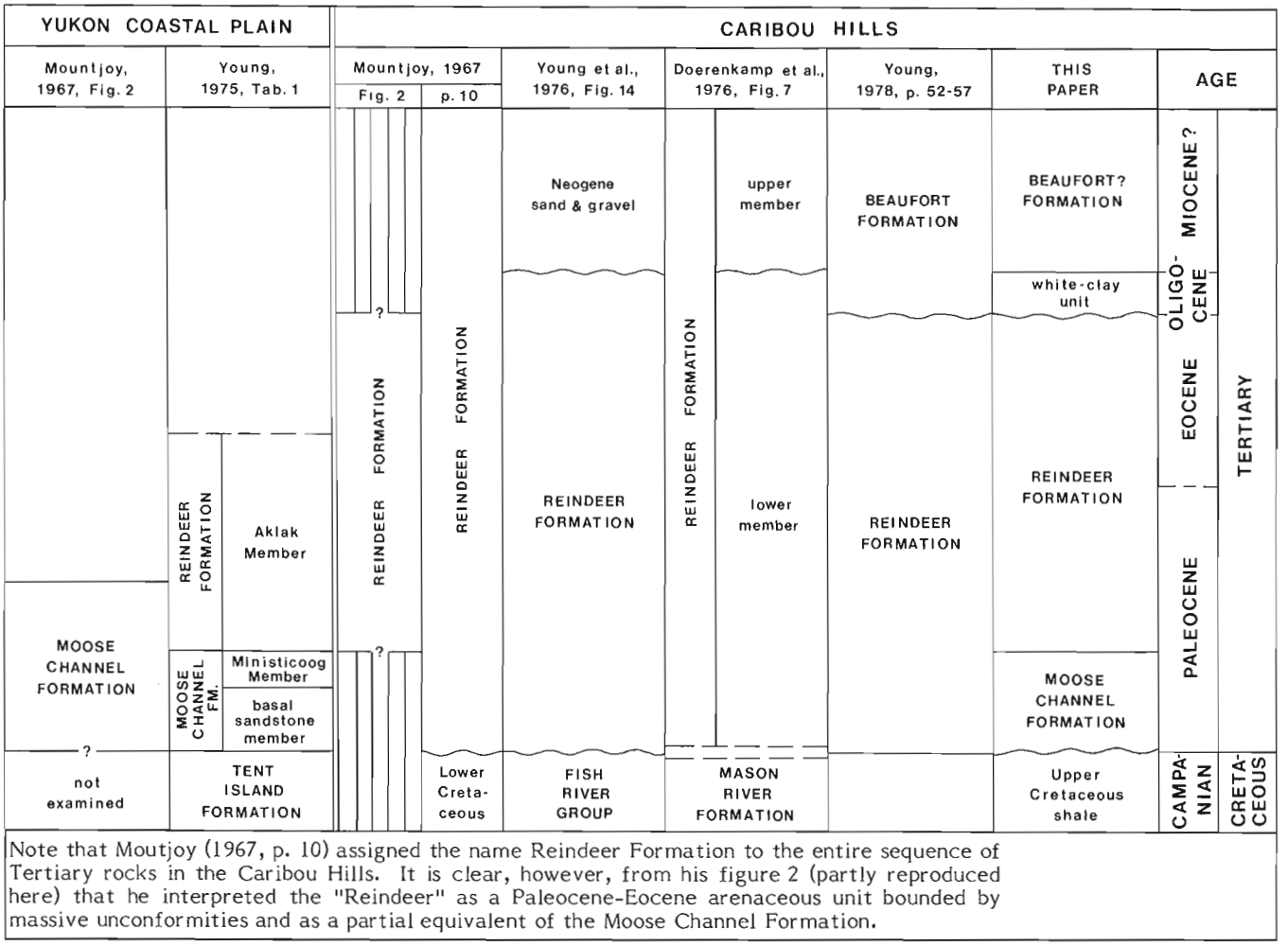

Note that Moutjoy (1967, p. 10) assigned the name Reindeer Formation to the entire sequence of Tertiary rocks in the Caribou Hills. It is clear, however, from his figure 2 (partly reproduced here) that he interpreted the "Reindeer" as a Paleocene-Eocene arenaceous unit bounded by massive unconformities and as a partial equivalent of the Moose Channel Formation.

The Revised Section

Units and Thickness of the Section

The Tertiary sequence in the Caribou Hills is here divided into four units (Fig. 19.2): a basal, coarse-grained unit (64 m) assigned to the Moose Channel Formation; a claystone, siltstone, sandstone, conglomerate, and lignite unit (657 m) constituting the revised Reindeer Formation; an unnamed, sandy, white-clay unit (40 m); and an upper unit (439 m) assigned questionably to the Beaufort Formation comprising gravel or conglomerate with minor lenses of white claystone. Total thickness of the Tertiary section is estimated at 1200 m. The composite type section for the Caribou Hills was constructed largely by direct correlation of beds between the outcrop sections shown in Figure 19.2. Where beds could not definitely be correlated, the measured 2 degree northwestward dip was used for reconstruction, modified slightly by interpreted faults in the section. Care was taken to distinguish between true and apparent dips and it was concluded that the escarpment is essentially a dip section on the northwest flank of Campbell Uplift.

In outcrop, the combined thickness of the Moose Channel and Reindeer formations has been measured at 721 m. This contrasts markedly with 1615 m which was measured for the equivalent units in the Ikhil I-37 well. Ikhil I-37, however, is located 5.0 km northeast of section 32 (Fig. 19.1) and correlations based on well-log data indicate that the Reindeer Formation and, to a lesser degree, the Moose Channel Formation almost double in thickness northward from Reindeer A-01 to Ikhil I-37. Figure 19.3 illustrates this as well as the stratigraphic overstep of Tertiary rocks on Cretaceous. In the subsurface, the unconformable Cretaceous-Tertiary contact dips to the northwest at just less than 4 degrees. The dip of the overlying Tertiary sediments becomes progressively less upsection from the unconformity, decreasing as the sequence progressively thickens north-northwestwards.

The preliminary thickness estimates (2500 m) for the exposed Tertiary sequence cited by Ioannides and McIntyre (1980) were based on an extrapolation through the Tertiary of the 4 degree dip of the Cretaceous-Tertiary contact and, therefore, should now be revised downward to correspond with the present determinations (1200 m).

Moose Channel Formation

The Moose Channel Formation consists of sandstone, pebbly in places or with minor dark clay interbeds. The lower contact is not exposed, but the formation may overlie unconformably Late Cretaceous shales of the Tent Island Formation. The upper contact is drawn at the top of a pebbly sandstone unit overlain by lignite at the base of the Reindeer Formation exposed in section 5 (Fig. 19.2). The Moose Channel Formation in the Caribou Hills is comparable lithologically to the basal sandstone member of the type Moose Channel. Shaly beds within the upper part of the

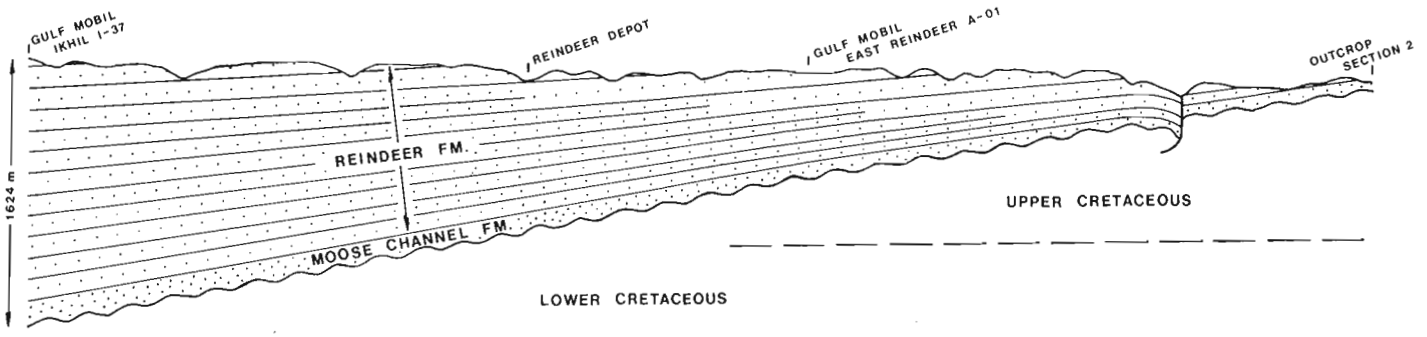

Figure 19.3. *Diagrammatic cross-section showing postulated Tertiary overstep of Cretaceous strata in the Caribou Hills subsurface. See Figure 19.1 for locations along line of section.*

formation, however, may be the feather edge of the Ministicoog Member or a facies equivalent of the Ministicoog based on the occurrence of **Cyclammina coksuvorovae** Ushakova in both the type Ministicoog and in the upper Moose Channel of the Caribou Hills. Palynomorphs recovered from the Moose Channel Formation are indicative of the Paleocene (Ioannides and McIntyre, 1980). A compatible age is suggested by **C. coksuvorovae** which is known to range from the Campanian to the Paleocene in the West Siberian Lowlands of the Soviet Unit (Subbotina, 1964).

Reindeer Formation

The revised Reindeer Formation consists of a lower part comprising carbonaceous claystone and shale, lignite, and lesser amounts of sand and pebbly sandstone and an upper part of similar lithologies but with proportionately less coal. Oxidation of many of the carbonaceous and lignitic beds has created prominent reddish bocanne units which dip gently northward across the face of the escarpment. The upper part of the Reindeer is also largely argillaceous and sandy, but with proportionately less lignite and bocanne. Its higher beds are distinguished by numerous coarsening upward cycles, diminishing in thickness from 30 m in the lower part to one to two metres in the upper part, consisting of lignite, shale, and pebbly sandstone. Many shales and fine grained sands or sandstones contain ferruginous concretions and concretionary layers; distinctive U-shaped burrows are preserved in one of these layers near the top of the unit. Marker beds are scarce in the Reindeer Formation, but a persistent, rusty-weathering bentonite occurring near the middle of the formation is traceable from outcrop locality 14 to locality 20, a distance of 8 km.

Many sandstones scattered through the lower part of the formation are conglomeratic, containing chert pebbles and cobbles and, less commonly, blade-shaped quartzite boulders up to 25 cm in length. Most sandstones shed copious gravel scree masking recessive units below. Some conglomeratic sands show steep crossbedding and are superficially indistinguishable from counterparts in the Moose Channel and in the upper part of the Reindeer.

Rich assemblages of Paleocene to Early Eocene palynomorphs occur in the Reindeer Formation. Preliminary results of a concurrent palynological study of the Tertiary sequence in the Caribou Hills have been published by Ioannides and McIntyre (1980). Although the Reindeer is largely of terrestrial origin (probably delta plain), occasional marine sedimentation is indicated by rare occurrences of the foraminifer, **Trochammina** sp. (= **Haplophragmoides** 4106 of Staplin, 1976), probably signifying brackish-water sedimentation, and by the occurrence of nearshore marine to estuarine dinoflagellates of the genus **Wetzeliella** in the upper part of the formation.

The upper contact of the Reindeer Formation is unconformable, drawn in outcrop section 32 (Fig. 19.1, 19.2; section 4 of Mountjoy, 1967) at the top of a thin carbonaceous clay and silt unit interpreted as a regolith. The uppermost beds of the Reindeer Formation contain the genera **Wetzeliella** and **Apectodinium,** suggesting an Early Eocene age. A seven metre thick conglomerate with a whitish-grey-weathering clay matrix overlies the regolith and marks the base of the unnamed sandy white-clay unit. The white-clay unit has yielded a palynomorph assemblage dated post-Eocene. A hiatus, representing at least Middle and Late Eocene time, separates the Reindeer Formation from the sandy, white-clay unit. In the subsurface to the northwest, the Reindeer Formation is not affected to such an extent, if at all, by this unconformity. Hence, a much more complete deltaic sequence there comprises the Reindeer Formation conformably overlain by the "Eocene shale unit".

White-Clay Unit

The sandy, white-clay unit (Fig. 19.2), 40 m thick, consists of silty and sandy kaolinitic claystone with conglomeratic sandstone, carbonaceous claystone, and lignitic beds. Conglomerate with greyish-white-weathering clay matrix occurs at the base and diminishes upwards into a distinctive, white, sandy claystone unit about 15 m thick. The upper part of the unit consists of claystone, sandy conglomerate, and lignite and is capped by an ochrous sandstone. The white kaolinitic clay of this unit contrasts markedly with the brownish grey claystones or shales of the Reindeer Formation, possibly signifying contrasting environments of deposition (fluvial-lacustrine versus delta plain). The contact with the conglomerate of the Beaufort(?) Formation is covered. The palynology of the white-clay unit has been outlined by Ioannides and McIntyre (1980) and a tentative Oligocene age has been determined.

The white-clay unit and the overlying Beaufort(?) Formation have some lithologic similarity, albeit one is clay-dominant, the other sand and gravel dominant. Further research may prove they are members of the Beaufort Formation. For the present, however, an apparent Oligocene age for the white-clay unit raises the possibility that the unit is separate from the Beaufort Formation, dated by Hills et al. (1974, p. 67) as probable Early to Middle Miocene on Banks Island.

Beaufort(?) Formation

The conglomerates overlying the white-clay unit have been assigned questionably to the Beaufort Formation. Gravel scree of the Beaufort(?) blankets much of the escarpment north of outcrop locality 32. The conglomerates are poorly exposed, limonitic, sandy, and interbedded with minor lenses of whitish claystone. Normal-graded, horizontal

bedding and crossbedding were observed. The Beaufort(?) is interpreted to be of fluvial, probably braided stream, origin with the lenses of white claystone representing channel fill. Neither foraminifers nor palynomorphs were recovered from the outcrops sampled. In the subsurface to the north (Richards Island area), however, sections of Beaufort Formation intertongue with marine shales and yield foraminifers and palynomorphs which for the most part indicate a Miocene age (Young and McNeil, in press).

Acknowledgments

The authors gratefully acknowledge F.G. Young who recommended that we undertake this project and who generously provided information in many phases of the study. We thank J. Dixon, A.R. Sweet, and numerous colleagues in the Institute of Sedimentary and Petroleum Geology for their helpful discussions on the geology of the region.

References

Brideaux, W.W. and Myhr, D.W.
1976: Lithostratigraphy and dinoflagellate cyst succession in the Gulf Mobil Parsons N-10 well, District of Mackenzie; in Report of Activities, Part B, Geological Survey of Canada, Paper 76-1B, p. 235-249.

Doerenkamp, A., Jardine, S., and Moreau, P.
1976: Cretaceous and Tertiary palynomorph assemblages from Banks Island and adjacent areas (N.W.T.); Bulletin of Canadian Petroleum Geology, v. 24, no. 3, p. 372-417.

Hills, L.V., Klovan, J.E. and Sweet, A.R.
1974: **Juglans eocinerea** n. sp., Beaufort Formation (Tertiary), southwestern Banks Island, Arctic Canada; Canadian Journal of Botany, v. 52, no. 1, p. 65-90.

Ioannides, N.S. and McIntyre, D.J.
1980: A preliminary palynological study of the Caribou Hills outcrop section along the Mackenzie River, District of Mackenzie, Canada; in Current Research, Part A, Geological Survey of Canada, Paper 80-1A.

Mountjoy, E.W.
1967: Upper Cretaceous and Tertiary stratigraphy, northern Yukon Territory and northwestern District of Mackenzie; Geological Survey of Canada, Paper 66-16, 70 p.

Shawa, M.S.
1978: Sedimentology, stratigraphy and diagenetic history of the Taglu member and equivalents, Mackenzie Delta area, Canada; unpublished Ph.D. thesis, University of St. Andrews, Scotland, 150 p.

Staplin, F.L. (ed.)
1976: Tertiary biostratigraphy, Mackenzie Delta region, Canada; Bulletin of Canadian Petroleum Geology, v. 24, no. 1, p. 117-136.

Subbotina, N.N.
1964: Foraminifery melovykh i paleogeonovykh otlozhenii zapadono-sibirskoi nizmennosti; Trudy VNIGRI, no. 234, 456 p. (Foraminifera of the Cretaceous and Paleogene deposits of the Western Siberian Lowland).

Tozer, E.T.
1955: Geological reconnaissance, Prince Patrick, Eglinton, and western Melville Islands, Arctic Archipelago, Northwest Territories; Geological Survey of Canada, Paper 55-5.

Young, F.G.
1975: Upper Cretaceous stratigraphy, Yukon coastal plain and northwestern Mackenzie Delta; Geological Survey of Canada, Bulletin 249, 83 p.

1978a: Tertiary succession of the Caribou Hills, in Geological and Geographical Guide to the Mackenzie Delta, ed., F.G. Young, Canadian Society of Petroleum Geologists, Calgary, p. 52-57.

1978b: Tertiary stratigraphy of the Mackenzie delta; in Geological and Geographical Guide to the Mackenzie Delta, ed., F.G. Young, Canadian Society of Petroleum Geologists, Calgary, p. 37-41.

Young, F.G. and McNeil, D.H.
Cenozoic stratigraphy of Mackenzie Delta, Northwest Territories; Geological Survey of Canada, Bulletin (in press).

Young, F.G., Myhr, D.W. and Yorath, C.J.
1976: Geology of the Beaufort-Mackenzie Basin; Geological Survey of Canada, Paper 76-11, 65 p.

Young, F.G. and Norris, D.K.
1978: Geological overview of the Mackenzie Delta area; in Geological and Geographical Guide to the Mackenzie Delta, ed., F.G. Young, Canadian Society of Petroleum Geologists, Calgary, p. 1-11.

20.

AGE AND Sr ISOTOPIC COMPOSITION OF THE PYROXENITE CREEK ULTRAMAFIC COMPLEX, SOUTHWESTERN YUKON TERRITORY: AN ALASKAN-TYPE ULTRAMAFIC INTRUSION

David L. Sturrock[1], Richard Lee Armstrong[2], and R.B. Maxwell[1]
Cordilleran Geology Division, Vancouver

Sturrock, David L., Armstrong, Richard Lee, and Maxwell, R.B., Age and Sr isotopic composition of the Pyroxenite Creek Ultramafic Complex, southwestern Yukon Territory: An Alaskan-type ultramafic intrusion; in Current Research, Part B, Geological Survey of Canada, Paper 80-1B, p. 185-188, 1980.

Abstract

The ultramafic rocks of the Pyroxenite Creek Alaskan-type ultramafic complex are late Early Cretaceous in age (K-Ar hornblende 124 ± 4 Ma, K-Ar biotite 113 ± 4 Ma, Rb-Sr biotite 116 ± 4 Ma). The initial $^{87}Sr/^{86}Sr$ isotope ratio for pyroxenite, 0.7027, is identical to values for mid-ocean ridge basalts indicating an origin direct from alkali-depleted mantle. Gabbro-diorite has a higher initial ratio, 0.7037, indicating a contaminated or hybrid origin and ruling out any simple magmatic fractionation relationship between the pyroxenite core and the younger surrounding gabbro-diorite bodies of the complex.

Introduction

The Pyroxenite Creek Ultramafic Complex is located approximately 19 km due west of Haines Junction, Yukon Territory, in the front ranges of the Saint Elias Mountains (Fig. 20.1). The body lies 8 km north of the confluence of the Kaskawulsh and Dezadeash rivers which combine to form the Alsek River. Relief in the area mapped (Fig. 20.2) is 1500 m. Access is provided by a gravel road branching off the Alaska Highway at Bear Creek, and by helicopter.

The complex was mapped by the senior author while participating in Operation Saint Elias (Campbell and Dodds, 1975, 1978) in the summer of 1974. A more detailed report on the geology, petrography, and preliminary geochronometry was submitted as an honours thesis to the University of British Columbia (Sturrock, 1975). The Sr isotope study was completed later by Maxwell and Armstrong.

Geological Setting

The Dalton Fault separates Cretaceous rocks, intruded by the Ultramafic Complex, from Paleozoic rocks that lie to the west (Fig. 20.2). In the mapped area the fault is a shear zone about 1 km wide striking 150°. On a larger scale this fault is part of the Denali fault system (Eisbacher, 1975; Campbell and Dodds, 1978). The Mush Lake Group (Read and Monger, 1975), which lies west of the Dalton Fault, is composed of andesite flows and pyroclastic rocks, limestone, and chert with complex structure. Fossils from areas farther south range from Ordovician to Devonian, but similar appearing rocks to the north are dated as Permian-Triassic (Muller, 1967).

The Dezadeash Group, which lies east of the Dalton Fault, is part of the Gravina-Nutzotin Belt (Berg et al., 1972) which contains sedimentary and volcanic rocks of Late Jurassic to Early Cretaceous age (Eisbacher, 1975). The Dezadeash rocks near the Pyroxenite Creek Complex are fine grained volcanic-fragment greywacke sandstone with a few graded beds and limestone lenses. Prehnite-pumpellyite grade regional metamorphism and multiple stages of folding and faulting obscure stratigraphic details in the Dezadeash Group surrounding the complex. A few bedding attitudes observed near the intrusive contact are parallel in strike to the contact and dip steeply towards it.

Intrusion of the ultramafic body has produced a contact metamorphic aureole approximately 30 m wide. Rocks at the contact were heated to about 800°C at a pressure of about 3 x 10^5 kPa* (Sturrock, 1975).

The Pyroxenite Creek Complex

Ultramafic rocks, discontinuously rimmed by gabbro-diorite, form an oblong body 6.5 km long and 2.5 km wide, oriented with long dimension northwest-southeast (Fig. 20.2). Aeromagnetic data suggest that the body extends, unexposed, further southeast under the Dezadeash River.

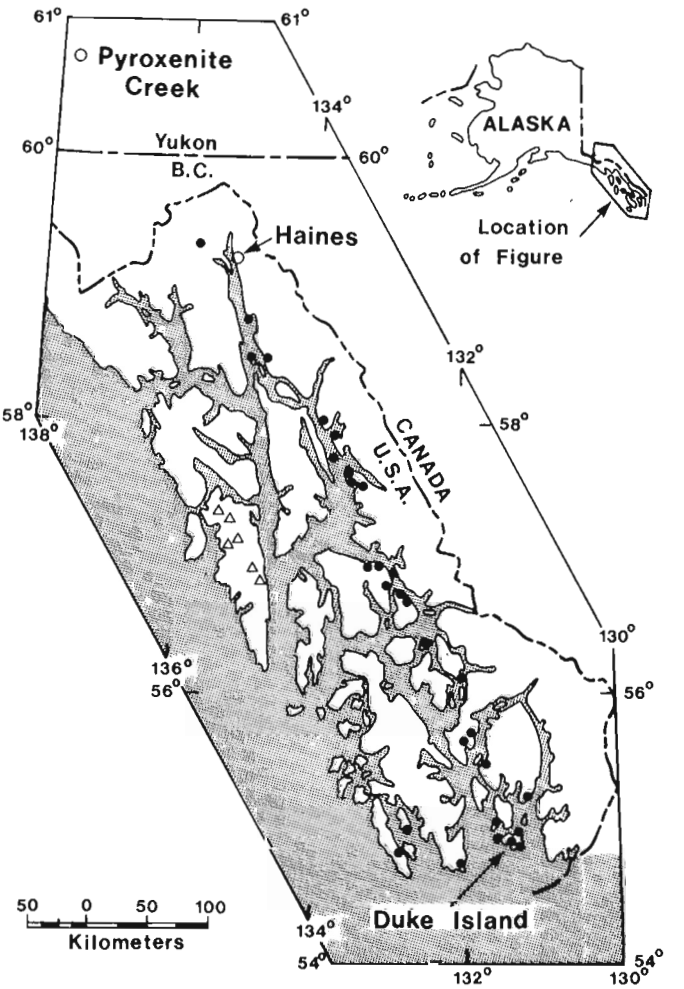

Figure 20.1. Distribution of Alaskan-type ultramafic complexes in southeastern Alaska and adjacent parts of Canada.

[1] Department of Geological Sciences, The University of British Columbia, Vancouver, B.C., Canada, V6T 1W5

[2] Shell Canada Resources Ltd., P.O. Box 880, Calgary, Alberta, Canada, T2P 2K3

* 1 kilobar = 10^5 kilopascal

Table 20.1

K-Ar Data

Sample	Rock Type & Location	Mineral	%K Radiogenic Ar ($cc_{STP} \times 10^6$)	% radiogenic	Date (Ma)
DS 12C	Hornblende Pyroxenite 137°47.9'W, 60°43.5'N	Hornblende	1.071 5.35	94.0	124 ± 4
DS 36	Biotite Pyroxenite 137°48.1'W, 60°43.4'N	Biotite	6.68 30.32	90.9	113 ± 4

K is determined in duplicate by atomic absorption using a Techtron AA4 spectrophotometer and Ar by isotope dilution using an AEI MS - 10 mass spectrometer and high purity ^{38}Ar spike. Errors reported are for one standard deviation. The constants used are:

$K\lambda_e = 0.581 \times 10^{-10} a^{-1}$, $K\lambda_\beta = 4.962 \times 10^{-10} a^{-1}$, $^{40}K/K = 0.01167$ atom per cent.

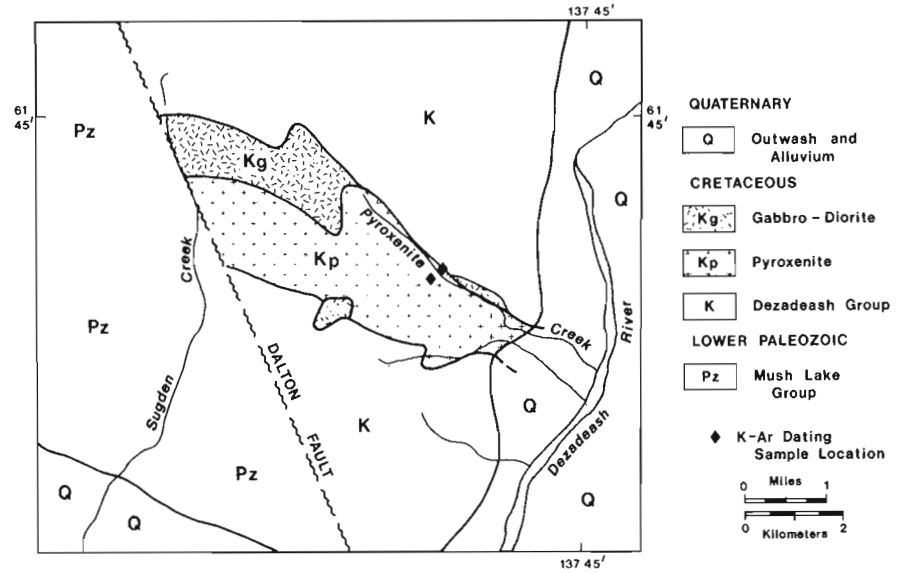

Figure 20.2. *Geological map of the Pyroxenite Creek Ultramafic Complex.*

The western to central interior of the pyroxenite body is composed of fine grained magnetite pyroxenite (85 per cent diopsidic augite, 15 per cent interstitial magnetite (with exsolved hercynite), and one or two per cent olivine and hornblende, while the eastern third of the exposed interior (the topographically and structurally lower part of the body) is coarse grained olivine pyroxenite (85 per cent diopsidic augite, 5 to 25 per cent serpentinized olivine, and minor interstitial biotite). Hornblende pyroxenite forms a border zone about 15 m thick separating the core pyroxenites from surrounding rocks. The modal composition is variable but averages 50 per cent diopsidic augite, 35 per cent hornblende and 15 per cent magnetite.

Gabbro-diorite occurs discontinuously around the ultramafic body. The largest exposure lies on the northwest side of the complex, a narrow band occurs north of Pyroxenite Creek, and a small body is situated on the southeast side of the ultramafic core. Numerous gabbro dykes cut the ultramafic rocks and xenoliths of pyroxenite and sedimentary rock occur within the gabbro-diorite. The gabbro-diorite is a texturally and compositionally variable mixture of euhedral hornblende, pyroxene (diopsidic augite mostly altered to hornblende), and biotite with interstitial plagioclase (An_{55} to An_{62}, extensively saussuritized). Accessory minerals are interstitial potassium feldspar, euhedral magnetite, and euhedral pyrite.

Anorthosite dykes and late pyroxenite dykes are the youngest igneous phases of the complex.

The Pyroxenite Creek Ultramafic Complex is the northernmost member of a 700 km long belt of intrusive complexes (Fig. 20.1) best known for examples studied in Alaska (Taylor, 1967; Irvine, 1973).

Age of the Complex

Both K-Ar (Table 20.1) and Rb-Sr (Table 20.2) dates for the pyroxenite body agree on an Early Cretaceous age. Biotite K-Ar and Rb-Sr (Table 20.2) dates are concordant at 113 ± 4 and 116 ± 4 Ma, respectively. Hornblende K-Ar is slightly older 124 ± 4 Ma. These indicate emplacement closely following deposition of the Dezadeash Group. Lanphere and Eberlein (1966) reported K-Ar dates of 102 to 112 Ma for several complexes in Alaska. The Sr isotope data for biotite and pyroxene of the Haines Complex (≈200 km south-southeast of Pyroxenite Creek) reported by Lanphere (1968) give a calculated Rb-Sr date of 120 ± 9 Ma. The Pyroxenite Creek and Haines complexes are either somewhat older, or have been less subject to later heating and Ar loss than the Alaskan complexes farther to the south. Irvine (1973) postulated an association of the Alaskan-type ultramafic bodies with a discontinuous volcanic belt, the Bridget Cove volcanics of the late Early Cretaceous age. The volcanic rocks show augite-magnetite-olivine phenocrysts in an alkalic trachyte matrix. The original composition is inferred to be a picritic ankaramite. The stratigraphic age of these volcanic rocks, a late accumulation in the Gravina-Nutzotin belt of Berg et al. (1972), is in accord with the isotopic dates that are mostly Albian with the K-Ar hornblende slightly older (Armstrong, 1978).

Sr Isotopic Composition

Mineral separates and whole rock samples of pyroxenite are in close agreement on an initial $^{87}Sr/^{86}Sr$ isotope ratio of 0.7027 which is remarkably low for igneous rocks intruded away from mid-ocean ridges. This is the same ratio as for mid ocean ridge basalt (0.7024 for fast spreading Pacific ridges according to Hart, 1971 and 0.7027 for Juan de Fuca Ridge basalts according to Hedge and Peterman, 1970) and much less than volcanic arc or ocean island igneous rocks (typically ≈0.7037 according to Pushkar, 1968; Peterman and

Table 20.2

Sr Isotope Data

Sample	Rock Type	Material Analyzed	ppm Rb	ppm Sr	Rb/Sr	Observed $^{87}Sr/^{86}Sr$	Initial $^{87}Sr/^{86}Sr$
DS 16	Gabbro	Whole Rock	34	1407	0.048	0.7039	0.7037
DS 29	Pyroxenite	Whole Rock	1	92	0.010	0.7026	0.7026
DS 12C	Hornblende Pyroxenite	Hornblende	3	575	0.005	0.7026	0.7026
DS Bi	Biotite Pyroxenite	Whole Rock	7	210	0.033	0.7029	0.7027
DS 36	Biotite Pyroxenite	Pyroxene	$\sim$ 0.1	95	0.001	0.7028	0.7028
DS 36	Biotite Pyroxenite	Biotite	112	84	1.34	0.7092	0.7028

Calculated biotite date 116 ± 4 Ma, using $^{87}Rb\lambda = 1.42 \times 10^{-11} a^{-1}$.

Rb and Sr concentrations were determined by replicate analysis of pressed powder pellets using X-ray fluorescence. U.S. Geological Survey rock standards were used for calibration; mass absorption coefficients were obtained from Mo Kα Compton scattering measurements. Rb/Sr ratios have a precision of 2% or ±0.3 ppm (1 σ). Sr isotopic composition was measured on unspiked samples prepared using standard ion exchange techniques. The mass spectrometer (60° sector, 30 cm radius, solid source) is of U.S. National Bureau of Standards design, modified by H. Faul. Data aquisition is digitized and automated using a NOVA computer. Experimental data have been normalized to a $^{86}Sr/^{88}Sr$ ratio of 0.1194 and adjusted so that the NBS standard $SrCO_3$ (SRM987) gives a $^{87}Sr/^{86}Sr$ ratio of .71022 ± 2 and the Eimer and Amend Sr a ratio of 0.70800 ± 2. The precision of a single $^{87}Sr/^{86}Sr$ ratio is 0.00013 (1 σ).

Hedge, 1971; and Gill and Compston, 1973). The conclusion that this leads to is of a completely uncontaminated, depleted mantle origin for the pyroxenite magma. The gabbro-diorite initial ratio, 0.7037, is distinctly higher than the pyroxenite ratio suggesting an origin involving contamination with crustal material, perhaps hybridization of pyroxenite magma with wall rocks in crustal magma chambers below the present level of exposure. Sr isotopic measurements for Alaskan complexes (Lanphere, 1968) indicate a scatter of initial ratios (0.7026 to 0.7068), some as low as the value we obtained.

Acknowledgments

G.H. Eisbacher provided supervision in the field. G.H. Eisbacher and R.B. Campbell of the Geological Survey of Canada provided helicopter and other logistical support for the field work. Krista Scott and J.E. Harakal assisted in the Sr and Ar dating, respectively. The Geochronometry program at the University of British Columbia is supported by NSERC operating grants to R.L. Armstrong.

References

Armstrong, R.L.
1978: The pre-Cenozoic Phanerozoic time scale – A computer file of critical dates and consequences of new and in-progress decay constant revisions; American Association of Petroleum Geologists, Studies in Geology, No. 6, p. 73-91.

Berg, H.C., Jones, D.L., and Richter, D.H.
1972: Gravina-Nutzotin belt – tectonic significance of an upper Mesozoic sedimentary and volcanic sequence in southern and southeastern Alaska; U.S. Geological Survey Professional Paper 800D, p. 1-24.

Campbell, R.B. and Dodds, C.J.
1975: Operation Saint Elias, Yukon Territory; in Report of Activities, Part A, Geological Survey of Canada, Paper 75-1A, p. 51-53.

1978: Operation Saint Elias, Yukon Territory; in Current Research, Part A, Geological Survey of Canada, Paper 78-1A, p. 35-41.

Eisbacher, G.H.
1975: Operation Saint Elias, Yukon Territory: Dezadeash Group and Amphitheatre Formation; in Report of Activities, Part A, Geological Survey of Canada, Paper 75-1A, p. 61-62.

Gill, J. and Compston, W.
1973: Strontium isotopes in island arc volcanic rocks, in, P.J. Coleman, editor, The western Pacific: island arcs, marginal seas, geochemistry; University of Western Australia Press, Nedlands, Western Australia, p. 483-496.

Hart, S.R.
1971: K, Rb, Cs, Sr and Ba contents and Sr isotopic ratios of ocean floor basalts; Royal Society of London Philosophical Transactions, Series A, v. 268, p. 573-587.

Hedge, C.E. and Peterman, Z.E.
1970: The strontium isotopic composition of basalts from the Gordo and Juan de Fuca Rises, northeastern Pacific Ocean; Contributions to Mineralogy and Petrology, v. 27, p. 114-120.

Irvine, T.N.
1973: Bridget Cove Volcanics, Juneau area, Alaska: Possible parental magma of Alaskan-type ultramafic complexes; Carnegie Institution of Washington, Year Book 72, p. 478-491.

Lanphere, M.A.
1968: Sr-Rb-K and Sr isotopic relationships in ultramafic rocks, southeastern Alaska; Earth and Planetary Science Letters, v. 4, p. 185-190.

Lanphere, M.A. and Eberlein, G.D.
1966: Potassium-argon ages of magnetite-bearing ultramafic complexes in southeastern Alaska (abs.); Geological Society of America Special Paper 87, p. 94.

Muller, J.E.
1967: Kluane Lake Map-area, Yukon Territory; Geological Survey of Canada, Memoir 340, 137 p.

Peterman, Z.E. and Hedge, C.E.
1971: Related strontium isotopic and chemical variations in oceanic basalts; Geological Society of America Bulletin, v. 82, p. 493-500.

Pushkar, Paul
1968: Strontium isotope ratios in volcanic rocks of three island arc areas; Journal of Geophysical Research, v. 73, p. 2701-2714.

Read, P.B. and Monger, J.W.H.
1975: Operation Saint Elias, Yukon Territory: The Mush Lake Group and Permo-Triassic rocks in the Kluane Ranges; in Report of Activities, Part A, Geological Survey of Canada, Paper 75-1A, p. 55-59.

Sturrock, D.L.
1975: The Pyroxenite Creek Ultramafic Complex: An Alaska-type ultramafic intrusion in the southwest Yukon; unpublished B.Sc. thesis, University of British Columbia, 90 p.

Taylor, H.P., Jr.
1967: The zoned ultramafic complexes of southeastern Alaska; in P.J. Wyllie, editor, Ultramafic and Related Rocks, New York, Wiley, p. 96-118.

21.

K-Ar, Rb-Sr AND FISSION TRACK GEOCHRONOMETRY OF THE BOCK'S BROOK STOCK, KLUANE RANGES, SOUTHWESTERN YUKON TERRITORY

Michael E. Downey[1], Richard Lee Armstrong[2], and Randall R. Parrish[2]
Cordilleran Geology Division, Vancouver

Downey, Michael E., Armstrong, Richard Lee, and Parrish, Randall R., K-Ar, Rb-Sr and fission track geochronometry of the Bock's Brook Stock, Kluane Ranges, southwestern Yukon Territory; in Current Research, Part B, Geological Survey of Canada, Paper 80-1B, p. 189-193, 1980.

Abstract

In the Kluane Ranges, southwestern Yukon Territory, a small zoned pluton, the Bock's Brook Stock, intrudes volcanic and sedimentary rocks of the late Paleozoic Skolai Group and Upper Triassic Nikolai Greenstone. The stock, a medium grained, biotite diorite with a narrow gabbroic border, is intruded by feldspar-porphyritic dykes probably related to Wrangell Lavas; many similar dykes intrude the adjacent Skolai Group and Nikolai Greenstone. Major element chemistry indicates a high-alumina, volcanic-arc tholeiite series classification for both the Bock's Brook Stock and Station Creek volcanics of the Skolai Group, in contrast with a calc-alkaline classification for the Neogene Wrangell Lavas that have been studied by J.G. Souther farther to the west. Concordant isotopic dates for the stock of 13.3 ± 0.5 Ma (K-Ar, biotite), 12.8 ± 1.5 Ma (Rb-Sr mineral isochron) and 14.3 ± 1.2 (fission track, apatite) indicate a mid-Miocene time of emplacement and rapid cooling, within the time span of eruption of Wrangell Lavas. $^{87}Sr/^{86}Sr$ initial ratios of 0.70414 ± 0.00007 for the stock and 0.7031 ± 0.0004 for the volcanics of the Skolai Group are within the normal range for circum-Pacific volcanic arcs.

Introduction

During the summer of 1977 the senior author mapped and collected samples from a small stock and its country rock at the head of Bock's Brook, in the Kluane Ranges of the Saint Elias Mountains. Petrographic, chemical, and isotopic studies of the material that had been collected provided the basis for an honours thesis submitted to The University of British Columbia (Downey, 1978).

The study was suggested by Peter Read, who first examined the stock in 1975 and reported it to be Late Tertiary, apparently intrusive into Wrangell Lavas. A specimen collected by Read produced discordant and contradictory K-Ar dates (R.K. Wanless, written communication to P.B. Read, 1977). Our objective was a more complete description of the stock and an in-depth geochronometric study.

Geological Setting

The Bock's Brook Stock occurs in a region being mapped by the Geological Survey of Canada in Operation Saint Elias (Read, 1976; Read and Monger, 1976; Campbell and Dodds, 1978). The stock itself covers about 2 km^2. Its local geological setting is shown on Figure 21.1. The surrounding rocks are part of the Taku-Skolai terrane (Berg et al., 1972), bounded on the northeast and southwest by the Denali and Duke River faults, respectively. The terrane consists of late Paleozoic arc volcanic and sedimentary rocks (Skolai Group) overlain by thick Upper Triassic tholeiitic basalts (Nikolai Greenstone), followed by Triassic through Cretaceous carbonate and clastics, and overlain by Tertiary sediments (Amphitheatre Formation) and volcanic rocks (Wrangell Lavas) (Jones et al., 1977; Read, 1976; Eisbacher, 1975). The strata are intruded by Cretaceous and Tertiary granitic rocks.

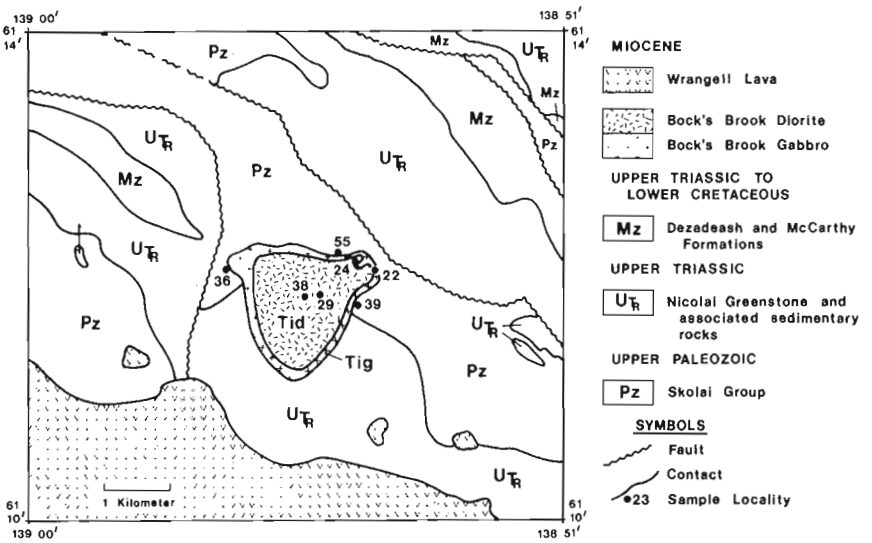

Figure 21.1. *Geological map of the Bock's Brook Stock and its surroundings (after Read, 1976).*

Enclosing Strata

The Station Creek and Hasen Creek formations of the Skolai Group surround the northern half of the stock (Fig. 21.1). The Station Creek is composed of plagioclase (An_{30}) > augite porphyritic volcanic rocks ranging from andesite to basalt in composition and from massive flow to pyroclastic breccia in depositional character. A weak subgreenschist or low greenschist grade regional metamorphism has been imposed on the volcanic rocks. Near the stock contact metamorphism produced a dark grey hornfels and biotitic alteration.

The Hasen Creek Formation in contact with the stock is a well bedded siliceous argillite. Contact metamorphism has produced a dark black to light grey, layered cordierite-quartz hornfels.

Nikolai Greenstone surrounds the southern half of the stock. The flows and breccias of dark to medium green and maroon basalt show greenschist facies metamorphism.

[1] Shell Canada Resources Ltd., P.O. Box 880, Calgary, Alberta, T2P 2K3

[2] Department of Geological Sciences, The University of British Columbia, Vancouver, B.C., V6T 1W5

Table 21.1

Chemical Analyses

	Station Creek Formation				Bock's Brook Stock		
Sample	36-MD-1 Andesite	39-MD-1 Andesite	55-MD-1 Andesite	22-MD-3 Gabbro	24-MD-2 Diorite	29-MD-2 Diorite	38-MD-1 Diorite
SiO_2	58.61	56.05	58.76	53.90	61.88	60.14	62.15
TiO_2	1.83	0.20	1.66	1.60	0.89	1.68	0.87
Al_2O_3	16.47	16.98	16.32	17.27	17.25	16.58	18.86
Fe_2O_3	3.20	4.10	3.69	2.52	1.80	2.15	1.47
FeO	5.04	6.46	5.81	6.41	4.60	5.49	3.74
MgO	1.45	1.97	1.77	3.37	0.90	1.39	0.94
CaO	4.38	6.83	4.73	8.79	3.80	5.05	4.39
Na_2O	5.89	5.13	4.81	4.67	5.35	5.33	4.62
K_2O	2.94	2.07	2.28	1.29	3.35	2.02	2.81
P_2O_5	0.19	0.21	0.17	0.18	0.18	0.17	0.15
L.O.I.	0.22	0.94	0.09	-0.07	-0.04	0.37	1.58

Major elements are reported as weight per cent on a volatile free basis recalculated to 100%.

Analyses by XRF following the procedure of Norrish and Hutton (1969). Procedural details are reported in Armstrong and Nixon (1980).

Table 21.2

K-Ar and Fission track data for Bock's Brook stock

Sample	Material Dated	%K	Radiogenic ^{40}Ar $x10^{6}$ cc STP	% Radiogenic	Date Ma**
38-MD-1	Biotite	6.69	3.482	36.5	13.3 ± 0.5

		Total tracks*		grains counted		average track density (cm^{-2})			
		s	i	s	i	s	i	s/i	
38-MD-1	Apatite	205	537	150	125	$3.137x10^{4}$	$9.862x10^{4}$	0.318	14.3 ± 1.2

*spontaneous = s; induced = i. $\Phi = 7.53 \pm 0.12x10^{14}$ n cm^{-2}

**One sigma errors are given.

K analysis supervised by K. Scott, Ar analysed by J.E. Harakal. K is determined in duplicate by atomic absorption using a Techtron AA4 spectrophotometer and Ar by isotope dilution using an AEI MS -10 mass spectrometer and high purity ^{38}Ar spike. Apatite etch for fission tracks was 30 seconds in 7% HNO at 22°C. The constants used are: $K_{\lambda e} = 0.581 \times 10^{-10}a^{-1}$, $K_{\lambda b} = 4.962 \times 10^{-10}a^{-1}$, $^{40}K/K = 0.01167$ atom per cent, $\lambda_f = 7.00 \times 10^{-18}a^{-1}$.

Wrangell Lavas

Wrangell lavas are exposed on the southwest side of the area studied, where they form one limb of a broad syncline. Flows, 1 to 10 m thick, vary from light to dark grey or brown in colour; the rocks are andesite porphyry with plagioclase phenocrysts (An_{52} to An_{38}) up to 5 mm long. The majority of specimens are vesicular or amygdaloidal with calcite and quartz fillings. Alteration is slight, with only local conversion of glassy matrix to epidote bearing assemblages. The base of the volcanic section is composed of breccia with volcanic clasts up to 2 m in diameter. Rhyolite to andesite dykes cut the Wrangell lavas and breccias. Some are presumably feeders for stratigraphically higher eruptive units.

The Bock's Brook Stock

The Bock's Brook Stock is nearly cylindrical, with a diameter of 1.5 km and is exposed for a vertical distance of 500 m. It is concentrically zoned with a narrow gabbroic border 50 m thick surrounding an interior of intermediate composition. Contacts are generally sharp and dykes of the plutonic rock cut the surrounding strata, including Wrangell volcanic rocks.

The basic border is a dark grey, medium to fine grained subophitic gabbro composed of plagioclase (An_{60} to An_{53}), and augite, with minor orthoclase, apatite, spinel, and opaque minerals. The gabbro is metamorphosed by the interior of the stock, producing secondary biotite plus epidote near the contact and epidote plus chlorite farther away.

Table 21.3

Sample location and Rb-Sr data

Sample numbers	Description	Latitude	Longitude	ppm Sr	ppm Rb	Rb/Sr	$^{87}Sr/^{86}Sr$
Station Creek Formation of Skolai Group							
36-MD-1	Meta-andesite breccia	61.200°	138.94°	443	57.8	0.131	0.7040
39-MD-1	Meta-andesite flow	61.196°	138.91°	672	33.8	0.050	0.7040
55-MD-2	Meta-andesite breccia	61.204°	138.91°	426	24.2	0.057	0.7042
Bock's Brook Stock							
24-MD-2	Augite-biotite-hornblende diorite	61.202°	138.91	450	63.3	0.141	0.7043
22-MD-3	Gabbro, basic border of pluton	61.201°	138.90°	512	16.7	0.033	0.7041
38-MD-1 W.R.	Biotite diorite	61.198°	138.92°	694	49.1	0.071	0.7042
38-MD-1 Plag	Plagioclase			830	16.9	0.020	0.7041
38-MD-1 Ksp	K-feldspar			451	154	0.342	0.7043
38-MD-1 Bi	Biotite			84.0	232	2.76	0.7056
38-MD-1 Ap	Apatite			190	1.2	0.006	0.7042

Rb and Sr concentrations were determined by replicate analysis of pressed powder pellets using X-ray fluorescence. U.S. Geological Survey rock standards were used for calibration; mass absorption coefficients were obtained from Mo Kα Compton scattering measurements. Rb/Sr ratios have a precision of 2% (1 σ) and concentrations a precision of 5% (1 σ). Sr isotopic composition was measured on unspiked samples prepared using standard ion exchange techniques. The mass spectrometer (60° sector, 30 cm radius, solid source) is of U.S. National Bureau of Standards design, modified by H. Faul. Data aquisition is digitized and automated using a NOVA computer. Experimental data have been normalized to a $^{86}Sr/^{88}Sr$ ratio of 0.1194 and adjusted so that the NBS standard $SrCO_3$ (SRM987) gives a $^{87}Sr/^{86}Sr$ ratio of 0.70122 ± 2 and the Eimer and Amend Sr a ratio of 0.70800 ± 2. The precision of a single $^{87}Sr/^{86}Sr$ ratio is 0.00013 (1 σ). Rb-Sr dates are based on a Rb decay constant of $1.42 \times 10^{-11} a^{-1}$. The regressions are calculated according to the technique of York (1969).

The core of the stock is a medium to light grey equigranular hypidiomorphic biotite diorite containing plagioclase (An_{56} to An_{25}), orthoclase, quartz, biotite, and augite with minor apatite and opaque minerals. Alteration consists of slight chloritizxation of biotite, saussuritization of plagioclase, and uralization of augite. Grain size increases toward the centre of the pluton.

Dykes

Diorite dykes 1 m thick with narrow (1-2 mm) chilled margins cut the basic border and surrounding strata.

Late granitic dykes cut both the core and border zones. These are thin (5 cm) hypidiomorphic granular granite (K-feldspar, quartz, biotite, and sodic plagioclase) with microgranite chilled margins.

A variety of dykes ranging from aphanitic rhyolite to basalt occur in the map area. Andesite porphyry is particularly common and was observed cutting both the stock and the Wrangell lavas.

Chemistry

Three samples of diorite and one of gabbro from the stock and three of Station Creek volcanic rocks were analyzed by XRF for purposes of classification and description (Table 21.1). On an alkali-silica plot the stock samples are mildly subalkaline, the Station Creek volcanics transitional subalkaline to alkaline in character. On an AFM plot the stock shows moderate iron enrichment (tholeiitic field) and the volcanics fairly strong iron enrichment. Silica compared to FeO/MgO (Miyashiro, 1974) indicates a tholeiitic

character for both suites but on Al_2O_3 vs normative plagioclase both suites plot in the calc-alkaline field of Irvine and Baragar (1971). These chemical characteristics indicate an affinity of both suites with arc tholeiites as defined by Jakes and Gill (1970), with slight alkali enrichment in the volcanics. The likely tectonic setting for arc tholeiites is an ensimatic, juvenile volcanic island arc.

The Wrangell Lavas are more typically calc-alkaline than the rocks analyzed in this study. Souther (1977 and unpublished data) shows that the Wrangell lavas are subalkaline to transitional alkaline-subalkaline on an alkali-silica diagram, show almost no iron enrichment on an AMF diagram, and are relatively low in silica relative to FeO*/MgO so that most samples plot in the tholeiitic field on Miyashiro's (1974) silica vs. FeO*/MgO diagram. The most striking contrast is the greater iron enrichment shown in the Bock's Brook Stock.

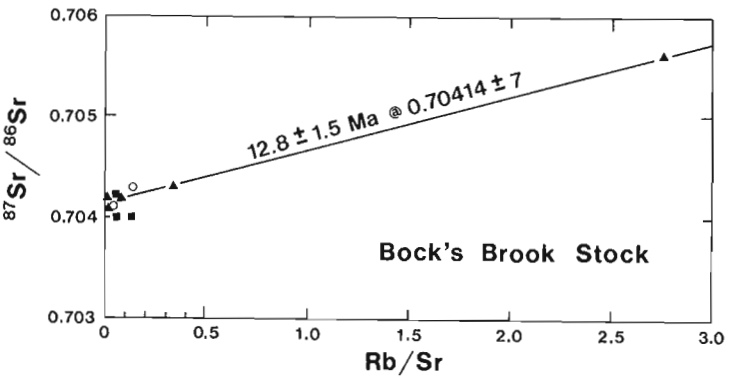

Figure 21.2. Mineral Isochron for the diorite (38-MD-1) of Bock's Brook Stock. Sample 38-MD-1 and its mineral separates are shown as circular spots and samples of country rock as squares.

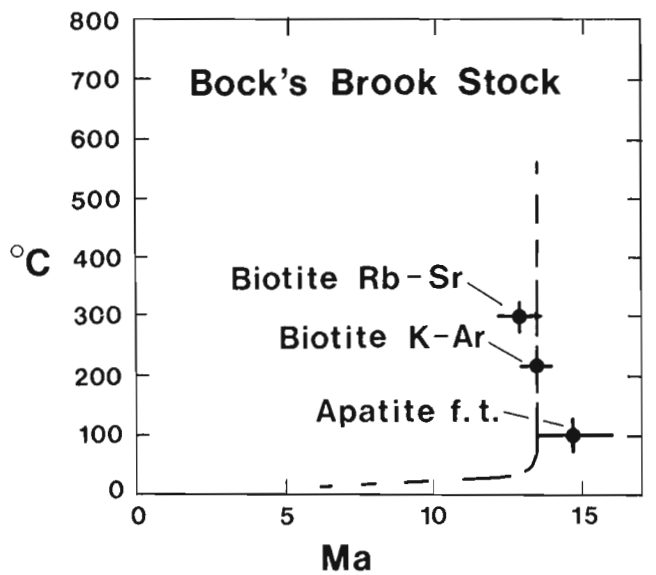

Figure 21.3. Cooling history for Bock's Brook Stock as given by mineral dates of this study and closure temperatures specified by Harrison et al. (1979).

Age of the Stock

Three different techniques used to date the stock all agree on an age of about 13 Ma. All mineral separates dated came from one sample of hypidiomorphic biotite diorite (38-MD-1). A K-Ar date of 13.3 ± 0.5 Ma was obtained for a biotite separate (Table 21.2). A Rb-Sr mineral isochron (Table 21.3, Fig. 21.2) gives a concordant date of 12.8 ± 1.5 Ma. This result is dominated by the Rb-enriched biotite. A fission track date of 14.3 ± 1.2 for apatite (Table 21.2) completes the geochronometry. The apatite was relatively low in U and young, so that track density was low. Abundant crystal defects added to the counting difficulties.

Because the three different dates represent cooling of the sample through different closure temperatures (Wagner et al., 1977; Harrison et al., 1979), a cooling history (Fig. 21.3) is obtained. In this case of concordance of all three dates the cooling must have been rapid (1 Ma to reach <100°C) and final. This is consistent with high level emplacement and an uncomplicated geologic history.

K-Ar dates for Wrangell lavas range from 17.3 to 1.6 Ma (Denton and Armstrong, 1969; Bingham and Stone, 1976; Eisbacher and Hopkins, 1977; unpublished University of British Columbia data cf. R.L. Armstrong and J. Souther). This, and the geological evidence, are consistent in correlating the stock with lower parts of the Wrangell volcanic succession.

Sr Isotopic Composition

The mineral isochron initial ratio of 0.70414 is in agreement with two other whole rock $^{87}Sr/^{86}Sr$ analyses of the stock (Table 21.3). This is similar to the average ratio of 0.7041 for six Wrangell lavas analyzed at the University of British Columbia (R.L. Armstrong and J. Souther, unpublished data) and within the range of values typical of modern volcanic arcs (Faure and Powell, 1972; Gill and Compston, 1973).

The Station Creek volcanic rocks had a $^{87}Sr/^{86}Sr$ ratio of 0.7041 13 Ma ago and 0.7031 ± 0.0004 in the Late Paleozoic. At the time of intrusion both stock and country rock isotopic compositions were identical, so that assimilation-contamination of the magma cannot be quantitatively evaluated using Sr isotopes. In Skolai time the initial ratio was relatively low for a volcanic arc, a ratio of 0.7030 being as low as can be found in modern circum-Pacific volcanic regions. A ratio of 0.7037 is more typical. Only a primitive magma source and ensimatic tectonic setting would be compatible with large-volume magmatism producing such low ratios. Low ratios also occur in areas of slow subduction and anemic volcanism within Phanerozoic sial – such as the Garibaldi Volcanic Belt of British Columbia (Green, 1977), over mantle hot spots such as the Anahim Volcanic Belt of B.C. (Bevier, 1978), and at rift zones, ocean ridges, and some ocean islands (Peterman and Hedge, 1971; Hedge, 1978), but these are all unlikely analogs for the Skolai terrane.

Acknowledgments

We thank P.B. Read for suggesting the project and providing advice and comment throughout. R.B. Campbell arranged helicopter support and was an additional source of field advice. C. Roots assisted in the field, K.L. Scott in the laboratory. J.G. Souther provided unpublished data for the Wrangell lavas, discussion during the study, and manuscript review. The geochronometry laboratory at the University of British Columbia is funded by a National Science and Engineering Research Council operating grant to R.L. Armstrong.

References

Armstrong, R.L. and Nixon, G.T.
1980: Chemical and Sr isotopic composition of igneous rocks from DSDP legs 59 and 60; Initial Reports of the Deep Sea Drilling Project, v. 60, in press.

Berg, H.C., Jones, D.L., and Richter, D.H.
1972: Gravina-Nutzotin Belt – Tectonic significance of an upper Mesozoic sedimentary and volcanic sequence in southern and southeastern Alaska; U.S. Geological Survey Professional Paper 800-D, p. D1-D4.

Bevier, M.L.
1978: Field relations and petrology of the Rainbow Range shield volcano, west central British Columbia; unpublished M.S. thesis, University of British Columbia, Vancouver, B.C., 100 p.

Bingham, D.K. and Stone, D.B.
1976: Evidence for geomagnetic field excursions and secular variation from the Wrangell Volcanics of Alaska; Canadian Journal of Earth Science, v. 13, p. 547-554.

Campbell, R.B. and Dodds, C.J.
1978: Operation Saint Elias, Yukon Territory; in Current Research, Part A, Geological Survey of Canada, Paper 78-1A, p. 35-41.

Denton, G.H. and Armstrong, R.L.
1969: Miocene-Pliocene glaciation in southern Alaska; American Journal of Science, v. 267, p. 1121-1142.

Downey, M.E.
1978: Geology, K-Ar and Rb-Sr geochronometry and chemistry of the Bock's Brook stock in the Kluane Ranges, southwestern Yukon Territory; unpublished B.Sc. thesis, University of British Columbia, 67 p.

Eisbacher, G.H.
1975: Operation Saint Elias, Yukon Territory: Dezadeash Group and Amphitheatre Formation; in Report of Activities, Part A, Geological Survey of Canada, Paper 75-1A, p. 61-62.

Eisbacher, G.H. and Hopkins, S.L.
1977: Mid-Cenozoic paleogeomorphology and tectonic setting of the St. Elias Mountains, Yukon Territory; in Report of Activities, Part B, Geological Survey of Canada, Paper 77-1B, p. 319-335.

Faure, G. and Powell, J.L.
1972: Strontium isotope geology; Springer-Verlag, New York, 185 p.

Gill, J. and Compston, W.
1973: Strontium isotopes in island arc volcanic rocks, in P.J. Coleman, ed., The western Pacific: island arcs, marginal seas, geochemistry; University of Western Australia Press, Nedlands, Western Australia, p. 483-496.

Green, N.I.
1977: Multistage andesite genesis in the Garibaldi Lake area, southwestern British Columbia; unpublished Ph.D. thesis, University of British Columbia, Vancouver, 246 p.

Harrison, T.M., Armstrong, R.L., Naeser, C.W., and Harakal, J.E.
1979: Geochronology and thermal history of the Coast Plutonic Complex near Prince Rupert, British Columbia; Canadian Journal of Earth Sciences, v. 16, p. 400-410.

Hedge, C.E.
1978: Strontium isotopes in basalts from the Pacific Ocean Basin; Earth and Planetary Science Letters, v. 38, p. 88-94.

Irvine, T.N. and Baragar, W.R.A.
1971: A guide to the chemical classification of the common volcanic rocks; Canadian Journal of Earth Sciences, v. 8, p. 523-548.

Jakes, P. and Gill, J.
1970: Rare earth elements and the island arc tholeiitic series; Earth and Planetary Science Letters, v. 9, p. 17-28.

Jones, D.L., Silberling, N.J., and Hillhouse, J.
1977: Wrangellia – A displaced terrane in the northwestern North America; Canadian Journal of Earth Sciences, v. 14, p. 2565-2577.

Miyashiro, A.
1974: Volcanic rock series in island arcs and active continental margins; American Journal of Science, v. 274, p. 321-355.

Norrish, K. and Hutton, J.T.
1969: An accurate X-ray spectrographic method for the analysis of a wide range of geological samples; Geochimica et Cosmochimica Acta, v. 33, p. 431-453.

Peterman, Z.E. and Hedge, C.E.
1971: Related strontium isotopic and chemical variations in oceanic basalts; Geological Society of America Bulletin, v. 82, p. 493-500.

Read, P.B.
1976: Operation Saint Elias, Yukon Territory: pre-Cenozoic volcanic assemblages in the Kluane Ranges; in Report of Activities, Part A, Geological Survey of Canada, Paper 76-1A, p. 187-193.

Read, P.B. and Monger, J.W.H.
1976: Pre-Cenozoic volcanic assemblages of the Kluane and Alsek Ranges, southwestern Yukon Territory; Geological Survey of Canada, Open File 381, 96 p.

Souther, J.G.
1977: Volcanism and tectonic environments in the Canadian Cordillera – A second look; Geological Association of Canada Special Paper 16, p. 3-24.

Wagner, G.A., Reimer, G.M., and Jager, E.
1977: Cooling ages derived by apatite fission-track, mica Rb-Sr and K-Ar dating: The uplift and cooling history of the Central Alps; Memoirs of the Institute of Geological Mineralogy, University of Padova, v. 30, 27 p.

York, D.
1969: Least squares fitting of a straight line with correlated errors; Earth and Planetary Science Letters, v. 5, p. 320-324.

22.

GEOCHRONOLOGY AND PETROLOGY OF THE TKOPE RIVER BATHOLITH IN THE SAINT ELIAS MOUNTAINS, NORTHWESTERN BRITISH COLUMBIA

Blair Jacobson[1], Randall R. Parrish[1], and Richard Lee Armstrong[1]
Cordilleran Geology Division, Vancouver

Jacobson, Blair, Parrish, Randall, R., and Armstrong Richard Lee, Geochronology and petrology of the Tkope River Batholith in the Saint Elias Mountains, northwestern British Columbia; in Current Research, Part B, Geological Survey of Canada, Paper 80-1B, p. 195-206, 1980.

Abstract

The informally named Kaskawulsh group (mainly Paleozoic) in the Saint Elias Mountains is intruded by the Tkope River batholith, a composite, epizonal pluton consisting of six phases ranging from gabbro to granophyre.

Major element chemistry shows a calc-alkaline trend for all the phases, starting with gabbro on the calc-alkaline-tholeiitic boundary of the AMF triangle. A first stage of fractionation removing amphibole, pyroxene, and calcic plagioclase can explain the trend from quartz diorite to granophyre. The large compositional gap between gabbro and quartz diorite and the very large volume of gabbroic magma that would be needed to produce the quartz diorite through granophyre suggest that two primary magmas may be involved.

The batholith was emplaced epizonally by a combination of assimilation, magmatic stoping, and forceful injection.

Isotopic dates of 26.9 ± 0.9 Ma (K-Ar, hornblende), 24.7 ± 0.9 Ma (K-Ar, biotite), 26.6 ± 0.7 Ma and 25.6 ± 0.8 Ma (Rb-Sr, mineral isochrons), 28.8 ± 1.9 Ma (Rb-Sr, whole rock isochrons, including some contaminated samples), 25.2 ± 2.8 Ma (fission track, zircon), and 14.5 ± 1.5 Ma (fission track, apatite), indicate an Oligocene age, and fairly rapid cooling to <200 C, followed by gradual uplift at a rate of 0.3 mm/year to present exposure.

Low initial $^{87}Sr/^{86}Sr$ ratios (0.7031) for two gabbros and several felsic phases suggest an indirect or direct mantle source for the magma. Variations in initial $^{87}Sr/^{86}Sr$ ratios reflect contamination of some rocks by radiogenic strontium from crustal rocks such as argillite of the Kaskawulsh group ($^{87}Sr/^{86}Sr$ = 0.7078 today).

Introduction

During the summer of 1978, geologic mapping was carried out by the Geological Survey of Canada (Operation Saint Elias) in the Saint Elias Mountains in the Tatshenshini map area (114 P) in extreme northwestern British Columbia (Campbell and Dodds, 1979). Tkope River batholith was suggested as a B.Sc. thesis problem by R.B. Campbell. By describing, dating, and analyzing the pluton, its age, origin, and mode of emplacement were determined. The thesis (Jacobson, 1979) contains detailed petrographic descriptions of rock units, chemical analyses, norms, and modes that are not included in this summary.

The Tkope River batholith underlies 160 km^2 of upland, bounded on the southwest by the Tkope River valley, and to the north and east by the O'Connor River valley (Figure 22.1). The area studied lies between 59°21' and 59°40'N and 136°45' and 137°05'W.

Access was by helicopter. The nearest road lies 20 km to the east at Chilkat Pass, milepost 90 of the Haines Road. Field work in the batholith took place during the first two weeks of August. The rugged terrain and extensive glacier cover limited sampling and mapping to traversable ridges. The valleys are all glacier-filled, but glaciation has created excellent exposure on cirque walls.

Enclosing Rocks

The Tkope River batholith occurs within the informally named Kaskawulsh group, which is part of the Alexander Terrane of Berg et al. (1972). The Kaskawulsh group is bounded on the northeast by the Denali and Duke River Fault systems and on the southwest by the Art Lewis or Hubbard Fault (Fig. 22.1). Both the Duke River and Denali Faults are believed to be major right lateral transcurrent faults (Campbell and Dodds, 1978). Read and Monger (1976) and Campbell and Dodds (1978) described the Kaskawulsh group.

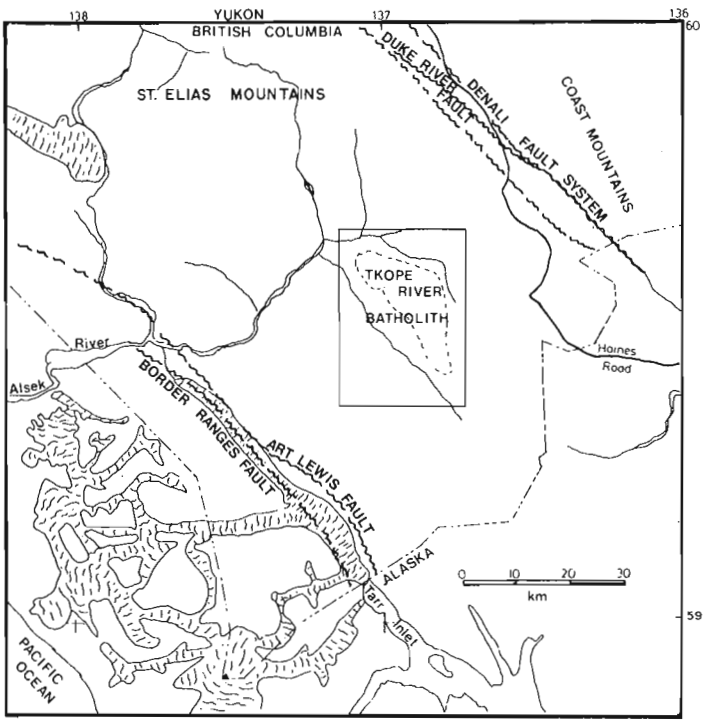

Figure 22.1. *Terrane bounding faults in the Saint Elias Mountains.*

[1]Department of Geological Sciences, The University of British Columbia, Vancouver, B.C., V6T 1W5

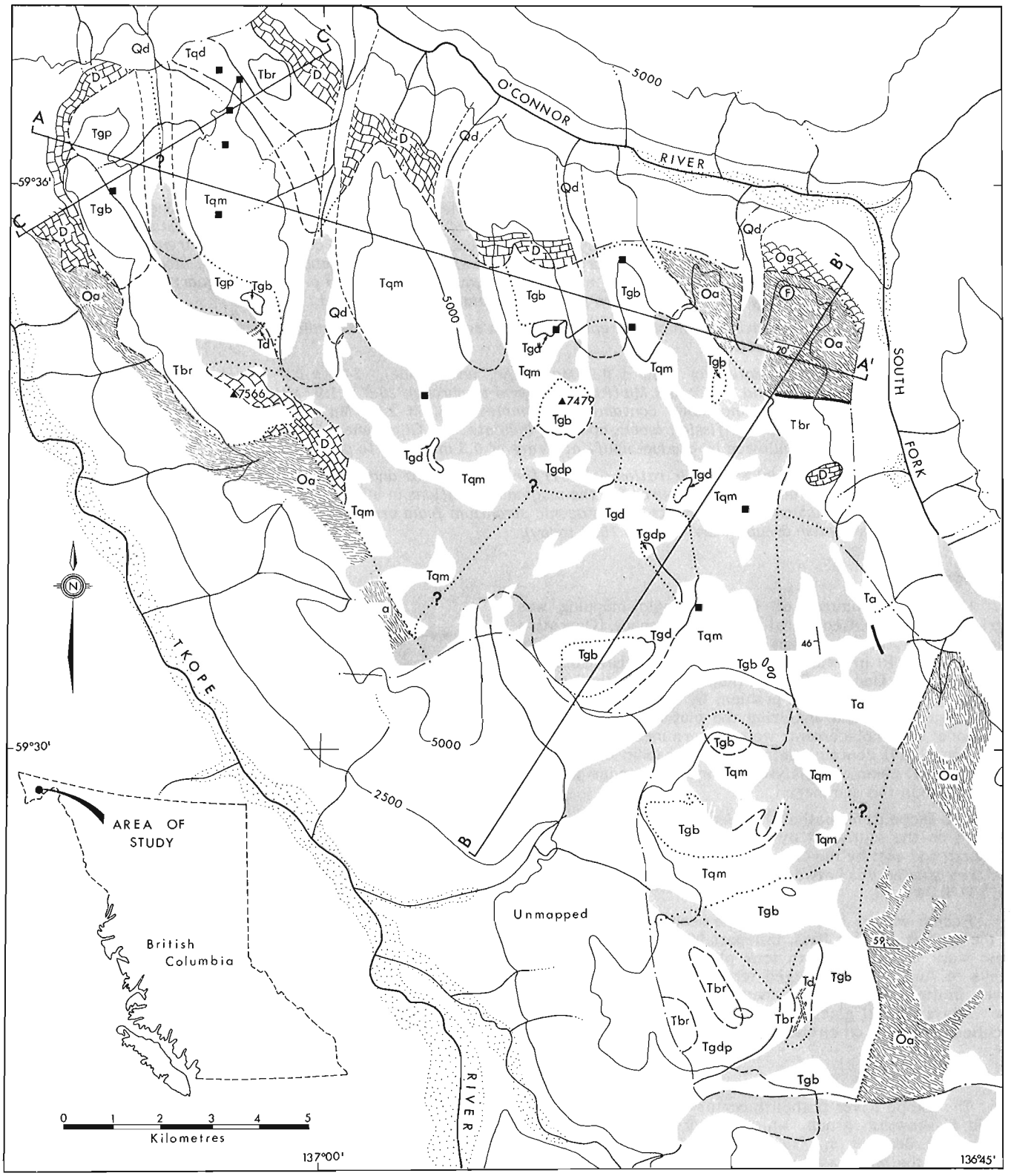
O'CONNOR
RIVER
SOUTH
FORK
TKOPE
RIVER
AREA OF
STUDY
British
Columbia
Unmapped
59°36'
59°30'
137°00'
136°45'
5000
2500
A
A'
B
B'
C
C'
Qd
Tqd
Tbr
Tgp
Tgb
Tqm
Td
Oa
Og
Tgd
Tgdp
Ta
Tbr
▲7566
▲7479
Kilometres
0 1 2 3 4 5

The group is dominated by greywacke-argillite and limestones ranging in age from Ordovician to Triassic. Local accumulations of basic volcanics are also present and in part are Cambrian to Ordovician in age. These are quite commonly pillowed and brecciated. Kaskawulsh group rocks are intruded and contact metamorphosed by plutons ranging in age from latest Paleozoic to Tertiary. They have undergone polyphase deformation, but regional metamorphism is generally no greater than lowest greenschist grade.

Within the study area (Fig. 22.2), Kaskawulsh group limestone of possible Devonian age and Ordovician-Silurian argillite-shale occur in contact with the batholith at its northeastern and southern margins. In addition a younger layered and possibly water-reworked volcaniclastic unit containing breccia, tuff, and poorly-sorted sandstones is present to the east, north, and west. The youngest rocks in contact with the batholith are interlayered andesite and andesite flow breccia that occur to the southeast.

All the enclosing rocks show contact metamorphism extending up to 50 m from the batholith. Argillite near the contact is hornfels. Intense deformation of argillite has created tight similar folds (50 cm amplitude) with sheared axial surfaces. Farther from the intrusive contact, argillite grades into less metamorphosed limy slates.

Recrystallized Devonian (?) limestone along the northwestern and eastern contacts of the batholith is dark grey to black in colour with areas of intense similar folding. No distinction was made between the deformation caused by intrusion and preexisting regional deformation.

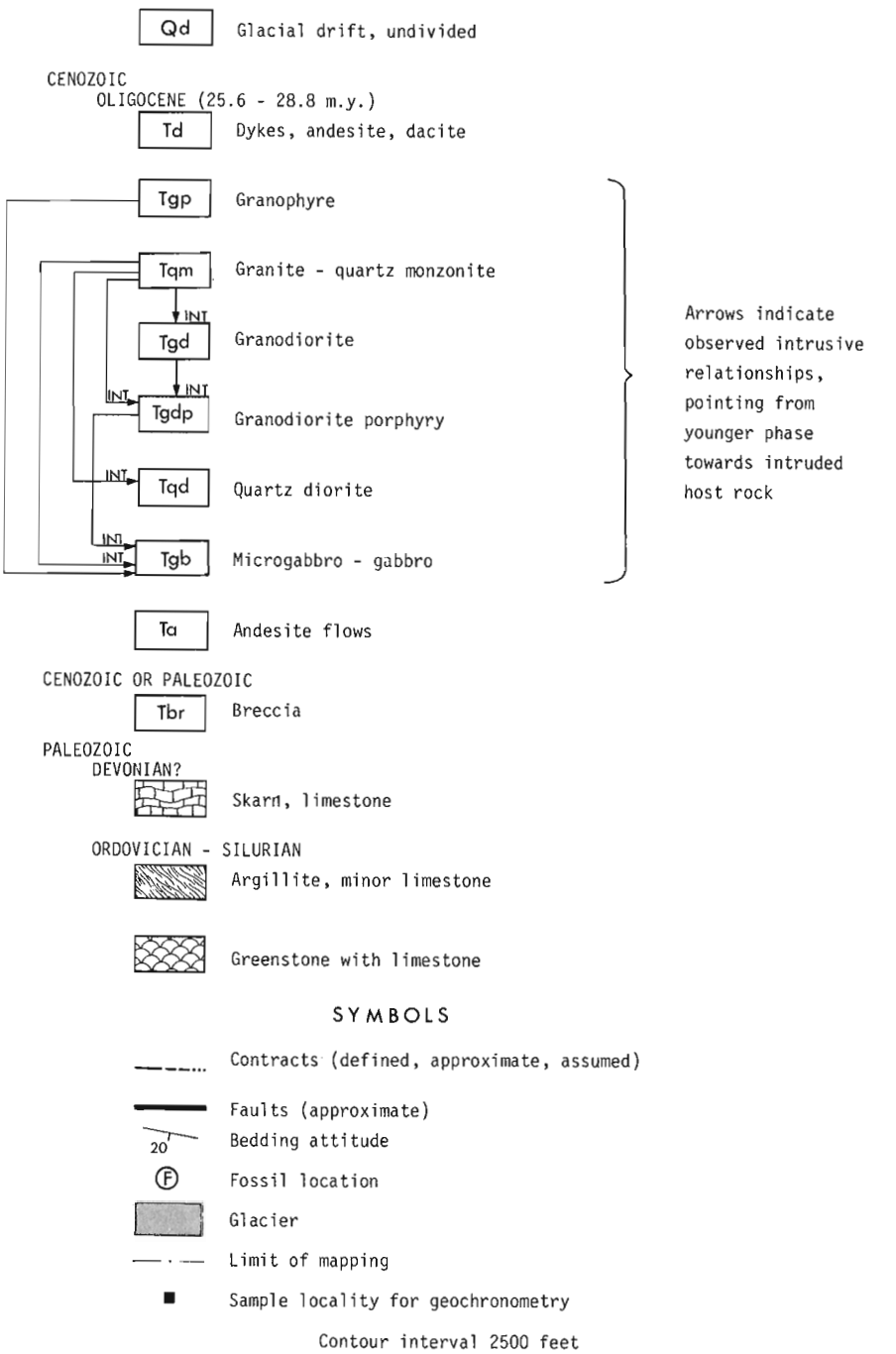

Figure 22.2. *Geologic map of the Tkope River Batholith.*

The age of layered breccia and tuff (Tbr) developed near the batholith margins is controversial. Campbell and Dodds (1979) stated that the breccias and tuffs are extrusive components of the Tkope River batholith and therefore Cenozoic. The volcaniclastic units comprise water-reworked layers containing limestone, siltstone, volcanic rock, and diorite clasts. Such diverse clast lithologies are difficult to explain if the volcaniclastic unit was an apron surrounding a volcanic centre. An alternate interpretation is that the volcaniclastic unit is much older and part of the Kaskawulsh group.

At the contact with the intrusion, limestone clasts in the breccia have been altered to grossularite, epidote, diopside, and sphene, which suggests hornblende hornfels facies metamorphism. Other clasts are silicified and partially recrystallized. One-half kilometre from the contact, thin sections of tuff show abundant subangular to angular fragments of plagioclase, quartzite, volcanic rock, diorite and microgabbro in an aphanitic, iron oxide stained matrix. All the fragments are altered, with plagioclase converted to sericite and epidote.

The andesite flows and flow-top breccias (Ta) occur as layers 5 to 6 m thick. Flattened, vesicle-rich andesite occurs near the top of the flows. The fresh nature of this sequence suggests that these are extrusive equivalents of intrusive phases of the Tkope River batholith.

Plutonic Rocks

Microgabbro-gabbro (Tgb)

The outer margin of much of the batholith and the tops of the ridges in its centre consist of dark grey to black microgabbro to gabbro (Fig. 22.2). In volume and areal extent, this phase is only exceeded by the granite-quartz monzonite. This initial phase intrudes the breccias, limestone, and argillite with sharp, discordant contacts. Neither screens of country rock nor xenoliths were observed in the gabbro.

Gabbro outcrops are extremely rugged, closely fractured, and black weathering. Texture is variable from subophitic in coarser varieties, to ophitic in microgabbro, to gabbro pegmatite. Plagioclase (An_{75-45}),

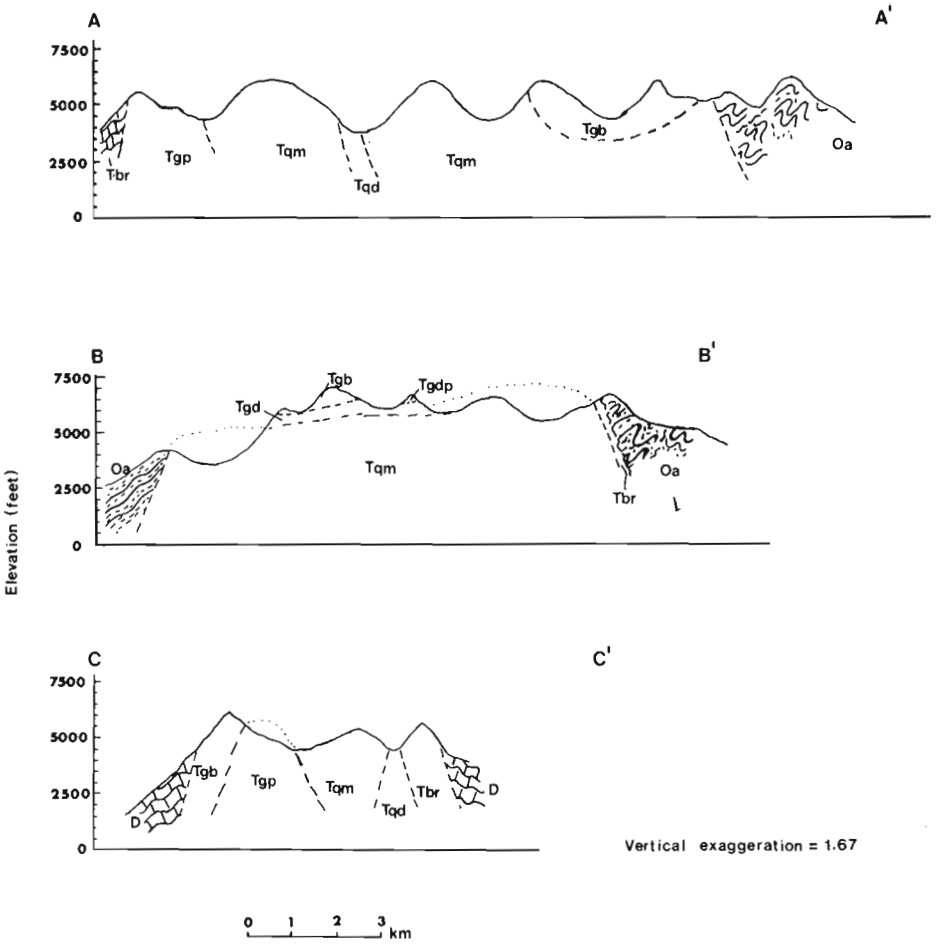

Figure 22.3. *Cross sections of the Tkope River Batholith.*

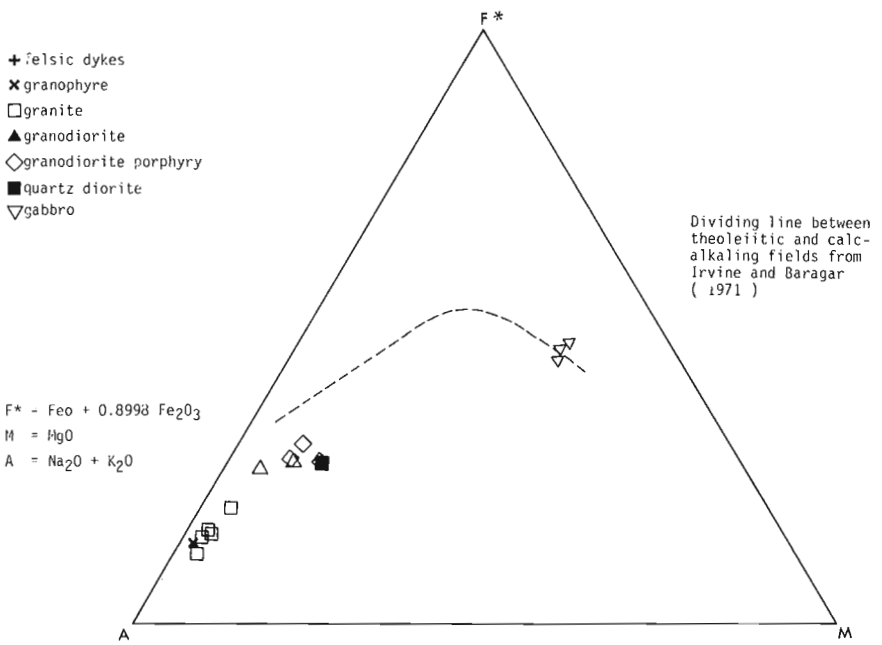

Figure 22.4. *AFM diagram for the six intrusive phases and one dyke phase in the Tkope River Batholith.*

augite, and hypersthene are the principal primary minerals. Secondary actinolitic hornblende, biotite, and chlorite are common. Many of the dark grey, massive augite crystals have uralitized outer margins. Hypersthene shows a greater amount of uralitic alteration. Alteration is manifest with chloritized mafics and fine grained, felted secondary biotite. The more calcic cores of plagioclase feldspars are saussuritized. Generally, the farther a sample is from a contact with a later phase, the less alteration is evident.

Quartz diorite (Tqd)

An elongate (3000 by 500 m) body of quartz diorite occurs in the northwest corner of the batholith (Fig. 22.2). This body has a southern contact that dips under the granite-quartz monzonite and a steeply dipping unexposed northern contact with the breccia.

The quartz diorite is massive, medium grained, and white to light grey on weathered and fresh surfaces. It is not resistant to erosion and forms rounded ridges.

The quartz diorite is hypidiomorphic and composed of quartz, plagioclase (An_{35-55}, with An_{15} rims), orthoclase, biotite, and hornblende. Alteration consists of chloritized mafics and saussuritized plagioclase cores.

Granodiorite porphyry (Tgdp)

Massive, grey, medium grained granodiorite porphyry occurs as three bodies; one is elongate (100 by 1000 m), another is circular (1500 m diameter), and the third is slightly elongated. They underlie the ridge-capping microgabbro-gabbro phase with sharp contacts and a narrow, poorly developed chill zone. This suggests little temperature contrast at the time of emplacement. Phenocrysts (up to 5 mm) of coarse grained plagioclase (An_{45-20}) and coarse grained anhedral quartz (up to 4 mm) occur in a very fine grained groundmass of plagioclase, orthoclase, quartz, biotite, and chlorite. There is a bimodal plagioclase phenocryst size distribution with the larger phenocrysts having highly corroded margins. Quartz occurs as highly anhedral phenocrysts and fine grained anhedral groundmass grains.

In the groundmass, fine grained felted biotite and chlorite exist in an equigranular allotriomorphic mosaic of quartz and orthoclase. Phenocrysts are embayed by material of the groundmass. Chlorite alteration of the fine grained groundmass is extensive; plagioclase is commonly saussuritized.

Granodiorite (Tgd)

Massive, dark grey, heterogeneous granodiorite occurs in the core of the batholith as a 20 to 40 m thick layer underlying the granodiorite porphyry and overlying the granite-quartz monzonite (Fig. 22.3, cross-section, B-B, Fig. 22.2).

At contacts with the overlying gabbro and granodiorite porphyry, the granodiorite contains rounded xenoliths of both phases. Contacts are sharp, with a narrow, weakly chilled margin. Euhedral plagioclase phenocrysts (An_{50-27}) occur in a fine grained to graphic groundmass of orthoclase and quartz with biotite, chlorite, abundant anhedral hornblende, and sparse augite.

The groundmass varies from very fine grained graphic quartz and orthoclase to fine grained, anhedral, almost graphic quartz and orthoclase. The graphic groundmass appears to radiate from the plagioclase phenocrysts, but the abrupt change in relief in thin section suggests the graphic feldspar is chemically distinct from the plagioclase.

Clay alteration of orthoclase, saussuritization of plagioclase, fine grained penninite after hornblende, minor uralization of sparse augite, and alteration of uralitized augite to chlorite occur throughout the unit.

Granite-Quartz Monzonite (Tqm)

The core of the batholith consists of a homogeneous, pink, medium grained granite-quartz monzonite (or simply granite in the I.U.G.S. Classification). This phase intrudes all other phases of the pluton except the granophyre. At contacts there is a reduction in grain size and rounded, recrystallized xenoliths of surrounding phases are very common. In contrast to most previously described phases, the granite has no visible lower contact.

Euhedral, white, medium grained plagioclase (An_{25-10}) crystals sit in a fine to medium grained groundmass of anhedral crystals of light pink orthoclase and grey quartz with minor hornblende and biotite. Accessory minerals are apatite, sphene, and magnetite. The common texture is hypidiomorphic granular, but it becomes porphyritic where anhedral quartz and orthoclase, in partially graphic intergrowth, surround coarser grained, euhedral plagioclase.

Alteration is weak, with potassium feldspar altered to clay and plagioclase to saussurite.

Granophyre (Tgp)

Light pink, fine grained granophyre occurs only at the extreme northwest corner of the pluton where a 1000 by 500 m body intrudes the gabbroic phase. The contact with the microgabbro-gabbro is sharp, with a narrow chill zone. A few xenoliths of microgabbro-gabbro occur in the granophyre. Medium grained, euhedral plagioclase (An_{18-10}) is surrounded by, and in some sections appears to be resorbed by, the much more abundant fine grained graphic orthoclase and quartz. Biotite, magnetite, and epidote comprise 5 per cent of the groundmass. Miarolitic cavities lined with quartz and magnetite are ubiquitous.

Alteration consists of minor replacement of orthoclase by clay, and biotite by chlorite.

Dykes (Td)

Diabase and feldspar quartz-eye porphyry dykes cut all the intrusive phases in the batholith. The dykes are up to 3 m wide, have well-developed chilled margins, and weakly developed alteration zones in the surrounding rock.

The relationship of the dykes to the batholith is unclear. The dykes do not fit the basic to acidic magma trend. They are not simply end-phase crystallization, and may be distinctly younger.

Intrusive Sequence

The intrusive sequence was deciphered using observed contact relationships, degree of alteration, texture, and the general trend from older basic to younger acidic phases with time.

The oldest phase, microgabbro-gabbro, occurs either as pendants on the highest ridges or as massive bodies near the pluton boundary. All other phases, except the quartz diorite, cut the gabbroic phase and contain xenoliths of it.

The quartz diorite is perhaps the second phase emplaced. Intruded only by granite, its sequential position is poorly defined. On the basis of a lesser degree of differentiation, the quartz diorite is placed before the granodiorite porphyry and granodiorite in order of intrusion.

The granodiorite prophyry and granodiorite are very distinctive in the field and crosscutting relationships are clear. Both phases underlie the microgabbro-gabbro and contain abundant gabbroic inclusions. The granodiorite postdates the granodiorite porphyry and at the contacts between these two phases, abundant granodiorite porphyry xenoliths exist in the granodiorite. The granite crosscuts all the previously mentioned phases; xenoliths of all of the more mafic phases occur in it.

The last phase is presumably the granophyre, but it only cuts the gabbro. The granophyric texture and miarolitic cavities suggest rapid cooling in contrast to the slower, deeper, and presumably earlier cooling hypidiomorphic granite.

Many characteristics of the batholith fit Buddington's (1959) criteria for high level emplacement.

Major Element Chemistry

Major element analyses for six intrusive phases and two dykes were provided by R.G. Garrett of the Geochemistry subdivision of the Geological Survey of Canada.

An AFM plot (Fig. 22.4) illustrates the typical tholeiitic and calc-alkaline fields as suggested by Irvine and Baragar (1971). The samples fall in two distinct groups. Granophyre to quartz diorite lie well within the calc-alkaline field. Three gabbro samples plot on the calc-alkaline-tholeiitic dividing line.

In Figure 22.5a, silica versus the total iron to MgO ratio is plotted with the dividing line between the tholeiitic and calc-alkaline fields from Miyashiro (1974). Normative plagioclase composition versus Al_2O_3 weight per cent are plotted on Figure 22.5b. The iron and magnesium depleted granophyre to quartz diorite samples plot in the calc-alkaline fields but show a nearly horizontal (tholeiitic) fractionation trend in Figure 22.5a. The gabbros are iron and magnesium rich and plot on or close to the transition between calc-alkaline and tholeiitic fields in all plots.

Ringwood (1974) outlined the differences between the tholeiitic and calc-alkaline trends. If the gabbro evolved to quartz diorite with little iron enrichment, this is a typical calc-alkaline suite. The strong iron enrichment trend from quartz diorite to granophyre may result from relatively shallow closed-system fractionation without magnetite removal.

Harker variation diagrams (Fig. 22.6) show a smooth decrease in CaO, FeO, and MgO, with differentiation for all phases. This is not observed in the Al_2O_3 versus SiO_2 diagrams, because the gabbros plot off the quartz diorite to granophyre trend. K_2O increases with differentiation, especially during later stages. In all variation diagrams, the gabbros are quite separate from the quartz diorite to granophyre series.

In the Tkope River batholith, Na/K and Ca/Na ratios in the gabbro differ from those of the quartz diorite. Green and Ringwood (1968) pointed out that amphibole fractionation alone could not alter the Na/K ratio of the residual melt. Because the Na/K ratio in the Tkope River batholith varies from the gabbro to quartz diorite, either pyroxene and plagioclase were also involved in early fractionation or the two magmas had independent origins.

A triangular plot of normative quartz-plagioclase-orthoclase (Figure 22.7a) again shows the gabbro distinctly separated from the rest of the phases. This figure also suggests a curved crystallization path from the gabbros to granophyres. The end product of the fractionation curve, the granophyres and granites, lies in the thermal valley very near the granite minimum.

Feldspars make up a large percentage of all phases. The normative anorthite-albite-orthoclase ternary diagram is shown in Figure 22.7b. Each melt in the ternary diagram should be in equilibrium with plagioclase crystals if the melt is on the plagioclase side of the cotectic trough. By estimating the anorthite content of plagioclase crystals in equilibrium with the melt, the trend in melt composition caused by plagioclase fractionation can be shown. The gabbro samples are in equilibrium with plagioclase crystals of An_{75} (C1) composition (Fig. 22.7b). Fractionation drives the melt towards granodiorite. The granodiorite melt is in equilibrium with plagioclase crystals of An_{56} composition (C2). Continued plagioclase fractionation drives the composition of the melt by way of paths P2 and P3 to the cotectic trough which corresponds to the granophyre composition. At this stage potassium feldspar forms simultaneously with plagioclase and the melt follows the cotectic trough to its minimum. Magma evolution of the Tkope River batholith can be largely explained by this simple system.

In the granodiorite porphyry, the coarse grained plagioclase phenocrysts are mottled and embayed, whereas their rims and fine grained plagioclase crystals are normally zoned.

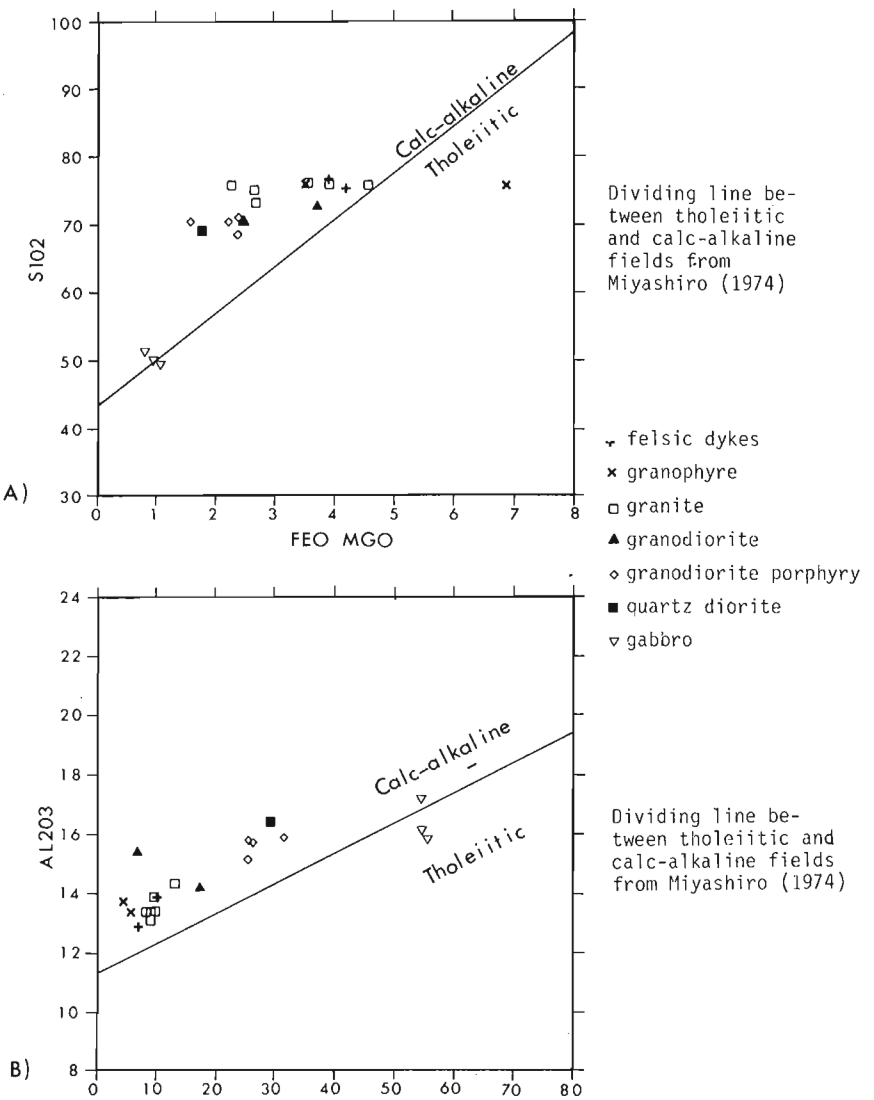

Figure 22.5.

a) SiO_2 (wt.%) versus FeO/MgO diagram.*

b) Al_2O_3 (wt.%) versus normative plagioclase diagram.

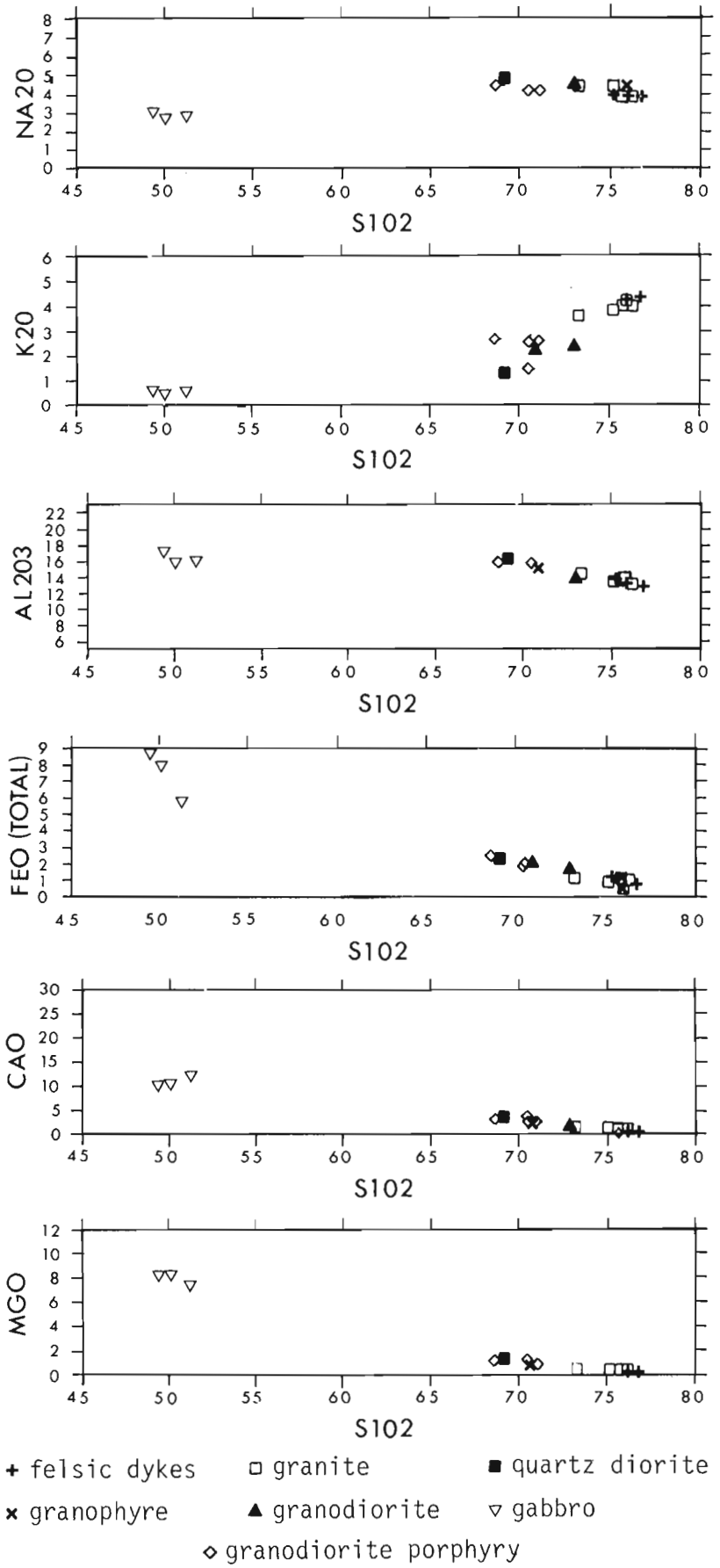

Figure 22.6. *Harker variation diagrams.*

The coarse grained plagioclase are probable relict crystals (restite of White and Chappell, 1977) formed much deeper than the epizonal level. The mottled cores would have formed in a deep magma chamber and the margins at a higher level with lower temperature and pressure.

The chemical data are consistent with a magma evolution similar to Northcote's (1968) model for the Guichon batholith. Separation of hornblende, pyroxene, and calcic plagioclase in the deeper magma chamber would drive the gabbroic liquid to a quartz dioritic liquid. Later this quartz diorite magma with minor mafic and dominant plagioclase segregation would produce the quartz diorite to granophyre series. The alternate view is that two separate magmas from the mantle formed the batholith. The very large volume of gabbroic magma necessary to generate granitic magmas makes the two magma interpretation attractive.

Geochronometry

The age of emplacement was sought using Rb-Sr, K-Ar, and fission track techniques. Conventional procedures for sample preparation and analyses are summarized in the Tables 22.1 to 22.4. Locations of all samples discussed are illustrated on Figure 22.2 and precise geographic coordinates are given in Table 22.1.

Rb-Sr Dates

Data for mineral isochrons and numerous Rb-Sr whole rock analyses are given in Tables 22.1 and 22.2.

The mineral isochron samples (granite 178-1) and quartz diorite 172-1) were chosen to represent different rock types with minimum alteration, and convenient crystal size and mineral abundance for sample preparation. The quartz diorite phase appears to be the second phase emplaced, whereas the granite was next to last. An age difference between the two samples might have been measurable.

The mineral isochrons give dates of 26.6 ± 0.7 Ma and 25.6 ± 0.8 Ma (Fig. 22.8). The older date was from the white, medium grained, pink, hypidiomorphic, inequigranular granite. Both isochrons show minimal scatter, with biotites having high Rb/Sr ratios that control the slopes and calculated dates.

For a whole rock isochron, a wide range of rock types in randomly scattered collecting sites were used. The whole rock Rb-Sr isochron gave 28.8 ± 41.9 Ma, for a regression using all points (Fig. 22.9). Scatter of the whole rock points about the calculated isochron is much greater than analytical error, and could be explained several ways. Metamorphic redistribution of radiogenic strontium in a partially reset older pluton might be suspected. The parent magma could have been inhomogeneous. Perhaps the best explanation is variable contamination with radiogenic strontium. The only argillite sample analyzed gave a high $^{87}Sr/^{86}Sr$ ratio and would be a likely contaminant.

The gabbros, with their low $^{87}Sr/^{86}Sr$ ratios, cannot be greatly affected by strontium contamination. Combining these low gabbro ratios with two granite samples (184-1, 191-1) having low $^{87}Sr/^{86}Sr$ ratios relative to their Rb/Sr ratios, a younger isochron of 28.0 ± 41.2 Ma is attained. This is a maximum age for those samples whether or not they are contaminated.

Samples thought to be contaminated (granites 177-1, 277-1, 178-1; granophyre 169-1; and quartz diorite 173-1) range in location from the batholith boundary (173-1, 169-1, 178-1) to its core (191-1, 227-1). There appears to be no correlation with the amount of contamination and the closeness to country rock. There is a general lack of country rock xenoliths.

The country rock sample (argillite 214-1) plots with a much higher $^{87}Sr/^{86}Sr$ ratio of 0.7078 (Figure 9). By assuming the batholith intruded country rock with a similar $^{87}Sr/^{86}Sr$ ratio as the argillite, the degree of contamination can be calculated (taking into account the relative strontium concentrations). Assimilation of 10 per cent argillite would account for the observed radiogenic strontium contamination if gabbro sample 196-1, contaminated quartz diorite 173-1, and the argillite are used for the calculation.

All samples of the same rock type plot in groups on the whole rock isochron diagram. Each rock type has similar $^{87}Sr/^{86}Sr$ and Rb/Sr ratios except for one granite sample (227-1) that has ratios intermediate to the quartz diorite and granite clusters. Assimilation of gabbro may have modified this sample because it is only 10 m from a gabbro body and abundant gabbro xenoliths surround the sample site.

K-Ar Dates

Two samples were picked for K-Ar dating (Table 22.3). Hornblende, from first phase gabbro, was separated because it has a high blocking temperature for Ar diffusion and should give the oldest mineral date for the batholith. Biotite, from the second phase quartz diorite, has a much lower blocking temperature and should give a younger age limit for the feldspathic rock series.

Hornblende from the medium grained, subophitic, in equigranular gabbro (196-1) gave a 26.9 ± 0.9 Ma date and biotite from the medium grained, hypidiomorphic, equigranular quartz diorite (172-1) gave a date of 24.7 ± 0.9 Ma (Table 22.3).

The gabbro from which the hornblende was separated was altered, with fine grained actinolitic hornblende after pyroxene. If the intensity of the alteration caused by later intrusive phases was great enough, the 26.9 ± 0.9 Ma date could be a time of resetting and alteration.

Fission Track

Zircon and apatite (Table 22.4) were separated from the coarser grained quartz diorite because of their larger crystal size. Biotite from the same rock specimen was dated by K-Ar and Rb-Sr.

The zircon fission track date is 25.2 ± 2.8 Ma. The large error reflects the limited number of grains that were suitable for counting in the irradiated grain mount, but nevertheless the result is similar to K-Ar and Rb-Sr dates for the same rock. In contrast the apatite date, 14.5 ± 1.5 Ma is only half the other dates for coexisting minerals.

Interpretation of Geochronometry

Age of Emplacement

Dates of 26.9 ± 0.9 Ma (K-Ar, hornblende), 24.7 ± 0.9 Ma (K-Ar, biotite), 26.6 ± 0.7 Ma and 25.6 ± 0.8 Ma (Rb-Sr, mineral isochrons), 25.2 ± 2.8 Ma (fission track, zircon), all indicate an Oligocene age for the Tkope River batholith.

This is not a unique Late Cenozoic intrusive event. Christopher (1973) dated biotite at 26.0 to 26.7 Ma from the Cork Molybdenum property, which is a quartz latite porphyry stock within the nearby Taku-Skolai Terrane. Read and Monger (1976) obtained a biotite K-Ar date of 26.0 Ma from quartz latite porphyry dykes intruding the Taku-Skolai Terrane, southwestern Yukon Territory.

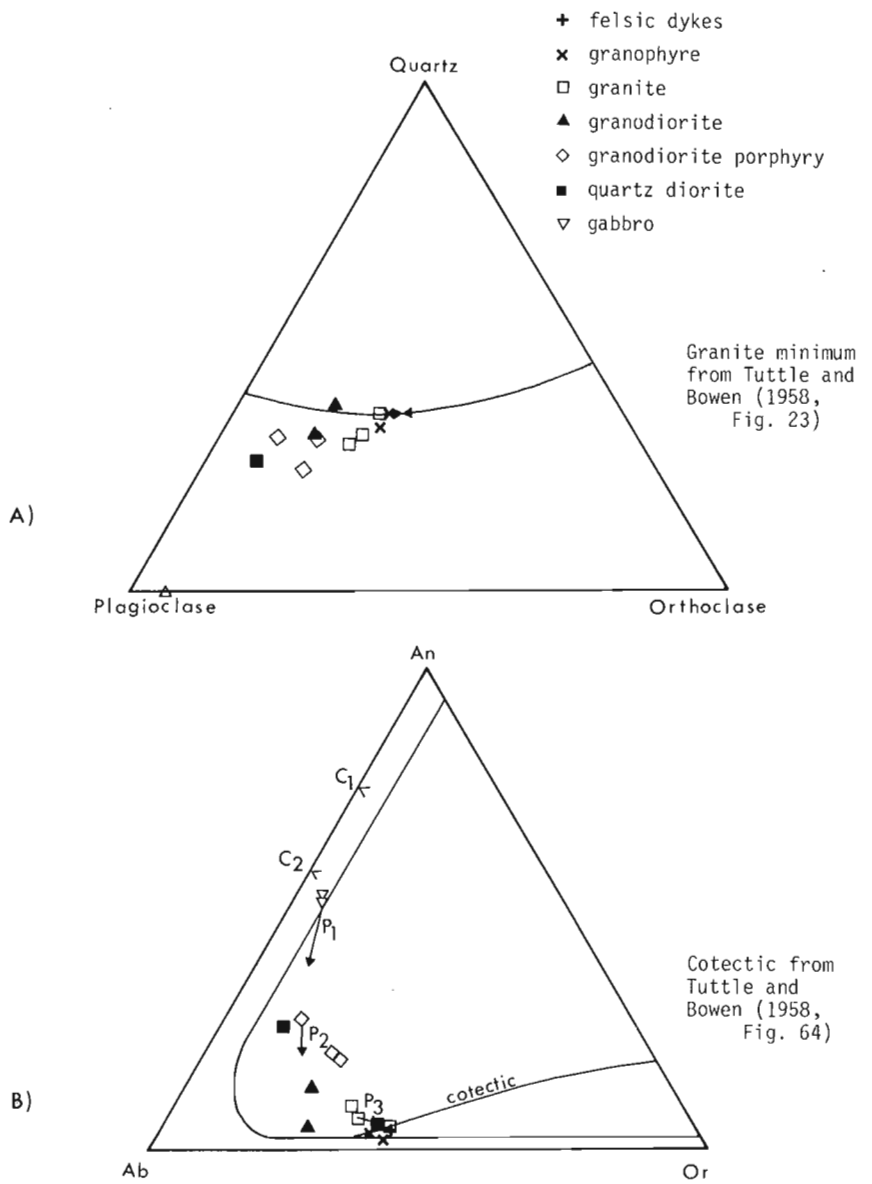

a) Normative quartz-plagioclase-orthoclase diagram.
b) Normative anorthite-albite-orthoclase diagram.

Figure 22.7

Table 22.1

Rb-Sr analyses, Sr isotopic compositions, and whole rock isochron for the Tkope River Batholith

Date Initial $^{87}Sr/^{86}Sr$	All whole rock data 28.2 ± 1.9 Ma 0.70346 ± 0.0002			Selected subset of whole rock data 28.0 ± 1.2 Ma 0.70306 ± 0.0002 0		
Sample Number Description	196-1 Gabbro	198-1 Microgabbro	203-1 Gabbro	172-1 Quartz Diorite	173-1 Quartz Diorite	177-1 Granite
N Latitude	59°34.4'	59°34.45'	59°35.4'	59°37.0'	59°37.4'	59°36.5'
W Longitude	136°53.1'	136°54.5'	136°53.2'	137°1.75'	137°2.4'	137°1.75'
ppm Sr	275	263	278	250	238	64.2
ppm Rb	13.6	11.8	39.5	42.1	62.1	134
Rb/Sr	0.0443	0.0445	0.1417	0.1679	0.2602	2.093
$^{87}Rb/^{86}Sr$	0.1426	0.1287	0.4097	0.4856	0.7521	6.055
$^{87}Sr/^{86}Sr$	0.7031	0.7031	0.7036	0.7038	0.7039	0.7067
Sample Number Description	178-1 Granite	184-1 Granite	191-1 Granite	227-1 Granite	169-1 Granophyre	214-1 Argillite
N Latitude	59°35.6'	59°33.5'	59°32.9'	59°31.75'	59°36.0'	59°34.0'
W Longitude	137°2.0'	136°57.5'	136°50.8'	136°51.2'	137°4.25'	136°49.7'
ppm Sr	52.9	44.5	41.9	118	25.2	106
ppm Rb	155	145	165	110	165	48.5
Rb/Sr	2.940	3.262	3.948	0.9263	6.57	0.4545
$^{87}Rb/^{86}Sr$	8.507	9.437	11.42	2.679	19.02	1.315
$^{87}Sr/^{86}Sr$	0.7072	0.7069	0.7075	0.7050	0.7113	0.7078

Analytical techniques:

Rb and Sr concentrations were determined by replicate analysis of pressed powder pellets using X-ray fluorescence. U.S. Geological Survey rock standards were used for calibration: mass absorption coefficients were obtained from Mo Kα Compton scattering measurements. Rb/Sr ratios have a precision of 2 per cent (1σ) and concentrations a precision of 5 per cent (1σ). Sr isotopic composition was measured on unspiked samples prepared using standard ion exchange techniques. The mass spectrometer (60° sector, 30 cm radius, solid source) is of U.S. National Bureau of Standards design, modified by H. Faul. Data acquisition is digitized and automated using a NOVA computer. Experimental data have been normalized to a $^{86}Sr/^{88}Sr$ ratio of 0.1194 and adjusted so that the NBS standard $SrCO_3$ (SRM987) gives a $^{87}Sr/^{86}Sr$ ratio of 0.71022 ± 2 and the Eimer and Amend Sr a ratio of 0.70800 ± 2. The precision of a single $^{87}Sr/^{86}Sr$ ratio is 0.00013 (1σ). Rb-Sr dates are based on a Rb decay constant of $1.42 \times 10^{-11} a^{-1}$. The regressions are calculated according to the technique of York (1967).

Table 22.2

Rb-Sr data for mineral isochrons

Tkope River Batholith Quartz Diorite Suite					
Date Initial $^{87}Sr/^{86}Sr$	26.6 ± 0.7 Ma = 0.7036 ± .0001				
Sample Number Description	172-1 Whole Rock			Plagioclase	Biotite
ppm Sr	250			276	28.4
ppm Rb	42.1			65.4	309
Rb/Sr	0.1679			0.0236	10.90
$^{87}Rb/^{86}Sr$	0.4856			0.0684	31.56
$^{87}Sr/^{86}Sr$	0.4856			0.0684	31.56
Tkope River Batholith Granite Mineral Suite					
Date Initial $^{87}Sr/^{86}Sr$	25.6 ± 0.8 Ma = .7044 ± .0002				
Sample Number Description	178-1 Whole Rock	Orthoclase	Hornblende and Biotite	Plagioclase	Biotite
ppm Sr	52.8	52.6	10.0	81.6	13.6
ppm Rb	155	297	100	94.9	585
Rb/Sr	2.940	5.643	10.24	1.163	43.30
$^{87}Rb/^{86}Sr$	8.507	16.33	29.65	3.363	125.8
$^{87}Sr/^{86}Sr$	0.7072	0.7013	0.7151	0.7059	0.7510

Table 22.3

K-Ar data and dates

Sample Description	172-1 Quartz Diorite	196-1 Gabbro
Minerals Present	Biotite and minor chlorite	Hornblende and minor pyroxene
K (%)	4.21, 4.19	0.494, 0.476
Ar^{40*} cc/gm (10^{-6}) 4	4.054	0.5120
Ar^{40*}/total Ar^{40*}	77.8%	29.3%
Date	24.7 ± 0.9 Ma	26.9 ± 0.9 Ma

K was determined in duplicate by atomic absorption using a Techtron AA4 spectrophotometer and Ar by isotope dilution using an AEI MS – 10 mass spectrometer and high purity ^{38}Ar spike. Errors reported are for one standard deviation. The constants used are:

$K\lambda_{\varepsilon} = 0.581 \times 10^{-10} a^{-1}$, $K\lambda_{\beta} = 4.962 \times 10^{-10} a^{-1}$,

$^{40}K/K = 0.01167$ atom per cent.

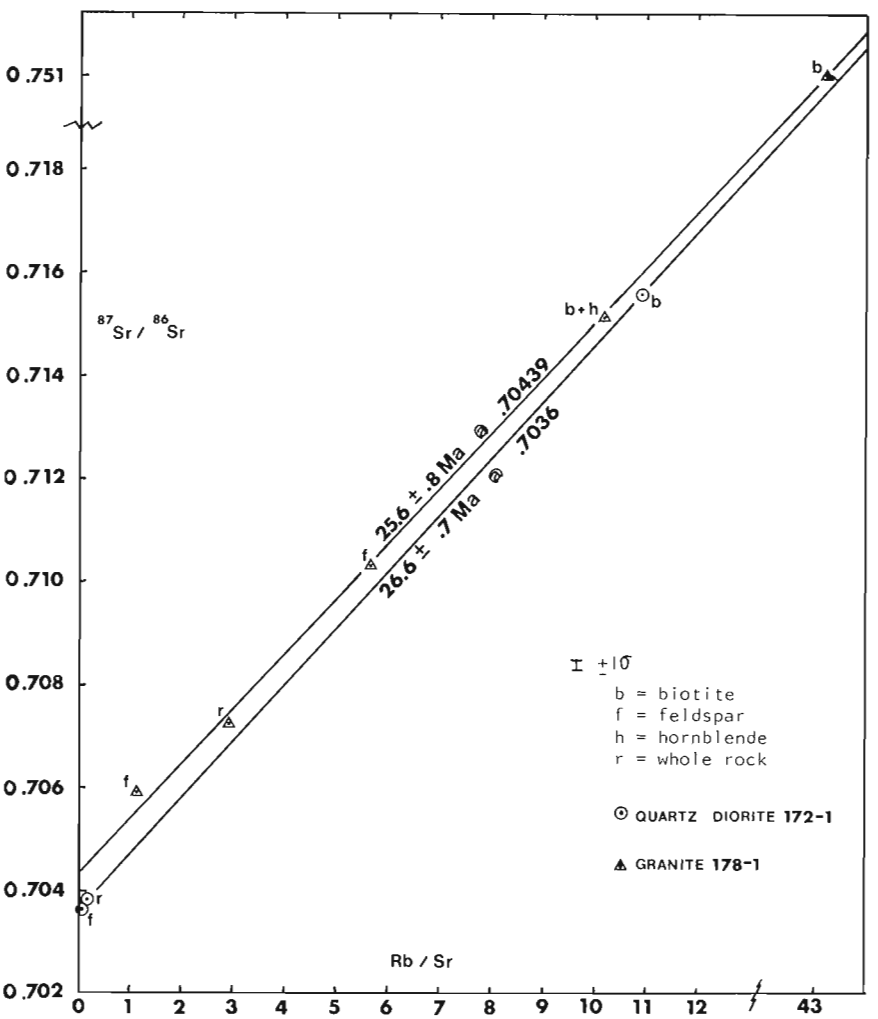

Figure 22.8. *Mineral isochrons.*

In the Yakutat-Saint Elias area, south-central Alaska, Hudson et al. (1977) have dated a Cenozoic intrusive suite that ranges from 30.6 to 24.1 Ma. Hudson (personal communication, 1979) dated Upper Oligocene epizonal to hypabyssal granite to porphyry stocks 70 km east of Ketchikan in southwestern Alaska.

The Oligocene was a time of widely scattered plutonic emplacement in southern Alaska and the Saint Elias region.

Cooling Curve

Harrison et al. (1979) constructed cooling curves – dates plotted against blocking temperature for different dating methods applied to one rock. Using Harrison's blocking temperatures, the various dates for the Tkope River batholith were plotted to construct a cooling curve (Fig. 22.10).

There was approximately a 500°C temperature drop in 1.5 Ma after emplacement. Such a steep cooling curve is consistent with high level emplacement and lack of metamorphic resetting. The apatite date of 14.5 Ma lies almost exactly on a straight line between the end of initial cooling and present day surface temperature (Fig. 22.10). The simplest interpretation is linear cooling at a rate of 7 to 8°C per/Ma. Given a geothermal gradient of 26°C/km (Mathews, 1972), this translates to an average uplift rate of 0.3 mm/year over the last 25 Ma.

Geologic evidence of recent uplift is provided by distortion of mid Tertiary erosion surfaces and uplifted mid to upper Tertiary sedimentary and volcanic rocks. Coal seems at Amphitheatre Mountain and Sheep Creek indicate a low-elevation, subtropical climate about 20 Ma ago (Muller, 1967). Uplift of the Saint Elias region from the low relief to exceptional altitude (>5 km) is thought to have occurred largely during the past 10 to 15 Ma (Eisbacher and Hopkins, 1977). If this is true, the cooling curve of Figure 22.10 would require modification to a sigmoidal shape – somewhat steeper (uplift >0.3 mm/year) in the last 10 Ma and flatter from 10 to 20 Ma (uplift <0.3 mm/year). This is entirely consistent with our data.

Initial $^{87}Sr/^{86}Sr$ Ratios

Granites can form by differentiation of a basaltic parent magma, or by granitization and partial melting of crustal rocks. The initial $^{87}Sr/^{86}Sr$ ratio of a mantle-derived magma or partial melt of lower crust will be low (<0.7040), whereas a granite derived even partly from older crust will have a higher initial $^{87}Sr/^{86}Sr$ ratio (<0.7050). Magma derived from the upper mantle could have a high initial $^{87}Sr/^{86}Sr$ ratio if contaminated by radiogenic strontium from assimilated wall rocks.

The Tkope River batholith initial $^{87}Sr/^{86}Sr$ ratios were all low at 0.7035 ± 0.0002 and 0.7031 ± 0.0002 for the whole rock isochrons, 0.7036 ± 0.0001 for a quartz diorite mineral isochron and 0.7044 ± 0.0002 for a granite mineral isochron. The differences between these initial ratios could be explained through erratic contamination by radiogenic strontium as the magmas rose in the crust.

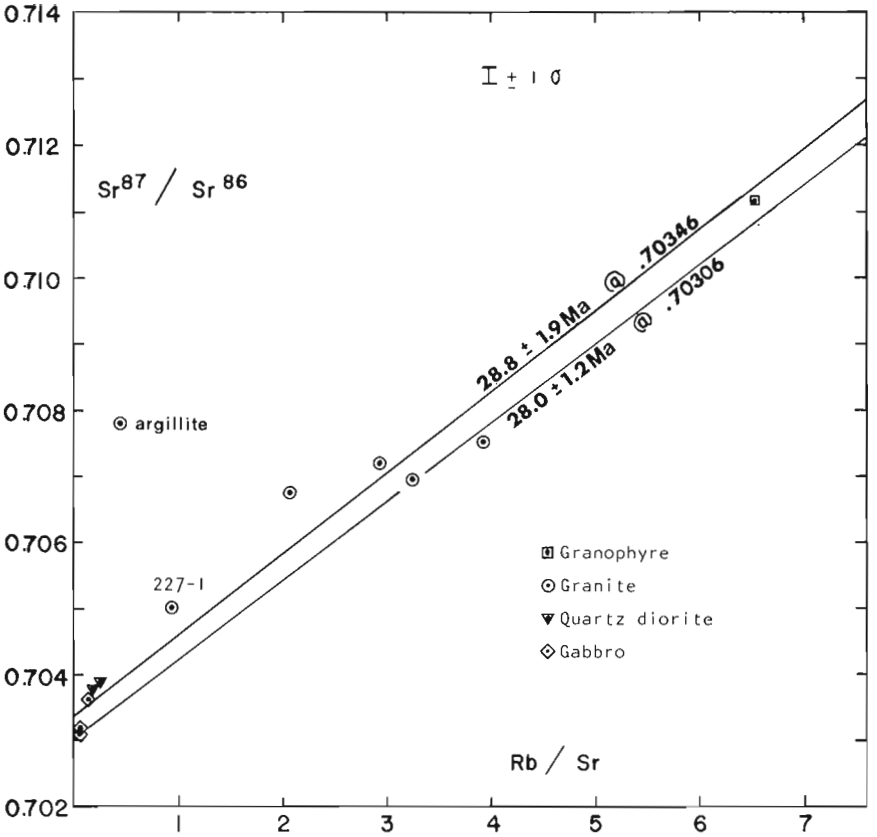

Figure 22.9. *Rb-Sr whole rock data and isochrons.*

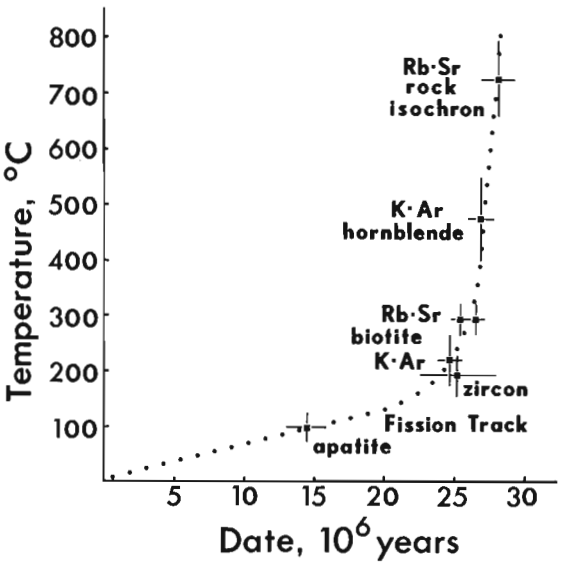

Figure 22.10. *Cooling curve for the Tkope River Batholith. Blocking temperatures are from Harrison et al. (1979).*

Table 22.4

Fission track data and date

Sample 172-1			
Total grains counted	Total track counted	P_s/P_i total	Date and Std. Dev. error
zircon 3	203	2.33	25.2 ± 2.8 Ma
apatite 50i, 75s	253		14.5 ± 1.5 Ma

Analytical Techniques:

The techniques used in the preparation and dating of apatite and zircon by the fission track method are outlined by Naeser (1976). SRM 962 fission track glass standards were used to calibrate the neutron flux from the U.S.G.S. TRIGA reactor in Denver, Colorado. The zircon sample was etched for 48 hours at 205-210°C in a eutectic mix of NaO-KOH. Its muscovite detector was etched for 13 minutes in 48% HF. Tracks were counted under 1600X (zircon) and 800X (apatite). Apatite grains (spontaneous and induced) were etched 30 seconds in 7% HNO_3 at 250°C. The age equation used to calculate dates is as follows:

$T = (6.446 \times 10^9) \ln (1 + 9.322 \times 10^{-18} (P_s/P_i)\Phi)$

Φ zircon = 1.80×10^{14} n/cm^2

Φ apatite = 3.08×10^{14} n/cm^2

$\lambda_F = 7.00 \times 10^{-17}$/year

$\lambda_D = 1.55125 \times 10^{-10}$/year

$U^{238}/U^{235} = 137.88$

All the whole-rock gabbros cluster at a low Rb/Sr ratio on the whole rock isochron. Their $^{87}Sr/^{86}Sr$ ratio is much less than 0.7040, suggesting the magma had a deep crust or upper mantle origin. Le Couteur and Tempelman-Kluit (1976) outlined a decrease in initial $^{87}Sr/^{86}Sr$ southwestward across the Yukon Crystalline Terrane, across a transition zone from plutons derived from or contaminated with old crust with high $^{87}Sr/^{86}Sr$ to plutons freshly derived from the mantle or derived from young and/or oceanic crust or contaminated with this same young and/or oceanic crust with low $^{87}Sr/^{86}Sr$. The Saint Elias rocks are on the low $^{87}Sr/^{86}Sr$ side of this transition zone.

Conclusion

The Tkope River batholith is a composite, epizonal pluton that intrudes argillite, limestone, and breccia units of the Kaskawulsh group (Paleozoic). During the Oligocene, six intrusive phases, distinguished on the basis of textural, chemical, and mineralogical differences and mapped contacts, were emplaced. Relative ages were established on the basis of xenoliths, position in the pluton, degree of alteration, chilled contacts, texture, and the general basic to acidic trend.

Evolution of the calc-alkaline magma was probably by fractional crystallization and multiple intrusion from one or two parental magmas. If fractionation of hornblende, pyroxene, and calcic plagioclase drove the melt from a gabbroic to quartz dioritic composition, only one magma would be required. The rest of the fractionation series can be explained by plagioclase removal.

Emplacement appears to be a combination of assimilation, magmatic stoping and forceful injection.

K-Ar, Rb-Sr and fission track dates indicate on Oligocene age. The Tkope River batholith is one of several Oligocene plutons that are widely scattered throughout southern Alaska and the Saint Elias region.

The cooling curve, with its rapid initial drop in temperature, supports high level batholith emplacement. Since emplacement and initial cooling, further cooling has been at an average rate of 7-8°C/Ma, corresponding to an uplift rate of 0.3 mm/year.

Low initial $^{87}Sr/^{86}Sr$ ratios indicate an indirect or direct upper mantle magma source, with variations in initial ratios reflecting different amounts of radiogenic strontium contamination by assimilation of Paleozoic crust relatively rich in radiogenic-strontium.

Acknowledgments

This study was mostly a B.Sc. Honours research project. We thank R.B. Campbell of the Geological Survey of Canada for suggesting the thesis problem and supporting the field work. Thanks are also due to R.G. Garrett of the Geochemistry subdivision of the Geological Survey of Canada for the chemical data and to D. Stone and W. Walker, who worked as field assistants.

R.L. Armstrong supervised the thesis work at U.B.C. K.L. Scott helped with the Rb-Sr analyses and sample preparation and determined the potassium for the two K-Ar dates. J.E. Harakal determined the argon for the K-Ar dates. R. Berman helped with chemical data manipulation. Laboratory work was funded by National Research Council operating grant G67-8841 to R.L. Armstrong.

References

Berg, H.C., Jones, D.L., and Richter, D.H.
1972: Gravina-Nutzotin Belt – Tectonic significance in southern and southeastern Alaska; U.S. Geological Survey of Professional Paper 800-D, p. D1-D24.

Buddington, A.F.
1959: Granite emplacement with special references to North America; Geological Society of America Bulletin, v. 70, p. 671-747.

Campbell, R.B. and Dodds, C.J.
1978: Operation Saint Elias, Yukon Territory; in Current Research, Part A, Geological Survey of Canada, Paper 78-1A, p. 35-41.

1979: Operation Saint Elias, British Columbia; in Current Research, Part A, Geological Survey of Canada, Paper 79-1A, p. 17-20.

Christopher, P.A.
1973: Application of K-Ar and fission track dating to the metallogeny of porphyry and related mineral deposits in the Canadian Cordillera; Ph.D. thesis, University of British Columbia, 161 p.

Eisbacher, G.H. and Hopkins, S.L.
1977: Mid-Cenozoic paleogeomorphology and tectonic setting of the Saint Elias Mountains, Yukon Territory; in Report of Activities, Part B, Geological Survey of Canada, Paper 77-1B.

Green, T.H. and Ringwood, A.E.
1968: Genesis of basaltic magma; Contributions to Mineralogy and Petrology, v. 18, p. 105-162.

Harrison, T.M., Armstrong, R.L., Naeser, C.W., and Harakal, J.E.
1979: Geochronology and thermal history of the Coast Plutonic Complex, near Prince Rupert, British Columbia; Canadian Journal of Earth Sciences, v. 16, p. 400-410.

Hudson, T., Plafker, G., and Lanphere, M.A.
1977: Intrusive rocks of the Yakutat-Saint Elias area, south-central Alaska; U.S. Geological Survey, Journal of Research, v. 5, p. 155-172.

Irvine, T.N. and Baragar, W.R.A.
1971: A guide to the chemical classification of the common volcanic rocks; Canadian Journal of Earth Sciences, v. 8, p. 523-548.

Jacobson, B.W.
1979: Geochronology and petrology of the Tkope River batholith in the Saint Elias Mountains, northwestern B.C.; B.Sc. thesis, University of British Columbia, 47 p.

Le Couteur, P.C., and Tempelman-Kluit, D.J.
1976: Rb/Sr ages and a profile of initial $^{87}Sr/^{86}Sr$ ratios for plutonic rocks across the Yukon crystalline terrane; Canadian Journal of Earth Sciences, v. 13, p. 319-330.

Mathews, W.H.
1972: Geothermal data from the Granduc area, northern Coast Mountains of British Columbia; Canadian Journal of Earth Sciences, v. 9, p. 1333-1337.

Miyashiro, A.
1974: Volcanic rock series in island arc and active continental margins; American Journal of Science, v. 274, p. 321-355.

Muller, J.E.
1967: Kluane Lake map-area, Yukon Territory; Geological Survey of Canada, Memoir 340, p. 137.

Naeser, C.W.
1976: Fission track dating; U.S. Geological Survey, Open File Report 76-190.

Northcote, K.E.
1969: Geology and geochronology of the Guichon Creek batholith, British Columbia; Ph.D. thesis, University of British Columbia, 190 p.

Read, P.B., and Monger, J.W.H.
1976: Pre-Cenozoic volcanic assemblages of the Kluane and Alsek Ranges, southwestern Yukon Territory; Geological Survey of Canada, Open File 381, 96 p.

Ringwood, A.E.
1974: The petrological evolution of island arc systems; Journal of Geological Society of London, v. 130, p. 183-204.

Tuttle, O.F. and Bowen, N.L.
1958: Origin of granites in the light of experimental studies in the system $NaAlSi_3O_8$-$KAlSi_3O_8$-SiO_2-H_2O; Geological Society of America, Memoir 74, 153 p.

White, A.J.R., and Chappell, B.W.
1977: Ultrametamorphism and granitoid genesis; Tectonophysics, v. 43, p. 7-22.

York, D.
1967: Least squares fitting of a straight line with correlated errors; Earth and Plantary Science Letters, v. 5, p. 230-324.

23.

UPPER PALEOZOIC VOLCANIC AND VOLCANICLASTIC ROCKS IN NORTHWEST TOODOGGONE MAP AREA, BRITISH COLUMBIA

Project 700047

L. Thorstad
Cordilleran Geology Division, Vancouver

Thorstad, L., Upper Paleozoic volcanic and volcaniclastic rocks in northwest Toodoggone map area, British Columbia; in Current Research, Part B, Geological Survey of Canada, Paper 80-1B, p. 207-211, 1980.

Abstract

A suite of volcanic and volcaniclastic rocks in the northwest Toodoggone map area (94E) was investigated during part of the 1979 field season. These rocks were correlated previously with the Permian Asitka Group on the basis of lithology but fossil evidence gives a Mississippian age for at least part of the sequence. Five stratigraphic units have been recognized, and are, from oldest to youngest, (1) feldspathic chlorite schist, (2) phyllite, sericite and calcareous sericite schist, (3) massive rhyolite, chert and sericite schist, (4) carbonate and (5) upper feldspathic, chlorite schist. The rocks are complexly folded and have undergone at least two phases of deformation. They are predominantly calc-alkaline with minor alkaline members. Two plutonic bodies, considered to be early Jurassic in age intrude the formation. Relations to other Paleozoic and Mesozoic rocks in the map area are not known. The sequence is similar in many respects to rocks of the 'Kutcho formation' which host massive sulphide deposits in southeastern Cry Lake map area.

Introduction

Geological mapping in the 1975 field season (Gabrielse et al., 1976) revealed a large area in northwest Toodoggone map area underlain by predominantly low grade metamorphic chloritic and sericitic schist, phyllite and carbonate. The age of these rocks was unknown and they were tentatively correlated with the Upper Paleozoic Asitka Group on the basis of lithology. Another possible correlation was suggested on the basis of lithological similarity with rocks of the 'Kutcho formation' in southeastern Cry Lake map area (Monger and Thorstad, 1978). The schist terrane was re-examined in 1979 with the objective of defining the stratigraphy and age of the sequence.

Regional Geology

Rocks in northwest Toodoggone map area are separated from the crystalline terrane of the Omineca Crystalline Belt, part of the continental margin, by a probable extension of the Kutcho fault mapped in the Cry Lake map area to the northwest (Fig. 23.1). Mesozoic rocks including the Upper Triassic Takla and lower Jurassic Hazelton formations are near but nowhere in contact with the schist terrane (Fig. 23.2).

Early Jurassic quartz monzonite and early Jurassic diorite plutons intrude and locally metamorphose volcaniclastic rocks in northwest Toodoggone map area.

Stratigraphy

Distinct lithological subdivisions can be recognized in rocks in northwest Toodoggone map area. An extreme degree of deformation and consequent structural repetition of units, however, make it difficult to establish a succinct stratigraphic sequence. Estimation of stratigraphic thickness is also precluded by structural complications.

Five units in probable stratigraphic sequence from oldest to youngest are: lower feldspathic, chlorite schist (Fig. 23.3, unit 1); phyllite, sericite and calcareous sericite schist (unit 2); massive rhyolite, chert and sericite schist (unit 3); carbonate (unit 4) and upper feldspathic, chlorite schist (unit 5).

Unit 1

The feldspathic, chlorite schist is predominantly volcaniclastic with transposed layering and abundant fragmental textures. The rocks weather dark to moss green to grey and are resistant, forming ridges or knobs on ridges characterized by massive to blocky talus.

Fragmental rocks range from ash fall to lapilli tuff and include fine to moderately coarse breccia. Lenses of sericite schist and chert, most abundant in the upper part of the unit, have gradational contacts with underlying greenstone. Sericite schist commonly contains abundant limonite, and upper contacts are generally sharp. Minor interlayered phyllite is also present. A layer of pillow basalt 2 m thick occurs in chloritic schist in the northern part of the area. Pillows are highly flattened in the foliation, having fine grained, dark green, recessive weathering rims. Amygdaloidal pillow cores are filled with epidote. Amygdules decrease in size outward from the centre of the core, and increase in concentration on the structural "tops" side. Overlying the pillowed unit is chlorite tuff and thinly laminated grey-black cherty tuff.

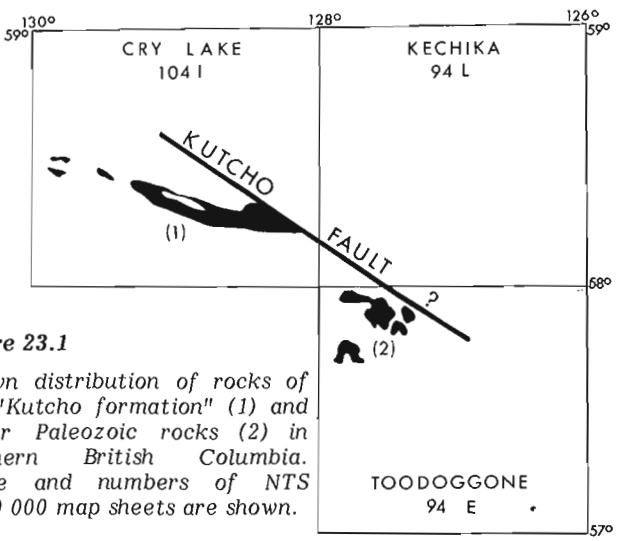

Figure 23.1

Known distribution of rocks of the "Kutcho formation" (1) and Upper Paleozoic rocks (2) in northern British Columbia. Name and numbers of NTS 1:250 000 map sheets are shown.

In thin section chlorite, epidote, feldspar and lesser sericite and carbonate are the dominant minerals. Feldspar is replaced by sericite, epidote and carbonate. Original mafics are altered to chlorite and epidote and the matrix is generally fine grained chlorite, epidote and feldspar.

Contacts with overlying silicic rocks are generally gradational. At some locations a thin member of distinctive olive to brown weathering, schistose tuff 3-4 m thick is present between chloritic schist and overlying silicic schist.

Unit 2

Interlayered white to pale grey-green quartz, sericite schist, calcareous sericite schist and grey phyllite constitute the major part of the unit. Layering, either tectonic or depositional, is on the scale of 1-2 m. Fragmental layers, with highly flattened, white to green clasts of sericite schist 1 to 8 cm long occur in a dark phyllitic matrix. Outcrops are recessive and form saddles in ridges.

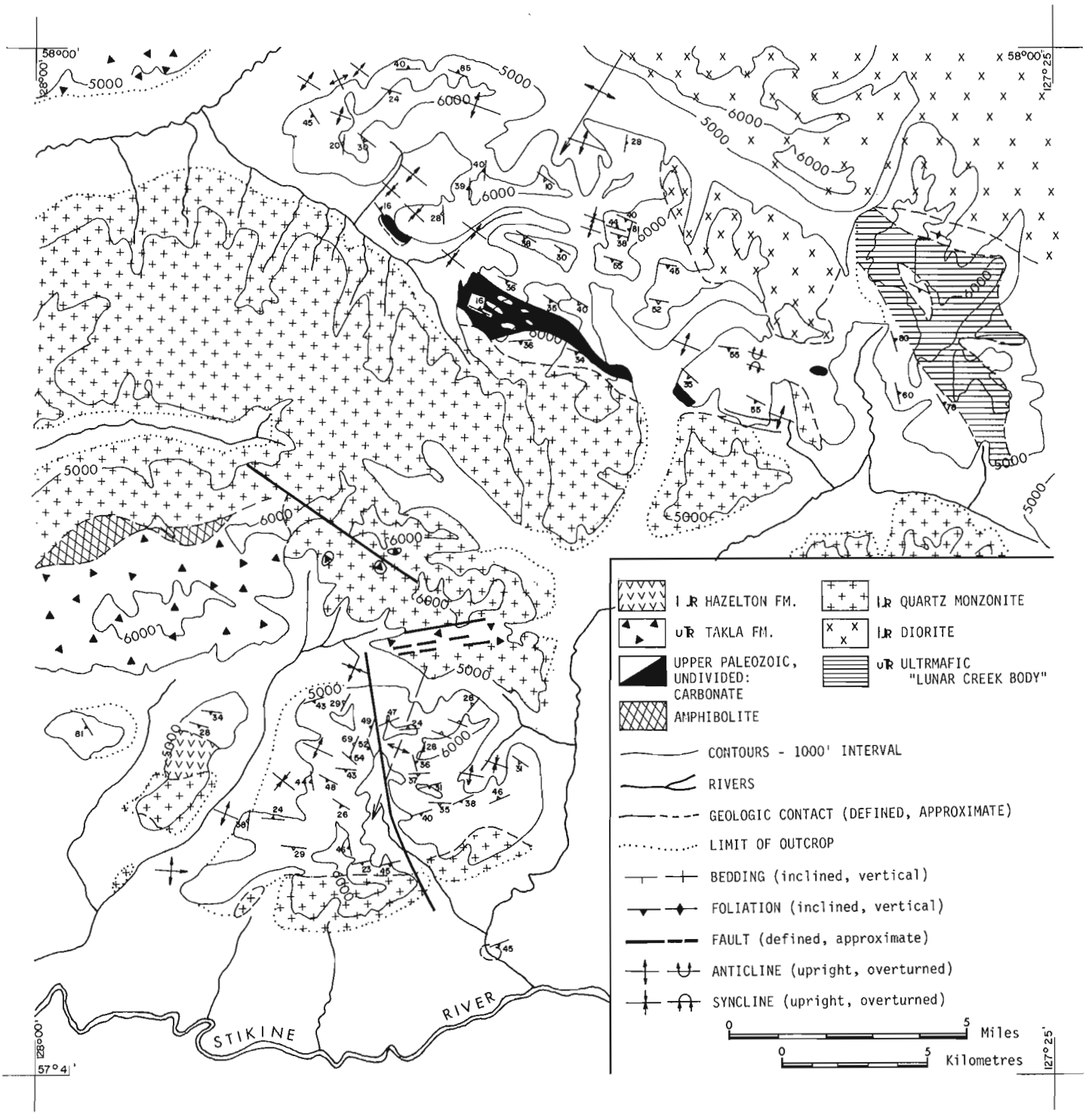

Figure 23.2. *Geologic sketch map showing distribution and major structural elements of Upper Paleozoic rocks and relations to other rocks in the northwest Toodoggone map area.*

Interlayered with sericite schist and generally near the contact with overlying schists of the silicic unit are thin, buff to orange weathering, dolomite beds 1 to 2 m thick containing abundant crinoidal debris.

In one location an upper phyllite and chlorite schist member grades into coarse conglomerate or breccia which is overlain by phyllite and possible metagreywacke.

In thin section sericite with lesser chlorite, and fine grained feldspar and quartz dominate.

Unit 3

Chert, rhyolite, quartzofeldspathic sandstone and sericite schist appear to overlie, and be intercalated with, phyllite and sericite schist, of unit 2. In places the unit rests directly on chloritic schist of unit 1. It is characterized by high silica content, brown to buff weathering, locally rusty, resistant knobs and ridges and very blocky talus. The chert is massive, commonly hematitic and pink weathering.

Rhyolite ranges from massive to well foliated. It is in part flow banded, and laminated. The rocks weather white, green, grey, pink and maroon. Some silicic rhyolitic tuff occurs as pink laminae with chloritic partings less than one mm thick.

Sericite schist with varying degrees of competency are generally white to pale green and may contain brilliant red to yellow gossans.

Intercalated with pink rhyolite and chert are rocks similar to feldspathic chlorite schists of unit 1. They are distinguished by the general presence of quartz and abundant coarse feldspar, by their blue-green weathering as opposed to the characteristic moss green of unit 1, and by the predominance of sericite over negligible amounts of chlorite.

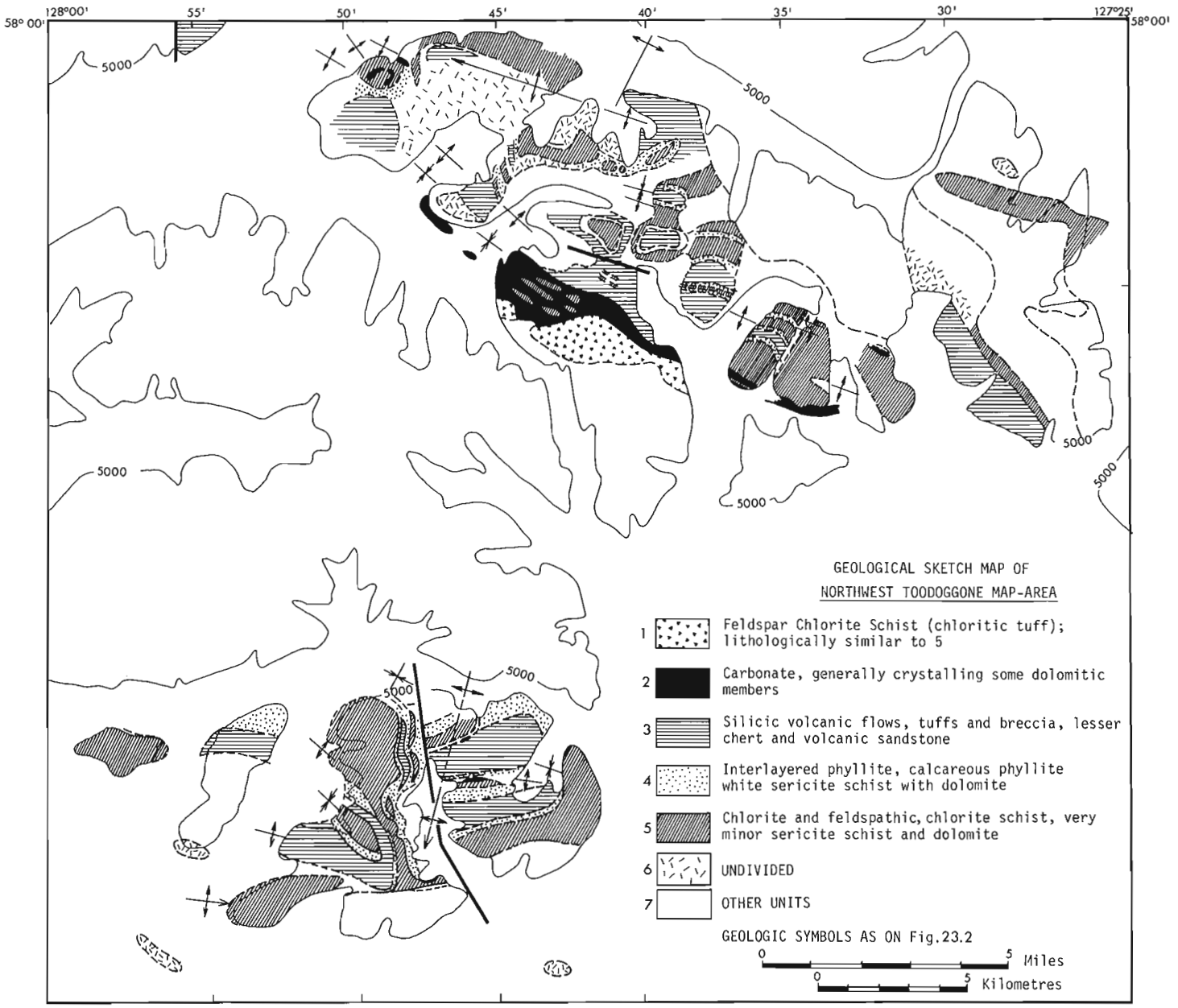

Figure 23.3. *Geological sketch map showing distribution of units within the Upper Paleozoic sequence.*

The lower part of unit three includes a few carbonate beds similar to those of unit 2.

White to tan weathering silicic tuff, sandstone and calcareous, tuffaceous sandstone are also interlayered with massive rhyolite and chert. The rocks are commonly well layered and variably foliated.

Hematite, both as specularite and red hematite, is abundant and imparts a red hue to many of the rocks. Specularite commonly coats fracture surfaces and hematitic blebs giving some chert and rhyolite a characteristic spotted appearance.

In thin section chert consists of fine crystalline quartz with disseminated opaques. Rhyolite textures ae not significantly different, but the presence of feldspar and sericite with quartz give the mineralogy and composition of rhyolite. Sericite schist is largely fine sericite with abundant fine quartz and feldspar grains.

Unit 4

Carbonate of unit 4, structurally overlies and is gradational with silicic rocks of unit 3. Gradational contacts are also evident at its upper contact with overlying basaltic rocks of unit 5. The carbonate ranges from massive, grey weathering, sucrosic limestone, showing little foliation in hand specimen to well foliated, interlayered limestone and calcareous chloritic schist. Buff to orange weathering, dolomitic layers and lenses are common throughout. No fossils have been found in the carbonate. Assuming no structural thickening the thickness of the limestone is thought to be about 25 m.

Unit 5

Resting on, and gradational with, the carbonate is a feldspathic, chlorite schist that is similar to rocks of unit 1. Rocks of unit 5 weather dark green, form resistant outcrops and are typified by very coarse feldspar fragmental rocks in which flattened, white feldspar crystals and crystal aggregates 2 to 20 mm long occur in a chloritic matrix. Chlorite schists are also common. Rocks are generally well foliated but little layering is evident.

Age

Three dolomitic members in the middle part of the sequence contain abundant crinoid debris and Mississippian (Visean) conodonts (M. Orchard, personal communication, 1979).

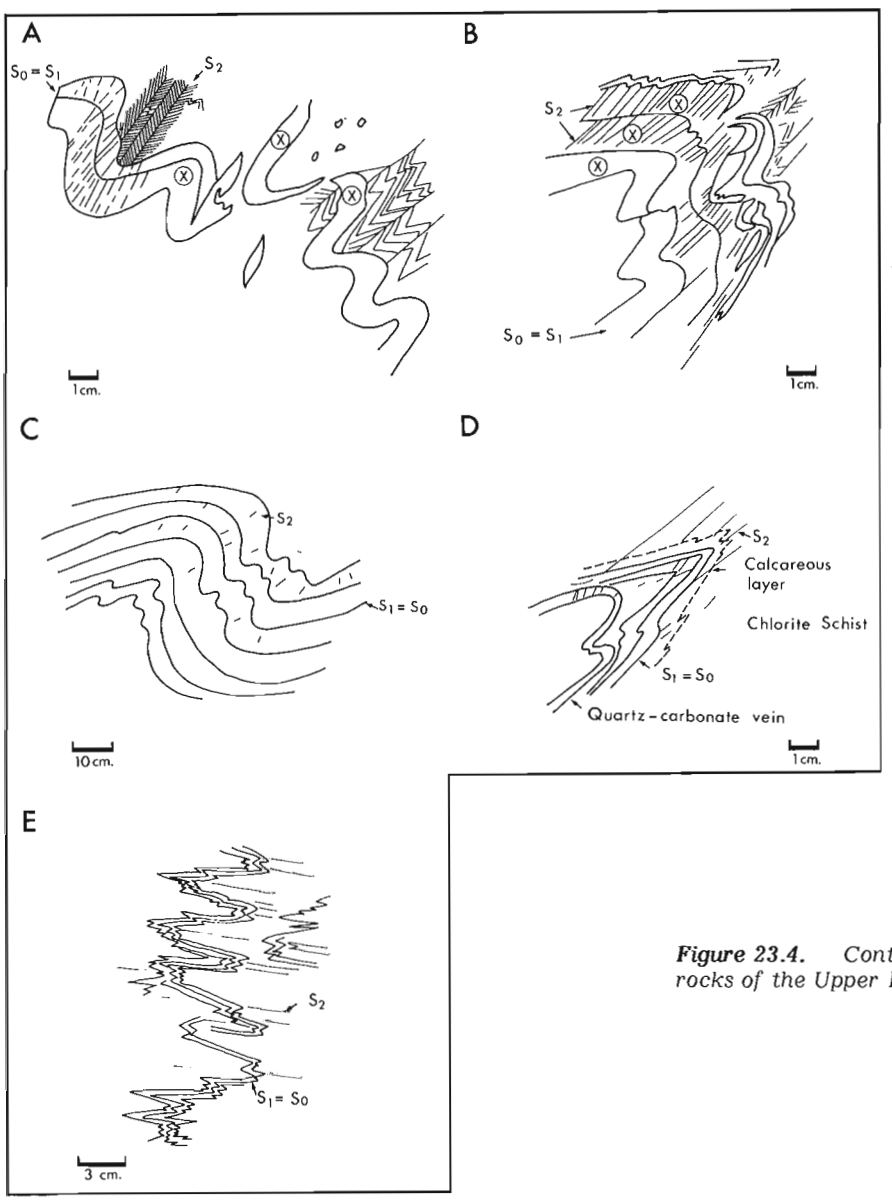

S_0 = *primary layering,*
S_1 = *first foliation,*
S_2 = *second foliation*

A,B: Contrast in fold styles between more competent silicic unit "X" and interlayered quartz-sericite schist. Note boudinage isolated fold hinges and more concentric style of folding in "X" in contrast to chevron style folding in sericite schists. Secondary cleavage is well developed in sericite schists in contrast to a coarse fracture cleavage in "X".

C: Folding in competent rhyolite tuff. A very poorly developed second foliation is superimposed on a folded first foliation and refolded primary layering.

D: Concentric folding in quartz-carbonate vein parallel with S_1 contrast with chevron type folds in chlorite schist.

E: Tight chevron folds in calcareous chlorite schist.

Figure 23.4. *Contrasting fold styles in rocks of the Upper Paleozoic sequence.*

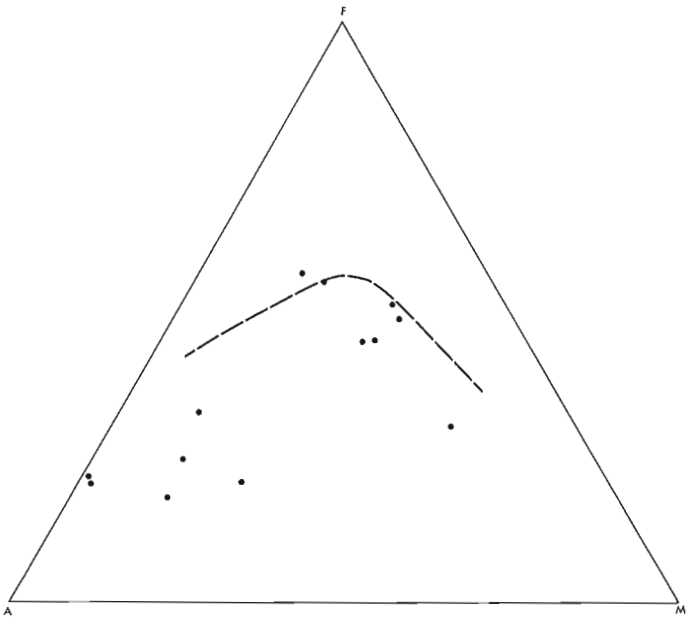

Figure 23.5a. *AFM diagram for rocks of the Upper Paleozoic sequence.*

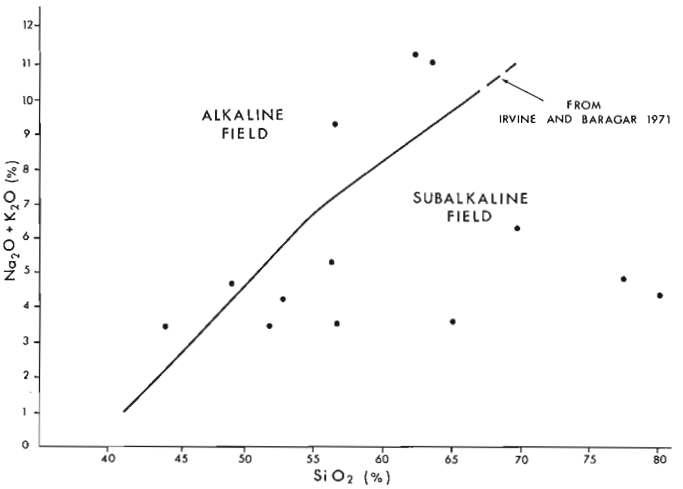

Figure 23.5b. *Alkalis vs. silica Diagram for rocks of the Upper Paleozoic sequence.*

Structure

Rocks in the northwest part of Toodoggone map area show evidence for at least two phases of deformation. Primary layering (S_o) is transposed to parallelism with a penetrative foliation (S_1). This foliation is folded and a second, somewhat less penetrative foliation overprints the first foliation. Folds related to the first deformation are isoclinal as evidenced by transposed layering. Folds related to the second deformation vary to some degree as a function of lithology but are commonly isoclinal to tight, overturned upright structures. In schistose rocks folds range from tight isoclines to en echelon chevron, both generally with a well developed axial planar cleavage (see Fig. 23.4A,B,D,E). In contrast, more competent silicic rich rocks generally form open isoclines to concentric folds with limbs and hinges commonly boudinaged resulting in fractured hinge zones and discontinuous structures (see Fig. 23.4A,B,C). Larger scale folds observed in the field mimic the small scale structures.

Two predominant fold axes directions and foliation orientations are evident. One trends roughly north-south, ranging from 150° to 020° with moderate to steep westerly dips of foliations. The other has west-northwesterly trends, ranging from 090° to 130° with shallow to moderately southwesterly dips of foliation (Fig. 23.2). It is difficult to ascertain which structural trends are oldest, although the second crenulation cleavage generally parallels west-northwesterly trends suggesting these trends may represent the last event.

Chemistry

A limited number of chemical analyses were obtained for the Mississippian rocks in the Toodoggone map area (Fig. 23.5a,b). Plots of this data on "AFM" and "Alkalis versus Silica" diagrams suggest the volcanic assemblage has both alkaline and calc-alkaline whereas more basic, chloritic schists are alkaline.

Plutonic Rocks

An early Jurassic quartz monzonite body and an early Jurassic diorite intrude rocks in the northwest Toodoggone map area. Rocks are locally metamorphosed and veined. Intrusion of the quartz monzonite predates at least one deformation event as evidenced by helicitic garnet observed within the contact metamorphic aureole.

Metamorphism

Volcanic and volcaniclastic rocks are variably metamorphosed generally having mineral assemblages of the lower greenschist facies but locally attaining higher grades near contacts with intrusive bodies.

Chlorite, epidote, feldspar, carbonate and lesser sericite dominate the mineralogy of basic to intermediate rocks whereas sericite, quartz, carbonate and feldspar are the predominant minerals in more silicic members. Local development of garnet, biotite, and staurolite is observed close to contacts with intrusions.

Summary

Rocks in the northwest Toodoggone map area can be divided into fairly persistent crude stratigraphic units. The prominent carbonate unit (unit 4) evident in the northern part of the map area is absent in the south and unit 5 is also apparently absent in southern exposures, suggesting nondeposition or erosion.

Rocks are highly deformed, showing evidence for at least two phases of deformation. Fossils suggest a Mississippian age for the assemblage. Chemically and lithologically the rocks resemble island arc derived volcanic suites.

References

Gabrielse, H., Dodds, C.J., and Mansy, J.L.
1976: Operation Finlay; in Report of Activities, Part A, Geological Survey of Canada, Paper 76-1A, p. 87-90.

Irvine, T.N. and Baragar, W.R.A.
1971: A Guide of the chemical classification at the common volcanic rocks; Canadian Journal of Earth Sciences, v. 8, p. 523-548.

Monger, J.W.H. and Thorstad, L.
1978: Lower Mesozoic Stratigraphy, Cry Lake (104I) and Spatsizi (104J) map areas; in Current Research, Part A, Geological Survey of Canada, Paper 78-1A, p. 21-24.

24.

GEOTHERMAL POTENTIAL OF THE CORYELL INTRUSIONS, GRANBY RIVER AREA, BRITISH COLUMBIA

Jane Leroux[1]
Cordilleran Geology Division, Vancouver

Leroux, Jane, Geothermal potential of the Coryell Intrusions, Granby River area, British Columbia; in Current Research, Part B, Geological Survey of Canada, Paper 80-1B, p. 213-215, 1980.

Abstract

Part of a pluton of the Tertiary Coryell Intrusions of southern British Columbia has been mapped at a scale of 1:50 000. Preliminary measurements by portable gamma ray spectrometer show that the abundant Coryell syenite contains up to 13 ppm uranium, which may account for local high heat flow.

Introduction

The western plutons of the Coryell Intrusions are exposed over an area of about 1000 km^2 in the Monashee mountain range, centred at approximately 118°30'W, 49°20'N, near Grand Forks, British Columbia (Fig. 24.1). They are in contact with the Valhalla Intrusions to the north and west, the Nelson Intrusions and Anarchist Group to the south, and are separated on the east by a fault from the Monashee and Grand Forks groups.

The area was first mapped by Little (1957), who described the Coryell Intrusions as a group of relatively young (Eocene or later) batholiths, stocks and plugs.

The purpose of the study is to determine the heat-producing potential of a pluton of the Coryell Intrusions. These intrusions were chosen for investigation because heat flow measurements in the vicinity are above normal, and several hot springs flow from the granitic and metamorphic rocks surrounding them (Lewis et al., 1979). The study therefore consists of mapping a pluton, measuring its radioactivity and studying its mineralogy and petrology.

Geologic mapping was conducted over a 100 km^2 area between Granby River and Burrell Creek (Fig. 24.1).

Description of Formations

Nelson Intrusions

Little (1957) described the dominant phase of the Nelson Intrusions as a nonporphyritic granodiorite. A porphyritic granite phase is common in the northeast part of the Kettle River map area. The granodiorite in the study area is a coarse grained, hypidiomorphic-granular rock consisting of andesine, orthoclase, quartz and biotite. Less abundant are augite and hypersthene. Granite is a medium grained, allotriomorphic-granular rock consisting of orthoclase, albite and quartz. Less abundant are chloritized biotite and magnetite. Both granodiorite and granite are foliated. The age relation between the granodiorite and granite is uncertain. The Nelson Intrusions are intruded by the Coryell Intrusions.

Coryell Intrusions

Little (1957) described the Coryell Intrusions as largely syenite, but with some granite, shonkinite and monzonite. The Coryell rocks in the map area range from fine grained to coarse grained, porphyritic to nonporphyritic and reddish to pale buff. The syenite consists of orthoclase, albite, quartz and chloritized biotite. The feldspar is commonly altered to carbonate and sericite and orthoclase replaces aplite. Quartz and orthoclase are graphically intergrown. Less abundant are hornblende and augite. Shonkinite, a medium grained dark rock, consists of much augite, biotite, hornblende and hypersthene, and less orthoclase, perthite, albite and quartz, with some graphically intergrown orthoclase and quartz. Diorite is porphyritic, with phenocrysts of plagioclase in a matrix of perthite, biotite, hypersthene and augite. Gabbro is a medium grained hypidiomorphic-granular rock with abundant plagioclase, biotite and augite. Also present is minor perthite, hypersthene, and magnetite. Porphyry dykes occur throughout the map area, but are concentrated in a few areas designated in Figure 24.1. The rock consists of phenocrysts of biotite and/or potassium or plagioclase feldspar embedded in a groundmass of quartz, feldspar, carbonate, biotite, chlorite and opaques. Feldspar phenocrysts are mostly chloritized. Small grains of apatite and biotite are later than the groundmass. The relations between the different phases of the Coryell Intrusions are uncertain.

Phoenix Volcanic Group

According to Little (1957), these rocks consist of andesitic and trachytic flows with interbedded sedimentary rocks and tuffs. In the map area, they consist of andesite, tuff and breccia. Phenocrysts of biotite mostly altered to zoisite, chlorite and carbonate are embedded in a groundmass of feldspar, carbonate, biotite and opaques. The formation has been folded or tilted; dips up to 60° have been recorded. The volcanics appear to overlie the Coryell but this relationship has not yet been proved.

Aplite

Granite aplite is abundant everywhere in the map area. It occurs as sheets and dykes intruding all of the above formations and is thus the youngest formation in the area. It is a fine- to medium-grained allotriomorphic-granular rock with abundant orthoclase, plagioclase and quartz. Orthoclase and quartz are graphically intergrown.

Radioactivity

Radioactivity was measured in the field using a portable gamma ray spectrometer. Gamma ray measurements were converted to ppm thorium and uranium and weight per cent potassium (Fig. 24.2). Preliminary results on a few samples show low values of uranium and thorium for the Nelson Intrusions. Coryell syenite is high in thorium and uranium with other phases showing a variety of values. The Phoenix Volcanic Group is low in thorium and uranium. Aplite shows high thorium values with correspondingly lower uranium values. However, uranium values for aplite are higher than the Nelson Intrusions and the Phoenix Volcanic Group. Coryell syenite shows consistently higher weight percentages potassium than other formations.

[1]Department of Geological Sciences, University of British Columbia, Vancouver, British Columbia, Canada V6T 2B4

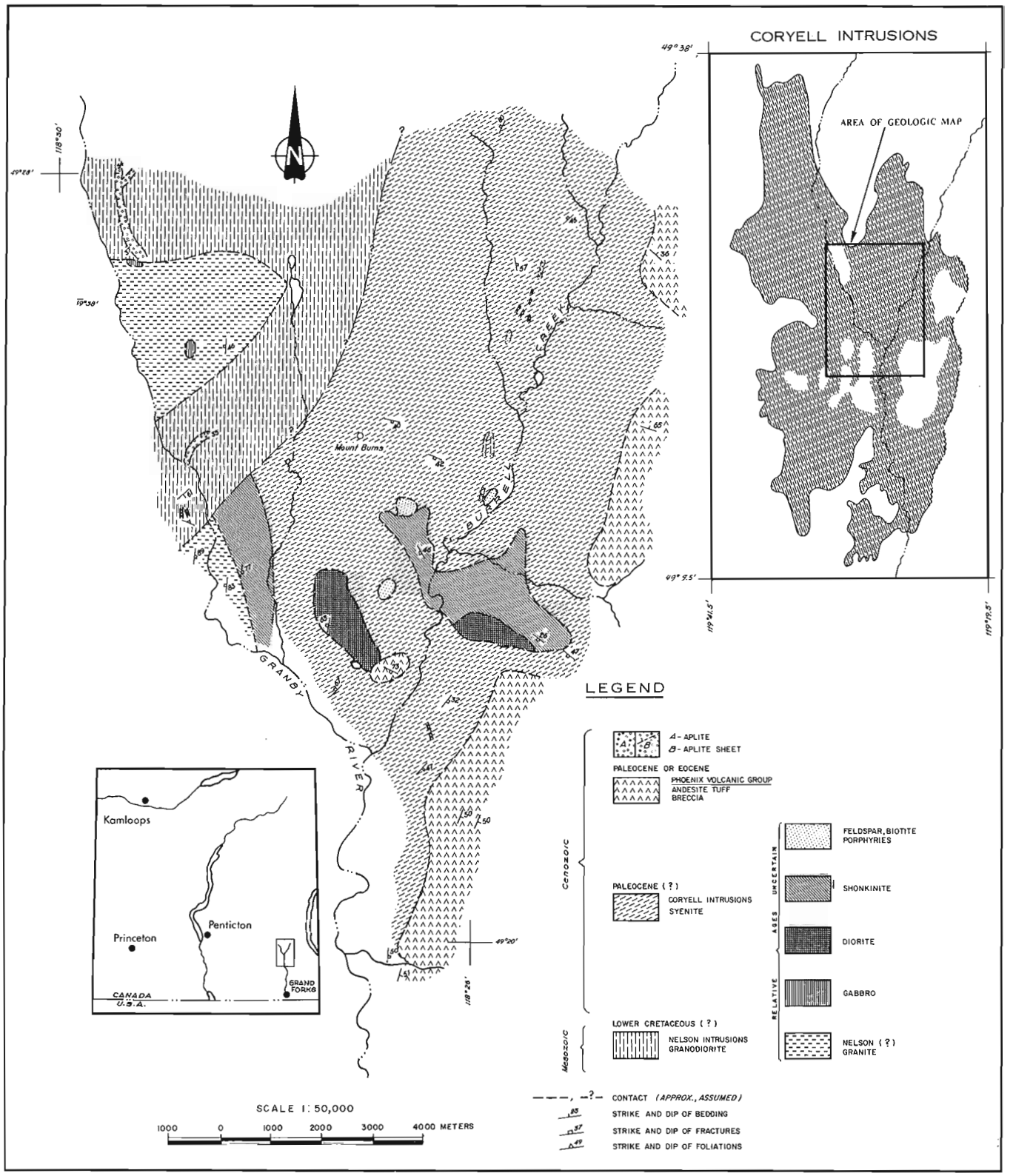

Figure 24.1. *Geology of study area.*

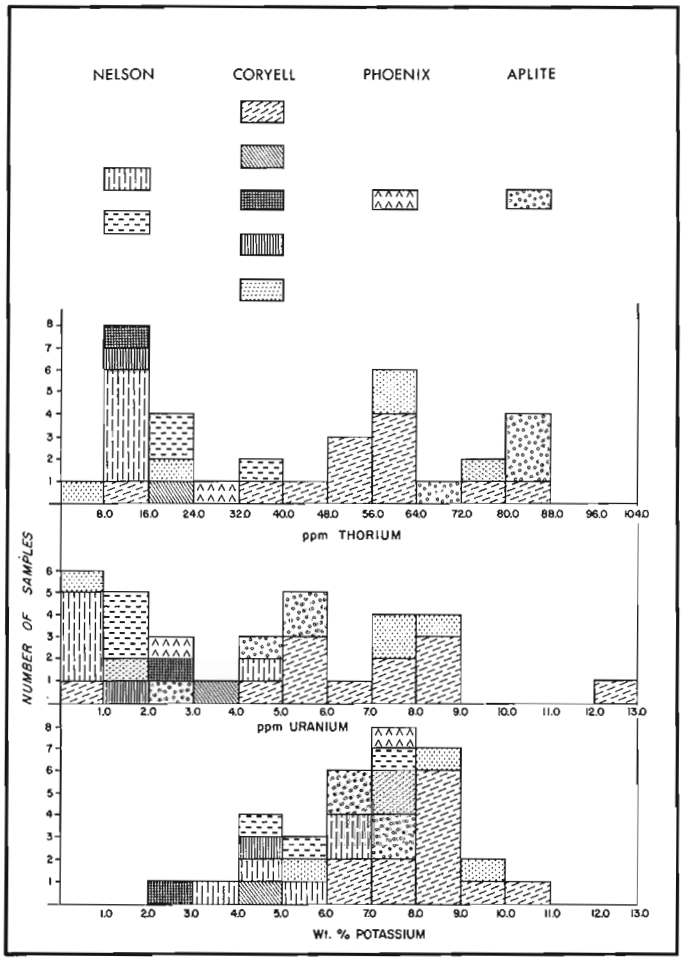

Figure 24.2. *Histograms showing distribution of radioactive elements. (Legend same as Figure 24.1).*

References

Lewis, T.J., Allen, V.S., Taylor, A.E., and Jessop, A.M.
1979: Temperature observations during drilling of two 400 m wells in the Coryell Intrusives North of Grand Forks, British Columbia, 1978; Earth Physics Branch Open File Number 79-4.

Little, H.W.
1957: Kettle River, British Columbia, Sheet 82 E (East Half); Geological Survey of Canada, Map 6-1957.

1960: Nelson map area, West Half, British Columbia (82 F W 1/2); Geological Survey of Canada, Memoir 308, 205 p.

25.

TWO NEW FORMATIONS IN THE LOWER CAMBRIAN ATAN GROUP, CASSIAR MOUNTAINS, NORTH-CENTRAL BRITISH COLUMBIA

Project 650024

W.H. Fritz
Institute of Sedimentary and Petroleum Geology, Ottawa

Fritz, W.H., Two new formations in the Lower Cambrian Atan Group, Cassiar Mountains, north-central British Columbia; in Current Research, Part B, Geological Survey of Canada, Paper 80-1B, p. 217-225, 1980.

Abstract

The Atan Group was known only from general descriptions until 1978 when the writer proposed a type section for the upper (carbonate) part of the group. The upper part is now assigned to the Rosella Formation (new), and the lower part to the Boya Formation (new). The Rosella Formation (690 m) is composed of light coloured limestone and subordinate siltstone, whereas the Boya Formation (400 m) is composed of siltstone and interbedded quartzite.

The Rosella Formation correlates with the Sekwi Formation in the Mackenzie Mountains, and the Boya Formation correlates with map unit 13 and probably part of map unit 12 of Blusson's Sekwi Mountain map area. In correlating formations of the Atan Group with formations of the Gog Group in the Mount Robson area, the Rosella Formation is equated with the Mural, Mahto, and Hota (Peyto) formations and the Boya Formation is correlated with the McNaughton Formation.

Introduction

The Atan Group was first used by H. Gabrielse in 1954 on the legend of a geological map of the McDame area and in accompanying marginal notes which state: "Fossiliferous rocks of the Atan group (1), comprising over 14 000 feet (4300 m) of sedimentary rocks, occupy a northwesterly trending, complex anticlinorium, and the southwest limb of a large syncline". In the legend the group is reported to contain "White and pink quartzite, limestone, dolomite, slate, red shale, argillite". Gabrielse later (1963, p. 26) greatly restricted the thickness of the group to "more than 3000 feet" (915 m), and divided it into two informal map units. Map unit 3 (lower) was reported to be composed of quartzite and map unit 4 (upper) was described as limestone. No type section was given for the group or its map units, but two reference areas were suggested (Gabrielse, 1963, p. 27) by the statement, "Excellent exposures occur in the mountains north and south of French River and near Atan Lake...". A generalized section 2700 feet (823 m) thick was described (op. cit., p. 29) from outcrops northwest of Atan Lake. Mansy and Gabrielse (1978, p. 9) helped to define the base of the Atan Group by reporting that "The Stelkuz Formation is in sharp contact with the basal sandstone of the overlying Atan Group..." in the Cassiar and Omineca mountains.

Six stratigraphic sections from the Atan Group have been described by the writer (Fritz, 1978a, Text-fig. 1a, 1b, sections 1 to 6). Of the six, section 1 was designated as the type section for the upper (carbonate) part of the Atan Group. A suggestion was also made that section 1 should be extended downward to include the lower, clastic part of the group, and thus allow section 1 to serve as the type section for the whole of the Atan Group. In 1979 this lower part (Fig. 25.2, section 1a, units 1B to 5B) was studied in the field and two additional sections (Fig. 25.2, sections 7, 8) in the Atan Group were measured. In the present paper section 1 is designated to serve as type section for the Atan Group, and the carbonate and clastic parts of the Atan Group in section 1 are designated to serve as type sections for the Rosella Formation and Boya Formation, respectively.

A fault has removed the upper strata of the Atan Group in section 1 and no nearby section containing these strata could be found. These strata are probably present in section 5 (Fritz, 1978a, Text-fig. 3.1b, units 6, 7), located 46 km southeast of section 1. No beds or stratigraphic units can be physically traced between sections 1 and 5 because of complex structural displacements. The upper part of section 5 (units 6R, 7R) is here designated as the reference section for the youngest strata in the Atan Group and in the Rosella Formation. This part of section 5 is reproduced from Fritz (1978a) and is shown on Figure 25.2. These strata in section 5 are deliberately assigned to a reference rather than a type section. This ensures that if at some future date the upper strata in reference section 5 (units 6R, 7R) are equated with part of type section 1, the author of the new correlation will not be confronted with two type sections for those strata that are (in his belief) common to the two sections.

Map co-ordinates for sections 1, 7, 8, and the upper part of section 5 are given in Figure 25.2 to the nearest 15 seconds which is the approximate limit of accuracy for the available maps (1:250 000). A local and more detailed map (1:50 000) of the area surrounding section 1 permits more accurate location of that section which is given in the text.

Acknowledgments

Field support and guidance to the various Atan sections were given in 1977 and 1979 by H. Gabrielse while he directed Operation Dease. Assistance with the measuring of section 1 in 1977 was provided by C.M. Henderson, and help with sections 1, 2, 4, 5 and 6 was given by P.W. Fritz. In 1979 G.J. Breaks provided assistance with the measuring of section 8 and the downward extension (units 1B to 5B) of section 1.

Boya Formation (Type Section 1a, Units 1B to 5B, 400.5 m)

Name and Location

This lower formation of the Atan Group is named for Boya Lake, which is centred 13 km northeast of the type section. Although the lake is unnamed on the present 1:250 000 topographic sheet (McDame sheet, 104P, 3rd edition), the name is scheduled to appear on the next edition (oral communication, Permanent Committee on Geographical Names, EMR) and is presently shown on the geological map (Gabrielse, 1963).

The type section is located (Fig. 25.1c, segment 1a; Pl. 25.1, fig. 5) southeast of Highway 37 (Stewart Highway). The distance from a point on the highway where it passes along the northwest shore of Good Hope Lake to the midpoint

of the type section is 2.7 km. The base of the formation is at latitude 59°17'06", longitude 129°12'33" and the top is at latitude 59°16'51", longitude 129°13'04".

A reference section for the Boya Formation is present at section 7 on the northwest slope of One Ace Mountain (Fig. 25.1b; Fig. 25.2; Pl. 25.1, fig. 1). There the lithology is known from quartzite outcrops, and is inferred from float originating from interbedded siltstone and thin bedded quartzite. At One Ace Mountain the base of the formation is at latitude 59°50'45", longitude 129°36'45" and the top is at latitude 59°50'15", longitude 129°36'15".

Lithology

A typical ridge underlain by the Boya Formation is mainly covered with float that weathers dark brown. The upper and middle parts of the formation consist of siltstone and minor interbedded quartzite that underlie a saddle between the overlying resistant limestone of the Rosella Formation and the underlying lower part of the Boya Formation, which has a higher quartzite to siltstone ratio. The base of the formation is the base of a resistant quartzite that is nearly white, but is typically covered by dark grey lichen. The Stelkuz Formation underlying the Boya Formation weathers medium brown to orange brown.

Map "a" gives locations for Lower Cambrian sections shown in Figure 25.3; Whitehorn Mountain-Cinnamon Peak section (W-C) near Mount Robson (MR), Ospika River section (OR), Mount Lloyd George section (LG), type section for Atan Group (A), and composite section for west-central Mackenzie Mountains (MM). Area outlined in north-central British Columbia is area shown in map "b".

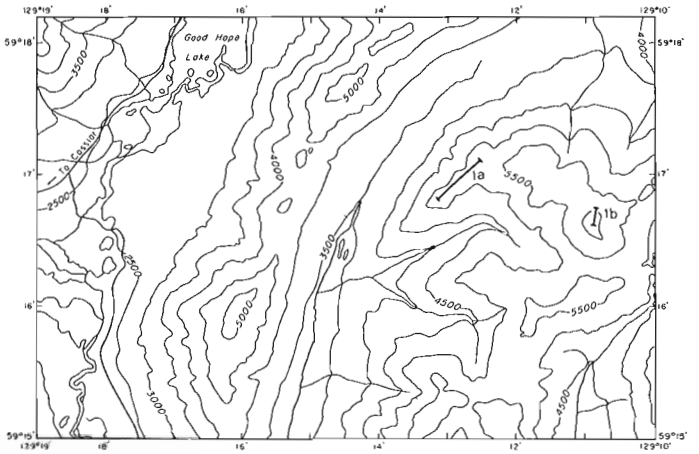

Map "c" locates lower segment (1a) and upper segment (1b) of section 1, which contains type sections for Boya Formation, Rosella Formation, and Atan Group.

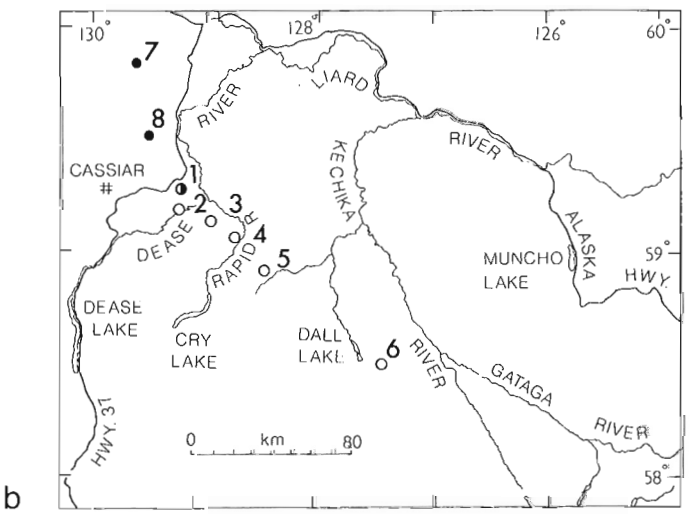

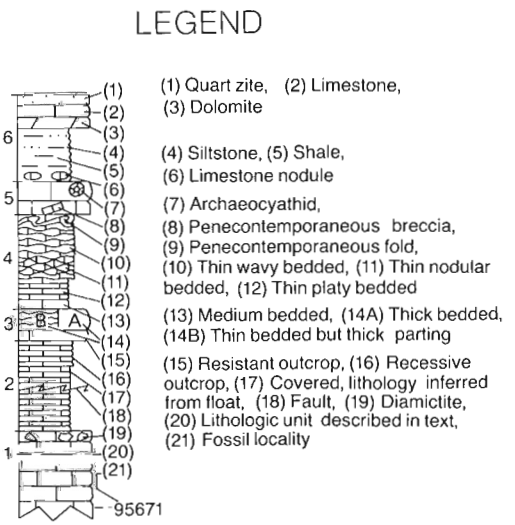

Map "b" locates Atan sections described in this report (solid circles) and those described earlier (Fritz, 1978a; open circles).

Figure 25.1. *Locality maps (a-c) for stratigraphic sections and legend (d) for stratigraphic sections shown in Figure 25.2.*

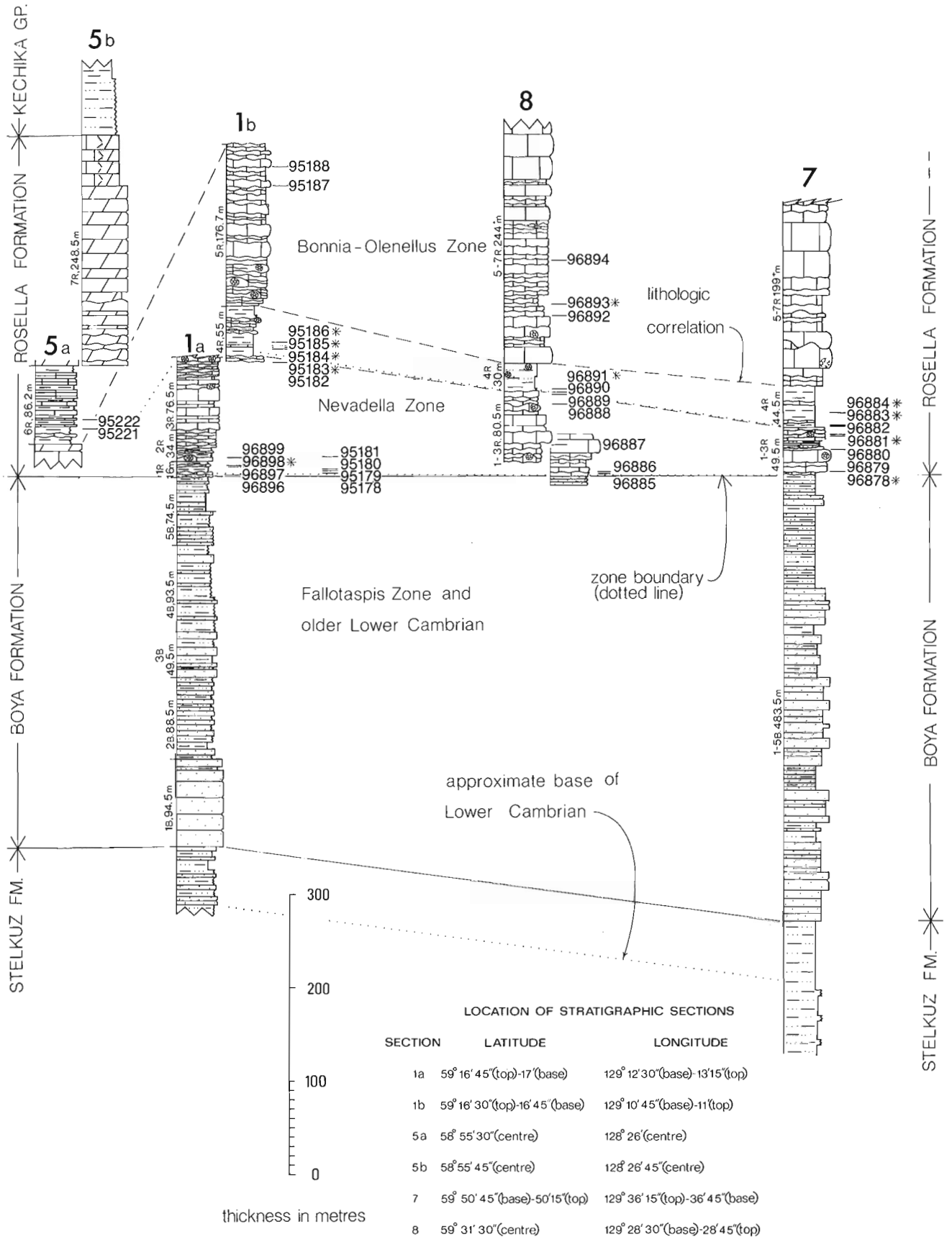

Figure 25.2. *Stratigraphic sections from Lower Cambrian Atan Group. Sections are located in Figure 25.1b. An asterisk following a fossil locality number indicates local float.*

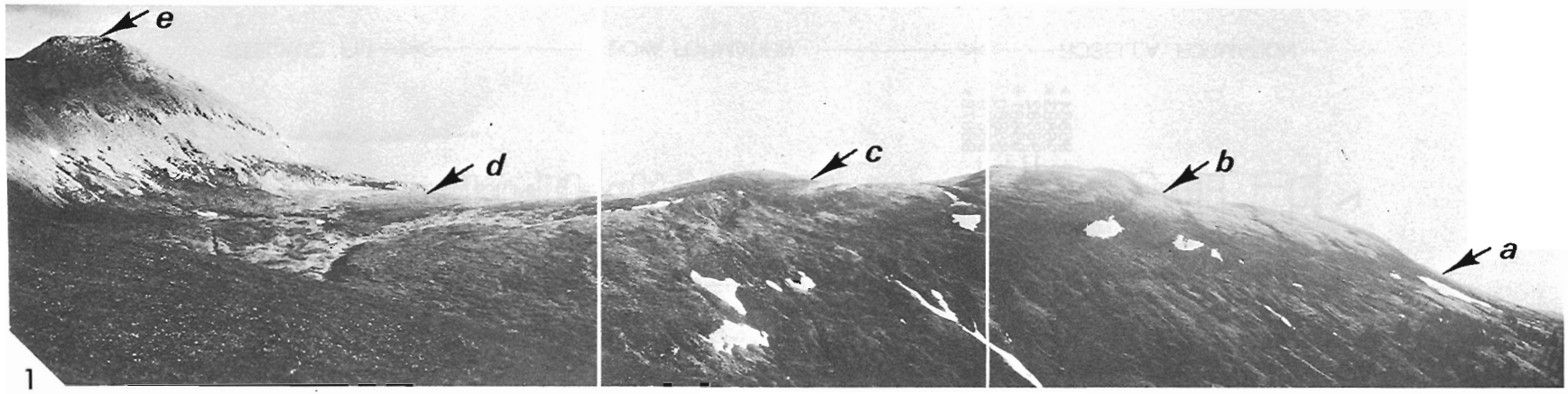
e
d
c
b
a
1

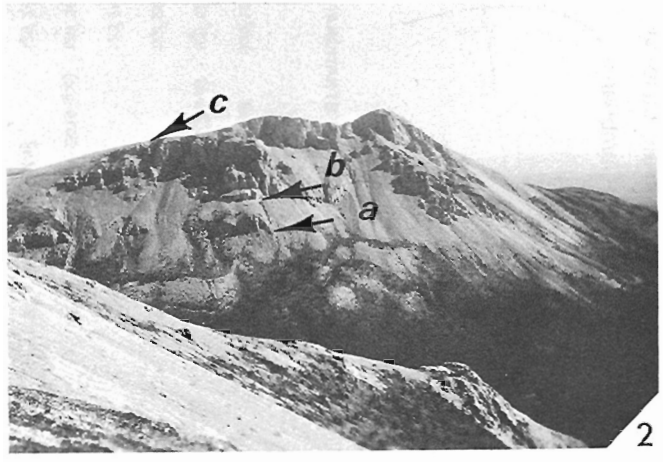
c
b
a
2

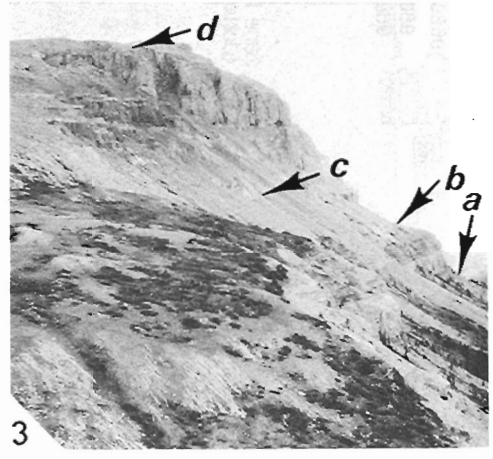
d
c
b
a
3

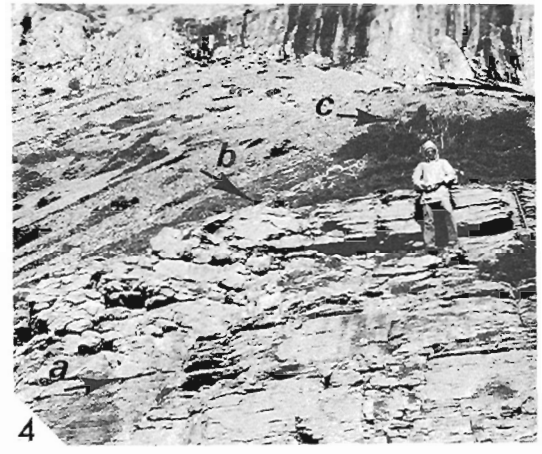
c
b
a
4

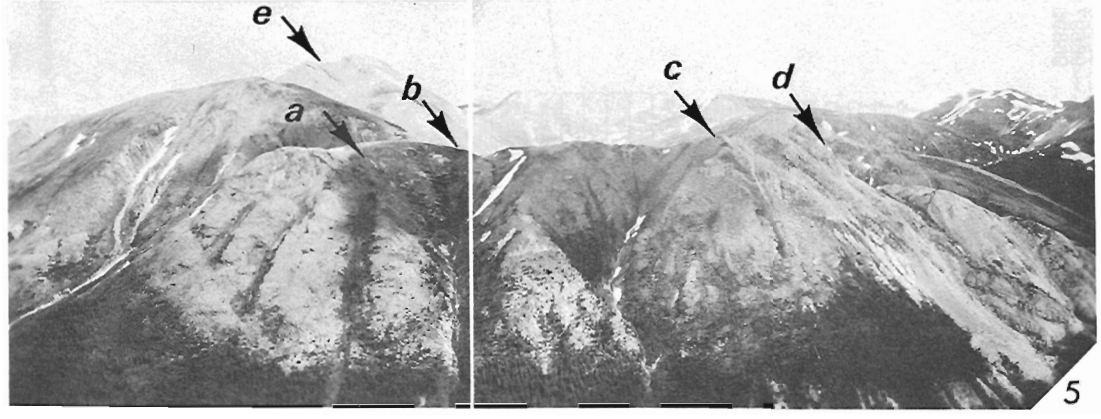
e
b
a
c
d
5


6

Plate 25.1

Figure 1. View looking southwest at section 7, northwest slope of One Ace Mountain. Base of Boya Formation is at "a", base of third quartzite subunit within Boya Formation is at "b" (167 m above base of Fm.), base of highest (fourth) quartzite subunit is at "c", base of Rosella Formation is at "d", cairn located on section and 254 m above base of Rosella Formation is located at "e". Composite from GSC photos 203474-G, 203474-H, 203474-I.

Figure 2. View looking northeast at Rosella Formation, section 8. Base of upper segment of section is at "a", base of unit 5-7R is at "b", point on section 198 m above base of unit 5R is at "c". GSC photo 203474-L.

Figure 3. View looking south at Rosella Formation, upper segment of section 8. Base of segment is at "a", base of unit 4R is at "b", base of unit 5R is at "c", and point on section 198 m above base of unit 5R is at "d". GSC photo 203474-J.

Figure 4. View of Rosella Formation, unit 1-3R, section 8. Small (3 m high by 7.5 m wide) bioherm composed of stacked limestone mounds averaging 0.2 m in height, bioherm base at "a" and top at "b". Top of unit 3R is at "c". GSC photo 203474-K.

Figure 5. View looking southeast at lower part (segment 1a between "a" and "d") of type section (section 1) for Atan Group. Type section for Boya Formation is between "a" and "c", basal quartzite of Boya Formation is between points "a" and "b", siltstone and interbedded quartzite part (2B-5B) are between points "b" and "c", basal strata (1R-3R) in type section for Rosella Formation are between points "c" and "d". Upper part of type Atan Group and type section (segment 1b) for medial strata in Rosella Formation (4R, 5R) is on ridge marked "e". Composite of GSC photos 203474-P, 203474-O.

Figure 6. Large burrows in Stelkuz Formation, local float, several hundred metres stratigraphically below Stelkuz-Atan boundary (below boundary at "a" in Fig. 5). GSC photo 203474-N.

At the type section the basal Boya stratigraphic unit (unit 1B, 94.5 m) is composed of thick beds of white weathered and unweathered quartzite. The quartzite is medium grained and is poorly or indistinctly crossbedded. In the uppermost 23 m of the unit the white quartzite is interbedded with some dark grey weathering and fresh shale and siltstone, and also with much light grey orange to rust weathering quartzite that is light orange brown on fresh surface. All of the quartzite in the upper 23 m is fine grained.

Strata in the next overlying unit (2B, 88.5 m) consist mainly of rust to greenish grey, brownish grey weathering quartzite in thin and very thin beds. The quartzite is medium dark grey on fresh surface and is very fine grained. Half of the basal 11 m of the unit is orange brown to rust weathering quartzite in thin and medium beds with crossbeds 12 cm high. Fresh surfaces are light brown and fine grained. The remaining half of the basal 11 m is composed of orange brown weathering and fresh shale. Strata in the interval 11 to 18 m above the base are covered, deeply recessive, and probably consist of shale.

More than one half of the strata in the third unit (3B, 49.5 m) are light greenish grey, light brownish orange weathering quartzite in thin to thick beds. The quartzite is medium grey to light brown on fresh surface. It is in part planar laminated and in part highly burrowed, and some of the bedding surfaces are marked by microripples. Ball and pillow structures up to 0.3 m thick are present in the quartzite 10 m above the base of the unit. Rust weathering siltstone and shale that are dark grey on fresh surfaces are interbedded with the quartzite.

Rust weathering siltstone that is dark grey on fresh surface predominates in the fourth stratigraphic unit (4B, 93.5 m). Minor (one-eighth) amounts of interbedded light brown to orange brown weathering quartzite in thin interbeds are also present. The quartzite is light brown on fresh surface and is very fine grained. A subunit 74.5 to 83.5 m above the base is half thin to thick bedded quartzite and half siltstone. Strata that are highly burrowed are present 34 m above the base.

Unit five (5B, 74.5 m) is one half light orange brown weathering quartzite in thin, platy beds. The quartzite has some laminae that parallel the bedding and some that are inclined at a low angle. Fresh surfaces are greenish light brown and are fine grained. The other half of unit 5B is composed of interbedded siltstone that is medium greenish grey on fresh and weathered surfaces. Burrows are present 20 m above the base and cross ripples and burrows are present 52 to 74.5 m above the base.

Below the white quartzite at the base of the Boya Formation (1B), the upper Stelkuz Formation (upper 70 m) is composed of two thirds rust weathering siltstone that is medium dark grey on fresh surface and one third interbedded light brown weathering and fresh quartzite in thin and medium beds. The quartzite is fine and very fine grained. Burrows are present in at least the upper several hundred metres of the Stelkuz Formation (Pl. 25.1, fig. 6).

Both the basal and upper contact of the Boya Formation are abrupt. The light brown quartzite and interbedded siltstone of the underlying Stelkuz Formation directly underlie the white, thick bedded quartzite of the lower Boya Formation with no interfingering of the two lithologies. At the upper contact, nonlimy siltstone and interbedded quartzite of the Boya Formation are abruptly overlain by a thick (1.2 m) bed of limy, crossbedded sandstone of the Rosella Formation. Observations suggesting that the Boya-Rosella contact represents a minor disconformity are given in the description of the Rosella Formation.

The Boya Formation at section 7 resembles the type section at section 1, and has a similar quartzite unit (85 m) at the base. At section 7, however, white quartzite is present in the interval 167 to 262.5 m above the base and in two-thirds of the interval 262.5 to 309.5 m above the base. At both sections the predominant lithologies are rust to medium brown weathering siltstone and fine grained quartzite.

Age

A minimum age for the type Boya Formation is provided by fossils in the lower beds of the overlying Rosella Formation. There the boundary between Lower Cambrian **Nevadella** and **Fallotaspis** zones lies in the interval 1.5 m to 1.6 m above the top of the Boya Formation. Burrows in the Boya and upper Stelkuz formations are the only fossils found thus far below the Rosella Formation. Pending further work, the Precambrian-Cambrian boundary is tentatively placed in the upper part of the Stelkuz Formation.

Rosella Formation (Type Section 1a-b, Units 1R to 5R, 358.2 m; Reference Section 5, Units 6R, 7R, 334.7 m)

Name and Location

The upper formation in the Atan Group is named for Rosella Creek, which is 23 km northwest of the closest point on the type section. The type section for the lowest part of the formation is in the upper part of the lower segment (section 1a, units 1R to 3R) in section 1. The next part of the type section is in the upper segment (section 1b, units 4R, 5R) of section 1, which is located 2 km to the east-southeast and along strike with the strata in the lower segment. The distances measured in a northwesterly direction from the lower (1a) and upper (1b) segments of the type section 1 to a point on Highway 37 near the north-western edge of Good Hope Lake is 2.7 km and 4.2 km respectively. A photo locating segments 1a and 1b of type section 1 is provided on Plate 25.1 (fig. 5), and segment 1b is also shown in an earlier publication (Fritz, 1978a, Pl. 3.1, fig. 1). The base of the formation in segment 1a is at latitude 59°16'51", longitude 129°13'04" and the top of the segment (top of unit R3) is at latitude 59°16'48", longitude 129°13'08". The base of segment 1b (base of unit 4R) is at latitude 59°16'46", longitude 129°10'52" and the top of the segment (top of unit 5R) is at latitude 59°16'37", longitude 129°10'55".

The upper part of the Rosella Formation is located in reference section 5 in the upper middle (unit R6) and upper (unit R7) segments of that section. The upper middle segment is located 4 km northwest of the Major Hart River and 0.2 km south of point "a" in a photo (Fritz, 1978a, Pl. 3.2, fig. 4) showing part of section 5. The upper segment is located 5 km northwest of the Major Hart River on a southwest facing dipslope, and downslope from a point on the ridge midway between points "b" and "d" in another photo (Fritz, 1978a, Pl. 3.2, fig. 3) illustrating section 5. The midpoint of the upper middle segment is at latitude 58°55'30", longitude 128°26'15" and the midpoint of the upper segment is at latitude 58°55'45", longitude 128°26'45".

Lithology

Resistant, light grey, thick bedded to massive limestone dominates typical exposures of this formation. Subordinate intervals containing thin bedded limestone or siltstone and shale are generally covered.

At the type locality the lowest stratigraphic unit (Fig. 25.2, unit 1R, 16 m) contains limy shale that is light brown on weathered and fresh surfaces, and some (10 per cent) limestone in thin, wavy interbeds and nodules. The limestone weathers medium brown and fresh surfaces are medium grey and bioclastic. A basal subunit (5 m) is more resistant than the overlying shale and is composed of a lower orange brown, limy quartz sandstone (1.2 m) that is coarse grained; a light brown weathering and fresh very fine grained sandstone (1.2 to 2.6 m) in thin, wavy beds; and a medium light grey weathering limestone (2.6 to 5 m) in thin and medium wavy beds. Fresh surfaces of the limestone are light grey to light brown and are coarse grained and bioclastic. Sparse grains of glauconite are present.

Medium dark grey weathering limestone in thin, wavy beds predominates in the second unit (2R, 34 m). On fresh surface the limestone is dark grey and finely crystalline. A subunit 4.2 to 17 m above the base contains some (one third) light brown weathering and fresh shale. Archaeocyathid bearing limestone mounds up to 1 m high are present in the lower part of the subunit where they are isolated or are locally concentrated in bioherms up to 3 m high. Penecontemporaneous slump structures and breccia are present in unit 2 of the Rosella Formation at section 5 (see extended section in Fritz, 1978a, Text-fig. 3.1b).

Unit 3 (3R, 76.5 m) is composed of medium light grey weathering limestone in thick to thin beds. Fresh surfaces are medium grey and are finely crystalline or fine- to coarse-grained. Medium dark grey limestone in thin beds is present 24.6 to 31.6 m and 66.5 to 76.5 m above the base. These beds are medium dark grey on fresh surface and fine- to coarse-grained. Archaeocyathids are present in the upper half of the unit.

Shale that weathers khaki (0 to 31.6 m), orange (40 to 43.6 m), and medium brown (43.6 to 55 m) are responsible for the recessive nature of unit 4 (4R, 55 m). About 5 per cent thin interbedded limestone is present in the lower part of the unit, and one subunit containing orange weathering and light grey weathering limestone is present 31.6 to 40 m above the base. Archaeocyathids are associated with the light grey limestone.

Unit 5 (5R, 176.7 m) is composed of thick to thin bedded limestone that is in part medium light grey weathering and fresh and in part medium grey weathering and fresh. The limestone is both finely crystalline and fine- to coarse-grained. Archaeocyathids are present in the lower 52.7 m. A fault at the top of the type section terminates unit 5, but as the thickness here is somewhat more than in section 4 and somewhat less than in section 5 (Fritz, 1978a; Text-fig. 3.1a-b), probably most of the unit is present. No favourable exposures of units 6 and 7 are present near the type section of the Rosella Formation, and therefore these units are described below from notes taken at section 4 and reference section 5 (Fritz, 1978a).

At reference section 5, unit 6 (6R, 86.2 m) consists of a lower subunit (0-32 m) containing light brown weathering and fresh shale, medium light grey weathering and fresh shale, and about 15 per cent orange weathering, medium grey fresh limestone in thin to thick interbeds. Thick, irregular beds of limestone are present 8.2 to 10.6 m above the base. The overlying subunit (32-86.2 m) comprises two thirds medium light grey weathering limestone in thin to thick beds that are medium grey and finely crystalline on fresh surface and one third shale that is medium light grey to orange weathering and light grey to medium brown fresh. At section 4 the shale in unit 6 is covered, and all of the limestone outcrops are thin bedded. This limestone weathers medium grey and fresh surfaces are either dark grey and finely crystalline or medium grey and fine- to coarse-grained.

Strata in unit 7 are slightly altered in a partial exposure at section 4 (78.5 m, see Fritz, 1978a) and moderately altered at a complete exposure at reference section 5 (7R, 248.5 m).

At section 4, the basal 56 m of the unit is composed of thin and medium bedded limestone with a medium blue grey and medium light grey mottled weathering surface. Fresh surfaces are medium grey and finely crystalline. One half of the overlying 22.5 m (below a covered top) is like the limestone just described, the other half being medium light grey limestone in thick beds that are dark grey on fresh surface. At section 5 the unit is mainly altered to cream or light brown weathering dolomite in thick and medium beds. Fresh surfaces are medium dark grey, medium grey or cream, and are finely or medium crystalline. The upper 53.6 m is comprised of medium blue grey weathering limestone in thick beds that changes laterally to cream weathering dolomite similar to that below. Fresh limestone surfaces are medium grey and finely crystalline.

As mentioned earlier, the Rosella-Boya formational contact at type section 1 is abrupt, with nonlimy siltstone and interbedded sandstone of the Boya Formation below and a thick (1.2 m) bed of limy sandstone of the Rosella Formation above. At section 7, local float suggests that the basal bed in the Rosella Formation is 15 cm thick and comprises quartz clasts up to 0.5 cm in diameter. At section 8 the basal contact is overlain by 0.8 m of fine to coarse quartz sandstone with grit sized clasts near the base.

At sections 3 and 4 medium light grey, greenish grey and pink weathering limestone immediately overlies typical siltstone and quartzite of the Boya Formation, and at section 5 similar Boya beds are overlain by limy siltstone of the Rosella Formation. The base of the Rosella Formation is not exposed at section 2. The abrupt change in lithology plus the coarse quartz sand or grit at the base of the Rosella Formation at three sections suggests that some erosion may have taken place after the deposition of the Boya Formation and before deposition of the Rosella Formation. No evidence of channeling or angularity was noted at the formational contact.

At section 6 (Fritz, 1978a) the basal Rosella formational contact differs from that in the sections just discussed. Here fine grained quartzite and interbedded siltstone that belong to the Boya Formation or older strata are overlain by approximately 26 m of white, fine grained Rosella quartzite. The next Rosella unit consists of 21.3 m of siltstone that contains **Olenellus**, and thus is the same age or younger than unit 4 in sections 1, 2, 4, 5, 7, and 8 to the northwest (unit 4 at section 3 not exposed). Because data are still meagre at section 6 and in the surrounding area, the interpretation of the contact at section 6 is open to question. One explanation is that clastics belonging to the Boya or an older formation were uplifted and in part eroded, and that the white quartzite represents the initial phase of a Rosella transgression. A modification of this concept that is equally likely, is that older Rosella beds (upper **Fallotaspis** and **Nevadella** Zone) were deposited over the Boya or older strata, and that these lower Rosella beds were uplifted and eroded before deposition of the white quartzite.

The top of the formation at section 5 is placed at a sharp and conspicuous lithological change. Below the Rosella-Kechika (Atan Group-Kechika Group) contact are thick, resistant beds composed of medium blue grey weathering limestone that in places has been altered to cream weathering dolomite. Above the contact is recessive siltstone that weathers medium rust brown and is rust brown to medium grey on fresh surface. Elsewhere the Rosella-Kechika contact was found to be erased by faulting except for a reported (Fritz, 1978a, Pl. 3.1, fig. 5, point "a") exposure that lies to the east and across the Rapid River from section 4. The lithologies on either side of the contact at this locality are the same as those at section 5.

Age

At type section 1 the Rosella Formation contains strata belonging to the Lower Cambrian **Fallotaspis, Nevadella,** and **Bonnia-Olenellus** zones. The boundary between the **Fallotaspis** and **Nevadella** Zone is between GSC localities 96897 and 95178 which are 1.5 m and 1.6 m above the base of the formation, respectively. GSC loc. 96897 contains **Fallotaspis** sp., and **Hyolithes** sp., and GSC locality 95178 contains **Keeleapis** sp. and **Holmiella** sp.

The boundary between the **Nevadella** Zone and the **Bonnia-Olenellus** Zone is near the base of unit 4R. In segment 1b it is between GSC loc. 95182, which contains **Nevadella** 6 m below the base, and local float locality GSC loc. 95183, which contains **Olenellus** sp. 9 m above the base. The zone boundary is closely located below reference section 5 where it is in the interval 3 m to 7.3 m above the base (extended section 5 in Fritz, 1978a, Text-fig. 3.1b, between GSC loc. 95219, 95220). At section 8 the boundary is between GSC loc. 96890, located 1.5 m below the base of unit 4R, and GSC loc. 96891, which is in local float 2.5 m above. The boundary at section 7 is between GSC loc. 96881 and 96882 which are 6.5 m below and 1.0 m above the base of unit 4R, respectively.

Some of the youngest fossils collected in the Rosella Formation are from the Lower Cambrian **Bonnia-Olenellus** Zone located in unit 5R of section 1b (GSC loc. 95187, 95188) and in unit 6R of section 5 (GSC loc. 95221, 95222). The collections in unit 5 contain **Proliostracus** sp., indicating a medial position in the zone. Collections in unit 6R contain **Olenellus** sp., a genus that ranges throughout the zone.

No fossils were found in unit 7R at reference section 5 or in unit 7R elsewhere, and none were found in the overlying Kechika Group. A speculation as to the age of unit 7R can be made by tentatively correlating this unit in the Cassiar Range with unit Z at section 6 (Fritz, 1978a, Text-fig. 3.1b) in the Kechika Range. There GSC loc. 95228 in the lower part of unit Z contains trilobite fragments with a **Wanneria**-like pattern and **Bonnia** pygidia with more than one pair of spines. These features are typical of the medial part of the **Bonnia-Olenellus** Zone. If the lithological correlation between unit 7R and unit Z is valid, and if the unit is not appreciably diachronous, then the lower part of unit 7R can be assumed to belong to the medial part of the **Bonnia-Olenellus** Zone. As this zone is known to be thick elsewhere, it would be reasonable to assume that at least the lower half of unit 7R belongs to the **Bonnia-Olenellus** Zone. In this paper the top of the Atan Group (top of unit 7) is tentatively equated with the top of the **Bonnia-Olenellus** Zone and therefore the top of the Lower Cambrian.

The reported presence of the Upper Cambrian trilobite **Hedinaspis** sp. a short distance above the Atan-Kechika contact (Gabrielse, 1963, p. 39; Fritz, 1978a, p. 7) is not strong evidence for placing the Lower-Middle Cambrian boundary at a lower horizon. It is important that this locality first be relocated and its position assessed in relation to local faults, unconformities, starved basin deposition, etc.

Regional Correlation

A correlation between the Atan Group and four other widely spaced Lower Cambrian stratigraphic sections is shown in Figure 25.3. These sections are briefly discussed, starting from the south, in order to relate the lithology and stratigraphic names to the Atan Group, and, when appropriate, to the Boya and Rosella formations. The locations for the various sections are shown in Figure 25.1a.

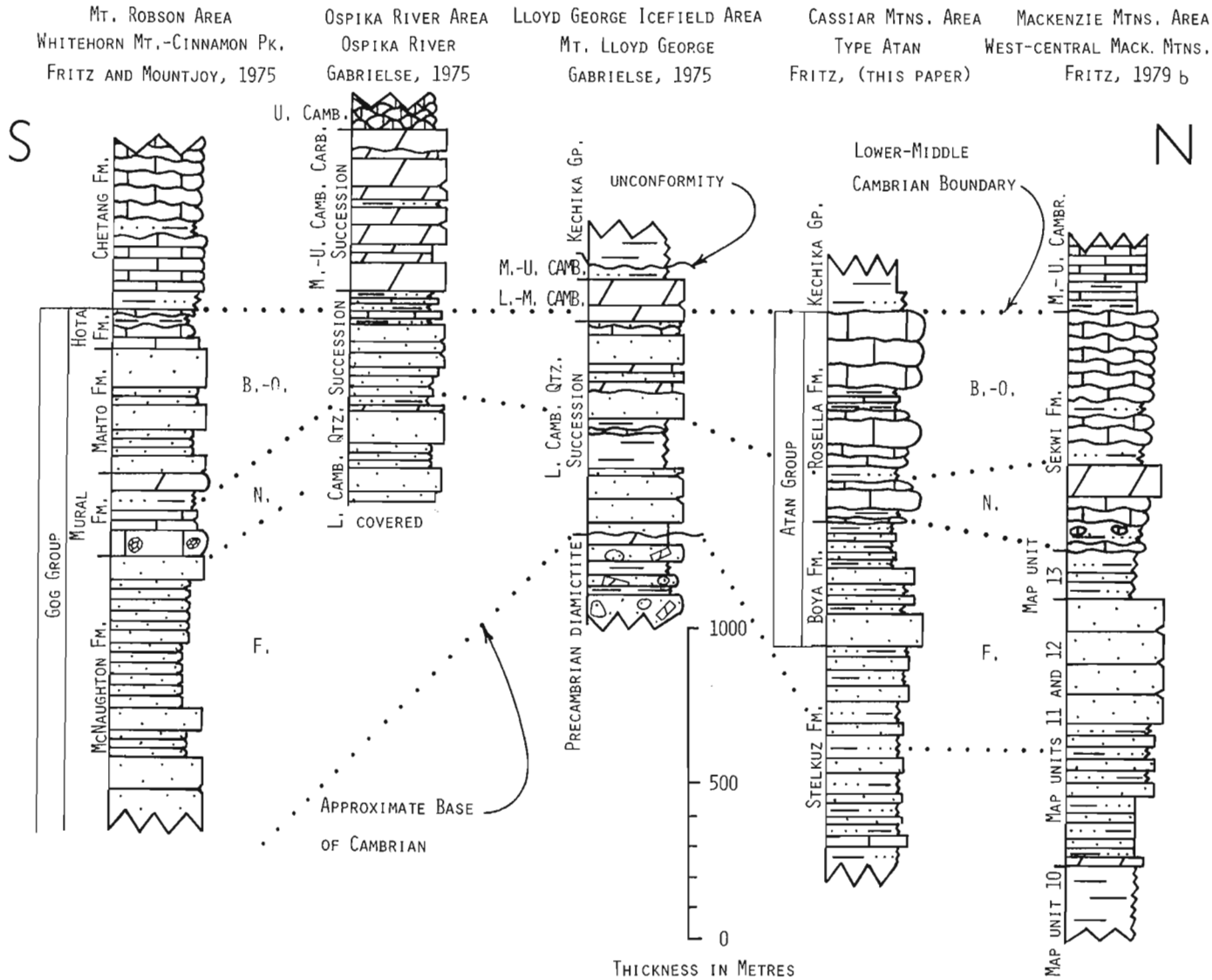

Figure 25.3. *Stratigraphic sections showing correlation between Atan Group (Boya and Rosella Formations) and Lower Cambrian strata in Rocky Mountains and Mackenzie Mountains. Sections are located in Figure 25.1a.*

The first section (redrafted from Fritz and Mountjoy, 1975) represents the Lower and early Middle Cambrian strata exposed between Whitehorn Mountain and Cinnamon Peak in the Mount Robson area. There the entire Lower Cambrian is assigned to the Gog Group, which is predominantly quartzite, but which contains some archaeocyathid bearing limestone well down in the section (Mural Formation) and some limestone at the top (Hota Formation=Peyto Formation).

The next section (redrafted from Gabrielse, 1975, section 4) is on the Ospika River and located northeast of Williston Lake. There the Lower Cambrian is probably thinner (base covered) than in the first section, but the ratio and distribution of quartzite to minor limestone is approximately the same. The third section (redrafted from Gabrielse, 1975, section 1; Fritz, 1979a, section 1) shows that the clastic-carbonate ratio continues into the Mount Lloyd George region, but within the clastic fraction more siltstone is present than to the south.

In contrast to the three sections to the south, the Atan Group (fourth section) in the Cassiar Mountains contains two distinct lithologies in the Lower Cambrian, one of which is consistently above the other. As it is the dual presence of the carbonate (Rosella Formation) and underlying clastics (Boya Formation) that characterizes the Atan Group, there is good reason not to extend the group into the regions occupied by the first three sections, where these two components are not distinctly separated.

The northernmost (fifth) section shown in Figure 25.3) is generalized from many sections (Fritz, 1976, 1978b, 1979b) in the west-central Mackenzie Mountains. There the carbonate and clastic lithological components are in the same relative position and are of the same age as those of the Atan Group in the Cassiar Mountains. The Mackenzie Mountains clastic succession has been assigned (Blusson, 1971) to map unit 13 and the upper part of map unit 12, and the carbonate succession to the Sekwi Formation (Handfield, 1968). The similarities between the fourth and fifth sections provide reason for suggesting the use of the Atan Group in the Mackenzie Mountains. However, it is presently doubtful that this would be practical, as the white quartzite marking the base of the group in the Cassiar Mountains may not be traceable into the Mackenzie Mountains. It should also be pointed out that the Sekwi Formation undergoes rapid facies

changes over a short lateral distance (Fritz, 1979b, fig. 4), and it contains only a small amount of light coloured, thick bedded limestone that is so typical of the upper Atan Group (Rosella Formation) in the Cassiar Mountains.

Additonal correlations for the Upper part of the Atan Group have been given in a previous paper (Fritz, 1978a, p. 14, 15).

References

Blusson, S.L.
1971: Sekwi Mountain map-area, Yukon Territory and District of Mackenzie; Geological Survey of Canada, Paper 71-22.

Fritz, W.H.
1976: Ten stratigraphic sections from the Lower Cambrian Sekwi Formation, Mackenzie Mountains, northwestern Canada; Geological Survey of Canada, Paper 76-22.

1978a: Upper (carbonate) part of Atan Group, Lower Cambrian, north-central British Columbia; in Current Research, Part A, Geological Survey of Canada, Paper 78-1A, p. 7-16.

1978b: Fifteen stratigraphic sections from the Lower Cambrian of the Mackenzie Mountains, northwestern Canada; Geological Survey of Canada, Paper 77-33.

1979a: Cambrian stratigraphy in the northern Rocky Mountains, British Columbia; in Current Research, Part B, Geological Survey of Canada, Paper 79-1B, p. 99-109.

Fritz, W.H. (cont'd.)
1979b: Eleven stratigraphic sections from the Lower Cambrian of the Mackenzie Mountains, northwestern Canada; Geological Survey of Canada, Paper 78-23.

Fritz, W.H. and Mountjoy, E.W.
1975: Lower and early Middle Cambrian Formations near Mount Robson, British Columbia and Alberta; Canadian Journal of Earth Science, v. 12, no. 2, p. 119-131.

Gabrielse, H.
1954: McDame, British Columbia (map with marginal notes); Geological Survey of Canada, Paper 54-10.

1963: McDame map-area, Cassiar District, British Columbia; Geological Survey of Canada, Memoir 319.

1975: Geology of Fort Grahame E 1/2 map-area, British Columbia; Geological Survey of Canada, Paper 75-33.

Handfield, R.C.
1968: Sekwi Formation, a new Lower Cambrian Formation in the southern Mackenzie Mountains, District of Mackenzie (95L, 105I, 105P); Geological Survey of Canada, Paper 68-47.

Mansy, J.L. and Gabrielse, H.
1978: Stratigraphy, terminology and correlation of Upper Proterozoic rocks in Omineca and Cassiar Mountains, north-central British Columbia; Geological Survey of Canada, Paper 77-19.

26.

REGIONAL RADIOGENIC HEAT PRODUCTION MAPPING BY AIRBORNE GAMMA RAY SPECTROMETRY

Project 740085

K.A. Richardson and P.G. Killeen
Resource Geophysics and Geochemistry Division

Richardson, K.A. and Killeen, P.G., Regional radiogenic heat production mapping by airborne gamma ray spectrometry; in Current Research, Part B, Geological Survey of Canada, Paper 80-1B, p. 227-232, 1980.

Abstract

In this paper the feasibility of compiling regional radiogenic heat production contour maps from reconnaissance airborne gamma ray spectrometric survey data is demonstrated. Such heat production maps clearly display the pattern of lateral variations in heat production and delineate anomalous areas. Quantitative information on the levels of heat production in the bedrock are obtained if the map values are increased by a factor which corrects for effects of overburden, vegetation and surface waters on the airborne radiometric measurements.

A regional heat production map covering 40 000 km^2 in the northwestern part of the Precambrian Canadian Shield shows that large lateral variations in surface heat production exist. A number of large belts of unusually high (>20 hgu or 8 μW/m^3) heat production are outlined on the map.

Introduction

Heat production in the earth's crust is an important factor necessary in heat flow studies and investigations of geothermal potential, and may also have application in the modelling of ore genesis. The major source of heat production in the crust is the radioactive decay of ^{40}K, and the radioactive nuclides in the uranium and thorium decay series. Radiogenic heat production can be calculated from potassium, uranium and thorium analyses of surface rocks.

Over the past 10 years, the Geological Survey of Canada has conducted extensive reconnaissance airborne gamma ray spectrometric surveys over the Canadian Shield. The presentation of survey results in units of concentration of radioelements was made possible by using calibrated airborne systems. The purpose of this paper is to demonstrate the feasibility and utility of compiling surface heat production contour maps from the reconnaissance airborne data. There are both advantages and limitations to this technique. The main advantage is the illustration of regional variations in the distribution of heat-producing elements. The limitation is the quantitative accuracy of the resulting heat production values.

Because the airborne determinations of radioelement concentration relate to the upper few tens of centimetres of the surface, which is generally some mixture of outcrop, overburden, vegetation and surface waters, the airborne measurements usually result in computed radioelement concentrations which are lower than the actual concentrations in bedrock. Consequently, a heat production map compiled from airborne data establishes a lower limit on heat production in the bedrock. Considerable work has been carried out over a period of years to quantify the relation between airborne and ground measurements. Comparison with ground measurements indicates airborne measurements are lower by a factor of about two to three over the range of radioelement concentrations normally found in rocks.

What is produced from airborne spectrometric data is a map which shows spatial variations in 'apparent' heat production. Such a map clearly indicates areas of anomalous heat production, and permits the estimation of the regional heat production in the upper crust.

Applications of Regional Heat Production Maps

(a) Heat Flow Studies

Heat production determinations are essential to heat flow studies and interpretations of crustal structure.

Birch et al. (1968) found that lateral variations in heat flow in New England and New York correlated with radioactivity of plutonic rocks in which the heat flow measurements were made according to the following relation:

$$Q = a + b\,A \qquad (1)$$

where Q is heat flow at surface
A is radiogenic heat production of surface bedrock
a is heat flow from lower crust and upper mantle
and b is the thickness of the heat producing layer of surface bedrock.

However, determination of representative heat production values often presents a problem. Roy et al. (1968) pointed out that many heat flow determinations in the Basin and Range province of southwestern United States for example, made in holes drilled for economic purposes, were less than satisfactory due to the possibility that heat production values were taken from unrepresentative regions of plutonic bodies. Similarly, Jessop and Lewis (1977) indicated the problem of determining representative heat production values at heat flow measurement sites in the Superior Province of the Canadian Shield. Regional heat production maps, which can be compiled from airborne gamma ray survey data, can be used to determine whether the heat production is representative and might also be used advantageously in selecting suitable sites for making heat flow-heat production measurements.

(b) Geothermal Potential

One requirement for the economic extraction of geothermal energy from hot dry granites is that the rock must reach a sufficiently high temperature at a reasonably shallow depth. Considering the geothermal potential of Caledonian granites in Britain, Brown et al. (1979) identified

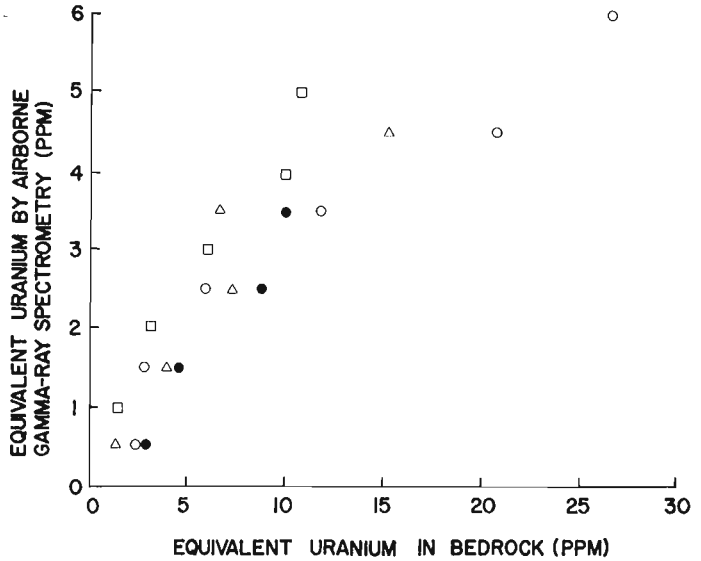

Figure 26.1. Relationship between gamma ray spectrometric determinations of uranium concentration, from airborne data and from in situ measurements on outcrop, for 4 areas of the Canadian Shield. Squares represent an area north of Great Slave Lake; open circles – Baffin Island north of Fury and Hecla Strait; solid circles – north of Elliot Lake, Ontario; triangles – Mont Laurier, Quebec.

three factors which favour high geothermal gradients in the upper crust. These are high background heat flow, high heat production, and large intrusive volumes indicated by negative Bouguer gravity anomalies. Examination of regional heat production maps, in conjunction with regional gravity anomaly maps, could be the first step in selection of areas having high geothermal potential.

(c) Mineral Deposits

Richardson and Oxburgh (1979), in conclusions regarding the heat flow field in Britain, suggested that granites at the time of intrusion may have initiated large scale convective circulations of water within the crust; these circulations, sustained by elevated heat production in the granites, could redistribute the heat-producing elements as well as other elements and ultimately concentrate them in ore deposits. Fehn et al. (1978) estimated the magnitude of hydrothermal convection cells and flow rates associated with radioactive plutons, and concluded that fluid convection is probably sufficient to develop hydrothermal uranium ore deposits. The close association of hydrothermal uranium deposits with uraniferous granites is not uncommon (e.g. Bräuer, 1970; Gangloff, 1970), and Richardson and Oxburgh (1979) found a weak correlation between areas of high heat flow and exposed zones of epigenetic mineralization. Thus information from heat production maps could be incorporated into the modelling of ore genesis and ultimately be applied as a guide to areas of potential mineral deposits.

Airborne Gamma Ray Spectrometric Data

Since 1970 the Geological Survey of Canada has been conducting high-sensitivity airborne gamma ray spectrometric surveys over Canada. From 1975 to 1978 under the Federal-Provincial Uranium Reconnaissance Program, extensive contract surveys were conducted, and presently approximately 2 000 000 km^2 of Canada, primarily over the Canadian Shield, have been surveyed.

The surveys were carried out systematically to uniform standards, using approximately 50 L of NaI(Tl) detectors flown at a terrain clearance of 122 m, with 5 km flight line spacing. This spacing was found to be suitable for determining regional radioelement distribution patterns in the Canadian Shield (Cameron et al., 1976). The spectrometer systems were calibrated (Grasty and Darnley, 1971; Grasty, 1976) and results were compiled in units of concentration of K, eU and eTh as recommended by the International Atomic Energy Agency (IAEA, 1976). In addition total gamma ray count rates over the range of 0.41 to 2.81 MeV were compiled in 'units of radioelement concentration'. The IAEA (1976) recommended this new unit, the 'ur' or 'unit of radioelement concentration', for total count gamma ray spectrometer or scintillometer results. The unit is described as follows: "A geological source with 1 unit of radioelement concentration produces the same instrument response (e.g. count rate) as an identical source containing only 1 part per million uranium in radioactive equilibrium". The 'ur' has been further discussed by Killeen (1979).

Charbonneau et al. (1976) reported on the relationship between contoured airborne measurements of radioelement concentration, and values measured in overburden and bedrock on the ground. Additional data subsequently acquired have been incorporated with the previous data and are presented in Figure 26.1. This diagram shows the average bedrock concentration of equivalent uranium for ground stations located within the various contour intervals of the airborne data, for four areas of the Canadian Shield. Over the normal range of uranium concentrations in rocks, the concentration of uranium in bedrock is about two to three times the value indicated by the airborne method. Results for thorium and potassium are similar. The points on Figure 1 indicated by square boxes represent the central part of the survey area to be discussed (Fig. 26.2, 26.3). This area is characterized by a higher percentage of outcrop than the other areas represented in Figure 26.1, and the data suggest that a factor of approximately two should be used to convert 'apparent' heat production values on Figure 26.2 to bedrock heat production.

Compilation of Contour Maps

Figure 26.2 is the 'apparent' heat production map covering an area of about 40 000 km^2 between Fort Smith and Port Radium, Northwest Territories compiled from reconnaissance airborne gamma ray spectrometric data. This surface heat production was calculated using conversion factors from Roy et al. (1968). Heat production, A, in heat-generation units (hgu) is calculated as

$$A = 0.23 \times (K\%) + 0.62 \times (U\ ppm) + 0.17 \times (Th\ ppm) \quad (2)$$

assuming a rock density of 2.67 g/cm^3. A heat generation unit (10^{-13}cal/cm^3 sec) is equal to 0.418 μW/m^3.

For comparison, the total count contour map of this same area is shown in Figure 26.3. The relative contributions of K, U, Th to the total count have been discussed by Grasty (1977); for the airborne survey data used to produce the contoured values in Figure 26.3.

$$TC\ (ur) = 3. \times (K\%) + 1. \times (U\ ppm) + 0.5 \times (Th\ ppm) \quad (3)$$

The above equations indicate that heat production is more sensitive to uranium and total count is more sensitive to potassium. When potassium, uranium and thorium occur in their normal crustal ratios (1.2×10^4/1/3.7, respectively) their relative contributions to heat production and to total count will be those shown in Table 26.1.

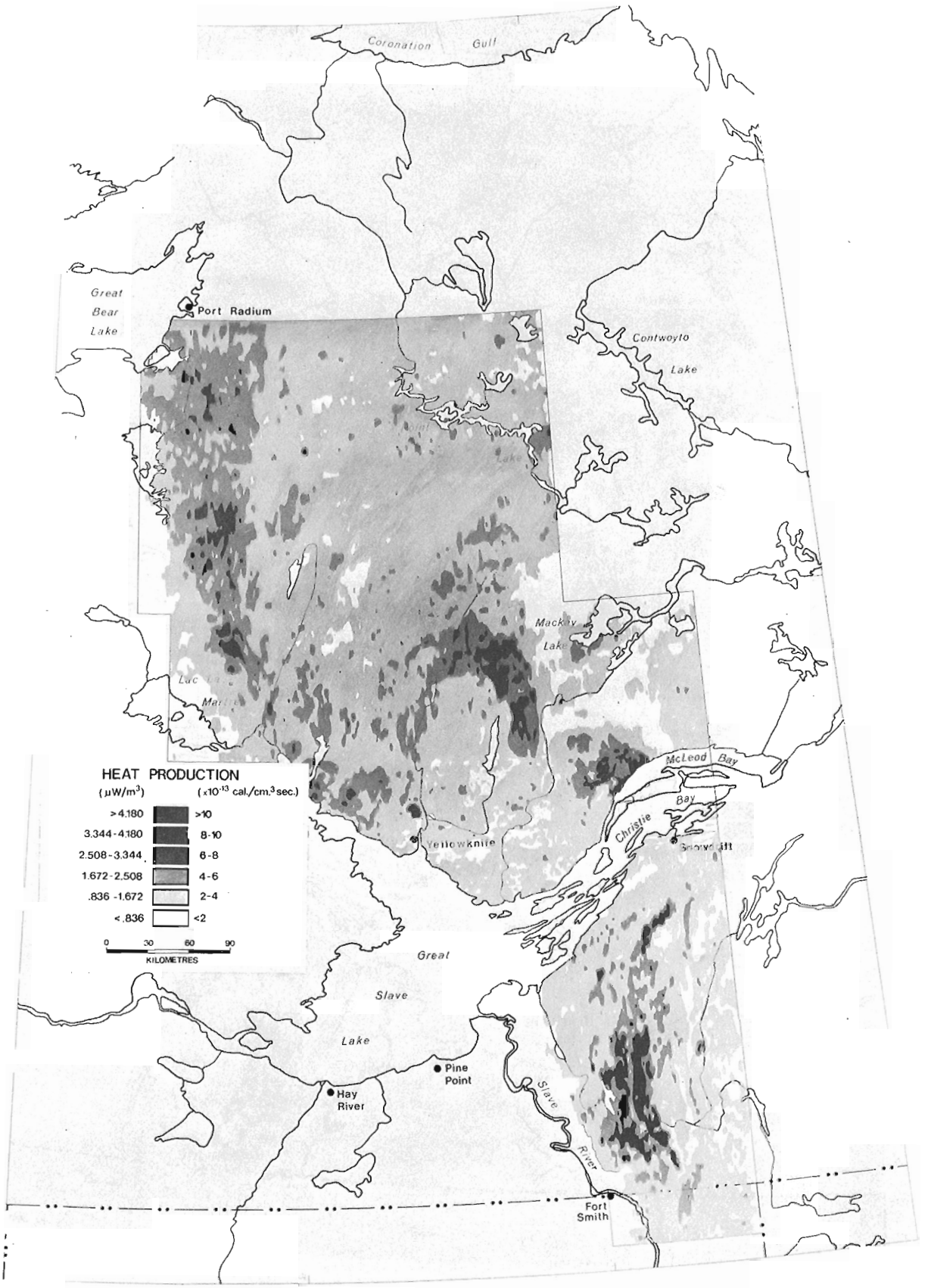

Figure 26.2. *Regional heat production map compiled from airborne gamma ray spectrometric data for northwestern part of the Canadian Shield.*

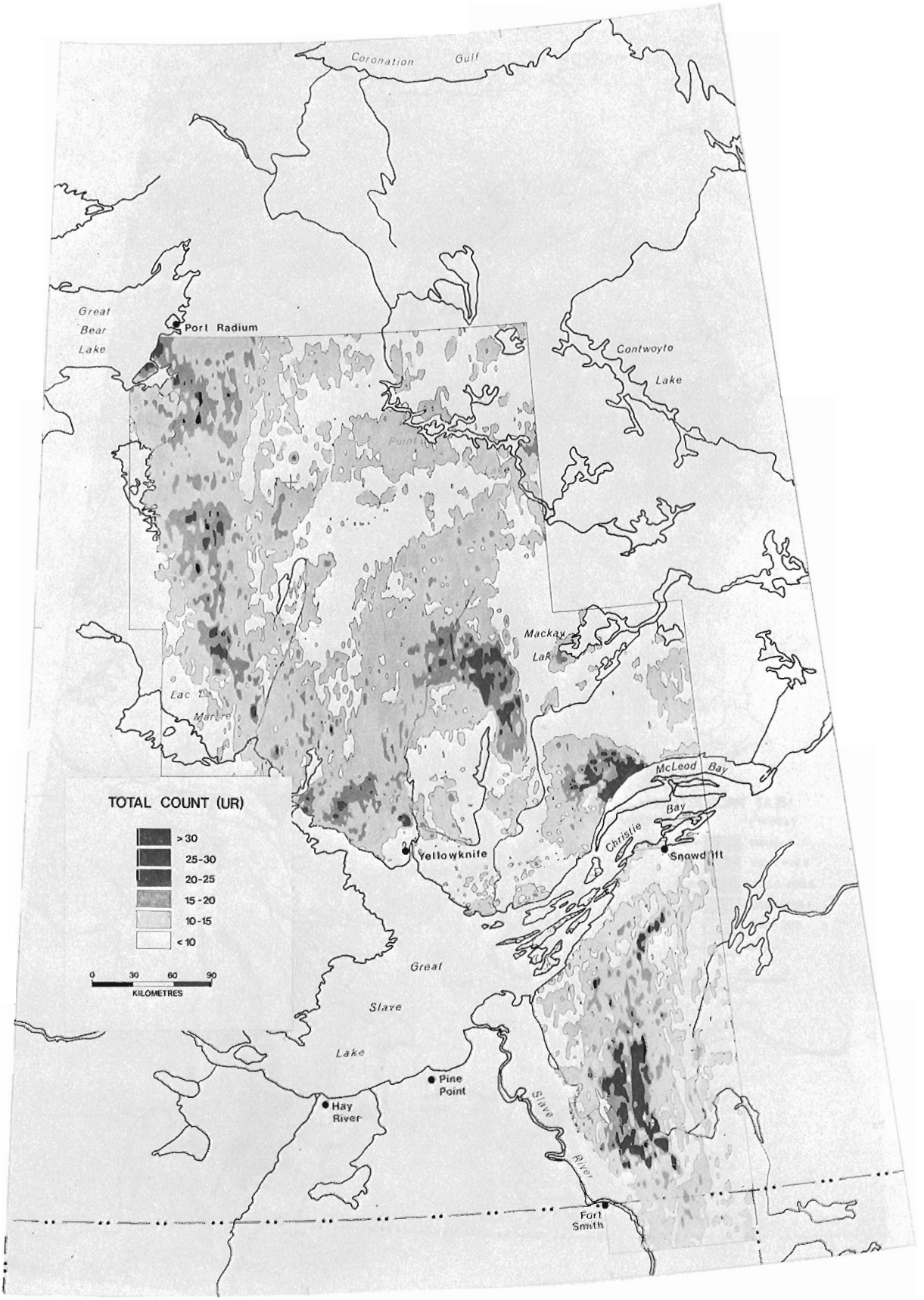

Figure 26.3. *Total count gamma ray contour map compiled from reconnaissance airborne surveys over northwestern part of the Precambrian Shield.*

Table 26.1

Relative contributions of potassium, uranium and thorium to heat production (A) and total gamma ray count rate (TC)

Normal Crustal Radioelement Ratio K/U/Th = 1.2 x 10^4/1/3.7		
	A	TC
K	18%	56%
U	41%	15.5%
Th	41%	28.5%

The strong influence of potassium on the total count map is evidenced by the similarity between Figure 26.3 and the previously published potassium map of the area (Killeen and Richardson, 1978). While the total count map appears adequate to indicate areas of anomalously high heat production, a more quantitative estimate of surface heat production can obviously be derived from the heat production map.

Discussion

The level of 'apparent' regional heat production over much of area shown in Figure 26.2 is between 2 and 4 hgu (0.836-1.67 $\mu W/m^3$). Conversion of this to bedrock heat production (increase by factor of 2 as described above) gives values of 4 to 8 hgu (1.67-3.34 $\mu W/m^3$), a range encompassing the heat production of the "continental crust" which was estimated by Heier and Rogers (1963) to be 4.4 hgu, and comparable to Jessop and Lewis' (1978) values for the Superior Province of the Canadian Shield.

Prominent features on both Figures 26.2 and 26.3 are areas of high heat production and radioactivity, respectively, which extend over several thousands of square kilometres. These include the western edge of the survey area between Lac La Martre and Port Radium (coincident with the Great Bear Batholith), an arcuate zone in the middle of the survey area (coincident with the Carp Lake Granite), an area on the north shore of McLeod Bay (underlain by granitic rocks) and a north-south trending area southeast of Great Slave Lake (over the highly thoriferous, granitoid Fort Smith Belt). Within these areas, 'apparent' regional heat production values exceed 4 hgu (1.67 $\mu W/m^3$) and reach values in excess of 10 hgu (4 $\mu W/m^3$). Applying the conversion factor to these values indicates bedrock heat production comparable to the highest values reported by Roy et al. (1968) for 38 localities in the United States. The northwestern part of the Canadian Shield contains some of the highest potassium, uranium and thorium contents found within the two million square kilometres of the Canadian Shield that have been surveyed by airborne gamma ray spectrometry.

Conclusion

This paper demonstrates the feasibility of compiling regional heat production contour maps from reconnaissance airborne gamma ray spectrometric survey data. Such a heat production map clearly displays the pattern of lateral variations in heat production and delineates anomalous areas. However to obtain more quantitative information on the levels of heat production in the bedrock, the map values must be increased by a factor which corrects for effects on the airborne measurement of overburden, vegetation and surface waters. This factor, which depends on the relative percentages of outcrop in a given region, can be determined by comparison of ground and airborne measurements.

A regional heat production map covering 40 000 km^2 in the northwestern part of the Canadian Shield shows that large lateral variations in surface heat production exist. These features must be taken into account in any interpretation of crustal structure and genesis.

References

Birch, F., Roy, R.F. and Decker, E.R.
1968: Heat flow and thermal history in New York and New England; in Studies of Appalachian Geology: Northern and Maritime, ed. E-an Zen, W.S. White, J.B. Haddley, and J.B. Thompson, Jr., John Wiley and Sons, Inc.-Interscience Publishers, New York.

Bräuer, H.
1970: Spurenelementgehalte in granitischen Gesteinen des Thüringer Waldes und des Erzgebirges; Freiberger Forschungshefte, v. C 259, p. 83-139.

Brown, G.C., Plant, Jane, and Lee, M.K.
1979: Geochemical and geophysical evidence on the geothermal potential of Caledonian granites in Britain; in Nature, v. 280, p. 129-130.

Cameron, G.W., Elliott, B.E., and Richardson, K.A.
1976: Effects of line spacing on contoured airborne gamma ray spectrometry data; in Exploration for Uranium Ore Deposits, International Atomic Energy Agency, Vienna, p. 81-91.

Charbonneau, B.W., Killeen, P.G., Carson, J.M., Cameron, G.W., and Richardson, K.A.
1976: Significance of radioelement concentration measurements made by airborne gamma ray spectrometry over the Canadian Shield; in Exploration for Uranium Ore Deposits, International Atomic Energy Agency, Vienna, p. 35-53.

Fehn, V., Cathles, L.M., and Holland, H.D.
1978: Hydrothermal convection and uranium deposits in abnormally radioactive plutons; in Economic Geology, v. 73, no. 8, p. 1556-1566.

Gangloff, A.
1970: Notes sommaires sur la géologie des principaux districts uranifères par la C.E.A.; in Uranium Exploration Geology, International Atomic Energy Agency, Vienna, p. 77-105.

Grasty, R.L.
1976: A calibration procedure for an airborne gamma ray spectrometer; Geological Survey of Canada Paper 76-16, 9 p.

1977: Calibration for total count gamma-ray surveys; in Report of Activities, Part B; Geological Survey of Canada, Paper 77-1B, p. 81-84.

Grasty, R.L. and Darnley, A.G.
1971: The calibration of gamma ray spectrometers for ground and airborne use; Geological Survey of Canada, Paper 71-17, 27 p.

Heier, K.S. and Rogers, J.J.W.
1963: Radiometric determination of thorium, uranium and potassium in basalts and in two magmatic differentiation series; Geochimica et Cosmochimica Acta, v. 27, no. 2, p. 137-154.

IAEA
1976: Radiometric reporting methods and calibration in uranium exploration; International Atomic Energy Agency, Vienna, Technical Reports Series no. 174, 57 p.

Jessop, Alan M. and Lewis, Trevor
1977: Heat flow and heat generation in the Superior Province of the Canadian Shield; in Tectonophysics, v. 50, p. 55-77.

Killeen, P.G.
1979: Gamma ray spectrometric methods in uranium exploration – application and interpretation; in Geophysics and Geochemistry in the Search for Metallic Ores; Peter J. Hood, ed., Geological Survey of Canada, Economic Geology Report 31, p. 163-229.

Killeen, P.G. and Richardson, K.A.
1978: The relationship of uranium deposits to metamorphism and belts of radioelement enrichment; in Current Research, Part B, Geological Survey of Canada, Paper 78-1B, p. 163-168.

Richardson, S.W. and Oxburgh, E.R.
1979: The heat flow field in mainland UK; in Nature, v. 282, p. 565-567.

Roy, R.F., Blackwell, D.D., and Birch, Francis
1968: Heat generation of plutonic rocks and continental heat flow provinces; in Earth and Planetary Science Letters, v. 5, p. 1-12.

27. URANIUM AND THORIUM VARIATIONS IN TWO MONZONITIC LACCOLITHS, EAST ARM OF GREAT SLAVE LAKE, DISTRICT OF MACKENZIE

Project 770024

S.S. Gandhi and N. Prasad
Economic Geology Division

Gandhi, S.S. and Prasad, N., Uranium and thorium variations in two monzonitic laccoliths, East Arm of Great Slave Lake, District of Mackenzie; in Current Research, Part B, Geological Survey of Canada, Paper 80-1B, p. 233-240, 1980.

Abstract

Two cogenetic monzonitic laccoliths, one hosting uraniferous actinolite-apatite-magnetite veins, were selected for a comparative petrochemical study. An unbalanced nested sampling design was adopted to estimate variability at four statistical levels within each laccolith and also between them. The laccoliths are roughly equal in area, approximately 2.5 km^2, and are represented by 53 and 59 samples. The data available to date are for uranium and thorium contents of the samples, specific gravity, and gamma ray spectrometer readings at the sample sites. The mean contents of uranium and thorium in the two sets of samples are 6.02 and 6.35 ppm U and 27.53 and 27.85 ppm Th. The corresponding means from the spectrometer readings are very close to these means. An analysis of variance shows that most of the variations in the contents of these elements occur at local rather than regional level in each of the laccoliths, and the variance between them is negligible. Specific Gravity ranges from 2.62 to 2.73. The two laccoliths are thus statistically very similar, and the present data suggest that uranium in the veins may have been derived from suitable country rock rather than the host intrusion.

Introduction

A string of more than 20 laccolithic intrusions of diorite-monzonite composition extends along the 225 km length of the East Arm of Great Slave Lake (Fig. 27.1). Their regional geology has been described by Stockwell (1936), Barnes (1953), Hoffman (1968, 1969, 1977), and Hoffman et al. (1977). Hoffman et al. (1977) recognized two compositionally distinguishable sets of laccoliths; those east of 110°30'W are predominantly monzonitic and those to the west of it are predominantly dioritic with more acidic dykes and veins at their borders. Badham (1978) presented chemical analyses of 17 samples from seven laccoliths, showing their subalkaline character and calc-alkaline differentiation trend.

Three laccoliths host veins of coarse actinolite, apatite and magnetite, carrying minor amounts of pitchblende and traces of copper sulphides (Lang et al., 1962; Badham, 1978). These veined laccoliths are at Regina Bay and Labelle Peninsula (Fig. 27.1). The veins are believed to be genetically related to the laccoliths (Lang et al., 1962; Badham, 1978; Gandhi, 1978; Bloy, 1979). The veins are more numerous, more extensive and are better explored at the Regina Bay laccolith than at the two other laccoliths on Labelle Peninsula. The Regina Bay laccolith therefore was selected for a detailed petrochemical study to determine chemical variation within it and possible significance of the variation to the origin of the uraniferous veins. For the purpose of a comparative study, another laccolith of approximately equal area (about 2.5 km^2) located at Meridian Lake (Fig. 27.1), which has no known uraniferous actinolite-apatite-magnetite veins associated with it, was selected.

Field observations by the writers show that the two laccoliths are very similar in composition and texture. They are predominantly monzonitic, medium to coarse in grain size, with well developed crystals of plagioclase approximately 1 cm long. Hornblende is the main mafic mineral, and biotite and quartz are encountered in minor amounts locally in both the laccoliths. The laccoliths are surrounded by brecciated sediments, mainly red shales, marl and limestone of the Stark Formation of Aphebian age. No contact metamorphic effects in the sediments were observed, not even in the sediments lying within the areas of the laccoliths. On the other hand, angular fragments of monzonite occur in the breccia along the margin of the laccoliths, indicating that brecciation postdates, at least in part, the emplacement of the laccoliths. These contact relations have been noted by previous workers in these and the other laccoliths. The mode of emplacement of the laccoliths, their relations to regional stratigraphy and structure, and brecciation of the sediments are discussed by Hoffman et al. (1977). Available K-Ar isotopic data on samples from the laccoliths and Pb-U isotopic data on samples from the uraniferous veins hosted by them, indicate a time range of 1850 to 1700 Ma for the emplacement of the intrusions as well as the veins (Hoffman, 1969; Gandhi, 1978; Bloy, 1979).

The present study was undertaken as a part of 'Canadian Granite Study' for an international collaborative research project on granites sponsored by Nuclear Energy Agency/International Atomic Energy Agency.

Sampling

A multi-stage stratified sampling design, as illustrated in Figure 27.2, was adopted for both the laccoliths in order to reasonably assure an unbiased selection of samples, to optimize the number of samples in each laccolith, and to apply a multi-level analysis of variance (Baird et al., 1967; Cameron et al., 1979; Garrett, 1979; Garrett and Goss, 1980). The successive levels of variation in chemical composition, from lower to higher levels of hierarchy, are: 'within outcrop', 'between outcrops', 'within a primary square' representing a large part of laccolith, 'between the primary squares' in a laccolith, and finally between the laccoliths. Analytical precision was estimated by splitting 10 per cent of the samples collected.

The area of each laccolith was divided into 19 primary squares as shown in Figures 27.3 and 27.4. This number of squares is regarded adequate for a reasonable estimate of variance, following Garrett (1979, p. 199) who pointed out that a sample population of 15 may be considered the minimum desirable as a compromise between precise values for mean and standard deviations and the costs of sample collection and analysis. The primary square size selected also provided a good chance for a pair of samples at the tertiary level (Fig. 27.2) to come from different outcrops.

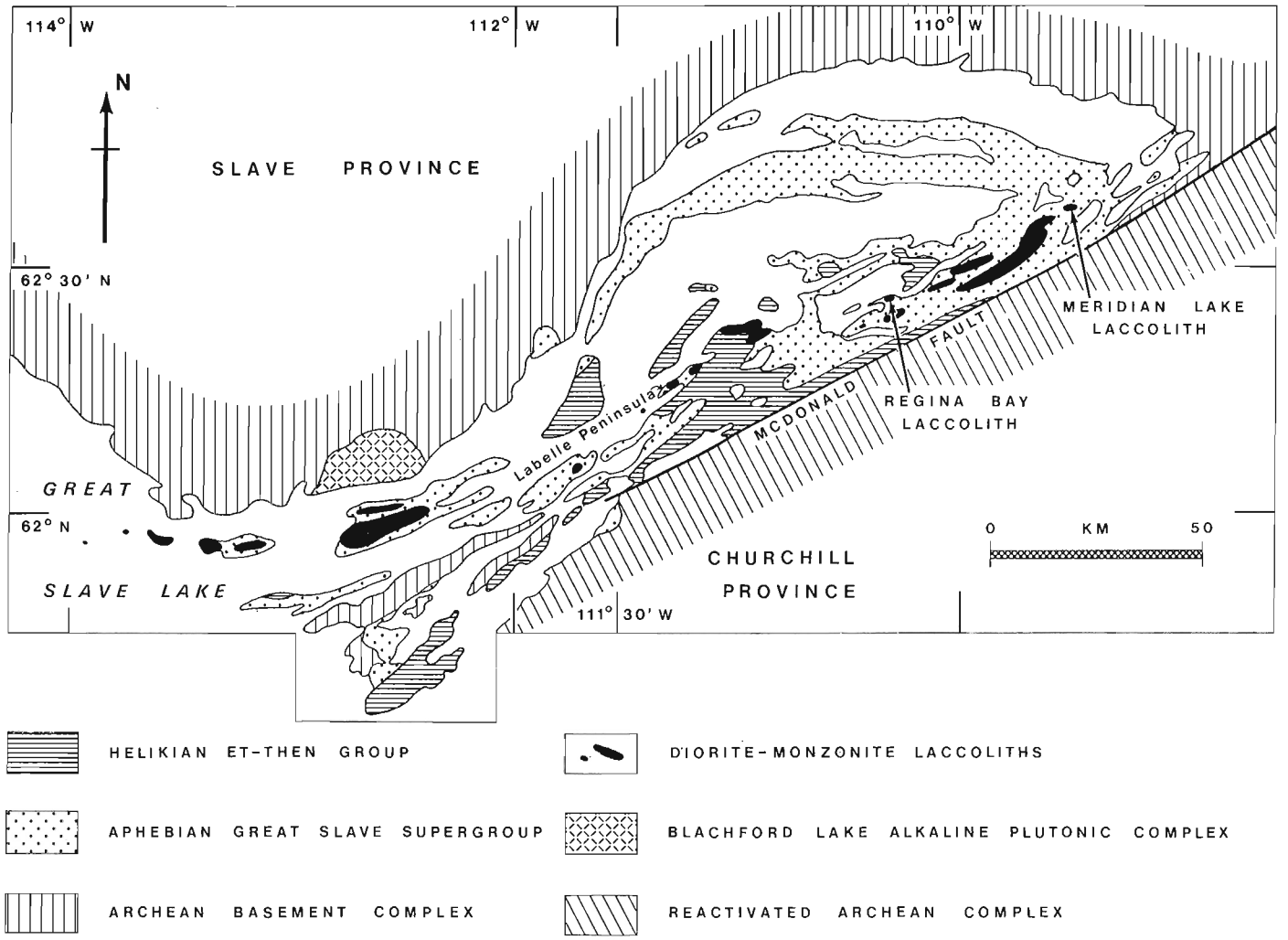

Figure 27.1. General geology of the East Arm of Great Slave Lake and location of the Meridian Lake and Regina Bay laccoliths.

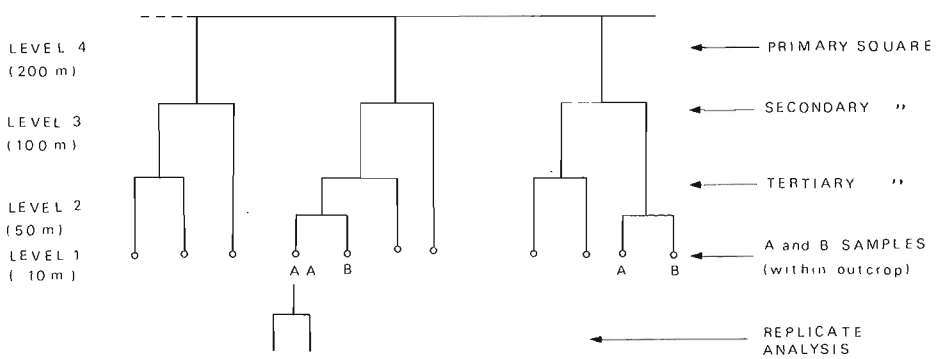

Figure 27.2. Hierarchical sample design for sampling of the two laccoliths in the East Arm of Great Slave Lake.

Each of the primary squares was divided into four secondary squares, two of which were selected randomly. One sample was collected from one of the two selected squares. The other square was further divided into four tertiary squares, and two of these were selected randomly, and sampled. This pair of samples was commonly from different outcrops, the sample sites being 50 to 60 m apart. Ten per cent of the total sample sites were chosen randomly for an additional sample within a 10 m distance (A and B) to estimate 'within outcrop' variation.

Both the laccoliths have a high topographic relief with respect to the surrounding sediments. Overburden is sparse, and exposures are good to excellent in this glaciated terrain. These features facilitated sampling of fresh rock. Approximately 1 to 2 kg of material was collected from one spot for each sample, and care was taken to avoid inclusions and vein material. At each sample site, radiometric readings of one minute duration were taken with a 4-channel gamma ray spectrometer (Model McPhar Spectra-44D). Readings were repeated at 4 sample sites and one background reading site for a duration of four minutes to check if the counts per minute differed significantly from the readings taken for one minute. The differences encountered were within the instrumental precision levels (± 1 ppm for U and ± 2.5 ppm for Th). Elevations were read with a barometer.

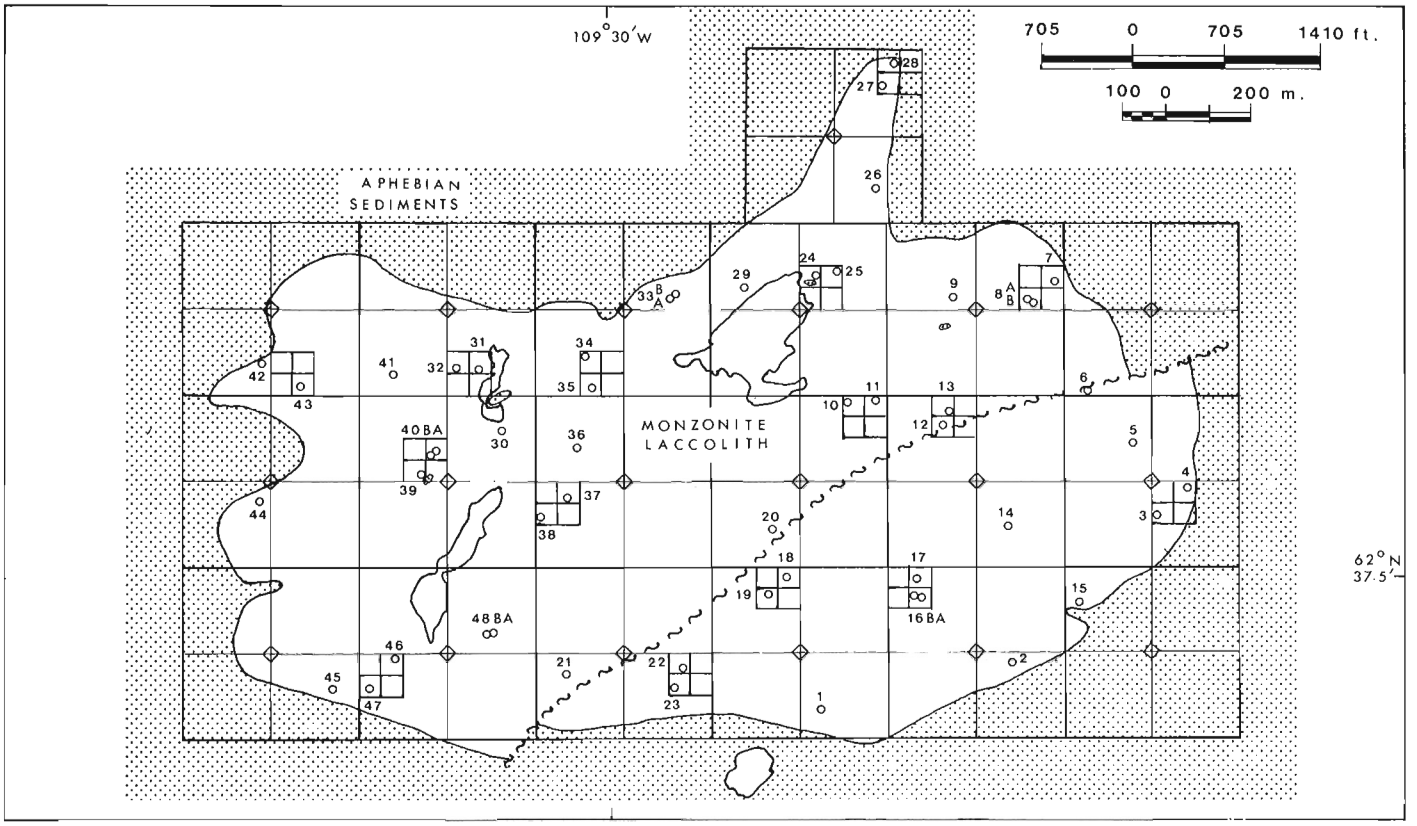

Figure 27.3. *Meridian Lake laccolith and sample locations. Primary squares marked by small diamond at their centre.*

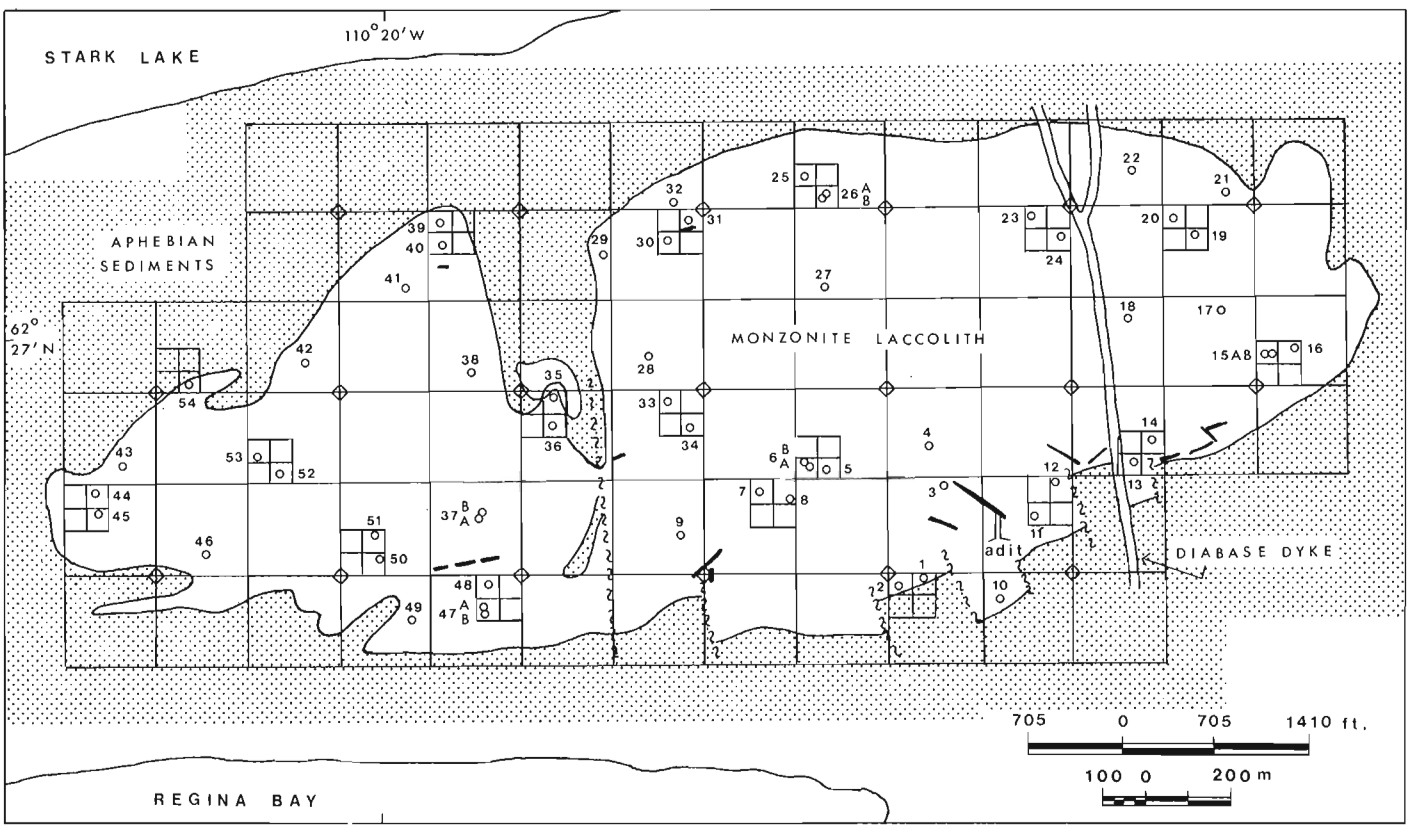

Figure 27.4. *Regina Bay laccolith and sample locations. Primary squares marked by small diamond at their centre. Uraniferous actinolite-apatite-magnetite veins represented by short heavy lines.*

Discussion of Results

The results obtained to date include spectrometer readings for U, Th, and K, specific gravity of samples, uranium content determined by delayed neutron counting and thorium content determined by X-ray fluorescence. These data are presented in Table 27.4. The data were treated statistically and the results are given in Tables 27.1, 27.2, and 27.3. Chemical analyses and petrographic study of the samples are underway.

Analysis of variance is sensitive to the homogeneity of variances of populations as well as to the normality of the population. The data on two laccoliths were checked for the homogeneity of variance using Burr-Foster Q test (Anderson and McLean, 1974). This showed that at 0.95 confidence limit, the variance of the two laccoliths are homogeneous. The Box-Cox parameters (Box and Cox, 1964) for optimal transformation of the raw data to normalize them were calculated. It was found that there was no advantage in any transformation, therefore the ANOVA (analysis of variance) was performed on the raw data.

The range and the mean values of the uranium and thorium contents are very similar for the two laccoliths, as seen in Tables 27.4 and 27.1. The mean uranium contents of the two laccoliths are 6.02 and 6.35 ppm (based on determinations by delayed neutron counting), and their mean thorium contents are 27.53 and 27.85 ppm (based on determinations by X-ray fluorescence), and the corresponding mean Th_{XRF}/U_{DNC} ratios are 4.85 and 4.73. The mean of contents of these elements as determined by the spectrometer are very close to the above means. The available data on the uranium and thorium contents of intermediate igneous rocks in various parts of the world are summarized by Nishimori et al. (1977, p. 7). These rocks commonly contain 2 ppm U, 7 ppm Th and 2 per cent K. Thus the two laccoliths in the East Arm are distinctly high in their mean uranium and thorium contents, compared to these global compilations. Examples of quartz monzonite distinctly enriched in uranium are Darby pluton in Alaska (Miller and Bunker, 1976) and a pluton in Stevens County, Washington (Nash, 1977); these contain 11.2 and 12.0 ppm U respectively. The Darby pluton has a Th/U ratio of 5.

Analysis of variance using UANOVA program (Garrett and Goss, 1980) was performed on the data (Table 27.4) to estimate degree of variance at 4 levels of hierarchy as illustrated in Figure 27.2. This program was written for carrying out ANOVA on unbalanced nested sampling design, like the one adopted for this study.

It can be seen from Table 27.2 that most of the variation in uranium and thorium contents in the two laccoliths occurs locally rather than regionally, viz. at outcrop level and between outcrop level rather than at levels involving greater distances. Specific gravity shows a negligible variance around the mean.

When the two laccoliths are compared, the percentage of total variance in the uranium and thorium contents at a 5th level or interlaccolith level, is negligible as seen in Table 27.3. Only the specific gravity shows a statistically significant variation at this level. The total variance of specific gravity however is so small that the percentage variances are quantitatively not significant.

Very small variation in specific gravity within each laccolith and between them reflects close similarities in composition of magma and little crystallization differentiation in situ of these intrusions.

The Regina Bay laccolith, although it hosts uranium-bearing veins, does not differ from the Meridian Lake laccolith in terms of overall uranium abundance and distribution. The present data therefore raise questions regarding the hypothesis that the intrusion is the source of uranium in the veins. Possibility of an external source of uranium cannot be ruled out and it is conceiveable that uranium was leached from suitable country rock by groundwater circulating in convection currents generated by heat of the intrusion. Further discussion on genesis of the veins will follow additional petrochemical studies underway.

Table 27.1

Some statistical parameters of two sample populations listed in Table 27.1

	MERIDIAN LAKE LACCOLITH						REGINA BAY LACCOLITH					
	U_{DNC}	Th_{XRF}	U_{SPEC}	Th_{SPEC}	K_{SPEC}	Sp.Gr.	U_{DNC}	Th_{XRF}	U_{SPEC}	Th_{SPEC}	K_{SPEC}	Sp.Gr.
UPPER*	6.33	28.82	6.74	29.65	2.08	2.702	6.92	28.74	7.68	29.06	2.09	2.676
MEAN	6.02	27.53	6.17	28.89	1.83	2.689	6.35	27.85	6.64	27.73	1.77	2.671
LOWER*	5.71	26.24	5.60	28.11	1.59	2.676	5.79	26.96	5.60	26.39	1.45	2.665
VARIANCE** AROUND MEAN	0.021	0.378	0.073	0.134	0.013	0.000	0.072	0.179	0.246	0.404	0.023	0.000
STANDARD*** DEVIATION	1.199	3.851	1.765	3.343	0.669	0.031	1.716	2.839	2.999	3.600	0.922	0.020
SKEWNESS***	-0.271	0.457	0.087	0.292	-0.641	-0.726	0.396	-0.032	1.080	-3.323	0.086	0.229
KURTOSIS***	4.981	-0.598	0.507	-0.237	0.473	0.435	0.260	0.257	2.909	0.119	-0.437	-0.352

*Upper and lower 95 per cent confidence limits for the mean.

**'Variance around mean' estimated by the UANOVA program (Garrett and Goss, 1980) which takes into account the sampling design.

***Calculated using SPSS (Statistical Package for Social Sciences), where all samples were considered to have equal weight, and the uneven distribution of samples imposed by the sampling design have not been taken into account.

Table 27.2

Analysis of variance in uranium and thorium contents and specific gravity in the Meridian Lake and Regina Bay laccoliths

Variable[1]		MERIDIAN LAKE LACCOLITH				REGINA BAY LACCOLITH				
	U_{DNC}	Th_{XRF}	U_{SPEC}	Th_{SPEC}	Sp.Gr.	U_{DNC}	Th_{XRF}	U_{SPEC}	Th_{SPEC}	Sp.Gr.
Total Variance	2.24	18.69	3.19	15.50	0.001	2.97	14.16	9.64	18.18	0.0005
Percentage of total variance at-										
Level 4 (200 m squares)	0.05^{N}	17.62^{N}	0.00^{N}	0.00^{N}	33.27^{N}	17.02^{N}	0.00^{N}	21.42^{N}	22.65^{N}	12.61^{N}
Level 3 (100 m squares)	0.00^{N}	0.00^{N}	26.75^{N}	0.00^{N}	21.04^{N}	3.67^{N}	29.39*	0.00^{N}	12.74^{N}	0.00^{N}
Level 2 (50 m squares)	87.51*	0.00^{N}	32.30^{N}	96.01***	0.00^{N}	7.77^{N}	0.00^{N}	70.61**	0.00^{N}	14.20^{N}
Level 1 (outcrop)	12.44	82.38	40.95	3.99	45.69	71.54	70.61	7.97	64.61	73.20

[1] Variables as in Table 27.1

***Significant at $\alpha = 0.001$; ** significant at $\alpha = 0.01$, and * significant at $\alpha = 0.05$ where α represents level of significance

N Not significant

Table 27.3

Analysis of variance in uranium and thorium contents and specific gravity between the Meridian Lake and Regina Bay laccoliths[1]

Variable	U_{DNC}	Th_{XRF}	U_{SPEC}	Th_{SPEC}	Sp. Gr.
Total Variance	2.554	15.564	6.270	12.566	0.0008
Percentage of total variance at -					
Level 5 (between laccolith)	0.28^{N}	0.00^{N}	0.00^{N}	3.03^{N}	17.89^{**}
Level 4 (200 m squares)	9.91^{N}	10.14^{N}	15.87^{N}	9.16^{N}	25.51^{*}
Level 3 (100 m squares)	0.00^{N}	8.26^{N}	0.83^{N}	3.38^{N}	2.77^{N}
Level 2 (50 m squares)	42.79^{N}	0.00^{N}	66.74**	35.24^{N}	0.00^{N}
Level 1 (outcrop)	47.02	81.60	16.56	49.19	53.82

[1] Symbols and abbreviations as in Tables 27.1 and 27.3

Table 27.4

Uranium and thorium contents and specific gravity of samples from the Meridian Lake and Regina Bay Laccoliths, East Arm of Great Slave Lake, District of Mackenzie

MERIDIAN LAKE LACCOLITH									
Sample Number	U_{DNC} ppm	Th_{XRF} ppm	U_{SPEC} ppm	Th_{SPEC} ppm	K_{SPEC} per cent	Sp. Gr. (gm/ml)	$\frac{Th_{XRF}}{U_{DNC}}$	$\frac{Th_{SPEC}}{U_{SPEC}}$	Elevation Metres
1	5.1	26.0	7.0	27.1	2.2	2.73	5.1	3.9	370
2	5.2	28.0	7.9	25.4	2.2	2.73	5.4	3.2	352
3	6.8	24.0	7.2	29.4	2.1	2.71	3.5	4.1	346
4	2.1	30.0	7.3	29.9	2.5	2.72	14.3	4.1	335
5	6.4	29.0	5.7	30.1	1.8	2.72	4.5	5.3	363
6	6.8	37.0	5.7	28.4	.3	2.69	5.4	5.0	372
7	4.9	27.0	7.2	24.0	1.8	2.69	5.5	3.3	358
8A	6.2	30.0	6.1	35.1	2.0	2.72	4.8	5.8	364
8B	6.1	22.0	6.1	35.1	2.0	2.70	3.6	5.8	364
9	6.8	27.0	6.7	28.2	1.1	2.68	4.0	4.2	355
10	5.2	22.0	6.5	26.2	1.6	2.71	4.2	4.0	367
11	6.2	29.0	7.0	29.6	1.7	2.69	4.7	4.2	367
12	5.5	24.0	8.3	24.9	1.7	2.72	4.4	3.0	381
13	2.4	27.0	7.4	26.8	2.0	2.69	11.2	3.6	393
14	6.4	24.0	5.4	32.9	1.1	2.69	3.7	6.1	349
15	7.0	23.0	6.0	27.9	2.8	2.72	3.3	4.6	322
16A	5.2	25.0	6.5	35.4	2.4	2.72	4.8	5.4	376
16B	4.9	23.0	6.3	34.1	2.8	2.72	4.7	5.4	373
17	6.2	28.0	6.8	26.8	1.9	2.70	4.5	3.9	378
18	6.3	33.0	3.3	30.0	2.4	2.72	5.2	9.1	367
19	5.1	24.0	5.7	23.4	1.7	2.73	4.7	4.1	373
20	6.5	33.0	8.3	28.7	1.9	2.70	5.1	3.5	367
21	4.5	25.0	5.9	27.5	2.3	2.69	5.6	4.7	361
22	5.5	27.0	3.3	29.0	2.1	2.71	4.9	8.8	373
23	7.0	26.0	5.0	27.4	2.6	2.70	3.7	5.5	367
24	7.9	30.0	3.5	30.9	.8	2.69	3.8	8.8	364
25	6.2	24.0	5.8	26.0	2.2	2.67	3.9	4.5	370
26	6.6	35.0	6.1	26.2	.5	2.68	5.3	4.3	370
27	6.1	33.0	8.4	27.1	2.0	2.62	5.4	3.2	343
28	6.7	26.0	4.3	30.0	2.6	2.65	3.9	7.0	352
29	5.3	30.0	7.9	22.6	3.4	2.68	5.7	2.9	349
30	5.0	27.0	5.5	24.0	1.9	2.75	5.4	4.4	383
31	5.9	22.0	6.8	27.9	1.6	2.66	3.7	4.1	386
32	6.3	29.0	4.8	29.9	1.5	2.66	4.6	6.2	392
33A	5.8	31.0	7.0	27.9	1.4	2.66	5.3	4.0	376
33B	5.8	32.0	3.4	29.4	2.1	2.69	5.5	8.6	376
34	5.6	27.0	5.7	34.9	2.1	2.69	4.8	6.1	373
35	6.2	32.0	7.2	29.0	1.3	2.70	5.2	4.0	367
36	5.6	32.0	3.7	26.8	.2	2.67	5.7	7.2	355
37	7.0	24.0	5.3	23.5	.5	2.64	3.4	4.4	358
38	5.1	23.0	8.0	30.4	2.0	2.69	4.5	3.8	358
39	10.3	28.0	6.9	28.8	1.3	2.64	2.7	4.2	358
40A	7.1	24.0	10.5	34.0	2.5	2.71	3.4	3.2	358
40B	6.1	31.0	10.8	32.5	2.0	2.65	5.1	3.0	358
41	7.1	27.0	5.8	36.0	1.1	2.64	3.8	6.2	367
42	6.0	22.0	1.9	29.0	2.1	2.70	3.7	15.3	352
43	6.4	25.0	4.4	22.9	2.2	2.68	3.9	5.2	358
44	5.4	35.0	5.5	26.9	.5	2.60	6.5	4.9	346
45	6.4	24.0	3.5	31.6	2.1	2.70	3.7	9.0	358
46	7.2	28.0	5.4	28.4	1.5	2.63	3.9	5.3	340
47	6.3	33.0	4.1	31.3	2.0	2.67	5.2	7.6	328
48A	7.3	23.0	8.1	29.7	2.4	2.69	3.2	3.7	346
48B	6.0	29.0	8.1	29.7	2.4	2.70	4.8	3.7	346
(Total 53)									

NOTES: U_{DNC} : Uranium determination using delayed neutron counting method, by Atomic Energy of Canada Limited, Ottawa

Th_{XRF} : Thorium determination using X-ray fluorescence method by Bondar-Clegg and Company Limited, Ottawa

U_{SPEC} : Uranium determination by gamma ray spectrometer (McPhar Spectra 44-D Model) in the field holding probe in contact with outcrop surface

Th_{SPEC} and K_{SPEC} : As in U_{SPEC}

Table 27.4 (cont'd)

REGINA BAY LACCOLITH

Sample Number	U_{DNC} ppm	Th_{XRF} ppm	U_{SPEC} ppm	Th_{SPEC} ppm	K_{SPEC} per cent	Sp. Gr. (gm/ml)	$\frac{Th_{XRF}}{U_{DNC}}$	$\frac{Th_{SPEC}}{U_{SPEC}}$	Elevation Metres
1	5.5	25.0	14.8	32.8	1.4	2.69	4.5	2.2	255
2	7.5	25.0	8.6	26.9	.8	2.68	3.3	3.1	244
3	7.8	31.0	9.1	27.4	1.2	2.69	4.0	3.0	264
4	5.3	28.0	5.6	26.5	.2	2.64	5.3	4.7	283
5	6.2	31.0	8.9	23.5	.9	2.66	5.0	2.6	293
6A	5.0	30.0	7.5	20.6	.9	2.66	6.0	2.7	296
6B	5.9	33.0	8.5	30.7	.9	2.67	5.6	3.6	296
7	6.5	27.0	5.4	19.6	0	2.64	4.2	3.6	296
8	5.2	27.0	4.8	18.2	.7	2.65	5.2	3.8	276
9	4.6	23.0	7.6	25.9	1.1	2.67	5.0	3.4	297
10	7.6	25.0	6.8	26.3	2.7	2.68	3.3	3.9	232
11	8.9	25.0	6.9	28.5	2.7	2.65	2.8	4.1	251
12	7.1	26.0	6.5	21.0	.6	2.66	3.7	3.2	277
13	7.9	28.0	7.2	24.9	2.5	2.67	3.5	3.5	259
14	7.9	21.0	8.7	29.6	2.1	2.70	2.7	3.4	274
15A	8.1	27.0	10.9	31.6	1.9	2.68	3.3	2.9	287
15B	8.7	32.0	10.3	30.0	2.3	2.68	3.7	2.9	287
16	8.1	31.0	7.6	28.1	.8	2.67	3.8	3.7	280
17	6.6	29.0	7.1	27.9	1.8	2.65	4.4	3.9	314
18	6.8	28.0	6.8	24.4	1.7	2.68	4.1	3.6	337
19	7.7	23.0	11.5	22.8	1.5	2.71	3.0	2.0	329
20	6.7	26.0	4.6	23.7	1.6	2.67	3.9	5.2	334
21	5.9	27.0	6.8	25.1	1.4	2.67	4.6	3.7	331
22	7.0	26.0	10.4	34.7	1.5	2.68	3.7	3.3	331
23	4.0	27.0	5.0	25.7	.6	2.65	6.8	5.1	337
24	7.3	27.0	6.2	24.1	1.2	2.69	3.7	3.9	334
25	4.0	28.0	4.0	25.6	1.2	2.66	7.0	6.4	326
26A	4.5	24.0	2.5	27.8	1.7	2.65	5.3	11.1	319
26B	5.5	32.0	3.7	27.2	2.3	2.66	5.8	7.4	319
27	4.8	27.0	5.0	26.0	1.8	2.66	5.6	5.2	317
28	6.0	29.0	3.3	30.0	2.2	2.68	4.8	9.1	326
29	7.3	27.0	10.2	33.4	3.4	2.66	3.7	3.3	277
30	8.1	25.0	9.3	34.9	3.4	2.64	3.1	3.8	280
31	5.7	30.0	8.6	32.1	2.8	2.72	5.3	3.7	277
32	6.3	35.0	3.4	29.7	2.7	2.69	5.6	8.7	255
33	3.9	30.0	1.9	27.1	2.0	2.65	7.7	14.3	334
34	3.7	28.0	.6	29.3	.7	2.66	7.6	48.8	326
35	6.4	30.0	5.0	31.3	4.0	2.69	4.7	6.3	283
36	9.2	29.0	6.2	28.5	.5	2.65	3.2	4.6	285
37A	6.0	29.0	7.1	25.9	2.2	2.63	4.8	3.6	302
37B	4.5	28.0	4.9	28.5	2.9	2.69	6.2	5.8	305
38	5.4	26.0	1.6	24.0	3.1	2.66	4.8	15.0	213
39	4.1	27.0	2.9	31.8	1.5	2.67	6.6	11.0	223
40	6.0	27.0	7.4	25.1	1.6	2.67	4.5	3.4	235
41	10.0	28.0	6.2	30.4	1.9	2.67	2.8	4.9	258
42	7.8	21.0	5.0	29.6	2.9	2.69	2.7	5.9	279
43	6.9	30.0	6.1	25.6	2.3	2.71	4.3	4.2	282
44	7.5	26.0	4.6	30.9	2.6	2.69	3.5	6.7	277
45	7.5	30.0	6.2	29.7	2.3	2.69	4.0	4.8	274
46	3.7	26.0	4.2	29.3	3.2	2.66	7.0	7.0	302
47A	3.4	30.0	6.3	29.6	0	2.65	8.8	4.7	283
47B	7.5	31.0	6.5	27.2	.1	2.66	4.1	4.2	283
48	4.6	29.0	4.3	27.1	1.5	2.68	6.3	6.3	288
49	4.5	26.0	5.2	33.2	3.0	2.69	5.8	6.4	276
50	5.8	32.0	7.0	30.9	1.8	2.65	5.5	4.4	276
51	11.6	33.0	9.6	32.6	2.1	2.69	2.8	3.4	277
52	6.1	26.0	17.9	28.5	1.7	2.67	4.3	1.6	323
53	3.7	29.0	6.4	26.6	1.9	2.64	7.8	4.2	323
54 (Total 59)	7.1	27.0	4.6	25.9	2.0	2.69	3.8	5.6	290

Precision - U_{SPEC} : ± 1 ppm
Th_{SPEC} : ± 2.5 ppm
K_{SPEC} : ± 0.2 ppm
U_{DNC} : ± 5 per cent at 10 ppm level at 0.95 confidence limit
Th_{XRF} : ± 1 ppm

Conclusions

Samples collected from the two cogenetic monzonitic laccoliths using a hierarchical sampling design, totalling 53 and 59 in number, yielded mean contents of uranium and thorium of 6.02 and 6.35 ppm U and 27.53 and 27.85 ppm Th respectively. An analysis of variance at different levels shows that most of the variances in the contents of these elements occur at local, viz. at outcrop and between outcrop levels, rather than at regional levels in each of the two laccoliths, and the variances between them are insignificant. Specific gravity shows a very small range in variations within each laccolith and between them. These data reflect statistically overall compositional similarities of the two laccoliths.

Acknowledgments

The writers are thankful to Dr. R.G. Garrett of the Geological Survey of Canada for his suggestions on sampling design for this study, and help in the analysis of variance. Discussions with J.A. Kerswill, also of the Geological Survey of Canada, on the statistical considerations have been very valuable. Responsibility for the opinions expressed and conclusions drawn here are, however, the writers' own. Capable assistance in the field work was provided by Craig Houle.

References

Anderson, V.L. and McLean, R.A.
1974: Design of Experiments; Marcel Dekker Inc. New York, p. 22-23 and 401-402.

Badham, J.P.N.
1978: Magnetite-apatite-amphibole-uranium and silver-arsenide mineralizations in lower Proterozoic igneous rocks, East Arm, Great Slave Lake, Canada; Economic Geology, v. 73, no. 8, p. 1474-1491.

Baird, A.K., McIntyre, D.B., and Welday, E.E.
1967: Geochemical and structural studies in batholithic rocks of southern California; Part II, sampling of the Rattlesnake Mountain pluton for chemical composition, variability, and trend analysis; Geological Society of America, v. 78, p. 191-222.

Barnes, F.Q.
1953: The Snowdrift and McLean Bay map-areas, Great Slave Lake, Northwest Territories; unpublished Ph.D. thesis, University of Toronto.

Bloy, G.R.
1979: U-Pb geochronology of uranium mineralization in the East Arm of Great Slave Lake, Northwest Territories; unpublished M.Sc. thesis, University of Alberta, 64 p.

Box, G.E.P. and Cox, D.R.
1964: An analysis of transformations; Journal of Royal Statistical Society, B-26, p. 211-243.

Cameron, E.M., Ermanovics, I.R., and Goss, T.
1979: Sampling methods and geochemical composition of Archean rocks in southeastern Manitoba, Canada; Precambrian Research, v. 9, p. 35-55.

Gandhi, S.S.
1978: Geological observations and exploration guides to uranium in Bear and Slave structural provinces and the Nonacho Basin, District of Mackenzie; in Current Research, Part B, Geological Survey of Canada, Paper 78-1B, p. 141-149.

Garrett, R.G.
1979: Sampling considerations for regional geochemical surveys; in Current Research, Part A, Geological Survey of Canada, Paper 79-1A, p. 197-205.

Garrett, R.G. and Goss, T.I.
1980: UANOVA: A FORTRAN IV program for unbalanced nested analysis of variance; Computers and Geosciences, v. 6, p. 35-60.

Hoffman, P.F.
1968: Stratigraphy of the Great Slave Supergroup (Aphebian), East Arm of Great Slave Lake, District of Mackenzie; Geological Survey of Canada, Paper 68-42, 93 p.

1969: Proterozoic paleocurrents and depositional history of the East Arm Fold belt, Great Slave Lake, Northwest Territories; Canadian Journal of Earth Sciences, v. 6, p. 441-462.

1977: Preliminary geology of Proterozoic Formations in the East Arm of Great Slave Lake, District of Mackenzie; Geological Survey of Canada, Open File 475 – G, K, and L (NTS 75 L/8, 75 K/11, and 75 K/12 respectively)

Hoffman, P.F., Bell, P.R., Hildebrand, R.S., and Thorstad, L.
1977: Geology of the Athapuscow aulacogen, East Arm of Great Slave Lake, District of Mackenzie; in Report of Activities, Part A, Geological Survey of Canada, Paper 77-1A, p. 117-129.

Lang, A.H., Griffith, J.W., and Steacy, H.R.
1962: Canadian deposits of uranium and thorium; Geological Survey of Canada, Economic Geology Report 16, 324 p.

Miller, T.P. and Bunker, C.M.
1976: A reconnaissance study of the uranium and thorium contents of plutonic rocks of the southeastern Seward Peninsula, Alaska; Journal of Research, United States Geological Survey, v. 4, p. 367-377.

Nash, J.T.
1977: Geology of the Midnite uranium mine area, Washington: maps, description and interpretation: United States Geological Survey Open File Report 77-592, 39 p.

Nishimori, R.K., Ragland, P.C., Rogers, J.J.W., and Greenberg, J.K.
1977: Uranium deposits in granitic rocks; United States Energy Research and Development Administration, Open File Report GJBX-13 (77), 311 p.

Stockwell, C.H.
1936: East Arm of Great Slave Lake; Geological Survey of Canada Map 377A (East Half) and 378A (West Half) (with descriptive notes).

28. PALEOLATITUDES AND POTENTIAL FOR PHOSPHORITE DEPOSITION IN CANADA

Project 760062

R.L. Christie
Institute of Sedimentary and Petroleum Geology, Calgary

Christie, R.L., Paleolatitudes and potential for phosphorite deposition in Canada; in Current Research, Part B, Geological Survey of Canada, Paper 80-1B, p. 000-000, 1980.

Abstract

Canada may have contained sites favourable to deposition of marine phosphates during long periods of the past when, according to paleopole calculations, northern North America lay at tropical to subtropical latitudes. The most favourable periods appear to have been between late Hadrynian and Triassic times.

Introduction

Sedimentary phosphate rock, or phosphorite, of Tertiary or Holocene ages evidently formed at tropical to subtropical latitudes and it seems clear that the paleolatitudinal distribution of ancient phosphorites similarly must fall within a few tens of degrees of the equator. Thus the paleolatitudes of sedimentary basins may be useful in determining probabilities for presence of phosphorite or in establishing targets for a phosphate search.

This paper is one of a series prepared by the Geological Survey of Canada on Canadian bedded phosphates and explores the use of published information on paleolatitudes in Canada. It begins with a brief review of phosphate genesis, occurrences, and the present state of the industry in order to provide background for discussion of paleolatitudes as a potential prospecting tool.

Canada has a well developed phosphate industry but at present produces no phosphate ore; the 'phosphate rock' required is imported, mainly from the United States. The discovery and development of domestic phosphate deposits can be viewed as a prime goal in Canadian mineral policy.

Phosphate Ores and Phosphate Rocks

The most widely used phosphate ore (more than 80 per cent of world production) is sedimentary phosphate rock, or phosphorite. Other phosphate ores include: phosphatized limestone, sandstones, shales, and igneous rocks; guano; and igneous and metamorphic apatite.

Phosphorites are indistinctive white to dark brownish grey, mainly light-coloured rocks; they are often featureless and easily overlooked. Some aids to recognition are the rounded, structureless pellets or nodules that are characteristic of certain phosphorites, or, for some other deposits, the presence of phosphatized bone fragments, fecal pellets, and fish teeth. Glauconite may be an accessory mineral. Other clues are a bluish white 'bloom' on weathered surfaces, and a bituminous odour produced on striking the (commonly) organic-rich phosphorite with a hammer. Marine phosphates usually contain small amounts of uranium and outcrops, samples, and drill cores can be scanned for gamma ray activity using a scintillometer or a gamma ray spectroscope. Chemical tests must be used as controls or to confirm the presence of phosphate. Gamma ray level can be used in places to obtain approximate P_2O_5 value, but is not always a reliable guide (Hale, 1967).

Phosphorite in Canada

Sedimentary phosphate deposits of possible economic grade and size were recognized in the southern Canadian Rockies shortly after the Western States phosphate field was developed about 1906 (see Telfer, 1933). Phosphatic beds at scattered localities in central and eastern Canada had been recognized earlier, but none approached useful thicknesses and grades (de Schmid, 1916).

Phosphatic beds of a wide range of ages have been reported in Canada from Proterozoic to Cretaceous in age. Mainly Cambrian, and some Ordovician, phosphate beds are known in the Maritimes: Matthew (1893) noted phosphate nodules in the Cambrian of southern New Brunswick; phosphatic nodules occur in a bed overlying Cambrian manganiferous deposits in Avalon Peninsula, Newfoundland (British Sulphur Corporation, 1971); phosphatic beds were noted in Ordovician limestones on the west coast of Newfoundland (British Sulphur Corporation, 1971); and coprolitic phosphate has been reported from Upper Cambrian limestones in Cape Breton and in Antigonish County, Nova Scotia (Spence, 1920). The phosphatic, hydrocarbon-rich shale of the Albert Formation of New Brunswick is early Mississippian in age (Greiner, 1962; R. Shaw, personal communication, 1979).

In Quebec, black phosphatic nodules have been reported in Cambrian limestone at Rivière Ouelle on the lower St. Lawrence River, and in Ordovician sandstone at Allumette Rapids and at Grenville, both on the Ottawa River (Spence, 1920).

Phosphatic nodules in Ordovician limestone also are reported at Hawkesbury and at Lochiel, Ontario (Spence, 1920). In the course of uranium exploration of Proterozoic beds, apatitic sediments have been discovered at several localities in the Canadian Shield. An example of such sediments occurs in the Aphebian Wollaston uranium subprovince, south of the Athabasca Basin in Saskatchewan where light green quartzites with disseminated uranium mineralization in places contain phosphates (Tremblay, 1978, p. 432). Whether the apatite is in all cases sedimentary in origin, however, is not clear.

Phosphatic nodules have been noted in beds of late Triassic (Schei Point Formation) and early Jurassic (Wilkie Point, Borden Island formations) ages in the Arctic Islands (Tozer, 1963, p. 368; Tozer and Thorsteinsson, 1964, p. 121-130).

Phosphorite occurs in beds of Proterozoic, Cambrian, Ordovician, Mississippian, Permian, Triassic, Jurassic, and Cretaceous ages in western Canada; these occurrences were reviewed by Christie (1979). In addition, phosphatic beds of Devonian age have recently been reported in the west (McIlreath, personal communication). The most promising deposits found to date, those of basal Jurassic beds in the Fernie synclinorium of southeastern British Columbia, have been explored intermittently several decades, but none has proven to be economically viable.

Phosphorite Deposition and Latitude

Some of the factors that affect the formation of phosphorite are: climate; ocean currents; basinal configuration; rate of downsinking and influx of clastic sediment; bottom chemical conditions and activity levels of physical processes at the bottom; and organic activity. Latitude at the site of deposition affects several of these factors. Hence, the paleolatitudes of exposed sedimentary basins may be a key to the discovery of ancient phosphorites.

Knowledge of paleogeographic and lithofacies relationships in sedimentary basins, in the light of sedimentological models for phosphate deposition, has led to discovery of phosphate deposits in Turkey and Peru (see McKelvey, 1963; Sheldon, 1964b). The 'Phosphoria model' has similarly proved useful in the discovery of new deposits in Saudi Arabia, Australia, India, and Colombia (Sheldon et al., 1967).

Origin of Phosphorite

From the observed abundance of organic remains in many phosphorites a biological phase in the formation of sedimentary phosphate seems necessary. Furthermore, a biogenic origin in a reducing environment is indicated by the chemical characteristics of phosphorites: the association of the elements Si-P-C and the strong – that is, low – C^{13} 'signal' (δC^{13})[1] in phosphatic sediments (Kolodny, 1979). A widespread consensus now is that upwelling of cold, phosphate-rich seawater at favourable sites (such as adjacent to a broad, stable marine platform) allows development of prolific biota, mainly phytoplankton, and that phosphate is leached from the organic remains during anoxic destruction of the dead organisms. A complex sequence of diagenetic phosphatization and upgrading of sediments through reworking finally produces economic phosphorite deposits (see Cook, 1976; Wang and McKelvey, 1976; Riggs, 1979).

Paleolatitudes of Phosphorite

The paleolatitudes of ancient (early Tertiary and older) phosphorities were determined by Sheldon (1964a), from selected paleomagnetic results, to lie within 40° of the equator. Sheldon used 'virtual geomagnetic poles'[2], taken from published lists, that most closely correspond to the ages of some 19 phosphorites. Both economic deposits and 'occurrences' were considered. In a recent re-evaluation of paleolatitudes and phosphorites Cook and McElhinny (1979) confirmed Sheldon's results and proposed new tectonic models for phosphate deposition. The new models take into account oceanic circulation and plate tectonics.

The recent compilation by Cook and McElhinny (1979) is based on paleolatitudes for 162 phosphorites from the Phanerozoic, among which are 72 major deposits. The paleolatitudes of all deposits range from about 0° to 70°, but a histogram shows a maximum within 20° of the paleoequator. Data from large deposits appear to form a peak, or preference, between 10° and 20° from the equator. Further analysis shows that: a) phosphate deposition may be favoured at sub-equatorial (10°-20°) rather than equatorial (0°-10°) latitudes; b) there may be a second favoured latitude at about 40°.

Much of the Canadian landmass may have lain at favourable latitudes at times in the past. A latitudinal belt favouring phosphate deposition is assumed, for purposes of this discussion, to lie between 30°N and 30°S, and the position of Canada at different times is represented by the paleopositions of a centre point (60°N, 100°W) arbitrarily chosen to be near the midpoint of the country. If this point were at latitude 30° or less, much of the landmass would lie in climatic zones favouring phosphate formation, and some part, at least, of any major Canadian sedimentary basin that lay poleward would be close to the possible temperate (40°) latitude favouring phosphate deposition. The azimuthal orientation of the continent need not, therefore, be considered here.

A favourable latitude alone, of course, will not result in the formation of major phosphate deposits. From the earlier remarks on the origin of phosphorite it is clear that one or more of the following conditions also must occur:

- favourable marine site, with currents bringing nutrient-rich water from oceanic depths;
- favourable climatic conditions (rainfall, pH and salinity of the sheltered marine terrace);
- favourable paleogeography - low hinterland possibly with topographic barriers to prevent influx of terrigenous sediment;
- favourable tectonic conditions: stable crust, with periodic small changes of sea level resulting in reworking of the phosphorites;
- favourable local structural features: gentle arches or 'highs' on the marine shelf that are either emergent or form shoals separating depressions for phosphate entrapment.

The tectonic features of seaways that might favour phosphate deposition were considered by Cook and McElhinny (1979, p. 318-323). These authors proposed two plate tectonic models, 'Spatial Models' A and B, to account for oceanic upwelling and phosphate deposition along the borders of seaways (with the exception of epeiric seas). Model A, in which lithospheric plates separate due to north-south movement, considers east-west seaways, and model B, in which plate movement is east-west, considers north-south seaways. Upwelling currents (and associated phosphorites) will develop at both early and late (narrow and wide seaways) stages where continental movements conform to model A, and at late stages in model B. The models serve to account for many phosphatic deposits of the world; examples are: Cretaceous phosphorites of the Tethys region – due to strong westerly currents in a narrow seaway at low latitude; certain Cambrian phosphorites of China – due to upwelling along a northern boundary of a wide seaway where the boundary has drifted into the latitude of westerly winds; and Eocene phosphorites of West Africa – due to upwelling on the east side of a seaway broad enough for the development of oceanic gyral currents. The models and examples given by Cook and McElhinny demonstrate the interrelationship of phosphorites, latitudinal position, and plate tectonic history.

---

[1] Variations in the ratio of C^{13} to C^{12} are reported as values of δC^{13}, in parts per thousand, relative to a standard. A strongly negative value for δC^{13} is characteristic of organic matter in general (Bender, 1972).

[2] A virtual geomagnetic pole is a 'spot' pole calculated for a single sample or site. It represents an instantaneous geomagnetic pole, and contrasts with a paleomagnetic pole, which represents a paleomagnetic field averaged over intervals in the order of 10^4 to 10^5 years (McElhinny, 1973, p. 26).

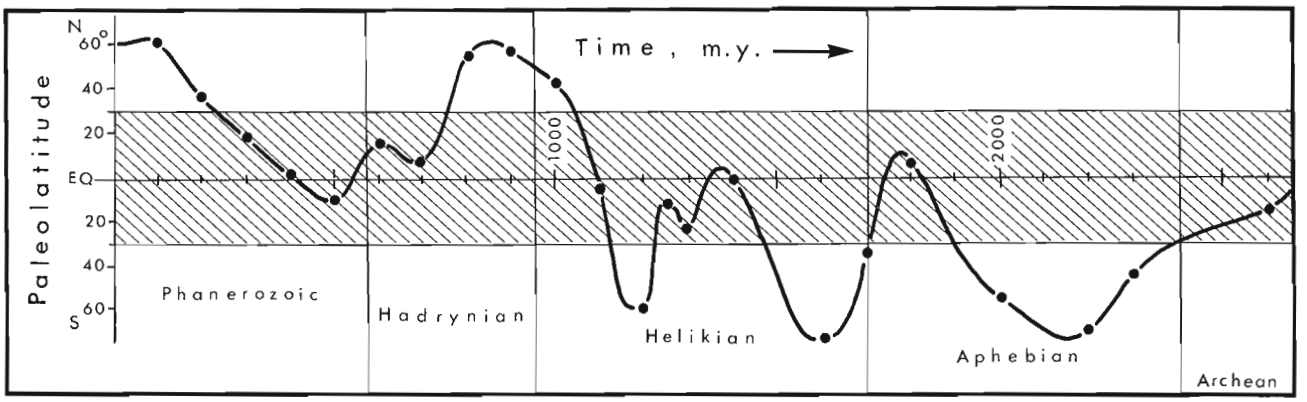

Figure 28.1. *Paleolatitudes for a locality west of Hudson Bay (60 N, 100 W); after Irving, 1979.*

Paleolatitudes and Paleogeography for Canada

Improved understanding of rock magnetization and refinements in procedures for the measurement of remanent magnetization have aided in the plotting of paths of 'apparent polar wandering', and, given certain assumptions (e.g. that the geomagnetic field on average conforms to a geocentric axial dipole), it has been possible to convert paleopole results to paleolatitudes and paleoazimuths (paleolatitude is the distance in degrees from a locality to the paleoequator, and paleoazimuth is the angle between the paleonorth and present north; Irving, 1979, p. 670-690). The latitudinal and angular positions of Canada (that is, central, stable parts of Canada) have recently been calculated back to 2800 Ma ago by Irving (1979) and shown graphically in his series of figures (op. cit., Fig. 14-19). Irving's reconstructions for Phanerozoic time broadly confirm positions for North America in figures drawn by Smith et al. (1973) using mainly geometric techniques based on topographic and tectonic data as well as paleomagnetic data from the ocean floors.

Paleolatitudes for Canada

Canada's present high-latitude position evidently is not typical of much of the time since late Archean (Irving, 1979, Fig. 14-19). Irving noted that a reference point such as that now occupied by the city of Winnipeg (latitude 50°N) spent about 45 per cent of the time in the last 2300 Ma (Proterozoic and later time) at latitudes less than 30°. A plot of the paleolatitudes of a more central Canadian locality (60°N, 100°W; the 'centre' of the country, mentioned earlier) suggests (by measurement) that much of Canada has been at subtropical to tropical latitudes for about the same proportion of Proterozoic and Phanerozoic time (see Fig. 28.1); that is, favourably positioned for deposition of phosphates.

Paleogeography and Phosphate Possibilities of Canada

The paleoposition of Canada, as proposed and figured by Irving (1979, Fig. 14-19) has broad implications for the paleoclimatic history of that region; indeed, close correlation between geological conditions and paleolatitudes for late Aphebian – early Helikian and Paleozoic times has already been noted by Irving: late Aphebian – early Helikian formations contain carbonate rocks, halite casts, and redbeds[1], and Paleozoic units in Canada contain, in addition, abundant reefal and evaporitic rocks. On the other hand, a precise estimation of paleoclimate and sedimentary conditions would require consideration of the relative positions or nearness of other landmasses, and the direction and strengths of winds and ocean currents. Such estimates have been made (e.g. Skevington, 1974; Jackson, 1975) to account for faunal affinities and distribution of certain graptolites. The approach could be profitable in the search for phosphorites, but will not be pursued further here.

Canada's positions relative to the 'phosphate zone', 30°S to 30°N latitude, since early Proterozoic time are reviewed in the following paragraphs and are based on Irving's (1979) constructions. Factors that are favourable to phosphate formation other than latitudinal position may also be considered. Some of these are: a) the probable presence of wide, shallow seas; b) the temporal relationship to recognized phosphogenic periods (Cook and McElhinny, 1979); and c) the changes with time of the chemical nature or balance of oceanic water.

Archean

The ancient nucleus of Canada (Laurentia) passed through the 'phosphate zone' in late Archean time according to the tentative reconstructions of Irving. However, Archean time appears to have been unproductive for phosphorite: no deposit of such great age has been discovered. Cook and McElhinny (1979, p. 326) speculated that before 3400 Ma B.P. phosphorus was present in the hydrosphere at a level sufficient to form the procaryotic fauna[2] characteristic of the Archean, but was not abundant enough to form phosphorites. Later in the Archean and in the earliest Proterozoic, the phosphorus content increased (derived from degassing and weathering of rocks) in both the hydrosphere and in the (increasing) biosphere, but a lack of shallow seas, an association with abundant iron, and a relatively small total biomass still precluded the formation of phosphorite.

[1] Evidence and opinions on the origin of redbeds were reviewed by Chandler (1980). Although there is controversy about some points, it seems clear that the red iron oxide (hematite) of redbeds is a diagenetic feature relating to hot conditions, whether desert or humid (op. cit., p. 4).

[2] The blue-green algae and bacteria; these cells lack nuclear membrane, well-defined chromosomes, and most components of the eucaryotic cells; included are anaerobic forms.

Proterozoic

Northern North America occupied tropical to temperate latitudes during about 40 per cent of Proterozoic time (Fig. 28.1). Early Proterozoic phosphorites are known elsewhere in the world, and peaks of phosphate deposition in later Proterozoic time are well defined (Cook and McElhinny, 1979). Proterozoic formations are widespread in Canada and thus may be promising targets for phosphate exploration.

Aphebian Canada approached the 'phosphate zone' after about middle Aphebian time, according to the paleopolar determinations, and occupied tropical latitudes until the Hudsonian Orogeny (1700 Ma), after which it drifted into high south polar latitudes. The Aphebian, between 1800 and 2200 Ma, is also the time of the first major phosphogenic episode; phosphorites of this age are known in Australia, in Finland, and in Michigan, U.S.A. The phosphorite of the Michigan locality occurs as carbonate-apatite in a cherty iron formation and as pebbles in a conglomerate. Both units are part of the Aphebian Marquette Range Supergroup of metasedimentary and metavolcanic rocks (Cannon and Klasner, 1976).

Cook and McElhinny (1979, p. 326) suggested that between 2200 and 1800 Ma the oceans 'overturned' (perhaps triggered by glaciation - upwelling was more intense because of a greater temperature differential); the deep oceanic water, rich in iron and phosphorus and in a reduced state, spread across shallow continental shelves. Phosphorus at this time precipitated together with iron to form phosphatic iron formations and a few thin phosphorite beds. Iron deposits contain small but significant amounts of phosphorus (0.02 to 2.63% P_2O_5 in average compositions listed by Gross, 1965, p. 13), and the total phosphate content of iron deposits is enormous (for quantitative estimates see Cook and McElhinny, 1979, p. 325). This phosphate, mainly in diluted form, cannot be considered phosphate ore, although bedded apatite segregations, as at the Michigan locality noted earlier, could be economic.

Helikian The Canadian nucleus, Laurentia, was in a state of general uplift following the Hudsonian Orogeny and occupied relatively high latitudes, according to 'low confidence level' determinations by Irving (1979). Throughout much of the Helikian, however, the northern North American continental mass lay at tropical and subtopical latitudes, well within the 'phosphate zone'. Southern high-latitude drift took place about 1200 Ma B.P., and northern high latitudes roughly coincided with the Grenville Orogeny, about 955 Ma ago. From age determinations (admittedly few and of uncertain reliability) it appears that a phosphogenic episode may have commenced at about 1600 Ma and ended at 1200 Ma; this episode would be represented by phosphorites at Pogoryy and Underly in the Yenisei Ridge district of the U.S.S.R. and Rajasthan in India, according to Cook and McElhinny (1979, p. 317). Low paleolatitudes for Canada in this period tend to be confirmed, as suggested by Irving (1979), by the occurrence of redbeds, halite casts, and carbonates in some Canadian basins of Helikian age (e.g. the Purcell System of the southern Rocky Mountains; see summary by Chandler, 1980, p. 18). The Purcell System is represented south of the International Boundary by the Belt Series (Supergroup), in which Gulbrandsen (1966) found dark, pelletal phosphorite. The apatitic rock occurs as laminae, up to 2.5 cm thick, in a 20 cm thick bed of coarse siltstone in a predominantly redbed unit, the Spokane Formation, in Montana.

Helikian basins on the western Canadian Shield contain mainly clastic rocks, but also stromatolitic dolomite, perhaps indicating a warm climate favouring production of organisms (see Stockwell et al., 1970, p. 89). Stromatolitic zones are common in the uppermost beds of the Athabasca Basin (op. cit., p. 94), and apatite forms a matrix in clastic rocks lower in the section, although it is not yet clear whether the phosphate is a primary sediment or due to later mineralization (P. Ramaekers, personal communication, 1980). Redbeds and calcareous cement characterize parts of the Dubawnt Group, and a shallow-marine environment of deposition under stable tectonic conditions is suggested for the upper part of the section in this basin (Stockwell et al., 1970, p. 99).

Helikian sediments in the Coppermine-Shaler Mountains (Victoria Island) region are marked by redbeds and stromatolite zones (op. cit., p. 81); these beds are included in a wide sedimentary province named the Amundsen Basin (Christie, 1972). Sedimentary units of this province have been correlated, on the basis of gross lithology and stromatolite assemblages, with Helikian strata of the Mackenzie Mountains (Aitken, et al., 1978b). A strong sequential similarity of clastic rocks, carbonate rocks, and evaporites is evident, although correlation of lower formations is unresolved.

The Proterozoic basin of the Mackenzie Mountains is characterized by abundant carbonate rocks, stromatolitic carbonate rocks including stromatolite reefs and biostromes, and a thick gypsum unit. The stromatolite forms and assemblages are taken, as in the Soviet Union, to be indicative of Helikian (basal Middle Riphaean, 1350 ± 50 Ma) and Helikian-Hadrynian (Basal Upper Riphaean, 950 ± 50 Ma) ages (Aitken et al., 1978a).

Sediments of Helikian age form great thicknesses in the southern Rocky Mountains (Purcell System) and, although carbonate units with stromatolitic and shallow-water features are present, the bulk of the section is terrigenous, ranging from quartzite to argillite. A carbonate shelf origin has been ascribed to the Waterton and Siyeh formations of the Clark Range, and redbeds, mudcracks, or casts of salt crystals are present in clastic units such as the Grinnell, Sheppard, and Gateway Formations (see Chandler, 1980, p. 18).

The Borden Basin of northern Baffin Island is intruded by dykes of Hadrynian age, and probably is itself Helikian in age (Blackadar, 1970; Jackson et al., 1978). The lowermost and uppermost units of the basin are reddish and orange-weathering quartzites and sandstone, whereas intervening units comprise predominantly dark to light grey dolomite, shale, and siltstone. Shallow-water and/or shelf deposition is indicated by algal carbonates of the Society Cliffs and Victory Bay formations, and these features, with gypsum beds of the Society Cliffs Formation (Geldsetzer, 1973) may be indicative of warm climate conditions. The Borden Basin, therefore, can be included among potentially phosphatic basins.

The Thule Basin of Northwest Greenland and Ellesmere Island is another sedimentary basin of Helikian age that might be considered for phosphorite, although few exposures of these rocks occur in Canada (see Christie, 1962a,b; Frisch et al., 1978; Dawes, 1976, p. 259-262). Carbonate-rocks, stromatolites, small reefs, redbeds, and gypsum suggest a general similarity in sedimentary conditions to those of the Amundsen and Cordilleran basins.

The six Canadian basins described above evidently lay at low latitudes during at least part of their histories and may be considered as favourable sites for phosphate deposition. The marine shelf parts of the basins, of course, are better targets for prospecting phosphate than some other facies that seem to suggest fluvial or continental conditions.

The geochemical character of oceanic water may have been 'improving' for phosphate deposition during Helikian time; Cook and McElhinny (1979, p. 327), in their Temporal Model C, speculated that the period from 1800 to 800 Ma ago was marked by an increase in phosphorus content of the hydrosphere, that the biota, now including the eucaryota[1] held an increasing amount of phosphorus, and that iron and phosphorus were sufficiently segregated (due to oxidizing conditions[2]) to allow the formation of phosphorites.

Hadrynian Laurentia occupied moderate to low latitudes during the later half of Hadrynian, or latest Proterozoic time, according to irving's (1979) calculations. (It should be noted, however, that the Hadrynian track was considered 'very speculative'.) This low-latitude interval began at about 800 Ma, which coincides with the beginning of a period of about 200 Ma duration, perhaps extending into the Cambrian, during which phosphogenesis may have been fairly continuous. Major phosphate deposits of late Hadrynian age are found in China and in the Volta area of northern Africa, and lesser deposits occur in central Siberia, Brazil, Mauritania, India, and central Australia (Cook and McElhinny, 1979, p. 317). No phosphorites of this age are yet known in Canada.

Cook and McElhinny (1979, p. 327) suggested that after 800 Ma, relatively large amounts of phosphorus were held in the biota, which then included metazoans. Large phosphorite deposits formed as a result of more productive biotic segregation and concentration of the phosphorus, while some phosphorus still was deposited with iron formations.

Canadian basins of Hadrynian age are mainly associated with the continental margins of that era: the Cordilleran, Franklinian, and Appalachian geosynclines. Hadrynian sediments are widely exposed in the western and northern geosynclines, but only a small area of late Precambrian sedimentary and volcanic rocks in southern and easternmost Québec represents deposits of the former eastern continental margin of North America (see Williams, 1979, p. 794).

Late Precambrian sedimentary and volcanic rocks of the Appalachian Orogen are widely exposed in southeastern Newfoundland, Cape Breton Island, and southeastern New Brunswick. The Hadrynian and Cambrian rocks of these areas are part of the Avalon Zone (see Williams, 1979), a stratigraphic-tectonic zone that formerly was part of an African - European continental landmass. This exotic element was attached to the Canadian nucleus during the Middle to Late Ordovician.

The geosynclinal sediments of the Cordilleran and Franklinian geosynclines are marine, and partly shallow-water and miogeosynclinal; they form an almost continuous linear belt in the eastern Cordillera, but to the north are exposed only in northern Ellesmere Island in the Innuitian (Franklinian) region. Relatively few facies types that are usually associated with phosphate deposition are known: bedded chert-hematite iron formations of the Rapitan Group in the Mackenzie Mountains might be considered to be favourable. Several carbonate formations of miogeosynclinal character were deposited in the Franklinian basin, and pisolitic limestone was noted by Kerr (1967, p. 16). In general, however, the two Canadian geosynclines were dominated in Hadrynian time by clastic or volcanic rocks; the seas and sedimentary basins had not yet achieved the productivity and variety of life forms that were to mark Paleozoic time.

Paleozoic

Reconstructions of continental positions in earliest Paleozoic time place Canada in equatorial latitudes, with today's lines of longitude lying subparallel to the paleoequator (Irving, 1979; Smith, et al., 1973). All the Canadian Paleozoic basins then lay within 30° of the equator; the abundant carbonates, evaporites, and fossil remains (including petroleum) of organisms of early and middle Paleozoic age in this country tend to confirm the paleolatitudinal reconstructions. By Permian time, however, northern North America had drifted into the northern hemisphere and by latest Triassic time only southern parts of Canada lay at 30° latitude.

Phosphorites, particularly with pelletal texture, were widely and abundantly deposited in Cambrian and later time. The abundance of phosphorite in Phanerozoic time coincides with other geochemical and lithological phenomena: e.g. massive formation of sedimentary sulphates (Cloud, 1974, p. 319); high phosphorus content (0.5 to 1.5%) in Clinton-type (Cambrian to Devonian) iron ores (Gross, 1965, p. 123); widespread oxidative enrichment of banded iron formations (Cloud, 1974, p. 319); and overall dominance of pelletal texture in both phosphorites and iron formations (Cook and McElhinny, 1979, p. 325). The interrelationships of features of this sort are not clear; for example, as noted by Cook and McElhinny, there are good matches for several peaks of deposition of phosphate and iron in the Phanerozoic (Cambrian, Ordovician, Jurassic, and upper Eocene), but there is no phosphate peak to match Devonian iron ore formation and no iron peak to match Miocene phosphorite. The authors conclude that phosphogenesis is only indirectly related to most of the other geochemical - lithological phenomena noted (e.g. evaporitic deposition) but that all are associated through plate tectonic history. Iron and phosphorus, on the other hand, are linked because upwelling ocean water is important to the formation of both. There appears to be a decreasing coincidence of phosphate and iron peaks of deposition after early Paleozoic time (see Cook and McElhinny, 1979, Fig. 5); this may be due to the increasing dominance and effects of the metazoans, these forms perhaps complicating the early, more direct chemical relationship between phosphorites and the oceans and atmosphere.

Phosphorites are known in Cambrian and Ordovician platformal and miogeosynclinal beds in the Canadian Cordillera (reviewed by Christie, 1979); in the Arctic Islands, phosphatic matrix and oolites have been identified in sandstone of the Cambrian Rabbit Point Formation (U. Mayr, personal communication).

A worldwide hiatus in phosphate deposition marked the Silurian, Devonian, and early Carboniferous periods. The reasons for this break in phosphogenesis are not known, although it may be relevant that the hiatus coincided with an interval lacking glacial events (see Cook and McElhinny, 1979, Fig. 5) and hence, perhaps, unfavourable conditions of oceanic overturning or circulation. Cook and McElhinny noted that few coasts were located at low, phosphate-favourable latitudes during Devonian to early Carboniferous times, according to the reconstructions of the continents by Smith et al. (1973).

The azimuthal direction of North America changed so that its long axis, which in Ordovician time lay parallel to the equator, by Silurian time lay approximately northeast (Irving, 1979); such major changes in crustal configuration clearly could alter the location of upwelling currents.

---

[1] Cellular life other than blue-green algae and bacteria; the presence of eucaryotes implies appreciable levels of free O_2 (Cloud, 1974).

[2] Iron retained in the rock weathering profile due to the buildup of O_2 in the atmosphere; large amounts of ferrous iron no longer transported to the sea by surface waters (Cloud, 1974).

Carboniferous and Permian times saw the Canadian Cordilleran sedimentary basin still in southern and phosphate-favourable latitudes, but with northerly trending coastlines. Sedimentological confirmation for this supposition is the shale beds of the Mississippian Exshaw Formation between the International Boundary and about 90 km north of the boundary in the southern Rocky Mountains. The productive, Permian Phosphoria Basin of the western United States also extends into Canada (as described by Telfer, 1933; also see Christie, 1979), but thicknesses and grades decrease northward and the known deposits are not economic.

The Mississippian Albert Formation of the Moncton Basin in New Brunswick includes dark grey, bituminous shales that contain phosphate nodules (R. Shaw, personal communication, 1979). The Albert Formation is characterized by a dominantly lacustrine facies that grades upsection into nonmarine evaporites near a depocentre in southeastern New Brunswick. The sediments are presumed to have accumulated in a narrow basin that formed along an orogenic 'suture' between continental plates. The younger Mississippian Windsor Group, higher in the section, contains anhydrite and salt deposits, from which it appears that a warm, arid climate was present in Mississippian time. The phosphate of the Albert Formation evidently was deposited in a nonmarine precurser of an east-west trending marine embayment (Greiner, 1962). With the exception of the Windsor Group, all the Carboniferous and Permian sedimentary units of the region are nonmarine; the Albert Formation appears to be distinctive and not to fit the usual models for phosphate depositon.

Mesozoic

Canada achieved increasingly higher latitudes during Triassic and Jurassic times according to paleopole reconstructions. By late Triassic time the entire Western Canada Sedimentary Basin (The Cordilleran Geosyncline and broad foreland basin onlapping the Canadian Shield) lay at and north of latitude 30°N. The Cordilleran seaway was by this time a tectonically complex region of eugeosynclinal troughs and geanticlines. Dark Triassic shales of the eastern Cordillera contain dispersed apatite and some higher concentrations – up to 30 per cent P_2O_5 (Gibson, 1975, p. 20; Telfer, 1933). The Triassic shales appear to have been deposited on the basinward side of an open marine shelf, with source areas mainly to the east and northeast. Deep basinal conditions lay to the west. Contemporary evaporites, redbeds, intraformational conglomerate, and solution breccias suggest evaporite conditions in a broad intertidal or tidal flat environment (Gibson, 1975, p. 30-33).

The extensive and volumetrically significant phosphatic formations of Triassic age in Canada are anomalous in world phosphogenesis: Triassic time is represented elsewhere by an important hiatus in phosphate deposition (Cook and McElhinny, 1979, Fig. 1). Phosphatic nodules in the Middle and Upper Triassic Schei Point Formation in the Canadian Arctic Islands (Tozer, 1963) are also notable; they formed during a phosphogenic 'low' time and at a high paleolatitude - over 40°N. Cook and McElhinny (1979, p. 318) have noted, however, that 40° latitude may be favoured for certain (usually Jurassic or Cambrian) phosphate deposits.

Canada occupied temperate latitudes (above 40°N in the western Canada Sedimentary Basin) in Jurassic time. This should not be a favourable period for phosphate deposition according to the rule of thumb adopted in this paper, yet the Jurassic Fernie Formation of southeastern British Columbia is one of the more phosphatic (though still economically marginal) units in Canada. A warm, continental climate must have prevailed, this apparently confirmed by evaporites in an adjacent cratonic basin, the Williston Basin of southern Saskatchewan and northern United States. Less easily explained are the phosphatic nodules of Jurassic formations in the high Arctic, the paleolatitudes of which must have been about 65°.

Phosphatic ironstones of mid-Cretaceous age with P_2O_5 values ranging up to 27 per cent occur in northern Yukon Territory and form perhaps the most enigmatic phosphate deposits in the light of their paleogeography; their paleolatitudinal position was calculated, according to Irving (1979) to be about 75°N, or at least 5° higher than at present! The deposit is distinctive in its iron and manganese association (phosphatic bedded ironstone and shale) and in being a facies equivalent of turbiditic sandstones and shales of the same basin. The deposits are subeconomic but have attracted interest because of excellent phosphate mineral specimens. At least four new mineral species have been named and described from the localities (Young, 1977).

A second Cretaceous phosphate locality, a layer of phosphatic fish remains of the Ashville Group (marine shale) of Manitoba, was formed at about its present latitude of 51°. This deposit, a thin (5 cm) black organic detrital bed, evidently resulted from a mid-Cretaceous marine transgression of the broad alluvial plain of the eastern part of the Western Canada Sedimentary Basin. A warm, continental climate must have prevailed during the Cretaceous: coal beds and dinosaur remains are found to the west. Thicker, more productive phosphate beds may occur basinward (to the southwest) in the subsurface.

Tertiary

Northern North America now stands relatively high compared to sea level and the few inland seas are arctic or subarctic. There appears to be little likelihood that substantial phosphate deposits formed during the Tertiary, when the climate, though warm (deciduous trees grew and coal formed on northern Ellesmere Island), was still temperate and continental. Only a few metres of Paleocene marine sediments are known in the Interior Plains (the Cannonball Sea), and up to 1800 m of clastic marine sediments on the Pacific Continental Shelf are interbedded with nonmarine sands and shales (Stott, 1970, p. 479). Up to 3000 m of sandstone, shale and coal of the early Cenozoic Eureka Sound Formation occur in scattered basins in the Arctic Islands. Both nonmarine and marine depositional environments are represented, but the general molassic character of the unit, together with its high latitude, precludes promise of significant phosphate deposits.

Miocene phosphorites occur along the east coast of the United States as far north as about latitude 35°, and some of these have been reworked in Holocene time. This continental shelf province could extend into offshore Nova Scotia (latitude 44°), but the probability of finding substantial deposits there seems slight.

Conclusions

Calculated paleopositions for Canada are approximate and the reliability for some data is low, as suggested by Irving (1979). In spite of these difficulties, it may be constructive to consider possibilities for phosphate deposition in the remote past in the light of calculated paleolatitudes.

Tentatively, it can be stated that:

1. Canada now occupies a tectonic and geographic position that is unfavourable for phosphate deposition. This position has prevailed since late Triassic or Jurassic time, although phosphatic beds of these and younger ages are known in the country.

2. Canada lay periodically in the 'phosphate zone' (with Canada's approximate centre between 30°N and 30°S latitudes) between late Hadrynian and Triassic time (Fig. 28.1). If other factors also were favourable to phosphate deposition then rocks of these ages should be targets for a phosphate search.
3. Hadrynian to Triassic rocks are widespread in Canada and, given that phosphorites are easily overlooked or misidentified, it seems possible that substantial phosphate deposits remain to be discovered.

References

Aitken, J.D., Long, D.G.F., and Semikhatov, M.A.
1978a: Progress in Helikian stratigraphy, Mackenzie Mountains; in Current Research, Part A, Geological Survey of Canada, Paper 78-1A, p. 481-484.

1978: Correlation of Helikian strata, Mackenzie Mountains - Brock Inlier -Victoria Island; in Current Research, Part A, Geological Survey of Canada, Paper 78-1A, p. 485-488.

Bender, M.L.
1972: Carbon isotope fractionation; in R.W. Fairbridge, ed; Encyclopedia of Geochemistry and Environmental Sciences; Van Nostrand Reinhold, p. 133-126.

Blackadar, R.G.
1970: Precambrian geology northwestern Baffin Island, District of Franklin; Geological Survey of Canada, Bulletin 191.

British Sulphur Corporation
1971: World Survey of Phosphate Deposits, 3rd edition; British Sulphur Corporation, London.

Cannon, W.F. and Klasner, J.S.
1976: Phosphorite and other apatite-bearing sedimentary rocks in the Precambrian of northern Michigan; United States Geological Survey, Circular 746.

Chandler, F.W.
1980: Proterozoic redbed sequences of Canada; Geological Survey of Canada, Bulletin 311.

Christie, R.L.
1962a: Geology, Alexandra Fiord, Ellesmere Island, District of Franklin (map with marginal notes); Geological Survey of Canada, Map 9-1962.

1962b: Geology, southeast Ellesmere Island, District of Franklin (map with marginal notes); Geological Survey of Canada, Map 12-1962.

1972: Central Stable Region; in The Canadian Arctic Islands and the Mackenzie Region; Guidebook for Field Excursion A-66, 24th International Geological Congress, Montreal, 1972; p. 40-87.

1979: Phosphorite in sedimentary basins of western Canada; in Current Research, Part B, Geological Survey of Canada, Paper 79-1B, p. 253-258.

Cloud, P.
1974: Development of atmosphere; in Encyclopedia Britannica, 15th edition, Warren E. Preece, general ed., Helen Hemingway Benton, publ., Macropaedia, v. 2, p. 313-319.

Cook, P.J.
1976: Sedimentary phosphate deposits; in Handbook of Strata-bound and Strataform Ore Deposits, K.H. Wolf, ed., Elsevier, Amsterdam, v. 7, p. 505-535.

Cook, P.J. and McElhinny, M.W.
1979: A reevaluation of the spatial and temporal distribution of sedimentary phosphate deposits in the light of plate tectonics; Economic Geology, v. 74, p. 315-330.

Dawes, P.R.
1976: Precambrian to Tertiary of northern Greenland; in Geology of Greenland, A. Escher and W.S. Watt, ed.; Geological Survey of Greenland, Copenhagen, p. 249-303.

de Schmid, H.S.
1916: Investigation of a reported discovery of phosphate in Alberta; Mines Branch, Department of Mines, Canada, Bulletin 12.

Frisch, T., Morgan, W.C., and Dunning, G.R.
1978: Reconnaissance geology of the Precambrian Shield on Ellesmere and Coburg Islands, Canadian Arctic Archipelago; in Current Research, Part A, Geological Survey of Canada, Paper 78-1A, p. 135-138.

Geldsetzer, H.
1973: The tectono-sedimentary development of an algal-dominated Helikian succession on northern Baffin Island, N.W.T.; in Canadian Arctic Geology, J.D. Aitken and D.J. Glass, ed.; Proceedings of the Symposium on the Geology of the Canadian Arctic, Saskatoon, May, 1973; Geological Association of Canada, Canadian Society of Petroleum Geologists, p. 99-126.

Gibson, D.W.
1975: Triassic rocks of the Rocky Mountain Foothills and Front Ranges of northeastern British Columbia and west-central Alberta; Geological Survey of Canada, Bulletin 247.

Greiner, H.R.
1962: Facies and sedimentary environment of Albert shale, New Brunswick; American Association of Petroleum Geologists, Bulletin, v. 46, p. 219-234.

Gross, G.A.
1965: Geology of iron deposits in Canada: Vol. I, General geology and evaluation of iron deposits; Geological Survey of Canada, Economic Geology Report No. 22, vol. I.

Gulbrandsen, R.A.
1966: Precambrian phosphate in the Belt Series in Montana; U.S. Geological Survey, Professional Paper 550-D, p. D199-D202.

Hale, L.A.
1967: Phosphate exploration using gamma-radiation logs, Dry Valley, Idaho; in Anatomy of the western phosphate field, L.A. Hale, ed., Intermountain Association of Geologists, 15th Field Conference, Salt Lake City, p. 147-159.

Irving, E.
1979: Paleopoles and paleolatitudes of North America and speculations about displaced terrains; Canadian Journal of Earth Sciences, v. 16, p. 669-694.

Jackson, D.E.
1975: A tropical Ordovician graptolite fauna from near the North Pole; in Report of Activities, Part B, Geological Survey of Canada, Paper 75-1B, p. 233-235.

Jackson, G.D., Ianelli, T.R., Narbonne, G.M., and Wallace, P.J.
1978: Upper Proterozoic sedimentary and volcanic rocks of northwestern Baffin Island; Geological Survey of Canada, Paper 78-14.

Kerr, J.Wm.
1967: Stratigraphy of central and eastern Ellesmere Island, Arctic Canada, Part I, Proterozoic and Cambrian; Geological Survey of Canada, Paper 67-27, Part I.

Kolodny, Y.
1979: Origin of phosphorites in light of recent studies of modern deposits; in Report on the Marine Phosphatic Sediments Workshop, Honolulu, February, 1979, East-West Center, Hawaii, p. 7, 8.

Matthew, G.F.
1893: On phosphate nodules from the Cambrian of southern New Brunswick; New York Academy of Science, Translation, v. XII, p. 108.

McElhinny, M.W.
1973: Palaeomagnetism and Plate Tectonics; Cambridge University Press.

McKelvey, V.E.
1963: Successful new techniques in prospecting for phosphate deposits: Science, Technology, and Development; U.S. papers prepared for the United Nations Conference on the application of science and technology for the benefit of the less developed areas, v. II, p. 163-172.

Riggs, S.R.
1979: Phosphorite sedimentation in Florida - a model phosphogenic system; Economic Geology, V. 74, p. 285-314.

Sheldon, R.P.
1964a: Paleolatitudinal and paleogeographic distribution of phosphorite; United States Geological Survey, Professional Paper 501-C, p. 106-113.

1964b: Exploration for phosphorite in Turkey - a case history; Economic Geology, v. 59, p. 1159-1175.

Sheldon, R.P., Maugham, E.K., and Cressman, E.R.
1967: Sedimentation of rocks of Leonard (Permian) age in Wyoming and adjacent states; in Anatomy of the Western Phosphate Field, L.A. Hale, ed.; Intermountain Association of Geologists, 15th Field Conference, Salt Lake City, Idaho, p. 1-13.

Skevington, D.
1974: Controls influencing the composition and distribution of Ordovician graptolite faunal provinces; in Graptolite Studies in Honour of O.M.B. Bulman, Palaeontological Association, London, Special Papers in Palaeontology, no. 13, p. 59-73.

Smith, A.G., Briden, J.C., and Drewry, G.E.
1973: Phanerozoic world maps; in Organisms and Continents through Time, N.F. Hughes, ed., The Paleontological Association, London, Special Papers in Palaeontology, no. 12, p. 1-42.

Spence, H.S.
1920: Phosphate in Canada; Mines Branch, Department of Mines, Canada, Publication 396.

Stockwell, C.H., McGlynn, J.C., Emslie, R.F., Sanford, B.V., Norris, A.W., Donaldson, J.A., Fahrig, W.F., and Currie, K.L.
1970: Geology of the Canadian Shield, Chapter IV; in Geology and Economic Minerals of Canada, Geological Survey of Canada, Economic Geology Report no. 1, 5th ed., p. 44-150.

Stott, D.F.
1970: Mesozoic; in Geology of Western Canada, by R.J.W. Douglas, H. Gabrielse, J.O. Wheeler, D.F. Stott, and H.R. Belyea; in Geology and Economic Minerals of Canada, Geological Survey of Canada, Economic Geology Report no. 1, 5th ed., Ch. VIII, p. 367-488.

Telfer, L.
1933: Phosphate in the Canadian Rockies; Canadian Institute of Mining and Metallurgy, Bulletin 260, p. 566-605.

Tozer, E.T.
1963: Northwestern Bjorne Peninsula; in Geology of the north-central part of the Arctic Archipelago, Northwest Territories (Operation Franklin), Geological Survey of Canada, Memoir 320, p. 363-370.

Tozer, E.T. and Thorsteinsson, R.
1964: Western Queen Elizabeth Islands, Arctic Archipelago; Geological Survey of Canada, Memoir 332.

Tremblay, L.P.
1978: Uranium subprovinces and types of uranium deposits in the Precambrian rocks of Saskatchewan; in Current Research, Part A, Geological Survey of Canada, Paper 78-1A, p. 427-435.

Wang, F.F.H., and McKelvey, V.E.
1976: Marine mineral resources; in World Mineral Supplies, Assessment and Perspective, G.J.S. Govett and M.H. Govett, eds., Elsevier, Amsterdam.

Williams, H.
1979: Appalachian Orogen in Canada; Canadian Journal of Earth Sciences, v. 16, p. 729-807.

Young, F.G.
1977: The mid-Cretaceous flysch and phosphatic ironstone sequence, northern Richardson Mountains, Yukon Territory; in Report of Activities, Part C, Geological Survey of Canada, Paper 77-1C, p. 67-74.

29.

OXIDATION CHARACTERISTICS OF SOME SHEARED COAL SEAMS OF THE MIST MOUNTAIN FORMATION, SOUTHEASTERN CANADIAN CORDILLERA

Project 780005

R.M. Bustin[1]
Institute of Sedimentary and Petroleum Geology, Calgary

Bustin, R.M., Oxidation characteristics of some sheared coal seams of the Mist Mountain Formation, southeastern Canadian Cordillera; in Current Research, Part B, Geological Survey of Canada, Paper 80-1B, p. 249-254, 1980.

Abstract

Tectonically deformed coal seams of the Mist Mountain Formation at Tent Mountain in the southeastern Canadian Cordillera are locally oxidized, even far from present weathering horizons. Oxidation, promoted by the fine grain size of the sheared coal, has resulted in a loss of coking power, a decrease in vitrinite reflectance, an increase in oxygen and decrease in carbon sulphur and hydrogen. Infrared spectroscopic analysis suggests a progressive decrease in alkanes and an increase in oxidation and aromaticity of the coal with increased weathering. Petrographically, the oxidized coal is characterized by the development of dark rinds and micropores and microfissures on vitrinite. The inertinite macerals show evidence of oxidation only in pervasively weathered coals. The oxidation tracks of the analyzed samples are nearly linear when plotted on a ternary C-H-O diagram, but they are oblique to those previously reported. Both the use of oxidation tracks and selective measurement of vitrinite reflectance may prove useful in predicting fresh coal characteristics from analysis of weathered samples, particularly when characteristic oxidation tracks and trends in vitrinite reflectance are established within the area of investigation.

Introduction

In the southeastern Canadian Cordillera, coal seams of the Mist Mountain Formation (formerly the Coal Bearing Member of the Kootenay Group; Gibson, 1979) were in part sheared and comminuted during Late Cretaceous and Tertiary tectonism. In many areas of active coal mining and exploration the sheared coal seams are extensively oxidized even when far from the present day weathering (soil) horizon. Oxidation of coal in such deposits is the result of the fine granular character of the tectonically sheared coal together with faults and fractures in the coal and adjacent strata, which have facilitated deep weathering accompanied by penetration of atmospheric oxygen and circulation of oxygenated waters (Bustin, 1979).

Oxidation markedly alters the physical and chemical characteristics of coal, resulting in poor flotation properties and lower than normal coking and calorific values (van Krevelan and Schuyer, 1957; Berkowitz, 1979; Crelling et al., 1979). Recognition and prediction of the distribution of even incipiently oxidized coal is therefore important during exploration and exploitation of coal deposits.

This paper documents some of the chemical and petrographic characteristics of oxidized coals from tectonically sheared coal deposits at Tent Mountain, and the depth of oxidation from present weathering horizons, and suggests methods of recognition of oxidized coal and prediction of fresh coal composition from oxidized coal samples.

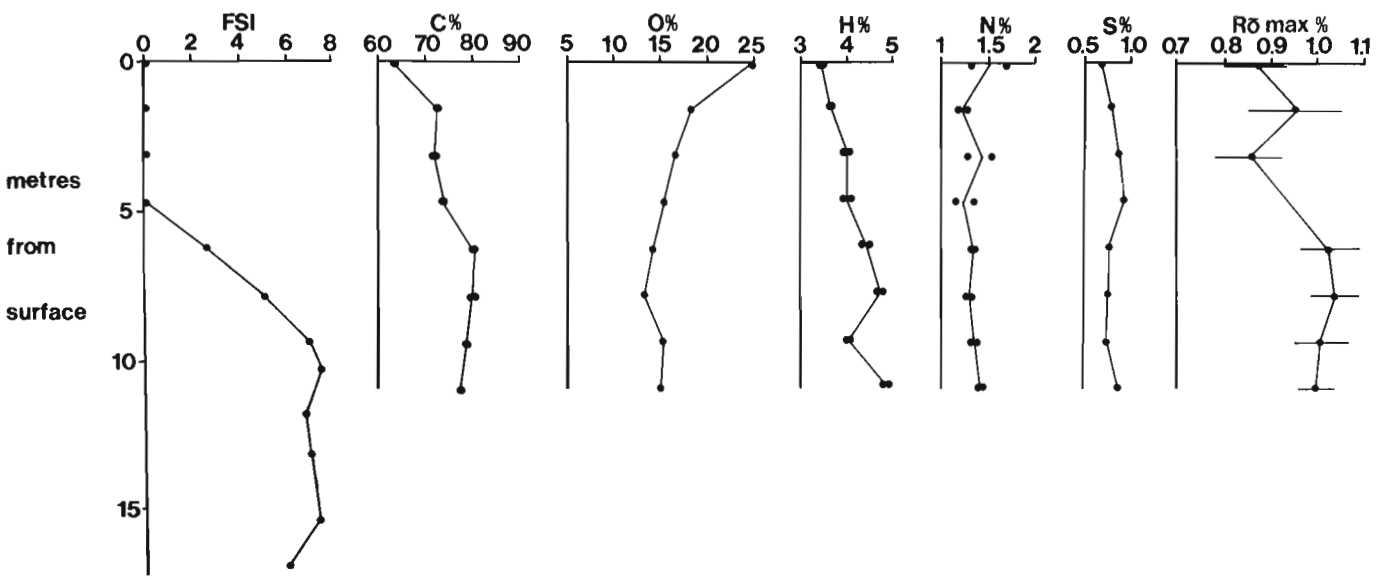

Figure 29.1. *No. 6 seam adit. Variation in Free Swelling Index (FSI), elemental analysis (dmmf), and vitrinite reflectance with increasing distance from the modern weathering surface. Oxygen determined by difference. Replicate analyses are shown for carbon, hydrogen and nitrogen. The mean (•) and standard deviation (⌙) of the maximum reflectance values are shown.*

[1]Department of Geological Sciences, The University of British Columbia, Vancouver, B.C., V6T 2B4

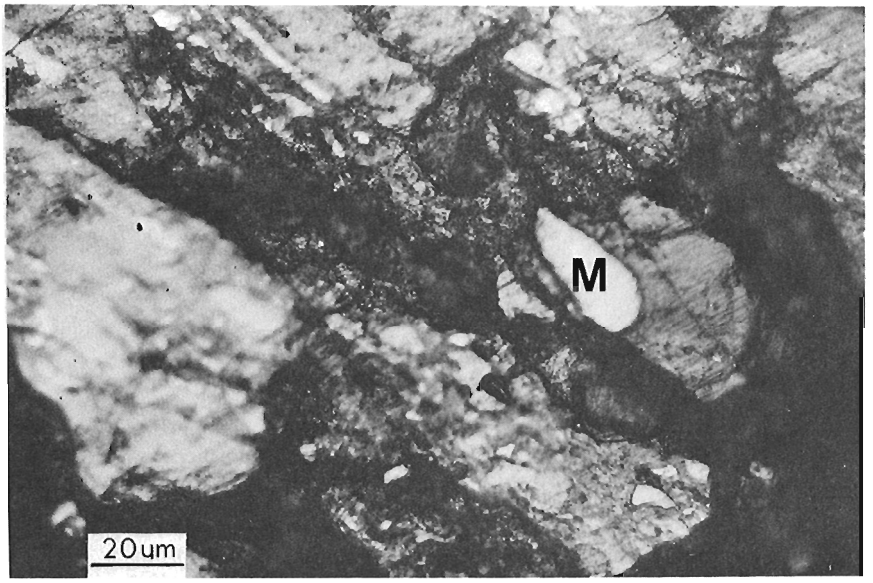

Figure 29.2

Photomicrograph of highly weathered vitrinite showing the development of microfractures and micropores. The more highly reflecting macrinite (M) shows little evidence of oxidation.

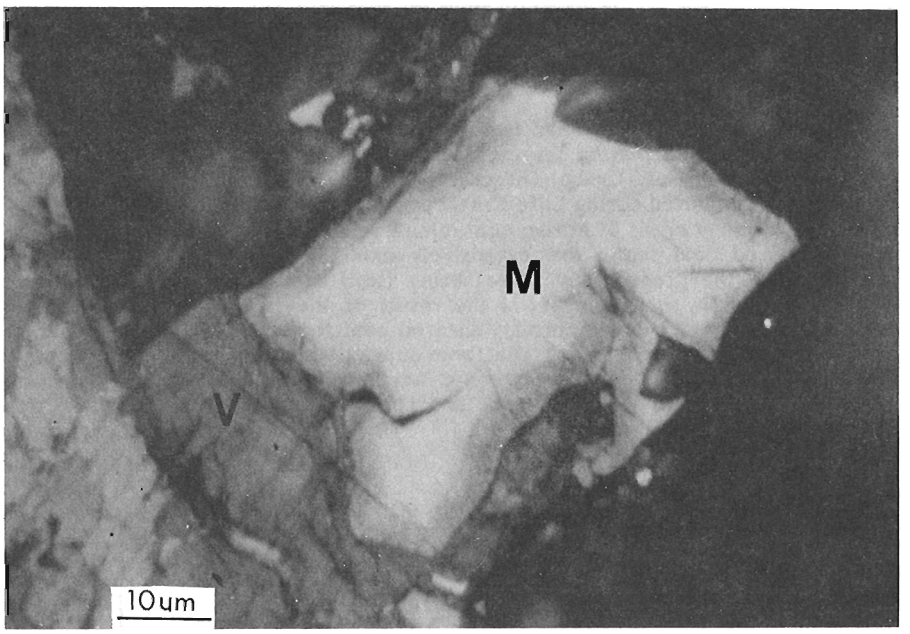

Figure 29.3

Photomicrograph of highly weathered coal particles. In this sample the vitrinite (V) is pervasively oxidized, and dark oxidation rinds are developed along the periphery and fractures of the macrinite (M).

Previous studies of oxidized coal of the Mist Mountain Formation include the studies of Wachowska et al. (1974) and Nandi et al. (1976) on the properties of laboratory oxidized coals of the Balmer Seam and the studies of Pearson and Kwong (1979) on the low temperature ash and associated properties of naturally oxidized coal seams of the Crowsnest Coalfield. Van Kreevlan and Schuyer (1957), Berkowitz (1979) and Crelling et al. (1979) have summarized many of the characteristics and properties of naturally and artificially oxidized coal.

Methods

Samples of weathered coal were collected from roadcuts and trenches, and unweathered (fresh) coal was collected from adits at Tent Mountain, north of Corbin, British Columbia, on the British Columbia-Alberta border. The samples were collected from three different seams, locally referred to as the No. 2, No. 4, and No. 6. One adit, driven along the footwall of the No. 6 seam, was sampled in greater detail for more comprehensive analysis. The roadcut, trench, and No. 6 seam adit samples were collected incrementally away from the present weathering horizon to establish variation in coal properties with different degrees of weathering. All the samples were collected from seams which were, at least in part, tectonically sheared.

The samples were examined microscopically using a reflecting light microscope. Mean maximum vitrinite reflectance was determined by measurement of 50 grains per sample, using established techniques (I.C.C.P., 1971). The ash was separated from all samples by using heavy liquid separation techniques and from some samples using a low temperature (plasma) furnace. The ash mineralogy was determined by X-ray diffractometry. Infrared spectroscopy of the No. 6 seam adit samples was determined using a double-beam grating infrared spectrophotometer and with pellets prepared using a mixture of 1.5 mg coal per 300 mg of KBr.

Results

General Characteristics

Near the present weathering horizon the coal is finely granulated and commonly permeated by roots of pine, spruce, or shrubs. Between 20 and 50 cm below the weathering horizon the size-consist of the coal coarsens and progressively grades to blocky coal at depths of 1 m. The tectonically sheared coal is either completely comminuted, consisting entirely of fragments less than 5 to 10 mm, or consists of a bimodal distribution of blocky fragments of coal up to 7 cm^3 and finely comminuted coal along shear zones.

The samples selected for analysis varied from pervasively weathered non-caking coals near the weathering horizon to normal (unweathered) coal with free-swelling indexes (FSI) between 4 and 8. All roadcut and trench samples were non-caking down to depths sampled, whereas the fresh adit samples had FSI's of 4 to 6, depending on the particular seam and local ash content. The No. 6 seam adit samples varied systematically from non-caking coal adjacent to the weathering horizon to an FSI of 8 at a distance of 10 m (Fig. 29.1). Beyond 10 m the FSI vaired between 6 and 8.

Petrography

Petrographic studies of the weathered coal revealed a characteristic microstructure consisting of a granular mosaic of micropores, and microfissures (Fig. 29.2) similar to those reported from experimentally and naturally weathered coals by Chandra (1962, 1975), Crelling et al. (1979), and others. Vitrinite shows evidence of weathering in almost all samples examined; in only slightly weathered coal (as between 5 and 10 m in Fig. 29.1), evidence of weathering is restricted to the periphery of the coal fragments and along fractures, whereas fresh surfaces showed no signs of weathering. The coarser blocky coal from areas of shearing similarly show no evidence of weathering; however, oxidation is commonly pronounced in the finely comminuted coal along the shear planes. In the more highly weathered coals the oxidation rinds have progressed throughout the grains, resulting in a darkish tint and high relief. The inertinite macerals show little evidence of oxidation with the exception of pervasively weathered coals proximal to weathering horizons, where distinct oxidation rinds are developed (Fig. 29.3). Under oil immersion, the oxidation rinds observed in this study have high relief and are darker than the internal portion of the particle, similar to naturally oxidized coals depicted by Crelling et al. (1979), but unlike the brighter oxidation rims observed in coals oxidized at elevated temperatures by Chandra (1975), Nandi et al. (1976), and others.

Vitrinite Reflectance

The mean maximum vitrinite reflectance (R_o max) of the No. 6 seam adit samples are shown in Figure 29.1, and roadcut and trench samples in Figures 29.4 and 29.5. In almost all the studied profiles R_o max decreases with proximity to the weathering horizon. The decrease in R_o max ranges from as much as 0.20% in profile F of Figure 29.4 to less than 0.05% in profile D of Figure 29.4. In some profiles (Fig. 29.4-E, Fig. 29.5) the variation in reflectance is not entirely consistent with proximity to the weathering horizon; however, the overall trend is to lower reflectances. The R_o max of individual grains of vitrinite in a particular sample was found to be inversely proportional to grain size. This relationship is demonstrated from analysis of two samples (Fig. 29.4-B at 2 m and Fig. 29.5 at 0.8 m), both of which were split into less than and greater than 1 mm fractions prior to analysis. The less than 1 mm fraction in both samples has a R_o max lower by 0.05% than the coarser fraction. Similarly large fragments of coal collected from highly weathered zones which were crushed prior to analysis had a correspondingly higher reflectivity than the associated finer grained coal.

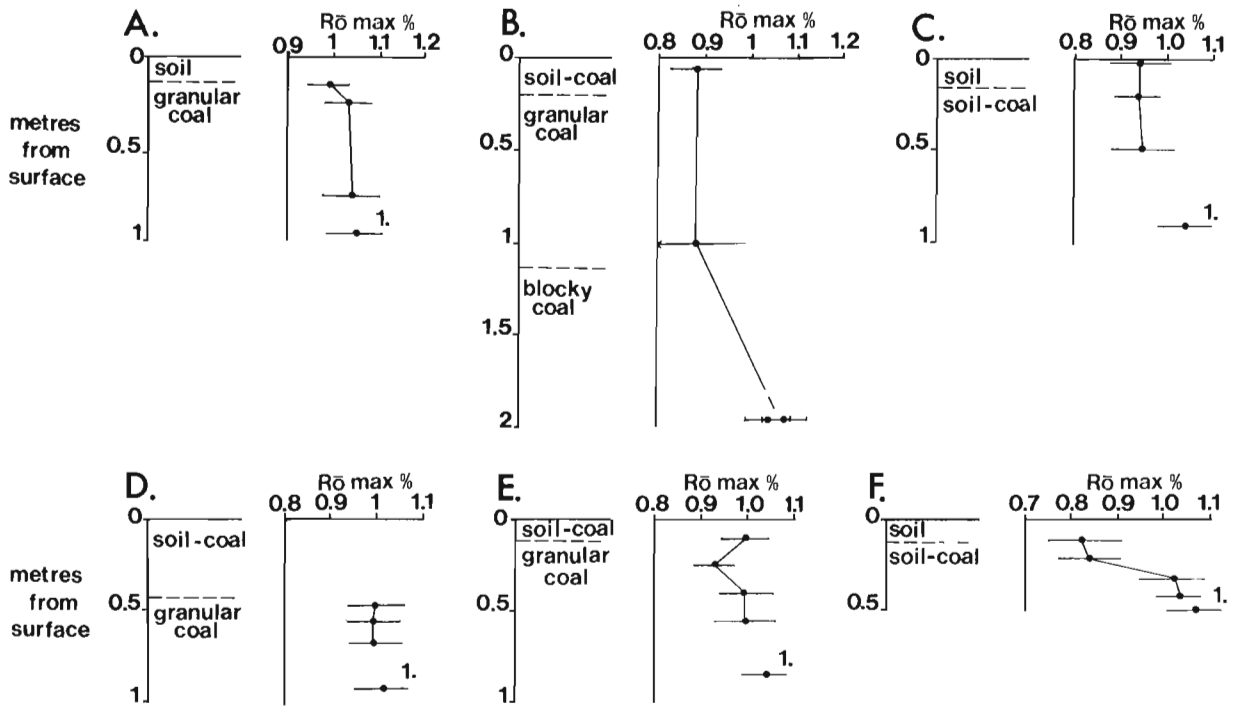

Figure 29.4. *Variation in vitrinite reflectance with distance from the modern weathering surface of roadcut and trench samples of No. 4 and No. 2 seams from various locations at Tent Mountain. The mean (•) and standard deviation (⊢⊣) of the maximum reflectance values are shown. Samples denoted by 1 are of fresh (normal) coal from adits.*

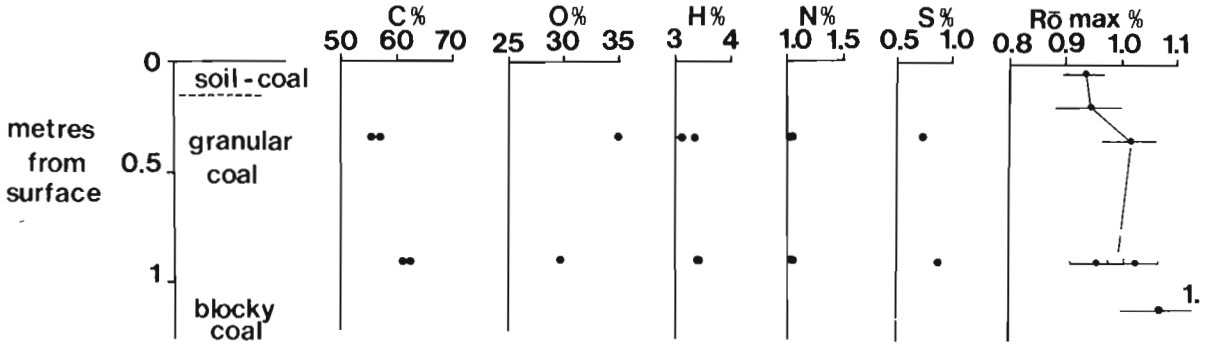

Figure 29.5. No. 4 seam roadcut profile. Variations in elemental composition (dmmf) and vitrinite reflectance with increasing distance from the modern weathering surface. Oxygen determined by difference. Replicate analyses are shown for carbon, hydrogen and nitrogen. The mean (•) and standard deviation (⊢⊣) of the maximum reflectance values are shown. Sample denoted by 1. is a fresh (normal) coal.

Chemistry

Ultimate analysis of two trench samples from No. 4 seam at Tent Mountain are shown in Figure 29.5 and for the No. 6 seam adit samples in Figure 29.1. In all of the analyzed samples an excellent correlation exists between the elemental analysis, degree of weathering as determined by FSI, and proximity to the weathering horizon. There is a consistent decrease in carbon and hydrogen, and a corresponding increase in oxygen. Sulphur and nitrogen content appear, from the analyzed samples, to be variable.

The infrared spectra of the No. 6 seam adit samples (Fig. 29.6) also show a progressive change with increasing proximity to the weathering horizon. The spectra, which were obtained from samples of vitrain-rich coal, were collected from the same stratigraphic horizon within the seam; the variation in the spectra is therefore principally the result of weathering, the only exception being the pronounced absorption near 1000 cm^{-1}, which is attributed to the presence of ash (Greenslade, 1975). In general, the absorption bands are broad; however, progressive changes are evident in the absorption bands in the regions of 2920 cm^{-1} to 2860 cm^{-1}, near 1700 cm^{-1} and 1600^{-1}. The absorption bands between 2920 cm^{-1} and 2860 cm^{-1} which is assigned to the alkanes (Baker, 1971) decreases with proximity to the weathering horizon, whereas the absorption band near 1700 cm^{-1} which is assigned to C=0 increases. The most pronounced change in absorption is the increase in the 1600 cm^{-1} band with increasing proximity to the weathering horizon. This absorption band in coal is generally attributed to aromatic C=C bonds, although some contribution to the absorption may result from oxygen-containing functional groups (Tschamler and De Ruiter, 1963; Greenslade, 1975).

The infrared spectra, considered in aggregate together with the ultimate analysis, indicates that there is a progressive decrease in the alkanes and an increase in oxidation and aromaticity with increasing weathering. Such results are similar to previous studies of coals oxidized at elevated temperatures, in which it was found that the relative aromaticity increases with oxidation, and which further suggests that the nonaromatic portion is more susceptible to attack and breakdown through oxidation (van Krevelen and Schuyer, 1957).

Ash Mineralogy

The ash mineralogy of the oxidized samples as determined by X-ray diffraction consists predominantly of quartz and kaolinite, with minor amounts of poorly-ordered illite. Bassinite ($CaSO_4 \cdot 1/2H_2O$) was found in the ash of oxidized coal samples of the No. 6 seam adit samples, which were separated using a low temperature (plasma) asher, but not present in ash separates prepared by heavy liquid separation. Such results concur with earlier studies of Pearson and Kwong (1979), who demonstrated the ubiquitous

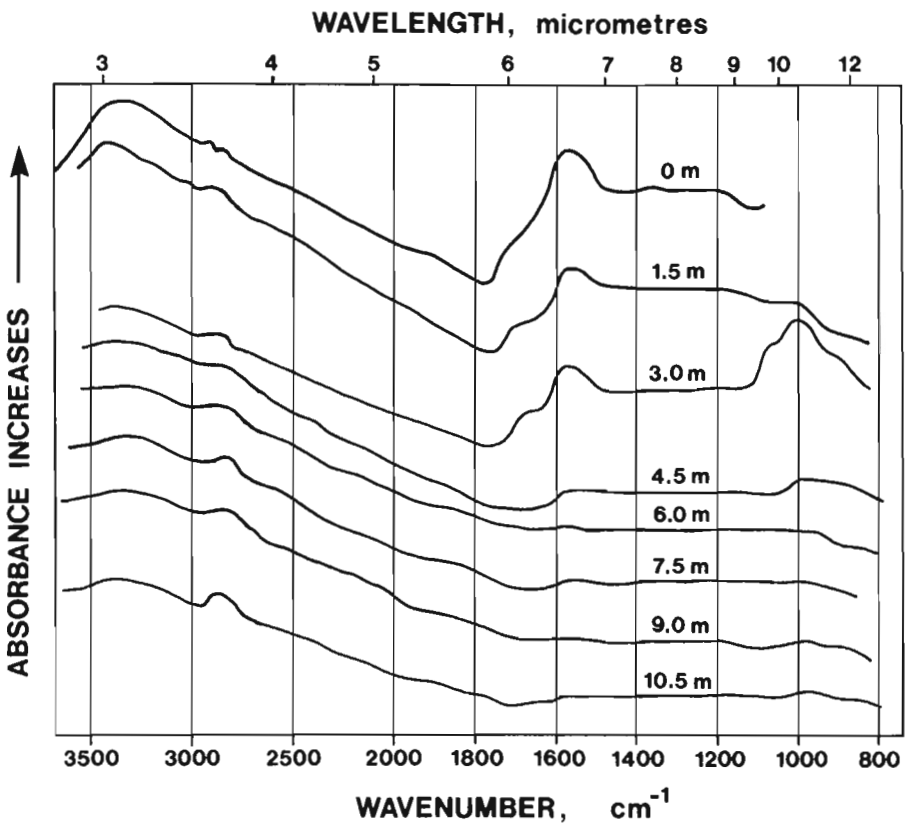

Figure 29.6. Infrared spectrum of the No. 6 seam adit examples shown in Figure 29.1. Refer to text for explanation.

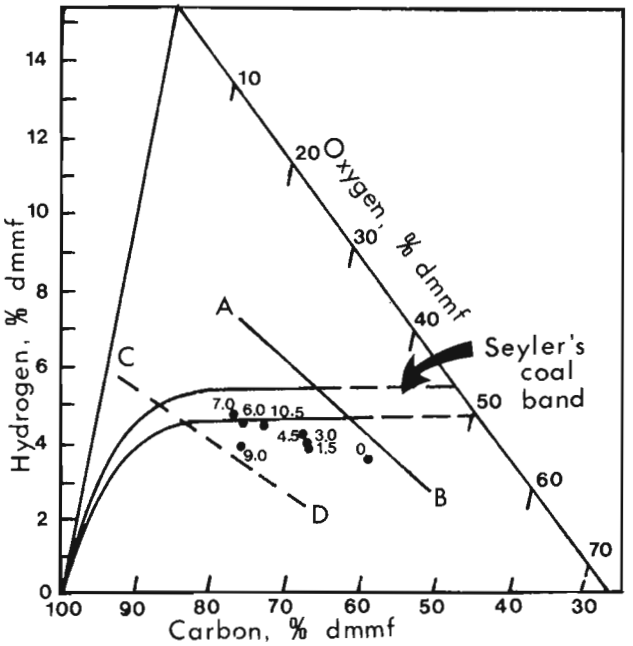

Figure 29.7. *C-H-O diagram showing the shifts in elemental composition of coal with progressive oxidation. Lines A-B and C-D are typical oxidation tracks of pure hydrocarbons (modified from Francis, 1961). Normal coal samples are expected to plot within Seyler's band of 'normal coal' and progressively shift, with oxidation, along tracks parallel to that of pure hydrocarbons and towards oxygen as shown by Francis (1961). Plotted are the No. 6 adit samples (•); the adjacent numbers indicate distance, in meters, from the modern weathering surface.*

occurrence of bassinite in oxidized samples of the Balmer Seam of the Mist Mountain Formation in the Crowsnest Coalfield. The absence of bassinite in ash separates prepared by heavy liquid separation further substantiates the suggestion by Miller et al. (1979) that bassinite forms during the plasma ashing process, although apparently its formation is restricted to the ash of oxidized coal.

Discussion and Conclusions

The results of this study generally concur with previous studies of naturally oxidized coal. Oxidation can be readily recognized and characterized from both chemical and physical characteristics of the coal. The presence of bassinite in ash separates prepared by low temperature (plasma) ashing also indirectly attests to oxidation of the coal. The petrography of the oxidized coal is distinct; even incipient oxidation can be recognized, particularly in the fine fraction of the sheared coals by the presence of microfissures, micropores, and oxidation rinds. The inertinite macerals petrographically appear much more resistant to oxidation, although they too are oxidized in highly weathered coals. In this study, FSI was found to be a more sensitive indicator of oxidation than reflectance, as previously concluded by Pearson and Kwong (1979). However, reflectance appears to be more responsive than reported by them, showing variations of up to 0.2% R_o max. The inverse relationship observed between reflectance and grain size is considered the result of the progressive centripetal oxidation of the coal particles; viz., the central portion of larger grains are less oxidized than the central portion of smaller grains. In less extensively weathered and sheared coals, evidence of oxidation is restricted to the fine fraction or along fractures in the coarser coal fragments. In the No. 6 seam, which is partly sheared partly sheared, the maximum depth of oxidation is about 9 m. It is unlikely, however, that any absolute depth of oxidation exists which can be extrapolated to adjacent areas; the susceptibility of coal to oxidation varies with rank and maceral content (Berkowitz, 1979) and such factors as topography, climate (Leythaeuser, 1973), and particularly, as found in this study, with particle size of the coal.

Predicting Fresh Coal Composition

In areas where fresh, unoxidized coal is not readily available for analysis, it may be desirable to predict the fresh coal composition. Methods for estimating fresh coal composition from oxidized samples have been proposed by Francis (1961) and Berkowitz (1979), based on the predictability of elemental shifts in oxygen, carbon, and hydrogen during oxidation. Naturally and artificially oxidized coal and pure hydrocarbons were shown by Francis (1961) to progressively change composition along predictable trends when plotted on a ternary diagram with oxygen, carbon and hydrogen as end members. Berkowitz (1979) has suggested that fresh coal composition can be estimated by plotting the composition of analyzed oxidized samples on such a diagram and extrapolating a line parallel to established oxidation tracks, back to the coal band of Seyler (Fig. 29.7).

In Figure 29.7 the analyzed samples from the No. 6 seam adit are plotted. With the exception of the sample at 9 m from the weathering horizon, the analyzed samples define a relatively straight oxidation track (Fig. 29.7). The oxidation track defined by the No. 6 seam adit samples is oblique to that reported by Francis (1961) but clearly demonstrates progressive change in chemistry with oxidation. Inasmuch as the extent of oxidation is at least in part a product of coal rank and the maceral composition, it is likely, and expected, that different coals will give different oxidation tracks. Nevertheless, such a method of predicting fresh coal composition from analysis of weathered samples could provide a good estimate of the fresh coal composition, particularly if the individual oxidation tracks of different seams are established in the area of investigation.

An additional method of estimating fresh coal composition from oxidized outcrop samples, based on measurement of vitrinite reflectance, has been proposed by Chandra (1958). In laboratory experiments, Chandra (1958) found essentially no change in reflectance of coals oxidized at temperatures of 110°C and 150°C and normal coals, which led him to suggest that it may be possible to predict fresh coal properties by measurement of vitrinite reflectance. The results of this study, however, show a notable reduction in reflectance with progressive natural oxidation. Because oxidation is centripetal and most pronounced in the finely sheared coal, closer approximations to fresh coal properties should be possible by selectively sampling larger coal fragments from oxidized zones and performing measurements only on fresh surfaces.

Acknowledgments

I thank Sally Finora of the Department of Mining Engineering, The University of British Columbia, for infrared spectroscopy and D.E. Pearson of the British Columbia Department of Energy, Mines and Petroleum Resources for use of equipment for reflectance measurements and for preparing the low temperature (plasma) ash separates. Coleman Collieries Ltd. provided access to adits on Tent Mountain and also some samples and analytical data. This research was supported in part by NSERC Operating Grant A-1107 to W.H. Mathews of the Department of Geological Sciences, The University of British Columbia. Alex Cameron and David Marchioni of the Geological Survey of Canada improved the manuscript with their critical comments.

References

Baker, B.R.
1971: Organic Chemistry; Wadsworth Publishing Co., Belmont, California, 506 p.

Berkowitz, N.
1979: An introduction to Coal Technology; Academic Press, New York, 345 p.

Bustin, R.M.
1979: Characterisitcs and mechanisms for the formation of structurally thickened coal deposits in the southeastern Canadian Cordillera; Ninth International Congress of Carboniferous Stratigraphy and Geology, Program with Abstracts, p. 27-28.

Chandra, D.
1958: Reflectance of oxidized coals; Economic Geology, v. 53, p. 102-208.

1962: Reflectance and microstructure of weathered coals; Fuel, 1962, v. 41, p. 185-293.

1975: Oxidized coals; in Stach, E., Mackowsky, M-Th., Teichmuller, M., Taylor, G.H., Chandra, D., and Teichmuller, R., Stach's Textbook of Coal Petrology; Gebruder Borntraeger, Berlin, p. 159-164.

Crelling, J.C., Schrader, R.H., and Benedict, L.G.
1979: Effects of weathered coal on coking properties and coke quality; Fuel, v. 58, p. 542-546.

Francis, W.
1961: Coal, its formation and composition; Edward Arnold Publishers Ltd., London, 806 p.

Gibson, D.W.
1979: The Morrissey and Mist Mountain Formations – newly defined lithostratigraphic unit of the Jura-Cretaceous Kootenay Group, Alberta and British Columbia; Bulletin of Canadian Petroleum Geology, v. 27, p. 183-208.

Greenslade, W.J.
1975: Surface studies on B.C. coals and their maceral constituents; unpublished M.Sc. thesis, The University of British Columbia, 28 p.

International Committee for Coal Petrology
1971: International handbook of coal petrography; supplement to the 2nd edition; Publications du Centre National de la Recherche Scientifique, Paris, France.

Krevelen, D.V. van and Schuyer, J.
1957: Coal Science; Elsevier Publishing Co., New York, 352 p.

Leythaeuser, D.
1973: Effects of weathering on organic matter in shales; Geochimica et Cosmochimica Acta, v. 37, p. 113-120.

Miller, R.N., Yarzab, R.F., and Given, P.H.
1979: Determination of the mineral-matter content of coals by low-temperature ashing; Fuel, v. 58, p. 4-10.

Nandi, B.N., Ciavaglia, L.A., and Montgomery, D.S.
1976: The variation of the microhardness and reflectance of coal under conditions of oxidation simulating weathering; Journal of Microscopy, v. 109, p. 93-103.

Nandi, B.N., Ghosh, A., and Ciavaglia, L.A.
1978: Anomalous microhardness impressions of some weathered coals; Fuel, v. 57, p. 317-319.

Pearson, D.E. and Kwong, J.
1979: Mineral matter as a measure of oxidation of a coking coal; Fuel, v. 58, p. 63-66.

Tschamler, H. and De Ruiter, E.
1963: Physical properties of coal; in Lowry. H.H., ed., Chemistry of Coal Utilization, Supplementary Volume; John Wiley and Sons, Inc., New York, p. 35-118.

Wachowska, H.M., Nandi, B.N., and Montgomery, D.S.
1974: Oxidation studies on coking coal related to weathering. 4. Oxygen linkages influencing dilatometric properties and the effect of cleavage of ether linkages; Fuel, v. 53, p. 212-219.

30. THE OCCURRENCE OF OSTRACODA WITH 'SOUTHERN' APPALACHIAN AFFINITIES IN THE LOWER DEVONIAN SHIPHEAD FORMATION, FORILLON PENINSULA, GASPÉ, QUÉBEC

Project 720072

M.J. Copeland and Pierre J. Lespérance[1]
Institute of Sedimentary and Petroleum Geology, Ottawa

Copeland, M.J. and Lespérance, Pierre J., The occurrence of Ostracoda with 'southern' Appalachian affinities in the Lower Devonian Shiphead Formation, Forillon Peninsula, Gaspé, Québec; in Current Research, Part B, Geological Survey of Canada, Paper 80-1B, p. 255-258, 1980.

Abstract

Ulsterian Ostracoda are highly endemic in the Appalachian Orogen. Based on distinctive taxa, they have been divided morphologically and paleogeographically into 'northern' beyrichiid-large palaeocopid and 'southern' bolliid-small palaeocopid-podocopid assemblages. This was interpreted as a result of paleogeographic endemism within the Appalachian Orogen during the Cayugan and Helderbergian but occurrences of the 'southern' assemblage in northeastern United States, New Brunswick and eastern Gaspé, Québec indicate that at that time water depth and substrate lithology were prime factors in the distribution of these facies controlled faunas.

Introduction

The Lower Devonian Upper Gaspé Limestone (Subgroup) exposed on Forillon Peninsula, Gaspé, Québec comprises the lower Forillon, middle Shiphead and upper Indian Cove formations, in all about 500 m thick (Lespérance, in press). The Forillon and Indian Cove formations are monotonous sequences of siliceous limestone whereas the strata of the intervening Shiphead Formation are generally less siliceous, heterogeneous, and have a higher content of terrigenous material, especially in their upper part. This mudstone contains a sparse, low diversity faunal assemblage of brachiopods, molluscs, trilobites and ostracodes, that constitute a distinctive community. In particular, the ostracode fauna is remarkable because certain of its taxa have been recorded only from widely separated areas of eastern North America in argillaceous calcilutite of late Silurian and Early Devonian age. The ostracode fauna of this 'marlstone' lithology is characterized by diagnostic bolliid-palaeocopid and podocopid genera of the Healdiacea and Thlipsuracea (Lundin, 1971) whereas ostracodes of this age from more calcareous lithologies are predominantly palaeocopid genera of the Beyrichiacea (Copeland and Berdan, 1977).

The 'marlstone' facies ostracode fauna that occurs at intervals throughout Upper Silurian and Lower Devonian rocks of the Appalachian Orogen has been described by Roth (1929), Coryell and Cuskley (1934) and Lundin (1968) from the Haragan Formation of Oklahoma, by Wilson (1935) from the Birdsong Shale of Tennessee, by Bassler (1941) and Swain (1953) from the Camden Chert of Tennessee, by Lundin and Petersen (1974) from the Rockhouse Formation of Tennessee, by Ulrich and Bassler (1913) from the Shriver Chert (therein termed the Oriskany Formation) of Maryland, by Swartz (1932, 1936) from the Shriver Chert of Pennsylvania, by Berdan (undescribed; personal communication) from the Kalkberg to Glenerie formations of New York and by Copeland (1962) from the Dalhousie beds of northern New Brunswick. The present occurrence of this fauna in the upper part of the Shiphead Formation extends its geographic limits some 300 km farther northeast to the extreme eastern part of Gaspé Peninsula, Québec.

Because this distinctive bolliid-podocopid ostracode assemblage is presently recorded only sporadically throughout Lower Devonian strata of the Appalachian Orogen, the ostracode fauna of the upper Shiphead Formation can only be

Table 30.1

Occurrence of Ostracoda in three collections of the upper Shiphead Formation, Forillon Peninsula, Gaspé, Québec

Ostracode species	Previous occurrence	Cap Gaspé (73F7)	Anse-aux-Sauvages (73F29A)	(73F28)
Palaeocopida				
Kloedeniopsis sp.*		X	X	X
Bollia sagittaformis Swartz, 1932	Shriver		X	
Bollia ungula Jones, 1889	Shriver		X	X
Bollia sp. cf. **B. zygocornis** Swartz, 1936	Shriver		X	
Podocopida				
Ranapeltis typicalis Bassler, 1941	Camden			X
Thlipsorothella cooperi (Bassler), 1941	Camden	X		
Strepulites bispinosus (Bassler), 1941	Camden		X	

*This species will be described later.

[1] Departement de Géologie, Université de Montréal, Montréal, Québec.

dated generically as Early Devonian of mid-Helderbergian to early Onesquethaw age and most similar specifically to forms from the Shriver Chert (mid Deerparkian) of Pennsylvania and Camden Chert (early Onesquethaw) of Tennessee. Based on its megafauna, however (Lespérance, in press), correlation of the upper Shiphead Formation with the Shriver Chert appears more plausible as both are contained within the Deerparkian **Rensselaeria** "zone" whereas the megafauna of the Camden Chert lies within the younger **Etymothyris** "zone" of Onesquethaw age.

Occurrence of the Shiphead Formation Ostracoda

Three collections of ostracodes are reported here. All were obtained by Lespérance in 1973 from mudstone and very fine grained argillaceous sandstone beds of the upper Shiphead Formation. One (73F7) occurs at Cap Gaspé, 28.5-29.2 m below the contact with the Indian Cove Formation; two are from the brook entering Anse-aux-Sauvages (Indian Cove) 3000 m northwest of Cap Gaspé near the shore of Baie de Gaspé. The Anse-aux-Sauvages brook occurrences are 15.5 m (73F29A) and 40.5 m (73F28) west-northwest of the highway to Cap Gaspé, 3 m and 6 m respectively below the contact with the Indian Cove Formation. Most of the specimens from the Anse-aux-Sauvages collections are preserved in sandstone as casts and molds. The beyrichiid ostracode specimens from Cap Gaspé occur in silty limestone; their shells are usually fractured and readily spall off leaving well preserved steinkerns of disarticulated valves. Only a specimen of **Thlipsorothella cooperi** (Bassler) is preserved as a carapace.

Paleogeographic Considerations

Lundin (1971, p. 865) sought to explain the apparent endemism of distinct 'southern' bolliid-podocopid (Bolliidae-Healdiacea-Thlipsuracea) and 'northern' palaeocopid (Beyrichiacea-Kloedenellacea) faunas within the Appalachian Orogen by paleogeographic separation and possibly by ecological barriers such as temperature and salinity. Even with the complex picture of large scale polar wandering through 15° of latitude (1500 km) between the Late Silurian and Early Devonian (Kent and Opdyke, 1978) no appreciable climatic change should be expected. Also, the appearance of the 'southern' fauna throughout the Appalachian Orogen from Oklahoma to Québec would dictate against permanent paleogeographic separation of the faunas during the Early Devonian.

These 'southern' and 'northern' Appalachian ostracode assemblages may be more readily explained by other means. Berdan (1964, p. B16), from studies in east-central New York, observed that a closely related beyrichiacean assemblage of large palaeocopid ostracodes predominated in that area throughout deposition of the early Helderbergian Manlius and Coeymans limestones. This shallow water 'northern' assemblage was replaced in the late Helderbergian and Deerparkian Kalkberg to Glenerie formations (Berdan, unpublished; personal communication) by an assemblage of small, deeper water bolliid-podocopid ostracodes in general generically similar to faunas from the southern Appalachian Haragan, Birdsong and Camden formations of Oklahoma and Tennessee. Fauna of these southern Appalachian strata developed directly from taxonomically similar older assemblages of the Late Silurian Henryhouse and Rockhouse formations of the same area, giving rise to the 'southern' Appalachian appellation used by Lundin and herein. All occurrences of this fauna in the southern Appalachians are in cherty or silty limestone and marlstone. These lithologies are the same as those containing the sporadic 'southern' ostracode fauna in the Shriver, Kalkberg to Glenerie (Berdan, personal communication), Dalhousie and Shiphead strata from West Virginia to Québec within the northern Appalachians.

PLATE 30.1 (GSC 202599-Z)

Figure 1. **Bollia sagittaformis** Swartz.
Impression of right valve, x 40, locality 73F29A, hypotype, GSC 64453.

Figure 2. **Strepulites bispinosus** (Bassler).
Rubber cast of impression of left valve, x 30, locality 73F29A, hypotype, GSC 64454.

Figure 3. **Bollia** sp. cf. **B. zygocornis** Swartz.
Left valve, x 40, locality 73F29A, hypotype, GSC 64455.

Figure 4. **Thlipsorothella cooperi** (Bassler).
Right view of carapace, x 30, locality 73F7, hypotype, GSC 64456.

Figure 5. **Bollia ungula** Jones.
Left valve, x 40, locality 73F29A, hypotype, GSC 64457.

Figure 6. **Bollia ungula** Jones.
Cast of left valve, x 40, locality 73F28, hypotype, GSC 64458.

Figure 7. **Ranapeltis typicalis** Bassler.
Right valve, x 40, locality 73F28, hypotype, GSC 64459.

Figure 8. **Bollia sagittaformis** Swartz.
Rubber cast of impression of right valve, x 40, locality 73F29A, hypotype, GSC 64460.

Figure 9. **Bollia ungula** Jones.
Left valve, x 40, locality 73F28, hypotype, GSC 64461.

Figures 10-19. **Kloedeniopsis** sp. (all specimens x10).

10. Left view of heteromorph, locality 73F29A, figured specimen, GSC 64462.
11. Right view of tecnomorph, locality 73F29A, figured specimen, GSC 64463.
12. Right view of tecnomorph, locality 73F29A, figured specimen, GSC 64464.
13. Right view of heteromorph, locality 73F29A, figured specimen, GSC 64465.
14. Left view of tecnomorph, locality 73F28, figured specimen, GSC 64466.
15. Right view of tecnomorph, locality 73F28, figured specimen, GSC 64467.
16. Right view of tecnomorph, locality 73F7, figured specimen, GSC 64468.
17. Left view of heteromorph, locality 73F7, figured specimen, GSC 64469.
18. Left view of tecnomorph, locality 73F28, figured specimen, GSC 64470.
19. Left view of tecnomorph, locality 73F7, figured specimen, GSC 64471.

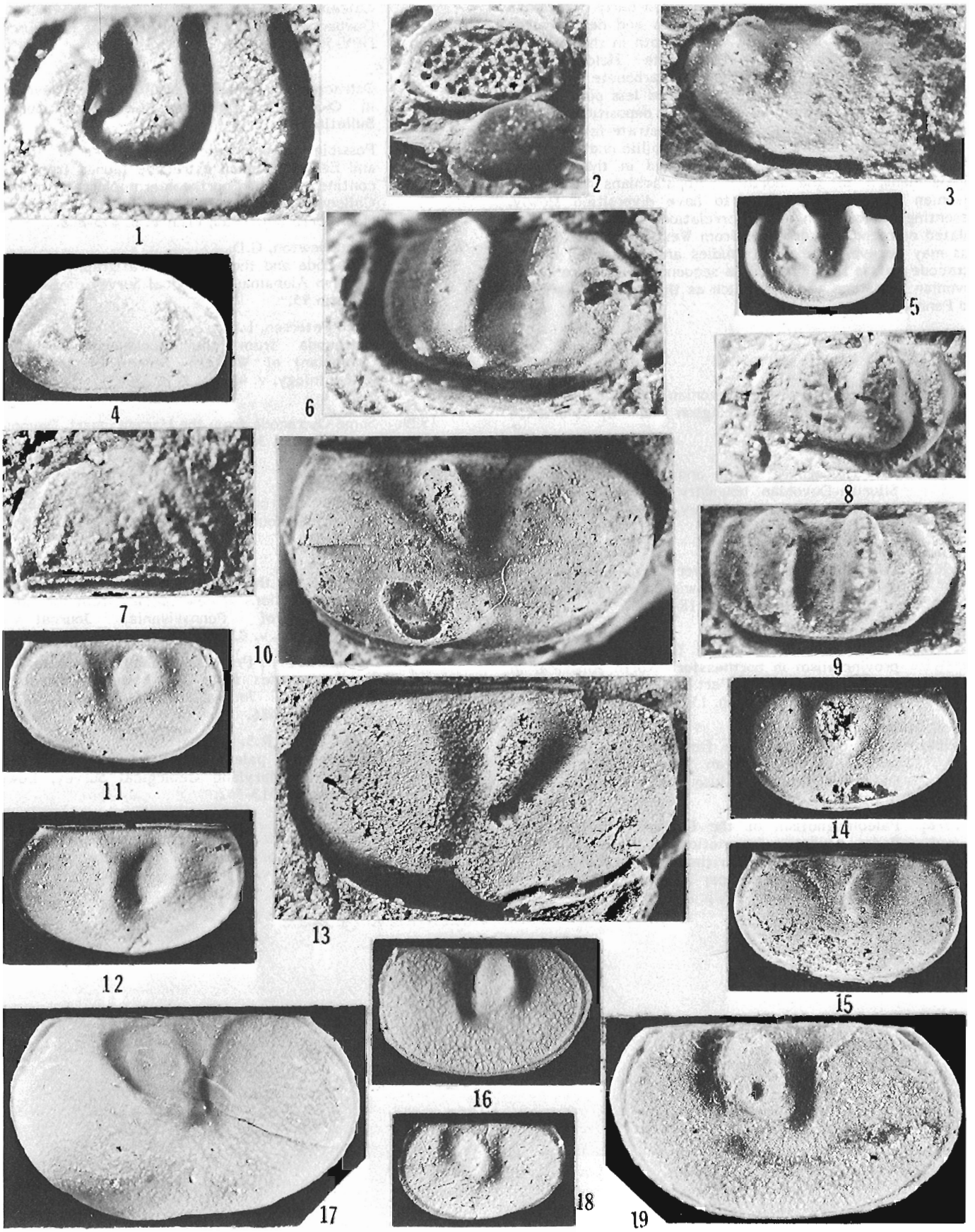
1
2
3
4
5
6
7
8
9
10
11
12
13
14
15
16
17
18
19

It seems more reasonable, therefore, to explain these 'southern' and 'northern' Late Silurian-Early Devonian ostracode faunas as controlled by facies and depth rather than by endemism. Increase in water depth in the northern Appalachian Orogen during the late Helderbergian-Deerparkian stages terminated the high carbonate deposition of the early Helderbergian and introduced less pure, cherty and argillaceous carbonate substrata deposition. The combination of deeper water and mud substrate favoured the migration of the possibly infaunal, small bolliid and podocopid ostracode fauna already well established in the southern Appalachians. In the northern Appalachians this Early Devonian assemblage appears to have diversified slowly, presenting difficulty in exact correlation among the various isolated ostracode occurrences from West Virginia to Gaspé. This may be overcome when studies are completed of the ostracode faunas from continuous sequences of impure Lower Devonian limestone and shale such as those from New York and Pennsylvania.

References

Bassler, R.S.
1941: Ostracoda from the Devonian (Onondaga) chert of west Tennessee; Washington Academy of Science Journal, v. 31, p. 21-27.

Berdan, J.M.
1964: The Helderberg Group and the position of the Silurian-Devonian boundary in North America; U.S. Geological Survey, Bulletin 1180-B, p. B-110B-19.

Copeland, M.J.
1962: Ostracoda from the Lower Devonian Dalhousie beds, northern New Brunswick; Geological Survey of Canada, Bulletin 91, p. 18-51.

Copeland, M.J. and Berdan, J.M.
1977: Silurian and Early Devonian ostracode provincialism in northeastern North America; in Report of Activities, Part B, Geological Survey of Canada, Paper 77-1B, p. 15-24.

Coryell, H.N. and Cuskley, V.A.
1934: Some new ostracodes from the "White Mound" section of the Haragan Shale, Murray County, Oklahoma; American Museum Novitates, no. 748.

Kent, D.V. and Opdyke, N.D.
1978: Paleomagnetism of the Devonian Catskill Red Beds: evidence for motion of the coastal New England-Canadian Maritime region relative to cratonic North America; Journal of Geophysical Research, v. 83, no. B9, p. 4441-4450.

Lespérance, P.J.
Calcaires Supérieurs de Gaspé; Province de Québec, Ministère de l'Energie et des Ressources, DPV-595. (in press)

Lundin, R.F.
1968: Ostracodes of the Haragan Formation (Devonian) in Oklahoma; Oklahoma Geological Survey, Bulletin 116.

1971: Possible paleoecological significance of Silurian and Early Devonian ostracode faunas from mid-continental and northeastern North America; Colloquium on the Paleoecology of Ostracodes, H.F. Oertli (ed.), Pau, France, p. 853-868.

Lundin, R.F. and Newton, G.D.
1970: Ostracoda and the Silurian stratigraphy of northwestern Alabama; Geological Survey of Alabama, Bulletin 95.

Lundin, R.F. and Petersen, L.E.
1974: Ostracoda from the Rockhouse Formation (Devonian) of Western Tennessee; Journal of Paleontology, v. 48, no. 2, p. 236-255.

Roth, R.
1929: Some Ostracoda from the Haragan marl, Devonian of Oklahoma; Journal of Paleontology, v. 3, no. 4, p. 327-372.

Swain, F.M.
1953: Ostracoda from the Camden Chert, western Tennessee; Journal of Paleontology, v. 27, no. 2, p. 257-284.

Swartz, F.M.
1932: Revision of the ostracode family Thlipsuridae, with descriptions of new species from the Lower Devonian of Pennsylvania; Journal of Paleontology, v. 6, no. 1, p. 36-58.

1936: Revision of the Primitiidae and Beyrichiidae, with new ostracodes from the Lower Devonian of Pennsylvania; Journal of Paleontology, v. 10, no. 7, p. 541-586.

Ulrich, E.O. and Bassler, R.S.
1913: Systematic paleontology, Lower Devonian Ostracoda; Maryland Geological Survey, Lower Devonian, p. 513-542.

Wilson, C.W.
1935: The ostracode fauna of the Birdsong Shale, Helderberg, of Western Tennessee; Journal of Paleontology, v. 9, no. 8, p. 629-646.

31. NONSORTED CIRCLES IN COHESIONLESS FINE SILTY SAND, NORTH-CENTRAL DISTRICT OF KEEWATIN

Project 730019

J.J. Veillette
Terrain Sciences Division

Veillette, J.J., Nonsorted circles in cohesionless fine silty sand, north-central District of Keewatin; in Current Research, Part B, Geological Survey of Canada, Paper 80-1B, p. 259-267, 1980.

Abstract

A site with 27 nonsorted circles in well sorted fine silty sand was investigated. The features have a late summer concave frost table, water available for ice lensing in the active layer, and a "loose" arrangement of soil particles (high void ratio, low total unit weight) compatible with disturbance by the annual freeze-thaw cycle. This suggests that the features result from heave (in winter) and subsidence (in summer) associated with ice lensing leading to the development of an upward cell circulation in the active layer similar to a model proposed for the growth and maintenance of hummocks in the western Arctic.

Surface and frost table topography and drainage conditions in and around the site are such that artesian or hydrostatic pressure cannot be generated where these nonsorted circles occur.

Similar grain-size distributions, void ratios, and total unit weights of undisturbed samples, obtained along a vertical axis within circles, indicate that diapiric expulsion of a lower layer of saturated mud at the surface through an upper carapace, by loading, such as occurs in some Keewatin mudboils, is not present.

Introduction

Recent studies (Shilts, 1973, 1974, 1978; Nicholson, 1976; Mackay and MacKay, 1976; Crampton, 1977; Egginton, 1978; Egginton and Shilts, 1978; MacKay, 1979) present field observations and measurements concerned primarily with the genesis of a type of patterned ground classified by Washburn (1973) as sorted and nonsorted circles. These features have been given a variety of names, derived from criteria as varied as inferred origin, association with perennial frost, and morphology; this has led to a confusing terminology discussed by Shilts (1978).

This paper describes nonsorted circles developed in well sorted, fine silty sand in north-central District of Keewatin, and discusses the models commonly invoked to explain their formation and that of related features. The term 'nonsorted circle' is retained to avoid addition to the already complex nomenclature. The following models are considered: (1) artesian and loading models proposed by Shilts (1974, 1978) to account for mudboils (sorted and nonsorted circles) in central and southern District of Keewatin and (2) an equilibrium model based on frost heave and subsidence proposed by Mackay (1979) for the growth and maintance of hummocks (nonsorted circles) on Garry Island, Northwest Territories, together with observations from Mackay and MacKay (1976). Models derived from cryostatic pressures are given less attention due to a lack of field studies in District of Keewatin based on this concept.

Sorted and nonsorted circles are widespread in the unconsolidated sediments of north-central District of Keewatin (Fig. 31.1) and are considered indicative of unstable soil conditions; mudboils largely on tills (diamicton) in central and southern Keewatin display such unstable conditions (Shilts, 1973, 1974, 1978). Mudboils commonly form a dense network (predominantly sorted circles) on till surfaces, but nonsorted circles on marine and shallow-water lacustrine silt and silty sand occur in clusters or as isolated features. Field work during summer 1976 at four locations in north-central District of Keewatin (Fig. 31.1, A-D) and observations from other locations throughout the map area (R.D. Thomas, and F.M. Nixon, personal communication, 1979) have shown that extensive, well vegetated, flat areas of poorly to moderately drained marine and shallow-water lacustrine silty sand, despite only a sporadic cover of nonsorted circles, also exhibit unstable soil conditions. Both the till described by Shilts and the silty sand considered here became "quick" when disturbed. A quick condition exists "when a cohesionless soil is subjected to a water condition that results in zero effective stress, the strength of the soil then becomes zero" (Lambe and Whitman, 1969, p. 263). The application of a shock to the ground surface, such as jumping several times at the same location, is sufficient in most cases to induce a quick condition in these Keewatin sediments.

To gain some insight into the conditions leading to the development of nonsorted circles in silty sand, a small area (Fig. 31.2) of lacustrine silty sand covered by 5 to 10 cm of moss and grass and containing 27 nonsorted circles was examined (Fig. 31.3). The bare soil patches are circular to subcircular, more rarely ellipsoidal, and rarely exceed 1 m in diameter. Surface elevation and depth to frost table (the surface that represents the level to which thawing of the seasonally frozen ground has penetrated at anytime in spring and summer) were recorded at 178 locations. Because of the sandy texture, probing to the frost table provided accurate depth measurement (Mackay, 1977). The 178 observations points, while adequate for surface topography, were not considered sufficient for a satisfactory contour map of the frost table, and consequently only selected profiles (Fig. 31.3) are shown for the frost table configuration. Thirty-two samples collected from pits dug to the frost table outside and within nonsorted circles and in boreholes drilled through circles below the frost table were analyzed to determine some volume and weight phase relationships. Grain-size and (to a lesser extent) mineralogical distributions were used in the interpretation of these relationships.

Frost Table and Permafrost

In general the frost table reflects surface topography and at the time of this investigation (mid August 1976) was at about 30 cm depth. The depth of thaw was thinnest over ice wedges and thickest in the centre of nonsorted circles.

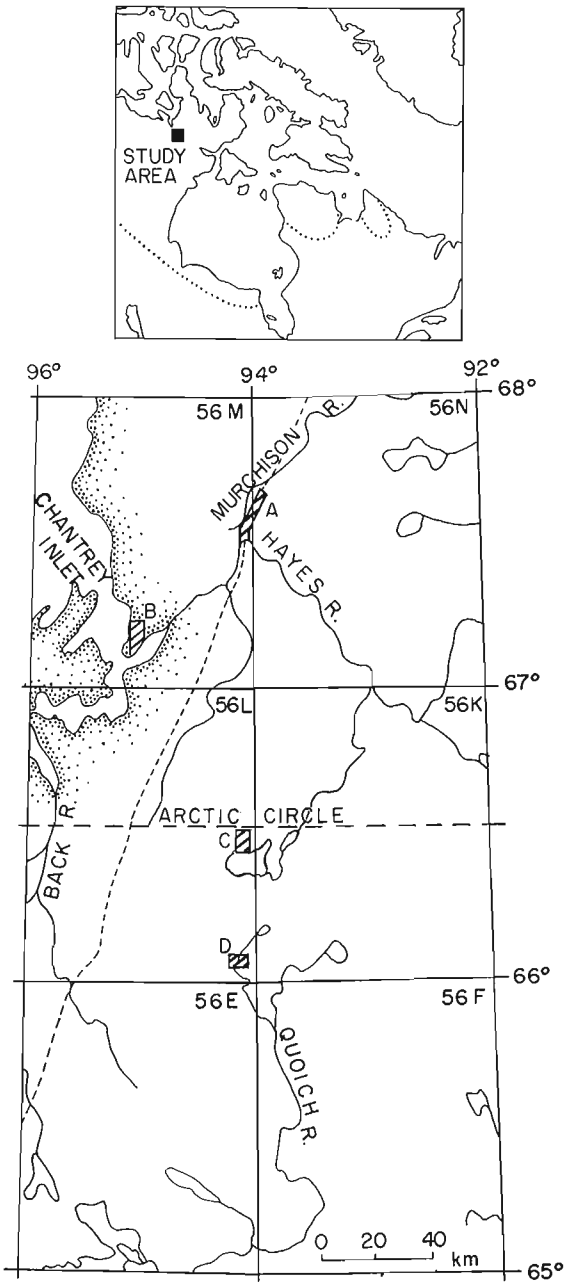

Figure 31.1. Map of a portion of north-central District of Keewatin; detailed field work was conducted at sites A, B, C and D; dashed line is the proposed Polar Gas pipeline route. Dotted line denotes southern limit of continuous permafrost zone.

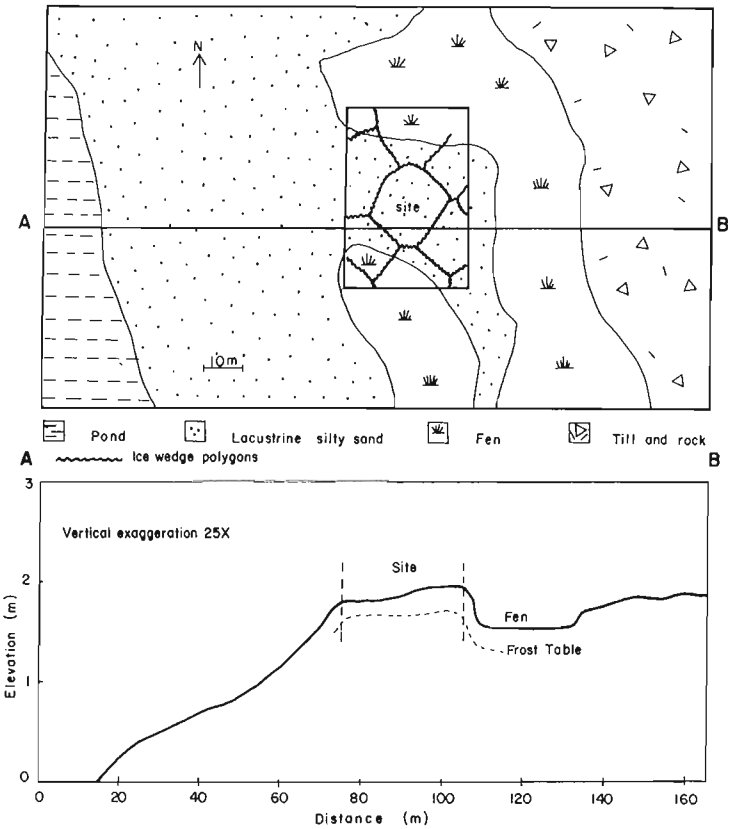

Figure 31.2. Distribution of surficial materials in the vicinity of site D (Fig. 31.1). The profile A-B (below) shows the topographic and frost table profiles for mid August, 1976.

The bare soil circle acts as a window through the vegetation mat and contributes to a local lowering of the frost table. The depression in the frost table under each circle is bowl-shaped with the deepest point directly under the centre of the circle. The frost table under circles 8, 22, and 23 is 33% to 50% lower than in the area surrounding them (Fig. 31.4) and as much as 90% lower under larger circles (e.g. 7). The diameters of depressions in the frost table are 4.5 to 7.8 times those of bare soil patches. Thus even though the surfaces patches are discrete features, the depressions in the frost table form an interconnecting network resulting in an overall greater depth of thaw under and around these features. This is illustrated by profiles C-D and E-F (Fig. 31.3) in the vicinity of circles 4 to 8. Depth of thaw measured in the centre of each circle (Fig. 31.5) increases exponentially with the area of the bare soil patch. This correlation is highest in the 36 to 46 cm depth range, and the data approximate a straight line on log-log paper. Although maximum depth of thaw varies from year to year, the data indicate that, for this particular site and time in the thaw season, the depth of thaw under large circles approaches a maximum (55-60 cm).

Figure 31.6. shows the stratigraphy and natural water (ice) contents from four boreholes drilled in the centre of circles 5, 14, 15, and 22 (Fig. 31.3). At circles 5 and 14 both holes bottomed in foliated ice. Ice at the 69-98 cm level of circle 5 is probably aggradational in origin; it lacks a foliated structure, is clear, contains elongated vertical bubbles, and truncates the underlying foliated ice. In circle 14, contorted bands of unweathered light grey sand mixed with rusty brown weathered sand and finely disseminated organic matter between 57 and 78 cm, and the lack of aggradational ice over the ice wedge suggest a maximum former depth of thaw of 78 cm. Ground ice in circles 15 and 22, at some distance from ice wedges, is mainly in the form of thin horizontal ice lenses.

Sediments below the frost table do not differ in texture from those above it (cf. Fig. 31.7, 31.8) fine sand and coarse silt being the dominant size fractions.

Physical Characteristics of the Silty Sand

The silty fine sand in the study area showed a lack of plasticity, and the large amount of fine sand and coarse silt made it difficult to perform reliable liquid limit tests. Hence, it is assumed that the plasticity index is close to 0. This property is characteristic of cohesionless soils.

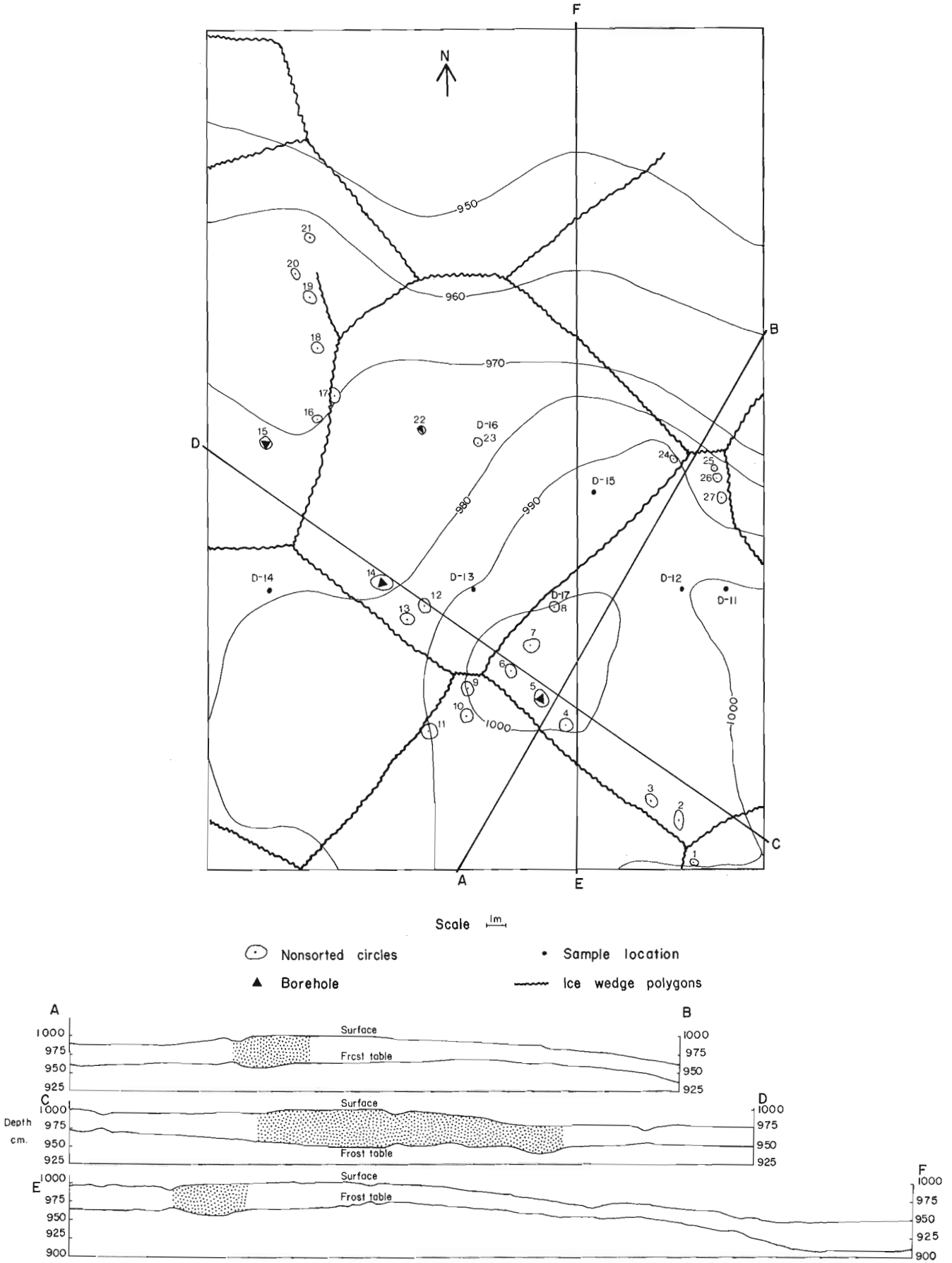

Figure 31.3. *Detailed map of site D (Fig. 31.1, 31.2) showing topography, ice wedge polygons, borehole and sample locations, and 27 nonsorted circles. Stippled areas in profiles show depressed parts of the frost table resulting from increased depth of thaw under closely spaced circles. Contour interval 10 cm; map based on 178 topographic measurements.*

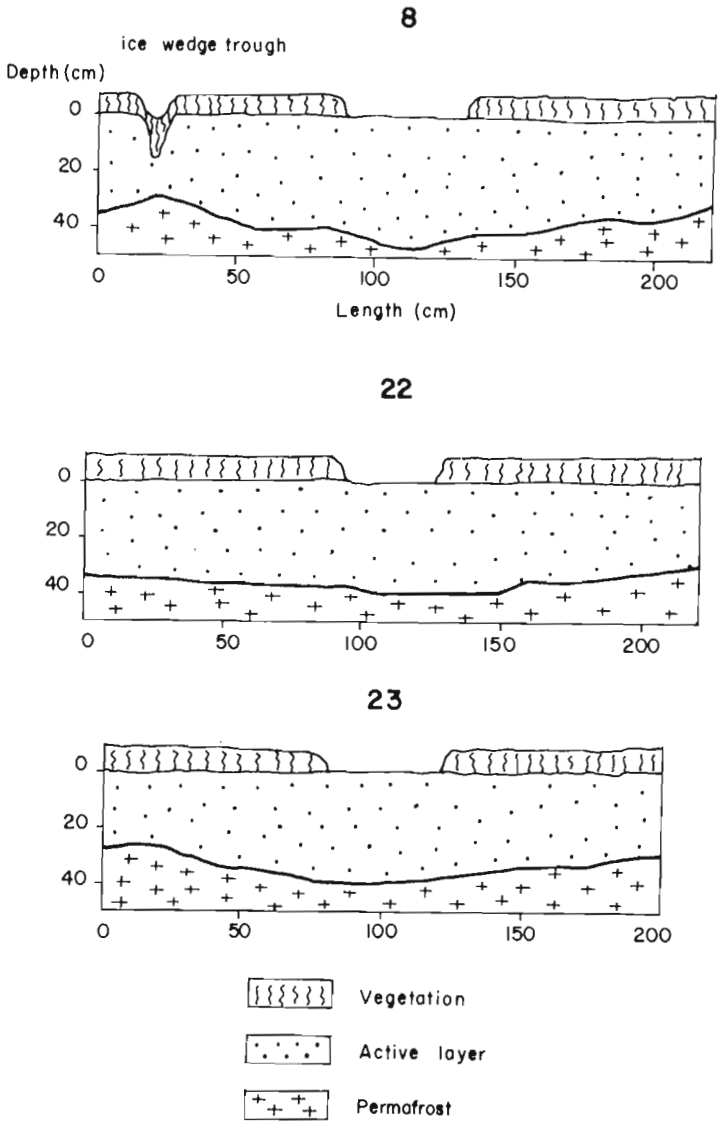

Figure 31.4. *Frost table configuration under circles 8, 22, and 23.*

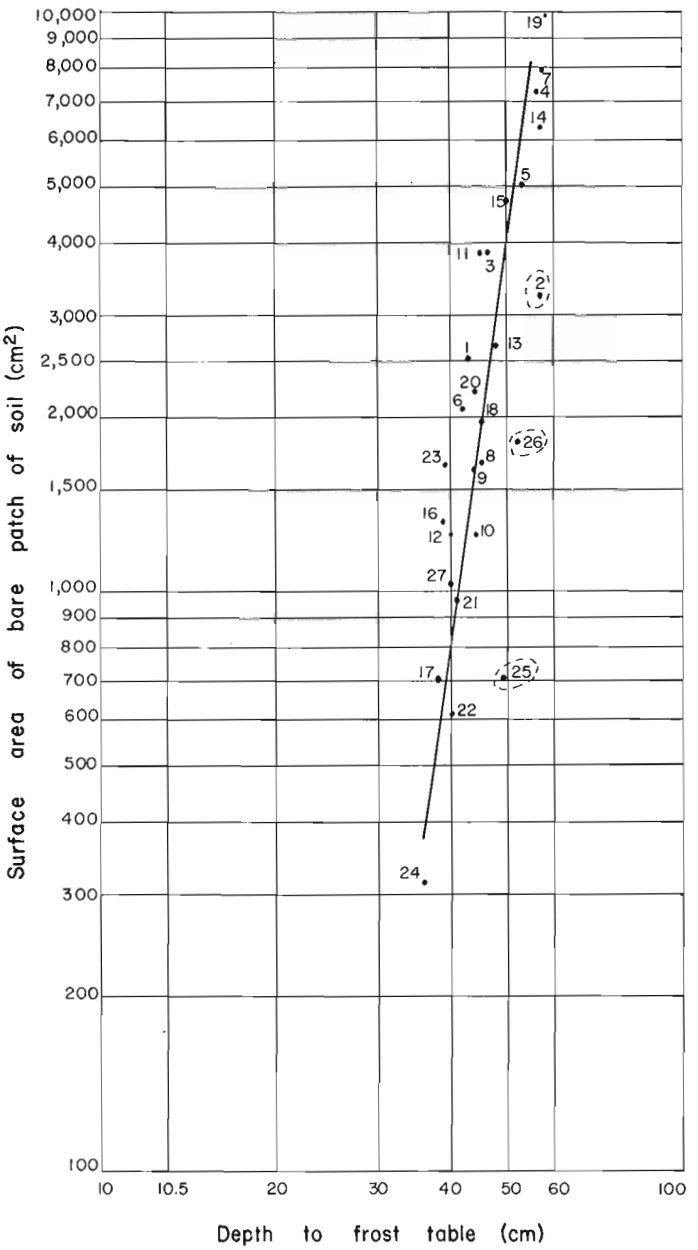

Figure 31.5. *Depth to frost table measured in the centre of each circle versus surface area of a bare soil patch on a circle for the 27 circles; 2, 25 and 26 are anomalous.*

Volume and weight phase relationships obtained from undisturbed samples collected both within and outside nonsorted circles at the site are given in Table 31.1.

Void ratios (e) for material outside the circles are higher than those from within circles, suggesting that the material is under greater confining pressure within circles or that the two sets of samples differ in texture and/or particle shape. The difference in texture must be rejected, however, given the similarity between grain-size curves for both sets of samples (Fig. 31.8). Sediments from within the circles are slightly drier than those outside (see mean saturation (S), Table 31.1). Water content of saturated soil (S = 100%) was computed to estimate the amount of water to be added to field water content (w) in order to fill all pore spaces and probably to induce a quick condition in the active layer.

Void ratio and porosity values both within and outside circles are typical of cohensionless soils in the "loose" state. Several factors contribute to a loose arrangement of soil particles: "The smaller the range of particle sizes present (i.e., the more nearly uniform the soil), the smaller and the more angular the particles, the smaller the minimum density (i.e., the greater the opportunity for building a loose arrangement of particles)" (Lambe and Witman, 1969, p. 31).

On the other hand, high pore pressures, if present, will cause poor interlocking between individual grains leading to a behaviour similar to that of a naturally "loose" soil. The site lacks conditions capable of generating artesian pressures (see discussion below); hence the loose arrangement of the particles possibly is due to other factors including: (1) a small range of particle size (Fig. 31.8), (2) small particles, i.e., very fine sand and coarse silt, and (3) particle shape. A grain count (1013 grains) on sample D-17-2 (28-36 cm depth) resulted in 17.2% of sheet-like minerals (biotite, muscovite, and vermiculite grains) in the silty sand. Micaceous sand in the loose state generally produces the highest void ratio and porosity values of all cohesionless soils (Lambe and Whitman, 1969, p. 31). The annual freeze and thaw cycle may prevent the soil from reaching a "normal" consolidation thus maintaining a loose arrangement of soil particles.

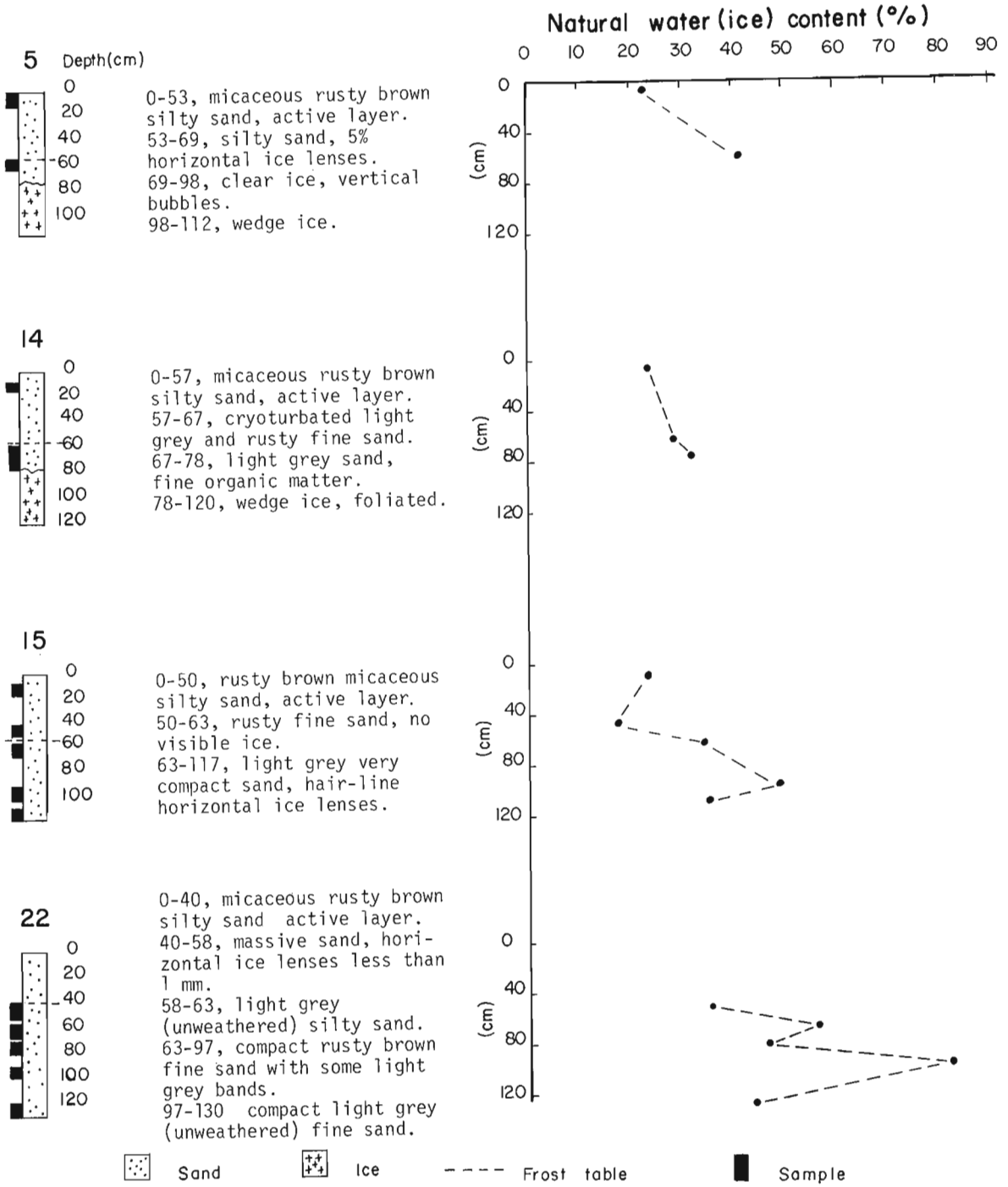

Figure 31.6. *Logs for boreholes drilled in the centre of circles 5, 14, 15, and 22. Note high water (ice) content immediately below the frost table.*

Models Invoked to Explain Sorted and Nonsorted Circles

General

Sorted and nonsorted circles in unconsolidated sediments are widespread throughout the Canadian Arctic, but the best descriptions are from District of Keewatin and western Arctic. Shilts (1974, 1978) applied the term "mudboils" to sorted and nonsorted circles on glacial and marine mud of central and southern District of Keewatin. The features are described as "round to elongate, 1-3 cm diameter bare soil patches that form on perennially frozen till, marine clayey silt, colluvium or other poorly sorted sediments (muds) with significant silt and (or) clay content" (Shilts, 1978, p. 1053). Allowing for variations in local soil and climatic conditions, the structural components of a mudboil can include: (1) an outer turf or stone ring; (2) a thawed mud substrate (TMS) lying between the permafrost table and a rigid surface layer; (3) a carapace, a semi-rigid, sandy, desiccated layer averaging 30 to 40 cm thick; and (4) a diapir, in the case of active mudboils, which marks a zone of intrusion of mud from the TMS through the carapace.

The soil properties responsible for mudboil formation are identified as a low liquid limit (20%), low plasticity index (<10%), and natural moisture content very near the liquid limit, so that slight changes in moisture content or slight changes in internal or external stresses cause the mud to

Table 31.1

Volume and weight phase relationships obtained for silty sand in the study area

Sample no. (see Fig. 31.3)	Depth cm	Specific gravity (G)	Total unit weight (γt) g/cm^3	Void ratio (e)	Porosity (n) %	Degree of saturation (S) %	Natural water content (w) %	Natural water content at S = 100% %
Samples outside nonsorted circles								
D-11-1	15-23	2.75	1.78	.98	49.0	79.0	28.3	35.6
D-11-2	25-33	2.75	1.93	.67	40.0	72.0	17.5	24.4
D-12-1	10-18	2.75	1.97	.72	41.9	88.8	23.3	26.2
D-12-2	26-34	2.75	1.91	.72	41.9	74.9	19.7	26.2
D-13-1	13-21	2.75	1.89	.83	45.0	86.0	26.1	30.2
D-14-1	16-24	2.75	1.91	.78	44.0	84.0	23.8	28.4
D-15-1	15-23	2.75	1.92	.81	45.0	90.6	26.7	29.5
			$\bar{x}$ = 1.90	$\bar{x}$ = .78	$\bar{x}$ = 43.8	$\bar{x}$ = 81.9	$\bar{x}$ = 23.6	$\bar{x}$ = 28.6
Samples within nonsorted circles								
D-16-1	1-9	2.75	1.93	.66	39.0	71.4	17.3	24.0
D-16-2	20-28	2.74	1.94	.66	39.0	74.3	17.9	24.0
D-16-3	31-39	2.76	1.85	.80	44.0	72.0	20.9	29.0
D-17-1	1-9	2.75	2.04	.57	36.5	80.4	16.8	20.7
D-17-2	28-36	2.75	1.93	.69	41.0	76.0	19.1	25.1
			$\bar{x}$ = 1.94	$\bar{x}$ = .68	$\bar{x}$ = 39.9	$\bar{x}$ = 74.8	$\bar{x}$ = 18.4	$\bar{x}$ = 24.6

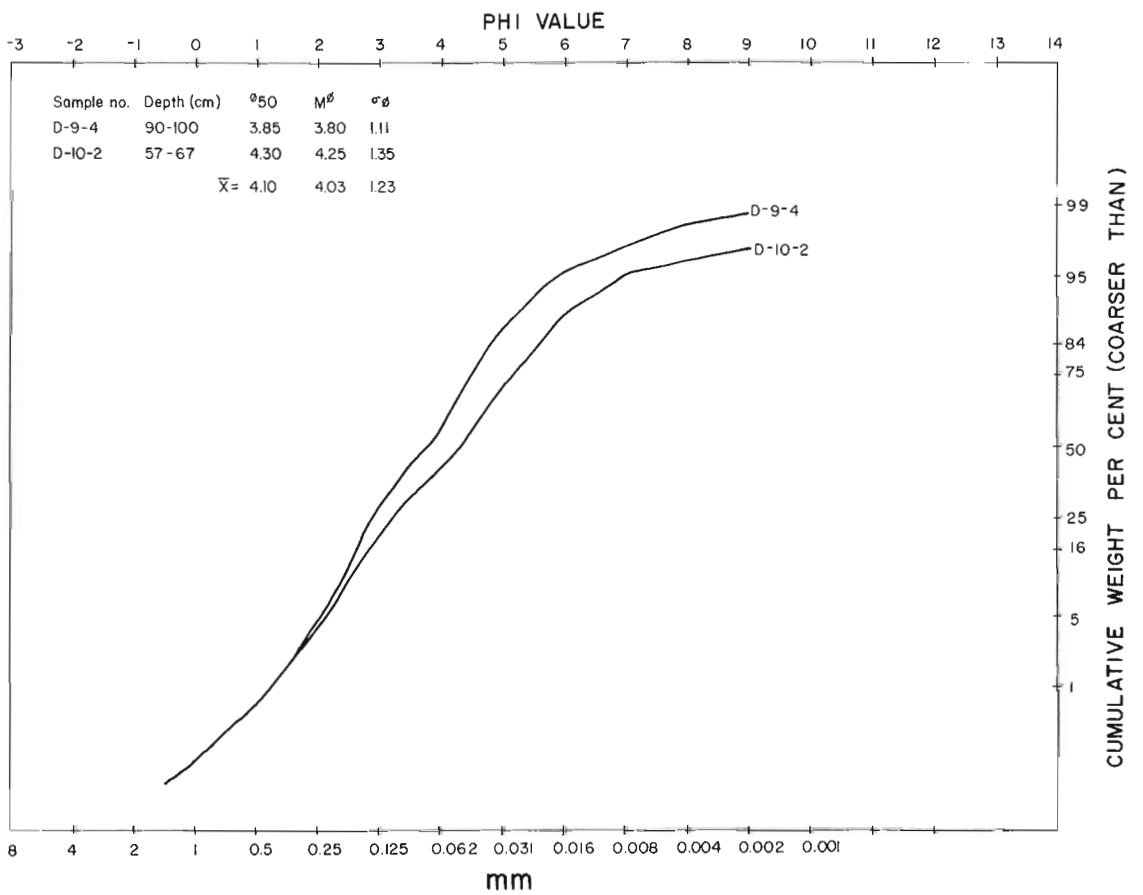

Figure 31.7. Grain-size distribution for sediments below the frost table under nonsorted circles 14 (D-10-2) and 15 (D-9-4) (see Fig. 31.3 for locations).

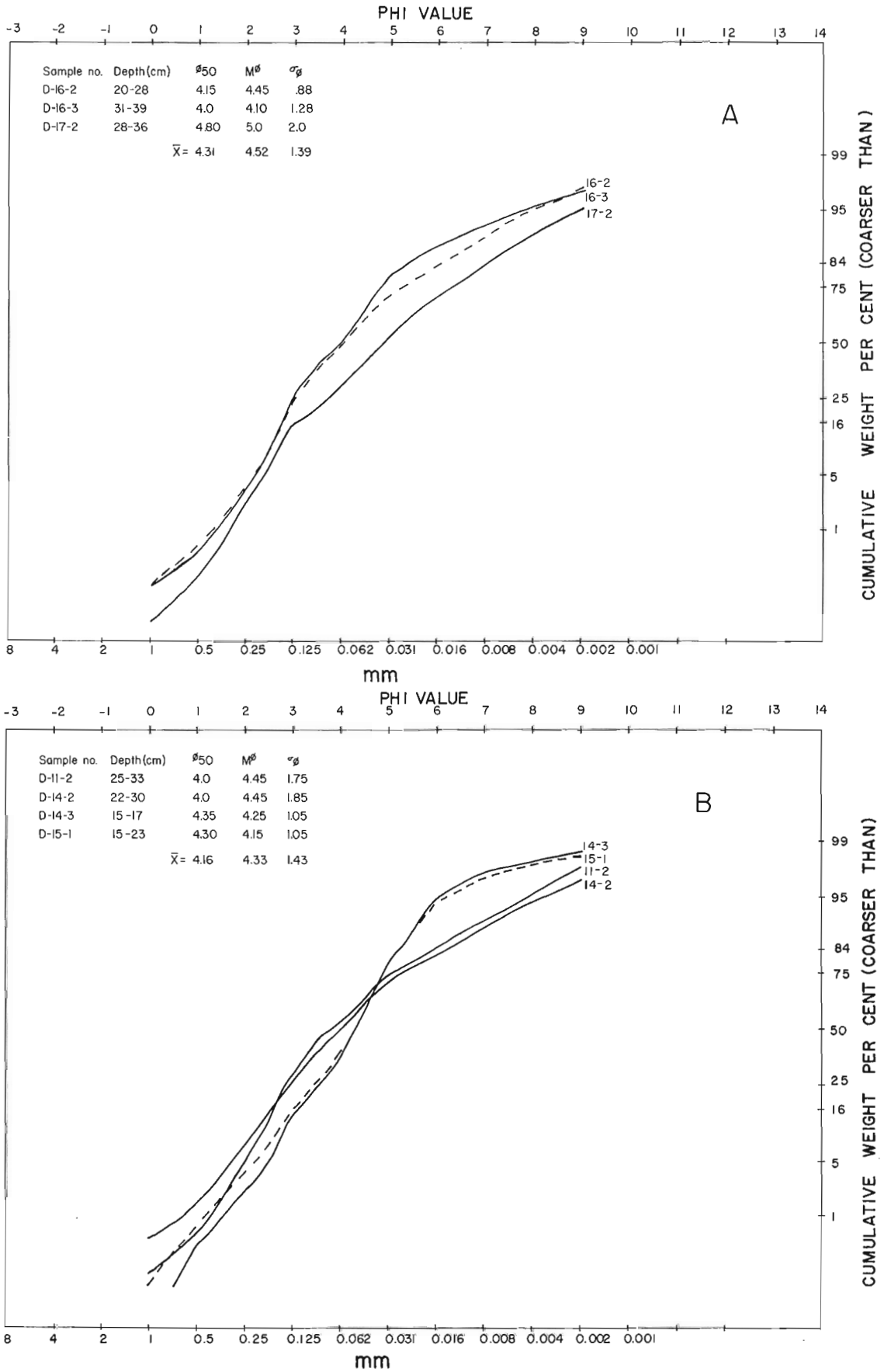

Figure 31.8. *Grain-size distribution for sediments above the frost table and within (A) (circles 8 and 23) and outside (B) nonsorted circles (see Fig. 31.3 for locations).*

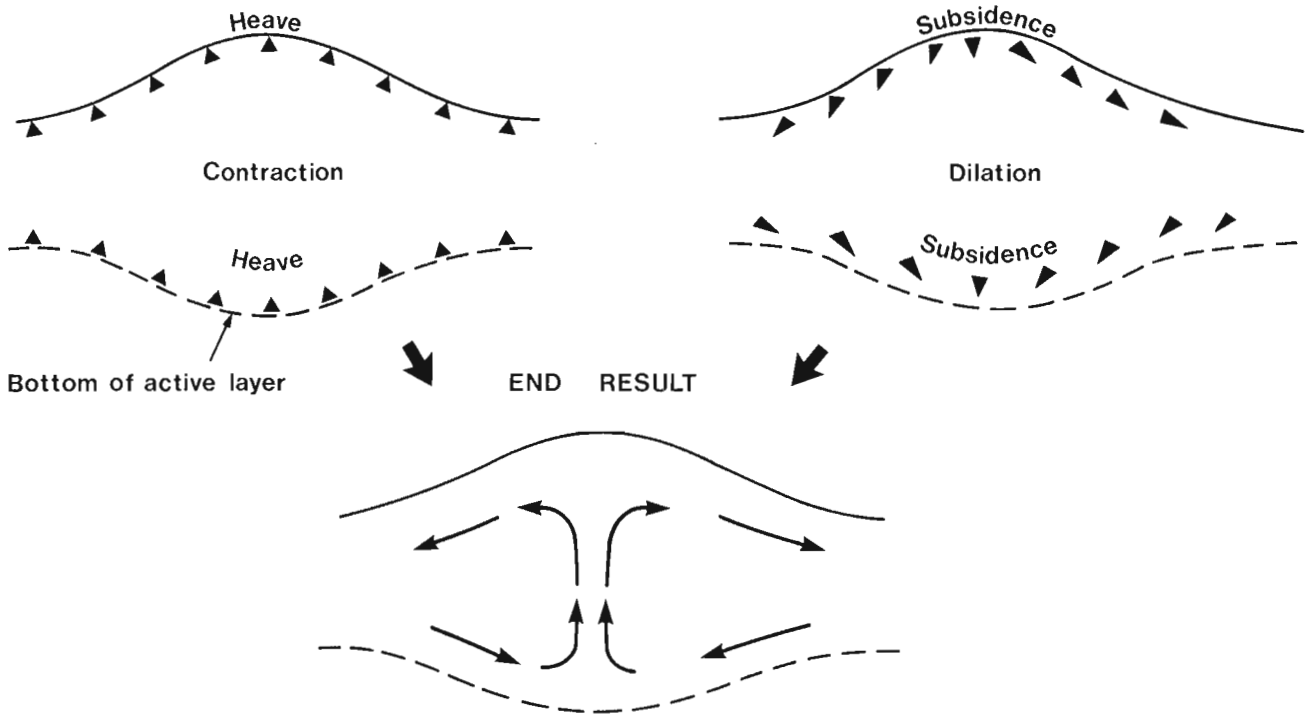

Figure 31.9. Equilibrium model proposed for the growth and maintenance of hummocks, Garry Island, Northwest Territories. Heave results from ice lensing at the base and top of the active layer, and subsidence from the thawing of the ice lenses (after Mackay, 1979).

liquefy and flow readily. Mudboils are created or maintained when the stresses cannot be relieved by downslope movement, causing mud to burst through a rigid surface layer or carapace. This diapirism may result from artesian or hydrostatic pressure on a slope, from excess porewater pressure due to rain or thawing of ice lenses, or from external loading.

Artesian pressure may also result from conditions analogous to that of the inclined confined aquifer model (Shilts, 1974). Essentially, the model requires an inclined surface, a lower impervious layer (frost table), an upper impervious layer (the rigid surface carapace), and an intermediate, confined, mobile material (liquefied mud).

Jahn (1968) suggested a mechanism whereby injection of material towards the surface, or diapiric action, could take place without having an inclined plane to generate hydrostatic pressure or without cryostatic stresses to force the fluid material upwards. He noted that tundra craters (mudboils) were found in sediments consisting of silt covered with a layer of sand or rock debris – similar to the carapace over mud described by Shilts (1973). Jahn observed pillars of silt at the surface which had emerged through the upper crust of sand and rock debris and attributed the process to a difference in specific gravity between the upper layer of gravel and sand and the lower silt layer. The load applied by the upper layer increases pore pressure in the bottom one and forces material upwards through points of weakness in the upper crust.

Some authors (Crampton, 1977; Nicholson, 1976) attributed the formation of sorted and nonsorted circles to cryostatic pressures. The theory rests on the basis that there is an upward injection of uniform material confined between the ground surface and a lower impermeable surface by progressive downward freezing that generates large hydrostatic pressures in pockets of such material (Gray et al., 1972, p. 169). Cryostatic pressures are most likely to develop in relatively coarse grained soils that are not frost susceptible; downward freezing can then lead to porewater expulsion and a saturated active layer at depth, particularly if there is some groundwater movement (Mackay, 1979).

An equilibrium model was proposed by Mackay (1979) for the growth and maintenance of hummocks (nonsorted circles) on Garry Island, Northwest Territories. Repeated cycles of winter freeze and summer thaw cause heave and subsidence, the end result being a slow cell-type internal movement of soil particles (Fig. 31.9). Heave results from ice lensing normal to the freezing plane both at the top and at the base of the active layer, and subsidence results from the thawing of the ice lenses. The Garry Island hummocks and a large proportion of Mackenzie Valley hummocks have a late summer frost table that is a mirror image of the ground surface.

Application of Models to Nonsorted Circles at the Study Site

A hydrostatic head cannot account for the development of the nonsorted circles at the study site in north-central District of Keewatin; in fact, the part of the site where they are the most numerous is also the highest ground in the immediate area (Fig. 31.3, circles 4 to 11). The fens located north, east, and south of the site are the only sources of water to cause a hydrostatic head. Figure 31.2 shows that the frost table within the site in mid-August 1976 was higher than the surface of the fen to the east, making it impossible for late summer drainage conditions to create a hydrostatic head. To saturate the active layer under the circles would require at least a 30 cm late season rise of water level in the fen. On the other hand, the water level in the fens is higher in early summer than in late summer. By attributing formation of nonsorted circles solely to a hydrostatic head in the active layer, the most likely time of formation would thus be limited to a short period in early summer or late spring. It is probable that a sufficient water head cannot exist at this time because the frost table early in the thaw season is shallow.

Both the loading and inclined confined aquifer models require the presence of a rigid upper carapace, which is absent from the nonsorted circles studied here. The 27 circles are in sediments that do not show significant vertical differences in total unit weight and in grain-size distribution from the ground surface to the frost table (Table 31.1). Also the material immediately above the frost table was not fluid, as is the TMS (thawed mud substrate) of a typical mudboil. It is suggested, therefore that the most likely mechanism left to explain their formation is associated with frost action.

Because the fine silty sand on which the 27 circles occur, although cohesionless, has a sufficient proportion of fine particles to be frost susceptible, it is unlikely that cryostatic pressures are adequate to explain their formation. Mackay and MacKay (1976) have shown that cryostatic pressures in hummocks of lower Mackenzie Valley during the freeze-back period play a minor role in hummock growth. The hummock centres were found to be desiccated, overconsolidated, and immobile rather than saturated and mobile. This is attributed to water loss to growing ice lenses at the top and bottom of the active layer. The material in the hummocks used for their field experiments has about 50% of particle sizes finer than 0.002 mm; thus the texture differs from that of the nonsorted circles studied here. A common factor between the lower Mackenzie Valley hummocks and the silty sand nonsorted circles, however, is their frost susceptibility, and as such, their susceptibility to ice lensing.

Conclusion

Mackay's (1979) model presents the most likely mechanisms to explain the growth and maintenance of the nonsorted circles described here: "The equilibrium model can be applied, with minor changes to take into account soil type and surface form, to some other types of patterned ground where the late summer frost table is concave upwards." (Mackay, 1979, p. 166.) The following observations and measurements support this model: (1) the presence of a late summer frost table that is concave upwards; (2) a lower void ratio (Table 31.1) in samples within the centres of circles compared with those outside circles, which may reflect the state of contraction left by winter freeze; (3) a natural water (ice) content, immediately below the frost table (probably close to the permafrost table in mid August) of circles, that is well in excess of the natural porosity of the thawed soil; further thawing would supply excess water available for ice lensing at the frost table; (4) available water (Table 31.1) within the thawed layer for ice lensing near the surface; (5) a "loose" arrangement of soil particles (high void ratio, low unit weight) compatible with disturbance resulting from the annual freeze and thaw cycle, thus preventing the soil from reaching a "normal" consolidation; (6) the inadequacy of artesian and loading models to explain the extrusion of active layer material in a diapiric fashion.

Stable "typical" Mackenzie Valley hummocks are commonly found in the Arctic Islands and in District of Keewatin near active "typical" Keewatin mudboils. Hummocks are restricted to predominantly clayey cohesive soils whereas mudboils (those with a carapace, thawed mud substrate, and other structural components described above) are characteristic of poorly sorted, cohesionless sediments. It is suggested that nonsorted circles in cohesive, impervious fine grained soils with high liquid limits will more readily retain a convex surface during the warm season. Despite a similar mode of circle formation, summer precipitation and wind action likely will prevent the retention of a convex surface on nonsorted circles in cohesionless, pervious fine sand and silty sand such as present at this site. If and when doming occurs, due to ice lensing, it probably disappears rapidly with early summer thawing of the upper active layer portion. On the other hand, if significant doming does not take place during winter freeze, the cell-type internal movement proposed by Mackay for hummocks likely occurs just the same in the nonsorted circles described here, because the bowl-shaped summer frost table causes movement of the soil particles towards the centre of the circle and eventually upwards.

References

Crampton, C.B.
1977: A study of the dynamics of hummocky microrelief in the Canadian North; Canadian Journal of Earth Sciences, v. 14, p. 639-649.

Egginton, P.A.
1978: Mudboil activity, central District of Keewatin; in Current Research, Part B; Geological Survey of Canada, Paper 79-1B, p. 359-356.

Egginton, P.A. and Shilts, W.W.
1978: Rates of movement associated with mudboils, central District of Keewatin; in Current Research, Part B; Geological Survey of Canada, Paper 78-1B, p. 203-206.

Gary, M., McAfee, R., Jr., and Wolf, C.L. (ed.)
1972: Glossary of Geology; American Geological Institute, Washington, D.C., 805 p.

Jahn, A.
1968: Patterned ground; in The Encyclopedia of Geomorphology, ed. R.W. Fairbridge; Reinhold, New York, p. 814-817.

Lambe, T.W. and Whitman, R.V.
1969: Soil Mechanics; Series in soil engineering, John Wiley and Sons Inc., New York, 553 p.

Mackay, J.R.
1977: Probing for the bottom of the active layer; in Report of Activities, Part A; Geological Survey of Canada; Paper 77-1A, p. 327-328.

1979: An equilibrium model for hummocks (nonsorted circles), Garry Island, Northwest Territories; in Current Research, Part A; Geological Survey of Canada, Paper 79-1A, p. 165-167.

Mackay, J.R. and MacKay, D.K.
1976: Cryostatic pressures in nonsorted circles (mud hummocks) Inuvik, Northwest Territories; Canadian Journal of Earth Sciences, v. 13, p. 889-897.

Nicholson, F.H.
1976: Patterned ground formation and description as suggested by Low Arctic and Sub-Arctic examples; Arctic and Alpine Research, v. 8, no. 4, p. 329-342.

Shilts, W.W.
1973: Drift prospecting; geochemistry of eskers and till in permanently frozen terrain, District of Keewatin, Northwest Territories; Geological Survey of Canada, Paper 72-45, 34 p.

1974: Physical and chemical properties of unconsolidated sediments in permanently frozen terrain, District of Keewatin; in Report of Activities, Part A; Geological Survey of Canada, Paper 74-1A, p. 229-235.

1978: Nature and genesis of mudboils, central Keewatin; Canadian Journal of Earth Sciences, v. 15, no. 7, p. 1053-1068.

Washburn, A.L.
1973: Periglacial Process and Environments; Edward Arnold, London, 320 p.

SCIENTIFIC AND TECHNICAL NOTES
NOTES SCIENTIFIQUES ET TECHNIQUES

REDATED HOLOCENE WHALE BONES FROM SOMERSET ISLAND, DISTRICT OF FRANKLIN

Arthur S. Dyke
Terrain Sciences Division

Dyke (1979) presented Holocene emergence curves for Somerset Island based on 36 radiocarbon dates on marine shells, whale and walrus bones, and driftwood. Of the thirteen whale bone samples that were dated, three were by far too young – that is, they plotted above the emergence curves. All three specimens had lichen and moss growing on them at time of collection, and this contamination was suspected as the cause of the anomalously young age determinations. These samples have since been redated (Table 1), and the results are briefly discussed in this note.

New Dates

The new dates were determined at the same laboratory as the original dates (Radiocarbon Dating Laboratory of the

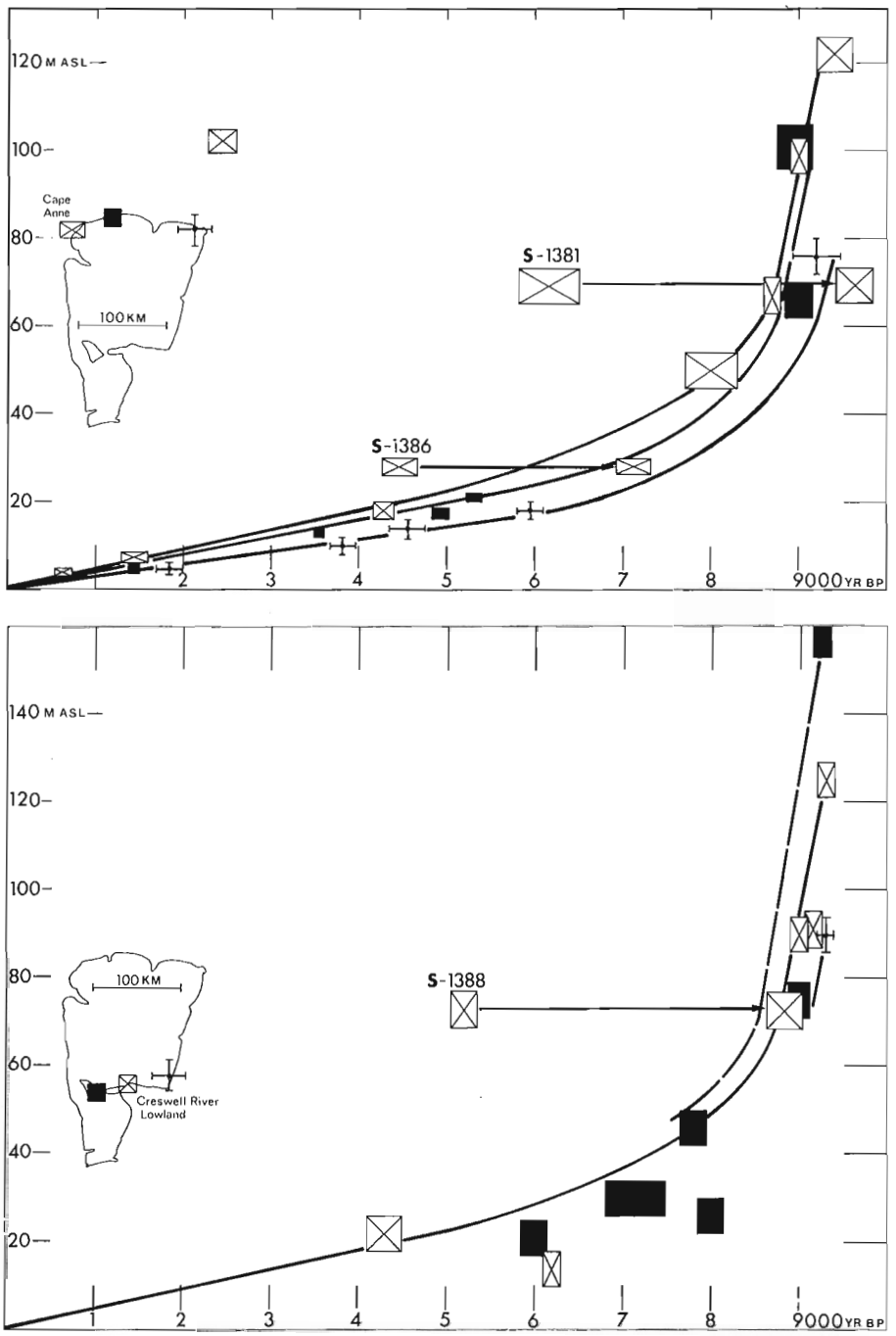

a – northern Somerset Island

b – southern Somerset Island

Figure 1

Holocene emergence curves for Somerset Island showing original and revised radiocarbon dates. The height of each symbol is the estimated error on elevation measurements, and the width is 2 sigma error on the radiocarbon age determination.

From: Scientific and Technical Notes in Current Research, Part B; Geol. Surv. Can., Paper 80-1B.

Table 1

Redated Holocene whale bones from Somerset Island

Laboratory no. (field no.)	Location	Original radiocarbon age determination (years B.P.)	New radiocarbon age determination (years B.P.)	Age expected according to emergence curves (years B.P.)
S-1381 (DCA-77-B21)	Cape Anne	6140 ± 165	9590 ± 115	>8800
S-1386 (DCA-77-B12)	Cape Anne	4465 ± 85	7105 ± 90	>6000
S-1388 (DCA-77-B1)	Creswell River lowland (West)	5205 ± 70	8805 ± 95	>8700

National Museums of Canada and the Saskatchewan Research Council). However, an extra step was used in the preparation of the samples for redating: after pretreatment with 1N HCl the softened material was hydrolized in a slightly acidic solution at 105°C for 16 hours. Then the collagen was dissolved in boiling H_2O and filtered to separate the impurities (J. Wittenberg, written communication to W. Blake Jr., January, 1980). The differences between the original and new dates testify to the efficiency of the revised pretreatment in removing plant and soil contaminants.

Discussion

The last column in Table 1 gives the ages expected according to the emergence curves constructed by Dyke (1979) and reproduced here as Figure 1. Because the whales could have died in some depth of water or on an actual beach, the new dates could plot either below or on the curves. In fact date S-1388 plots on the curve, and the other two dates fall below the curve. Hence no revision of the emergence curves is warranted by the new dates.

Sample S-1381, which yielded an age of 9590 ± 115 years, may be the oldest Holocene sample known from Somerset Island, although the age overlaps with that of the oldest Holocene shell sample from the island (GSC-319, 9380 ± 180 years). Seven other shell samples and one whale bone sample pertaining to the marine limit on the north, east, and south coast of the island all fall in the 9200 ± 100 year age range (see Dyke, 1979, Fig. 34.4); hence, that seems to be a reasonable date for deglaciation of the marine limit sites. If S-1381 gives the true radiocarbon age of the whale bone, whales and open water existed off northern Somerset Island before deglaciation of most marine limit sites.

Reference

Dyke, A.S.
1979: Radiocarbon-dated Holocene emergence of Somerset Island, central Canadian Arctic; in Current Research, Part B, Geological Survey of Canada, Paper 79-1B, p. 307-318.

RADIOCARBON-DATED MUDBOILS, CENTRAL CANADIAN ARCTIC

Project 750071

Arthur S. Dyke and S.C. Zoltai[1]
Terrain Sciences Division

Introduction

Mudboils, a type of sorted or nonsorted circle, are probably the most common patterned ground features in the central Canadian Arctic. They are ubiquitous on till and on diamictic residual soils formed by weathering of bedrock. Related raised, hemispherical forms, referred to as earth or mud hummocks, occur on marine silts and clays in the central Arctic and on clay-rich tills and colluvium in the western Arctic (Mackay and MacKay, 1976; Tarnocai and Zoltai, 1978). Buried organic materials are common in earth hummocks; most are less than 4500 years old (Zoltai et al., 1978).

Several workers have discussed the pattern of movement of sediments in mudboils and hummocks. Among these, Shilts (1978) has shown that sediment moves upward as plumes, which he referred to as diapirs, in the central portions of mudboils and spreads laterally at the surface, and Mackay (1979) has proposed an upward cell-type circulation for earth and mud hummocks of the western Arctic. Because individual mudboils are essentially closed sediment systems, sediment must move downward at or near the edges of boils. Many mudboil edges are outlined by vegetation or turf, and these organic materials are carried under by the subducting sediment. Material can be carried no deeper than the permafrost table, which marks the base of the active layer.

Three mudboils in till, excavated on Boothia Peninsula, Somerset Island, and central District of Keewatin (Fig. 1), had well developed subducted organic layers. The organic materials were sampled for radiocarbon dating to determine long-term average rates of subduction of material in mudboil edges, and the tills were sampled to measure their physical properties.

Mudboil 1

Mudboil 1 was excavated at 71°04'N, 95°36'W on Boothia Peninsula on July 19, 1978, in the early part of an abnormally late and cold summer. The boil occurred on a 1° to 2° well drained slope, with a 50 per cent vegetation cover and 5 per cent boulder cover. The vegetation forms nearly circular rims around the bare mudboil centres, which comprise the remaining 45 per cent of the ground surface. The mudboil chosen for study was typical of others in the area, except perhaps in that its vegetation rim was more distinct than that of most boils. Frost table was encountered at 50 cm depth, and the frozen ground was excavated to a depth of 110 cm with an electric jackhammer.

The pit wall that bisected the mudboil exposed a core of till lined with a mixture of till and fine grained vegetal organic material (Fig. 2). The organic content of the 'lining' was 10-20 per cent. The presence and shape of the organic lining clearly demonstrate that material moves downward at the boil edge, and there is little, if any, exchange of sediment between the boils and the surrounding soil. Hence the boil is a closed system, and material must return to the surface through its central part.

Seven samples of till were collected between the surface and 110 cm depth, including two samples below the base of the organic layer. Roughly 20 to 50 per cent of the till consists of gravel (larger than 2 mm fragments), and the matrix (less than 2 mm fragments) is highly calcareous silty sand. The two samples taken below the organic layer were slightly richer in clay (Table 1). This possibly indicates a slight depletion of fines from the upper till, probably by slopewash and deflation.

The natural moisture contents that mark the boundaries between the solid and plastic and the plastic and liquid states of a soil are referred to as the plastic and liquid Atterberg limits, which are loosely related to texture. In Mudboil 1 the sample with the highest clay content had a plastic limit of 11.8 per cent and a liquid limit of 13.0 per cent; the sample with the least clay content was too coarse for testing (Table 1). Hence, the till has a very limited range of plasticity and liquefies at low moisture content. In this regard it is typical of tills on Boothia Peninsula and Somerset Island and similar to the tills of southern District of Keewatin (Shilts, 1978; Egginton and Shilts, 1978). Natural moisture contents at time of excavation were close to the liquid limit, but the unfrozen sediment showed no tendency to flow. Field observations throughout the region indicate that tills in well drained areas behave as solids through most of the summer but are quite liquid during the period of snowmelt.

Mudboil 2

Mudboil 2 was excavated at 72°52'N, 93°37'W on Somerset Island on July 24, 1977, in the middle of a long and relatively dry summer. The boil occurred on a 2° to 3° seepage slope with a 30 per cent vegetation cover and about 5 per cent boulder cover. The vegetation outlines elongated mudboils with downslope lengths two to four times their widths. Boils of similar shapes are common on gentle seepage slopes in the study area. The shape indicates that the convection process is accompanied by downslope movement of the boils. Frost table was encountered 58 cm below the moss cover at the boil edge and 68 cm below the unvegetated boil centre (Fig. 3). The frozen ground was excavated to a depth of 180 cm.

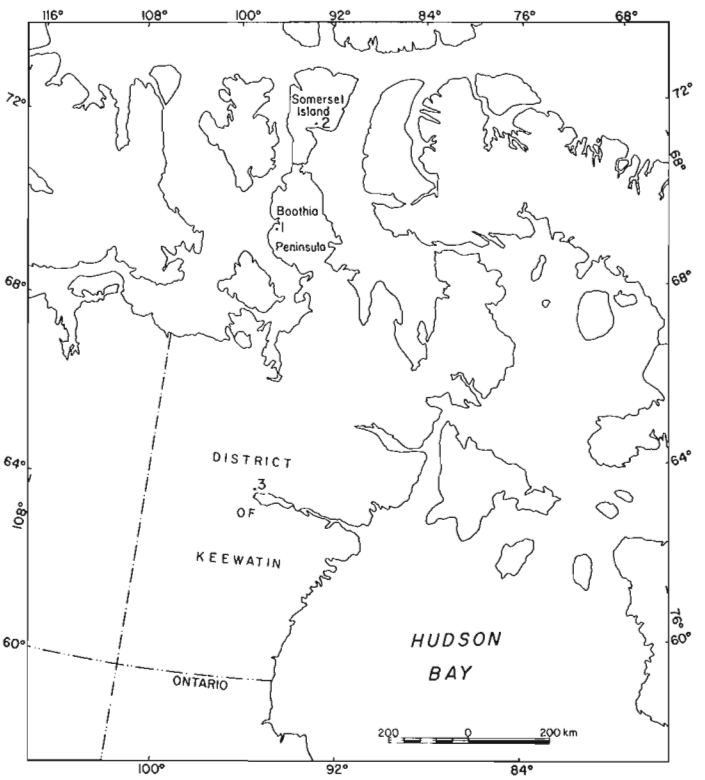

Figure 1. Locations of radiocarbon-dated mudboils, central Canadian Arctic.

From: Scientific and Technical Notes in Current Research, Part B; Geol. Surv. Can., Paper 80-1B.

[1]Canadian Forestry Service, 5320-122 Street, Edmonton, Alberta T6H 3S5

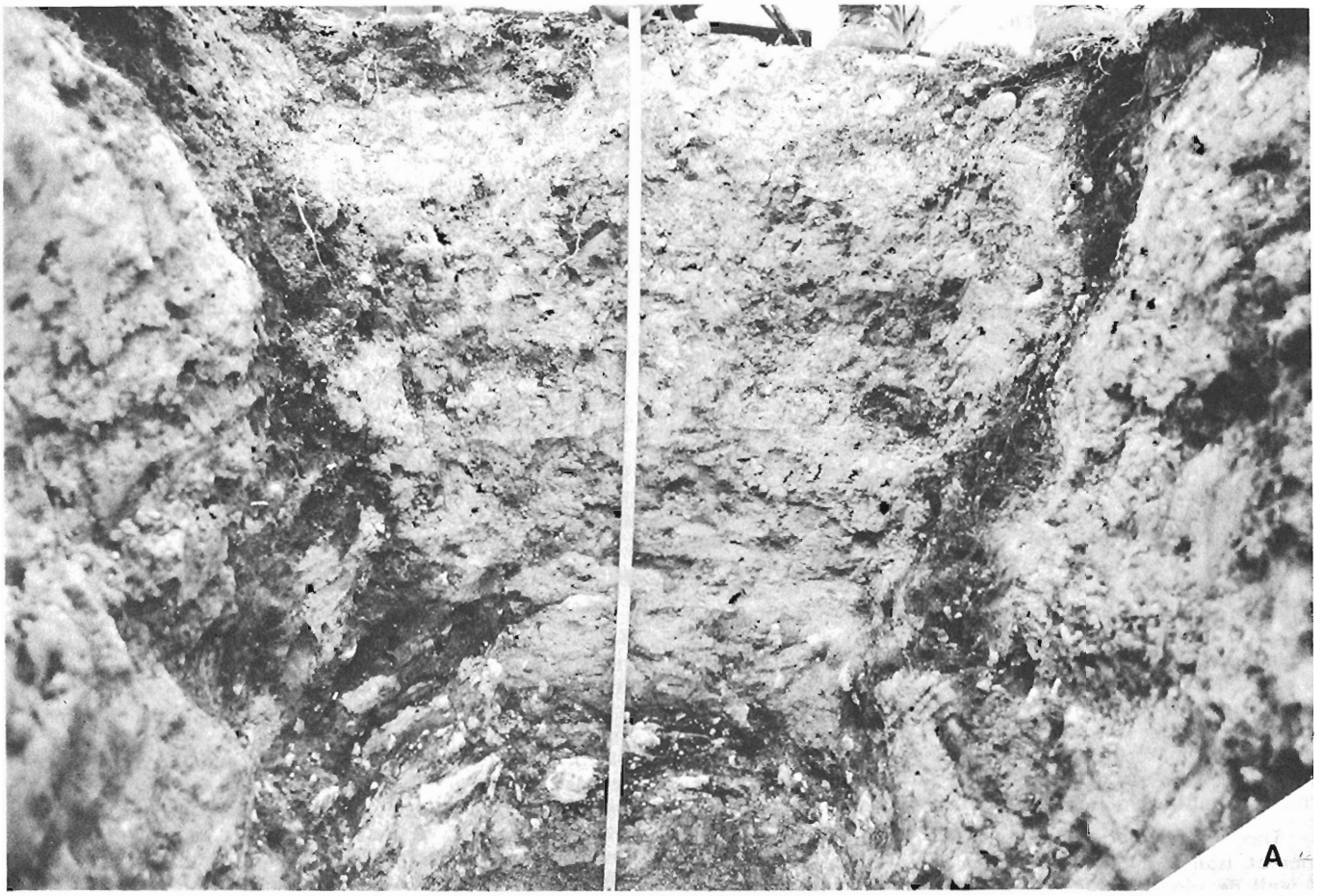
A

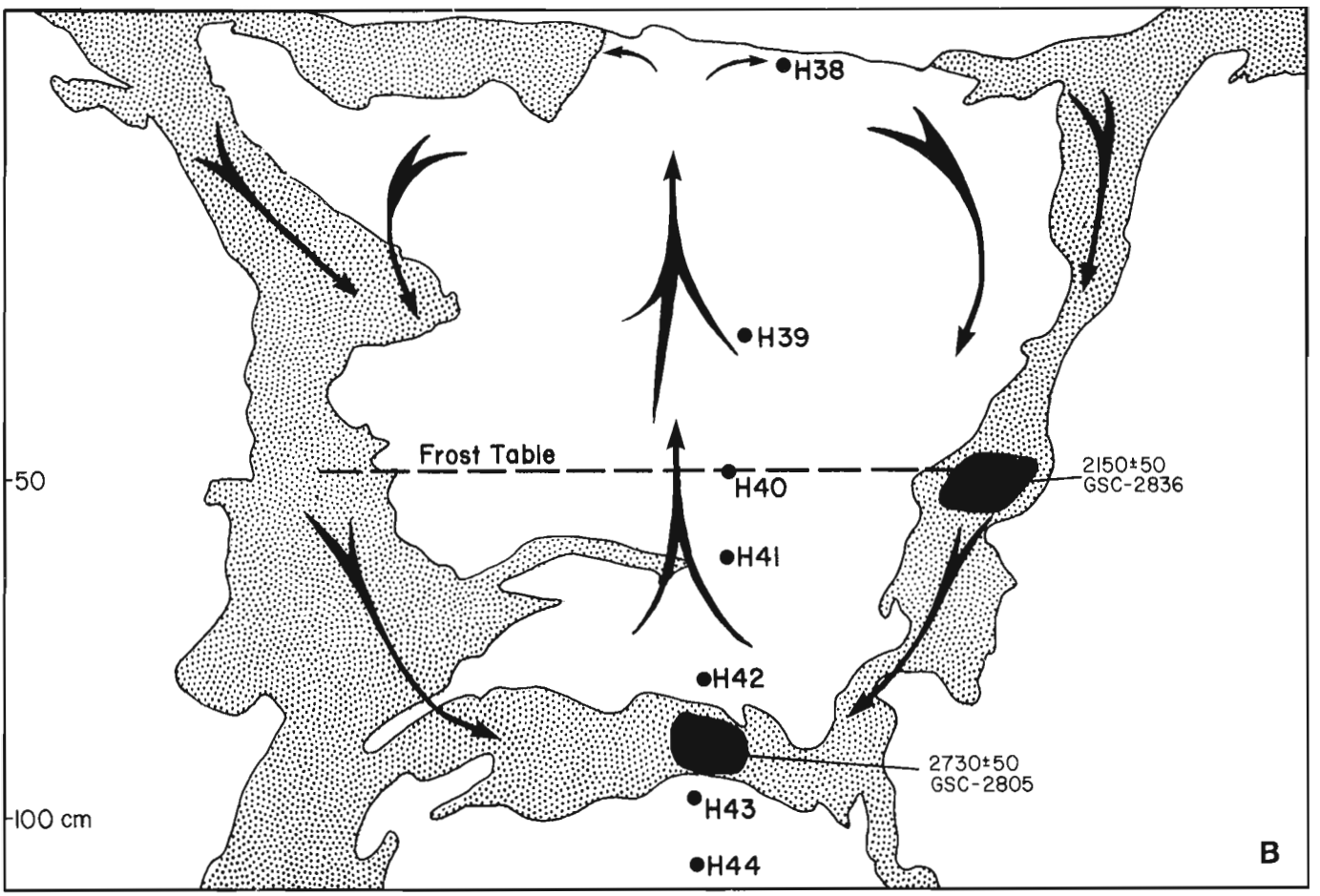
H38
H39
Frost Table
-50
H40
H41
2150±50
GSC-2836
H42
2730±50
GSC-2805
H43
-100 cm
H44
B

Table 1

Properties of till samples from Mubdoils 1, 2, and 3

Sample	Depth (cm)	% Sand	% Silt	% Clay	%$CaCO_3$	Plastic Limit %	Liquid Limit %	Water Content by weight
Mudboil 1								
78-H38	0-5	53	39	8	66	too	sandy	11
78-H39	35	55	35	9	57			9
78-H40	50	46	43	11	58			10
78-H41	60	50	40	10	59			10
78-H42	75	52	39	10	56			10
78-H43	95	44	42	14	60			14
78-H44	110	40	44	16	63	11.8	13.0	16
Mudboil 2								
77-H44	20-30	55	31	14	26	15.4	19.4	
77-H35	58-67	62	26	12	21			38
77-H36	73-79	59	27	14				45
77-H37	87-95	64	24	12	29			27
77-H38	100-109	62	27	11				35
77-H39	115-121	52	36	12				38
77-H40	143-152	79	22	8				37
77-H41	167-176	60	29	14				98
Mudboil 3								
ZS4-B_5	0-5	76	17	7	0			9
ZS4-B_4	15-18	76	19	5	0			10
ZS4-B_3	23-30	71	25	4	0			9
ZS4-B_2	33-39	69	24	7	0			8
ZS4-B_1	45-50	74	18	8	0			10

The pit wall, which extended little more than halfway across the boil and slightly into an adjacent boil (normal to long axes of boils), exposed cores of till separated by a mixture of till and fine grained vegetal organic material. The till cores are underlain by an organic rich layer just below the frost table. Another parallel organic layer occurs 20 cm below the first and is connected to it by a vertical organic layer. This structure suggests that the lower layer could have been emplaced by subduction at a time when the base level for subduction, the permafrost table, was farther beneath the surface than it is at present.

Eight samples of till were collected from and beneath the mudboil. Gravel contents of the till samples range from 12 to 80 per cent; the matrix is a moderately calcareous silty sand, with sand-silt-clay ratios similar to those from Mudboil 1. The detailed grain-size characteristics, however, differ somewhat from those of Mudboil 1 in that there is a distinct peak in the medium sand fraction. This characteristic is due to the provenance of the till; it was derived from sandstone bedrock.

***Figure 2A** (opposite)*

Photograph of a vertical section through Mudboil 1. (GSC-203359-Z)

Figure 2B

Sketch of the section shown in Figure 2A. Stippled areas represent organic-rich material; blank areas represent till with little or no admixed organics; H38, etc. locate till samples; black areas locate radiocarbon-dated organic materials; arrows show inferred pattern of movement of materials within the mudboil.

Plastic and liquid limits were determined for the sample from the core of the mudboil (Table 1, Fig. 3). Although these values are slightly higher than those for Mudboil 1, the material still classifies as a silty sand of slight plasticity. Samples taken at and below the frost table had natural moisture contents considerably in excess of the liquid limit, and the active layer at time of excavation was saturated and prone of liquefaction. This mudboil, because of its situation on a seepage slope, unlike Mudboil 1, is probably saturated beyond its liquid limit during much of the summer.

Mudboil 3

Mudboil 3 was excavated at 63°39'N, 95°50'W in central District of Keewatin on July 9, 1976. Being in the early part of the thaw season, the frost table was reached by the excavation, but the pit rapidly became flooded with water, preventing deeper penetration. The low centre mudboil occurred on a flat, imperfectly to poorly drained area that had a 75 per cent vegetation cover, the rest being bare in the centres of mudboils. Vegetation and peat formed a 25 cm high ring around the boil (Fig. 4). Excavation showed the presence of peat-covered rocks under the rim but not in the central part of the mudboil.

In the central part of the mudboil thin, elongated layers of organic material were found at various depths. The material consisted of comminuted, somewhat humified vegetal organic matter. The layers appeared to be smeared into the mineral soil, without sharp boundaries. One of the layers was a loop of organic matter that appeared to be connected to the unexcavated rim, whereas the lower layer was probably connected to the excavated rim behind the excavated face.

Five till samples were collected between the surface and 50 cm depth. Between 12 and 34 per cent of the till consists of stones and gravel (larger than 2 mm fragments), and the matrix is a noncalcareous silty sand to loamy sand (Table 1). The organic layer was sampled at 57 cm below the surface, but 40 cm above the frost table. Another sample was taken from beneath the rim at 57 to 63 cm below the surface and 25 cm below the frost table.

Subduction Rates

In calculating subduction rates the soil residence age is ignored; that is, the material at the top of the subducted organic column is considered modern, or 0 radiocarbon years old. The distance that any piece of organic material has travelled down the column divided by its radiocarbon age gives the rate of subduction.

The effect of residence time of the organic material on the surface can be eliminated if the subduction rate is calculated between the dated sampling points. This assumes that the lower sample originated from the region of the upper sample, but the effect of initial age of the organic material is discounted.

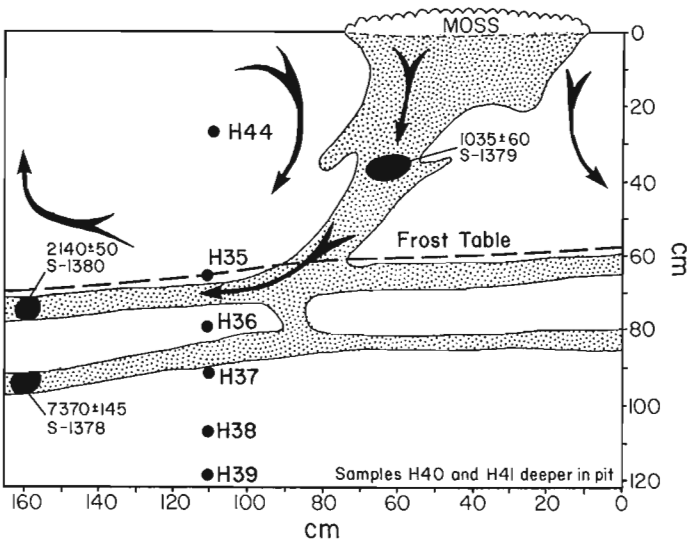

Figure 3. Field sketch of a section through part of Mudboil 2 and part of an adjacent mudboil; symbols as in Figure 2B.

Mudboil 1

Two samples from this mudboil were radiocarbon dated (Fig. 2). The upper sample came from an average depth of 52 cm, which corresponds to a distance of travel along the slightly inclined subduction path of about 56 cm. Dividing this by the age of the material, 2150 years, gives an average rate of subduction of 0.26 mm per year. The lower sample came from the base of the mudboil at an average depth of 85 cm. It had travelled about 110 cm along the inclined subduction path and yielded a radiocarbon age of 2730 years. The average rate of subduction is, therefore, 0.40 mm per year. The indicated average rate of subduction from the upper to the lower sample, a distance of 44 cm, is 0.92 mm per year.

Mudboil 2

Three samples from Mudboil 2 were radiocarbon dated (Fig. 3), but only two can be used to calculate subduction rates; the lowest sample (S-1378) has probably been immobilized within the upper permafrost for several thousand years due to permafrost aggradation. The uppermost sample came from an average depth of 45 cm, which is about 48 cm along the inclined subduction path. Dividing this by its age of 1035 years gives an average rate of subduction of 0.46 mm per year. The other sample came from an average depth of 73 cm but had been carried about 150 cm from its point of origin in the moss at the boil edge. The sample yielded a radiocarbon date of 2140 years. Hence, the average rate of subduction is 0.70 mm per year. However, the average subduction rate from the upper to lower sample, a distance of 102 cm in 1105 years, is 0.92 mm per year.

Mudboil 3

The organic material obtained from the rim of the mudboil from an average depth of 60 cm (Fig. 4) yielded an age of 1310 ± 80 years (BGS-501). The indicated average subduction rate from the surface is 0.46 mm per year. This figure, however, is a minimal rate, because the rate of accumulation and residence time of peat is not taken into consideration. The sample from the centre of the mudboil, about 190 cm from the edge of the rim, yielded an age of 3800 ± 80 years (BGS-402). The indicated average subduction rate from the rim to the centre is 0.76 mm per year.

Summary and Implications

The three mudboils studied occurred in materials that have low plasticity and can become liquefied at or slightly below their saturation point with water. Such soils are shock-sensitive (Zoltai and Woo, 1978), as spontaneous

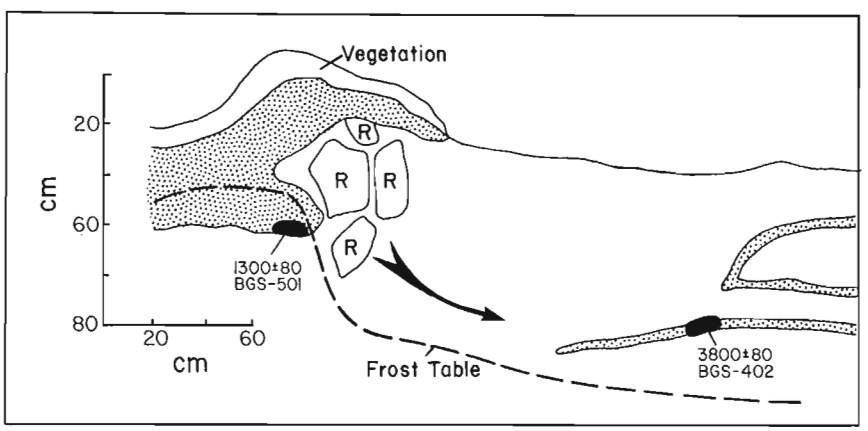

Figure 4

Sketch of a section through part of Mudboil 3; symbols as in Figure 2B; R represents rock.

liquefaction occurs upon disturbance, such as changes in internal pressure or external vibrations. The liquefaction is followed by rapid solidification as the disturbance is removed. The inclusion of organic materials indicates that the material of the mudboils flowed as a viscous, semi-liquid mass. The buried organic materials suggest a downward movement around the periphery of the mudboils and a possible upward movement in the centre.

The long term average rate of subduction of material is less than 1 mm per year. The calculated average subduction rate between samples is 0.92 mm per year – almost twice as high as the rate from the surface to the upper sample. This indicates either that the residence time of organic material at the surface must be taken into consideration or that subduction rates are slower near the surface than at greater depth. Both the structures and the subduction rates imply that the studied mudboils, and certainly many others in the central Arctic, have occupied the same sites for several thousand years.

References

Egginton, P.A.
1979: Mudboil activity, central District of Keewatin; in Current Research, Part B, Geological Survey of Canada, Paper 79-1B, p. 349-356.

Egginton, P.A. and Shilts, W.W.
1978: Rates of movement associated with mudboils, central District of Keewatin; in Current Research, Part B, Geological Survey of Canada, Paper 78-1B, p. 203-206.

Mackay, J.R.
1979: An equilibrium model for hummocks (nonsorted circles), Garry Island, Northwest Territories; in Current Research, Part A, Geological Survey of Canada, Paper 79-1A, p. 165-167.

Mackay, J.R. and MacKay, D.K.
1976: Cryostatic pressures in nonsorted circles (mud hummocks), Inuvik, Northwest Territories; Canadian Journal of Earth Sciences, v. 13, p. 889-897.

Shilts, W.W.
1978: Nature and genesis of mudboils, central Keewatin, Canada; Canadian Journal of Earth Sciences, v. 15, p. 1053-1068.

Tarnocai, C. and Zoltai, S.C.
1978: Earth hummocks of the Canadian Arctic and Subarctic; Arctic and Alpine Research, v. 10, p. 581-594.

Zoltai, S.C. and Woo, W.
1978: Sensitive soils of permafrost terrain; in Proceedings, Fifth North American Forest Soils Conference, ed. C.T. Youngberg, Fort Collins, Colorado, p. 410-424.

Zoltai, S.C., Tarnocai, C., and Pettapiece, W.W.
1978: Age of cryoturbated organic materials in earth hummocks from the Canadian Arctic; Proceedings, Third International Conference on Permafrost (Edmonton), v. 1, p. 325-331.

WANGOCERAS, A NEW NAME FOR PSEUDOTIBETITES TOZER 1980, NON JEANNET 1959 (CEPHALOPODA, TRIASSIC)

Project 670576

E.T. Tozer
Institute of Sedimentary and Petroleum Geology, Ottawa

Dr. Wang Yi-gang of the Nanjing Institute of Geology and Palaeontology, Academia Sinica, Nanjing, People's Republic of China, has kindly drawn my attention to the fact that the genus **Pseudotibetites** Tozer (1980, p. 110), for which the type species is **Pseudotibetites pax** Tozer, is a junior homonym of **Pseudotibetites** Jeannet (1959, p. 157), for which the type species is **Paratibetites (Pseudotibetites) tinkari** Jeannet. The new name **Wangoceras** Tozer (type species **Pseudotibetites pax** Tozer) is accordingly proposed.

References

Jeannet, A.
1959: Ammonites Permiennes et faunes Triasiques de l'Himalaya Central (Expedition Suisse Arn. Heim et A. Gansser, 1936); Palaeontologia Indica, New Series, vol. 34, number 1.

Tozer, E.T.
1980: New Genera of Triassic Ammonoidea; in Current Research, Part A, Geological Survey of Canada, Paper 80-1A, p. 107-113.

From: Scientific and Technical Notes in Current Research, Part B; Geol. Surv. Can., Paper 80-1B.

GEOLOGICAL SURVEY OF CANADA-ESSO MINERALS CANADA JOINT RESEARCH PROJECT

D.F. Sangster[1] and G. de Mille[2]

A research project on lead-zinc in carbonate rocks has been initiated as a joint venture between the Geological Survey of Canada and Esso Minerals Canada. Objective of the research, initially envisaged as a 3-4 year effort, is a better understanding of Canadian carbonate-hosted lead-zinc deposits, particularly the recognition of permissive areas and an understanding of the mechanism(s) of formation of the deposits. At present, the initial object of research is the determination of geochemical background values of approximately two dozen elements (major as well as minor) in selected carbonate formations.

The method of study is to sample, from core and/or well-exposed sections, selected carbonate formations. These will be chosen such that close stratigraphic, lithologic, and facies control can be maintained. The objective is to determine element distribution in a multifacies carbonate formation capable of being studied in three dimensions as in standard paleogeographic fence diagrams. Careful stratigraphic and contamination control will be maintained throughout by restricting sampling to only core or carefully selected outcrop sections; standard oil drilling chip samples will not be used.

Stratigraphers, geochemists, geostatisticians, and economic geologists from both organizations are participating in the project. Some initial sampling has already been completed and chemical analysis has begun. Publication of results will occur as soon as possible after the data are received; they will appear either as GSC Open File Reports and/or in future issues of "Current Research". A final, interpretive report will be published upon completion of the research project.

[1] Economic Geology Division, Geological Survey of Canada
[2] Esso Minerals Canada

DECOMPOSED GRANITE, BIG BALD MOUNTAIN AREA, NEW BRUNSWICK

Project 760008

Claude Gauthier[1]
Terrain Sciences Division

Introduction

Big Bald Mountain region of New Brunswick, with its extensive area of decomposed granite, is unique within the glaciated portion of North America. Despite abundant evidence of glacial activity present throughout the study area, features normally connected with prolonged weathering are surprisingly well preserved. Tors, weathering pits, and other surface features on the granite, in addition to thick grus, suggest a long weathering period. Despite the preservation of these easily destroyed features, till commonly overlies the grus, suggesting that active glacier ice has covered the area following alteration of the granite. This report presents a brief description of this area of "decomposed" granite.

Big Bald Mountain is located in the New Brunswick Highlands (Bostock, 1969) of north-central New Brunswick (Fig. 1). It is associated with the eastern extension of a large Devonian granitic batholith. The study area extends eastward and southward from Big Bald Mountain (47°11'40"N, 66°25'20"W) and comprises approximately 20 km^2 of exposed solid granite and grus accumulation (Fig. 2). Maximum relief is of the order of 150 m, with Big Bald Mountain at 675 m a.s.l. the highest point. This is one of six rock summits (average elevation 600 m a.s.l.) with low angle slopes surrounded by an undulating plain. Big Bald Mountain is the only summit with steep rock cliffs of sound granite that appears to be undergoing active dissection. In areas where the bedrock surface is at shallow depth, creeks are deeply entrenched (up to 20 m) in the unweathered granite. In areas where grus has accumulated, a shallow and broad valley has developed. South Sevogle River heads on the southeast side of these summits, which act as a trifold divide between the Sevogle, the Miramichi and the Nepisiguit drainage basins.

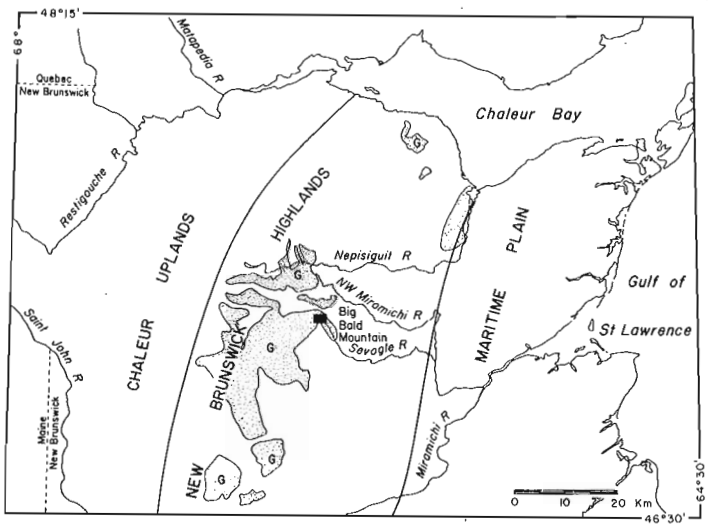

Figure 1. *Location map showing physiographic subdivisions (Bostock, 1969), major river systems surrounding the study area (black rectangle), and outcrops of granite (stippled) including Big Bald Mountain (modified from Potter et al., 1968).*

[1] Department of Geology, University of Western Ontario, London, Ontario N6A 5B8.

From: Scientific and Technical Notes in Current Research, Part B; Geol. Surv. Can., Paper 80-1B.

Bedrock has been mapped by both the Geological Survey of Canada (Anderson, 1969) and the New Brunswick Department of Natural Resources (McNutt, 1961; Fyffe, 1972a, b; Irrinki, 1972). The intrusive Devonian granite batholith with "chilled" margins is surrounded by greywackes, metabasalts, schists, and phyllites of the Ordovician Tetagouche Group. The homogeneous pink biotite granite in the Big Bald Mountain area is massive and coarse grained. In the southern part of the study area, the contact between granite and metasediments is shown by Anderson as being farther south (Fig. 2) than that shown by Fyffe and Irrinki who may have been influenced by the presence of metasedimentary erratics within the area of the batholith.

Studies in Progress

Following field work in 1978 Needham (1979) produced a brief description of the area. A second field season in 1979 included a seismic refraction program (R.M. Gagné, unpublished report, 1979), as well as systematic sampling of the surface material from shothole pits (0 to 5 m depth), dug with shovels and a powered auger. Three dimensional till fabrics were obtained at 10 sites from the walls of the shotholes. An overall detailed mapping and sampling program of the granite and the grus was also undertaken. Through geochemical analyses, weathering phases and stratigraphy of the grus are determined. All these data will aid our understanding of the type of granite weathering that has affected the area and of the geomorphological role of glacial activity.

Description of Rock Features

Sound granite is exposed on top of the six summits shown in Figure 2. This occurs in jointed blocks, undercut pinnacles, and isolated rounded knobs which in places resemble tors. These features are the most striking phenomena in the area; they stand out in the landscape, having local relief of up to 3 m. Figures 3 to 5 illustrate the variety of sizes and shapes of knobs on Colonels Mountain which has a major concentration of tors. The bedrock surface is coarse and rough, controlled by the high relief of individual crystals of the granite. A thin cover of grus laps up onto the sloping sides (5 to 15°) of the tors. The tors are well rounded, show evidence of exfoliation, and their orientation reflects the control of the regional fracture systems. The two regional fracture systems, trending at 045° and 140°, control the orientation of tor walls and alignment of the long axis of the features. The tors occur both as isolated features and in groups of several knobs of different size and surface characteristics.

Weathering pits (Fig. 6) are present on virtually all the granite summits shown in Figure 2. These basins vary between 20 and 150 cm in diameter and 2 to 50 cm deep. They commonly have overhanging walls. In places weathering pits are coalescent or are superimposed, with smaller ones formed in the base of older ones. The density of pits varies considerably from site to site. Summit 3 (Fig. 2) exhibits the largest concentration of weathering pits. They also occur as tafoni (cavities, with depth greater than diameter, formed by cavernous weathering) along steep sides of outcrops or tors. Rillen-like features (Fig. 7) have been observed at one locality along the south slope of Big Bald Mountain. They occur as repetitive rows of dimples, oriented towards the maximum slope direction.

Linear Rock Features

Trends of linear rock features based on different scales of observation are presented in Figure 8. The rose diagrams present a more realistic appraisal of orientations of linear features and relative density over a larger area than a

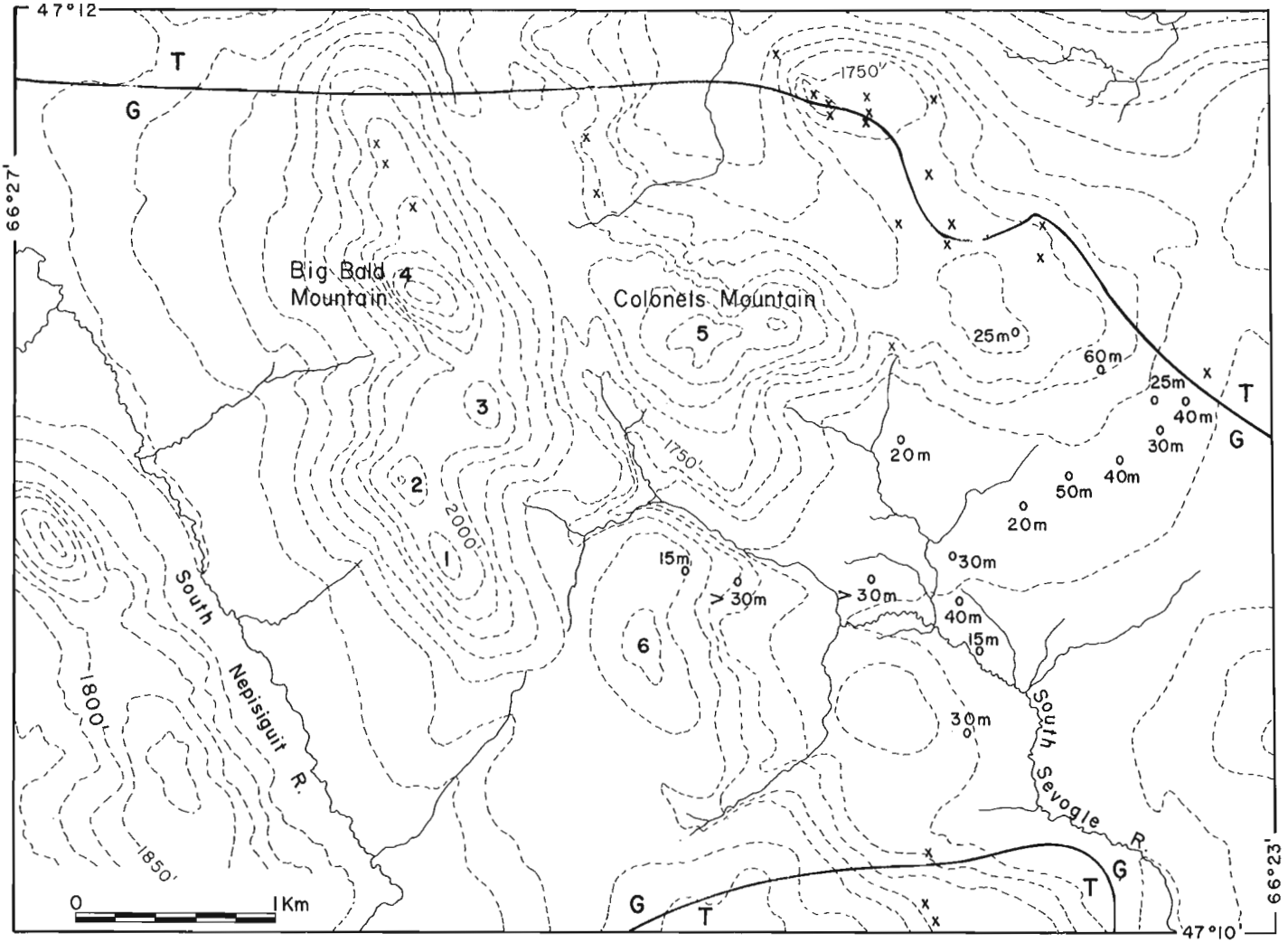

Figure 2. Topographic map (contour interval 50 feet) of the study area, showing the major summits numbered 1 to 6. Colonels Mountain (5) has the best developed tors; summit 2, the highest concentration of weathering pits; and Big Bald Mountain (4) has an actively exfoliating slope. Open circles represent seismic depth determinations, x's are outcrops, G is an area of granite, and T is an area of Tetagouche Group rocks.

standard numerical compilation. Summits, depressions, and straight fluvial stretches show similar alignments, predominantly at 150° to 180°; however more variation occurs in the alignment of straight fluvial stretches than of summits and depressions. The trends of lineations and of individual fractures measured on rock in different areas show strong similarity.

The difference between the pairs of rose diagrams A-B (alignments of summits and depressions and of water course segments) and C-D (lineations and rock fractures) is striking. Summits, depressions, and water course segments show a single dominant trend at 170°, as opposed to right angle dual trends at 050° and 140° for lineations and rock fractures. The right angle bimodal distribution of lineations and rock fractures is expected and corresponds to the distribution of fractures in a tectonic system, with stress vectors bisecting the two populations of fractures. The 170° structural orientation might be attributable to a regional tectonic trend, since this value also corresponds to the contact orientation of the granite batholith to the south. This 170° trend is not a dominant orientation in the smaller scale features.

Grus

Grus mantles the surface in areas of low relief (5 m), which are characterized by rolling topography. Grus consists mainly of granule and sand-sized angular quartz and feldspar crystals. Mineral grains in the grus remain of similar size to those in the sound rock. Limited mechanical breakdown has affected the individual crystalline fragments; polycrystalline agglomerate of various minerals account for less than 5% of the total fragments in the 0.5 to 1.0 mm grain size fraction. On average, the grus consists of more than 75% sand and less than 10% clay. From mineral counts on 35 samples of grus (fraction 0.5 to 1.0 mm) and 5 thin sections of sound rock, the ratios of quartz to potassium feldspar to plagioclase were 4:4:1 for grus and 2.5:2.5:1 for sound rock. In the small grain size fractions, quartz concentration decreased as the plagioclase increased; this reflects the mechanical and chemical resistance of quartz, concentrated in the larger fraction (1 mm), as opposed to the chemical susceptibility of plagioclase. The differences in mineral concentrations between grus and sound rock confirm this conclusion.

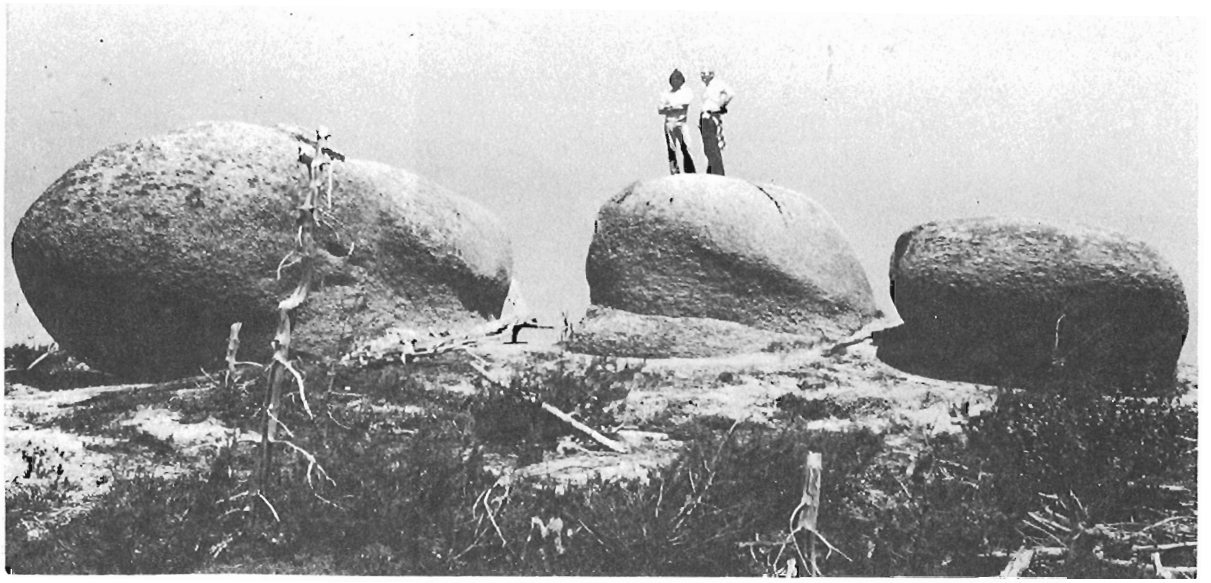

Figure 3. *A group of three woolsack tors on the sound granite summit of Colonels Mountain (summit 5, Fig. 2). View towards the northeast.*

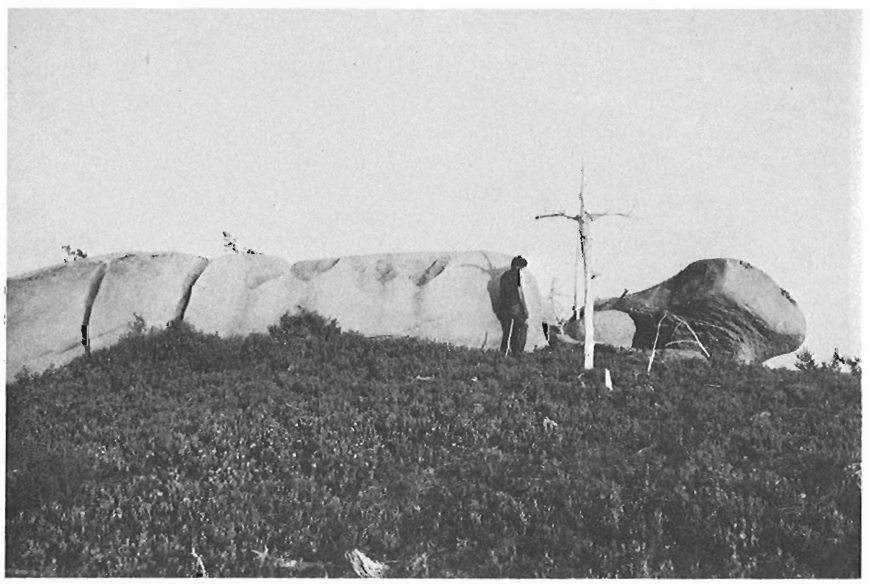

Figure 4

Elongated tor, oriented at 045° and cut by fracture planes at 140°, on Colonels Mountain. Weathering pits can be seen on the feature. Photograph taken towards the southeast.

The thickness of the grus mantle has been determined by seismic refraction and locally reaches 60 m (R.M. Gagné, unpublished report, 1979). The contact between high and low velocity layers is sharp (sound granite from 3960 to 6860 m/s, in situ grus from 1500 to 2740 m/s). This type of abrupt transition corroborates studies from tropical areas, where drilling and exposures indicate a transition zone less than 1 m thick between fresh granite and grus (Feininger, 1971; Ruxton and Berry, 1957). Seismic velocities in surface layers vary between 900 and 1300 m/s.

A siliceous glaze can be observed on thin grus mantles on hilltops. Erratics are scattered on them, but till is absent. Podzolic soil profiles are well developed, even in sloping areas, attesting to the present stability of the grus. Fresh and weathered flat outcrops and core rocks are present locally.

Till

Basal till was observed in most holes dug for seismic profiling. Systematic sampling of till and of underlying grus indicates that a high percentage of the erratic granules and pebbles in the till are fragments of parasedimentary, volcanic, and schist rocks, lithologies outcropping adjacent to the granite batholith. From preliminary results, a faint textural difference can be established between till and grus samples; granulometric curves show a lower sand content with respect to silt and clay in the till, in contrast with a higher sand content in the grus. Ten sites were selected for till fabric studies which showed an "a" axis orientation (070°-110°, dip 05°-14°) in accordance with other regional ice flow indicators.

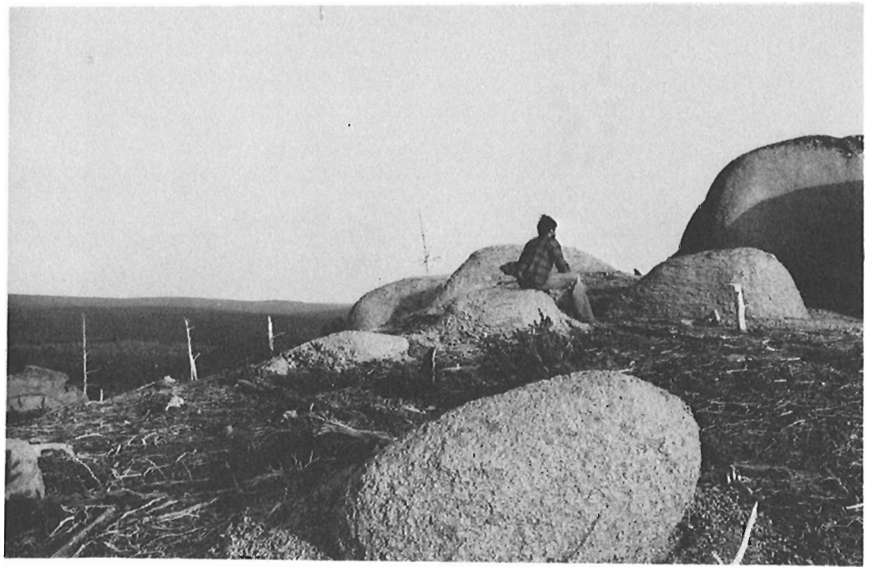

Figure 5

A family of tors on Colonels Mountain showing various degrees of weathering and development. Exfoliation layers are visible on most; grus mantles the ground surface. Photograph taken towards the southeast.

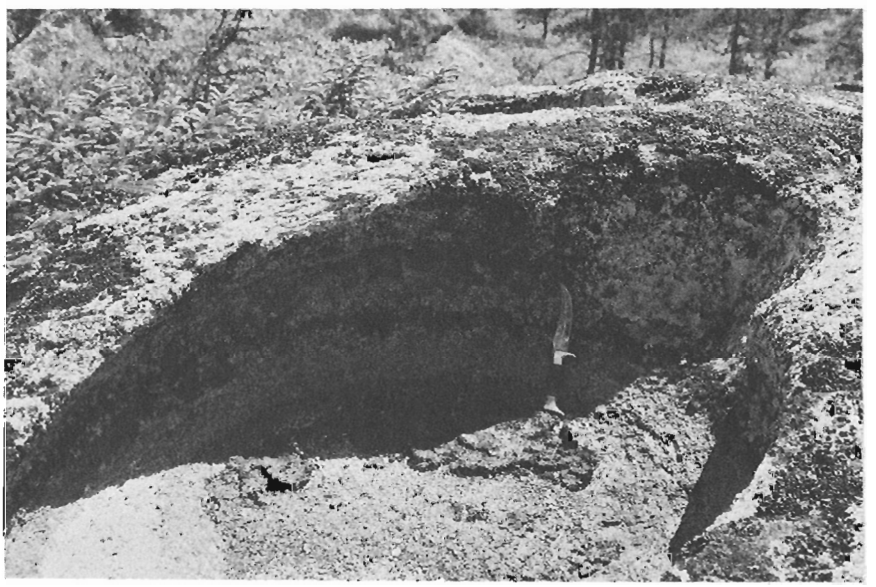

Figure 6

Subcircular weathering basin in coarse granite (summit 2, Fig. 2); knife is 25 cm long.

Figure 7

Successive rows of dimples (rillens?), some are branching, located on the south slope (inclination ~35°) of Big Bald Mountain at an elevation of about 635 m (2080 ft) a.s.l. The knife, 25 cm long, is oriented west-southwest towards the maximum slope.

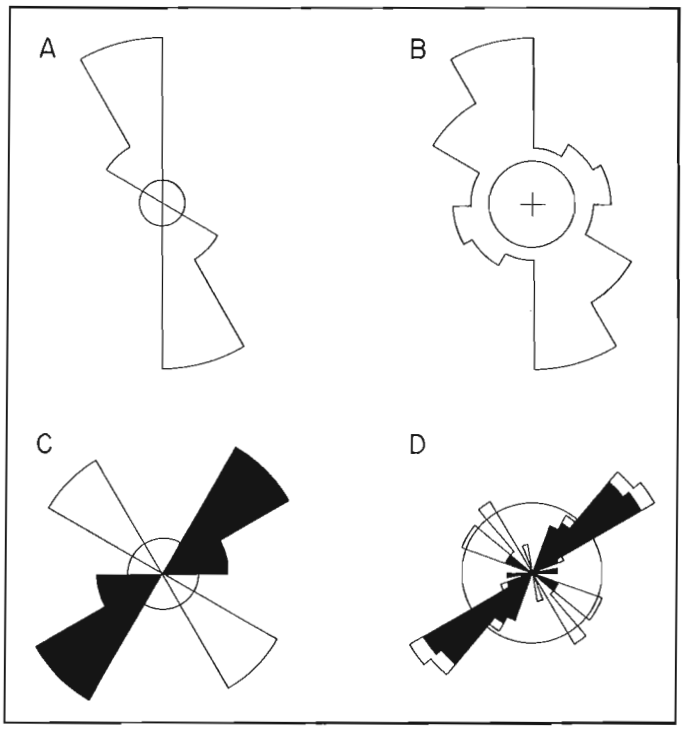

Figure 8. *Rose orientations showing orientations of fractures and linear features observed in the study area (Fig. 2). The radius of the inner circle is equal to 10% of the total weighted measurements. A: Large scale summit and depression alignments based on the 1:50 000 scale topographic map. B: Straight water course segments longer than 0.2 km weighted by the length of each segment (total length 82 km); compilation from 1:20 000 aerial photographs. C: Other lineations taken from 1:20 000 aerial photographs, weighted by their length (total length 12 km); dark area: Big Bald Mountain; light area: Colonels Mountain. D: Rock fractures measured on the ground (weighting factor varies from 1 for microfractures to 5 for rock walls larger than 50 m^2); 57 individual readings are presented for a total weighted population of 156 units; dark area from Big Bald Mountain, light area from Colonels Mountain. Data in A, B, and C are grouped in 30° sectors, those in D are at 10° intervals.*

Discussion: Glacial Implications

Tors and associated weathering phenomena have been described elsewhere in Canada, but the intensity of weathering and the amount of grus encountered in the Big Bald Mountain region is believed to be unique. Bostock (1966) noted the presence of tors as well as thin and discontinuous accumulations of grus in areas of pre-late Wisconsin surfaces in Yukon Territory. Dyke (1976) described a variety of tors from Somerset Island that either escaped glacial erosion, under a protective cold-based ice, or that were beyond the margin of late Wisconsin ice. Pheasant and Andrews (1972) reported tors on pre-late Wisconsin surfaces on Baffin Island. Sugden and Watts (1977) and Watts (1979) described two groups of tors from Cumberland Peninsula, a group below 750 m a.s.l. showing signs of some glacial erosion, and a group situated above the limit of glacial erosive activity, showing none.

The question of tor development is part of a debate centred around the weathering zones (Ives, 1978; Grant, 1977) as opposed to the idea of a cold- and warm-based ice (Sugden, 1978). The discovery of tors in central New Brunswick adds to our knowledge of tor distribution.

Surrounded by regions of strong glacial imprint (Gauthier, 1978, 1979, 1980), the New Brunswick Highlands, despite their low relief, present a contrasting set of geomorphic features where abraded rock surfaces, till, and weathering phenomena occur. Questions have been repeatedly raised in scientific literature concerning the absence of obvious glacial activity on the New Brunswick Highlands (Alcock, 1948). According to Gauthier's mapping, the Highlands consist of two types of areas: the low-lying areas, mostly valleys, show numerous evidence of glacial activity followed by glacial lake damming; in contrast, higher areas, including Big Bald Mountain, show evidence of limited glacial activity, and yet basal till and erratics are more or less ubiquitous. The pattern suggested to account for these observations is as follows: complete ice cover followed by a vertical deglaciation affecting the uplands of New Brunswick; meanwhile the borderlands (Chaleur Bay and Saint John, Nepisiguit, and Miramichi valleys) remain ice covered and are influenced by a multiplicity of independent, localized ice flows. This suggests that all parts of the area were occupied by active ice, but the Highlands were affected to a lesser extent and during an earlier phase than the lowlands. It also implies that most of the effective glacial erosion in the lowlands took place during the last late glacial period. Because of the intensity of weathering, Big Bald Mountain area is seen as representing a relict of pre-Wisconsin weathering. Other areas in New Brunswick present isolated profiles of similar weathering (Anderson, 1968; Lee, 1962); Anderson suggested that weathering may have been active as early as the Carboniferous Period in order to form the present profiles.

References

Alcock, F.J.
1948: Problems of New Brunswick geology; Royal Society of Canada, Transactions, v. XLII, Series III, p. 1-15.

Anderson, F.D.
1968: Woodstock, Millville, and Coldstream map-areas, Carleton and York counties, New Brunswick; Geological Survey of Canada, Memoir 353, 67 p.

1969: Geology of Big Bald Mountain, New Brunswick; Geological Survey of Canada, Map 1220A, scale 1:50 000.

Bostock, H.S.
1966: Notes on glaciation in the central Yukon Territory; Geological Survey of Canada, Paper 65-36, 18 p.

1969: Physiographic Regions of Canada; Geological Survey of Canada, Map 1254A, scale 1:5 000 000.

Dyke, A.S.
1976: Tors and associated weathering phenomena, Somerset Island, District of Franklin; in Report of Activities, Part B, Geological Survey of Canada, Paper 76-1B, p. 209-216.

Feininger, T.
1971: Chemical weathering and glacial erosion of crystalline rocks and the origin of till; United States Geological Survey, Professional Paper 750-C, p. C65-C81.

Fyffe, L.
1972a: Geology of lower North Branch Little S.W. Miramichi River; Mineral Resources Branch, New Brunswick Department of Natural Resources, Plate 72-80, Map M-10, scale 1:15 625.

Fyffe, L. (cont'd.)
1972b: Upper parts South Branch Sevogle River; Mineral Resources Branch, New Brunswick Department of Natural Resources, Plate 72-89, Map M-9, scale 1:15 625.

Gauthier, R.C.
1978: Quelques interprétations de l'inventaire des dépôts de surface, Péninsule Nord-est du Nouveau-Brunswick; dans Recherches en cours, Partie A, Commission géologique du Canada, Étude 78-1A, p. 409-412.

1979: Aspects of the glacial history of the north-central Highlands of New Brunswick; in Current Research, Part B, Geological Survey of Canada, Paper 79-1B, p. 371-377.

1980: Existence of a central New Brunswick ice cap based on evidence of northwestward-moving ice in the Edmundston area, New Brunswick; in Current Research, Part A, Geological Survey of Canada, Paper 80-1A, p. 377-378.

Grant, D.R.
1977: Altitudinal weathering zones and glacial limits in western Newfoundland, with particular reference to Gros Morne National Park; in Report of Activities, Part A, Geological Survey of Canada, Paper 77-1A, p. 455-463.

Irrinki, R.R.
1972: Upper parts of South Branch Sevogle River; Mineral Resources Branch, New Brunswick Department of Natural Resources, Plate 72-82, Map N-10, scale 1:15 625.

Ives, J.D.
1978: The maximum extent of the Laurentide Ice Sheet along the east coast of North America during the last glaciation; Arctic, v. 31, no. 1, p. 24-53.

Lee, H.A.
1962: Surficial geology of Canterbury, Woodstock, Florenceville, and Andover map-areas, York, Carleton and Victoria counties, New Brunswick; Geological Survey of Canada, Paper 62-12, 8 p.

McNutt, J.R.A.
1962: Upper parts North Big Sevogle and N.W. Miramichi Rivers; Mineral Resources Branch, New Brunswick Department of Natural Resources, Plate 61-2, Map N-9, scale 1:15 625.

Needham, R.B.
1979: Physical and chemical aspects of granite weathering in north central New Brunswick; unpublished B.Sc. thesis, McMaster University, 201 p.

Pheasant, D.R. and Andrews, J.T.
1972: The Quaternary history of northern Cumberland Peninsula, Baffin Island, N.W.T., Part VIII: Chronology of Narpaing and Quajon Fiords during the past 120 000 years; 24th International Geological Congress (Montreal), Section 12, p. 81-88.

Potter, R.R., Jackson, E.V., and Davis, J.L.
1968: Geological map of New Brunswick; New Brunswick Department of Natural Resources, Map NR-1, scale 1:500 000.

Ruxton, B.P. and Berry, L.
1957: Weathering of granite and associated erosional features in Hong Kong; Geological Society of America Bulletin, v. 68, p. 1263-1292.

Sugden, D.E.
1978: Glacial erosion by the Laurentide Ice Sheet; Journal of Glaciology, v. 20, p. 367-391.

Sugden, D.E. and Watts, S.H.
1977: Tors, felsenmeer, and glaciation in northern Cumberland Peninsula, Baffin Island; Canadian Journal of Earth Sciences, v. 14, p. 2817-2823.

Watts, S.H.
1979: Some observations on rock weathering, Cumberland Peninsula, Baffin Island; Canadian Journal of Earth Sciences, v. 16, p. 977-983.

NATURE AND DISTRIBUTION OF SAND AND GRAVEL, NORTHEASTERN MANITOBA

Project 750072

L.A. Dredge and F.M. Nixon
Terrain Sciences Division

Introduction

In northeastern Manitoba sources of coarse aggregate are geographically restricted. Many deposits are shallow, isolated, and contain aggregate of variable quality. In the past, the major use of sand and gravel was for roadbeds and building pads between the townsite of Churchill and a rocket range 23 km to the east, and along some portions of the Hudson Bay Railway (Canadian National Railways) which constitutes the only year-round ground link between the port of Churchill and southern transportation systems. Additional aggregate will be required for further economic development and for upgrading present facilities in the region. This note describes the nature of aggregate sources and shows their distribution for areas in Manitoba north of latitude 57° and east of longitude 96°. Data were compiled from airphoto interpretation and from 1978 field mapping of surficial deposits. Comments on texture and petrology are based on field observations of shallow (less than 2 m deep) boreholes and river cuts.

The principal sand and gravel deposits are eskers, kame moraine, and beach ridges, all of which are products of the last stages of glaciation and the postglacial marine episode. Minor deposits are associated with sandy till or alluvium. Figures 1 to 4, each covering one 1:250 000 National Topographic System (NTS) map area, show the distribution of sand and gravel, as well as bedrock outcrop. Major deposits occur along the northern coast, in a grand arc crossing the west half of the area, and in a band parallel to the east coast. Smaller linear deposits are found in a zone east of the railway, along the lower reaches of North and South Knife rivers and Owl River, and as small isolated patches. Bedrock outcrop, a potential source for crushed rock, is widespread in the northwest, but is otherwise limited to a single prominent ridge at Churchill and to exposures along upper Churchill River. The remainder of the area consists of deposits of silty till, lacustrine clay, and marine silt-clay, with a combined thickness commonly exceeding 15 m. About 90 per cent of the study area, including sand and gravel deposits, is overlain by wet, poorly drained forested bog, tundra peat, or fen. The region lies along the southern limit of continuous permafrost, but coarse grained deposits not overlain by peat are unfrozen in summer.

Acknowledgments

Serge Paradis, Department of Geography, University of Ottawa, provided data for the Churchill area east of 94°30'W and north of 58°30'N. Douglas Hodgson, Geological Survey of Canada, reviewed the manuscript.

Gravel and Sand Deposits

Eskers and Glaciofluvial Features

The esker that crosses Seal River (Fig. 1) is one of the major sources of sand and gravel. The deposit is a prominent linear feature approximately 10 m thick. It consists primarily of well sorted, stratified, medium to coarse sand with Precambrian granitic and gneissic lithologies, but small sections are composed of rounded cobbles. Other less extensive glaciofluvial masses are scattered over the map area (NTS 54 L). These also consist primarily of moderately to well sorted sand and gravel with Precambrian lithologies.

Large esker-like ridges are associated with meltwater channels along Churchill and Little Churchill rivers in the southwest corner of Figure 3 (NTS 54 E). These deposits exceed 10 m in thickness and appear (from airphoto interpretation) to contain large amounts of sandy material. Where examined on the ground, however, they consist of loose silty micaceous sand with a considerable amount of fine grained carbonate (strong reaction to HCl). This material grades downwards to poorly sorted sand and gravel, containing excess fines. The ridges may have sand and gravel cores, but this type of material was not found in the sections observed. Additional esker remnants (Fig. 3) are capped by lacustrine clay and may have a high volume of fines.

Modified esker remnants are present as broad flat ridges between Norton Lake and Marantz Lake (Fig. 2). They consist of massive sand and gravel, with high percentages of Precambrian clasts. Portions of some ridges and of local prominences (former moulins) are strewn with rounded cobbles, but generally the upper metre of these ridges consists of sorted, stratified beach sand, with lithologically mixed (igneous, metamorphic, and carbonate sedimentary clasts) gravels.

Kame Moraine

The largest continuous feature composed of coarse aggregate is a subdued ridge about 500 m wide and 2 to 15 m high which stretches for 200 km from South Knife River to Cooper Creek (Fig. 1, 3). The moraine consists of variably sorted ice contact material. Its surface has been subjected to reworking by littoral lacustrine processes and below an elevation of 130 m, by marine processes as well, so that beach ridges are prevalent along most of the feature. The texture and petrographic character of the moraine vary along its length according to differences in source rocks and the degree of subsequent modification.

In the extreme northwest the feature consists of up to 15 m of stratified medium grained sand; for the remainder of its length it consists of either massive or bedded, moderately sorted sand and rounded pebble gravel with few fines. Where the ridge has been reworked (i.e., below 120 m a.s.l.), the upper 2 m consists of beds of well sorted medium sand and small gravel clasts. This material grades downwards into less well sorted and more poorly stratified sand and gravel. In the north gravel-sized clasts consist entirely of Precambrian lithologies, including significant amounts of schists, phyllites, and basalt as well as the granitic and gneissic types mentioned above. South of Churchill River about 50 per cent of the gravels consist of Paleozoic limestone and dolomite.

For most of its length the feature is cored by silt-clay till; hence, the volume of sand and gravel is less than the volume of the morphological feature. The thickness of potential aggregate ranges from greater than 4 m (in the northwest) to about 1 m (in the extreme south).

Beach Ridges and Blanket Beach Deposits

Coastal Ridges. Extensive beach ridge sequences, formed during the postglacial emergence of the land, lie parallel to the present coast between Cape Churchill and Nelson River (Fig. 2, 4). The ridges are 10 to 20 m wide and 1 to 3 m thick; they consist of stratified sand and gravel mixtures, characteristically medium to coarse, sorted sand, and rounded pebble-sized clasts. About 90 per cent of the clasts are carbonate. The deposits grade laterally and vertically into silty marine sands.

From: Scientific and Technical Notes in Current Research, Part B; Geol. Surv. Can., Paper 80-1B.

Figure 1-4

Distribution of surficial sand, gravel, and bedrock outcrop in northeastern Manitoba. (Legend common to all figures.)

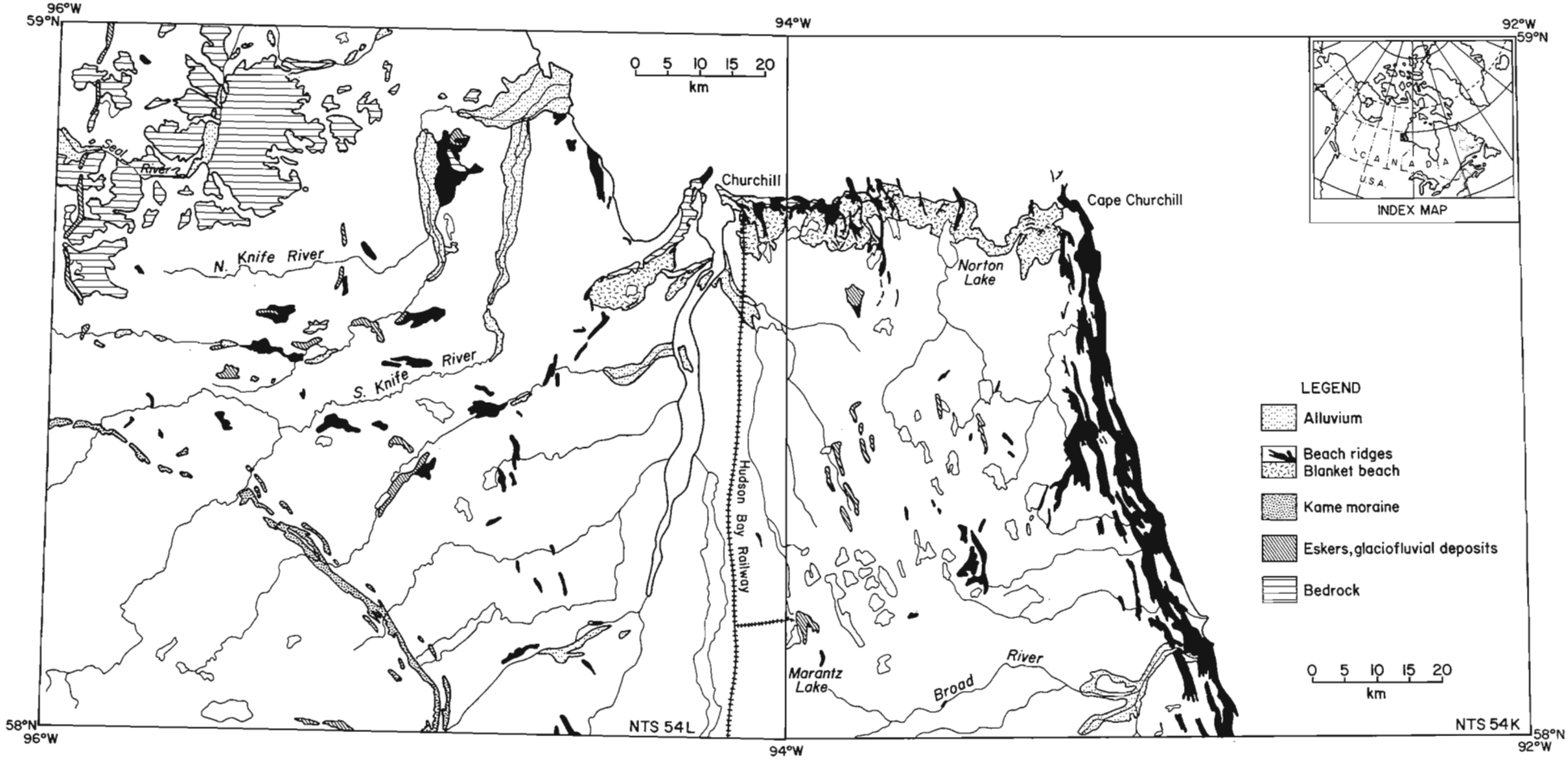

Figure 1 ***Figure 2***

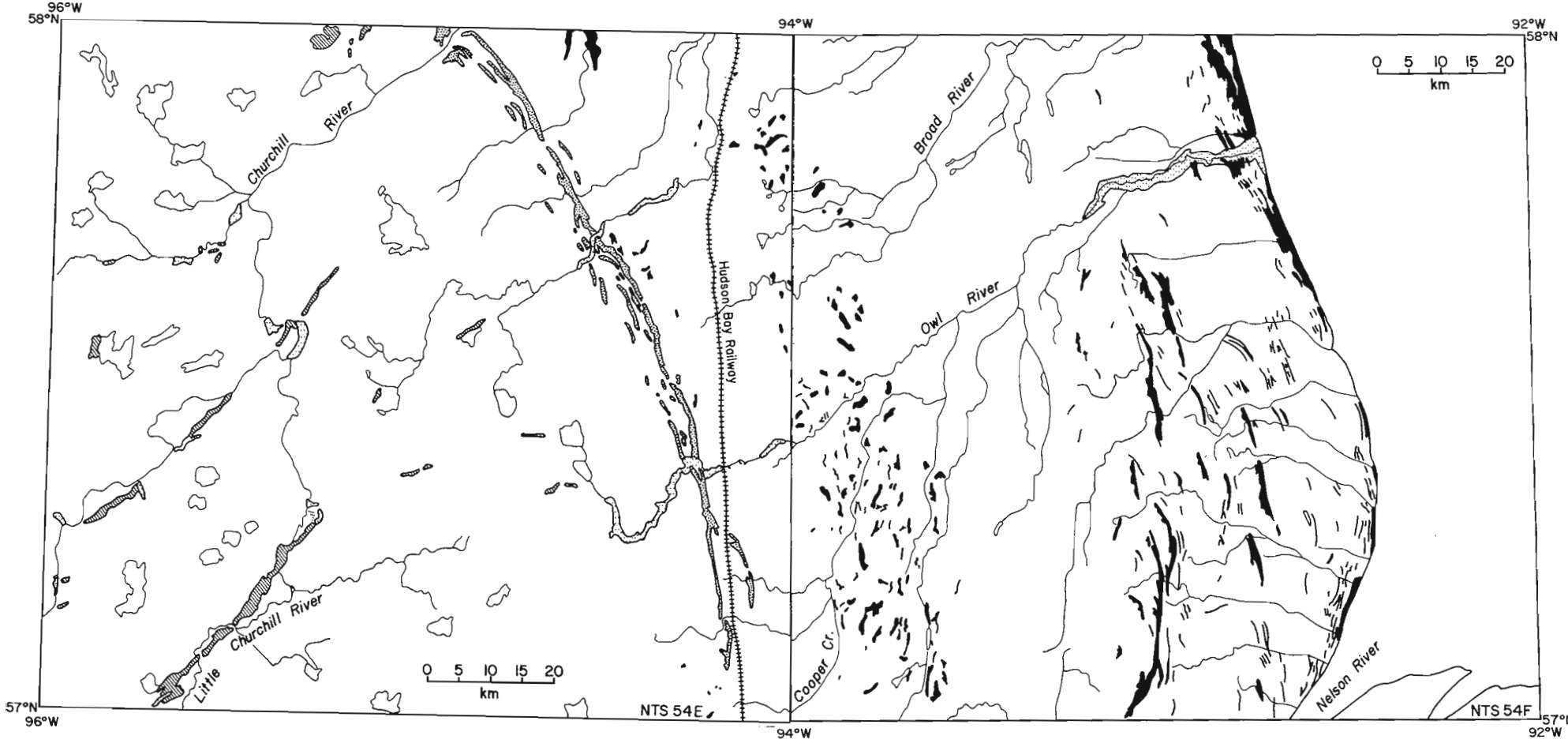

Figure 3

Figure 4

Inland Ridges. These ridges lie inland in a 40 km wide zone east of the railway and are chiefly found along the west boundary of NTS 54 F (Fig. 4). The linear deposits may have originated as ice contact stratified drift but later were reworked by marine processes and reformed into beach ridges. The deposits differ from regular beach deposits in that they are less sorted, are massive in places, contain some subangular or angular clasts, and consist of 10 to 40 per cent Precambrian lithologies. The granular deposits are generally 1 to 2 m thick and are underlain by clay till.

Blanket Beach Deposits. Blanket deposits of calcareous sand with minor gravel underlie much of the organic terrain below 150 m elevation. They are visible at the surface around the beds of drained tundra lakes in all areas east of the kame moraine. Rounded cobble gravel and sand occur as surficial materials in a zone along the north coast between Churchill and Cape Churchill (Fig. 1, 2). Despite their widespread occurrence, most blanket deposits are poor aggregate sources because they are commonly extremely shallow (less than 1 m thick), grade downwards rapidly into sandy silt or silt till, and are overlain by 2 to 4 m of permanently frozen peat.

Alluvium

Alluvial deposits are restricted to active channels and floodplains of the lower reaches of North and South Knife, Broad, and Owl rivers, to the Churchill estuary, and to small point bars (unmapped). Over most reaches major rivers are incised into either bedrock or till and do not have floodplains. The deltas of North and South Knife rivers consist of well sorted granitic sand and minor gravel. Owl River delta and Churchill estuary consist of poorly sorted subround limestone gravel and sand. Other alluvial deposits have a high silt component, contain organic-rich layers, or are extremely shallow.

Gravel deposits 1 to 3 m thick were observed in section along North and South Knife rivers and in some places along Churchill River. These deposits are dominantly massive gravels, with some sand and a few fines. They have Precambrian lithologies which are highly oxidized and which contain limonite and secondary products formed by the weathering of ferromagnesian minerals.

Alternate Sources of Aggregate: Crushed Rock

Bedrock outcrop is extremely limited in this region, the main areas being in the northwest (Seal River area), around Churchill, and along Churchill River. Outcrop in the Seal River area consists of medium grained granitic gneiss and quartz monzonite. Typically it has a blocky joint structure and splits or frost shatters into blocks 0.5 to 2 m on a side. Little surface chemical weathering occurs. The ridge at Churchill is characterized by grey, fine- to medium-grained quartzose metasedimentary rock (subgreywacke) containing hematite laminae and minor amounts of sericite and chlorite. This rock type is subject to some frost heaving. Cemented limestone and dolomite of Silurian and Ordovician age outcrop in section along Churchill River.

STUDIES IN QUATERNARY GEOLOGY: AN APPROACH USING REMOTE SENSING INFORMATION

Project 780035

J.R. Bélanger
Terrain Sciences Division

Introduction

During the past year Terrain Sciences Division has initiated a project to evaluate the possibilities of using remote sensing data in Quaternary geology studies. The objectives of the project are to survey the various sources of remote sensing information and the techniques of processing and displaying data, and to study the use of remote sensing in geological research mainly as it applies to the Canadian context.

Once the initial survey was completed, a more detailed study of selected sources of information and processing techniques was undertaken. This report describes 1) the sources of remote sensing information used, 2) the approach used to analyze the MSS video data, and 3) how the data will be used in projects related to Quaternary geology. All computer software developed for this project is available from the author. The programs are written in FORTRAN using the Computer Science Centre CDC computer and NOS/BE Operating System.

Source Data

Both airborne and space flight data have been evaluated as sources of remote sensing information. Although airborne operations offer advantages, such as fine resolution and numerous sensors, the prohibitive costs of data acquisition and of processing time limit its use to special and localized projects. On the other hand, the coarse resolution of the multispectral scanners of Landsat[1] and the frequent passes of the space craft over the country provide an inexpensive source of data that can be used for large scale studies and for remote areas which would be difficult to reach using airborne operations.

The MSS data are available in digital form on Computer Compatible Tapes (CCT). The format permits analysis of the video data using in-house computer facilities. This approach allows for more control and a better understanding of the data by the user.

The first step in processing the original information is to transform the bit structure of the CCT to CDC standards. This operation is essential because the original recording is done using an 8-bit configuration compared to the 6-bit structure of the Computer Science Centre computer. When decoding the original tape, only the MSS video data are conserved, by-passing the header and transformation records and tables. This section of the tape is by-passed since all pertinent information is given on a listing accompanying the CCT. The transformation program, called CCRSDEC, is written in FORTRAN and uses many CDC dependent features.

Histograms

The role of histograms in remote sensing is to display the frequency distributions of reflectance levels of pixels. Analysis of histograms is of importance in the early stages of a study in order to be acquainted with the type of distribution pattern of the reflectance levels for the area of interest. The use of histograms facilitates the discrimination of ground features based on their spectral signature using enhancement techniques.

[1] The Landsat scenes are formed of pixels corresponding to an area on the ground of 57 by 79 m.

Figure 1 shows examples of histograms produced by a computer program developed for this project. They show two distribution patterns for the Thetford Mines, Quebec area for different dates; note how much the distribution pattern of reflectance levels of a given area can vary from one season to another. In this case, the variation is due mainly to seasonal changes of vegetation. In the summer scene (Fig. 1a) the healthy vegetation reflects the near infrared to a higher degree than the senescent vegetation (Fig. 1b) of the autumn scene.

Pixel Classification

The purpose of pixel classification is to form broad spectral classes from individual spectral signatures. It is necessary to group similar signatures into larger classes since the intensities for each of the four MSS bands vary from 0 to 255, thus giving a possible 256^4 single signatures, which would make the analysis and cartographic display virtually impossible.

Two different approaches are used for pixel classification: supervised and unsupervised methods. Unsupervised classification groups classes of similar signatures based only on statistical characteristics. Supervised methods use sample areas for which a spectral signature is defined based on ground or other information.

Both supervised and unsupervised classification schemes are used in this project for the analysis of remote sensing information.

Unsupervised Maps

Unsupervised maps resulting from this project provide documents on which the maximum amount of spectral information can be portrayed. Although not all spectral features on the maps may be of importance in geological studies, it is important to enhance all spectrally separable phenomena because they can bring out features that could otherwise be overlooked. Furthermore, the use of unsupervised classification eliminates the problems of choosing representative sample areas and of class overlap and variability by discriminating classes according to their spectral characteristics rather than from ground information.

Unsupervised maps are produced prior to the field season in order to give an overview of the study area from a remote sensing standpoint and to identify sites that could serve as indicators to the geology. The maps are then taken into the field to locate the pixels and thereby study the influence of geological factors on the Landsat imagery.

A large number of mathematical algorithms exists to group individual signatures into broad classes. Most of these algorithms rely on finding areas of high pixel density (statistically cohesive clusters in feature space) which are separated by regions of low density (Alföldi, 1978). The problem with cluster algorithms is to define a proper threshold value to separate the significant classes. Since the classification relies only on mathematical assumptions, the classes formed do not necessarily relate to ground reality and minor classes may be ignored. Another pitfall lies in the grey zones located between the major clusters; because each class is identified as being discrete, there is no smooth transition between adjacent classes.

The method used to produce unsupervised maps is a multiband classification (three bands) where the class limits depend on the combination of subclasses which are defined for each band. This is obtained by assigning a primary colour to each band, by dividing the band into subclasses (maximum of 17) according to their reflectance level, and by assigning a colour intensity to each subclass of the band. The histogram

From: Scientific and Technical Notes in Current Research, Part B; Geol. Surv. Can., Paper 80-1B.

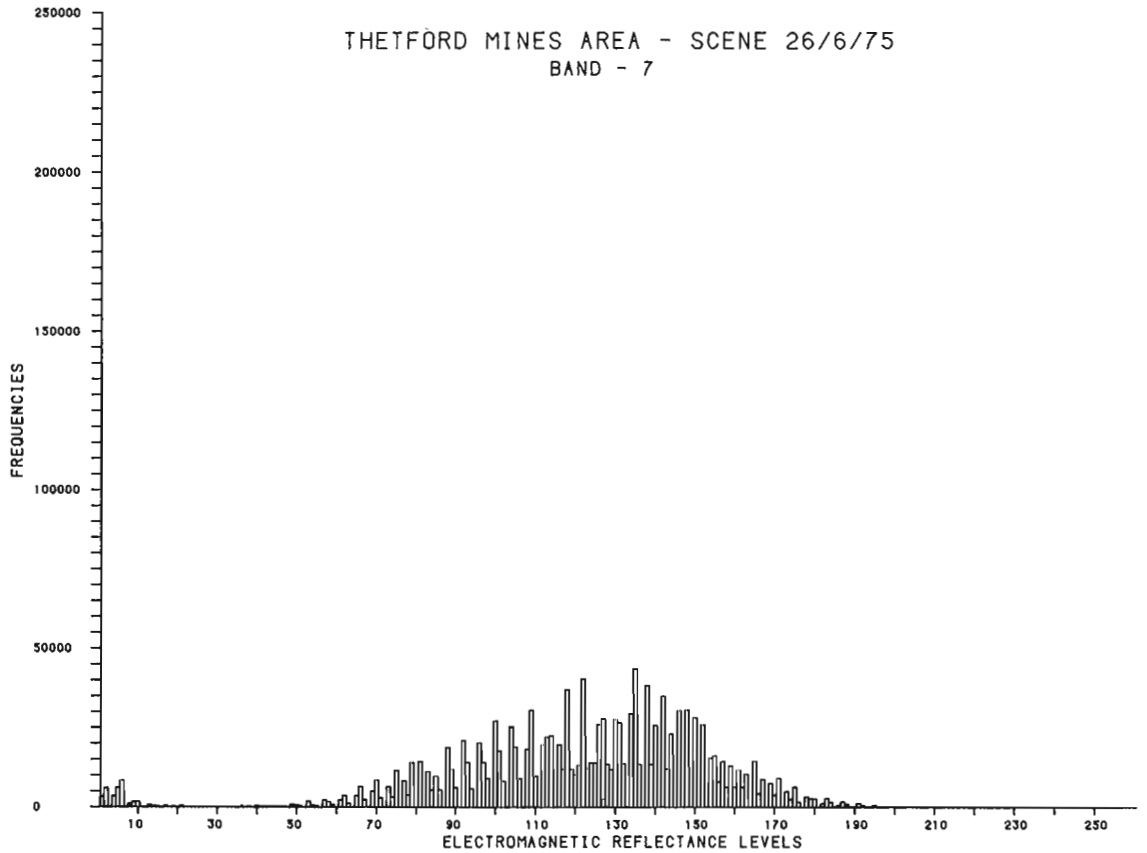

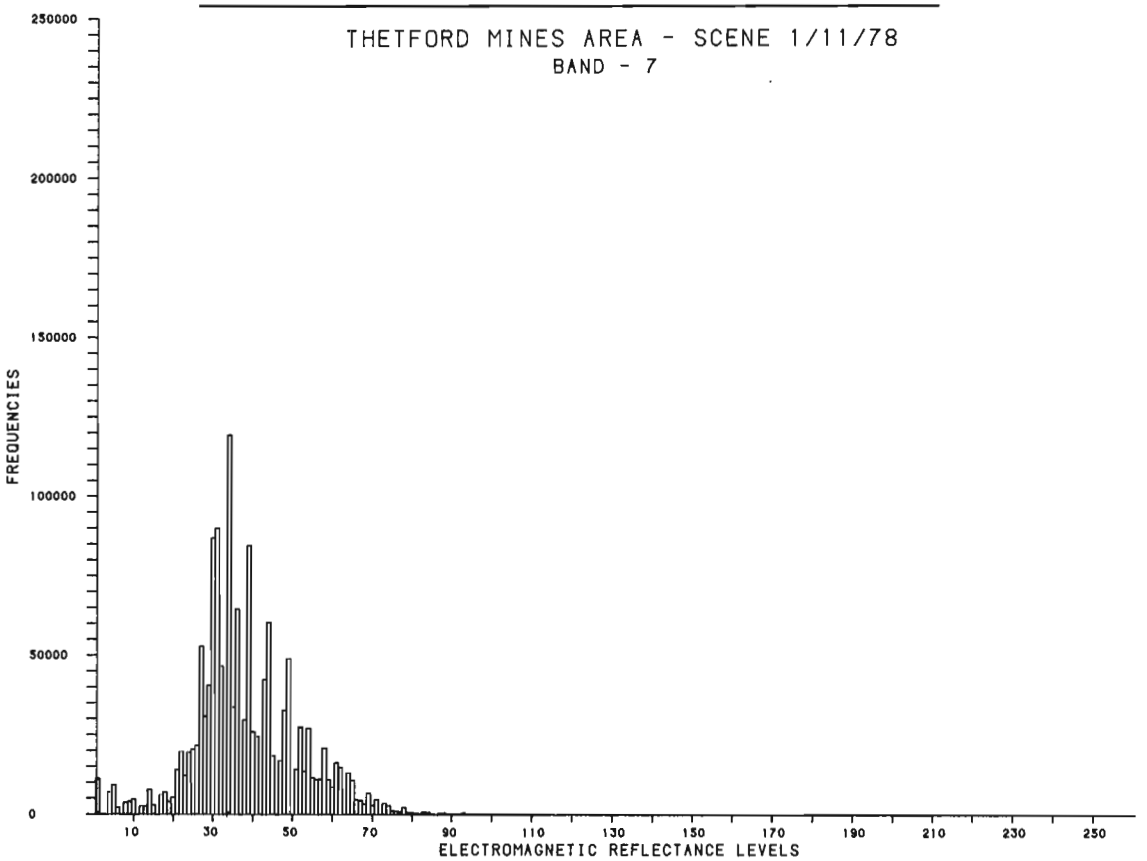

Figure 1. *Histograms of Band-7 from a Landsat scene taken over the Thetford Mines area of Quebec on June 26, 1975 (1a) and November 1, 1978 (1b). Note the variation in distribution of reflectance levels for the two seasons.*

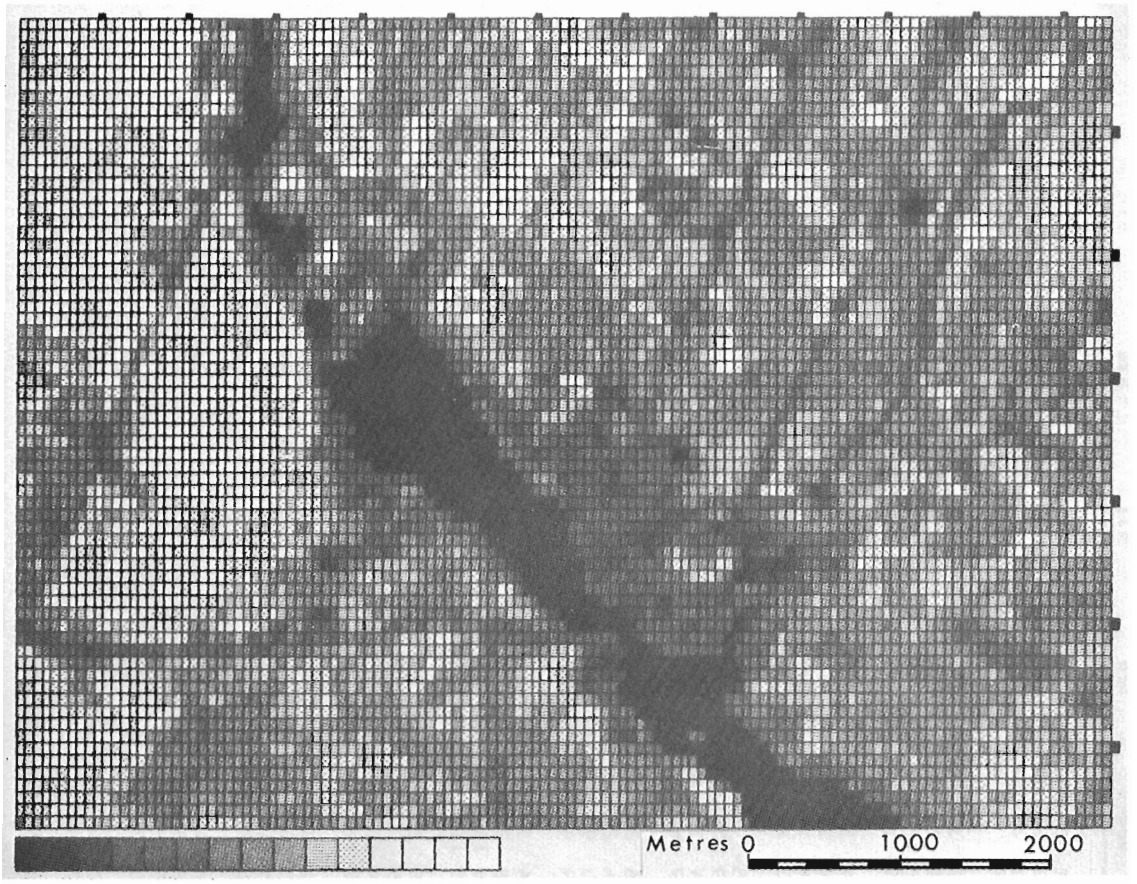

Figure 2

Example of a pixel location map; each rectangle on the map corresponds to a Landsat pixel.

for each band is used to assign an equal number of pixels to each subclass, which permits better enhancement of the high frequency levels. Because the classes are formed by combining subclasses from each band, a smooth gradation is obtained between the major classes, revealing the minor classes.

The maps are produced on an Applicon Color plotter using the software operating at the raster scan level. Software has been developed to produce maps at scales of 1:285 000, 1:250 000, and 1:125 000 using a maximum of 100 possible classes and at scales of 1:71 250, 1:50 000, and 1:25 000 permitting a maximum of 17 x 17 x 17 subclass combinations.

Supervised Maps

Once a preliminary study using unsupervised maps has been completed, the second stage is to reduce the number of spectral classes in order to produce a document on which only the phenomena of interest are presented. This is achieved by relating spectral signatures to ground information and then by eliminating the minor or insignificant classes.

The first step in supervised classification is to locate the pixels on the ground to correlate their signature with ground data. To do this, a pixel location map and a listing of the reflectance values are necessary.

The pixel location map (Fig. 2) is produced on the colour plotter at 1:50 000 scale so that the map can be used as an overlay on a standard National Topographic System (NTS) map. Once the pertinent pixels are identified, i.e., scan line (row) and pixel number (column), a listing of reflectance levels for different MSS bands for each pixel is produced (Fig. 3).

Next, spectral classes are created based on ground information. A number of training samples are selected and analyzed to evaluate the separability of the classes and to find the statistical parameters of each class. Both parametric and nonparametric methods are used to classify pixels.

The classification scheme produces three confidence levels for spectral classes: high confidence, intermediate, and unclassified pixels. The classes of intermediate confidence relate to the high confidence classes but have a lower confidence level. By including classes of intermediate confidence, the user can interpret the classes based on experience and context.

Application

Studies in remote sensing currently are being applied to three different aspects of Quaternary research: the study of geobotanical indicators in drift prospecting, erosion and sedimentation in a drainage basin, and mapping of surficial materials.

A study of geobotanical indicators is being conducted in the Thetford Mines area of Quebec to evaluate the effect of high concentrations of certain metals on species composition and vigour of vegetation and to determine how metal-induced vegetation anomalies are reflected in Landsat imageries (Bélanger et al., 1979). This region was chosen because of the ideal context offered by the presence of large ultrabasic outcrops which were partly eroded during the last glaciation forming a train of debris rich in heavy metals, particularly nickel.

```
**********************************************************************************************************************************
                                        REFLECTANCE VALUE  MAP - G.S.C. - T.S. - 1979
**********************************************************************************************************************************

+++++ TITLE = THETFORD MINES AREA - SCENE OF JUNE 26, 1975

          +++++ SCAN LINES TO BE LISTED ARE, FROM  560 TO  569

          +++++ PIXEL   510 TO   539 ON EACH SCAN LINE WILL BE LISTED


---------------------------------------------------------------------------------------------------------------------------------
        510         513         516         519         522         525         528         531         534         537
---------------------------------------------------------------------------------------------------------------------------------

560 -   35  38  35  35  38  35  35  35  35  38  41  51  44  33  30  33  30  30  33  33  38  41  48  54  41  35  35  35  38  38
        25  27  25  25  25  25  25  25  25  27  30  51  45  22  22  22  22  22  22  25  30  33  42  51  30  25  25  25  25  27
       109 105 109 114 109 105 109 119 114 114 119 105  82  34  21  23  21  19  21  45  85  92  92  96 100 105 105 105 109 119
       122 126 137 137 122 118 137 149 137 141 137 107  69  16   8   8   4   4   8  50  99 107  92  96 126 122 126 122 126 141

561 -   35  35  35  35  35  38  38  38  38  35  38  40  51  45  35  33  30  33  35  42  45  42  40  45  45  40  35  35  38  38
        25  25  23  23  23  25  23  25  25  25  28  33  48  39  25  23  23  23  30  36  39  36  33  45  42  33  25  28  25  25
        95  99 107  99 103 103 103 111 116 122 116 116 107  95  60  25  19  23  56  99  91  87  99  91  79  83  95 107 116 127
       107 123 127 123 119 115 123 143 131 143 135 123 107 100  49  13   5   9  52 107 103 100 103  92  88  92 107 127 139 151

562 -   36  39  36  36  36  39  36  36  36  36  36  39  42  47  39  36  33  42  44  42  36  36  36  39  39  44  42  33  36  39
        26  26  24  24  24  26  24  26  26  24  24  29  38  45  29  32  26  38  41  32  26  24  29  32  32  38  29  24  24  26
       116 116  98  90 103  98 103  98 103 107 103 120 107 103  94  79  30  62  90  90 107 111 103  94  94  82  98 107 116 120
       134 139 113 108 117 121 121 121 126 126 121 143 130 113 113  78  18  65 100 104 117 134 121 113 104  87 108 121 134 134

563 -   37  37  37  37  37  37  37  37  34  37  37  40  48  54  45  42  37  42  48  40  34  34  37  42  37  37  42  42  42  45
        24  27  24  24  24  24  24  24  27  27  27  27  39  49  39  36  32  39  42  27  24  27  27  30  27  30  36  30  39  39
       121 132 116 102  98 102  94  94 102 106 111 116 111 102  94  78  48  74  98  98 111 121 121 102 102  98  94  98 102 102
       147 159 134 121 112 121 108 112 117 125 129 138 125  99  99  82  39  87 104 121 142 142 142 117 117 112  91 117 108 112

564 -   34  36  36  36  36  36  36  36  44  50  50  47  39  36  39  34  32  36  41  41  44  44  44  41  41  44  47  44  41
        28  26  26  21  26  26  26  28  26  43  53  46  37  26  26  28  23  26  31  31  34  37  34  34  31  31  37  46  34  34
       132 121 110 106 106  98  94  94 106 106  98 102 106 121 110  90  41  62 106 110 115 115 126 115 106 110 106  94  94  94
       161 145 141 129 125 113 105 109 121 113  97  97 113 137 129  97  40  76 125 137 129 133 145 133 121 121 113  97 105 101

565 -   36  39  36  36  33  36  36  36  36  36  39  42  39  36  36  39  36  29  31  36  42  44  39  44  44  47  44  44  42  39
        26  26  23  23  23  26  26  23  28  26  28  37  28  26  28  28  26  21  23  28  37  39  34  37  39  39  37  39  31  26
       125 114 101 101 105 110 110 101  97 101 105 105 110 114 120 101  45  18  35  86 105 110 114 114 110 114 120 105  97  97
       149 141 112 112 128 124 128 120 116 120 124 120 133 137 145 112  41   7  32  91 120 124 133 128 120 128 133 116 108 103

566 -   35  35  35  38  35  35  35  35  38  38  41  41  44  38  35  38  41  33  30  30  30  30  30  33  44  48  44  41  44  38
        25  25  25  22  25  25  25  25  27  30  36  36  33  27  25  30  33  22  20  20  22  25  22  27  39  39  36  33  36  30
       119 119 109 105 105 109 109 109 109 109 100 100 114 114 114 109  75  25  17  19  27  42  27  61 105 114 105  96  96 114
       141 137 130 126 122 134 134 134 126 122 103 111 134 141 137 122  61   8   4   8  23  31  16  77 126 122 118  99  99 130

567 -   38  38  35  38  40  45  48  42  40  45  45  38  38  42  42  38  42  38  30  30  30  28  28  30  38  45  45  40  38  42
        25  25  25  25  28  39  45  39  30  39  39  25  28  33  33  30  33  25  21  21  21  21  21  21  28  36  39  33  30  42
       127 116 111  99  99 107 111 107 107  99  99 111 116 107 111 111 107  53  14  19  19  16  16  25  79 111 103  79  75 107
       151 147 127 107 115 123 127 119 119 107 107 135 139 135 123 131 119  45   1   5   1   5   5  17  96 127 111  76  80 123

568 -   36  39  39  39  39  42  44  44  44  47  44  39  36  36  36  44  44  44  42  31  28  31  31  31  33  36  42  44  50  44
        26  26  26  26  29  32  32  38  41  41  35  24  26  24  26  38  38  41  38  21  21  21  21  21  24  26  29  38  45  35
       128 120 116 120 120 111 103 111 107 103  98 111 116 103 116 120 116 111  72  22  15  17  19  32  70 107 133 116  90  94
       160 147 139 139 134 117 121 121 117 113 108 139 139 126 143 134 130 121  65   9   5   9   5  26  74 134 156 126  95 108

569 -   37  37  37  37  42  45  48  48  48  45  37  37  34  37  37  40  45  48  48  40  29  29  32  40  40  34  40  45  51  51
        24  24  27  27  39  46  46  46  46  39  27  24  24  24  27  30  42  46  39  32  19  19  21  30  27  24  30  36  49  52
```

Figure 3. *Computer printout showing the reflectance values for the four MSS bands. Pixel 560 (row) and 510 (column) corresponds to the pixel located on the upper left hand corner of Figure 2.*

Erosion and sedimentation problems triggered by man's activities in the Swan Hills area of Alberta is a matter of major concern because of their high impact on the environment. A remote sensing study, using Landsat data, is being conducted in order to evaluate its potential to monitor erosion problems.

Mapping using Landsat data has been attempted in numerous fields of activity. Because Landsat imageries reflect bedrock lithologies, vegetation types, and moisture conditions associated with surficial materials, the resulting maps show a wide variety of phenomena of which only a small portion may be related to the theme of a particular study. A pilot project aimed at integrating related phenomena, such as vegetation with the nature of the surficial materials, so that the final maps are oriented mainly towards Quaternary geology is underway. The mapping project using remote sensing data is being undertaken in the Kaminak Lake area, District of Keewatin, because this area has already been mapped in appropriate detail using conventional airphoto interpretation and field mapping techniques.

Remote sensing can be applied to a variety of activities in Quaternary geology. Although not an end in itself, remote sensing can be used advantageously to facilitate and increase the efficiency of currently used approaches to terrain studies. The use of in-house computer facilities to analyze and display remote sensing information permits a better control and understanding of the data by the user and also permits the development of programs specifically designed to meet the needs of a project.

References

Alföldi, T.T.
1978: Introduction to digital images and digital analyses techniques; Canada Centre for Remote Sensing (CCRS); Technical Note 78-1, Energy, Mines and Resources.

Bélanger, J.R., Rencz, A.N., and Shilts, W.W.
1979: Patterns of glacial dispersal of heavy metals as reflected by satellite imagery; Télédétection et gestion des ressources, Association québecoise de télédétection, Ste-Foy, P.Q.

NEW EVIDENCE ON THE ORIGIN OF THE SEPTEMBER 6, 1978 JOKULHLAUP FROM CATHEDRAL GLACIER, BRITISH COLUMBIA

Project 780045

Lionel E. Jackson, Jr.
Terrain Sciences Division
Calgary, Alberta

Introduction

On September 6, 1978, a jökulhlaup from Cathedral Glacier triggered a debris flow which closed the Canadian Pacific Railroad mainline and the Trans Canada Highway (Fig. 1) in Kicking Horse Pass, British Columbia (Jackson, 1979). Furthermore, evidence was presented indicating that Cathedral Glacier had produced jökulhlaups in 1925 and 1946, but no definite cause for the events was determined. A small lake on the margin of the glacier, however, was implicated as being the source of jökulhlaup waters. Possible causes for the jökulhlaup involve progressive modification of the hydrostatic conditions which permit the lake to form or a through-going system of fissures which could open suddenly and allow drainage (Jackson, 1979).

In order to shed further light on the origin of these jökulhlaups, a helicopter visit was made to the lake on September 13, 1979 in the company of Dr. B. Leeson of Parks Canada and Messrs J. Edworthy and M. Bourns of Snow and Ice Division, National Hydrology Research Institute.

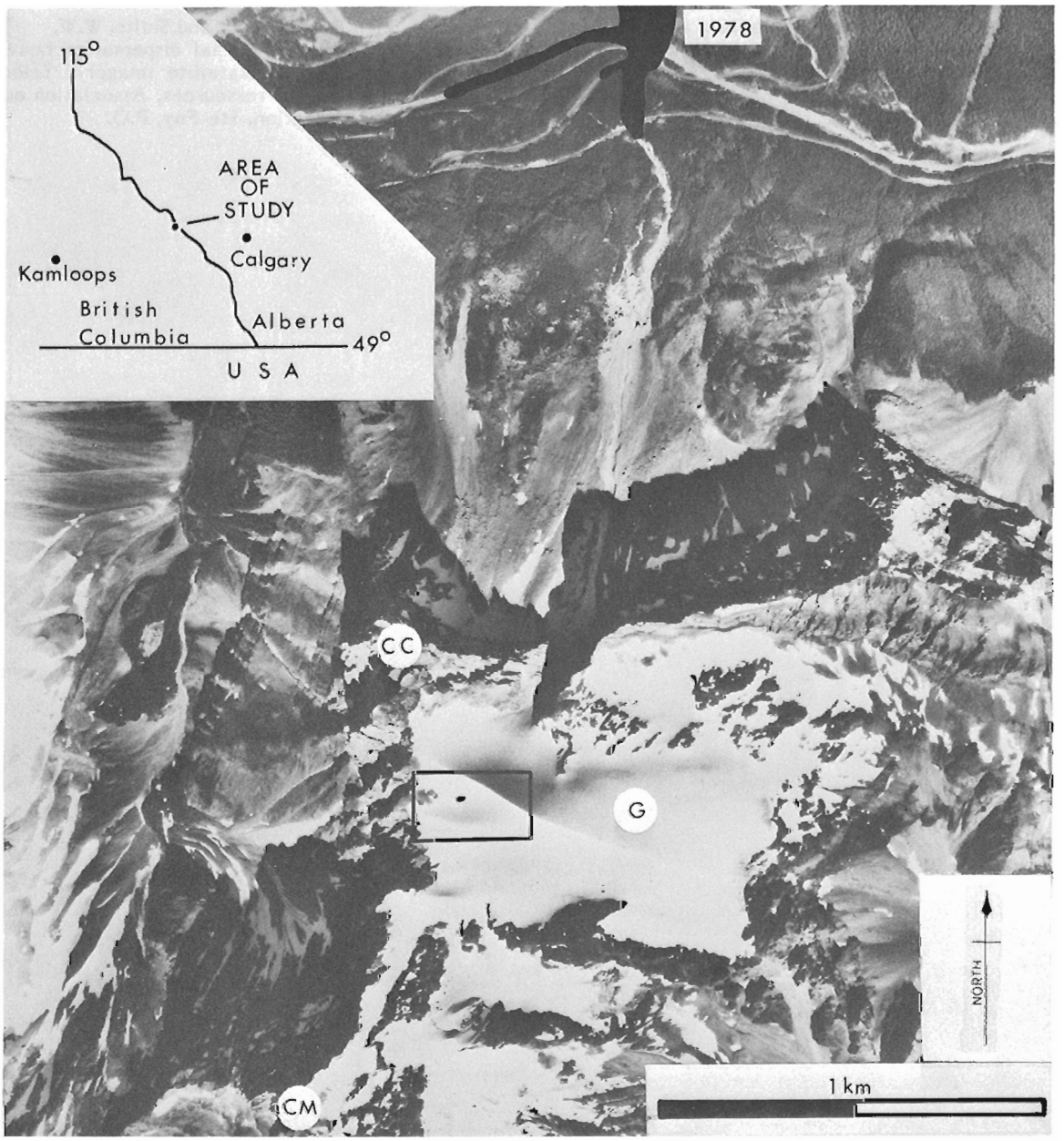

G - Cathedral Glacier *CM - Cathedral Mountain* *CC - Cathedral Crags*

Figure 1. *Aerial photograph of the Cathedral Glacier area. The rectangle includes the bowl-like depression in which the glacial lake is located. The lake was touched up to appear darker on this photo. 1978 refers to the dark area to the west which indicates the general area of Kicking Horse Valley affected by the 1978 debris flow. (NAPL A23408-73)*

From: Scientific and Technical Notes in Current Research, Part B; Geol. Surv. Can., Paper 80-1B.

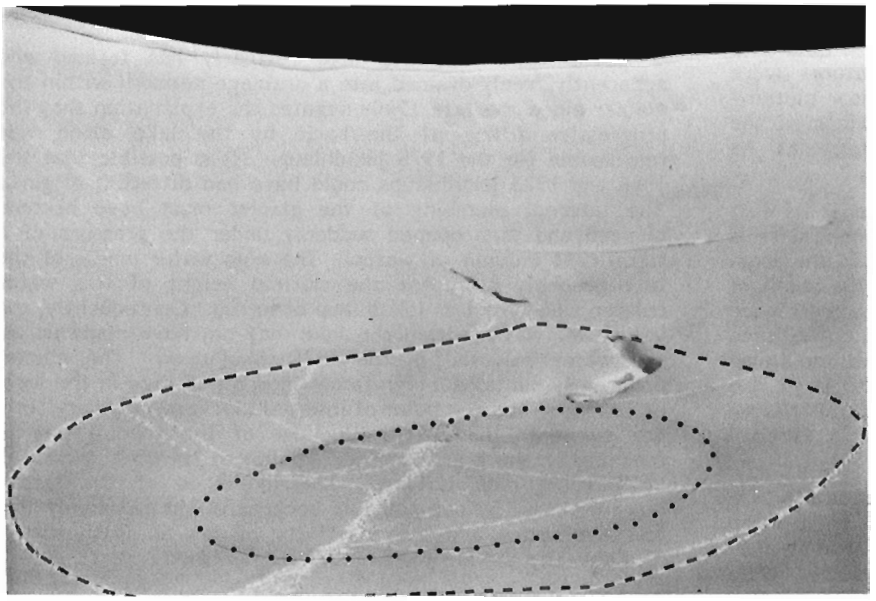

Figure 2

Looking approximately west to east along the long dimension of the glacial lake. The high water marks (dashed line) are about 73 m across in the direction of view and about 35 m in width; the dotted line denotes the low water marks created by the lake during the summer season 1978. The outlet fissure is visible at the end of the lake. Part of the fissure is covered by a snowbridge. Relief from the top of the fissure to the base is about 5 m. A crevasse trending at 90° to the fissure can be seen in the upper right of the photo.

Figure 3

A close-up view of the lower part of the outlet fissure.

Acknowledgments

I am indebted to Mr. J. Edworthy and Mr. M. Bourns for their consultation, to Dr. B. Leeson for this help in the field, and to Parks Canada for arranging helicopter transportation to Cathedral Glacier.

Setting

Cathedral Glacier rests on Cathedral Mountain – Cathedral Crags Massif on the south side of Kicking Horse Valley between approximately 2410 m and 2900 m elevation. A small lake is situated in a bowl-like depression on the northwestern margin of the glacier (Fig. 1). The depression is about 140 m wide, about 320 m long, and oriented east-west. Winds have built two ridges of snow around the depression: one on the north side rising to about 20 to 30 m above the floor of the bowl and one on the south side rising to about two thirds of this height.

The Lake

The presence of a small lake at the bottom of the depression along the northwest margin of Cathedral Glacier was first reported in 1949 (F.J. Stevens, personal communication, 1978). It is visible on an aerial photograph (National Airphoto Library A23408-73, scale 1:30 000) taken on July 24, 1973 (Fig. 1). Consequently, it has existed at least part of the time during the summer months for at least the last 30 years.

The lake depression was partly filled with snow at the time of inspection, but two sets of water level marks associated with the lake were apparent – a low level with lake dimensions of about 20 by 33 m marking the boundary of the present slush-filled lake and a level about 2 m higher with lake dimensions of about 35 by 73 m (Fig. 2). The high marks probably indicate the highest level reached by the lake in the last one or two years. The total volume of the lake basin up to the high water marks was estimated to range between 2260 and 3532 m^3 (J. Edworthy and M. Bourns, 1979; unpublished report). Probing of the lake bottom within the upper water marks indicated that about one sixth of the lake was floored by bedrock rather than glacial ice.

The anomalous ability of this lake to form well above the firn line, at about 2890 m elevation, can be attributed to the concave shape of the surrounding bowl which acts as a parabolic reflector. Although no air temperatures were taken at the time of the inspection, heavy outdoor clothing was required for comfort during windless conditions on the bowl's rim, whereas shirt-sleeves were adequate at its bottom.

A fissure outlet of the lake was discovered at its east end (Fig. 2, 3). The fissure is not a crevasse because it is oriented at right angles to the crevasse system in the area. The most probable explanation for it is that it is the result of water drainage through a zone of weakness over a protracted period of time (J. Edworthy and M. Bourns, 1979; unpublished report). Mr. Bourns was lowered into the fissure and found that the lake depression was freely draining into it at the time. It was also discovered that the floor of the fissure sloped away from the lake and terminated in a vertical moulin descending farther into the glacier.

The upper limit of the fissure is approximately 5 m above the floor of the lake. From the water-cut features on the wall of the fissure, from top to bottom, it appears that the lake basin has melted downward into the glacier while overflow from it has kept pace by deepening the outlet fissure.

Implications for the Origin of Jökulhlaups from Cathedral Glacier

The fact that the lake regularly has formed and apparently freely drained into a drainage network within the glacier since the late 1940s negates the explanation that the progressive filling of the basin by the lake alone was responsible for the 1978 jökulhlaup. (It is possible that the 1946 and 1925 jökulhlaups could have had different origins.) The internal plumbing of the glacier must have become plugged and then opened suddenly under the pressure of a significant column of water. The high water marks of the lake probably represent the critical height of this water column when the last jökulhlaup occurred. Consequently, the volume of water within the lake may not have made up all the water released in the 1978 jökulhlaup. The glacier apparently contains a significant internal storage in the form of conduits, and the point of internal blockage may vary from one event to the next. Blockage of the conduit due to freezing or the plastic squeezing shut of its walls appear to be possible explanations. The likelihood of the latter, however, may be questionable because of the relatively thin ice overburden and the inactivity of ice at this altitude (J. Edworthy and M. Bourns, 1979; unpublished report).

Reference

Jackson, L.E., Jr.
1979: A catastrophic glacial outburst flood (Jökulhlaup) mechanism for debris flow generation at the Spiral Tunnels, Kicking Horse River basin, British Columbia; Canadian Geotechnical Journal, v. 16, no. 4, p. 806-813.

A TRICLINIC UNIT CELL FOR OBOYERITE

Project 680023

A.C. Roberts
Central Laboratories and Technical Services Division

Oboyerite, $H_6Pb_6(TeO_3)_3(TeO_6)_2 \cdot 2H_2O$, is an extremely rare mineral found in the waste dumps of the Grand Central Mine, Tombstone, Arizona. Originally described by Williams (1979), it has been completely characterized except for the indexing of the powder diffraction pattern. Concerning this, Williams stated, "Despite determined efforts, the powder pattern could not be indexed by the Ito method and, due to the minute crystal size, single crystal work was impossible. Failure to index the pattern seems reasonable because the optics strongly suggest triclinic symmetry". The purpose of this short note is to report a possible triclinic cell which is consistent with the powder pattern and other mineralogical data.

The powder pattern of oboyerite, presented in Table 1, was indexed by the Ito method using the powder data reported by Williams (1979). The approximate cell deduced from theoretical calculations was refined on 16 lines between 9.038Å[1] and 1.911Å for which unambiguous indexing was possible. The refined triclinic unit cell parameters are:

a = 12.249(8) Å	α = 116.45(4)°
b = 15.113(6) Å	β = 98.58(4)°
c = 6.868(3) Å	γ = 85.82(4)°

The space group is $P\bar{1}(1)$ or P1(2) and the computed cell volume is 1125.6Å^3. With Z=2, the calculated density is 6.66 g/cm^3, in good agreement with the measured density of 6.4 ± 0.6 g/cm^3 obtained by Williams using Thoulet's method.

Reference

Williams, S.A.
1979: Girdite, oboyerite, fairbankite, and winstanleyite, four new tellurium minerals from Tombstone, Arizona; Mineralogical Magazine, v. 43, no. 328, p. 453-457.

[1] 1Å = 0.1 nm

Table 1

Triclinic indexing of oboyerite*

I est	dÅ meas	dÅ calc	hkl
3	9.038	9.056	110
1/2	6.752	6.765	020
3	6.077	6.096	001
		6.056	200
1	4.819	4.819	011
2	4.534	4.528	220
2	3.710	3.723	$31\bar{1}$
3	3.600	3.598	211
2	3.388	3.395	$02\bar{2}$
		3.383	040
3	3.273	several poss.	
7	3.180	3.180	301
10	3.040	3.041	031
5	2.976	2.976	$15\bar{1}$
5	2.927	2.926	$\bar{3}3\bar{1}$
5	2.862	2.865	$\bar{4}01$
		2.864	$24\bar{2}$
1/2	2.788	2.789	$\bar{2}2\bar{2}$
		2.786	$\bar{2}31$
1	2.646	2.645	150
3b	2.540	several poss.	
1	2.415	several poss.	
3b	2.264	2.264	440
		2.264	$03\bar{3}$
2	2.206	2.206	$22\bar{3}$
3	2.140	2.140	530
		2.140	053
		2.139	$\bar{2}6\bar{2}$
1	2.088	2.088	$41\bar{2}$
1	2.062	2.063	$45\bar{1}$
3	2.026	2.025	450
1/2	1.911	1.911	170
1/2	1.871	1.872	$07\bar{3}$
		1.870	$\bar{2}13$
1/2	1.842		
4b	1.804		
2	1.753		
2	1.728		
2	1.692		
2	1.663		
2	1.625		

*powder data taken from Williams (1979), CrKα radiation, 114 mm camera, indexed on a triclinic cell with a=12.249(8) Å, b=15.113(6) Å, c=6.868(3) Å, α=116.45(4)°, β=98.58(4)°, γ=85.82(4)°.

From: Scientific and Technical Notes in Current Research, Part B; Geol. Surv. Can., Paper 80-1B.

DETERMINATION OF YTTRIUM AND RARE-EARTH ELEMENTS IN ROCKS BY GRAPHITE-FURNANCE ATOMIC-ABSORPTION SPECTROMETRY

Project 690090

J.G. Sen Gupta
Central Laboratories and Technical Services Division

The high sensitivities of rare-earth elements in pyrolytically coated graphite-furnace atomization makes it possible to determine these elements in a variety of rocks using small amounts of sample. Traces of praseodymium, gadolinium, terbium and lutetium in some rocks, which cannot be determined by flame atomic-absorption because of insufficient sensitivities, can be determined accurately without difficulty by furnace atomization. Moreover, traces of yttrium, neodymium and samarium in rocks can be determined with greater accuracy by furnace atomization than by the flame.

The rare-earth elements are pre-concentrated from rocks by decomposition with hydrofluoric, nitric and perchloric acids, co-precipitation with calcium as oxalates and with iron as hydroxides (Sen Gupta, 1976, 1977). The concentrate is dissolved in dilute nitric acid, diluted to suitable volumes with water, and yttrium, praseodymium, neodymium, samarium, europium, gadolinium, terbium, dysprosium, holmium, erbium, thulium, ytterbium and lutetium are determined by graphite-furnace atomic-absorption spectrometry using an Instrumentation Laboratory Model 555 controlled-temperature furnace atomizer and a Model 151 atomic-absorption spectrophotometer. The method has been tested with synthetic solutions of rare-earth elements and iron simulating the rare-earth concentrates of international reference rocks GA (granite), NIM-G (granite), SY-2 (syenite) and SY-3 (syenite). Inter-element effects are negligible when dilute solutions are used.

The furnace atomization method has been used to determine yttrium and rare-earth elements in Canadian reference rock SY-2 (syenite), U.S.G.S. reference rocks W-2 (diabase), DNC-1 (diabase) and BIR-1 (basalt), and South African reference rock NIM-18/69 (carbonatite). The results are in satisfactory agreement with flame atomic-absorption and other values, where available.

References

Sen Gupta, J.G.

1976: Determination of lanthanides and yttrium in rocks and minerals by atomic-absorption and flame-emission spectrometry; Talanta, v. 23, p. 343-348.

1977: Determination of traces of rare-earth elements, yttrium and thorium in several international geological reference samples and comparison of data with other published values; Geostandards Newsletter, v. 1, p. 149-155.

From: Scientific and Technical Notes in Current Research, Part B; Geol. Surv. Can., Paper 80-1B.

DISCUSSIONS AND COMMUNICATIONS
DISCUSSIONS ET COMMUNICATIONS

THE PALEOLATITUDE AND PALEOMAGNETIC AGE OF THE ATHABASCA FORMATION, NORTHERN SASKATCHEWAN – FURTHER DISCUSSION

Paul Ramaekers
Saskatchewan Geological Survey
201 Dewdney Avenue East
Regina, Saskatchewan S4N 4G3

Fahrig et al. (1978) claimed to be able to date the Athabasca Sandstone by paleomagnetic means and suggested that samples showing reversed polarity indicated the possibility of chronostratigraphic correlation of redbed units within this sandstone.

In my discussion (Ramaekers, 1979) of their paper I presented evidence to show that neither claim is likely to be valid because: 1) petrographic evidence shows that much of the hematite in the Athabasca sediments is of late diagenetic origin, 2) Fahrig et al.'s (1978) data show so much scatter that they cannot be distinguished from a random distribution, 3) they have ignored the data with shallow magnetic inclinations, 4) their group of samples with steep inclinations, on which they based their age, is itself bimodal, showing a greater gap between the modes than exists between their group of samples with shallow and those with steep inclinations, 5) four of their samples are not of Athabasca Sandstone, as claimed, but are taken from basement rock, or have their footages mislabelled, 6) to date the Athabasca Sandstone, out of a total of 21 samples, Fahrig et al. (1978), used at least three and possibly up to six samples of altered basement, which they claimed to have been weathered 80 Ma before the deposition of the Athabasca Sandstone, 7) three of five of the samples used by them to obtain the date of weathering of the basement were virtually unaltered and their date probably reflects a basement tectonic event rather than a weathering event.

In their reply Fahrig et al. (1979) ignored the first four points in my discussion but reiterated 1) that their samples were all correctly identified and labelled, 2) that all the samples used to obtain the date of weathering of the basement were severely altered, 3) that diagenesis in the Athabasca Sandstone was a matter of at the most 'a few tens of millions of years', 4) that it was unlikely that dyke intrusion could affect Fe diagenesis.

Identification of Samples

As a core laboratory should be able to offer assurance to the public that due care is taken of the cores, Fahrig et al.'s (1979) claim that the cores they sampled were mixed after they studied them deserves some attention. Any discussion of this point must fit the following facts, readily verifiable by reference to the Saskatchewan Department of Mineral Resources Assessment File 74H15-0002, and the complete HL-1, HL-2, HL-3 cores in the Subsurface Geological Laboratory. All of these materials are accessible to the public. (1). The assessment file shows HL-1, HL-2, and HL-3 to bottom at 1115', 781', and 1117' respectively. (2). The company geologist at the drill site, who studied these cores before they were transported, reported the basement contact in these cores at 1087', 744', and 1048'. This means that the basement sections were 28', 37', and 69' long respectively, if this geologist's placement of the Athabasca-basement contact was correct. (3). At present there are 25', 34½', and 60½' of basement rock present in the respective cores, and these show no evidence of disruption (e.g. the regolith profiles are in their normal sequence). (4). The cores do not display evidence of major faults through the basement. None are noted by any geologist thus far. In particular, no evidence of post-Athabasca thrusting is present.

Thus, the sample footages HL-1 1092, HL-2 762, HL-3 1064, and HL-3 1072 fall a minimum of 2', 15½', 7½', and 15½' below the Athabasca-basement contact respectively, and are not Athabasca Sandstone as claimed by Fahrig et al. (1978 and 1979). Any core loss (and this often occurs at the top of the regolith, which is generally poorly recovered) would increase the depth of Fahrig et al.'s samples below the basement contact. Note that these measurements were made without reference to core footage indicators and are independent of possible errors in these. However, the drillsite geologist's report and the available footage indicators agree with the cores as they exist in our laboratory. Thus, if the footage indicators mislead Fahrig et al. then a rather severe core rearrangement occurred between the drillsite and La Ronge, and somehow undid itself between La Ronge and Regina. The application of Ockham's Razor suggests a simpler solution.

If we take Fahrig et al.'s footages as correct, they have mistaken basement core for Athabasca Sandstone. Listing where and who made the identifications (Fahrig et al., 1979) does not shed light on this problem; only the publication of a detailed petrographic description of their samples will do so. Examination of the footages used by Fahrig et al. (1978) indicates that in the case of HL-1 and HL-3 they sampled altered metaquartzite, the constituents of which, nearly exclusively quartz, clays, and hematite, are identical to those of the Athabasca Sandstone. This metaquartzite can be distinguished from the latter by its banding inclined at angles greater than 25° to the core axis, the presence of thin pegmatites, and by texture in thin section (paleosol textures). Well-exposed outcrops of it may be found, more or less on strike, near Rabbit Lake.

The Significance of the Rb/Sr Date on Basement Samples from the RL Core and Their Degree of Weathering

In that the Rb/Sr work of Wanless (written communication) yielded an "isochron age of 1631 ± 30 Ma" (reported as 1633 Ma in Fahrig et al., 1978), Fahrig et al.'s (1978) age of 1550 Ma for the deposition of the Athabasca Sandstone must have an error range of at least ±50 Ma associated with it, if they assumed that there is negligible difference between these two ages. Under the circumstance to regard these ages as equal (as evidenced by their use of regolith data to establish the age of the Athabasca Sandstone) is exactly as justifiable (or rather, as unjustifiable) as assuming the correct ages to be at least 160 Ma apart. Fahrig et al.'s (1978) Fig. 1.5 indicates a difference in paleolatitude of about 15° for a 80 Ma difference in age and about 35° for a 160 Ma age difference. These are not negligible values.

From: Discussions and Communications in Current Research, Part B; Geol. Surv. Can., Paper 80-1B

Table 1

Chemical analyses of the samples used in the Rb/Sr isochron date on the RL core

Sample No.	CaO	Al_2O_3
RL 4797	0.0	26.9
RL 4816	0.2	14.9
RL 4878	0.1	17.6
RL 4910	3.3	16.5
RL 4920	1.3	13.7
RL 4915	3.0	16.9

GSC Project No. 680135; Batch No. 73-29; Submitter's Name: W. Fahrig.

If, according to Fahrig et al. (1979), we cannot "speculate too intelligently regarding the exact size of the gap between weathering and sedimentation" then their use of regolith data to establish the age of deposition of the Athabasca Sandstone is astounding, as this clearly indicates that Fahrig et al. (1978) have not only speculated on this difference, but, for reasons unstated, have decided that it was negligible.

The main problem with Fahrig et al.'s use of the Rb/Sr data lies in their interpretation that the 1631 Ma date represents a weathering event. They base this on a claim that the samples were "all intensely weathered" as shown by their 'extremely low' calcium and "correspondingly high" alumina content. Fahrig et al. (1979) did not present the data on which they based this claim. They are presented here (Table 1) through the kindness of R.K. Wanless. These data, alluded to by Fahrig et al. (1979) and which were used as input to my description of these samples in the discussion (Ramaekers, 1979) show that: 1) The 3 deepest samples are virtually unaltered in CaO content. The Handbook of Geochemistry (p. 20-M-1) gives a weight per cent of 3.0 as the average abundance of CaO in Proterozoic 'banded gneiss, migmatite gneisses, granitic gneiss, minor amphibolitic inclusions' of the Canadian Shield, quoting Eade and Fahrig, (1971). For the 921 samples used these authors give no dispersion statistics, so that it is not easy to evaluate the significance of the value of 1.3 for sample RL 4920. However, Ronov and Migdisov (1970) obtained an average CaO content of 2.3 weight per cent on 460 samples of this type of Proterozoic rock from the Russian Platform. Evaluation of the values of the other major elements in sample RL 4920 strongly suggests that the value of 1.3 falls within the normal range of CaO content in unaltered rocks of this type; indeed, the average for the three deepest samples is higher than Ronov and Migdisov's average CaO value. 2) Only the stratigraphically highest sample in the RL core shows any enrichment in alumina. The average for this rock type of this age is 16.0 weight per cent (Eade and Fahrig, 1971). The Handbook of Geochemistry (p. 13-M-2) shows that in gneisses the value of alumina commonly ranges between 12 and 20 weight per cent around an average of about 16 weight per cent. 3) The same pattern holds for the other major elements not shown here; i.e. the deepest samples are virtually unaltered. Of the three deepest samples the only major element to indicate any sign of alteration is Na in RL 4910, which is depleted; H_2O^T is higher in this sample as well, but much less so in the two deeper samples. These values probably reflect the slight sericitization evident in thin section. 4) Sample 4878, the one sample not used in the isochron, and visually the most severely altered is also the most altered chemically.

Thus, as stated in my discussion (Ramaekers, 1979), the three deepest samples seem virtually unaltered in visual appearance, in thin section (less altered than most samples of the Mackenzie dykes in the Athabasca Basin which give normal Mackenzie event ages), and the chemical analyses confirm this. In view of this, Fahrig et al. may be assured that not only is material from below the zone of weathering in the RL core available, but that they have used it in their isochron. As with the Kenoran provenance ages obtained from the actual Athabasca Sandstone (Ramaekers, 1979), the fact that the two clearly altered samples of this core, but not the most altered one, fall on the same isochron as the unaltered samples, is in itself evidence that the Rb/Sr method is able to look through a considerable amount of weathering. Interpreting the 1631 Ma date as a late stage event of the basement rock (perhaps an episode of tectonic activity) fits in well with the other basement dates cited, which were not questioned by Fahrig et al. in their reply.

Duration of Diagenesis in the Athabasca Sandstone

Fahrig et al. failed to demonstrate, either in their paper or reply, 1) the existence of stratigraphic redbed units in the Athabasca Sandstone, 2) continuity of deposition in the Athabasca Sandstone, 3) age equivalence of the sandstone deposition and the oldest generation of hematite, and 4) immobility of the hematite after precipitation. Failure on any one of these points invalidates chronostratigraphic correlation of hematite-rich zones by magnetic reversals. As all evidence presented by me on these points (Ramaekers, 1979) was unchallenged by Fahrig et al. in their reply, their reassertion of their claim in this respect is hollow.

It is not just simply a matter that "some Phanerozoic sequences ... progressively reddened during time". Many such sequences show well defined magnetic poles indicating relatively shortlived, thorough going alteration events hundreds of millions of years after deposition. Others show modern poles. Ample examples of these and of other types of alteration are found in the references cited in my discussion. To say that "little is known about this possibility in Proterozoic sequences" is to ignore a considerable body of work, two of which were cited in my discussion. As Fahrig et al. (1979) point out "it is important to remember the scale of time involved"; however, diagenesis in the Athabasca Sandstone is not a matter of just a few "tens of millions of years". Dahlkamp (1978), cited in my discussion, establishes that pitchblende, in places intergrown with quartz overgrowths is of Permian to cretaceous age in the Athabasca Sandstone, about 1400 Ma younger than Fahrig et al.'s date for deposition of that sequence, thus showing that quartz diagenesis was still proceeding then. Hematite is also intergrown with pitchblende in many of the uranium shows and orebodies within the Athabasca Sandstone. Virtually all of these reveal Paleozoic or Mesozoic ages: e.g. Stewart Island, 400 Ma (Wanless, in Fahrig, 1961); Middle Lake, 100 Ma (Fahrig, 1961). The high Fe content of deep formation waters (10 ppm with a pH of 7.5; very high values in this pH range, Handbook of Geochemistry, p. 26-I-2) is evidence that Fe is still moving in the Athabasca Sandstone.

That the demagnetization events do not show more than one component, at any one sample is quite compatible with the mechanism of chemical remobilization of the Fe oxides that Fahrig et al. so steadfastly refused to consider in their paper or reply. This mechanism also explains why reversed and nonreversed samples of strikingly different magnetic inclinations lie so close together in the Athabasca Sandstone, something that is otherwise hard to explain without invoking otherwise detectable discontinuities, which Fahrig et al.

cannot do because it would make their proposed chronostratigraphic correlations impossible. The wide scatter of magnetic inclinations (0° – 80°) and their distribution through the Athabasca Sandstone (Fahrig et al., 1978) provides clear paleomagnetic evidence of Fe remobilization. For them to claim otherwise is to ignore their own data.

Effect of Dykes on Fe Diagenesis

The mobility of Fe in low temperature groundwater systems is well documented in the literature and needs no further comment. Thus it is surprising that the possibility of Fe remobilization as a result of stimulation of groundwater circulation by dyke intrusion seems "remote" to Fahrig et al. (1979). Groundwater circulation around dykes is widely recorded by students of geothermal systems (Ellis and Mahon, 1977, p. 33 and the many references therein). It is supported by simulation studies (Cathles, 1976), and by the study of connate waters (Roedder, 1979), which suggest that heat input into a basin will destabalize stagnant groundwater systems. Such a mechanism may also account for the correlation between the "oldest" uranium ages in the Athabasca Basin and the ages of dyke intrusion, a relation noted by virtually all authors in the literature on the Athabasca deposits.

Despite Fahrig et al.'s (1979) claims to the contrary, there is evidence of polarity reversal with Mackenzie event dykes. Within the Athabasca Basin occur Mackenzie event dykes with associated negative magnetic anomalies rather than the usual positive ones. Personen and Halls (1979) report Mackenzie dykes with reversed polarity elsewhere. However, the polarity of Mackenzie dykes is irrelevant to the point under discussion, which is the times of groundwater movement. Dykes will affect the movement of groundwater physically and chemically long after the former have cooled. Knowledge of the sampling density of the Sudbury dykes (Fahrig et al., 1979) is equally impertinent to understanding of Fe diagenesis within the Athabasca Basin. A discussion of sampling density, but more important of post-intrusive alteration of Mackenzie dykes within the Athabasca Basin, of which our mapping (Ramaekers and Hartling, 1979) has increased the number of known exposures by a factor of ten, would have been more to the point. Such work reveals intensive alteration of these dykes after intrusion, and hence the importance of late diagenetic alteration and of late Fe mobilization around the sites from which Fahrig et al. (1978) obtained most of the samples used in their attempt to find a depositional age for the Athabasca Sandstone.

References

Cathles, L.M.
1976: A physical model for pluton driven groundwater convection; Geological Society of America, Abstracts with Programs, p. 805-806.

Eade, K.E. and Fahrig, W.F.
1971: Geochemical evolutionary trends of continental plates – a preliminary study of the Canadian Shield; Geological Survey of Canada, Bulletin 179.

Ellis, A.J. and Mahon, W.A.J.
1977: Chemistry and geothermal systems; Academic Press, N.Y.

Fahrig, W.F.
1961: The Geology of the Athabasca Formation; Geological Study of Canada, Bulletin 68.

Fahrig, W.F., Christie, K.W. and Freda, G.
1978: The paleolatitude and paleomagnetic age of the Athabasca Formation, northern Saskatchewan; in Current Research, Part C, Geological Survey of Canada, Paper 78-1C, p. 1-6.

1979: The paleolatitude and paleomagnetic age of the Athabasca Formation, northern Saskatchewan – Reply; Geological Survey of Canada, Paper 79-1C, p. 119-120.

Ramaekers, Paul
1979: The paleolatitude and paleomagnetic age of the Athabasca Formation, northern Saskatchewan – Discussion; Geological Survey of Canada, Paper 79-1C, p. 117-119.

Ramaekers, Paul and Hartling, A.A.
1979: Structural geology and intrusive events of the Athabasca Basins and their bearing on uranium mineralization; Saskatchewan Geological Society, Special Publication Number 4, p. 221-234.

Roedder, E.
1979: Fluid inclusion evidence on the environments of sedimentary diagenesis, a review; Society of Economic Paleontologists and Mineralogists, Special Publication No. 26, p. 89-107.

Ronov, A.B. and Migdisov, A.A.
1970: Evolution of the chemical composition of the rocks in the shields and sediment cover of the Russian and North American Platform; Geochemistry, v. 7, p. 294.

Wedepohl, K.H. (ed.)
1969-1979: Handbook of Geochemistry; Springer-Verlag, Berlin.

Note from Chief Scientific Editor

This contribution terminates the discussion generated by the short papers by W.F. Fahrig, K.W. Christie and G. Freda published in Current Research, Part C, Geological Survey of Canada, Paper 78-1C.

NOTE TO CONTRIBUTORS

Submissions to the *Discussion* section of *Current Research* are welcome from both the staff of the Geological Survey and from the public. Discussions are limited to 6 double-spaced typewritten pages (about 1500 words) and are subject to review by the Chief Scientific Editor. Discussions are restricted to the scientific content of Geological Survey reports. General discussions concerning branch or government policy will not be accepted. Illustrations will be accepted only if, in the opinion of the editor, they are considered essential. In any case no redrafting will be undertaken and reproducible copy must accompany the original submissions. Discussion is limited to recent reports (not more than 2 years old) and may be in either English or French. Every effort is made to include both *Discussion* and *Reply* in the same issue. *Current Research* is published in January, June and November. Submissions for these issues should be received not later than November 1, April 1, and September 1 respectively. Submissions should be sent to the Chief Scientific Editor, Geological Survey of Canada, 601 Booth Street, Ottawa, Canada, K1A 0E8.

Avis aux auteurs d'articles

Nous encourageons tant le personnel de la Commission géologique que le grand public à nous faire parvenir des articles destinés à la section discussion *de la publication* Recherches en cours. *Le texte doit comprendre au plus six pages dactylographiées à double interligne (environ 1500 mots), texte qui peut faire l'objet d'un réexamen par le rédacteur en chef scientifique. Les discussions doivent se limiter au contenu scientifique des rapports de la Commission géologique. Les discussions générales sur la Direction ou les politiques gouvernementales ne seront pas acceptées. Les illustrations ne seront acceptées que dans la mesure où , selon l'opinion du rédacteur, elles seront considérées comme essentielles. Aucune retouche ne sera faite aux textes et dans tous les cas, une copie qui puisse être reproduite doit accompagner les textes originaux. Les discussions en français ou en anglais doivent se limiter aux rapports récents (au plus de 2 ans). On s'efforcera de faire coincider les articles destinés aux rubriques* discussions *et* réponses *dans le même numéro. La publication* Recherches en cours *paraît en janvier, en juin et en novembre. Les articles pour ces numéros doivent être reçus au plus tard le 1er novembre, le 1er avril et le 1er septembre respectivement. Les articles doivent être renvoyés au rédacteur en chef scientifique: Commission géologique du Canada, 601, rue Booth, Ottawa, Canada, K1A 0E8.*

ERRATUM

The legend for Figures 46.1 and 46.2 in Current Research, Part A, Paper80-1A (p. 320-322) was incomplete.

The complete legend and figures follow.

Figure 46.1.

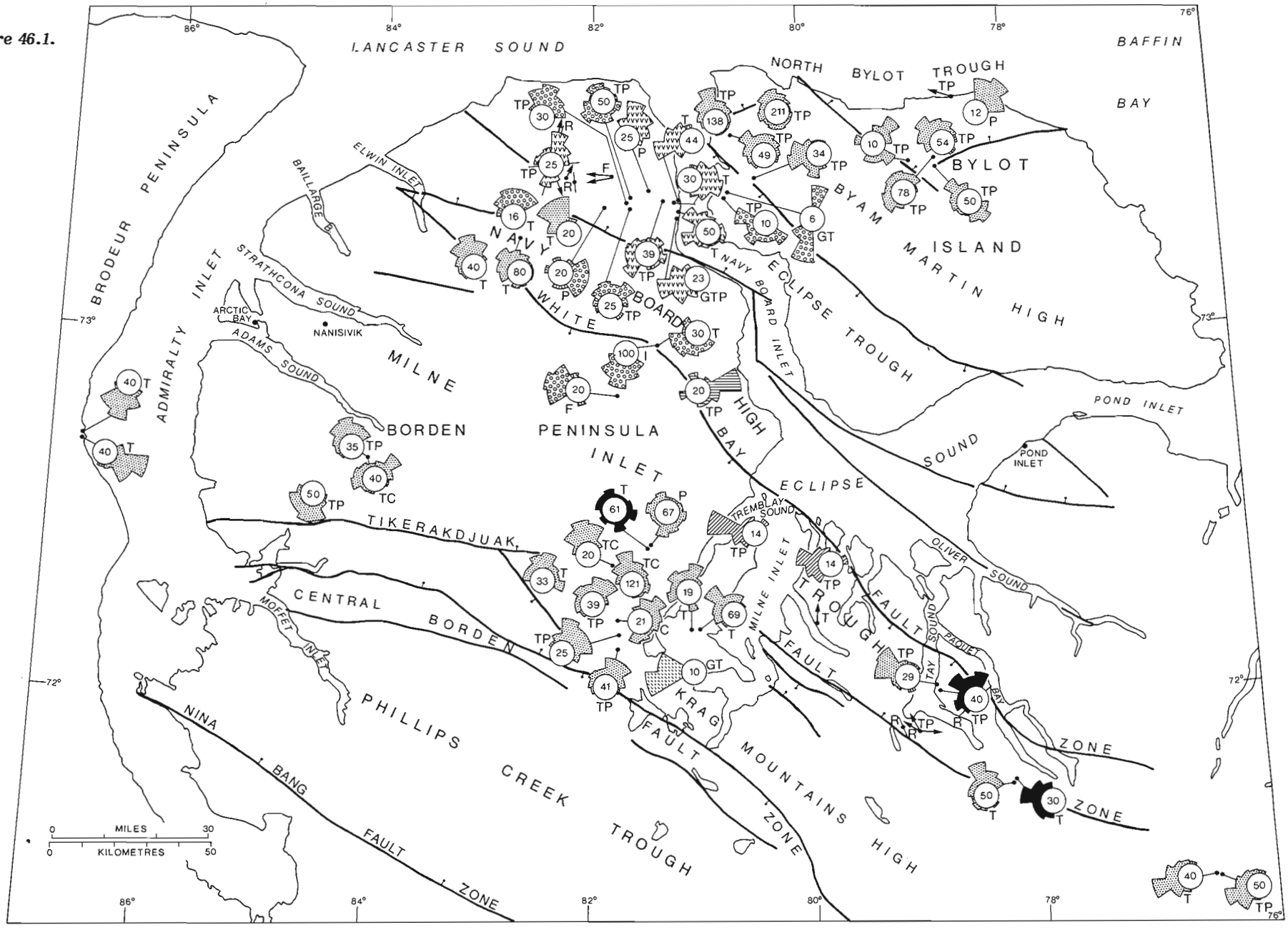

Figure 46.2.

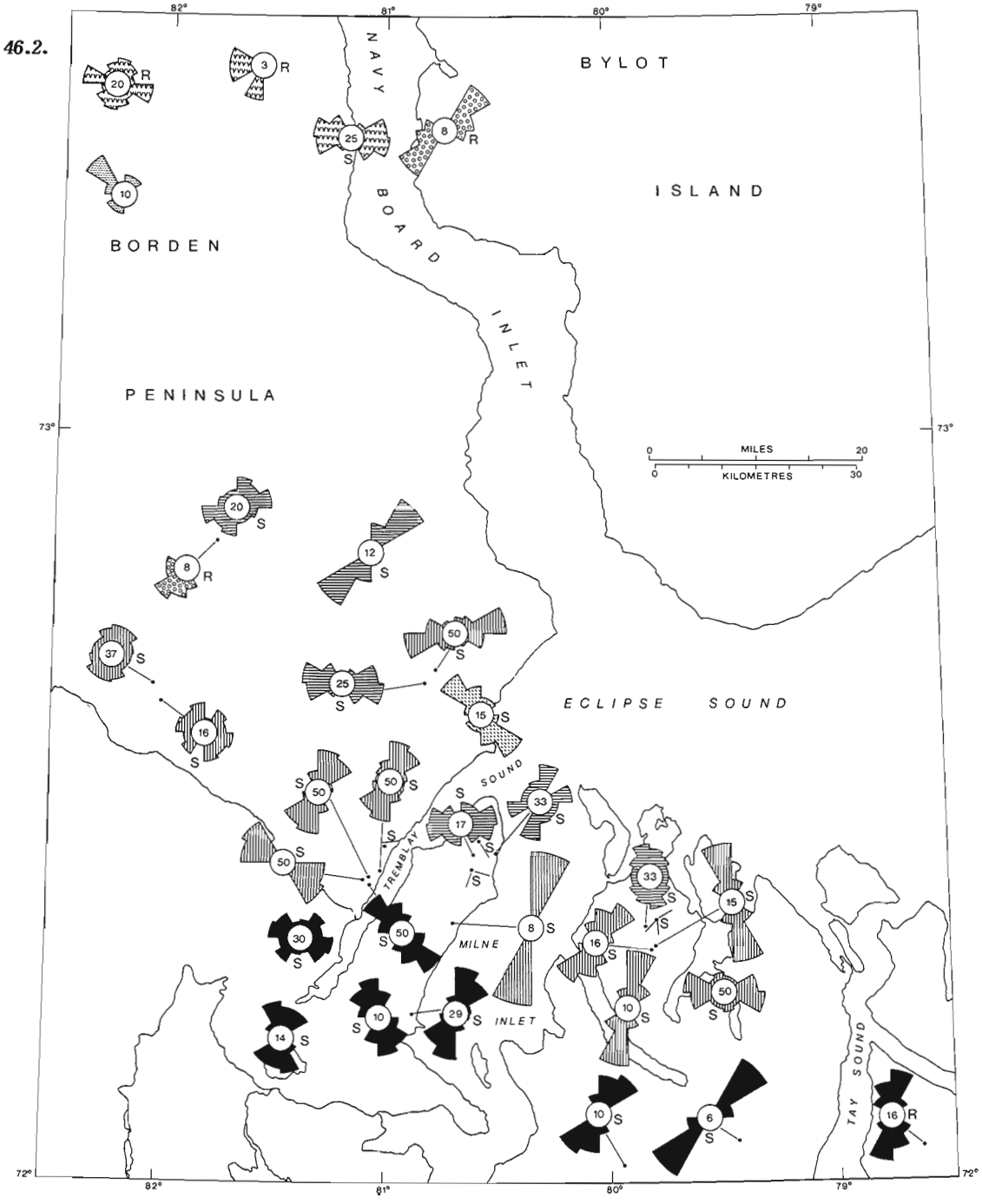

Legend for Figures 46.1 and 46.2

As a scale reference the radius of center circle in each row is 20 per cent, readings start on the circumference.
Numbers in circle indicate the number of readings.
Single determinations are indicated by a straight line or arrow.

- *Adams Sound Formation*
- *Arctic Bay Formation*
- *Fabricius Fiord Formation*
- *Society Cliffs Formation*
- *Victor Bay Formation*
- *Athole Point Formation*
- *Strathcona Sound Formation*
- *Elwin Formation*

C - channels
F - flutes
G - giant trough crossbeds
I - imbricate clasts
P - planar crossbeds
R - ripple marks
S - stromatolite elongations
T - trough crossbeds

AUTHOR INDEX